

LDEF- 69 Months in Space

NASA Conference Publication 3275

Part 2

Third Post - Retrieval Symposium

Edited by

Arlene S. Levine

NASA Langley Research Center

Hampton, Virginia

Proceedings of a symposium sponsored by the National Aeronautics and Space Administration, Washington, D.C., and the American Institute of Aeronautics and Astronautics, Washington, D.C., and held in Williamsburg, Virginia November 8-12, 1993



National Aeronautics and
Space Administration

Office of Management

Scientific and Technical
Information Program

1993

The use of trade names of manufacturers in this report does not constitute an official endorsement of such products or manufacturers, either expressed or implied, by the National Aeronautics and Space Administration.

This publication is available from the following sources:

NASA Center for AeroSpace Information
800 Elkridge Landing Road
Linthicum Heights, MD 21090-2934
(301) 621-0390

National Technical Information Service (NTIS)
5285 Port Royal Road
Springfield, VA 22161-2171
(703) 487-4650

FOREWORD

The third LDEF Post-Retrieval Symposium was held at the Williamsburg Lodge in Williamsburg, Virginia, November 8–12, 1993. Approximately 140 papers, posters, and demonstrations were presented. The Symposium represents the transition from focusing solely on a single spacecraft (LDEF) and its exposure to the low Earth orbit, to focusing on a broad approach to study the space environment and its effects. The LDEF program has provided a benchmark and means of comparison for other programs defining the low Earth orbit environment and its effects on spacecraft materials, systems, and structures. This Symposium included the preliminary results of European Retrievable Carrier (EURECA), the Evaluation of Oxygen Interactions with Materials III (EOIM-III) flight experiment, Salyut-7, and future flight experiments.

We have been challenged to design cheaper, better, and longer lasting spacecraft. NASA, other domestic and foreign agencies, and industry have contributed to the experiments and technologies now used to provide more accurate environmental definition and life prediction, lighter, long-lasting materials and structures, and more efficient systems. NASA's mission has always been to disseminate knowledge, and now we have been challenged to see that this knowledge is transformed into relevant technology.

The editor would like to thank all participants at the third Post-Retrieval Symposium for their contributions leading to the transfer of this technology. I would also like to thank all the contributing authors, as well as all those researchers who performed peer reviews of the enclosed papers. A special word of thanks goes to Bland Stein, Don Humes, and Steve Koontz, who reviewed more than their fair share of papers. I would like to thank the Symposium session chairs:

Darrel Tenney, *Opening Session*
Gale Harvey, *Induced Environment*
Alan Dover, *EURECA*
Thomas Parnell and James Adams, *Ionizing Radiation*
Friedrich Hörz, Dale Atkinson, J.A.M. McDonnell, Michael Zolensky, Donald Kessler,
Donald Humes, and Jean-Claude Mandeville, *Meteoroid and Debris*
Philip Young, Ann Whitaker, Gary Pippin, James Zwiener, Joan Funk, and Bruce
Banks, *Materials*
Steve Koontz and Wayne Stuckey, *EOIM-III*
James Mason, *Systems*
Ranty Liang and William Kinard, *Future Activities*

Many thanks to Susan Hurd (Mason and Hanger) for her patient, gracious, and invaluable editing and to Maureen Sgambelluri (Troy Systems) for her patience and skill in reformatting papers to meet our requirements.

NASA CP-3275 is the third LDEF Post-Retrieval Symposium. The first Symposium, NASA CP-3134, was held in 1991 in Kissimmee, Florida, and the second Symposium, NASA CP-3194, was held in San Diego, California, in 1992. You may request copies of either or both proceedings. For information please contact

Arlene S. Levine
Mail Stop 404
NASA Langley Research Center
Hampton, Virginia 23681-0001
phone: 804 864-3318/fax: 804 864-8094
e-mail: a.s.levine@larc.nasa.gov

CONTENTS

FOREWORD	iii
Author Index	xv

PART 1*

NATURAL AND INDUCED ENVIRONMENTS

LDEF Environment Modeling Updates	3
Tim Gordon, Ray Rantanen, Ann Whitaker	
Outgassing Products from Orbiter TPS Materials	13
Gale A. Harvey, Tom J. Lash, J. Richard Rawls	

EUROPEAN RETRIEVABLE CARRIER (EURECA)

EURECA 11 Months in Orbit: Initial Post Flight Investigation Results	23
Alan Dover, Roberto Aceti, Gerhard Drolshagen	
Dosimetric Results on EURECA	37
G. Reitz	
Preliminary Results of Radiation Measurements on EURECA	43
E.V. Benton, A.L. Frank	
Performance Characterizations of EURECA Retroreflectors with Fluoropolymer-Filled SiO_x Protective Coatings	51
Bruce A. Banks, Sharon K. Rutledge, Michael Cales	
Effect of the Space Environment on Materials Flown on the EURECA/TICCE-HVI Experiment	65
Carl R. Maag, William G. Tanner, Tim J. Stevenson, Mare Crisium, Janet Borg	
Material Inspection of EURECA: First Findings and Recommendations	71
Marc Van Eesbeek, Michael Froggatt, Georges Gourmelon	

IONIZING RADIATION

LDEF Contributions to Cosmic Ray and Radiation Environments Research	89
Thomas A. Parnell	
Trapped Iron Measured on LDEF	91
R. Beaujean, D. Jonathal, S. Barz, W. Enge	
Characteristics of Low Energy Ions in the Heavy Ions in Space (HIIS) Experiment	101
Thomas Kleis, Allan J. Tylka, Paul R. Boberg, James H. Adams, Jr., Lorraine P. Beahm	

*Part 1 is presented under separate cover.

1984 14

Results from the Heavy Ions in Space (HIIS) Experiment on the Ionic Charge State of Solar Energetic Particles	113
Allan J. Tylka, Paul R. Boberg, James H. Adams, Jr., Lorraine P. Beahm, Thomas Kleis	
Early Results from the Ultra Heavy Cosmic Ray Experiment	129
D. O'Sullivan, A. Thompson, J. Bosch, R. Keegan, K.-P. Wenzel, F. Jansen, C. Domingo	
Absorbed Dose and LET Spectra Measurements on LDEF	135
E.V. Benton, I. Csige, A.L. Frank, E.R. Benton, L.A. Frigo, T.A. Parnell, J. Watts, A. Harmon	
Fission Foil Measurements of Neutron and Proton Fluences in the A0015 Experiment	149
A.L. Frank, E.V. Benton, T.W. Armstrong, B.L. Colborn	
Measurement of Trapped Proton Fluences in Main Stack of P0006 Experiment	159
N. Nefedov, I. Csige, E.V. Benton, R.P. Henke, E.R. Benton, L.A. Frigo	
Contribution of Proton-Induced Short Range Secondaries to the LET Spectra on LDEF	167
E.R. Benton, I. Csige, E.V. Benton, L.A. Frigo	
Charge, Energy and LET Spectra of High LET Primary and Secondary Particles in CR-39 Plastic Nuclear Track Detectors of the P0006 Experiment	179
I. Csige, L.A. Frigo, E.V. Benton, K. Oda	
Predictions of LET Spectra Measured on LDEF	181
T.W. Armstrong, B.L. Colborn, E.V. Benton	
Doing Photons with Merlin II at Oroville	189
Alan R. Smith, Donna L. Hurley	
Status of LDEF Activation Measurements and Archive	199
B. Alan Harmon, Thomas A. Parnell, Christopher E. Laird	
Predictions of LDEF Radioactivity and Comparison with Measurements	203
T.W. Armstrong, B.L. Colborn, B.A. Harmon, C. E. Laird	
Status of LDEF Radiation Modeling	217
John W. Watts, T.W. Armstrong, B.L. Colborn	
¹⁰Be in Terrestrial Bauxite and Industrial Aluminum: An LDEF Fallout	227
J.C. Gregory, A. Albrecht, G. Herzog, J. Klein, R. Middleton, B.A. Harmon, T.A. Parnell	
Germination, Growth Rates, and Electron Microscope Analysis of Tomato Seeds Flown on the LDEF	231
Ernest C. Hammond, Jr., Kevin Bridgers, Cecelia Wright Brown	

SPACE ENVIRONMENTS
Meteoroid and Debris

Status of LDEF Contributions to Current Knowledge of Meteoroid and Manmade Debris Environments and Their Effects on Spacecraft in LEO	255
William H. Kinard	
LDEF Meteoroid and Debris Special Investigation Group Investigations and Activities at the Johnson Space Center	257
Thomas H. See, Michael E. Zolensky, Ronald P. Bernhard, Jack L. Warren, Clyde A. Sapp, Claire B. Dardano	
Micrometeoroids and Debris on LDEF: Comparison With MIR Data	275
Jean-Claude Mandeville, Lucinda Berthoud	
Small Craters on the Meteoroid and Space Debris Impact Experiment	287
Donald H. Humes	
Long-Term Microparticle Impact Fluxes on LDEF Determined from Optical Survey of Interplanetary Dust Experiment (IDE) Sensors	323
C.G. Simon, J.P. Oliver, W.J. Cooke, K.I. Downey, P.C. Kassel	
Penetration Rates Over 30 Years in the Space Age	337
J.A.M. McDonnell, J.M. Baron	
LDEF Interplanetary Dust Experiment (IDE) Results	353
John P. Oliver, S.F. Singer, J.L. Weinberg, C.G. Simon, W.J. Cooke, P.C. Kassel, W.H. Kinard, J.D. Mulholland, J.J. Wortman	
The Orbital Characteristics of Debris Particle Rings as Derived from IDE Observations of Multiple Orbit Intersections with LDEF	361
William J. Cooke, John P. Oliver, Charles G. Simon	
Orbital Debris and Meteoroid Population as Estimated from LDEF Impact Data	373
Jingchang Zhang, Donald J. Kessler	
Hypervelocity Impact Survivability Experiments for Carbonaceous Impactors: Part II	385
T.E. Bunch, Julie M. Paque, Luann Becker, James F. Vedder, Jozef Erlichman	
Analytical Electron Microscopy of LDEF Impactor Residues	401
Ronald P. Bernhard, Ruth A. Barrett, Michael E. Zolensky	
Natural and Orbital Debris Particles on LDEF's Trailing and Forward-Facing Surfaces	415
Friedrich Hörz, Ronald P. Bernhard, Thomas H. See, Donald E. Brownlee	
Debris and Meteoroid Proportions Deduced from Impact Crater Residue Analysis	431
Lucinda Berthoud, Jean-Claude Mandeville, Christian Durin, Janet Borg	
Micro-Abrasion Package Capture Cell Experiment on the Trailing Edge of LDEF: Impactor Chemistry and Whipple Bumper Shield Efficiencies	445
Howard J. Fitzgerald, Hajime Yano	

Secondary Ion Mass Spectrometry (SIMS) Analysis of Hypervelocity Microparticle Impact Sites on LDEF Surfaces	459
C.G. Simon, A.J. Buonaquisti, D.A. Batchelor, J.L. Hunter, D.P. Griffis, V. Misra, D.R. Ricks, J.J. Wortman, D.E. Brownlee, S.R. Best, M.S. Crumpler, B. Arad, S. Eliezer, S.E. Moshe, S. Maman, I. Gilath	
SIMS Chemical and Isotopic Analysis of Impact Features from LDEF Experiments AO187-1 and AO187-2	461
Frank J. Stadermann, Sachiko Amari, John Foote, Pat Swan, Robert M. Walker, Ernst Zinner	
Image and Compositional Characteristics of the "Big Guy" LDEF Impact Crater	475
T.E. Bunch, Julie M. Paque, Michael Zolensky	
The Effect of Impact Angle on Craters Formed by Hypervelocity Particles . .	483
David C. Hill, M. Frank Rose, Steve R. Best, Michael S. Crumpler, Gary D. Crawford, Ralph H-C. Zee, Michael J. Bozack	
Experimental Investigation of the Relationship Between Impact Crater Morphology and Impacting Particle Velocity and Direction	499
N.G. Mackay, S.F. Green, D.J. Gardner, J.A.M. McDonnell	
Determining Orbital Particle Parameters of Impacts into Germanium Using Morphology Analysis and Calibration Data from Hypervelocity Impact Experiments in the Laboratory	509
Klaus G.Paul	
Cratering and Penetration Experiments in Teflon Targets at Velocities from 1 To 7 KM/S	521
Friedrich Hörz, Mark J. Cintala, Ronald P. Bernhard, Thomas H. See	
Dimensional Scaling for Impact Cratering and Perforation	523
Alan J. Watts, Dale Atkinson	

PART 2

MATERIALS

Summary and Review of Materials Special Investigation Group Evaluations of Hardware from the Long Duration Exposure Facility	539-1
Ann F. Whitaker, Joan Funk, Gary Pippin and Harry Dursch	
Recent Results from Long Duration Exposure Facility Materials Testing	555 -2
H.G. Pippin, H.W. Dursch	
LDEF Polymeric Materials: A Summary of Langley Characterization	567 -3
Philip R. Young, Wayne S. Slemple, Karen S. Whitley, Carol R. Kalil, Emilie J. Siochi, James Y. Shen, A. C. Chang	
Surface Characterization of LDEF Carbon Fiber/Polymer Matrix Composites	601 -4
Holly L. Grammer, James P. Wightman, Philip R. Young, Wayne S. Slemple	

Space Environmental Effects on Polymer Matrix Composites as a Function of Sample Location on LDEF	613	5
R.C. Tennyson, G.R. Cool, D.G. Zimcik		
Nonlinear Viscoelastic Characterization of Polymer Materials Using a Dynamic-Mechanical Methodology	631	6
Thomas W. Strganac, Debbie Flowers Payne, Bruce A. Biskup, Alan Letton		
The Effect of Simulated Low Earth Orbit Radiation on Polyimides (UV Degradation Study)	645	7
John S. Forsythe, Graeme A. George, David J.T. Hill, James H. O'Donnell, Peter J. Pomery, Firas A. Rasoul		
The Surface Properties of Fluorinated Polyimides Exposed to VUV and Atomic Oxygen	657	8
John S. Forsythe, Graeme A. George, David J.T. Hill, James H. O'Donnell, Peter J. Pomery, Firas A. Rasoul		
Collection and Review of Metals Data Obtained from LDEF Experiment Specimens and Support Hardware	667	9
Roger Bourassa, Gary Pippin		
Measurements of the Optical Properties of Thin Films of Silver and Silver Oxide	689	10
Palmer N. Peters, Robert C. Sisk, Yolanda Brown, John C. Gregory, Pallob K. Nag, Ligia Christl		
Changes in Chemical and Optical Properties of Thin Film Metal Mirrors on LDEF	703	11
Palmer N. Peters, James M. Zwiener, John C. Gregory, Ganesh N. Raikar, Ligia C. Christl, Donald R. Wilkes		
Further Investigations of Experiment AO034 Atomic Oxygen Stimulated Outgassing	727	12
Roger C. Linton, Miria M. Finckenor, Rachel R. Kamenetzky		
Atomic Oxygen Interactions with Protected Organic Materials on the Long Duration Exposure Facility (LDEF)	737	13
Bruce A. Banks, Kim K. de Groh, Justine L. Bucholz, Michael R. Cales		
Trend Analysis of In-Situ Spectral Reflectance Data from the Thermal Control Surfaces Experiment (TCSE)	755	14
D.R. Wilkes, P.S. LeMaster, R.J. Mell, E.R. Miller, J.M. Zwiener		
Whisker/Cone Growth on the Thermal Control Surfaces Experiment #S0069	771	15
James M. Zwiener, James E. Coston, Jr., Donald R. Wilkes, Edgar R. Miller, Richard J. Mell		
Durability of Reflector Materials in the Space Environment	791	16
Ann F. Whitaker, Miria M. Finckenor, David Edwards, Rachel R. Kamenetzky, Roger C. Linton		

Four Space Application Materials Coatings on the Long-Duration Exposure Facility (LDEF)	803	-17
John J. Scialdone and Carroll Clatterbuck		
Organic Matrix Composite Protective Coatings for Space Applications	825	-18
Harry Dursch and Pete George		
Structure and Properties of Polymeric Composite Materials During 1501 Days Outer Space Exposure on the "Salyut-7" Orbital Station	843	-19
Oleg V. Startsev, Eugene F. Nikishin		
Overview of the LDEF MSIG Databasing Activities	859	
Joan G. Funk		

PART 3*

EVALUATION OF OXYGEN INTERACTIONS WITH MATERIALS III (EOIM-III)

An Overview of the Evaluation of Oxygen Interactions with Materials III Experiment: Space Shuttle Mission 46, July - August 1992	869
Steven L. Koontz, Lubert J. Leger, James T. Visentine, Don E. Hunton, Jon B. Cross, Charles L. Hakes	
Evaluation of Oxygen Interactions with Materials III — Mission and Induced Environments	903
Steven L. Koontz, Lubert J. Leger, Steven L. Rickman, Charles L. Hakes, David T. Bui, Donald Hunton, Jon B. Cross,	
Spacecraft Materials Studies on the Aerospace Corporation Tray on EOIM-III	917
Wayne K. Stuckey, Carol S. Hemminger, Gary L. Steckel, Malina M. Hills, Michael R. Hilton	
Exposure of LDEF Materials to Atomic Oxygen: Results of EOIM-III	931
C.H. Jagers, M.J. Meshishnek	
Atomic Oxygen Dosimetry Measurements Made on STS-46 by CONCAP-II	957
J.C. Gregory, G.P. Miller, P.J. Pettigrew, G.N. Raikar, J.B. Cross, E. Lan, C.L. Renschler, W.T. Sutherland	
Inflight Resistance Measurements on High-T_c Superconducting Thin Films Exposed to Orbital Atomic Oxygen on CONCAP-II (STS-46)	971
J.C. Gregory, G.N. Raikar, J.A. Bijvoet, P.D. Nerren, W.T. Sutherland, A. Mogro-Campero, L.G. Turner, Hoi Kwok, I.D. Raistrick, J.B. Cross, D.W. Cooke, C. Mombourquette, R.J. Houlton, F.H. Garzon, R. Herschitz	
LEO Degradation of Graphite and Carbon-Based Composites Aboard Space Shuttle Flight STS-46	989
Blaine R. Spady, R.A. Synowicki, Jeffrey S. Hale, M.J. De Vries, John A. Woollam, Arthur W. Moore, Max Lake	

*Part 3 is presented under separate cover.

Orbital Atomic Oxygen Effects on Materials: An Overview of MSFC Experiments on the STS-46 EOIM-3	999
Roger C. Linton, Jason A. Vaughn, Miria M. Finckenor, Rachel R. Kamenetzky, Robert F. DeHaye, Ann F. Whitaker	
Effects of Atomic Oxygen on Polymeric Materials Flown on EOIM-3	1011
Rachel R. Kamenetzky, Roger C. Linton, Miria M. Finckenor, Jason A. Vaughn	
Thermal Control Materials on EOIM-3	1025
Miria M. Finckenor, Roger C. Linton, Rachel R. Kamenetzky, Jason A. Vaughn	
Solid Film Lubricants and Thermal Control Coatings Flown Aboard the EOIM-3 MDA Sub-Experiment	1037
Taylor J. Murphy, Kaia E. David, Hank W. Babel	
Evaluation of Space Environmental Effects on Metals and Optical Thin Films on EOIM-3	1053
Jason A. Vaughn, Roger C. Linton, Miria M. Finckenor, Rachel R. Kamenetzky	
Analysis of Selected Specimens from the STS-46 Energetic Oxygen Interaction with Materials-III Experiment	1067
Johnny L. Golden, Roger J. Bourassa, Harry W. Dursch, H. Gary Pippin	
Molecular Beam Scattering from ¹³C-Enriched Kapton and Correlation with the EOIM-3 Carousel Experiment	1095
Timothy K. Minton, Teresa A. Moore	
BMDO Materials Testing in the EOIM-3 Experiment	1115
Shirley Y. Chung, David E. Brinza, Timothy K. Minton, Ranty H. Liang	
STS-46 Plasma Composition Measurements Using the EOIM-3 Mass Spectrometer	1129
Donald E. Hunton, Edmund Trzcinski, Roger Gosselin, Steve Koontz, Lubert Leger, Jim Visentine	
Point Defect Formation in Optical Materials Exposed to the Space Environment	1131
J. L. Allen, N. Seifert, Y. Yao, R.G. Albridge, A.V. Barnes, N.H. Tolk, A.M. Strauss, R.C. Linton, R.R. Kamenetzky, J.A. Vaughn, M.M. Finckenor	
SYSTEMS	
LDEF Systems Special Investigation Group Overview	1149
Jim Mason, Harry Dursch	
System Results from FRECOPA	1153
Christian Durin, Lucinda Berthoud, Jean-Claude Mandeville	
Space Environmental Effects on Solar Cells: LDEF and Other Flight Tests . .	1167
Peter Gruenbaum, Harry Dursch	
A Final Look at LDEF Electro-Optic Systems Components	1179
M.D. Blue	

Effects of the LDEF Orbital Environment on the Reflectance of Optical Mirror Materials	1189
Howard Herzig, Charles M. Fleetwood, Jr.	
Effects of Low Earth Orbit on the Optical Performance of Multilayer Enhanced High Reflectance Mirrors	1205
Terence Donovan, Linda Johnson, Karl Klemm, Rick Scheri, Jean Bennett, Jon Erickson, Filippo di Brozolo	
Effects of Long Term Space Environment Exposure on Optical Substrates and Coatings (S0050-2)	1227
John Vallimont, E. Steven Brandt, Keith Havey, Arthur Mustico	
Long Duration Exposure Facility (LDEF) Space Optics Handbook	1229
William T. Kemp, Edward Taylor, Robert Champetier, Alan Watts, Dale Atkinson	
Space Environmental Effects Observed on the Hubble Space Telescope	1231
Joel E. Edelman, James B. Mason	
Hardware Cleanliness Methodology and Certification	1237
Gale A. Harvey, Thomas J. Lash, J. Richard Rawls	
FUTURE ACTIVITIES	
From LDEF to a National Space Environment and Effects (SEE) Program: A Natural Progression	1247
David E. Bowles, Robert L. Calloway, Joan G. Funk, William H. Kinard, Arlene S. Levine	
Long Duration Exposure Facility (LDEF) Archive System	1249
Brenda K. Wilson	
The Long Duration Exposure Facility (LDEF) Annotated Bibliography	1263
Arlene S. Levine	
The Long Duration Exposure Facility (LDEF) Photographic Survey Special Publication	1267
Robert L. O'Neal, Arlene S. Levine, Carol C. Kiser	
SPACE STATION	
LDEF's Contribution to the Selection of Thermal Control Coatings for the Space Station	1273
Henry W. Babel	
Space Station Program Status and Research Capabilities	1285
Alan C. Holt	
Space Station as a Long Duration Exposure Facility	1289
Adrienne Folley, Jim Scheib	
A Materials Exposure Facility	1301
Wayne S. Slemple, Don E. Avery	

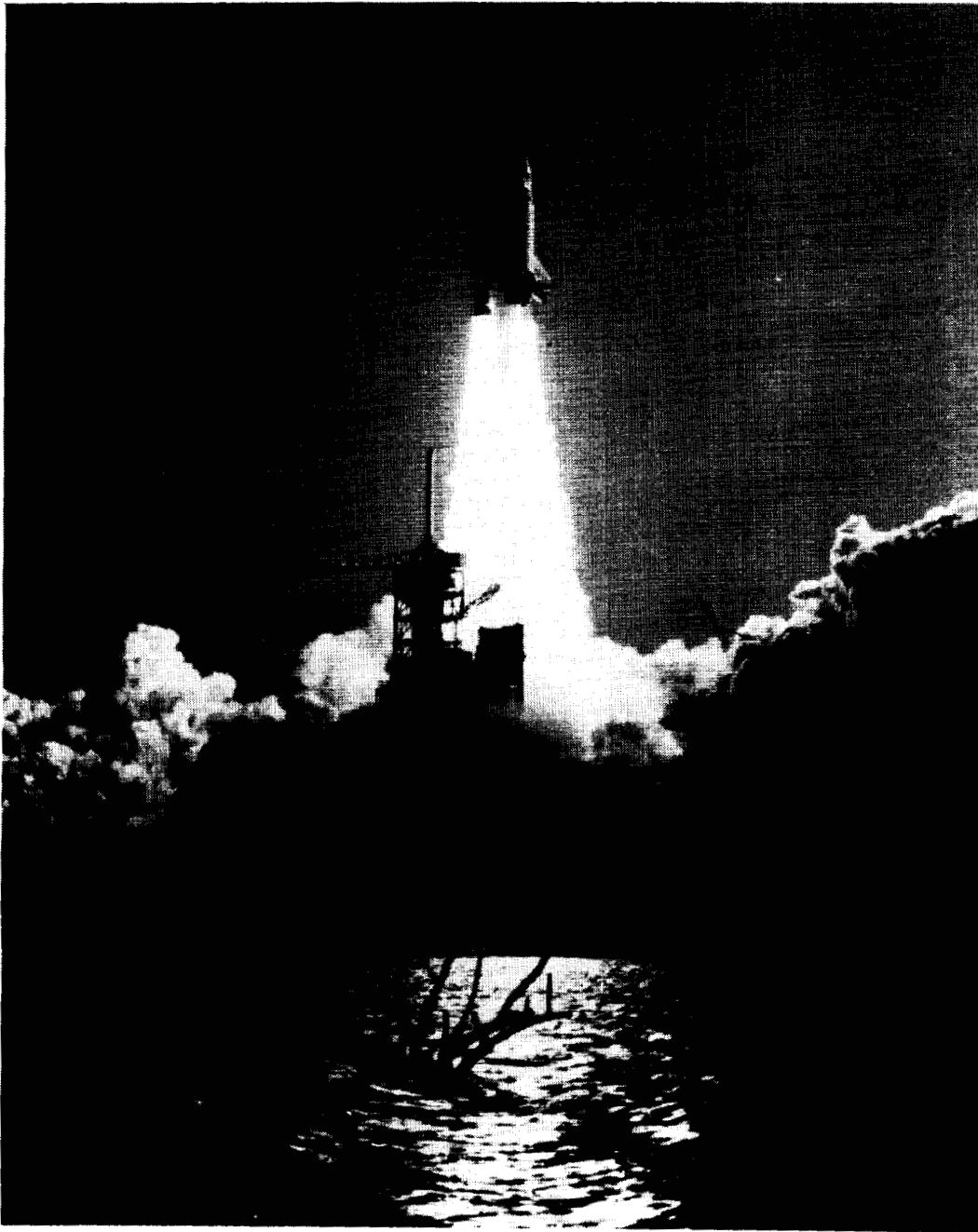
OTHER SPACECRAFT

- An LDEF Follow-on Spacecraft Concept** 1307
Vernon Keller, Larry Breazeale, Don Perkinson, William H. Kinard
- Long Duration Exposure Facility Post-Flight Data as It Influences
the Tropical Rainfall Measuring Mission** 1309
Sharon A. Straka

EXPERIMENTS

- Element Material Exposure Experiment by EFFU** 1321
Yoshihiro Hashimoto, Masaaki Ichikawa, Mitsuru Takei, Yoshihiro Torii, Kazuo Ota
- Orbiting Meteoroid and Debris Counting Experiment** 1331
William H. Kinard, Dwayne Armstrong, Sharon K. Crockett, James L. Jones, Jr.,
Philip C. Kassel, Jr., J.J. Wortman
- The Strategic Technologies for Automation and Robotics (STEAR)
Program Protection of Materials in the Space Environment Subprogram** 1341
L R. Schmidt, J. Francoeur, A. Agüero, M.R. Wertheimer, J.E. Klemberg-Sapieha,
L. Martinu, J. W. Blezius, M. Olivier, A. Singh
- The Orbital Debris Detector Consortium: Suppliers of Instruments for
In Situ Measurements of Small Particles in the Space Environment** 1361
C.G. Simon, R. Münzenmeyer, W.G. Tanner, Jr., O.M. Uy, R.A. Skrivanek, Jr.,
A.J. Tuzzolino, C. Maag, J.J. Wortman
- A New Technique for Ground Simulation of Hypervelocity Debris** 1379
R. Roybal, J. Shively, C. Stein, C. Miglionico, R. Robertson

AUTHOR INDEX



84-5648

100-174

xv

PRECEDING PAGE BLANK NOT FILMED

AUTHOR INDEX

Part 1 — pages 1—536
Part 2 — pages 537—866
Part 3 — pages 867—1388

A

Aceti, Roberto 23
Adams, James H., Jr. 101, 113
Agüero, A. 1341
Albrecht, A. 227
Albridge, R.G. 1131
Allen, J.L. 1131
Amari, Sachiko 461
Arad, B 459
Armstrong, Dwayne 1331
Armstrong, T.W. 149, 181, 203, 217
Atkinson, Dale 523, 1229
Avery, Don E. 1301

B

Babel, Henry W. 1037, 1273
Banks, Bruce A. 51, 737
Barnes, A.V. 1131
Baron, J.M. 337
Barrett, Ruth A. 401
Barz, S. 91
Batchelor, D.A. 459
Beahm, Lorraine P. 101, 113
Beaujean, R. 91
Becker, Luann 385
Bennett, Jean 1205
Benton, E.R. 135, 159, 167
Benton, E.V. 43, 135, 149, 159, 167, 179, 181
Bernhard, Ronald P. 257, 401, 415, 521
Berthoud, Lucinda 275, 431, 1153
Best, Steve R. 459, 483
Bijvoet, J.A. 971
Biskup, Bruce 631
Blezius, J.W. 1341
Blue, M.D. 1179
Boberg, Paul R. 101, 113
Borg, Janet 65, 431
Bosch, J. 129
Bourassa, Roger 667, 1067
Bowles, David E. 1247
Bozack, Michael J. 483
Brandt, E. Steven 1227
Breazeale, Larry 1307

Bridgers, Kevin 231
Brinza, David E. 1115
Brown, Cecelia Wright 231
Brown, Yolanda 689
Brownlee, Donald E. 415, 459
Bucholz, Justine L. 737
Bui, David T. 903
Bunch, T.E. 385, 475
Buonaquisti, A.J. 459

C

Cales, Michael 51, 737
Calloway, Robert L. 1247
Champetier, Robert 1229
Chang, A.C. 567
Christl, Ligia 689, 703
Chung, Shirley Y. 1115
Cintala, Mark J. 521
Clatterbuck, Carroll 803
Colborn, B.L. 149, 181, 203, 217
Cooke, D.W. 971
Cooke, William J. 323, 353, 361
Cool, G.R. 613
Coston, James, E., Jr. 771
Crawford, Gary D. 483
Crisium, Mare 65
Crockett, Sharon K. 1331
Cross, Jon B. 869, 903, 957, 971
Crumpler, Michael S. 459, 483
Csige, I. 135, 159, 167, 179

D

Dardano, Claire B. 257
David, Kaia E. 1037
de Groh, Kim K. 737
DeHaye, Robert F. 999
DeVries, M.J. 989
di Brozolo, Filippo 1205
Domingo, C. 129
Donovan, Terence 1205
Dover, Alan 23
Downey, K.I. 323
Drolshagen, Gerhard 23
Durin, Christian 431, 1153
Dursch, H.W. 539, 555, 825, 1067, 1149, 1167

E

Edelman, Joel E. 1231
Edwards David 791
Eliezer, S. 459
Enge, W. 91

Erickson, Jon 1205
Erlichman, Jozef 385

F

Finckenor, Miria M. 727, 791, 999, 1011, 1025, 1053, 1131
Fitzgerald, Howard J. 445
Fleetwood, Charles M., Jr. 1189
Folley, Adrienne 1289
Foote, John 461
Forsythe, John S. 645, 657
Francoeur, J. 1341
Frank, A.L. 43, 135, 149
Frigo, L.A. 135, 159, 167, 179
Froggatt, Michael 71
Funk, Joan G. 539, 859, 1247

G

Gardner, D.J. 499
Garzon, F.H. 971
George, Graeme A. 645, 657
George, Pete 825
Gilath, I. 459
Golden, Johnny L. 1067
Gordon, Tim 3
Gosselin, Roger 1129
Gourmelon, Georges 71
Grammer, Holly L. 601
Green, S.F. 499
Gregory, J.C. 227, 689, 703, 957, 971
Griffis, D.P. 459
Gruenbaum, Peter 1167

H

Hakes, Charles L. 869, 903
Hale, Jeffrey S. 989
Hammond, Ernest C., Jr. 231
Harmon, B. Alan 135, 199, 203, 227
Harvey, Gale A. 13, 1237
Hashimoto, Yoshihiro 1321
Havey, Keith 1227
Hemminger, Carol S. 917
Henke, R.P. 159
Herschitz, R. 971
Herzig, Howard 227, 1189
Herzog, G. 227
Hill, David C. 483
Hill, David J.T. 645, 657
Hills, Malina M. 917
Hilton, Michael R. 917
Holt, Alan C. 1285

Hörz, Friedrich 415, 521
Houlton, R.J. 971
Humes, Donald H. 287
Hunter, J.L. 459
Hunton, Don E. 869, 903, 1129
Hurley, Donna L. 189

I

Ichikawa, Masaaki 1321

J

Jaggers, C.H. 931
Jansen, F. 129
Johnson, Linda 1205
Jonathal, D. 91
Jones, James L. Jr. 1331

K

Kalil, Carol R. 567
Kamenetzky, Rachel R. 727, 791, 999, 1011, 1025, 1053, 1131
Kassel, P.C. 323, 353, 1331
Keegan, R. 129
Keller, Vernon 1307
Kemp, William T. 1229
Kessler, Donald J. 373
Kinard, W.H. 255, 353, 1247, 1307, 1331
Kiser, Carol 1267
Klein, J. 227
Kleis, Thomas 101, 113
Klemberg-Sapieha, J.E. 1341
Klemm, Karl 1205
Koontz, Steven L. 869, 903, 1129
Kwok, Hoi 971

L

Laird, Christopher E. 199, 203
Lake, Max 989
Lan, E. 957
Lash, Tom J. 13, 1237
Leger, Lubert J. 869, 903, 1129
LeMaster, P.S. 755
Letton, Alan 631
Levine, Arlene S. 1247, 1263, 1267
Liang, Ranty H. 1115
Linton, Roger.C. 727, 791, 999, 1011, 1025, 1053, 1131

M

Maag, Carl R. 65, 1361
Mackay, N.G. 499

Maman, S. 459
Mandeville, Jean-Claude 275, 431, 1153
Martinu, L. 1341
Mason, James B. 1149, 1231
McDonnell, J.A.M. 337, 499
Mell, Richard J. 755, 771
Meshishnek, M.J. 931
Middleton, R. 227
Miglione, C. 1379
Miller, Edgar R. 755, 771
Miller, G.P. 957
Minton, Timothy K. 1095, 1115
Misra, V. 459
Mombourquette, C. 971
Mogro-Campero, A. 971
Moore, Arthur W. 989
Moore, Teresa A. 1095
Moshe, S.E. 459
Mulholland, J.D. 353
Murphy, Taylor J. 1037
Münzenmeyer, R. 1361
Mustico, Arthur 1227

N

Nag, Pallob, K. 689
Nefedov, N. 159
Nerren, P.D. 971
Nikishin, Eugene F. 843

O

Oda, K. 179
O'Donnell, James H. 645, 657
O'Neal, Robert L. 1267
O'Sullivan, D. 129
Oliver, John P. 323, 353, 361
Olivier, M. 1341
Ota, Kazuo 1321

P

Paque, Julie M. 385, 475
Parnell, Thomas A. 89, 135, 199, 227
Paul, Klaus G. 509
Payne, Debbie F. 631
Perkinson, Don 1307
Peters, Palmer N. 689, 703
Pettigrew, P. J. 957
Pippin, H. Gary 539, 555, 667, 1067
Pomery, Peter J. 645, 657

R

Raikar, G.N. 703, 957, 971
Raistrick, I.D. 971
Rantanen, Ray 3
Rasoul, Firas A. 645, 657
Rawls, J. Richard 13, 1237
Reitz, G. 37
Renschler, C.L. 957
Rickman, Steven L. 903
Ricks, D.R. 459
Robertson, R. 1379
Rose, M. Frank 483
Roybal, R. 1379
Rutledge, Sharon K. 51

S

Sapp, Clyde A. 257
Scheib, Jim 1289
Scheri, Rick 1205
Schmidt, L.R. 1341
Scialdone, John J. 803
See, Thomas H. 257, 415, 521
Seifert, N. 1131
Shen, James Y. 567
Shively, J. 1379
Simon, Charles G. 323, 353, 361, 459, 1361
Singer, S.F. 353
Singh, A. 1341
Siochi, Emilie J. 567
Sisk, Robert C. 689
Skrivanek, R.A. 1361
Slemp, Wayne S. 567, 601, 1301
Smith, Alan R. 189
Spady, Blaine R. 989
Stadermann, Frank J. 461
Startsev, Oleg V. 843
Steckel, Gary L. 917
Stein, C. 1379
Stevenson, Tim J. 65
Straka, Sharon A. 1309
Strauss, A.M. 1131
Strganac, Thomas W. 631
Stuckey, Wayne K. 917
Sutherland, W.T. 957, 971
Swan, Pat 461
Synowicki, R.A. 989

T

Takei, Mitsuru 1321
Tanner, W.G. 65, 1361

Taylor, Edward 1229
Tennyson, R.C. 613
Thompson, A. 129
Tolk, N.H. 1131
Torii, Yoshihiro 1321
Trzcinski, Edmund 1129
Turner, L.G. 971
Tylka, Allan J. 101, 113
Tuzzolino, A.J. 1361

U

Uy, O.M. 1361

V

Vallimont, John 1227
Van Eesbeek, Marc 71
Vaughn, Jason A. 999, 1011, 1025, 1053, 1131
Vedder, James F. 385
Visentine, James T. 869, 1129

W

Walker, Robert M. 461
Warren, Jack L. 257
Watts, Alan J. 523, 1229
Watts, John W. 135, 217
Weinberg, J.L. 353
Wenzel, K.-P. 129
Wertheimer, M.R. 1341
Whitaker, Ann F. 3, 539, 791, 999
Whitley, Karen S. 567
Wightman, James P. 601
Wilkes, Donald R. 703, 755, 771
Wilson, Brenda K. 1249
Woollam, John A. 989
Wortman, J.J. 353, 459, 1331, 1361

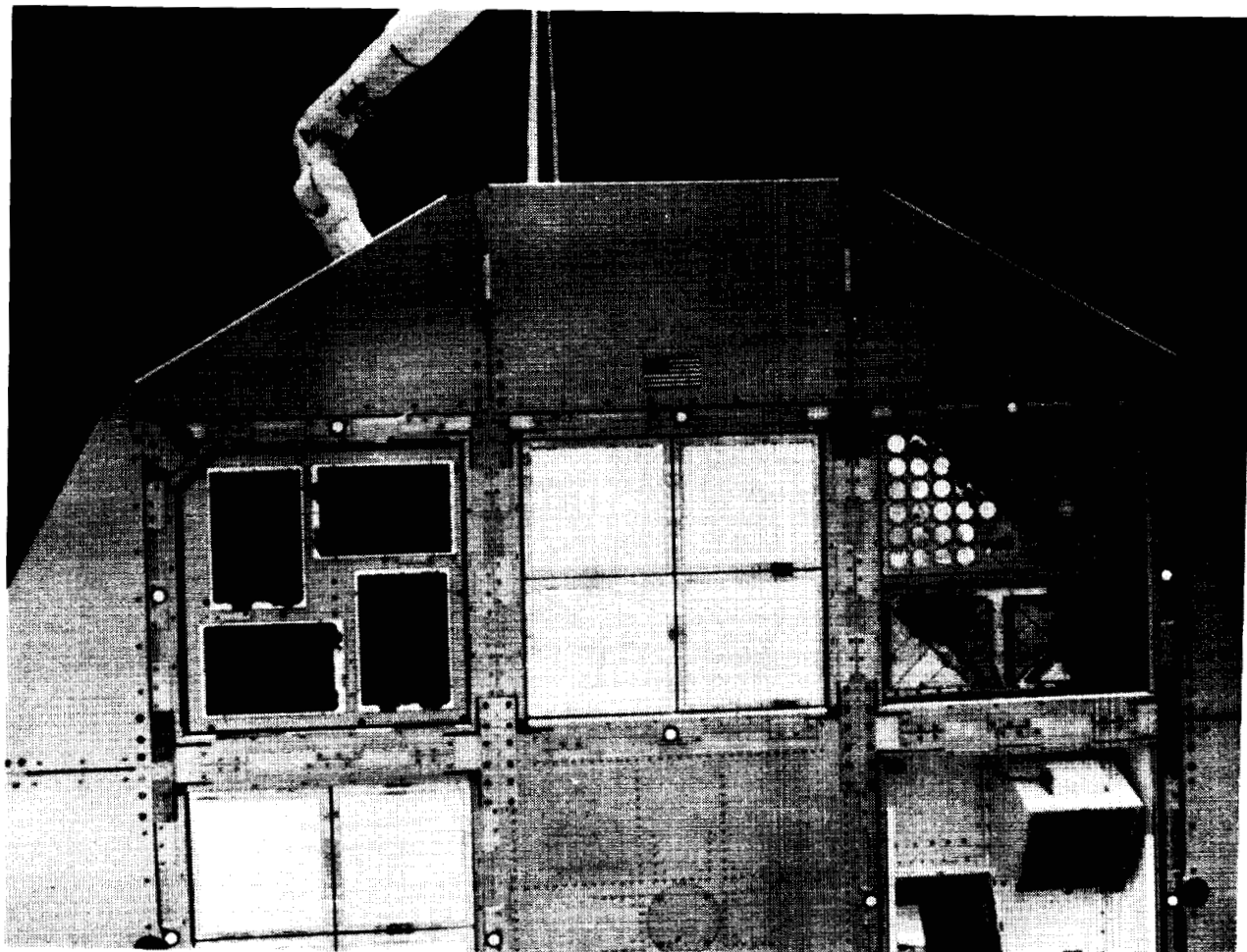
Y

Yao, Y. 1131
Yano, Hajime 445
Young, Philip R. 567, 601

Z

Zee, Ralph H-C. 483
Zhang, Jingchang 373
Zimcik, D.G. 613
Zinner, Ernst 461
Zolensky, Michael E. 257, 401, 475
Zwiener, James M. 703, 755, 771

PART 2
MATERIALS



L-84-4335

SUMMARY AND REVIEW OF MATERIALS SPECIAL INVESTIGATION GROUP
EVALUATIONS OF HARDWARE FROM THE LONG DURATION EXPOSURE FACILITY

Ann F. Whitaker
NASA/Marshall Space Flight Center
Huntsville, AL 35812
Phone: (205) 544-2510

51-25

2/10/90

15f

Joan Funk
NASA/Langley Research Center
Hampton, VA 23681-0001
Phone: (804) 864-3092

Gary Pippin*
Harry Dursch
Boeing Defense and Space Group
P.O. Box 3999
Seattle, WA 98124-2499
Phone: (206) 773-2846

ABSTRACT

Major materials findings obtained during LDEF post-flight investigations over the past three and one-half years are reported. The summary of findings to date includes results for thermal control coatings, thin polymeric films, composites, metals, adhesives, contamination, and environments definitions. Reaction rates of selected materials exposed to atomic oxygen are presented. Results useful for model verification and comparison with ground based facility data are specifically highlighted. Potential areas for future work are described. In conclusion, a rationale for a second long term flight experiment is presented.

INTRODUCTION

The Materials Special Investigation Group (MSIG), formed by NASA to direct the analysis of materials from the Long Duration Exposure Facility (LDEF), has supported numerous activities since the LDEF retrieval in January 1990. These efforts have included materials analyses, contamination analyses, and definition of the specific LDEF environmental exposure. This exposure over 5.8 years was dominated by ultraviolet radiation (UV) effects at the beginning of the mission. As the orbit decayed near the end of the mission, atomic oxygen (AO) dominated the low Earth orbital effects. Examinations have confirmed the expected performance of selected materials and demonstrated that effects on passive thermal control systems are quite dependent

* Boeing Defense and Space Group activities were funded by NASA Langley Research Center contract NAS1-19247, Task 8.

upon the exact exposure sequence. The LDEF materials database has supported some important conclusions about engineering uses of selected paints, coated composites, thin polymeric films, adhesives, seals, lubricants, and metals in long term LEO exposures. Detailed reviews of these investigations have been presented at the first three LDEF post-retrieval symposia (refs. 1-3) and two materials workshops (refs. 4-5). Comprehensive reports on these same subjects are nearing completion.

Current (as of November 1993) results of studies of thermal control paints, silverized Teflon™, thin polymeric films, composites, adhesives, lubricants, composites, anodized aluminum, glassy ceramic materials, and effects of contamination on the performance of certain materials are summarized in this paper. This work includes recession rate determinations of some thin polymeric films, silverized Teflon, and composites, embrittlement and/or darkening of thermal control materials under solar exposure, and deposition and subsequent darkening of a number of contaminant films. Some evaluations are extensive and quantitative enough to provide baselines for comparison with ground-based exposure results.

In addition to the extensive investigations already completed, there are still several areas with the potential for providing useful information. Examinations of changes in the thin binder layer in the A-276 paint buttons subsequent to UV exposure will provide information on polymer breakdown mechanisms, structural changes with depth, and clues for manufacturing inherently resistant materials. Selected S13G/LO samples may also be studied in the same manner. UV induced changes in the resin systems of composite materials, Kapton, and Mylar are other subjects which have not been examined in detail. The contamination deposition around vents, near selected outgassing sources, and inside the canisters which opened in stages may be compared to existing contamination models. This activity would require additional analyses to define the amount and nature of the surface deposits in these areas.

ENVIRONMENTS

The values for atomic oxygen and solar UV fluences around the LDEF are reproduced in figure 1. These values include the integrated fluence over all portions of the flight, including the brief exposure in the orbiter cargo bay after retrieval. Detailed information regarding other exposure environments, thermal cycling, meteoroid and space debris impacts, and particulate radiation are found in reports and papers (refs. 6-8) produced by other special investigation groups.

OBSERVED MATERIALS EFFECTS

Thermal Control Paints

White thermal control paints with organic binders retained their optical properties under combined atomic oxygen and UV exposure. However, as the organic binder was eroded by AO, the mechanical integrity of the paint was lost. Trailing edge A-276 specimens, mainly exposed to solar UV and thermal cycling, had a darkened thin outer layer of binder. Specimens taken from

trailing edge locations on the LDEF and reflight on the Evaluation of Oxygen Interaction with Materials-3 experiment (EOIM-3) on the STS-46 shuttle flight partially recovered their initial low absorptance as the damaged binder layer was eroded by atomic oxygen. Exposure to atomic oxygen simultaneous with, or following, solar UV-induced darkening of low absorptivity organic paints can reverse this increased absorptivity leading to performance lifetimes much greater than expected for diffuse paints.

The Z-93 inorganic paint specimens remained white under AO and UV exposure, while the S13G/LO binder darkened, limiting its performance lifetime as the absorptance increased. The black Z-306 paint maintained its optical properties but lost mechanical integrity in the same manner as the A-276. At certain locations on the leading edge the ring of Z-306 surrounding the white A-276 paint buttons was almost completely removed. Z-302 on the leading edge lost binder and pigment essentially down to the substrate. This material retained its absorptance; however, it became diffuse and the emittance was reduced, thus limiting the use of this material for thermal control applications in an AO environment.

Silverized Teflon

The Teflon layer of the nominally 5 mil thick Ag/FEP thermal control blankets used on the A0178 and P0004 experiments recessed under atomic oxygen exposure. Optical property changes as a result of this exposure include an increase in the diffuse component of the reflectance but no change in either solar absorptance or infrared emittance. Specimens from the trailing edge blankets showed no change in their optical properties but did show considerable embrittlement as evidenced by their decreased elongation and ultimate tensile strength values in comparison with leading edge, unexposed, and ground control specimens.

Adhesive backed silverized Teflon tape used on the M0001 experiment, located on the space end of LDEF, ripped along a 90° bend where the tape fastened multi-layer insulation to the aluminum substrate. These failures, shown in figure 2, were most likely caused by the repeated thermal cycling coupled with the associated mechanical motion. The tape was bonded without any allowance for stress relief, and the UV embrittlement lowered the strength of the material. Areas of Ag/FEP bonded to a rigid aluminum substrate, shown in figure 3, increased in solar absorptivity during UV exposure. The application procedure resulted in cracks in the extremely thin (few hundred angstroms) silver and inconel layers. This allowed the adhesive to pass through the metal layers and collect under the FEP layer, where it was darkened by the solar exposure.

Polymeric Films

Thin polymeric films exposed on leading edge locations were eroded significantly and often removed completely under combined AO, solar UV, and thermal cycling exposure. The recession of such films caused failure of the film materials and loss of its engineering function. Failed metallized films produced significant particulate contamination as the loss of the polymer layer allowed the vacuum deposited metals to disperse. Films or coatings which contained inert particle fillers were damaged less severely under the same exposure conditions. This implies that the performance lifetimes of some films may be extended by the atomic oxygen shielding effect of inert particles. Pure organic polymeric films have erosion rates which are linear with exposure to atomic oxygen. This means that the lifetime and performance of such materials is relatively predictable.

Recession rates for Kapton and FEP Teflon, as determined by profilometry, cross-section photomicrographs, or weight change, are given in Table 1.

Composites

Uncoated composite materials eroded under atomic oxygen attack. The organic resins eroded faster than the fibers. Carbon fiber composite erosion rates approached the erosion rate of carbon as the outer resin layer was removed. Recession rates for selected composites are given in Table 1. The recession rate values are averages, since the resins react faster than the carbon fibers. Fiberglass composites became self-protecting as the reactive resin portions were eroded away, exposing the inert glass fibers. As expected, coated composites retained their mechanical properties even when the coatings were degraded over a range of AO and UV exposures. Thin coatings of nickel, SiO₂, and paints all protected composites effectively; no erosion of the coated composites was observed except at meteoroid and space debris impact sites. The significance of these observations is that light-weight composite structures with thin coatings may be used for non-contamination critical LEO applications. Use of such structures in a contamination-sensitive application would be dictated by the properties of the coating material.

Lubricants and Adhesives

Most adhesives and lubricant materials on LDEF were shielded from atomic oxygen and UV radiation and only exposed to vacuum and thermal cycling. Most adhesives used on the LDEF worked well, and post-flight peel strengths were similar to those for control specimens. The LDEF experience verified the use of adhesive tapes for non-structural spacecraft applications. Use of Velcro™ was also verified as an easy method to attach and detach hardware. All Velcro used on LDEF remained functional, although the Dacron thread used to attach Velcro on experiment S1005 failed due to atomic oxygen attack. DC6-1104 RTV adhesive was used successfully to bond Velcro to aluminum and to Z-306 painted blankets. Acrylic adhesive used with UV transparent materials darkened with no change in functional properties. For lubricant materials used on fasteners, the performance was a materials usage issue. The lubricant must be carefully selected if on-orbit cycling is required. Silver plating and MoS₂ on bolts prevented galling (ref. 9).

Chromic Acid Anodized Aluminum

Chromic acid anodized (CAA) aluminum was virtually unchanged by exposure to LEO conditions. This material showed only a slight increase in absorptance at trailing edge locations, attributed to contamination films. CAA aluminum has good potential for long-term space applications. Black chromium plated aluminum, used on experiment A0076 (tray F9) and on Earth end panels, showed large variations in post-flight optical properties. Much of this variation was associated with complex exposure histories, such as shielding by the Earth end support beam and failed aluminum film folding over onto the chromium plating. Figure 4 shows an on-orbit photograph of experiment A0076 and a post-flight close-up of the black chrome plated solar collector.

Metals

Certain metals were affected by the long term exposure to LEO. Atomic oxygen and thermal cycling-induced mechanical stress played major roles in the magnitude of degradation. Thin films of aluminum and tantalum failed under thermal cycling. Leading edge copper straps

darkened, and the absorptance increase correlates with atomic oxygen fluence. The oxidation is superficial; copper would survive if used bare as an interconnect material but would probably operate at a higher temperature over time. Bare 6061-T6 aluminum remained significantly discolored relative to anodized aluminum under both high UV and high AO exposures.

Glassy Ceramics

Glassy ceramics used as mirror coatings increased in film density with reduction in thickness when exposed to AO and solar UV. SiO was converted to SiO₂, and MgF₂ surfaces lost fluorine. These materials had small decreases in solar reflectance. Defects were noted in materials which were not completely oxidized. Coatings for solar mirrors must be selected carefully based on their potential for being oxidized and their susceptibility to densification and reduction in film thickness.

CONTAMINATION

Contamination was present in both particulate and molecular form. A wide variety of particulate contaminants were observed on the LDEF. The distribution of particles include contributions from pre-flight, on-orbit, and post-flight exposures. Debris from failed materials or hardware was transported to other locations during flight, causing large and unpredicted effects in specific areas. The transport mechanisms for this particle movement are not well understood. Particulate debris preferentially collected in the LDEF wake. Aluminizations on thin Mylar and Kapton films created significant particulate contamination after the polymeric material completely eroded away.

Contamination films are common to all materials. Such films may particularly affect short term recession rate measurements. Contaminants may oxidize and act as a sacrificial material to AO erosion or physically block oxygen access to the substrate material. This may be temporary, until the contaminant is oxidized to a volatile species and evaporates, or it may have long term influences if the reaction product, such as SiO_x, is not volatile under the particular flight conditions. Thin molecular film contaminant layers were produced from multiple local sources on the LDEF, including: 1) materials from end structure reflectors, 2) the unbaked Z-306 paint used on the interior of the LDEF structure, and 3) several organic and silicone based materials used on or as part of various experiments. The potential sources and the associated deposited films were subjected to the full range of LDEF exposures depending on their location. The influences of such films on the electrical and optical properties vary with silicone and hydrocarbon sources and exposure. There are a number of competing post-deposition processes which either fix material in place or remove material. Such processes may form films through UV induced reactions which darken and attach material firmly to the substrate or AO oxidation to non-volatile products. Oxidized film layers may also trap materials, allowing subsequent UV darkening of underlying contaminant layers. Silicon was detected at many locations on LDEF but appears to always be associated with a localized source.

MODELING OF SPACE ENVIRONMENT EFFECTS

Figures 5 and 6 show the atomic oxygen fluence vs. time as a percent of total exposure and as a function of incidence angle. The observations of the condition of materials on LDEF are dominated by the fact that the spacecraft experienced over half its oxygen fluence in the last six months of the mission. Materials performance lifetimes are influenced not only by the exposures but the sequence of exposures. The thermal velocity spread among atomic oxygen atoms allows significant amounts of oxygen to reach positions in excess of 100° from the ram direction. Details of the atomic oxygen environment models have been presented in detail in previous reports (ref. 10). LDEF data is available in sufficient amounts to verify atomic oxygen exposure, UV exposure, and contamination deposition models and to predict property changes associated with these types of exposures. Also available are recession rates of FEP, TFE, several composites, and paint systems due to AO exposures, and changes in optical properties due to UV exposures. Using in-flight and post-flight measurements of thermal control coatings, degradation trend analyses were performed for extrapolation of solar absorptance values for Z-93, S13G/LO, A-276 with RTV670 overcoat, A-276 with OI650 overcoat, and chromic acid anodized aluminum (ref. 11). Outgassing of RTV silicones, Z-306 paints, and heat shrink tubing have been measured. Thermal models of the entire spacecraft and selected surfaces have been carried out (ref. 6).

LDEF results allow for many benchmark comparisons with ground-based test facilities. Dimensional changes in various composite laminates due to moisture outgassing in vacuum were measured both during the LDEF flight for the first 370 days and in the laboratory (ref. 12). Diffusion coefficients were also predicted using control and LDEF flight specimens. Atomic oxygen interaction with polymers at defect sites in protective coatings have been studied by Banks, et al. (ref. 13). Using LDEF flight samples and samples exposed in RF plasma ashers in the laboratory, a Monte Carlo model was developed for predicting undercut cavities and atomic oxygen scattering.

Further investigation of simulated space environment, particularly synergistic effects, is needed. Such comparisons could include atomic oxygen recession on composites, Kapton, and FEP Teflon; solar UV darkening of white thermal control paints; mechanical property changes in composites and FEP Teflon including percent elongation to failure and tensile strength; solar cell performance; physical degradation of paints under atomic oxygen exposure; fixing of silicone contaminants on substrates; and specular changes in materials.

RATIONALE FOR FUTURE FLIGHT TESTING

There exists a continuing need for long term LEO exposure testing. Spacecraft missions are being extended to longer and longer times to obtain the maximum return on capital investment, and extended missions cannot rely on design concepts which work for brief exposures. New design concepts must be verified prior to in-service use. The materials flown on LDEF were from the late 1970s and early 1980s, and not all these materials are in current use. Some materials flown which remain in use have been superseded by newer materials with better intrinsic properties but without a flight history. Existing materials must be qualified for longer durations, and new

materials must be qualified where current materials do not suffice. Demonstration of hardware performance identifies any concerns in the development stage and increases the reliability of the spacecraft and its systems. In addition to these program needs, there are supporting technical reasons for flight testing. These included developing the environmental monitoring capability and hardware performance sensors to better define refurbishment schedules, eliminate unnecessary maintenance, and give forewarning of developing hardware or material problems. Flight demonstrations increase the reliability of spacecraft in-service and verify ground-based tests. Flight testing reduces the uncertainty ranges on the engineering design models, leading to increased confidence in the design parameters and reducing risk of performance failure.

Technical considerations for long term test flights include active monitoring of the spacecraft temperatures and ambient environments, and obtaining time-resolved data to separate the ground and on-orbit effects. A polar or near-polar orbit would provide a much higher particulate radiation exposure than was received by the first LDEF, allowing evaluation of materials and systems performance in a new environmental regime. A second extended duration flight would take advantage of a new generation of candidate materials for use as coatings, structural materials, seals, adhesives, optical ports, lubricants, antennas, and communications hardware. Investigations would focus on determination of degradation mechanisms, their temperature dependence, specific exposures, performance characteristics under selected varying environments and the time dependence of property changes. Verification of models for contamination and space debris are high priority items. On-orbit testing would also define acceptable exposure sequencing for combined effects ground based testing. A long term flight test would also qualify accelerated testing methodology for both on-orbit and ground applications.

REFERENCES

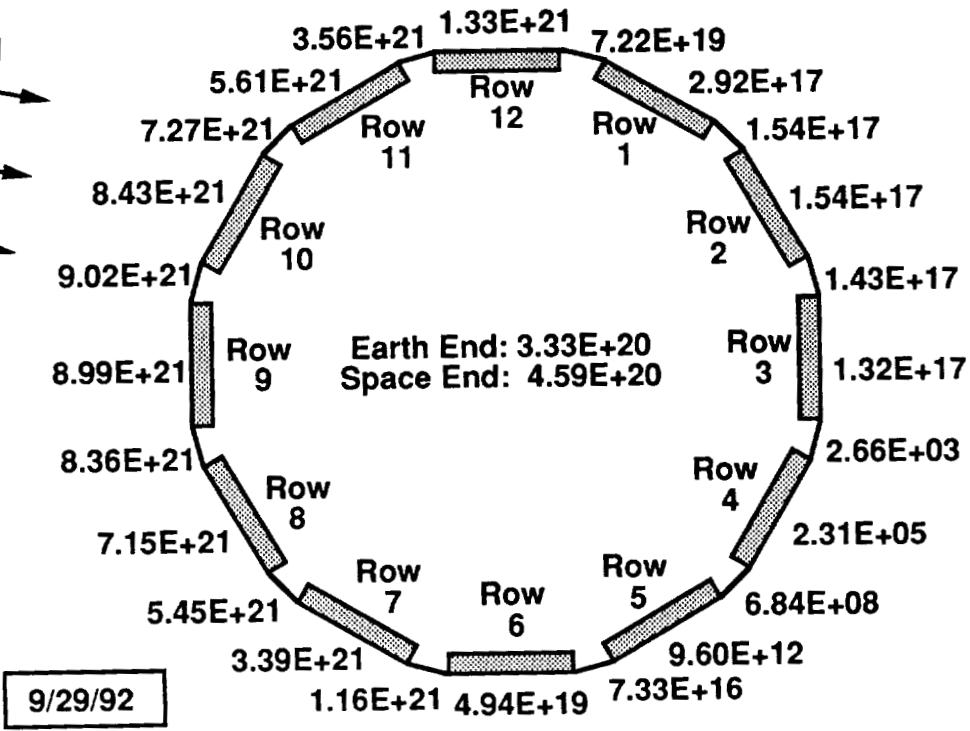
1. Stein, B.A. and H.G. Pippin, "Preliminary Findings of the LDEF Materials Special Investigation Group," LDEF-69 Months in Space-First Post-Retrieval Symposium, NASA CP-3134, Part 2, A.S. Levine, ed., Kissimmee, FL, June 1991.
2. Stein, B.A., "LDEF Materials Overview," LDEF-69 Months in Space-Second Post-Retrieval Symposium, NASA CP-3194, Part 3, A.S. Levine, ed., San Diego, CA, June 1992.
3. Whitaker, Ann F., Wayne K. Stuckey and Bland A. Stein, "What LDEF Means for Development and Testing of Materials," LDEF Materials Results for Spacecraft Applications, NASA CP-3257, A. F. Whitaker and J. Gregory, eds., Huntsville, AL, October 1992.
4. Stein, B.A., "LDEF Materials: An Overview of the Interim Findings," LDEF Materials Workshop '91, NASA CP-3162, B.A. Stein and P.R. Young, eds., Hampton, VA, November 1991.
5. Dursch, Harry and Dr. Gary Pippin, "Summary of Materials and Hardware Performance on LDEF," LDEF Materials Results for Spacecraft Applications, NASA CP-3257, A.F. Whitaker and J. Gregory, eds., Huntsville, AL, October 1992.

6. Berrios, W.M., "Use of LDEF's Thermal Measurement System for the Verification of Thermal Models," LDEF-69 Months in Space-First Post-Retrieval Symposium, NASA CP-3134, Part 2. A.S. Levine, ed., Kissimmee, FL, June 1991.
7. See, T.H., M.A. Allbrooks, D.R. Atkinson, C.G. Simon, and M. Zolensky, Meteoroid and Debris Impact Features Documented on the Long Duration Exposure Facility, A Preliminary Report, Publication #84, JSC #24608, August 1990.
8. Parnell, T.H. "Status of LDEF Ionizing Radiation Measurements and Analysis," LDEF-69 Months in Space-Second Post-Retrieval Symposium, NASA CP-3194, Part 1. A.S. Levine, ed., San Diego, CA, June 1992.
9. Dursch, H.W., W.S. Spear, E.A. Miller, G.L. Bohnhoff-Hlavacek, and J. Edelman, Analysis of Systems Hardware Flown on LDEF-Results of the Systems Special Investigation Group, NASA CR-189628, April 1992.
10. Bourassa, R.J., H.G. Pippin, and J.R. Gillis, "LDEF Microenvironments, Observed and Predicted," LDEF-69 Months in Space-Second Post-Retrieval Symposium, NASA CP-3194, Part 1, A.S. Levine, ed., San Diego, CA, June 1992.
11. Wilkes, Donald R., Edgar R. Miller, James M. Zwiener, and Richard J. Mell, "The Continuing Materials Analysis of the Thermal Control Surfaces Experiment S0069," LDEF-69 Months in Space-Second Post-Retrieval Symposium, NASA CP-3194, Part 1. A.S. Levine, ed., San Diego, CA, June 1992.
12. Tennyson, R.C. and R. Matthews, "Thermal-Vacuum Response of Polymer Matrix Composites in Space," LDEF Materials Results for Spacecraft Applications, NASA CP-3257, A.F. Whitaker and J. Gregory, eds., Huntsville, AL, October 1992.
13. Banks, Bruce A., Kim K. de Groh, Bruce M. Auer, Linda Gebauer, and Jonathan L. Edwards, "Monte Carlo Modeling of Atomic Oxygen Attack of Polymers With Protective Coatings on LDEF," LDEF-69 Months in Space-Second Post-Retrieval Symposium, NASA CP-3194, Part 1, A.S. Levine, ed., San Diego, CA, June 1992.

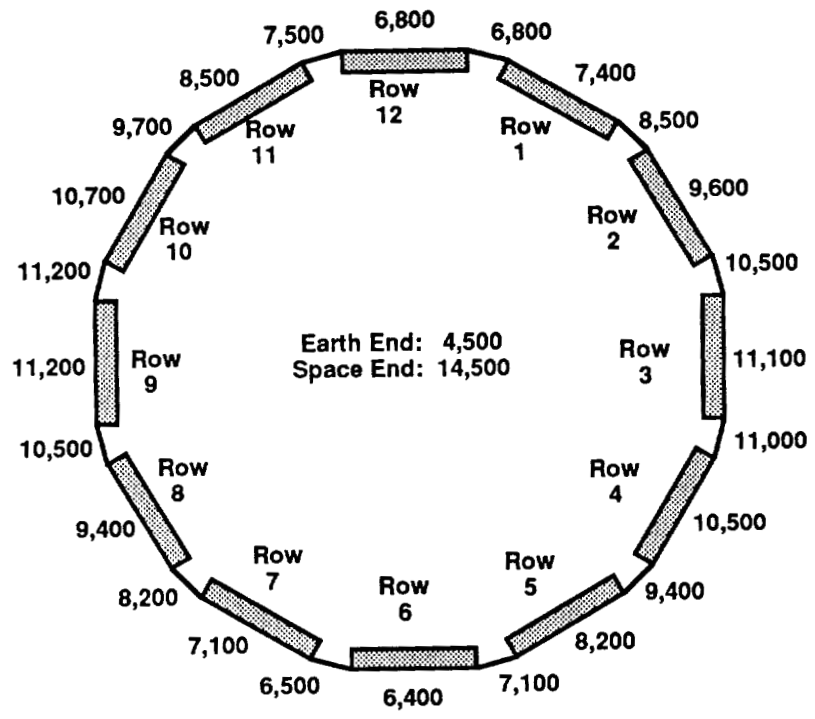
Table 1. Atomic oxygen induced recession rates.

Composites	R_e (10^{-24} cm ³ /atom)
T300/934 (Graphite/Epoxy)	0.56-1.12
Gr/P1700 (Graphite/Polysulfone)	1.05
Gr/Bismaleimide	1.26
Thin Polymeric Films	
Ag/FEP	0.34
Kapton TM (Space end-Grazing angle incidence)	1.75

RAM
DIRECTION



ATOMIC OXYGEN FLUENCES (ATOMS/CM²) AT END OF MISSION,
INCLUDING EXPOSURE DURING RETRIEVAL



CUMULATIVE EQUIVALENT SUN HOURS EXPOSURE AT END OF MISSION

Figure 1. Mission atomic oxygen and solar exposures for LDEF.



Figure 2. Failure of adhesive backed silverized teflon tape on M0001 experiment located on space end of LDEF.

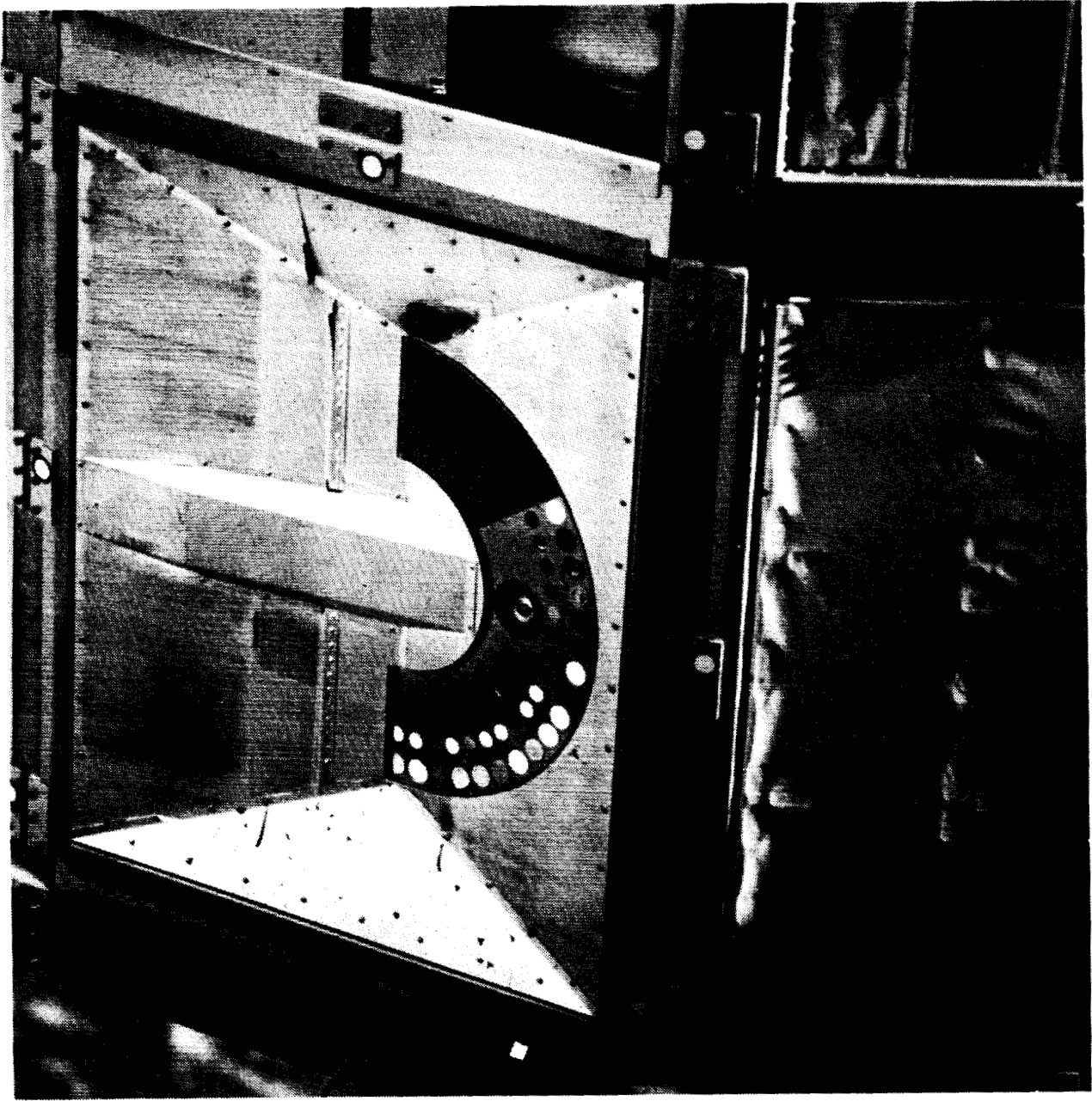


Figure 3. Ag/FEP bonded to rigid aluminum substrate on experiment AO069 located on tray A9.

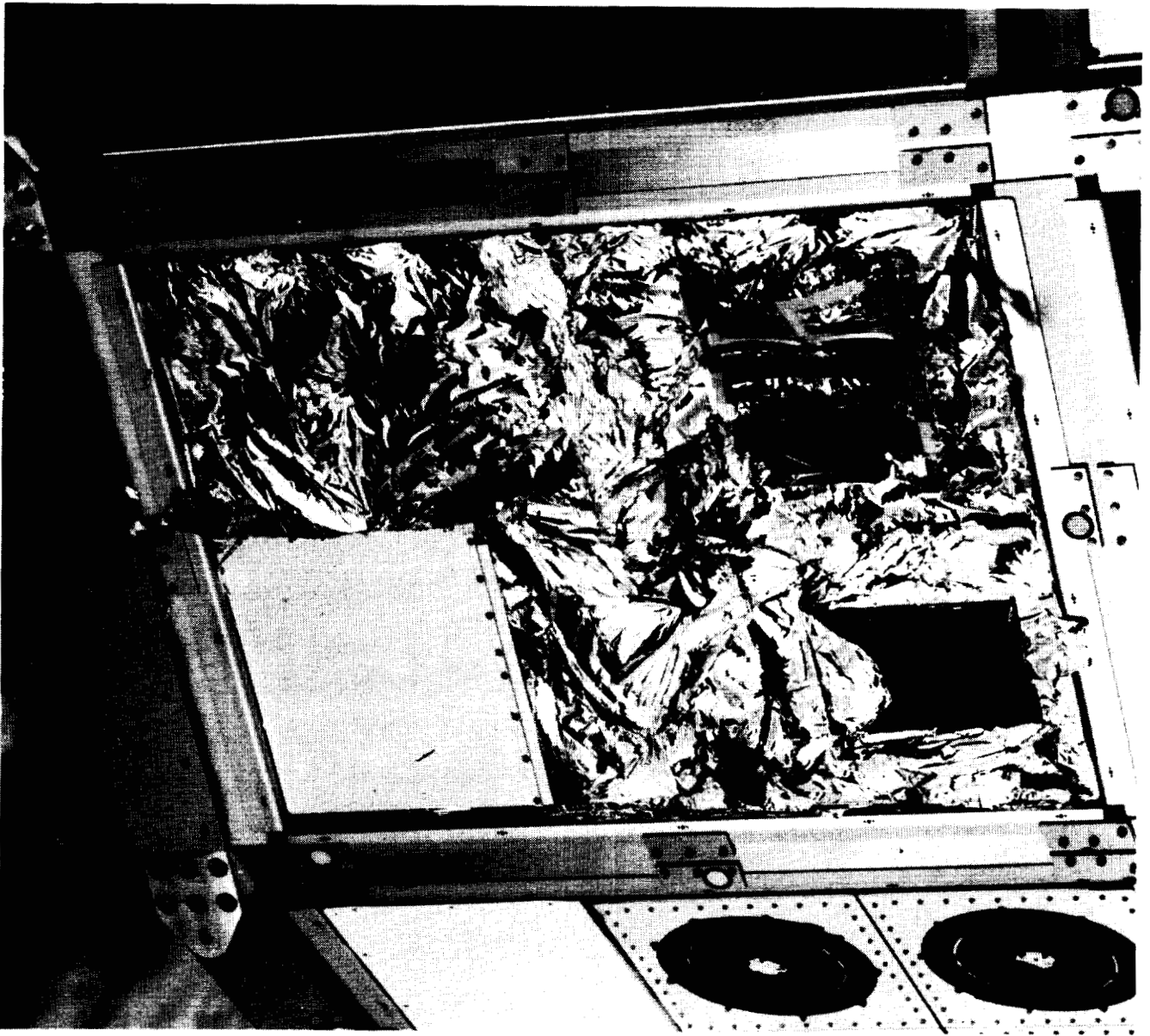


Figure 4a. On-orbit photograph of experiment AO076 showing failed aluminum film folding over chrome plated solar collector.

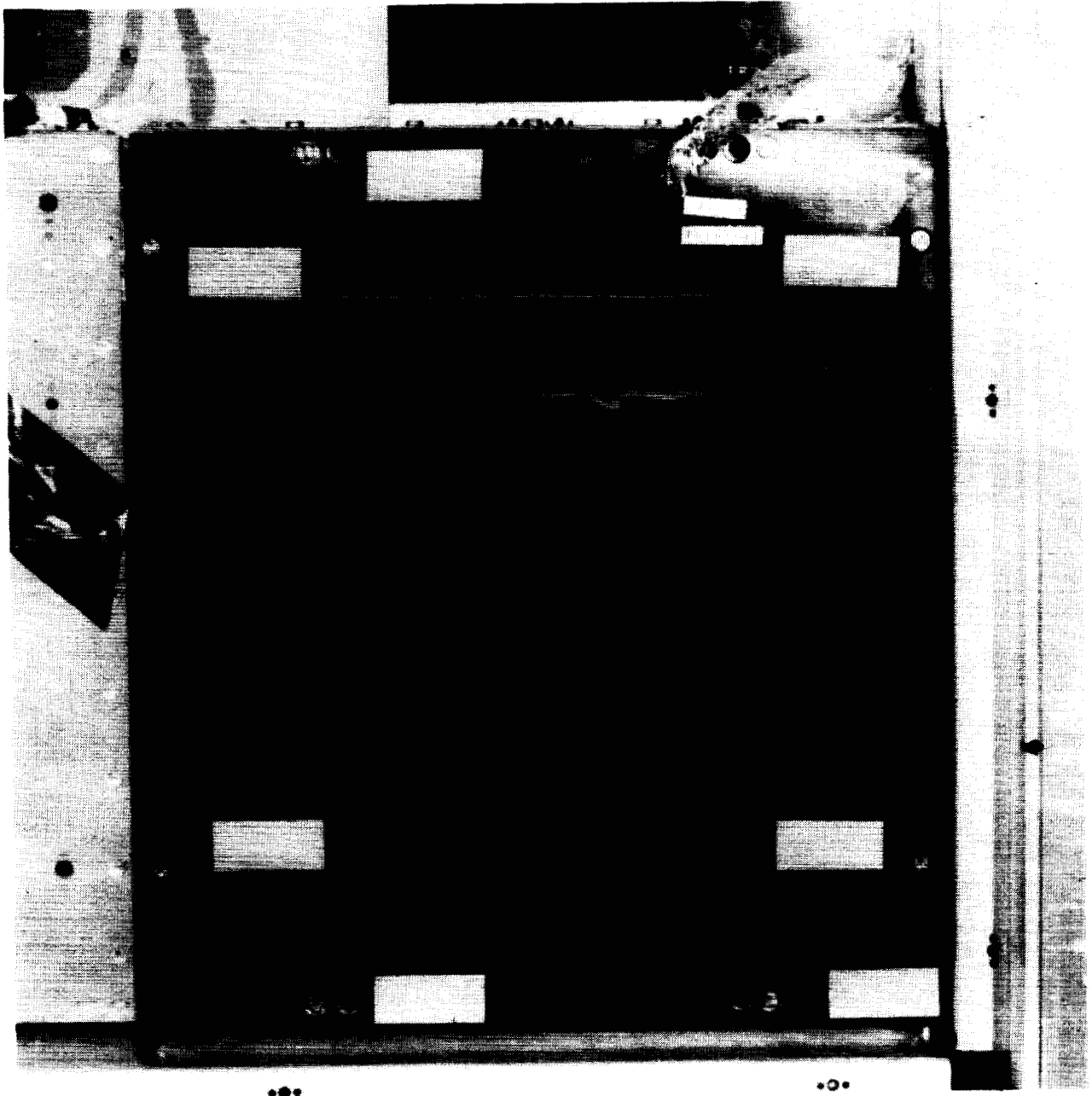


Figure 4b. Post-flight photograph of black chrome plated solar collector.

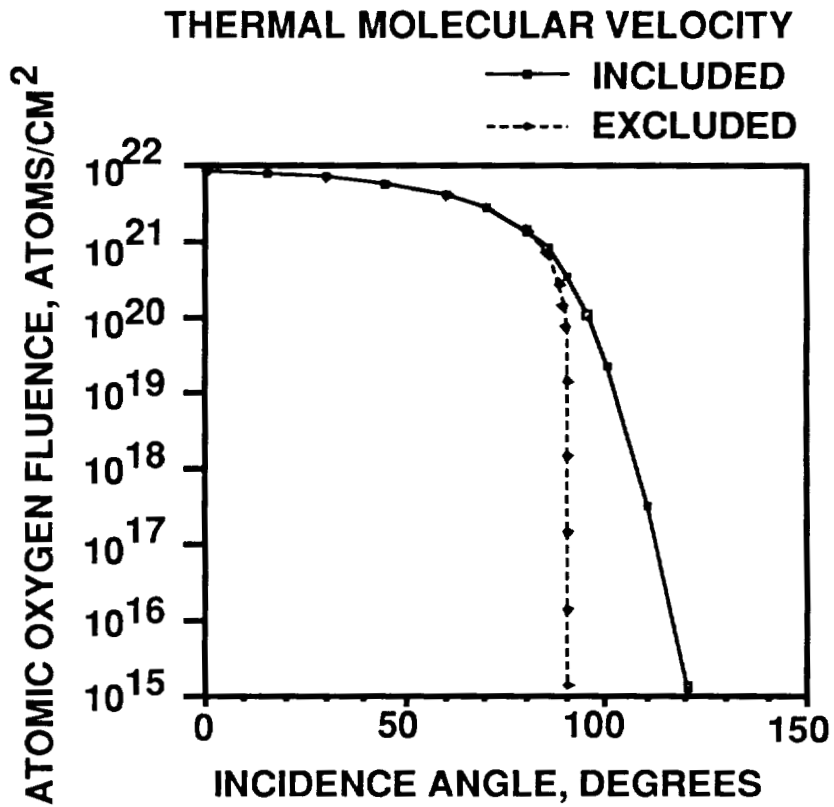


Figure 5. Atomic oxygen fluence as a function of angle of incidence.

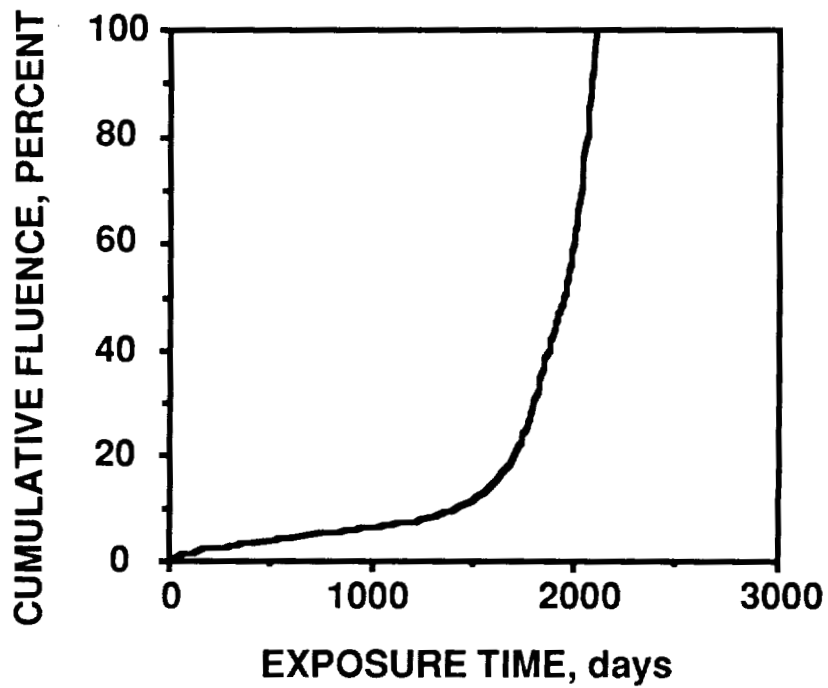


Figure 6. Percent cumulative atomic oxygen fluence as a function of exposure time.

Recent Results from Long Duration Exposure Facility Materials Testing*

H.G. Pippin and H.W. Dursch
Boeing Defense & Space Group
 Seattle, WA. 98124-2499
 (206) 773-2846

52-25
 4
 118

The overall goals of the Long Duration Exposure Facility (LDEF) investigations, established by the Materials Special Investigation Group (MSIG) prior to LDEF retrieval, are to provide useful engineering data to people designing and building spacecraft and, secondarily, to obtain data of potential interest to materials researchers.

The specific objectives are to support predictions of materials lifetimes under the various low earth orbit (LEO) environments to determine how long the material will physically survive; to estimate the engineering performance lifetimes of these same materials under specific LEO exposures; to identify materials and processes by which given materials degrade; and to provide insights into development of new, more inherently LEO environmentally resistant materials.

To achieve the established objectives, two criteria were established to select which materials had the highest priorities for analyses. The first criteria was to examine materials which are still being used on new spacecraft. The second priority was to examine materials with multiple exposure locations on LDEF, because this provided opportunity to develop predictions on how a material will behave as the exposure environment varies.

The goals as defined led to the identification of silverized Teflon™ (Ag/FEP), chromic acid anodized aluminum, and certain thermal control paints used on LDEF as the material types of highest priority for examination. Ag/FEP was chosen because of an excellent a/e ratio (extremely low), and extensive flight history. Also influencing the decision was the fact that the Hubble Space Telescope uses Ag/FEP as its primary passive thermal control system (and was launched shortly after LDEF retrieval) and that a number of other spacecraft are using, or considering this material for use. The various forms of Ag//FEP were used on virtually every side of the LDEF except the earth end. The potential uses of this material, and the location distribution and therefore, exposure conditions, have provided the rationale and opportunity for a comprehensive study of this material.

The performance of anodized aluminum is of significance to Space Station because of the planned wide use of treated aluminum to achieve desired optical properties. The anodizing process allows good control and tailoring of optical properties (Ref. 1). Aluminum is widely used on spacecraft because of its relative inertness and low density.

A276, S13/GLO, and a variety of additional thermal control paints were used on selected experiments and flown as test specimens on other experiments. These paints are used for many spacecraft, under many different exposures, and continue to be considered for future missions. The many observed changes seen on LDEF post-flight have raised concerns about the suitability of a number of these materials for longer term missions and is the reason for the high priority in characterizing the observed degradation.

*These activities were supported by NASA Langley Research Center under contract NAS1-19247

A number of additional types of materials were flown in-service or as specimens in multiple locations. These materials include various composites, copper, stainless steel, and a variety of different adhesives, seal materials, and lubricants. These materials all have practical significance for spacecraft design and have been examined and reported on by various investigators.

Materials present in only one or a very few locations were considered lowest priority for MSIG activities. A number of optical materials, one of a kind coating materials, hardware used on only one experiment tray, and materials in well shielded areas fall into this category.

Reports on specific materials are being completed describing our investigations on chromic acid anodized aluminum, thermal control coatings, materials from internal locations, seals and lubricants, adhesives, silverized Teflon, composites and metals flown on LDEF. In addition, user guides are being prepared for existing models which predict atomic oxygen and solar ultraviolet radiation fluences at arbitrary, but specific, locations on spacecraft.

The primary atomic oxygen model used to predict the direct fluence to LDEF surfaces has also been used to make estimates for a nominal space station trajectory.

The microenvironments atomic oxygen (AO) fluence model has been applied to selected surfaces on the LDEF and to two other spacecraft, the Tropical Rainfall Measurement Mission (TRMM) and the All-Composite Experimental Spacecraft Structure (ACCESS). The LDEF applications include predicting exposures on a space end clamp and bolts, a pair of specimens from A0171, an angle bracket on A0076, a copper grounding strap, selected areas on blankets from trays B7, D7 and D11, the S0069 experiment tray and a module from the M0001 experiment. Figure 1 shows the results of the AO microenvironments model calculation on a representative ACCESS geometry structure.

The solar UV model has been applied to the LDEF to determine the equivalent sun hours (ESH) of solar radiation, including both direct solar and earth albedo contributions. These results were compared with an earlier analytical calculation of the ESH and are in agreement. The solar model was also used for the TRMM spacecraft, and for S0069 and M0001 experiments on LDEF. Thermal models have also been applied to an M0003 composite panel and to tray clamps from rows 9 and 4 to examine thermal loads on the adhesive holding the paint buttons on these clamps.

Boeing Defense & Space Group has produced both IBM Compatible and Macintosh™ versions of data bases covering four material types from LDEF. The subjects are thermal control paints, optical material, Ag/FEP, treated aluminum, and LDEF environments. These data bases are complete through the 2nd Post Retrieval Symposium and include some information from the 1992 Huntsville LDEF materials conference and are available to the user community free of charge.

Materials analysis continued on a variety of LDEF materials in 1993. These materials included a copper grounding strap, unanodized aluminum, yellow paint surfaces on the scuff plates, stainless steel bolts, DC6-1104 adhesive, heat shrink tubing and additional Ag/FEP from the S1005, M0001 and S1002 experiments.

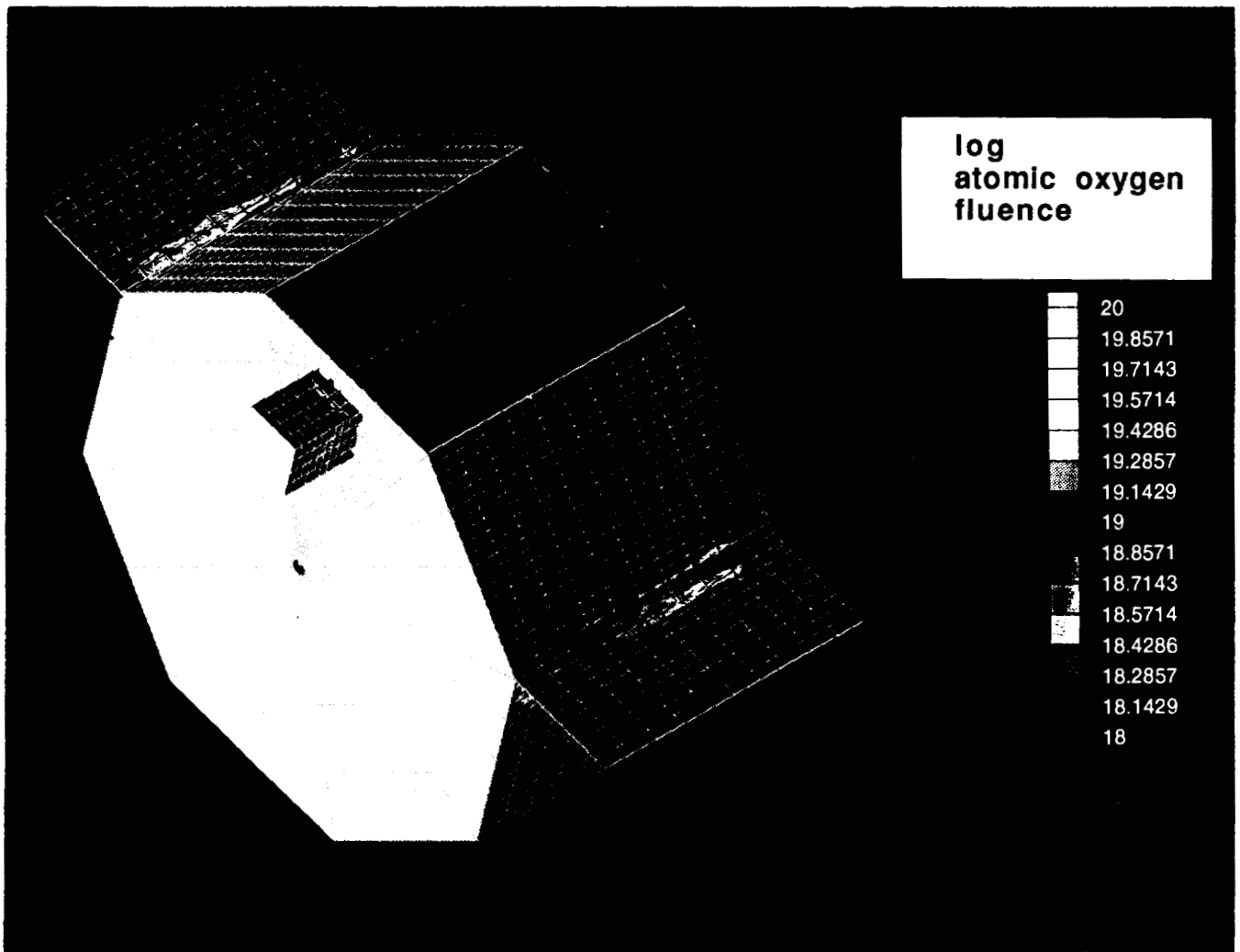


Figure 1. Computer generated plot of the atomic oxygen exposure over the surface of the All-Composites Experimental Spacecraft Structure (ACCESS). The atomic oxygen microenvironments model used for this prediction was verified through comparisons with LDEF flight data.

Materials from "interior" locations, which were only directly exposed to vacuum and mild thermal cycling conditions, generally appeared in excellent condition post-flight. All the heat shrink tubing, nylon grommets, Teflon-coated wire bundles and multi-layer insulators (MLI) were intact and functioning. A slight increase in brittleness was observed for the nylon grommet flight specimens relative to ground control material. Selected fiberglass shims associated with the heat shrink tubing were evaluated and had slightly lower Total Mass Loss (TML) and Collectable Volatile Condensable Materials (CVCM) in comparison with ground specimens. These results are detailed in a NASA Contractor Report on LDEF Internal Materials.

Figure 2 shows the points of attachment of the velcro fastening material with the AO178 tray frame from location C11. The DC6-1104 RTV silicone adhesive used showed significantly increased TMLs relative to a ground reference value. The CVCMs were virtually identical for flight and ground specimens. For selected LDEF locations, samples were taken from both the vacuum exposed bond line of flight specimens and the center of the velcro covered area on these same specimens. No difference could be determined between outgassing properties of pairs of samples from different areas of the same adhesive specimen.

Figure 3 shows a photo of aluminum wire harness clamps partially covered with heat shrink tubing, nylon grommets and a wire harness bundle.

Outgassing data for heat shrink tubing specimens are shown in figures 4 and 5. The results show no significant difference in CVCM for flight vs. ground specimens, although the average for each flight location is slightly lower than for the ground control specimens. The average TML's for two distant flight sample populations, samples from rows 3, 4, 8, and 9 compared with specimens from all other locations (different to >95% confidence level), are about 30% lower than the ground control TML. One Earth end clamp showed anomalously high results. An additional set of specimens were run on this particular clamp and showed the same high TML as the original measurement. The reason for the anomaly is not known.

The surface of Ag/FEP specimens from a M0001 module on the space end and the Environmental Exposure Control Canister (EECC) from experiment S0002 on tray E03 showed the expected changes in structure associated with solar exposure. The relative environmental susceptibility of functional groups under LEO exposure conditions, in increasing order, is CF to CF₂ to CF₃. Changes in relative amounts of CF, CF₂ and CF₃ functional groups vs. solar exposure are summarized in figures 6 and 7. The results indicate that changes in the FEP structure accelerate over the UV exposure range for which data is available. It cannot be assumed that the trend towards more rapid degradation will continue indefinitely because the cross-linked structure may achieve more stability with time. In addition, the sequence of environmental exposures is critical; an initial exposure to a relatively high dose of atomic oxygen is probably less damaging to this material than an equivalent dose later in a mission. By contrast, under high particulate radiation environments, such as the SCATHA experiment flown at geosynchronous altitudes, this material changed a by ~0.2 over 10 years (Ref. 3).

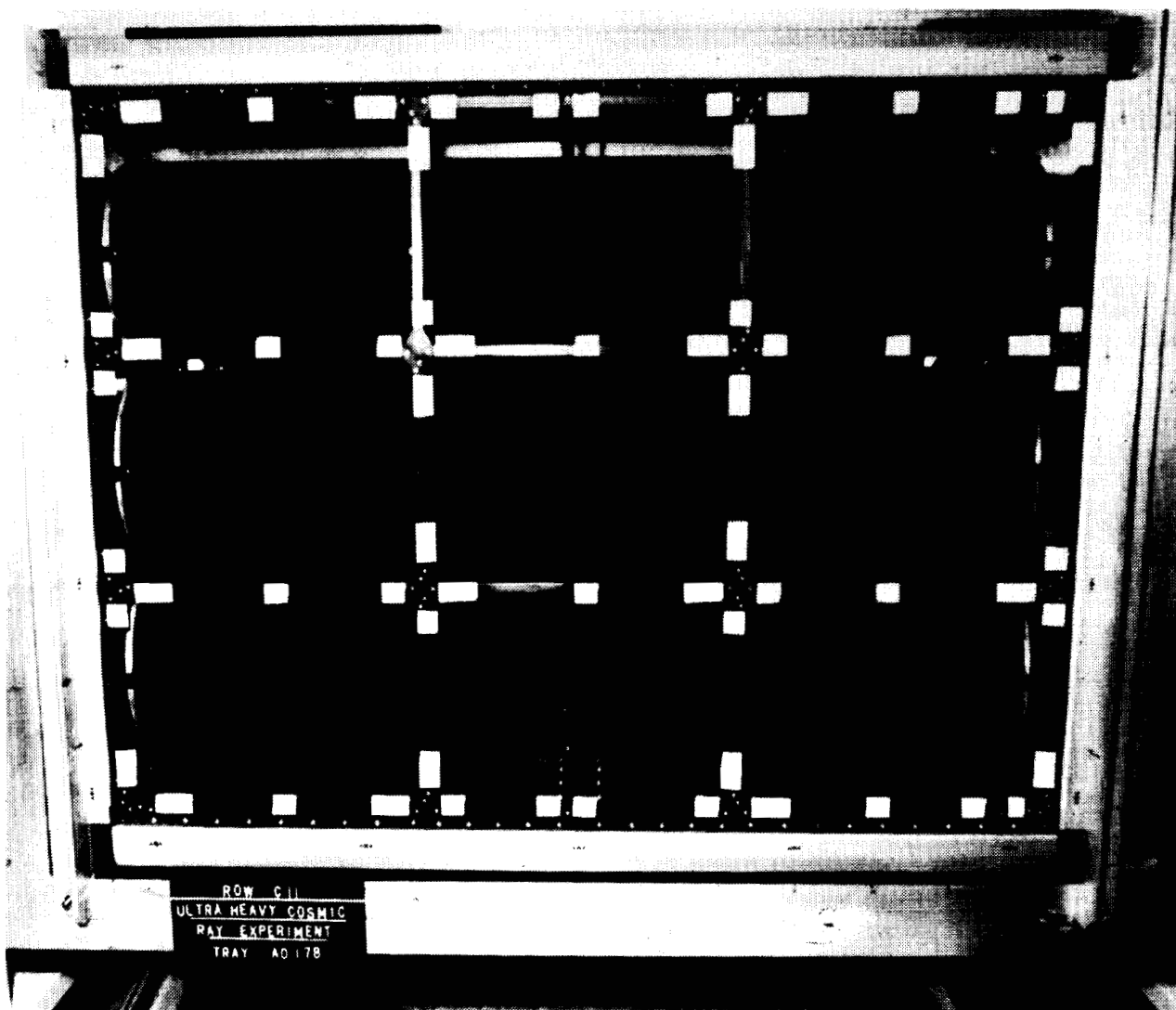


Figure 2. NASA photograph of open tray from location C11 showing the points of attachment of the thermal control blanket to the tray. The white rectangular areas are the velcro strips attached to the tray frame.

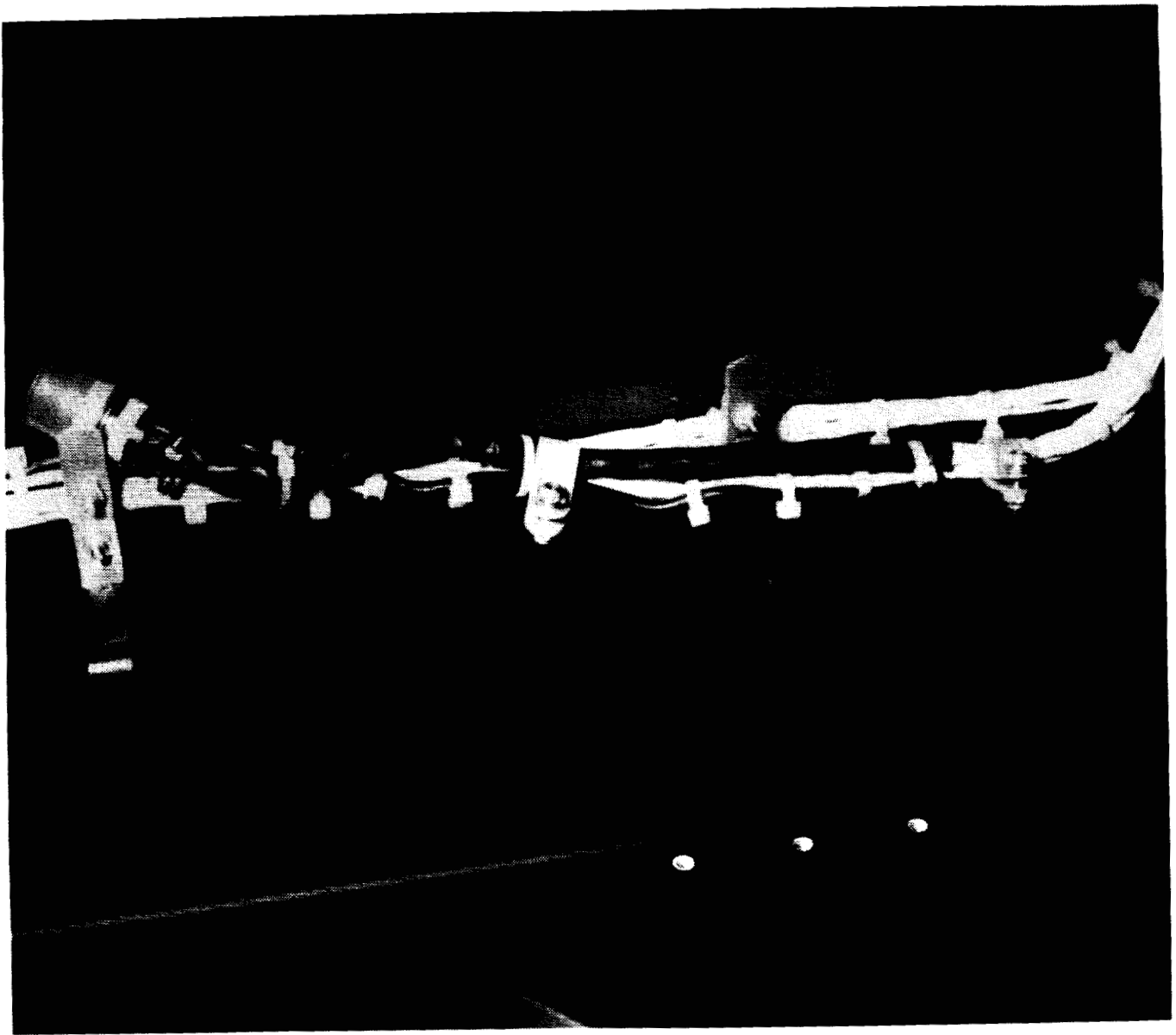


Figure 3. NASA photograph of a portion of the LDEF interior showing the wire harness bundles, nylon grommets, aluminum clamps, and heat shrink tubing on the aluminum wire harness bundle clamps.

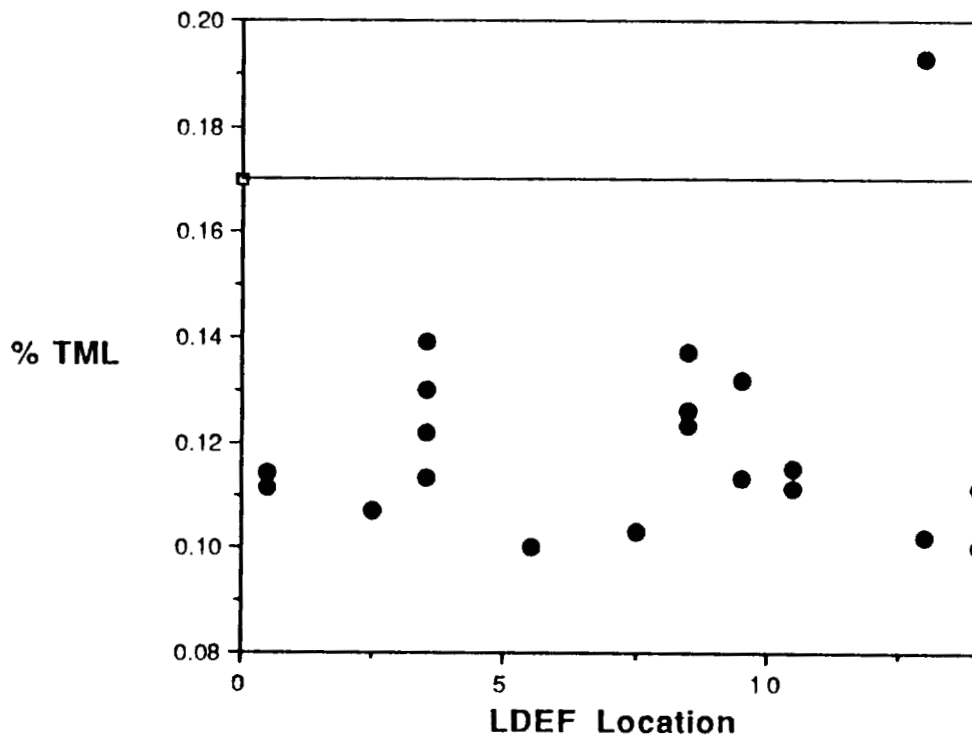


Figure 4. Total Mass Loss (%TML) of heat shrink tubing as a function of location on the LDEF interior. The horizontal line at 0.17% is the TML average for the ground control specimens.

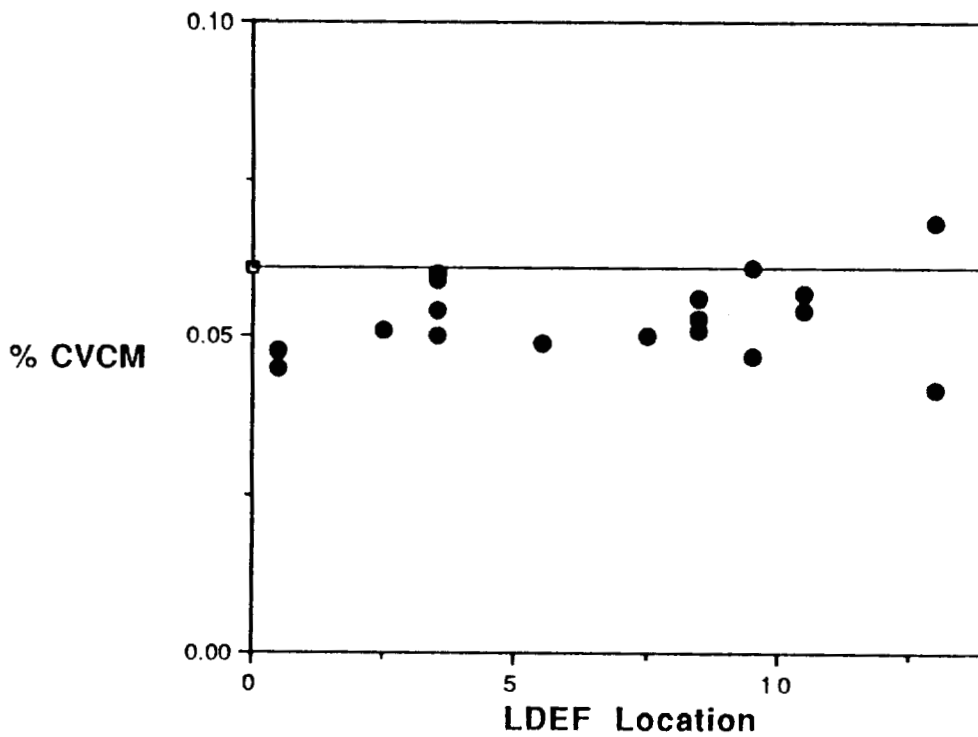


Figure 5. Collectable Volatile Condensable Materials (%CVCM) of heat shrink tubing as a function of location on the LDEF interior. The horizontal line at ~0.06 is the average % CVCM for the ground control specimens.

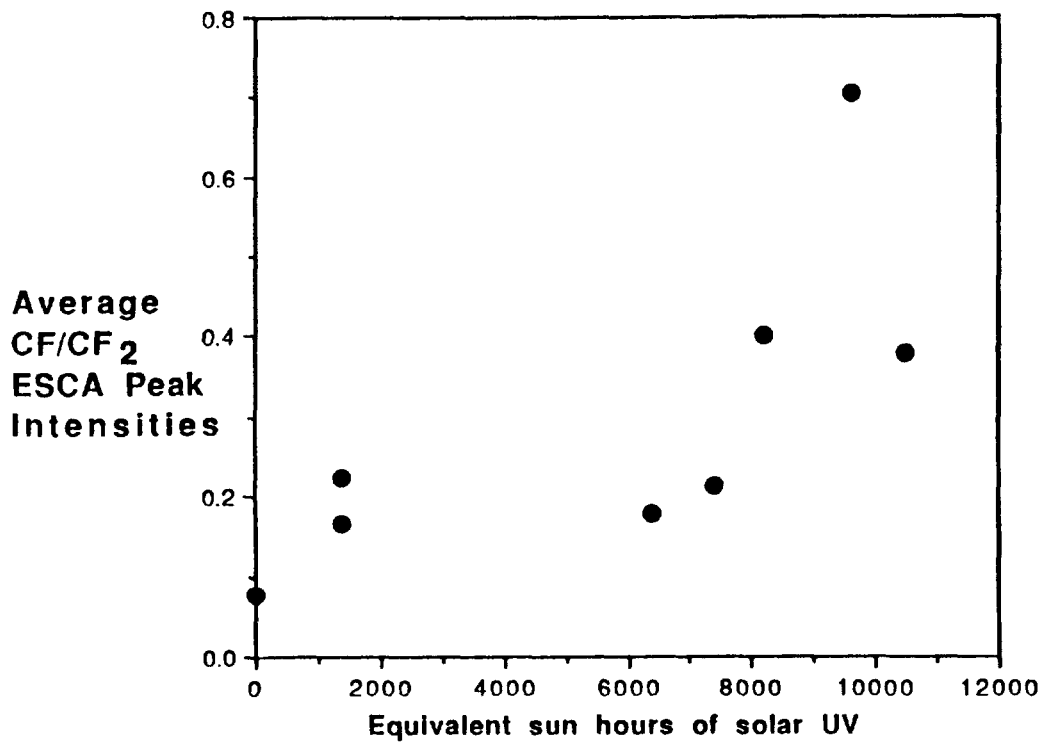


Figure 6. Ratio of CF to CF₂ ESCA peak heights as a function of hours of solar exposure.

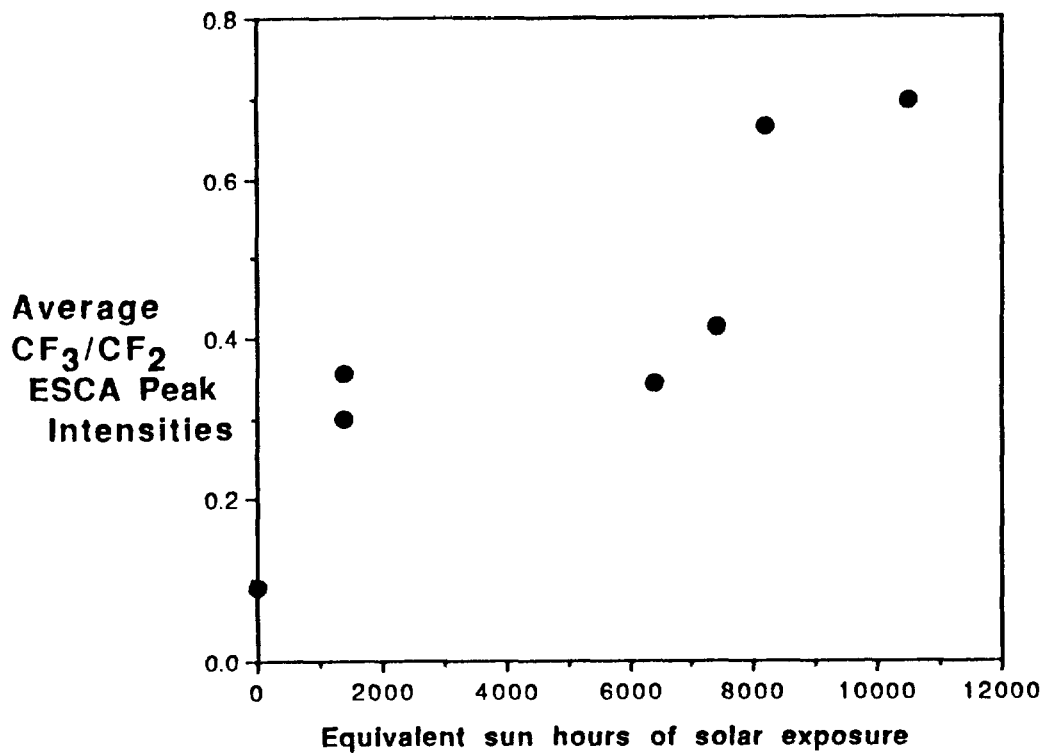


Figure 7. Ratio of CF₃ to CF₂ ESCA peak heights as a function of hours of solar exposure.

Because the exposure cycle was different on the Solar Max Satellite than for LDEF, the Solar Max Ag/FEP specimens may have high information content regarding environmental effects on materials. This depends partially on how well the orbit and satellite motions can be estimated.

Goddard Space Flight Center also flew vapor deposited aluminum coated FEP tape on rows 9 and 12. The row 9 specimen exposed side shows less carbon and increased oxygen relative to the shielded side. Row 12 specimens show silicon contamination on exposed surfaces and small amounts of silicon on shielded surfaces.

The effects of contaminant film range from optical properties changes to influencing the apparent recession rate of other materials. The chromic acid anodized aluminum surfaces on the trailing edge appeared slightly darkened and showed a 3-4% increase in absorbency relative to the control specimens. This increase is attributed to solar darkened contaminant films and is not considered a significant engineering change. Localized deposits of outgassed products from silicone adhesive increased the absorbency of Ag/FEP from 0.07 up to 0.25 in a few areas. Similar changes were also seen on Solar Max specimens (Ref. 2). Severe darkening was also associated with small areas around vent paths from interior locations. While the discoloration is severe, and these areas appear visibly dark, the total area is a small fraction of the surface.

Deposited material lowers the apparent recession rate of the substrate material by acting as a sacrificial material which consumes oxygen and may also physically block the oxygen from reaching some reactive sites.

Degraded materials are also potential sources of particles which may block lenses, mirrors and thermal control surfaces. These films may also alter properties on these critical surfaces.

Silicone has been detected on many LDEF surfaces. These surfaces include each stainless steel bolt head examined, both exposed and shielded FEP surfaces on the trailing edge, 22 of 24 aluminum tray clamps examined using ESCA, numerous clamps examined using IR spectroscopy, stainless steel bolt tips and silver coated hex nuts on the interior of LDEF, each copper strap examined, and on the surface of specific experiments.

A number of potential sources have been identified, but in every case determined to date, the outgassing source has been very localized and/or the contaminant was present from the manufacturing process.

The adhesive used on AO178 and P0004 experiment trays to fasten velcro to the tray frame and back side of the thermal control blankets outgassed and left stains around the corners and sides of these trays and on the surfaces of the blankets themselves. The bicycle reflectors and a number of specimens from certain experiments were silicone coated. The area around the reflectors was not analyzed for Si content. Where specimens adjacent to silicon containing specimens were examined, any silicon based contamination was shown to be extremely local. Small amounts of silicon based adhesive used on specific experiments contaminated areas on those same experiments. There is no evidence of serious cross contamination from one tray to another.

The copper grounding straps were made by bonding two strips of adhesive-backed copper tape together. This tape as manufactured has a silicon based release coating on the cover paper protecting the adhesive. When the tape is rolled this paper comes in contact with the copper side and a thin silicone film is deposited on the copper. The shuttle is also a potential source of silicon. However, the results of our examination of the stainless steel bolts were not conclusive because the silicon levels were small and any films were extremely thin. The A286 type alloy stainless steel bolts, as manufactured, contain about 1% silicone by weight. The presence of this source and the carbon based contamination on the bolt heads mask the deposition of Si on orbit.

Property changes observed on LDEF are a function of the specific environmental exposure. The Ag/FEP optical properties did not change under AO and UV exposure. The structural changes in the FEP increased with UV exposure in a non-linear fashion.

The discoloration of the A276 paint buttons due to UV exposure is irreversible. The damage to this material is to the resin system. By contrast, the "bleaching" of paints in air, after vacuum exposure to protons, electrons, and UV, is a result of changes of the pigment.

The total amount of Si on LDEF surfaces is quite small. There were a number of localized sources.

There are specific materials and surfaces on LDEF which still have a high information content. The Ag/FEP specimens from the M0001 modules and the AO069 experiment, and the A276 paint binders all contain materials whose chemical structure has been altered and could provide clues as to the actual UV damage mechanisms. Most of the time resolved exposures on LDEF have not yet been analyzed. The inside surfaces of canisters which were opened in stages provide time resolved information about the deposition of contaminant films.

Application of the AO and UV microenvironments models continue to show that for complex shaped surfaces, the indirect scattering makes a significant contribution to the total intensity. This is significant because the interpretation of materials data from the LDEF only has meaning in the content of the specific environmental exposure.

Post flight measurements are integrated results which reflect the net changes induced by several uncontrolled environments. The sequencing of the exposure conditions determines the observed results.

References

1. Duckett, R.J. and Gilliland, C.S., Variable Anodic Thermal Control Coating on Aluminum, AIAA 18th Thermophysics Conference, June 1-3, 1983, AIAA-83-1492.
2. Proceedings of the SMRM Degradation Study Workshop, May 9-10, 1985, NASH-GSFC, 408-SMRM-79-0001.
3. Hall, D.F. and Fote, A.A., 10 Year Performance of Thermal Control Coatings at Geosynchronous Altitude, AIAA 26th Thermophysics Conference, June 24-26, 1991, Honolulu, Hawaii.

LDEF POLYMERIC MATERIALS: A SUMMARY OF LANGLEY CHARACTERIZATION

Philip R. Young, Wayne S. Slemp, Karen S. Whitley, Carol R. Kalil,¹
 Emilie J. Siochi,² James Y. Shen,² and A. C. Chang²
 NASA Langley Research Center
 Hampton, VA 23681-0001

53-27

4447

33P

SUMMARY

The NASA Long Duration Exposure Facility (LDEF) enabled the exposure of a wide variety of materials to the low Earth orbit (LEO) environment. This paper provides a summary of research conducted at the Langley Research Center into the response of selected LDEF polymers to this environment. Materials examined include graphite fiber reinforced epoxy, polysulfone, and additional polyimide matrix composites, films of FEP Teflon, Kapton, several experimental high performance polyimides, and films of more traditional polymers such as poly(vinyl toluene) and polystyrene. Exposure duration was either 10 months or 5.8 years.

Flight and control specimens were characterized by a number of analytical techniques including ultraviolet-visible and infrared spectroscopy, thermal analysis, scanning electron and scanning tunneling microscopy, x-ray photoelectron spectroscopy, and, in some instances, selected solution property measurements. Characterized effects were found to be primarily surface phenomena. These effects included atomic oxygen-induced erosion of unprotected surfaces and ultraviolet-induced discoloration and changes in selected molecular level parameters. No gross changes in molecular structure or glass transition temperature were noted.

The intent of this characterization is to increase our fundamental knowledge of space environmental effects as an aid in developing new and improved polymers for space application. A secondary objective is to develop benchmarks to enhance our methodology for the ground-based simulation of environmental effects so that polymer performance in space can be more reliably predicted.

1.0 INTRODUCTION

The 69-month low Earth orbit (LEO) flight and subsequent January 1990 return to Earth of the NASA Long Duration Exposure Facility (LDEF) provided a novel opportunity for the aerospace community to examine the effects of long-term space exposure on a variety of materials. The saga of this remarkable vehicle is continuing to unfold through a series of symposia, workshops, and journal articles (1-5). The 11-ton satellite shown in Figure 1 contained 57 experiments to assess the effects of the space environment on materials, living matter, and various space systems (6). Perhaps as much as 90% of our first-hand knowledge of LEO space environmental effects rests with the LDEF and its contents (7).

The Langley Research Center actively pursued the chemical characterization of polymeric materials which flew on LDEF (8-20). The present paper summarizes almost 5 years of LDEF-related polymer research at this facility. It represents the collective efforts of a number of individuals and organizations in both assembling and analyzing a broad variety of control and exposed specimens.

1. Analytical Services and Materials, Inc., Hampton, VA 23666
2. Lockheed Engineering and Sciences, Co., Hampton, VA 23666

The intent of this activity is to increase our fundamental understanding of space environmental effects on polymeric materials and to develop benchmarks to enhance our methodology for the ground base simulation of those effects so that polymer performance in space can be more reliably predicted.

Initial planning for the chemical characterization of LDEF polymeric materials was guided by a number of anticipated environmental effects. Table I, taken from a presentation given at the LDEF Materials Data Analysis Workshop just prior to deintegration activities at the Kennedy Space Center (21), summarizes many of these effects. Modifications to molecular structure and molecular weight, changes in surface chemistry, surface erosion, optical property changes, and a deterioration in various mechanical properties were among more dominant effects to be examined. An analysis plan, summarized in Table II, was developed to address these anticipated effects. Extensive use was planned for selected solution property measurement techniques, spectroscopic analyses, thermomechanical analyses, and techniques to assess surface chemistry. Analytical methods to characterize the molecular level response to environmental exposure, in addition to more obvious physical and mechanical effects, would be emphasized.

Table III lists LDEF polymeric materials assembled for analysis. These materials were provided by several Principal Investigators, and depending on LDEF row and tray location, experienced somewhat different environments. Specimens were exposed for either 10 months or 5.8 years as noted. Materials ranged from early 1980 state-of-the-art graphite fiber reinforced polymer matrix composites, to space films and coatings, high performance polymer films, and more traditional polymers. Representative data obtained on these materials is given in this paper. A more complete data presentation can often be found in accompanying referenced reports.

2.0 EXPERIMENTAL

Most materials identified in Table III were originally obtained from commercial sources. The fabrication, quality control, specimen preparation, and baseline testing of Langley-supplied P1700/C6000, 934/T300, and 5208/T300 composite materials is discussed in references 22 and 23. Polyimide-polysiloxane copolymer films were synthesized under NASA Grant NAG-1-343 with Virginia Polytechnic Institute and State University, Blacksburg, Virginia. Several high performance polyimide films were synthesized in-house (24-26).

As noted in the text, some specimens were exposed for only 10 months while other materials received the full 5.8-year exposure. Specimens exposed for 10 months were inside an Experimental Exposure Control Canister (EECC) (6). The EECC was closed when LDEF was launched. It opened 1 month after deployment and closed 10 months later. Various environmental exposure parameters are included with Figures 1 and 2.

2.1 Instrumental Methods of Analysis

Thermal analyses were conducted using a DuPont 9900 Computer/Thermal Analyzer to process data from a DuPont 943 Thermomechanical Analyzer operating in the expansion mode. The glass transition temperature (T_g) was obtained by noting the point of inflection from the thermogram baseline. Ultraviolet-Visible (UV-VIS) transmission spectra were scanned on a Perkin-Elmer Lambda 4A Spectrophotometer. Infrared spectra were recorded on a Nicolet 60SX Fourier Transform Infrared System (FTIR) using a diffuse reflectance technique (27). X-ray Photoelectron Spectroscopy (XPS) measurements were conducted under NASA Grant NAG-1-1186 at the Virginia Tech Surface Analysis Laboratory, VPI&SU, Blacksburg, VA. Measurements were made on a

Perkin-Elmer PHI 5300 Spectrometer equipped with a Mg K α x-ray source (1253.6 eV), operating at 15 kV/120mA. Scanning Tunneling Microscopy (STM) was performed in air on a NanoScope II instrument (Digital Instruments, Inc., Santa Barbara, CA) using a tungsten tip and G-Head accessory. Specimens were prepared by coating with 5-7 nm of gold-palladium using a Hummer IV sputtering system (Anatech, Ltd., Alexandria, VA). Transmission Electron Microscopy (TEM) analyses were conducted under NASA Contract NAS1-19656 at the Virginia Institute of Marine Science, Gloucester Point, VA. A Cambridge StereoScan 150 (Cambridge Instruments, Deerfield, IL) equipped with an EDAX S150 detecting unit (EDAX International, Inc., Prarie View, IL) performed Scanning Electron Microscopy (SEM) analyses. Various photographic techniques were used to document specimen appearance.

2.2 Solution Property Measurements

Molecular weight measurements for LDEF polystyrene specimens were determined on a Waters 150-C Gel Permeation Chromatograph (GPC) interfaced with a Viscotek (Viscotek Corp., Porter, TX) Model 150R Differential Viscometer (DV). The general technique used to make these measurements has been previously described (28). Experiments were conducted in toluene at 40°C using a Waters 10³/10⁴/10⁵/10⁶Å MicroStyragel HT column bank. The flow rate was 1.0 ml/min. A universal calibration curve was constructed using Polymer Laboratories (Polymer Laboratories, Inc., Amherst, MA) narrow dispersity polystyrene standards. Polyimide films were analyzed at 35°C in 0.0075M LiBr in DMAc. GPC-DV measurements on all polysulfone specimens were determined on a standard Waters Associates chromatograph at room temperature using a 10³/10⁴/10⁵/10⁶Å MicroStyragel HT column bank. The solvent was chloroform.

GPC sample solutions were prepared 1 day prior to analysis by dissolving specimens in the appropriate solvent. The soluble portion was filtered through 0.2 mm PTFE filters before injection into the chromatograph. Insoluble gel was decanted into tared beakers, rinsed several times, and allowed to dry for about 2 hours before placing in an oven at 100°C and drying to constant weight. GPC sample concentrations were then adjusted to correct for removal of insoluble gel. Molecular weight parameters reported are averages obtained from two or three GPC-DV analyses.

2.3 Mechanical Property Measurements

Measurements on 4-ply ($\pm 45^\circ$)_s composite tensile specimens were performed according to ASTM D3039-76. Test specimens were cut to standard dimensions and tapered end-tabs machined from epoxy/glass cloth were adhesively applied prior to integration onto the LDEF experimental tray. A detailed description of composite test specimen preparation and testing is given references 15, 22, and 23.

3.0 RESULTS AND DISCUSSION

A precise orbital orientation was achieved by the LDEF spacecraft. As a result, the environmental exposure a sample received often depended on where it was located on the vehicle. Figure 1 depicts the spacecraft and its flight orientation. The 30 foot long by 14 foot in diameter gravity gradient stabilized structure had 12 sides or rows with 6 experimental trays per row. Additional trays were mounted on the Earth and space-pointing ends (6). The location of polymeric materials in this report will be identified by Tray and Row. For example, B9 identifies a specimen from Tray B on Row 9.

The Row 9 leading edge nominally faced the RAM or velocity vector direction and the Row 3 trailing edge faced the WAKE direction. A detailed analysis of several factors determined that the actual RAM direction was about 8° of yaw from the perpendicular to Row 9 in the direction of Row 10, with 1° of pitch (29). This orientation was sustained throughout flight, from deployment in April 1984 until retrieval in January 1990.

Figure 2 gives additional environmental parameters. The procedure for calculating total atomic oxygen (AO) fluence and equivalent ultraviolet (UV) sun hours may be found elsewhere (30-31). The asymmetrical AO fluence around the vehicle is partly due to the 8° of yaw and a short excursion during which the vehicle received exposure while in the Shuttle payload bay after retrieval. A further discussion of orientation and environments may be found in several references (1, 3, 4, 6).

3.1 Films

The primary environments of concern for polymeric films in low Earth orbit are AO and UV. The most dominant visual effect for exposed films was AO-induced surface erosion which generally resulted in a diffuse or frosted appearance. This visual effect was readily apparent with silvered fluorinated ethylene propylene (FEP) teflon thermal blanket material which provided thermal protection for 17 underlying experiment trays distributed around LDEF. Blankets located near Row 9 were opaque while blankets located near Row 3 remained highly specular. Figure 3 shows on-orbit photographs of F4 and E10 thermal blankets which illustrate this phenomenon. The change from specular to diffuse correlated with the change in AO fluence at various LDEF locations.

Atomic-oxygen-eroded thermal blankets changed from specular reflectors of solar radiation to diffuse reflectors (9). The total reflectance, specular plus diffuse components, which determines solar absorptance (α_s), remained virtually constant. The thermal emissivity (ϵ) was also virtually unchanged. Thus, the α_s/ϵ parameter, which influences equilibrium temperatures for passive thermal control coatings in space, was largely unaffected. This fortuitous result meant that the thermal performance of frosted and specular thermal blankets were probably the same. While surface atomic carbon to fluorine ratios, as determined by XPS, changed with exposure and UV-induced surface crosslinking no doubt occurred, various infrared and thermal analyses failed to detect significant molecular structural changes in the bulk FEP polymer (9).

The AO-induced erosion of films has been described as producing a textured, carpeted, or "christmas tree" morphology (32). Figure 4 gives SEM photomicrographs of the edge of a 5 mil Kapton film specimen which flew on the space end of LDEF at H7. This specimen was oriented such that the AO flow was perpendicular to the film edge and in the plane of the film surface. Figure 4a shows the "christmas tree" morphology associated with the leading edge of this film. The trailing edge, shown in 4b, did not receive direct exposure and remained fairly smooth.

Figure 5 gives the SEM photomicrograph of polysulfone film exposed for 10 months on Row 9 (11). AO exposure for this specimen was essentially orthogonal to the film surface. Evidently, surface contamination partially protected underlying resin from AO to produce the relief pattern apparent in this figure. This phenomenon provides a perspective on the depth of erosion for this 10-month specimen.

The roughened surface dramatically reduced the ultraviolet-visible transmission properties of exposed film. Figure 6 gives before and after UV-VIS spectra between 200 and 600 nm for 5 high performance polyimide films (19). Kapton was included as a reference. The molecular structure of each polyimide is identified in Table IV. All films received 10 months of Row 9 exposure and, thus, experienced the environment summarized in Figure 2d. While some UV and AO degradation of the

polymer molecular backbone no doubt occurred, the decrease in transmittance with exposure is considered to be largely due to physical roughening of the film surface by AO. The uneven surface reflected and/or refracted the impinging radiation and, thus, less light was transmitted.

Scanning Tunneling Microscopy (STM) has proven to be an effective tool for profiling the surface of space-exposed films. Figure 7 shows STM line plots for unexposed and exposed BTDA-ODA and exposed BTDA-ODA- Al^{3+} , two high performance polymer films included in a previous study (19). The smooth surface shown in 7a is typical of that observed for other unexposed LDEF specimens. Minor undulations in the x-direction likely resulted from the drawing procedure used during casting when the film was doctored onto a glass plate. The egg-crate-like appearance of exposed BTDA-ODA is also typical of the "christmas tree" morphology observed for several other LDEF films. The mechanism by which polymeric materials develop this conical shape upon exposure to AO is not adequately understood. VUV-induced surface crazing/crosslinking may play a role in this phenomenon.

The BTDA-ODA- Al^{3+} specimen shown in 7c also exhibited erosion but the appearance is different from that observed in 7b for the undoped film. An obvious conclusion is that aluminum ions had an effect on how the film surface responded to the LEO environment. A protective aluminum oxide phase may have formed with exposure. STM has provided insight into the erosion of additional 10-month exposed Row 9 films (10). The technique could not be used on many 5.8-year exposed films on or near Row 9 because the specimens were too rough. The STM probe tip tended to "crash" with the irregular surface of these full-exposure samples. Ten month-exposed Row 9 films received approximately 2.6×10^{20} AO atoms/cm² while 5.8-year exposed Row 9 films received up to 8.99×10^{21} AO atoms/cm². These results suggest the upper limit of directional AO exposure for characterization by the STM technique is intermediate between these two fluences.

Transmission Electron Microscopy (TEM) also proved to be an effective tool for characterizing AO erosion of polymer films. Figure 8 shows TEM photomicrographs of the five experimental polyimide films and Kapton. Prior to analysis, a segment of each film was cast into an epoxy potting resin, the resin cured, and then carefully microtomed. Irregular features emanating from the darkened films are artifacts of this potting procedure. A constant magnification was used for all specimens in Figure 8. The righthand portion of each micrograph in the figure indicates the original thickness of each film. This portion was protected from direct exposure by an aluminum retaining template which held the films in place during exposure. The diminished film thickness due to AO erosion is noted by the lefthand portion. The PMDA-DAF film was partially eroded through. The aluminum ion-containing film shows little effect at this magnification.

Figure 9 shows three TEMs at progressively higher magnifications for BTDA-ODA- Al^{3+} . The 3675X micrograph given in 9a clearly shows the smooth back and eroded front film surfaces. The arrow to the left in the figure denotes the original uneroded surface. The textured morphology is clearly apparent in 9b and 9c. The survival of small strands of polymer in such a hostile environment, particularly as depicted in Figure 9b, is astonishing.

3.2 Composites

Unprotected composites were also affected by LEO exposure. Figure 10 shows the SEM of T300 carbon fiber reinforced 934 epoxy matrix specimens for two exposures. The 10-month and 5.8-year samples were placed adjacent to each other in the SEM to enable simultaneous analyses. The left side, low magnification photomicrograph shows both exposed surface and surface protected from direct exposure by an aluminum retaining template. The fabric-appearing pattern visible in the micrograph was transferred to the composite surface by a glass cloth peel-ply during processing.

The right side photomicrograph shows a higher magnification SEM of exposed regions of two specimens. Individual carbon fibers apparent with the 10-month composite are no longer distinguishable after 5.8 years.

Table V gives XPS data for control, 10-month, and 5.8-year T300-934 epoxy composites. Surface carbon content increased in the first 10 months of exposure. This probably reflects increased carbon fiber content due to an initial preferential erosion of matrix resin. Oxygen and sulfur did not appear to change significantly. Fluorine on the control likely resulted from release agent used during processing. Fluorine was not detected on exposed composites because this outer surface was eroded away by AO. The increased silicon content with exposure is no doubt due to a well-documented LDEF contamination to be discussed later. Additional chemical characterization including FTIR, TMA, and DSC failed to detect significant differences between the two specimens.

The loss of both resin and fiber is clearly illustrated by the SEM in Figure 11. This figure gives photomicrographs at two magnifications for a 4-ply $[\pm 45^\circ]_s$ 5208/T300 epoxy composite which received 5.8 years of Row 9 exposure. The righthand micrograph shows the interface between the top ply and the second ply in some detail.

As expected, the loss of fiber and matrix due to flight exposure affected selected mechanical properties. Figure 12 and Figure 13 give ultimate tensile strength and tensile modulus for five different composite materials flown on a Langley experiment (15). No major differences are noted between baseline values obtained when the composites were tested in 1983, ground control composites which remained at Langley, and composites which flew on LDEF as flight control specimens, protected from direct exposure. However, specimens which flew exposed experienced a deterioration in tensile strength and tensile modulus. No doubt, more than resin loss contributed to this phenomenon since the thickness loss was not proportional to the loss in tensile properties by rule of mixtures. The P1700/C6000 specimens lost least in thickness and retained more ultimate tensile strength than other specimens. No explanation for this has been found.

PMR-15 and LARCTM-160 are two similar addition polyimides of considerable promise in the early 1980's when LDEF experiments were being designed. Celion 6000 graphite fiber reinforced composites of these polymers were flown on a Row 1 and Row 7 experiment (33). Specimens of these two materials were made available to Langley for chemical characterization. Figure 14 summarizes selected analyses performed on a PMR-15/C6000 composite. Inspection of the TMA thermogram suggests no difference in T_g for control and exposed specimens. Long-term isothermal weight loss also failed to detect significant effects due to exposure. Exposed and unexposed composite specimens were also examined by DR-FTIR spectroscopy. Spectra given in Figure 14 suggest little difference. A new absorption band at 1650cm^{-1} was anticipated for the exposed specimen. This band would have been indicative of oxidation of a methylene group in the polymer molecular backbone. This band along with an accompanying band at 930cm^{-1} had been detected in the spectrum of thermally aged LARCTM-160 composites (27). The two bands are missing in the spectra shown in Figure 14. The band at 1684cm^{-1} is due to the anhydride portion of the polymer backbone and is supposed to be present. Similar FTIR analyses of other LDEF-exposed composites have failed to detect significant molecular level differences as a result of exposure. Figure 15 gives a typical example of spectra obtained for a P1700/C6000 polysulfone composite. Spectra of exposed and protected composite specimens are virtually identical.

One of the unsolved mysteries concerning materials on LDEF were "stripes" and/or "gray ash" associated with selected epoxy matrix composites. This phenomenon was investigated in some detail. Figure 16 gives a photograph of a striped 5.8-year exposed 934/T300 epoxy composite specimen and also SEM photomicrographs of a sample of the gray ash. Projections rising from the composite surface were apparently caused by contamination protecting underlying material from AO attack. The righthand photograph, obtained by overlaying three individual micrographs, shows

graphite fiber presumably sheared off by AO. The gray ash in question is visible at the base of the finger-like projection.

Figure 17 provides additional information on the 934/T300 flight specimen. The upper righthand portion shows a high resolution SEM of the ash. The residue appears to contain crystals on the order of 0.1 μ m in diameter. EDS and XPS analyses on these crystals, given in Figure 17, revealed sulfur to be a significant component. This was an unexpected result. However, sulfur is present in the diaminodiphenylsulfone (DDS) cured epoxy matrix resin. Similar-appearing residues have been noted for DDS-cured 5208 epoxy composites. The exact chemical nature of this sulfur-containing species has not been established; sodium may be a counter ion. XPS data in Table V for another epoxy flight specimen shows no unusual sulfur content. Apparently this analysis was not conducted on an ash-rich portion of the exposed composite.

Figure 18 contains information on a striped 5208/T300 epoxy composite. Optical and SEM micrographs are given at the top of the figure. The slightly recessed dark stripe is on the order of a tow wide. XPS analysis of a 1mm² spot size failed to note significant differences between white and dark areas. Why one tow of the epoxy composite behaved differently from adjacent tows has not been adequately explained.

The composites addressed in this paper were uncoated materials. They were intentionally left uncoated in order to maximize the effects of long term LEO exposure. Identical materials protected with thin coatings, such as 1000 Å of nickel followed by 600 Å of silicon dioxide, exhibited outstanding resistance to surface erosion (8, 15, 16). Several additional inorganic coatings were found to be effective in preventing surface degradation (17).

3.3 Glass Transition Temperature

Table VI summarizes glass transition temperature (T_g) measurements conducted on a series of composites and films which flew on LDEF along with selected data obtained on films flown on STS-8 and STS-46 experiments. Exposure duration, row, and tray location are identified in the table. A careful inspection of T_g values for control and flight specimens suggests no significant change as a result of exposure. T_g effects do not appear to be an issue for polymeric materials in LEO, at least for polymers exposed for 69 months or less.

3.4 Solution Property Measurements

Selected solution property measurements have been conducted on several polymeric materials which flew on LDEF. The most extensively studied material is a thermoplastic polysulfone resin designated P1700. Both film and graphite fiber reinforced composites have been examined. Table VII summarizes molecular weight data for P1700 film and composite specimens and Figure 19 gives typical molecular weight distribution curves for 10-month exposed film. All data was obtained by Gel Permeation Chromatography-Differential Viscometry (GPC-DV). Several points concerning these data are evident.

A decrease in solubility was noted in testing control film, then a template-protected specimen cut from around the yellowed edge of a flight specimen, and finally a directly exposed center-cut specimen. This decreased solubility with exposure along with a significant decrease in number average molecular weight (M_n) and increase in weight- and z-average molecular weights (M_w and

Mz) is evidence for chain scission plus crosslinking. This behavior confirms predictions derived from ground-based simulation of space environmental effects on this material (34-38).

Table VII also includes molecular weight data obtained on the top ply of 4-ply composites flown on Row 9 and exposed for 10 months or 5.8 years. Data for the 5.8-year sample reflects no molecular weight change when compared with the control composite while the 10-month exposed specimen suggests the same molecular level trends observed with the film sample. This potentially contradictory observation is best understood by considering the orbit of the spacecraft during its flight. LDEF was deployed in an essentially circular orbit of 257 nautical miles on April 7, 1984 (39). It was retrieved 69 months later at an altitude of 179 nautical miles. Only about 2 months of orbit lifetime remained at retrieval. The atomic oxygen fluence differs greatly at these two altitudes.

Figure 20 is the approximate cumulative percent RAM AO fluence as a function of time. Exact AO exposure for these specimens is given in reference 30. The 10-month specimens were exposed early in the mission when AO fluence was at a minimum. The 5.8-year specimens received significant AO near the end of the mission. As much as 50% of total AO was received during the last 6 months in orbit. The molecular level effects observed after 10 months, primarily related to changes in surface chemistry, had most likely been eroded away by the time the satellite was retrieved. An earlier retrieval from a higher orbit may have provided different results. Subtractive FTIR spectroscopy gave additional insight into the molecular level response of P1700 film to LEO exposure. Since the LDEF specimen was too thick for good quality transmission studies, somewhat poorer quality spectra of control and exposed specimens were obtained by diffuse reflectance (DR). Differences between the two spectra were difficult to establish until they were subtracted. Figure 21 is the result of subtracting the DR-FTIR spectrum of the control film from that of the exposed. A downward inflection in the curve is indicative of a larger amount of a particular species in the exposed spectrum.

The band centered around 3400cm^{-1} is most likely due to -OH. Bands at 1485 and 1237cm^{-1} may also be associated with that group. Reports in the literature have noted the 3400cm^{-1} -OH band for polysulfone film exposed to UV (40) and also to 3-MeV protons (37). Additionally, the loss of the 1385cm^{-1} methyl band was noted in at least one study (40). Methyl does not appear to have been lost in the present study. A diminished -CH₃ content would have resulted in an upward inflection in the subtraction spectrum at 1385cm^{-1} ; no band is present around 1385cm^{-1} in Figure 21.

The presence of -OH has been explained by cleavage of the ether oxygen in the backbone of the polymer followed by abstraction of a proton (37), or by a photo Claisen rearrangement of the ether oxygen to produce an ortho-hydroxy substituted biphenyl linkage (36). We made no determination in this study of the origin of the -OH group.

Solution property measurements were also conducted on polystyrene specimens exposed for 5.8 years on LDEF Row 9 and Row 3. Table VIII gives various molecular weight parameters for these two specimens. Only a slight reduction in M_n was observed with exposure while M_w and M_z increased dramatically. This behavior is indicative of crosslinking and is the predicted response to UV for polystyrene. FTIR and UV-VIS spectra of this polymer will be included in a future report.

Additional solution property measurements were conducted on two polyimide films exposed for 10 months on Row 9. The molecular structure of the two polyimides, 6F-BDAF and 6F-DDSO₂, is included with structures given in Table IV. The two 6F-anhydride polymers were the only potentially soluble polyimides flown on LDEF. Table IX summarizes molecular weight data determined by GPC-DV. Analyses were conducted on a control film, the edge of a flight specimen shielded from direct exposure, and a 10-month exposed specimen cut from the center of the film. All

samples contained residual insoluble material. The insoluble gel was recovered by filtration and dried to constant weight. Analyzed concentrations were then adjusted to account for the insoluble portion.

An inspection of data for 6F-BDAF suggests that various molecular weight parameters were not affected by the 10-month LEO exposure provided by LDEF. In contrast, 6F-DDSO₂ exhibited significant changes at the molecular level. Solubility decreased from 94.5% to 60.9% with exposure. The number average molecular weight (M_n) remained fairly constant while the z-average molecular weight (M_z) doubled. Changes in the polydispersity ratio (M_w/M_n) are also noted for this material. These observations, particularly solubility and M_z behavior, are considered evidence that the 6F-DDSO₂ structure crosslinked during exposure. The z-average molecular weight (M_z) is probably a neglected parameter for evaluating crosslinking in environmentally exposed polymers (41). Figure 22 gives GPC-DV molecular weight distributions for 6F-DDSO₂. They show the broadening with exposure and shift to higher molecular weight documented in Table IX. The molecular weight distributions for control and exposed 6F-BDAF were virtually superimposable. The change in molecular weight for 6F-DDSO₂ is considered primarily a result of VUV damage to the -SO₂- group in the polymer backbone.

3.5 Additional Studies

Polyimide-polysiloxane copolymers. The chemical characterization of a series of polyimide-polysiloxane copolymers which received 10 months of Row 9 exposure also provided molecular level insight into LEO space environmental effects. Preliminary results obtained on these experimental materials have been given in previous reports (10, 13, 18). In general, the films discolored somewhat with exposure but did not exhibit significant weight loss. SEM, STM, and limited XPS data may be found in the referenced reports.

Table X gives detailed XPS results for three different siloxane-containing copolymers. Data for both control and exposed film is included in the table. Several points are made concerning these data. Note the decrease in surface carbon content with exposure and concurrent increase in surface oxygen content. Note also the increase in silicon and that the silicon to oxygen ratio is about 1:2 after exposure. Finally, note the increase in the silicon 2p electron binding energy with exposure from approximately 102 electron volts to 103 eV. This data is consistent with the following interpretation. Upon AO exposure, the surface of these siloxane-containing copolymers eroded to expose silicon atoms. These atoms were initially present as an organically-bound silicon, as evidenced by the 102 eV binding energy. Upon exposure to AO, organic silicon (102 eV B.E.) was oxidized to inorganic silicon (103 eV B.E.), most likely an SiO₂ type of silicate. At this point, further AO erosion was retarded. Inorganic silicates are known to be effective barriers to AO erosion. These observations suggest an exciting potential for designing AO protection into the backbone of certain polymers. This protection could likely be achieved by periodic incorporation of siloxane groups into the molecular structure of the host polymer.

RTV-511 Silicone. Several polymeric materials which flew on a Row 8 experiment were characterized. Figure 23 summarizes selected information on one of these materials, an RTV-511 silicone specimen. SEM revealed topography typical of embrittlement. Surface carbon and oxygen content changed with exposure but silicon did not. The 102.5 eV binding energy for this element for both unexposed and exposed specimens suggests no change in chemical state of Si with exposure. Thermogravimetric analysis included in Figure 23 revealed that the exposed sample exhibited 2-3% less weight loss prior to decomposition than the unexposed sample. Apparently the flight sample had outgassed low molecular weight species while in space. This phenomenon no doubt contributed to the general contamination observed on the LDEF spacecraft.

Contamination. As documented in numerous LDEF publications, much of the vehicle surface was coated with varying amounts of a molecular contamination film commonly referred to as the "nicotine stain." Figure 24 summarizes XPS results obtained on an optical window flown on a Row 9 experiment. One side of the window received 5.8 years of RAM exposure while the reverse side was vented to the inside of the experiment tray. Approximately 20% silicon was detected on the exposed surface while only 3.3% was found on the vented side. The control contained no silicon. The 102.9 eV binding energy for the Si 2p electron indicates that exposed surface silicon was present as inorganic silica/silicate. The 101.9 eV binding energy for the vented side is indicative of organic silicone.

This contamination layer likely had an effect on the behavior of polymeric materials on LDEF. UV probably contributed to the discoloration of contaminated specimens. Upon exposure to AO, the silicon-containing contamination was oxidized from silicone to silicate. The resultant AO-resistant protective layer likely affected the manner in which the material eroded. Contaminated samples probably performed differently than had they not been contaminated.

Post Exposure Effects. The possibility that some LDEF polymeric materials have changed or degraded after the spacecraft was returned to Earth has been raised on several occasions. At the First Post Retrieval Symposium, we reported that two thin films flown on STS-8 in 1983 had changed significantly in appearance since they were initially examined (12). Additional information on these two films was presented at the LDEF Materials Workshop '91 (13). One of the films flown on STS-8, an experimental polyimide designated PMDA-DAF, was reflighted on LDEF. By visual inspection, the exposed area of this film is noticeably more opaque now than it was when the experiment was deintegrated from LDEF in Spring 1990.

Selected Ag/FEP Teflon thermal blanket specimens have changed in appearance with time. Figure 25 shows photographs of a micrometeoroid impact on a thermal blanket flown on Row 11. Both photographs were obtained on an optical microscope at the same magnification. The photograph on the left was taken in April 1990, shortly after the analysis of LDEF materials began at the Langley Research Center. The same specimen area was located and photographed again in November 1991. A careful inspection of the two photographs in Figure 25 will reveal that cracks on the vapor deposited silver side of the thermal blanket material had continued to form and intensify. The aged specimen had also become duller in appearance.

Thus, some polymeric materials no doubt continued to age after environmental exposure. Quantified information is needed to define the chemical and/or mechanical mechanisms associated with this phenomenon. The prudent analyst must be aware that certain characterized effects may have become exaggerated during the interval between when the specimen was returned to Earth and when it was analyzed. In retrospect, Electron Spin Resonance (ESR) should have been used to investigate the formation and lifetime of free radicals which likely contributed to various observed post exposure effects. Including ESR with other characterization techniques outlined in Table II would have strengthened our understanding in this particular area.

3.6 A Perspective

A significant amount of fundamental information has been generated on several polymers which received 10 months or 5.8 years of LEO exposure. For example, Table VII gives molecular weight data on P1700 polysulfone film and composite specimens. Table VIII gives similar data for polystyrene specimens flown on Row 3 and Row 9 of LDEF. Additional unreported molecular weight measurements were conducted on 5.8-year exposed Row 3 poly(vinyl toluene). Polystyrene and poly(vinyl toluene) are two well-characterized polymers. Finally, Table IX contains molecular weight data for two 10-month exposed experimental polyimide films.

All polysulfone, polystyrene, and polyimide specimens were extensively characterized by UV-VIS and FTIR spectroscopy, thermal analysis, SEM, STM, and in most cases, XPS. Thus, a thorough understanding has been obtained of the molecular level response of these polymers to extended LEO exposure. Additional polysulfone and polystyrene data has been obtained on samples flown on recent Space Shuttle experiments.

Can this data be used as a benchmark to calibrate the ground-based simulation of LEO space environmental effects? If effects on materials described in this report can be simulated, then the same conditions can be used to simulate the effects of LEO exposure on new and emerging polymeric materials of current interest for space application. Synergistic and accelerated effects may also then be better understood. Such understanding will significantly enhance our ability to predict the long-term performance of polymeric materials in low Earth orbit.

4.0 CONCLUDING REMARKS

Current studies indicate LDEF to be the definitive source for long-term exposure verification of LEO environmental effects on polymeric materials. A wide variety of materials has been characterized. Exposure to atomic oxygen led to changes in the physical appearance of most flight specimens and reductions in selected mechanical properties. Other environmental effects are considered to be primarily surface phenomena. Changes in various molecular weight parameters, attributed to ultraviolet degradation, were documented for several soluble polymers. Many environmental effects for specimens located on or near Row 9 were lost to increased AO erosion near the end of the LDEF mission. An ubiquitous silicon-containing contamination likely affected the behavior of many polymeric materials. Finally, the possibility that selected LDEF polymers have changed since they returned to Earth in January 1990, was addressed.

The Long Duration Exposure Facility provided a once-in-a-career opportunity for the first-hand examination of effects of long-term space exposure on a variety of polymeric materials. As a result, research on space environmental effects has taken a forward leap past pre-LDEF levels of analytical procedures, data acquisition, modeling, and understanding of degradation mechanisms in low Earth orbit.

ACKNOWLEDGMENT

A significant portion of this research was made possible by the generous contribution of LDEF specimens by a number of individuals. The authors express appreciation to John C. Gregory, The University of Alabama in Huntsville; James B. Whiteside, Grumman Aerospace Corporation; Richard F. Vyhna, Rockwell International Corporation; Michael G. Grote, McDonnell Douglas Astronautics Company; Ann F. Whitaker and James M. Zwiener, NASA Marshall Space Flight Center; H. Gary Pippin, Boeing Defense and Space Group; Anne K. St. Clair and Bland A. Stein, NASA Langley Research Center.

REFERENCES

1. A. S. Levine, ed.: LDEF-69 Months in Space. First Post Retrieval Symposium, Kissimmee, FL, June 2-8, 1991. NASA CP-3134, Parts 1, 2, and 3.
2. B. A. Stein and P. R. Young, comp.: LDEF Materials Workshop '91. Langley Research Center, Hampton, VA, November 18-21, 1991. NASA CP-3162, Parts 1 and 2.

3. A. S. Levine, ed.: LDEF-69 Months in Space. Second Post Retrieval Symposium, San Diego, CA, June 1-5, 1992. NASA CP-3194, Parts 1, 2, 3, and 4.
4. J. C. Gregory, ed.: LDEF Materials Results for Spacecraft Applications Conference, Huntsville, AL, October 27-28, 1992. NASA CP-3257.
5. L. E. Murr and W. H. Kinard: Effects of Low Earth Orbit. American Scientist, **81**, 152 (1993).
6. L. G. Clark, W. H. Kinard, D. J. Carter, and J. L. Jones, ed.: The Long Duration Exposure Facility (LDEF). NASA SP-473, 1984.
7. T. Stevenson: LDEF Comes Home. Aerospace Composites and Materials, **2(2)** May-June (1990).
8. P. R. Young, W. S. Slemp, W. G. Witte, and J. Y. Shen: Characterization of Selected LDEF Polymer Matrix Resin Composite Materials. SAMPE International Symposium, **36(1)**, 403(1991).
9. P. R. Young and W. S. Slemp: An Analysis of LDEF-Exposed Silvered FEP Teflon Thermal Blanket Material. NASA TM 104096 (1991).
10. P. R. Young, W. S. Slemp, and C. R. Gautreaux: Characterization of Selected LDEF Exposed Polymer Films. SAMPE International Symposium, **37**, 159 (1992).
11. P. R. Young, W. S. Slemp, E. J. Siochi, and J. R. J. Davis: Analysis of a Space-Exposed Thermoplastic Resin. SAMPE Intl. Tech. Conf., **24**, T174 (1992).
12. P. R. Young and W. S. Slemp: Chemical Characterization of Selected LDEF Polymeric Materials. NASA CP-3134, Part 2, 687 (1991).
13. P. R. Young and W. S. Slemp: Characterization of Selected LDEF-Exposed Polymer Films and Resins. NASA CP-3162, Part 1, 1992, 357 (1992).
14. P. R. Young and W. S. Slemp: Space Environmental Effects on Selected LDEF Polymeric Materials. American Chemical Society Book Series 527, Radiation Effects on Polymeric Materials, E. Reichmanis, C. W. Frank, J. H. O'Donnell, eds., ACS, Washington, DC, 1993.
15. W. S. Slemp, P. R. Young, W. G. Witte, and J. Y. Shen: Effects of LDEF Flight Exposure on Selected Polymer Matrix Resin Composite Materials. NASA CP-3134, Part 2, 1149 (1992).
16. P. R. Young, W. S. Slemp, and A. C. Chang: LDEF Polymeric Materials: 10 Months vs. 5.8 Years of Exposure. NASA CP-3194, Part 3, 827 (1993).
17. W. S. Slemp and P. R. Young: LDEF Thermal Control Coatings Post-Flight Analysis. NASA CP-3194, Part 3, 1093 (1993).
18. P. R. Young, W. S. Slemp, and B. A. Stein: Performance of Selected Polymeric Materials on LDEF. NASA CP-3257, 125 (1992).
19. P. R. Young, A. K. St. Clair, and W. S. Slemp: Response of Selected High Performance Films to LEO Exposure. SAMPE International Symposium, **38(1)**, 664 (1993).
20. C. R. Kalil and P. R. Young: Scanning Tunneling Microscopy Analysis of Space-Exposed Polymer Films. 39th Intl. Instrument Symposium, ISA 39, 445 (1993).
21. B. A. Stein and P. R. Young, comp: LDEF Materials Data Analysis Workshop. NASA CP-10046, 1990.
22. W. G. Witte, Jr.: Manual for LDEF Tensile Tests. NASA TM 87624, 1985.
23. W. G. Witte, Jr.: Baseline Tensile Tests of Composite Materials for LDEF Exposure. NASA TM 89069, 1987.
24. A. K. St. Clair, T. L. St. Clair, and K. I. Shevet: Synthesis and Characterization of Essentially Colorless Polyimide Films. Proceedings of the ACS Division of Polymeric Materials: Science and Engineering, **51**, 62(1984).
25. Aluminum Ion-Containing Polyimide Adhesives. U.S. Patent 4,234,461 to NASA, Aug. 13, 1981.
26. V. L. Bell: Polyimide Structure-Property Relationships. I. Polymers from Fluorene-Derived Diamines. J. Polym. Sci.: Polym. Chem. Ed., **14**, 225(1976).

27. P. R. Young, B. A. Stein, and A. C. Chang: Resin Characterization in Cured Graphite Fiber Reinforced Composites Using Diffuse Reflectance FTIR. National SAMPE Symposium, **28**, 824 (1983).
28. P. R. Young, J. R. J. Davis, and A. C. Chang: Molecular Weight Characterization in Advanced Thermoplastic Resins. SAMPE International Symposium, **34(2)**, 1450 (1989).
29. P. N. Peters, P. L. Whitehouse, and J. C. Gregory: Refinements on the Pinhole Camera Measurements of the LDEF Attitude. NASA CP-3194, Part 1, 3 (1993).
30. R. J. Bourassa and J. R. Gillis; Atomic Oxygen Exposure of LDEF Experiment Trays. NASA CR 189627, Contracts NASI-18224 and NASI-19247, May 1992
31. R. J. Bourassa and J. R. Gillis: Solar Exposure of LDEF Experiment Trays. NASA CR 189554, Contract NASI-18224, February 1992.
32. S. L. Koontz: Atomic Oxygen Effects on Spacecraft Materials-The State of the Art of Our Knowledge. NASA CP-3035, Part 1, 241 (1989).
33. R. F. Vyhnal: The Effects of Long-Duration Space Exposure on the Mechanical Properties of Some Carbon-Reinforced Resin Matrix Composites. NASA CP-3194, Part 3, 941 (1993).
34. J. R. Brown and J. H. O'Donnell: Effects of Gamma Radiation on Two Aromatic Polysulfones. J. Appl. Polym. Sci., **19**, 405 (1975).
35. J. R. Brown and J. H. O'Donnell: Effects of Gamma Radiation on Two Aromatic Polysulfones II. A Comparison of Irradiation at Various Temperatures in Air-Vacuum Environments. J. Appl. Polym. Sci., **23**, 2763 (1979).
36. S. Kuroda, A. Nagura, K. Horie, and I. Mita: Degradation of Aromatic Polymers III. Crosslinking and Chain Scission During Photodegradation of Polysulfones. Eur. Polym. J., **25(6)**, 621 (1989).
37. D. R. Coulter, M. V. Smith, F. Tsay, and A. Gupta: The Effects of 3-MeV Proton Radiation on an Aromatic Polysulfone. J. Appl. Polym. Sci., **30**, 1753 (1985).
38. B. Santos and G. F. Sykes: Radiation Effects on Four Polysulfone Films. SAMPE Technical Conference, **13**, 256 (1981).
39. R. L. O'Neal and E. B. Lightner: Long Duration Exposure Facility-A General Overview. NASA CP-3134, Part 1, 3 (1991).
40. B. D. Gesner and P. G. Kelleher: Thermal and Photooxidation of Polysulfone. J. Appl. Polym. Sci., **12**, 1199 (1968).
41. D. J. T. Hill, D. A. Lewis, J. H. O'Donnell, P. J. Pomery, C. L. Winzor, D. J. Winzor, and A. K. Whitaker: Recent Advances in the Radiation Chemistry of Polymers. First Pacific Polymer Conference, Maui, December 12-15, 1989. Pacific Polymer Preprints, **1**, 67 (1989).

TABLE I. ANTICIPATED ENVIRONMENTAL EFFECTS FOR LDEF POLYMERIC MATERIALS

Chemical

- Modification to molecular structure
- Molecular weight/distribution change
- T_g /crystallinity effects
- Formation of volatile/degradation products
- Changes in surface chemistry

Physical

- Resin loss/erosion
- Dimensional changes (CTE ...)

Optical

- Change in transparency
- α_s/ϵ
- Contamination

Mechanical

- Deterioration in strength, modulus, toughness ...

TABLE II. RECOMMENDED CHARACTERIZATION

Chemical

Solution property measurements

- Gel permeation chromatography (GPC)
- Low Angle Laser Light Scattering (LALLS)
- Differential Viscometry (DV)
- Osmometry
- GPC/LALLS, GPC/DV
- High Pressure Liquid Chromatography (HPLC)

Spectroscopy

- Fourier transform infrared spectroscopy
- UV-VIS-NIR
- Mass Spectroscopy (SIMS)
- Magnetic resonance
- Thermal emittance

Physical

Thermal/thermomechanical

- Thermomechanical Analysis (TMA)
- Dynamic Mechanical Analysis (DMA)
- Differential Scanning Calorimetry (DSC)
- Thermogravimetric Analysis (TGA)

Surface Analysis

- X-Ray Photoelectron Spectroscopy (ESCA)
- Energy Dispersive Spectroscopy (EDAX)
- Scanning Electron Microscopy (SEM)
- Scanning Tunneling Microscopy (STM)

Objective: Molecular level response to environmental exposure

TABLE III. LDEF POLYMERIC MATERIALS

Composites:	Films:
^a P1700/C6000 Polysulfone	^a FEP Teflon
^a 934/T300 Epoxy	^c Silvered FEP Teflon
^a 5208/T300 Epoxy	^a Kynar Fluorocarbon
^b PMR-15/C6000 Polyimide	^a P1700 Polysulfone
^b LARC-160/C6000 Polyimide	^{a,d} Kapton Polyimide
^e High Performance Polymers:	^f Traditional Polymers:
Polyimide-Polysiloxane Copolymer	Polystyrene
BTDA-ODA Polyimide	Polyvinyl toluene
BTDA-ODA-Al ³⁺ Doped polyimide	Polytetrafluoroethylene
6F-DDSO ₂ Soluble polyimide	Polymethylmethacrylate
6F-BDAF Soluble polyimide	Nylon
PMDA-DAF Polyimide	Polyethylene terephthalate
^g Polyetheretherketone (PEEK)	^g Various Silicones
	^g Polyurethane

Source: ^a W. Slemp, PI, Expts. A0134/S0010 (B9).
^b R. Vyhnal, PI, Expt. A0175 (A1 and A7).
^c LDEF MSIG (various LDEF locations).
^d J. Whiteside, PI, Expt. A0133 (H7).
^e W. Slemp and A. St. Clair, PI, Expt. S0010 (B9).
^f J. Gregory, PI, Expt. A0114 (C9/C3).
^g A. Whitaker, PI, Expt. A0171 (A8).

TABLE IV. MOLECULAR STRUCTURE OF 10-MONTH EXPOSED POLYIMIDE FILMS

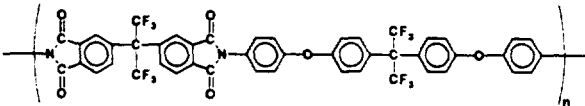
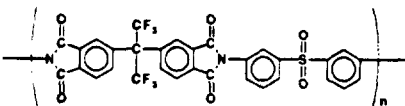
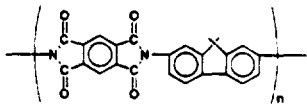
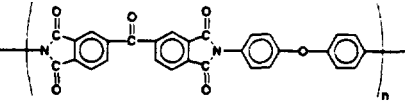
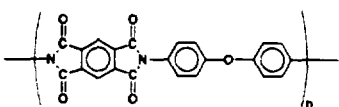
SAMPLE	STRUCTURE	COLOR
6F-BDAF		pale yellow
6F-DDSO ₂		colorless
PMDA-DAF		reddish-yellow
BTDA-ODA		yellow
BTDA-ODA-Al ³⁺	BTDA-ODA + Al(acac) ₃	brownish-yellow
KAPTON		yellow

TABLE V. XPS ANALYSIS OF 934/T300 COMPOSITES

Photopeak	Control	10-Month Exposed	5.8-Year Exposed
C 1s B.E. ^a (eV)	285.0 ... 292.3 ^c	283.6 ... 289.7	283.9 ... 288.5
A.C. ^b (%)	68.9	73.3	72.1
O 1s B.E. (eV)	531.5/532.7/533.9	531.3 ... 534.0	531.1/532.5/534.8
A.C. (%)	18.1	18.8	19.7
S 2p B.E. (eV)	168.4	168.6	170.0
A.C. (%)	1.1	0.8	0.9
N 1s B.E. (eV)	399.9	399.6	400.6
A.C. (%)	3.4	5.5	0.8
Si 2p B.E. (eV)	103.2	103.7	104.0
A.C. (%)	1.0	0.9	6.4
Na 1s B.E. (eV)	1072.2	—	—
A.C. (%)	2.0	NSP ^d	—
F 1s B.E. (eV)	689.3	—	—
A.C. (%)	5.5	NSP	NSP

^a Binding Energy.

^b Atomic Concentration.

^c Multiple Peaks.

^d No Significant Peak.

TABLE VI. GLASS TRANSITION TEMPERATURE*

Composite	Exposure Condition	T _g , °C		Film/Resin	Exposure Condition	T _g , °C	
		Control	Exposed			Control	Exposed
P1700/C6000	1	164	164	P1700	1	184	184
P1700/C6000	2	171	171	P1700	5	185	185
PMR-15/C6000	3	343	342	PET	6	85	86
LaRC-160/C6000	4	356	357	PEN-2,6	7	131	131
5208/T300	2	214	215	6F-BDAF	1	259	255
934/T300	1	202	209	6F-DDSO ₂	1	270	273
Exposure Conditions:				PMDA-DAF	1	331	—
1. 10-Month LDEF, Row 9, Tray B				BTDA-ODA	1	271	269
2. 5.8-Year LDEF, Row 9, Tray B				BTDA-ODA-AP ⁺	1	295	290
3. 5.8-Year LDEF, Row 7, Tray A				PEEK	8	164	166
4. 5.8-Year LDEF, Row 1, Tray A				Polystyrene	5	99	97
5. STS-46 EOIM-III, 40 hr RAM				Polystyrene	6	92	93
6. 5.8-Year LDEF, Row 3, Tray C				Polyvinyl toluene	6	85	85
7. STS-8 EOIM-II, 40 hr RAM				Polymethylmethacrylate	6	119	119
8. 5.8-Year LDEF, Row 8, Tray A							

*Thermomechanical Analysis

TABLE VII. MOLECULAR WEIGHT OF LDEF-EXPOSED P1700 SPECIMENS

Film	¹ Solubility	² M _n	M _w	M _z	M _w /M _n	³ IV
Control	100	18,100	53,600	92,600	2.97	0.48
10 month, edge	96	12,700	73,500	183,000	5.77	0.47
10 month, center	87	12,500	90,900	326,000	7.27	0.49
Composite	% Resin					
Control, top ply	30.3	15,800	57,400	100,600	3.62	0.43
10 month, top ply	27.5	14,300	61,200	115,600	4.28	0.39
5.8 year, top ply	32.9	15,400	57,300	99,800	3.71	0.45

¹ Solubility in Chloroform, %

² All molecular weight in grams/mole

³ Intrinsic viscosity, dL/g

TABLE VIII. MOLECULAR WEIGHT OF LDEF-EXPOSED POLYSTYRENE

Experiment	Origin	Sample	¹ Solubility	² M _n	M _w	M _z	M _w /M _n	³ IV
LDEF, Row 3	⁴ UAH, 30 mil	Control	95	79,900	289,900	754,200	3.63	0.68
		Exposed	95	65,700	410,500	1,422,000	6.25	0.77
LDEF, Row 9	⁴ UAH, 30 mil	Control	100	69,300	310,000	1,099,900	4.47	0.74
		Exposed	90.6	57,600	474,500	1,903,000	8.24	0.85

¹ Solubility in Toluene, %

² All molecular weight in grams/mole

³ Intrinsic viscosity in dL/g

⁴ University of Alabama in Huntsville, John C. Gregory, PI.

TABLE IX. MOLECULAR WEIGHT OF LDEF-EXPOSED POLYIMIDE FILMS

SAMPLE	¹ SOLUBILITY	² M _n	M _w	M _z	M _w /M _n	³ I.V.
6F-BDAF						
Control	98.8	85,600	218,000	710,000	2.54	0.829
		87,500	218,000	659,000	2.49	0.816
⁴ Edge	98.7	76,500	212,000	767,000	2.77	0.846
		84,000	225,000	800,000	2.68	0.805
⁵ Center	96.8	80,500	219,000	651,000	2.72	0.824
6F-DDSO₂						
Control	94.5	66,900	181,000	438,000	2.70	0.715
		46,500	176,000	407,000	3.79	0.732
⁴ Edge	86.8	80,700	302,000	904,000	3.74	1.048
		76,200	309,000	966,000	4.06	1.042
⁵ Center	60.9	41,800	306,000	1,110,000	7.32	0.619
		52,200	274,000	802,000	5.25	0.598

- ¹ Solubility in DMAc, %
- ² All molecular weight in grams/mole
- ³ Intrinsic Viscosity, dL/g
- ⁴ Shielded from direct exposure
- ⁵ 10-month direct exposure

TABLE X. XPS ANALYSIS OF 10-MONTH EXPOSED POLYIMIDE-POLYSILOXANE COPOLYMERS

PHOTOPEAK	PIPSX-6		PIPSX-9		PIPSX-11	
	CONTROL	EXPOSED	CONTROL	EXPOSED	CONTROL	EXPOSED
C 1s B.E. ^a (eV)	285.0/287.6/288.7	285.0/286.1	284.7	284.6	285.0/286.5/288.6	283.7 ... 287.8 ^c
A.C. ^b (%)	57.5	15.5	54.4	16.8	69.2	19.0
O 1s B.E. (eV)	532.6	532.9/533.8	532.5	533.0	532.2/533.7	532.7/533.8
A.C. (%)	23.4	53.8	23.7	52.4	19.2	53.0
N 1s B.E. (eV)	400.1	—	—	—	400.4	—
A.C. (%)	1.6	NSP ^d	NSP	NSP	2.5	NSP
Si 2p B.E. (eV)	102.6	103.8	102.2	103.4	102.2	103.6
A.C. (%)	17.6	27.1	21.6	30.8	9.2	28.0
F 1s B.E. (eV)	—	—	—	—	—	—
A.C. (%)	NSP	—	—	—	NSP	NSP
Na 1s B.E. (eV)	—	1073.1	—	—	—	—
A.C. (%)	—	2.1	—	—	—	—
Cl 2p B.E. (eV)	—	200.1	—	—	—	—
A.C. (%)	—	1.3	—	—	—	—

^a Binding Energy

^b Atomic Concentration

^c Multiple Peaks

^d No Significant Peak

LDEF IN ORBIT

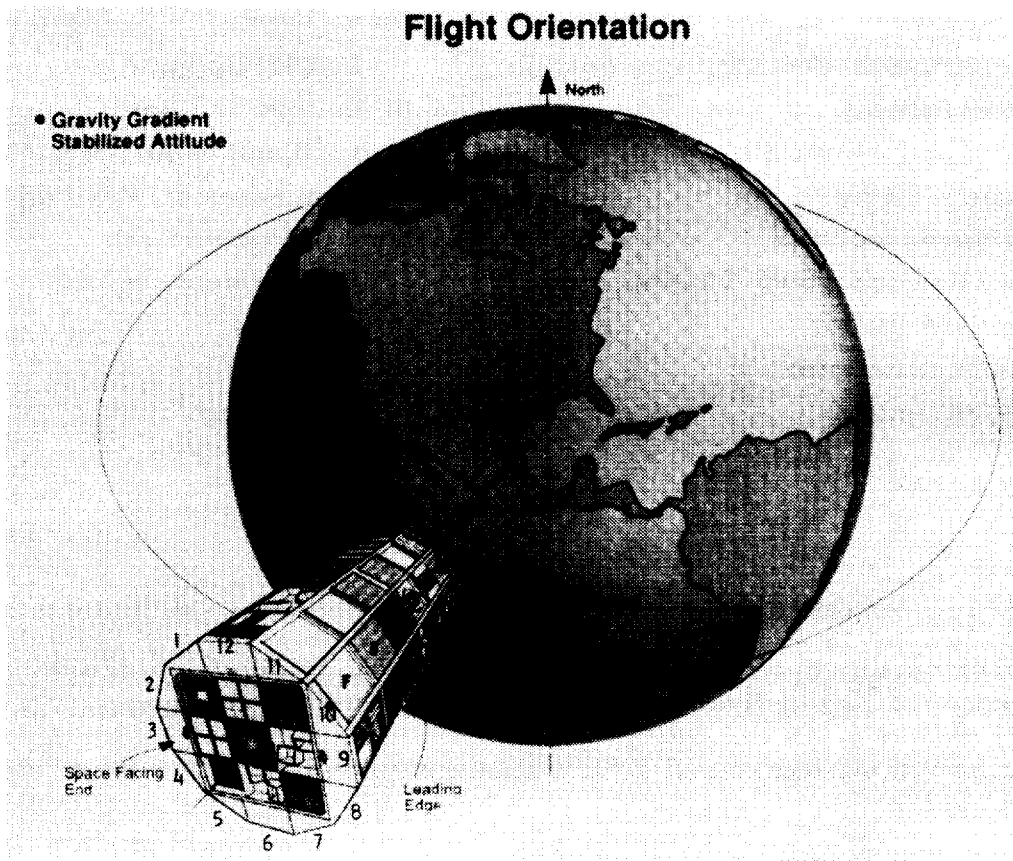
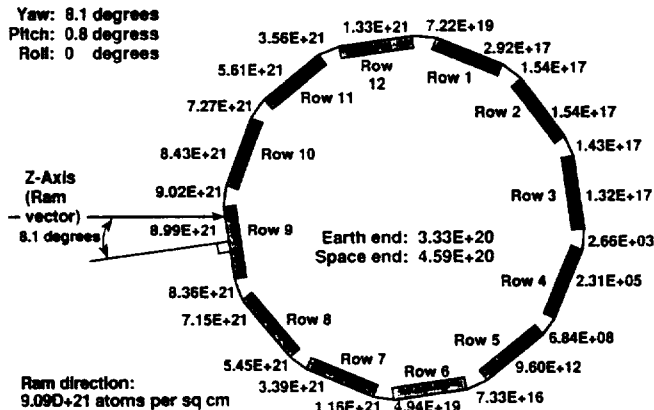
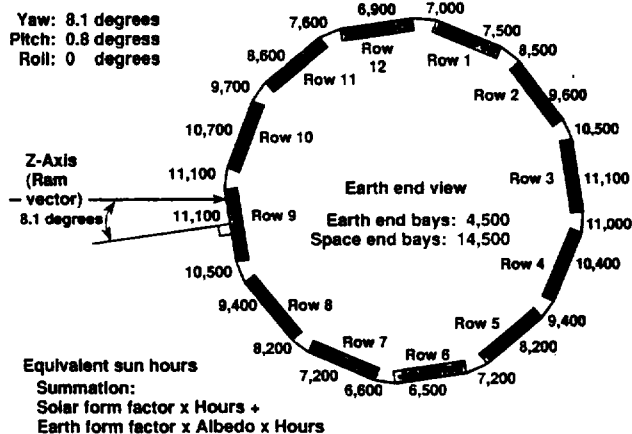


Figure 1. The LDEF and flight orientation.

(a) Atomic Oxygen Fluence Summary



(b) Equivalent Sun Hours Summary



(c) Integrated 5.8-Year Parameters

Thermal Cycles:
~34,000 (-20 to 160°F, $\pm 20^\circ$)

Particulate Radiation:
e⁻ and p⁺: 2.5×10^5 rad
Cosmic: <10 rad

Micrometeoroid and Debris:
34,336 Impacts (0.5mm - 5.25mm)

Vacuum: 10^{-6} - 10^{-7} torr

Altitude/Orbital Inclination:
255-180 nm/28.5°

(d) Selected 10-Month Parameters

Atomic Oxygen:
 2.6×10^{20} atoms/cm²

UV Radiation: ~2,300 hrs

Thermal Cycles: ~4,900 (-20 to 140°F)

Particulate Radiation: ~ 4×10^4 rad

Micrometeoroid and Debris:
No Visual Impacts on Test Specimens

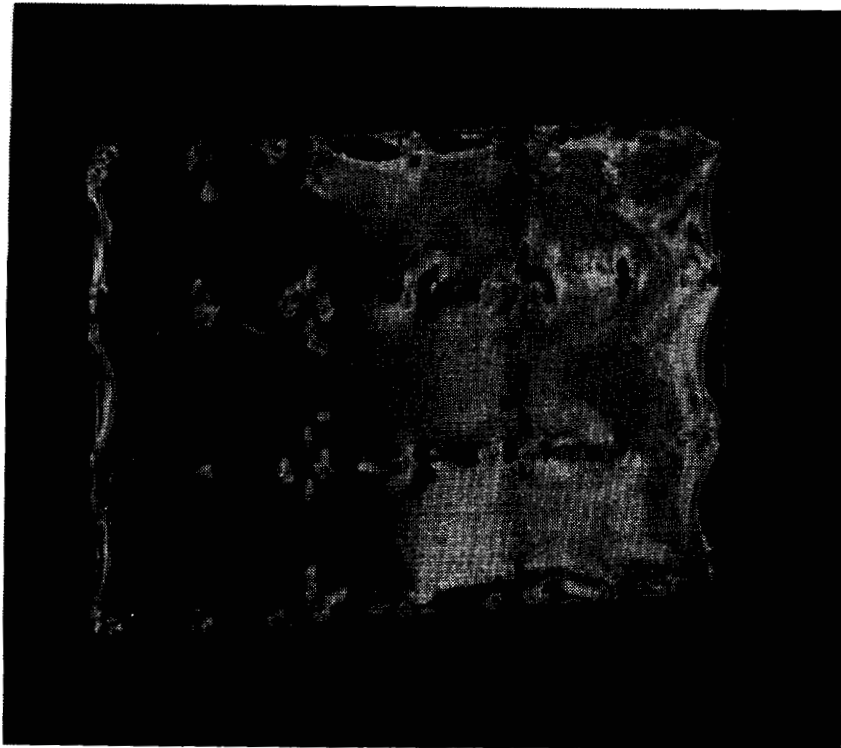
Figure 2. LDEF environmental exposure parameters.

(a) atomic oxygen fluences at end of 5.8-year mission for all row, longeron, and end-bay locations including the fluence received during the retrieval attitude excursion (30).

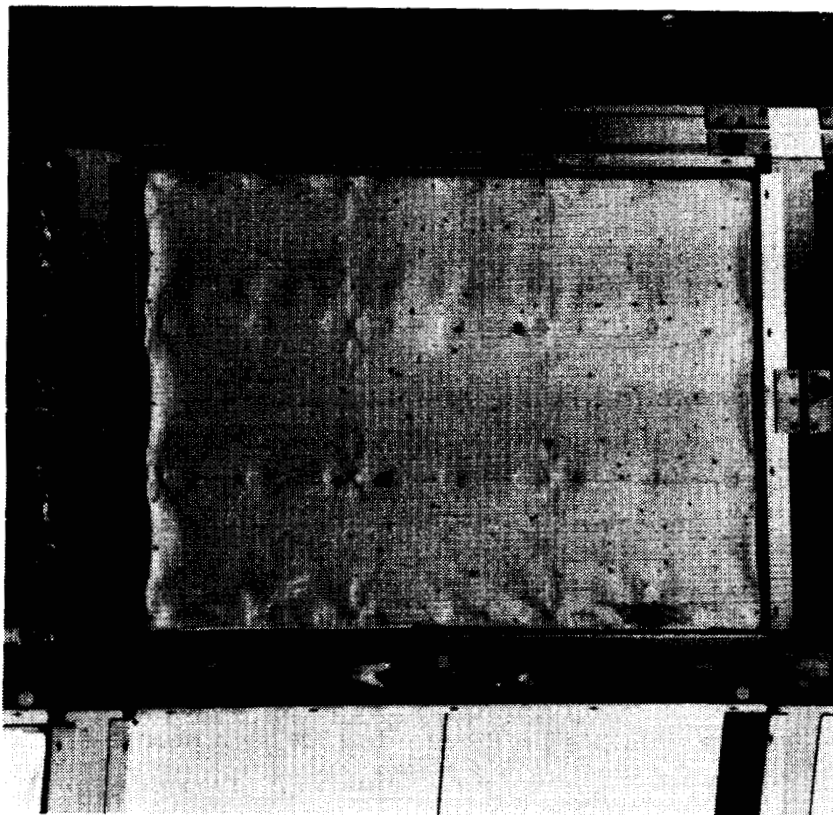
(b) equivalent sun hours at end of 5.8-year mission for each row, longeron, and end-bay location (31).

(c) additional integrated 5.8-year exposure parameters.

(d) selected 10-month exposure parameters.



(a) F4 thermal blanket



(b) E10 thermal blanket

Figure 3. On-orbit retrieval photographs of (a) F4 and (b) E10 silvered FEP teflon thermal blankets.

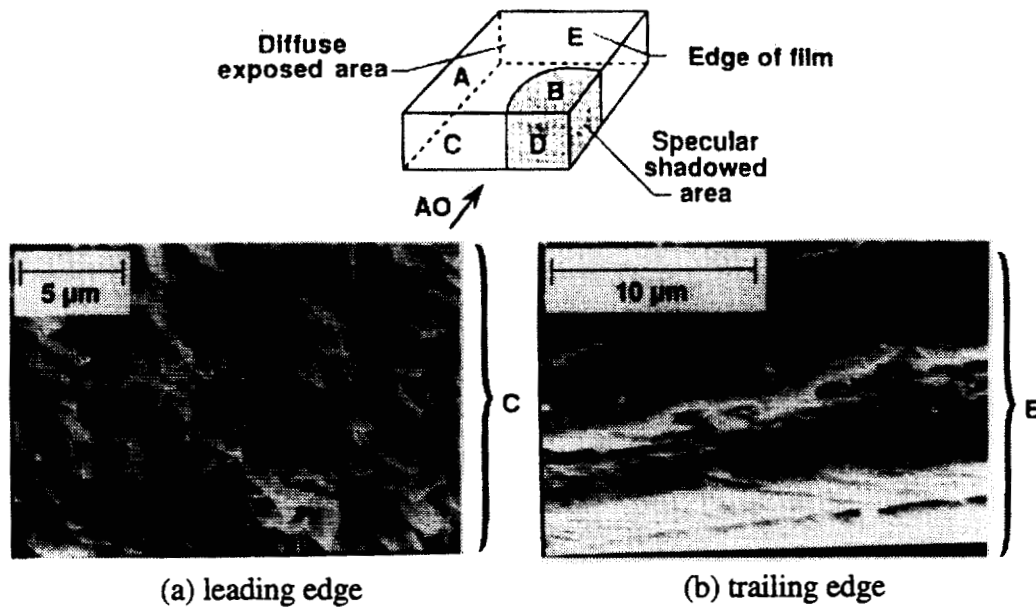


Figure 4. SEM photomicrographs of exposed Kapton film.

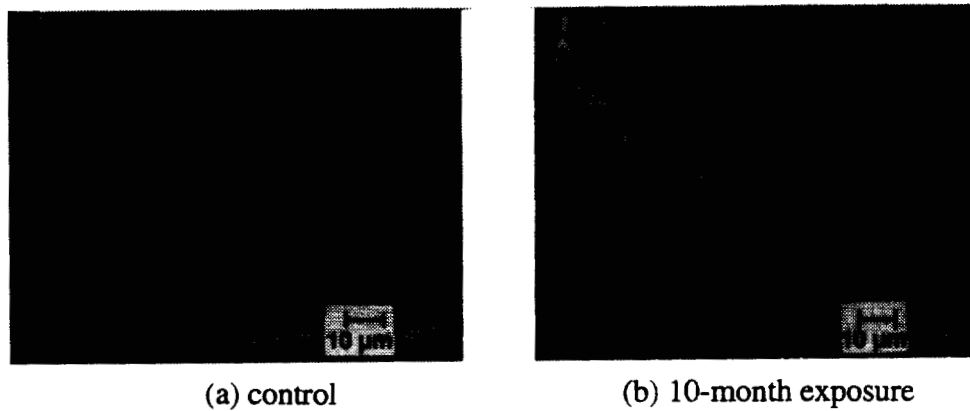


Figure 5. SEM photomicrographs of control and 10-month exposed polysulfone film.

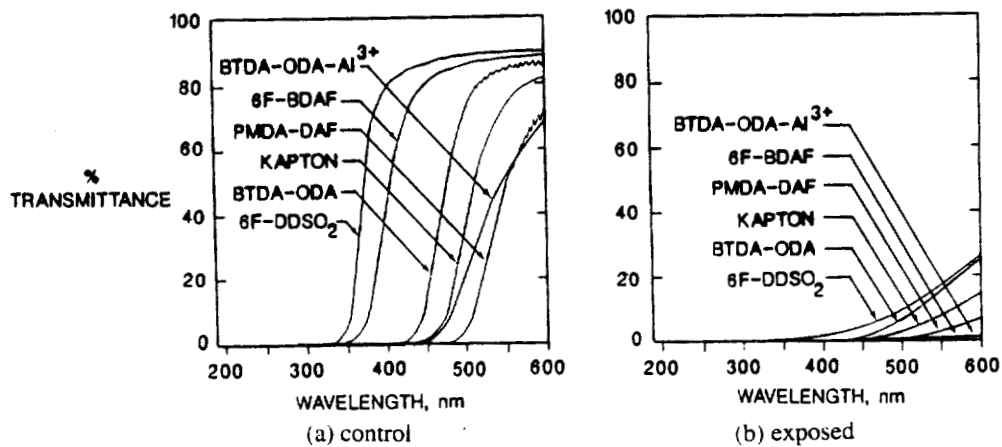
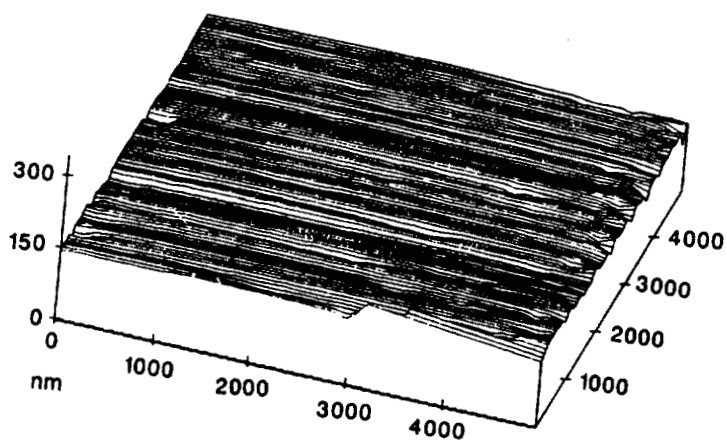
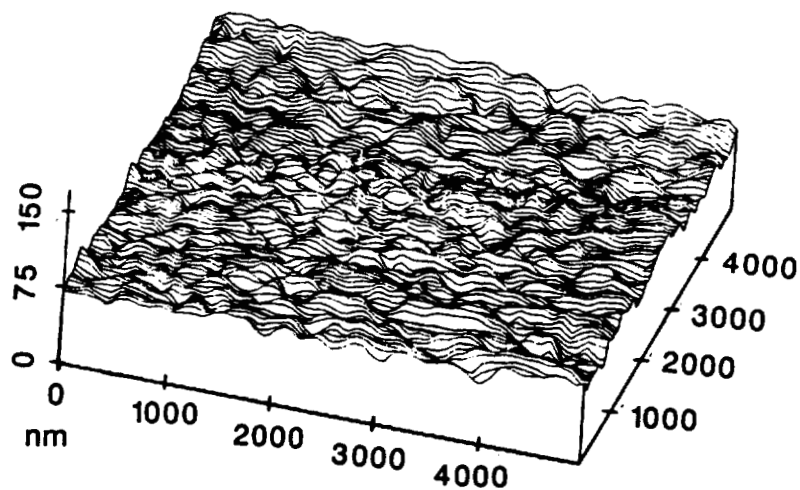


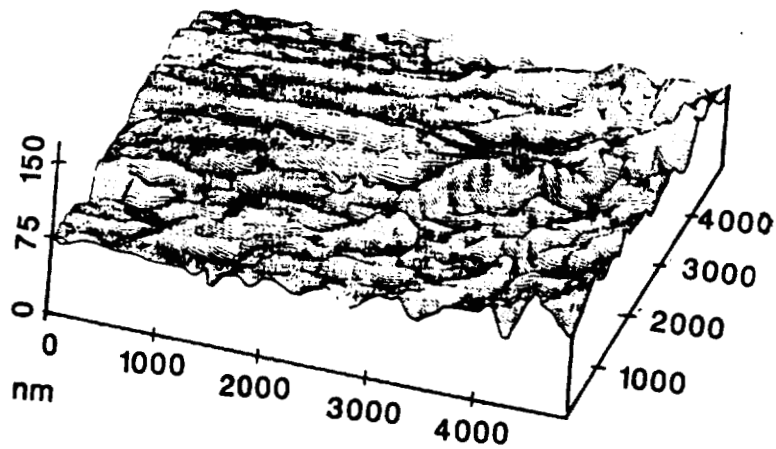
Figure 6. UV-VIS spectra of 10-month exposed polyimide films.



(a) BTDA-ODA unexposed



(b) BTDA-ODA exposed



(c) BTDA-ODA-Al³⁺ exposed

Figure 7. STM analysis of BTDA polyimide films.

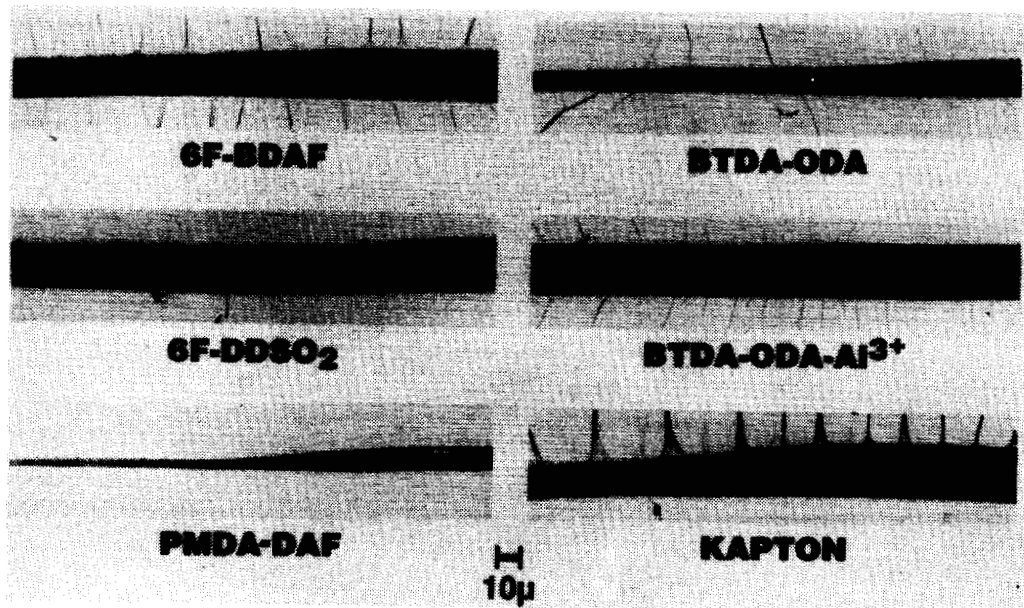


Figure 8. TEM analysis of exposed polyimide films (770X).

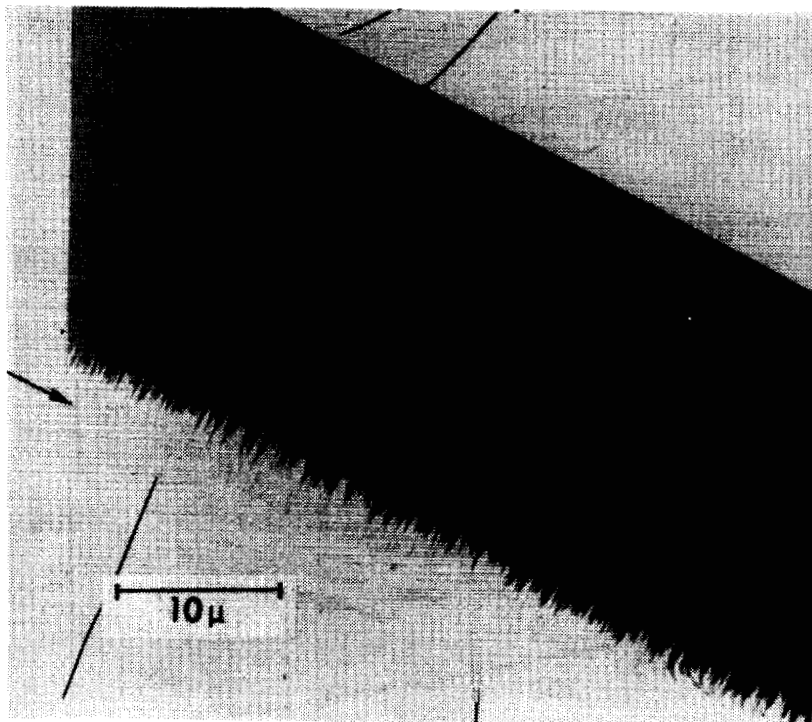


Figure 9a. TEM of exposed BTDA-ODA-Al³⁺ (3675X).

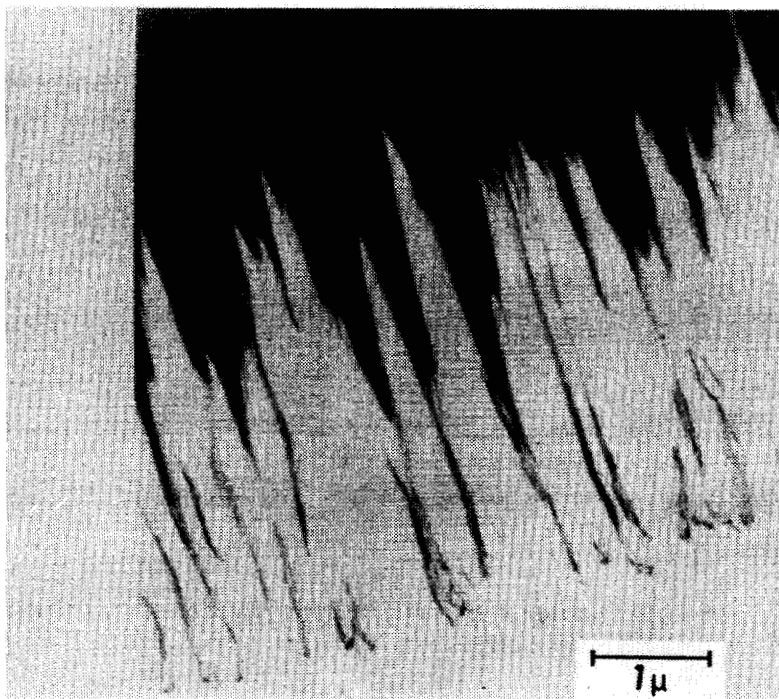


Figure 9b. TEM of exposed BTDA-ODA-Al³⁺ (25,200X).

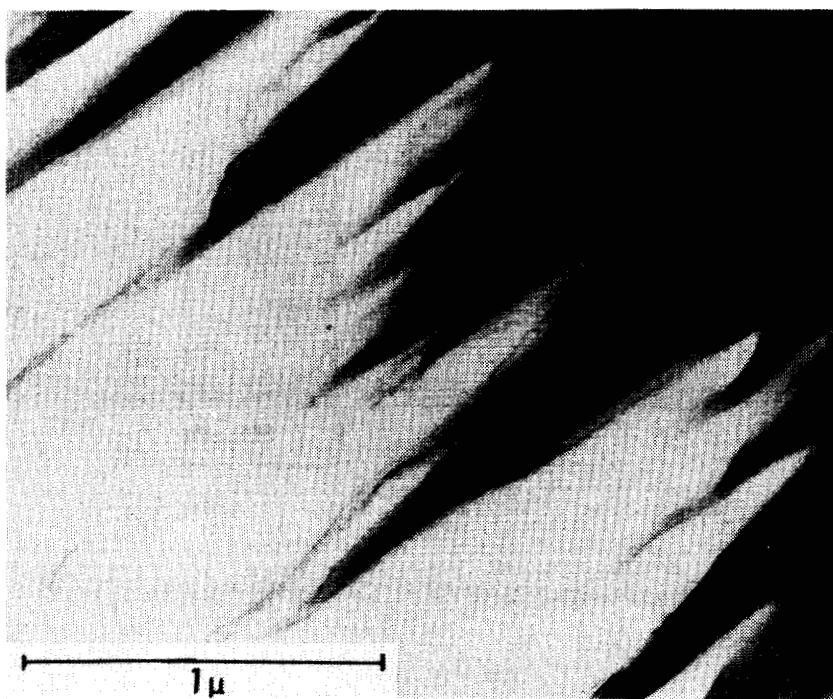


Figure 9c. TEM of exposed BTDA-ODA-Al³⁺ (81,375X).

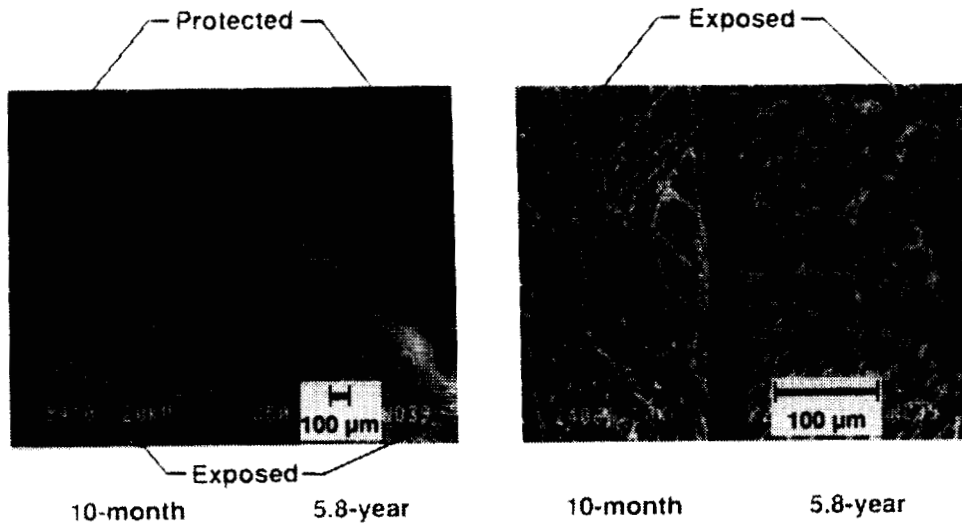


Figure 10. SEM photomicrographs of 934/T300 epoxy/graphite composites after 10-month and 5.8-year LDEF exposures.

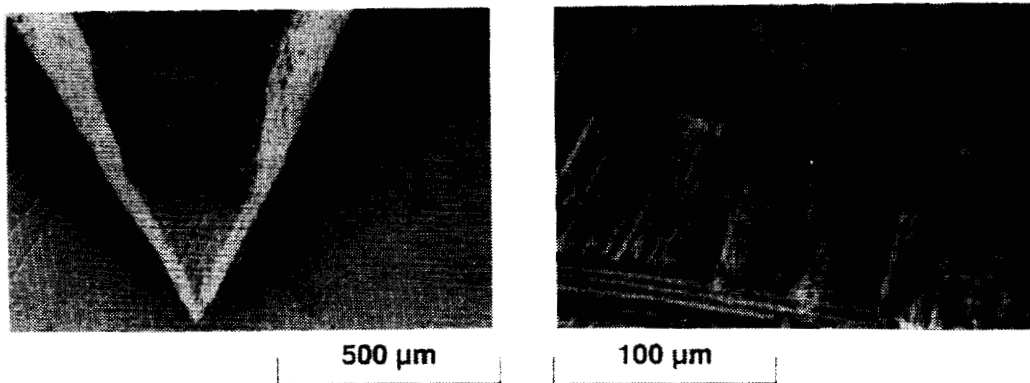


Figure 11. SEM photomicrographs of 5208/T300 epoxy/graphite $[\pm 45]_s$ composite after 5.8-year exposure.

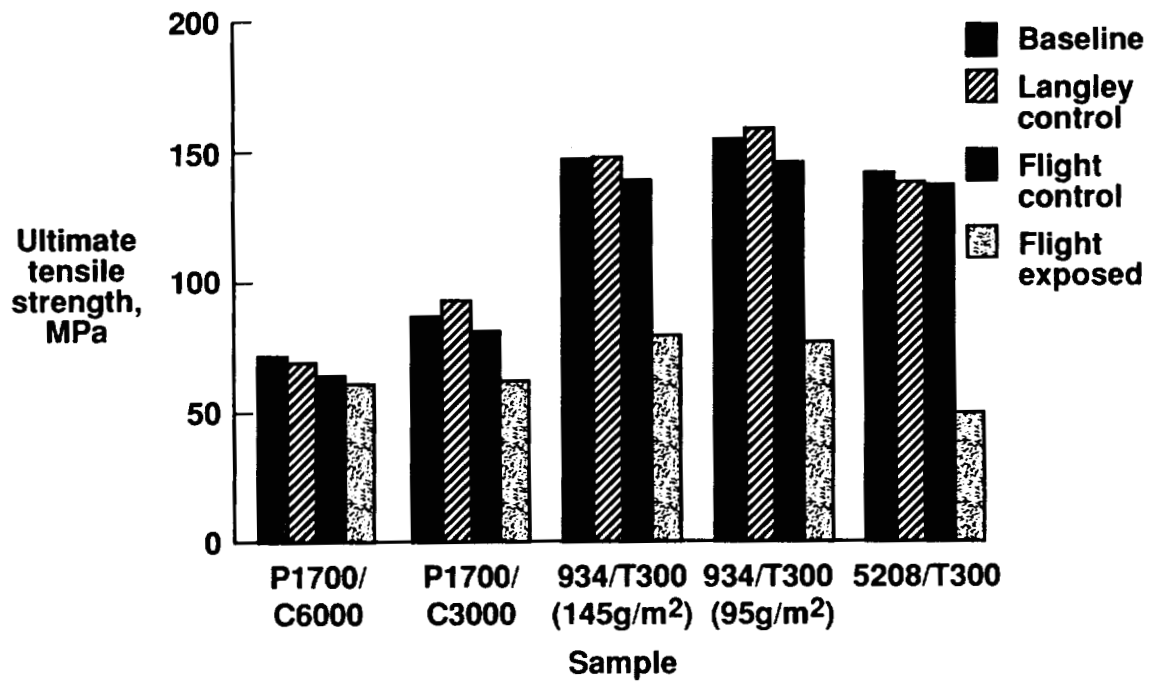


Figure 12. Effects of 5.8 years of LDEF flight exposure on tensile strength of composite materials.

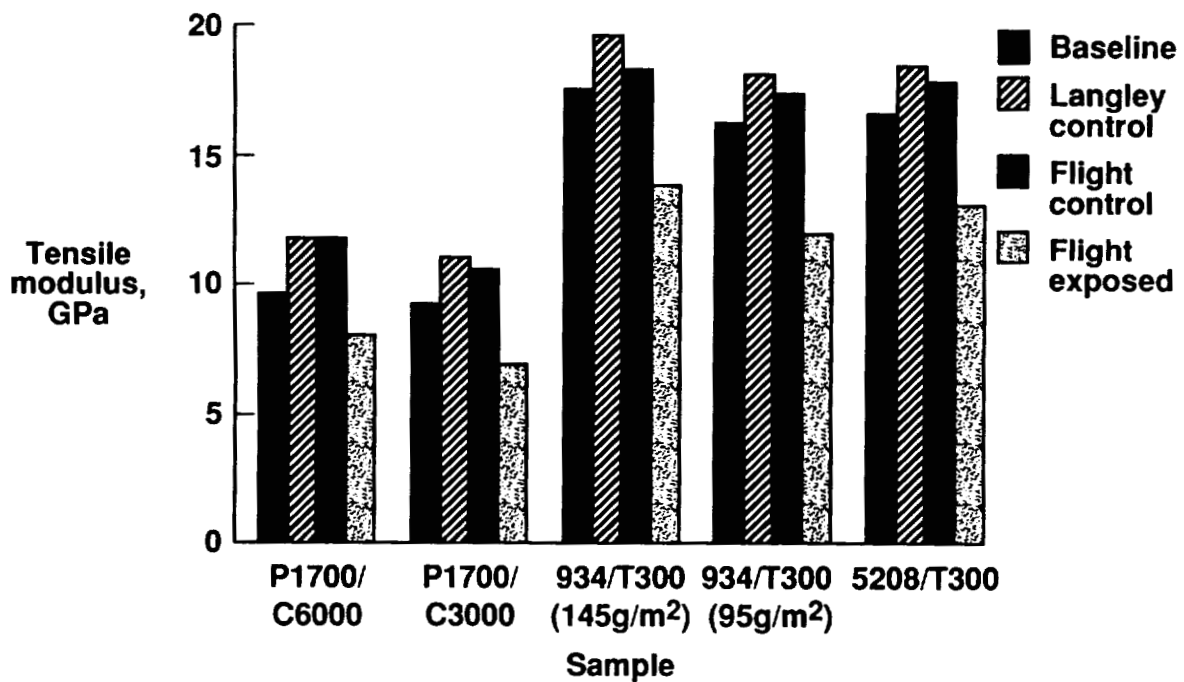


Figure 13. Effects of 5.8 years of LDEF flight exposure on tensile modulus of composite materials.

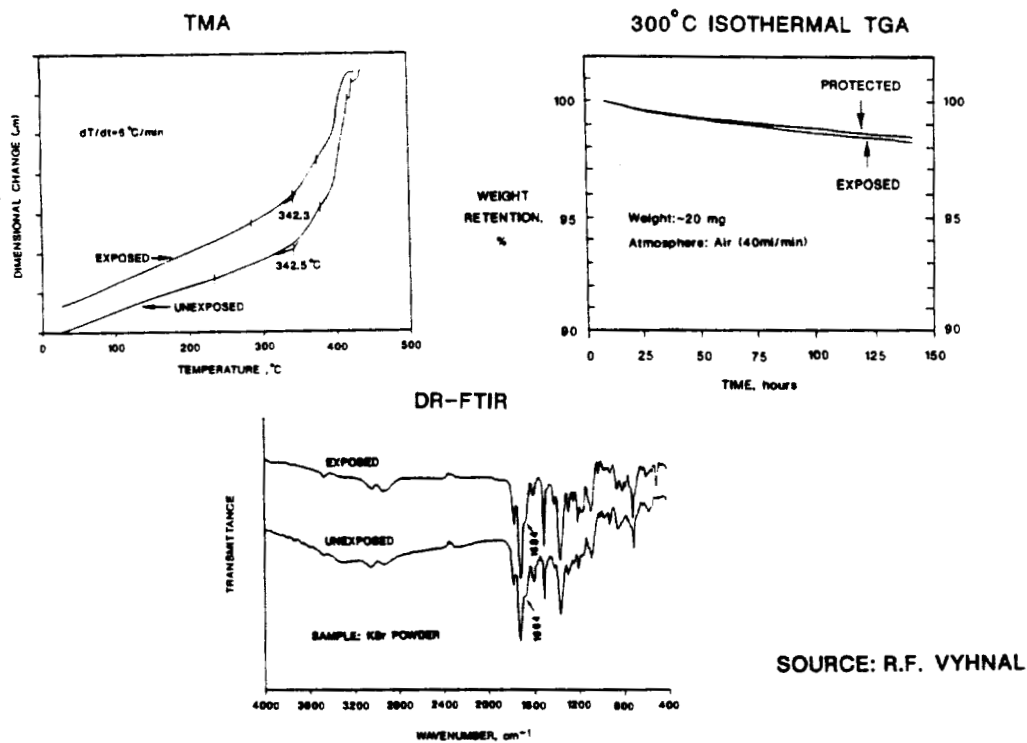


Figure 14. Characterization of PMR-15/C6000 polyimide composites.

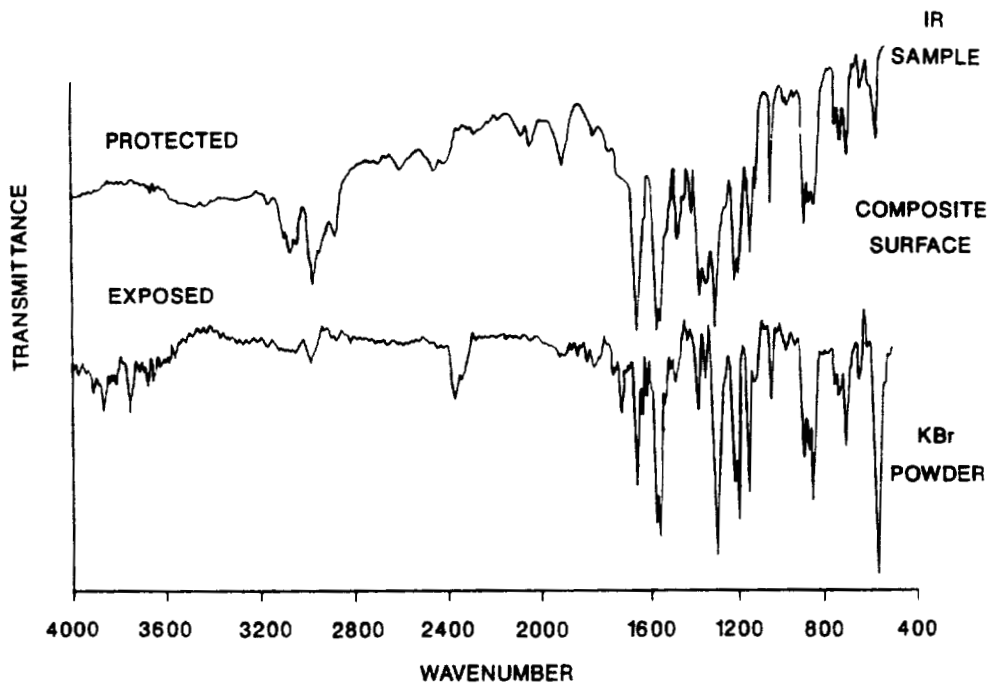


Figure 15. DR-FTIR spectra of LDEF-exposed P1700/C6000 polysulfone composite.

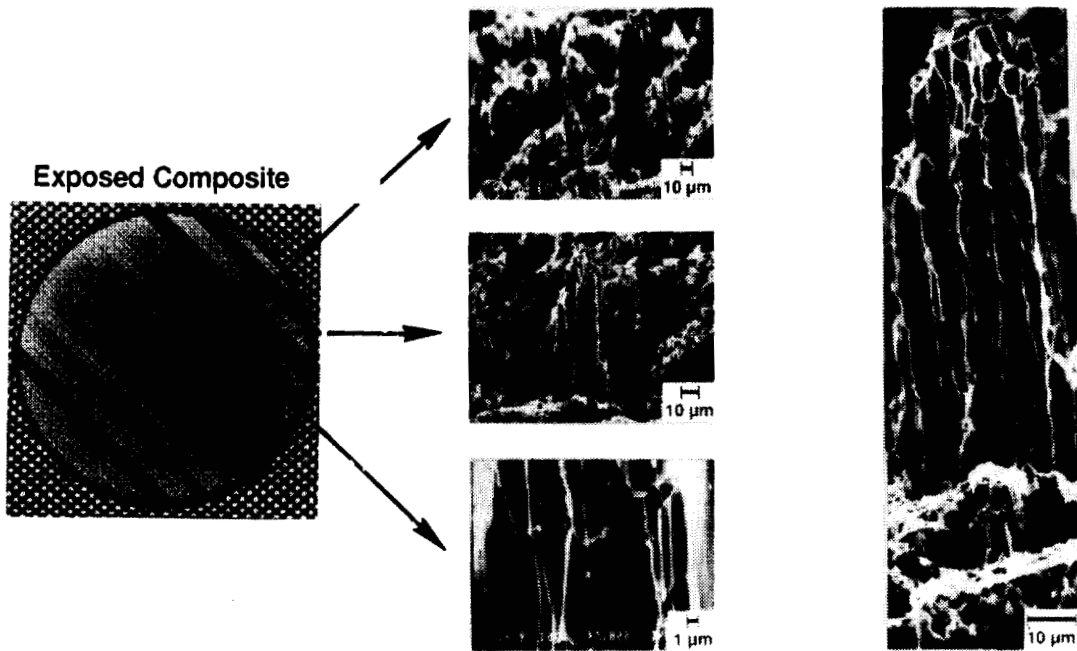


Figure 16. Photograph and SEM photomicrographs of 5.8-year exposed 934/T300 epoxy composite.

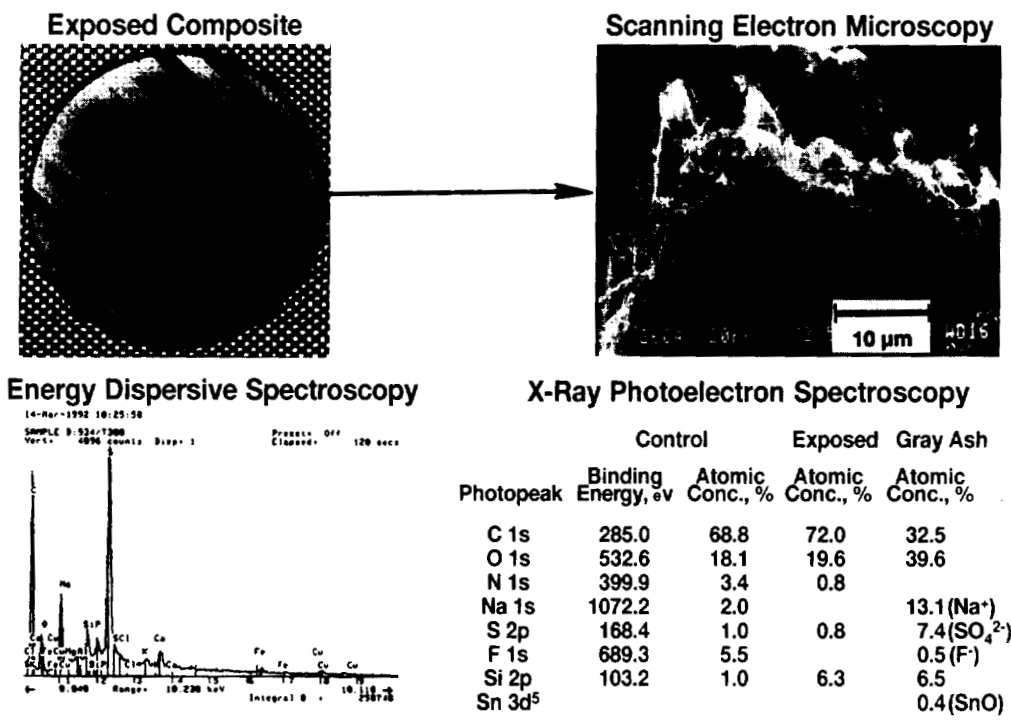


Figure 17. Characterization of 934/T300 epoxy composite.

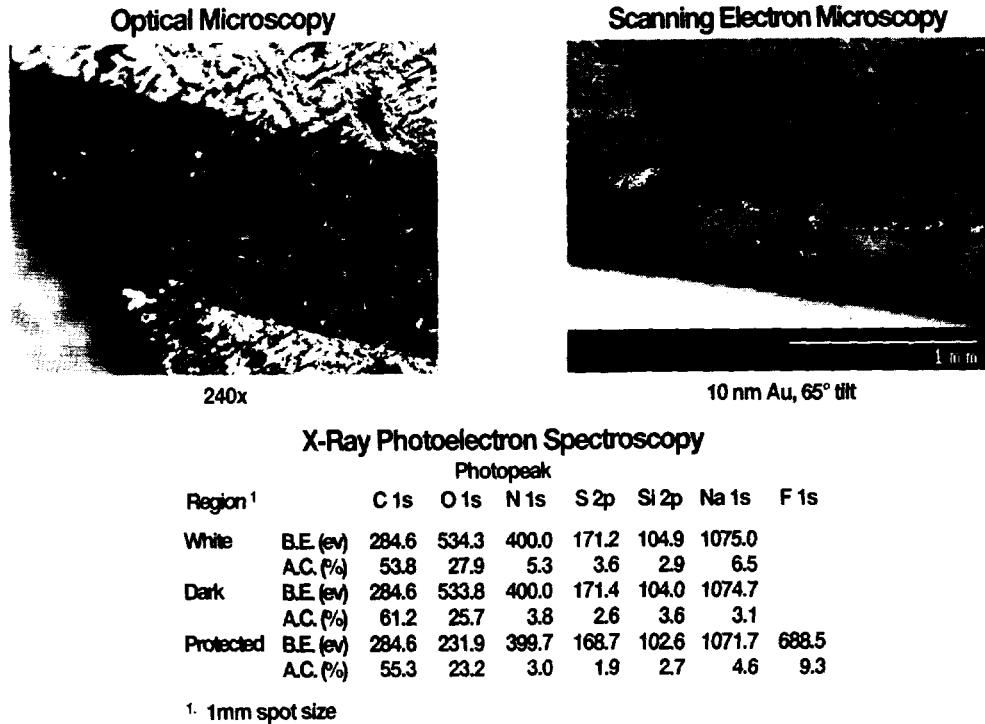


Figure 18. Characterization of 5208/T300 epoxy composite.

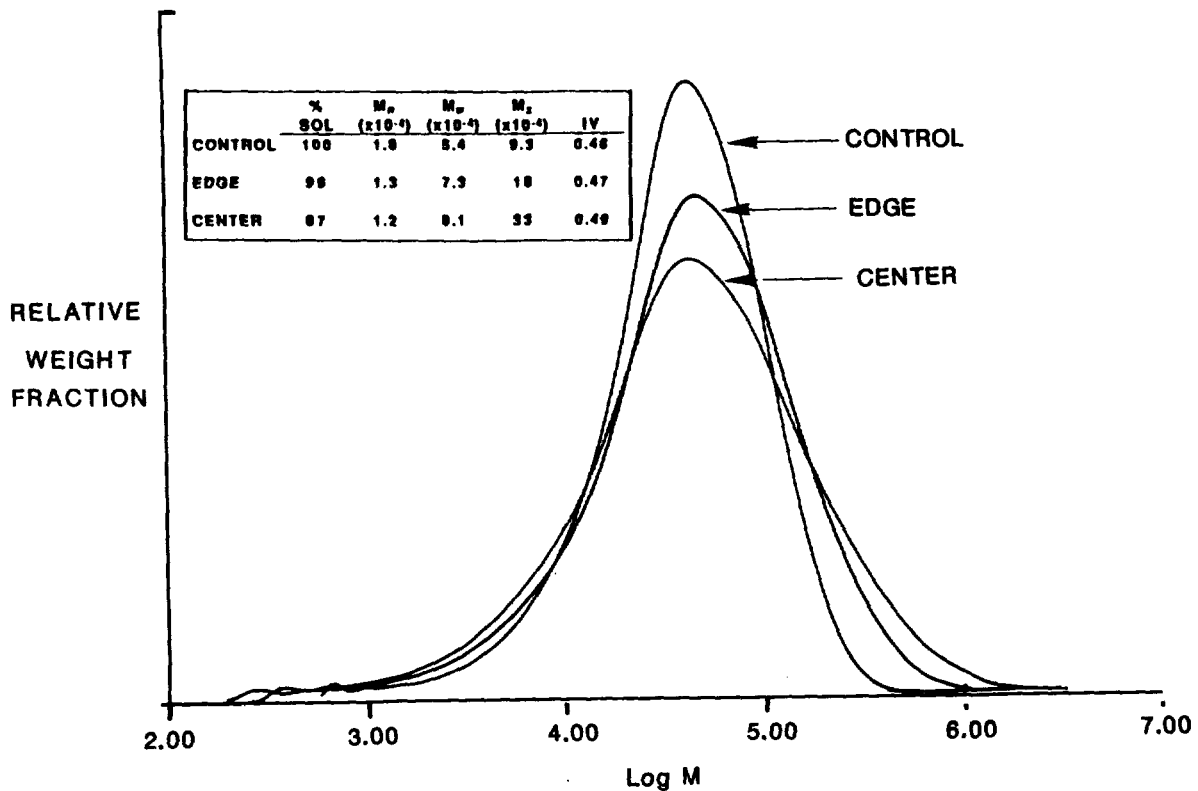


Figure 19. GPC-DV molecular weight distribution of 10-month exposed polysulfone film.

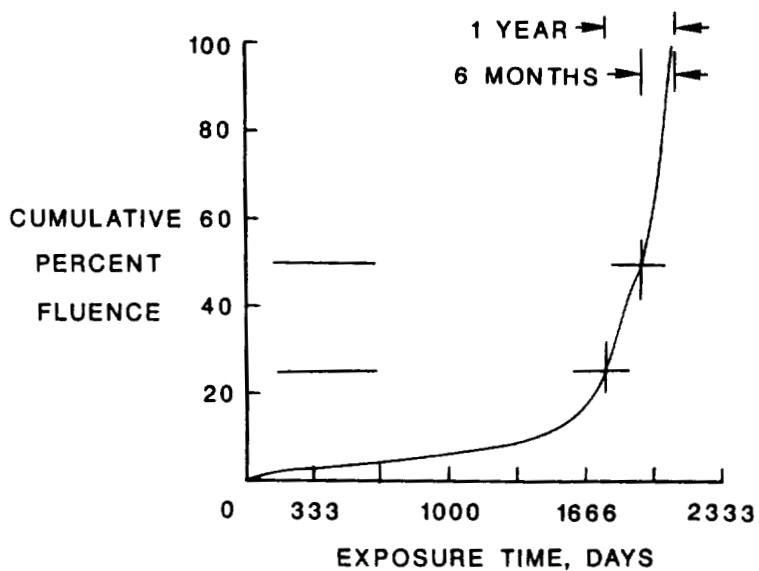


Figure 20. Approximate LDEF cumulative atomic oxygen fluence as a function of exposure time.

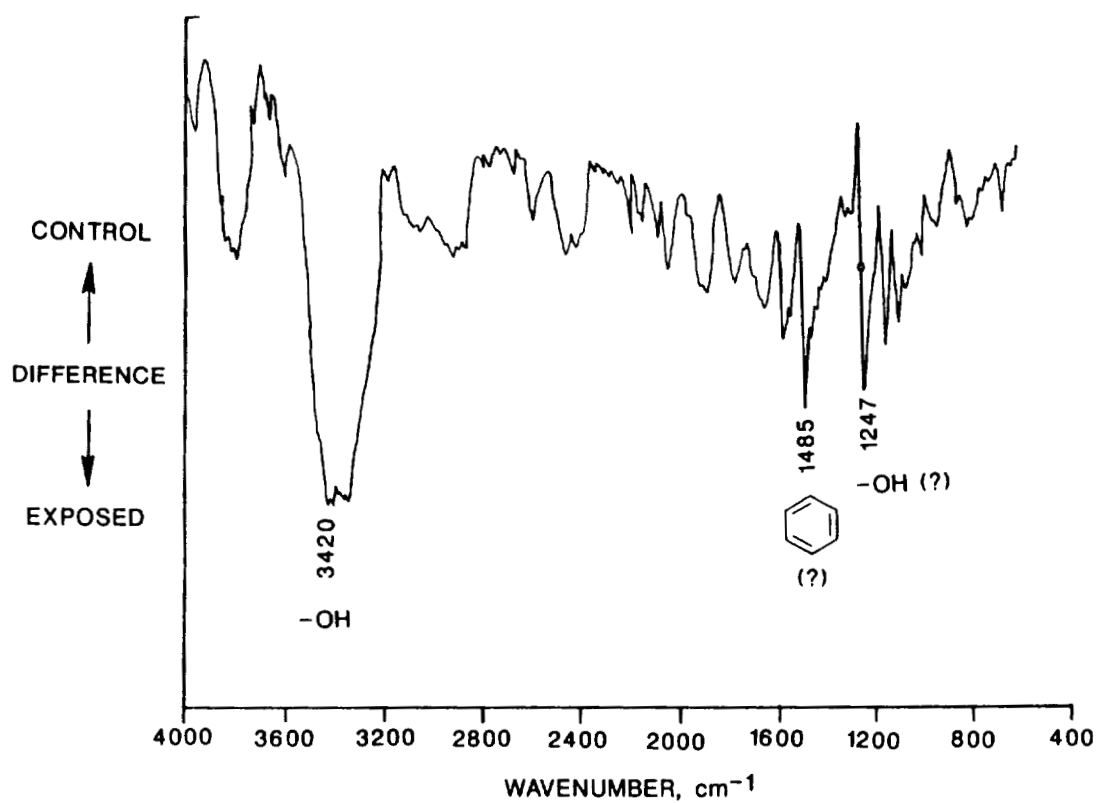


Figure 21. DR-FTIR subtraction spectrum of 10-month exposed polysulfone film.

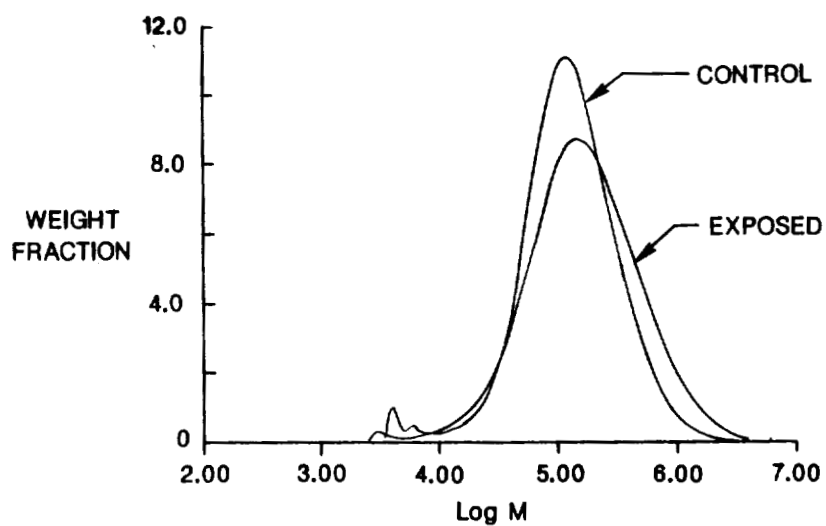
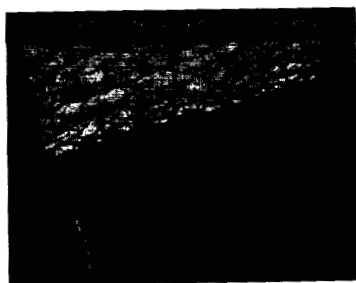
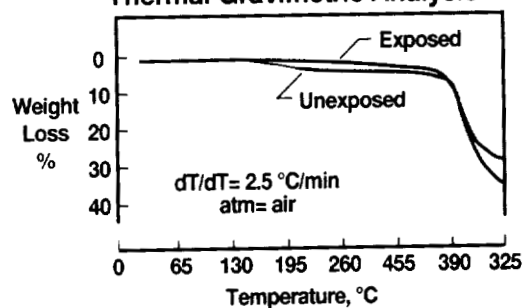


Figure 22. GPC-DV molecular weight distribution of 10-month exposed 6F-DDSO₂ film.

Scanning Electron Microscopy



Thermal Gravimetric Analysis



X-Ray Photoelectron Spectroscopy

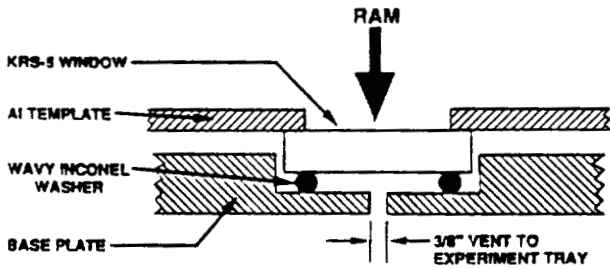
Sample		C1s	O1s	Si2p
Unexposed	¹ B.E.	285.0	532.6	102.5
	² A.C.	56.0	21.8	22.2
Exposed	B.E.	285.0	532.7	102.5
	A.C.	49.9	28.3	21.8

1. Binding Energy, eV
2. Atomic Concentration, %

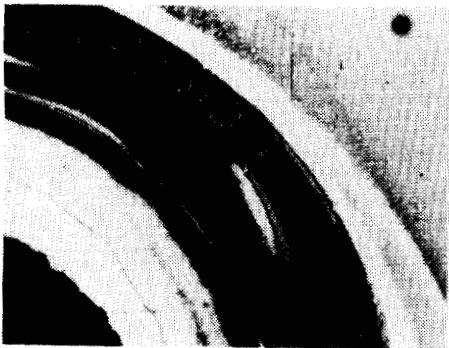
Figure 23. Characterization of RTV-511 silicone.

X-RAY PHOTOELECTRON SPECTROSCOPY

EXPERIMENT DESIGN



<u>Photo Peak</u>	<u>Binding Energy (eV)</u>	<u>Atomic Conc. (%)</u>
<u>DIRECT EXPOSURE SIDE</u>		
C 1s	284.6	15.8
O 1s	529.3/532.5	54.5
Ti 4f 7, 5	118.0/122.3	9.2
I 3d 5, 3	618.7/630.2	0.5
Si 2p	102.9	20.0
<u>NO DIRECT EXPOSURE (VENTED)</u>		
C 1s	284.6	36.1
O 1s	529.5	36.3
Ti 4f 7, 5	118.6/123.1	23.2
I 3d 5, 3	618.7/629.5	1.1
Si 2p	101.9	3.3
<u>CONTROL</u>		
C 1s	284.6/286.5	42.2
O 1s	533.0	21.7
Ti 4f 7, 5	118.3/122.7	25.8
I 3d 5, 3	619.0/630.5	10.1
Si 2p	-----	---



April 1990



November 1991

Figure 25. Photographs of micrometeoroid impact on Ag/FEP teflon thermal blanket (100X).

SURFACE CHARACTERIZATION OF LDEF
CARBON FIBER/POLYMER MATRIX COMPOSITES

Holly L. Grammer and James P. Wightman
Virginia Polytechnic Institute and State University
Department of Chemistry
Blacksburg, VA 24061
Phone: 703/231-5854, Fax: 703/231-3971

34-24
444-3
12f

Philip R. Young and Wayne S. Slemp
NASA Langley Research Center
Mail Stop 226
Hampton, VA 23665-5225
Phone: 804/864-4265, Fax: 804/864-8312

SUMMARY

XPS (x-ray photoelectron spectroscopy) and SEM (scanning electron microscopy) analysis of both carbon fiber/epoxy matrix and carbon fiber/polysulfone matrix composites revealed significant changes in the surface composition as a result of exposure to low-Earth orbit. The carbon 1s curve fit XPS analysis in conjunction with the SEM photomicrographs revealed significant erosion of the polymer matrix resins by atomic oxygen to expose the carbon fibers of the composite samples. This erosion effect on the composites was seen after 10 months in orbit and was even more obvious after 69 months.

INTRODUCTION

One of the tasks of the MSIG (Materials Special Investigation Group) is the detailed analysis of LDEF composites. Stein presented a summary of the findings of the LDEF materials studies on polymer-matrix composites and noted that atomic oxygen causes surface degradation of uncoated composites but that thin inorganic coatings prevent atomic oxygen erosion [1]. George and Hill [2] using SEM reported a similar highly eroded topography for both epoxy matrix and polysulfone matrix/carbon fiber composites due to reaction with atomic oxygen. A lack of resin on the exposed (leading edge) surfaces was determined by infrared spectroscopy. Sulfur present in the curing agent of the epoxy resin and sulfur in the polysulfone backbone was presumed to react with atomic oxygen to produce sulfate species on the exposed surfaces of both composites.

Measured decreases in the thickness of epoxy and polysulfone matrix/carbon fiber composites on the leading edge have been reported by Slemp et al. [3] in the range of 75 - 115 mm. Whitaker et al. [4] noted that the measured thickness decrease for the polysulfone matrix (110 mm) was about 50% greater than for the epoxy matrix (70 mm). It was also noted that erosion due to atomic oxygen was much greater for the matrix resin than for the carbon fibers. A detailed XPS study of poly(arylacetylene) matrix/carbon fiber composites on the leading edge has been reported by Mallon et al. [5]. The presence of inorganic silicon at 103.5 eV was noted on the exposed surface.

The objective of the present work was to document changes in the surface chemistry of composite samples taken from LDEF. Surface characterization results obtained using x-ray photoelectron spectroscopy (XPS) and scanning electron microscopy (SEM) are reported. These results

are a part of a larger study [6] where surface characterization techniques were used to examine polymer films and aluminum tray clamps taken from LDEF.

EXPERIMENTAL

Materials

An epoxy matrix composite (934/T300) and a polysulfone matrix composite (P1700/C6000) were studied. The epoxy and polysulfone matrix resins were produced by Fiberite and Union Carbide, resp. The T300 and C6000 carbon fibers were produced by Union Carbide and Celanese, resp. A control and two flight samples exposed for 10 and 69 months of each composite were studied. The flight samples were located on Tray B, Row 9 of the LDEF. The flight samples were cut from larger panels processed at the NASA - Langley Research Center using prepreg manufacturer's specifications. Control samples were cut from the same panel as the flight specimens. The control samples remained at the NASA - Langley Research Center in a low humidity environment.

Procedures

Extreme care was used when preparing the composite samples for surface characterization. Lint free nylon white gloves from Fisher Scientific Company were used to prevent sample contamination. The gloves, prior to use, were washed in solvent grade hexane, also obtained from Fisher Scientific, to remove any silicon contamination. The gloves were then subsequently washed with soap and water and allowed to dry. Scotch Magic Tape[®] was used to secure samples for XPS and SEM analysis. Preparation of the composites for XPS and SEM analysis required cutting of the samples using an Exacto-knife. Typical sample dimensions were 13 mm x 13 mm.

Analysis Techniques

XPS (x-ray photoelectron spectroscopy) analysis was performed on a Perkin-Elmer PHI 5400 spectrometer with a magnesium Ka achromatic X-ray source (1253.6 eV) operated at 15 keV and 400 watts with an emission current of 30 mA. The spectrometer was calibrated to the 4f_{7/2} photopeak of gold. Atomic concentrations were determined using PHI software, version 3.0. Curve fitting was carried out by using PHI software, version 3.0. All photopeaks were fitted with Gaussian curves. The peak positions, indicative of the type of chemical functionality present, were assigned using known literature values [7]. The various peak positions were held at a constant value and were referenced to the C1s photopeak characteristic of adventitious carbon-containing organic species taken at 285.0 eV. The full width at half maximum for the C1s photopeaks was held constant at 1.70 eV. Curve fit photopeaks contributing less than 5% to the total carbon content were neglected.

SEM (scanning electron microscopy) photomicrographs were obtained using an International Scientific Instrument ISI SX-40 scanning electron microscope operated at a beam voltage of approximately 20kV. All samples were sputtered for approximately two to three minutes with gold to reduce charging.

RESULTS/DISCUSSION

The surface analysis results for the two composites are discussed separately.

Atomic Composition

The XPS results for the surface composition of the control, 10- and 69-month flight samples are shown in Table I. Elemental photopeaks are listed in the first column followed by the binding energy (in eV) and atomic concentration (in %) for each element. Carbon, oxygen, and nitrogen are expected for an epoxy composite which has a resin-rich surface. For example, the XPS composition of a BASF epoxy composite has been determined [8] to be 67.5% carbon, 14.2% oxygen, and 2.2% nitrogen in reasonable agreement with the present results for the control sample. The organo-fluorine photopeak at 689.3eV present on the composite surface most likely resulted from the transfer of a fluorinated release agent used in the fabrication of the composite. Moyer and Wightman [9] reported a 30% organo-fluorine content on the surface of a carbon fiber/polyimide composite. It is noted that the control sample has a 1.1% silicon characteristic of inorganic silicon at 103.2eV but the source is not identified. The small amounts of sodium (2.0%) and sulfur (1.1%) are not identified although Mallon et al. [5] have reported similar concentrations of minor contaminants on carbon fiber/polymer matrix composites.

As shown in Table I, the surface composition of the 10- and 69-month samples parallels that of the control which might appear at first to be a surprising result. The O/C atomic ratios were essentially the same for the three samples. However, some significant changes were observed. The loss of organo-fluorine was obvious for the two flight samples compared to the control. It is assumed that exposure to atomic oxygen results in the formation of volatile fluorine-containing species. Silicon contamination of LDEF samples is widely reported [1]. It is only noted that the 69-month sample has the highest silicon content (6.3%) with a binding energy characteristic of inorgano-silicon. It is well established that organo-silicon compounds when subjected to atomic oxygen are converted to inorgano-silicon containing materials [5].

Curve Fit Analysis

The results of the curve fit analysis for the three samples are summarized in Table II. Significant differences are observed in the carbon 1s curve fit region for the three samples showing different contributions (percentages) as well as different types of carbon functionality under the carbon 1s envelope. Although the atomic compositions of the three samples were similar (see Table I), the types of carbon functionality for each sample are very different. These results reinforce the necessity of curve-fitting photopeaks obtained in XPS measurements. Information obtained from proper curve fitting procedures is useful and critical in describing the surface chemistry of materials.

The carbon 1s photopeak of the control sample revealed a resin rich surface. The carbon 1s photopeak (C2) corresponding to hydrocarbon functionality accounted for 55.7% of the total carbon. The carbon-oxygen functionality (peaks C3, C4 and C5) accounted for 38.0% of the total carbon.

A dramatic shift in the curve fit analysis is seen for the 10- and 69-month flight samples. In both cases, a new major photopeak (C1) appeared with a binding energy of 283.7 eV assigned to a graphitic type carbon [10]. The appearance of the graphitic type carbon is a direct result of the degradation/erosion of the epoxy matrix to expose the carbon fibers of the composite. The curve fit analysis supports the argument that significant erosion of the epoxy matrix occurred within the first ten months of exposure in low Earth orbit.

The degradation/erosion of polymer matrix composite samples flown on the LDEF, particularly on the leading edge, has been discussed previously [11]. Here, atomic oxygen reaction results in polymer bond breaking and subsequent molecular fragmentation leading to erosion of the materials.

SEM Photomicrographs

The SEM photomicrographs of the control, 10- and 69-month flight samples are shown in Figure 1. Three very different surface topographies are observed in Figure 1 and support the results obtained from the XPS curve fit analysis.

The SEM photomicrograph of the control sample (see Fig. 1A) shows an apparent resin rich surface. The weave pattern seen on this control sample is not the weave pattern of the carbon fibers within the composite but rather the impression left from the scrim cloth used in the consolidation of the composite.

The SEM photomicrograph of the 10-month flight sample (see Fig. 1B) suggests some erosion of the matrix resin. The curve fit analysis of the 10-month flight sample showed carbon functionality that is consistent with the presence of both resin and carbon fiber. Photopeaks C2 - C5 for the 10-month flight sample are attributed to the resin since these photopeaks were also observed in the control sample. However, photopeaks C3-C5 have been reported for carbon fibers [12]. On the other hand, photopeak C1 is uniquely assigned to the carbon fibers. This significant photopeak, accounting for 46% of the total carbon signal, was absent in the control sample.

The SEM photomicrograph of the 69-month flight sample (see Fig. 1C) shows significant continued erosion of the matrix resin. The 69-month flight sample exhibits similar topography as reported previously for composite samples from the LDEF [2]. The carbon 1s curve fit analysis for the 69-month flight sample again suggests that the surface composition results from a combination of both resin and carbon fibers. However, the contribution of the C1 photopeak would suggest the composition is predominantly due to carbon fibers. The SEM photomicrographs are consistent then with the XPS curve fit analysis for the control, 10- and 69-month flight samples.

The SEM photomicrographs and the curve fit analysis support the degradation/erosion of the epoxy matrix within the first 10 months of the mission as well as further degradation for the remaining 59 months. Tennyson [13] reported that an atomic oxygen fluence of 1.33×10^{21} atoms/cm² on Row 12 was sufficient to erode the epoxy layer and a portion of the reinforcing graphite fibers. The epoxy samples discussed in the present study were located on the leading edge (Row 9) of the LDEF where the atomic oxygen fluence was 8.99×10^{21} atoms/cm². Thus, the higher atomic oxygen fluence for Row 9 would facilitate the degradation/erosion of the matrix to expose the carbon fibers as seen in Figure 1.

P1700/C6000 Polysulfone Composite

Atomic Composition

The XPS results for the surface composition of the control, 10- and 69-month flight samples are shown in Table III. Carbon, oxygen, and sulfur are expected for a polysulfone composite which has a resin-rich surface. For example, the XPS composition of a polysulfone film has been determined [14] to be 82% carbon, 15% oxygen, and 3.0% sulfur. Although the concentrations of carbon and sulfur are in good agreement, the sulfur concentration for the composite sample is considerably lower than expected. The organo-fluorine photopeak at 688.9 eV present on the control composite surface most likely resulted from the transfer of a fluorinated release agent used in the fabrication of the composite. This is similar to the concentration of organo-fluorine noted and discussed above for the control epoxy composite.

The control sample has a 1.2 atomic % silicon characteristic of organo-silicon at 102.4 eV but the source is not identified. The sources of the small amounts of aluminum (1.6%) and calcium (1.3%) are

also not identified. George and coworkers [11] have reported similar concentrations of minor contaminants on P1700 polysulfone/T300 composites.

As shown in Table III, the oxygen content of the 10- and 69-month samples differs significantly from that of the control sample. The O/C atomic concentration ratio increases from 0.19 (control) to 0.36 (10 month) to 2.08 (69 months) in sharp contrast to the constancy of the same ratio for the epoxy composite. George et al. [11] have also reported a trend of decreasing carbon content and increasing oxygen content for flight composite samples compared to control composite samples. The loss of organo-fluorine was obvious for the two flight samples compared to the control as was the case for the epoxy composites.

It is noted that the 69-month sample again has the highest silicon content (17.3%) with a binding energy at 103.7 eV characteristic of inorgano-silicon. A similar result was observed on the 69-month epoxy composite. George et al.[11] also reported an increase in silicon content for the flight samples. A possible SiO_x non-volatile contamination layer on the 69-month flight sample is consistent with the observed increase in the oxygen and silicon contents as well as the shift in the binding energy of the silicon 2p photopeak.

Sulfur is noted on the two flight samples at a higher concentration than for the control and closer to the value of 3.0% expected for neat polysulfone. However, the binding energy increased from 167.9 eV (organo-sulfur) for the control to 169.75 eV (inorgano-sulfur) for the two flight samples. The conversion of organo-sulfur to inorgano-sulfur in the presence of atomic oxygen has been documented [2]. The sources of the small amounts of aluminum (1.9%), calcium (0.1%), and sodium (0.8%) are not identified.

The appearance of nitrogen in both the 10-month and 69-month samples and its absence in the control sample may be due to uncovering of the PAN-based carbon fibers following matrix erosion by atomic oxygen. The nitrogen content of PAN-based T300 carbon fibers as determined by XPS has been reported [15] as 2.1% in fair agreement with the value of 1.1% observed in the present work.

Curve Fit Analysis

The carbon 1s curve fit analysis of the control and two flight samples is shown in Table IV. The curve fit analysis of the control sample again revealed a resin rich surface. Hydrocarbon functionality corresponds to 91% of the total photopeak area. The remaining area corresponds primarily to carbon-oxygen functionality.

The curve fit analysis of the 10-month flight sample showed a three-fold decrease in the hydrocarbon functionality and a two-fold increase in the carbon-oxygen functionality. The appearance of the C1 photopeak at 283.5 eV is taken as supporting evidence the carbon fibers were uncovered as the polysulfone matrix resin was eroded by reaction with atomic oxygen. This is the same striking result as was obtained for the epoxy composite.

The curve fit analysis for the 69-month polysulfone composite shows some difference from the epoxy composite. Carbon-oxygen functionality accounted for 50% of the total carbon content for the polysulfone composite compared to only 9% for the epoxy composite. No definitive conclusion is drawn from this result.

ACKNOWLEDGEMENTS

The authors (H. L. G. and J. P. W.) acknowledge the support of this research under NASA Grant NAG-1-1186.

REFERENCES

- [1] Stein, B. A.: LDEF Materials Overview. In LDEF -69 Months in Space, NASA Conference Publication 3194 (Arlene S. Levine, editor), Part 3, 1992, p. 741.
- [2] George, P. E. and Hill, S. G.: Results from Analysis of Boeing Composite Specimens Flown on LDEF Experiment M0003. In LDEF -69 Months in Space, NASA Conference Publication 3134 (Arlene S. Levine, editor), Part 2, 1991, p.1115.
- [3] Slemp, W. S.; Young, P. R.; Witte, jr., W. G. and Shen, J. Y.: Effects of LDEF Flight Exposure on Selected Polymer Matrix Resin Composite Materials. In LDEF -69 Months in Space, NASA Conference Publication 3134 (Arlene S. Levine, editor), Part 2, 1991, p.1149.
- [4] A. F. Whitaker, A. F.; R. R. Kamenetzky, R. R.; M. M. Finckenor, M. M.; and J. K. Norwood, J. K.: Atomic Oxygen Effects on LDEF Experiment A0171. In LDEF -69 Months in Space, NASA Conference Publication 3194 (Arlene S. Levine, editor), Part 3, 1992, p.1125.
- [5] J. J. Mallon, J. J.; J. C. Uht, J. C. and C. S. Hemminger, C. S.: Surface Analysis of Composites Exposed to the Space Environment on LDEF. In LDEF -69 Months in Space, NASA Conference Publication 3194 (Arlene S. Levine, editor), Part 3, 1992, p.963.
- [6] Grammer, H. L.: Surface Characterization of LDEF Materials. M. S. Thesis, Virginia Polytechnic Institute and State University, Blacksburg, VA, 1993.
- [7] High Resolution XPS of Organic Polymers, G. Beamson and D. Briggs, ed., p.277, John Wiley & Sons, Chichester (1992).
- [8] Chin, J. W. and Wightman, J. P.: Surface Pretreatment and Adhesive Bonding of Carbon Fiber-Reinforced Epoxy Composites. In Composition Bonding ASTM STP 1227, D. J. Damico, J. M. Prandy and S. L. F. Niks, Eds., Am. Soc. Testing & Materials, Philadelphia, PA, in press.
- [9] Moyer, D. J. D. and Wightman, J. P.: Characterization of Surface Pretreatments of Carbon Fiber-Polyimide Matrix Composites. Surface & Interface Analysis, **14**, 496-504 (1989).
- [10] Handbook of X-ray Photoelectron Spectroscopy, G. E. Muilenberg, ed., p. 38, Perkin-Elmer Corp., Eden Prarie, MN (1979).
- [11] George, P. E., Dursch, H. W. and Hill, S. G.: Space Environmental Effects on LDEF Composites: A Leading Edge Coated Graphite Epoxy Panel. In LDEF -69 Months in Space, NASA Conference Publication 3194 (Arlene S. Levine, editor), Part 3, 1992, p.923.
- [12] Commercon, P. and Wightman, J. P. : Surface Characterization of Plasma Treated Carbon Fibers and Adhesion to a Thermoplastic Polymer. J. Adhesion, **38**, 55 (1992).

[13] Tennyson, R. C.: Additional Results on Space Environmental Effects on Polymer Matrix Composites - Experiment A0180. In LDEF Materials Workshop '91, NASA Conference Publication 3162, (Bland A. Stein and Philip R. Young, compilers), Part 2, 1992, p. 593.

[14] Hollenhead, J. B. and Wightman, J. P.: The Adhesive Bonding of Steel with Polysulfone. J. Adhesion, 37, 121 (1992).

[15] DeVilbiss, T. A.: Carbon Fiber Surface Treatments for Improved Adhesion to Thermoplastic Polymers. Ph.D. Dissertation, Virginia Polytechnic Institute and State University, Blacksburg, VA, 1987.

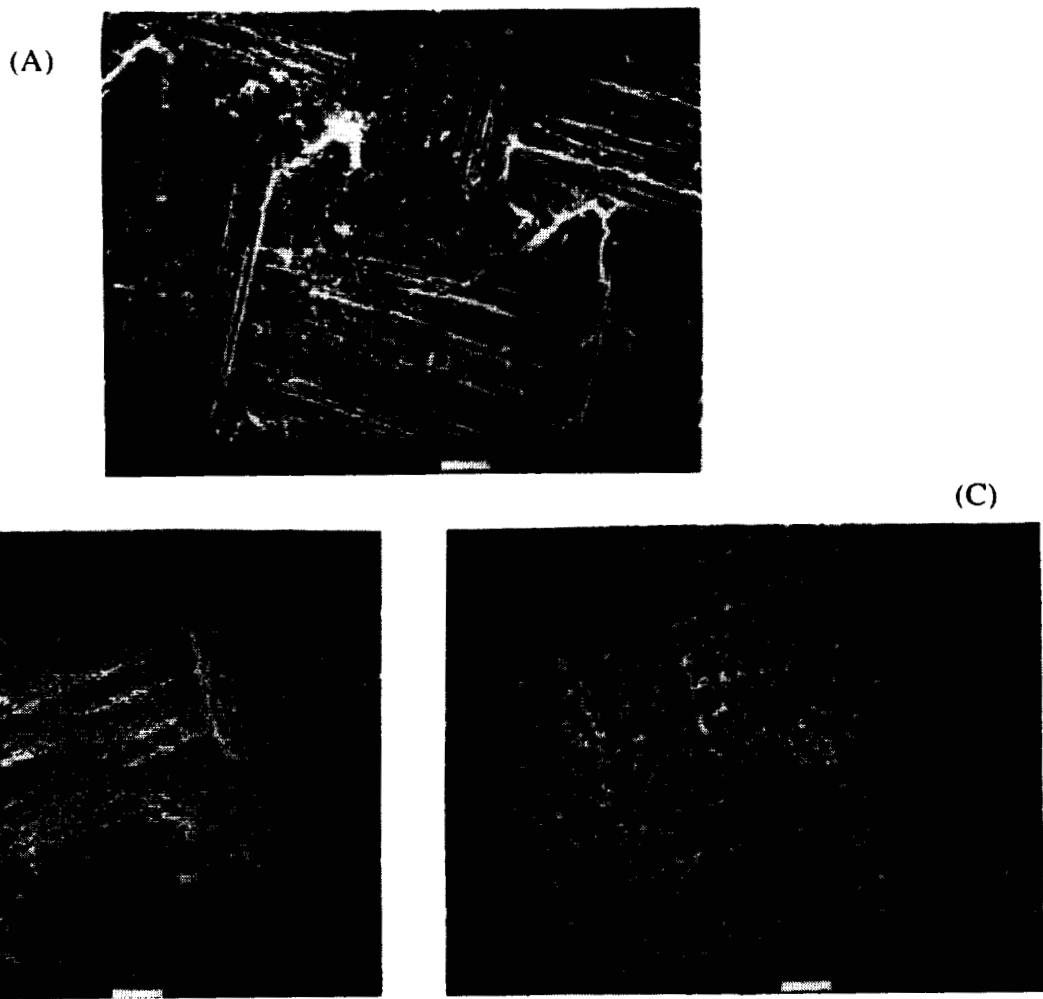


FIGURE 1: SEM PHOTOMICROGRAPHS OF 934/T300 EPOXY COMPOSITE SAMPLES

(A) CONTROL (B) 10 MONTH (C) 69 MONTH.

TABLE I: XPS ANALYSIS OF 934/T300 EPOXY COMPOSITES

CONTROL

<u>PHOTOPEAK</u>	<u>BINDING ENERGY(eV)</u>	<u>ATOMIC CONC(%)</u>
C 1s	285.0	68.8
O 1s	532.6	18.1
N 1s	399.9	3.4
F 1s	689.3	5.5
Si 2p	103.2	1.1
Na 1s	1072.2	2.0
S 2p	168.4	1.1

10 MONTH

<u>PHOTOPEAK</u>	<u>BINDING ENERGY(eV)</u>	<u>ATOMIC CONC(%)</u>
C 1s	285.0	73.3
O 1s	531.9	18.7
N 1s	399.6	5.5
F 1s	688.2	0.2
Si 2p	103.7	0.8
Na 1s	1071.9	0.5
S 2p	168.4	0.8

69 MONTH

<u>PHOTOPEAK</u>	<u>BINDING ENERGY(eV)</u>	<u>ATOMIC CONC(%)</u>
C 1s	285.0	72.0
O 1s	533.3	19.6
N 1s	400.6	0.8
F 1s	nsp*	--
Si 2p	104.0	6.3
Na 1s	nsp	--
S 2p	170.0	0.8

*nsp-no significant peak

TABLE II: CARBON 1s CURVE FIT ANALYSIS OF 934/T300 EPOXY COMPOSITES

CONTROL

<u>PHOTOPEAK</u>	<u>BINDING ENERGY(eV)</u>	<u>% AREA</u>	<u>CARBON TYPE</u>
C2	285.0	55.7	<u>C</u> -H
C3	286.3	25.0	<u>C</u> -O
C4	287.8	7.8	<u>C</u> =O
C5	289.4	5.2	O- <u>C</u> =O

10 MONTH

<u>PHOTOPEAK</u>	<u>BINDING ENERGY(eV)</u>	<u>% AREA</u>	<u>CARBON TYPE</u>
C1	283.6	46.4	graphitic
C2	285.0	30.8	<u>C</u> -H
C3	286.6	11.8	<u>C</u> -O
C4	288.1	7.3	<u>C</u> =O

69 MONTH

<u>PHOTOPEAK</u>	<u>BINDING ENERGY(eV)</u>	<u>% AREA</u>	<u>CARBON TYPE</u>
C1	283.9	49.8	graphitic
C2	285.0	38.9	<u>C</u> -H
C3	286.4	8.6	<u>C</u> -O

TABLE III: XPS ANALYSIS OF P1700/C6000 POLYSULFONE COMPOSITES

CONTROL

<u>PHOTOPEAK</u>	<u>BINDING ENERGY(eV)</u>	<u>ATOMIC CONC(%)</u>
C 1s	285.0	76.9
O 1s	532.1	14.5
S 2p	167.9	0.4
F 1s	688.9	4.1
Al 2p	74.7	1.6
Ca 2p	347.6, 351.1	1.3
Si 2p	102.4	1.2

10 MONTH

<u>PHOTOPEAK</u>	<u>BINDING ENERGY(eV)</u>	<u>ATOMIC CONC(%)</u>
C 1s	285.0	67.0
O 1s	531.2	24.5
S 2p	168.4	2.4
Si 2p	102.0	2.3
Al 2p	73.8	1.9
Na 1s	1071.3	0.8
N 1s	398.2	1.1

69 MONTH

<u>PHOTOPEAK</u>	<u>BINDING ENERGY(eV)</u>	<u>ATOMIC CONC(%)</u>
C 1s	285.0	25.0
O 1s	533.1	51.9
S 2p	169.6	2.9
Si 1s	103.7	17.3
N 1s	400.6	1.2
Ca 2p	348.5, 352.0	0.1

TABLE IV: CARBON 1s CURVE FIT ANALYSIS OF P1700/C6000
POLYSULFONE COMPOSITES

CONTROL

<u>PHOTOPEAK</u>	<u>BINDING ENERGY(eV)</u>	<u>% AREA</u>	<u>CARBON TYPE</u>
C 2	285.0	90.8	<u>C</u> -H
C 3	288.9	2.8	O- <u>C</u> =O

10 MONTH

<u>PHOTOPEAK</u>	<u>BINDING ENERGY(eV)</u>	<u>% AREA</u>	<u>CARBON TYPE</u>
C 1	283.5	53.3	graphitic
C 2	285.0	27.1	<u>C</u> -H
C 3	286.1	12.2	<u>C</u> -O

69 MONTH

<u>PHOTOPEAK</u>	<u>BINDING ENERGY(eV)</u>	<u>ATOMIC CONC(%)</u>	<u>CARBON TYPE</u>
C 1	283.6	22.4	graphitic
C 2	285.0	18.6	<u>C</u> -H
C 3	286.6	33.3	<u>C</u> -O
C 4	288.0	12.4	<u>C</u> =O
C 5	289.5	4.7	O- <u>C</u> =O

SPACE ENVIRONMENTAL EFFECTS ON POLYMER MATRIX COMPOSITES AS A
FUNCTION OF SAMPLE LOCATION ON LDEF

R. C. Tennyson and G. R. Cool
University of Toronto Institute for Aerospace Studies
North York, Ontario, Canada, M3H 5T6

D. G. Zimcik
Canadian Space Agency, Space Mechanics Directorate
Ottawa, Ontario, Canada, K2H 8S2

SUMMARY

This paper presents results on the effect of circumferential location on the variation in solar absorptance (α_s) and infrared emittance (ϵ) for five different polymer matrix composites (PMC), and variations in erosion depth due to atomic oxygen (AO) for fourteen different PMC materials. In addition, a chemical content design parameter (γ) has been found that correlates well with the erosion yield obtained from space flight data and hyperthermal AO tests for hydrocarbon polymeric materials. This parameter defines the ratio of the total number of atoms in a repeat monomer unit to the difference between the total carbon content and the total number of intermolecular oxygen atoms in the same repeat unit.

INTRODUCTION

The purpose of this report is to present a survey of the polymer matrix composite materials that were flown on LDEF with particular attention to the effect of circumferential location (θ) on the measured degradation and selected property changes (see Fig. 1). Specifically, it is known that atomic oxygen fluence (AO), VUV radiation dose and number of impacts by micrometeoroids/debris vary with θ . Thus it should be possible to assess material degradation and property changes with θ for those materials that are common to three or more locations. Once the θ -dependence functions have been defined, other material sample data from any location can then be used to predict damage and property changes as a function of θ as well.

Table 1 summarizes the polymer matrix composite samples analysed at UTIAS. It can be seen that they were distributed over seven circumferential locations around LDEF. Also shown is the variation in atomic oxygen fluence (atoms/cm²) and the total VUV radiation exposure at each location, measured in *equivalent sun hours* (ESH). It should be noted that one material (934/T300) was present at seven of the locations.

The properties that were measured include the solar absorptance (α_s), the infrared emittance (ϵ) and the erosion depth. Tables 2a, 2b and 2c summarize all the data obtained from these samples.

SOLAR ABSORPTANCE (α_s) AND INFRARED EMITTANCE (ϵ)

Measurement Procedures

Absorptance and emittance measurements were carried out on all samples received. Absorptance measurements were performed using a Beckman DK-2A integrating sphere ratio recording spectrophotometer with a magnesium oxide reference. Solar absorptance is calculated from the relative absorptance spectrum, according to ASTM E 424 and ASTM E 903, across the range of 250 to 2400 nm. IR emittance was measured using a Gier-Dunkle DB100 infrared reflectometer with appropriate calibrating standards and in accordance with ASTM E 408.

Experimental Results

Tables 3 and 4 present the solar absorptance (α_s) and emittance data (ϵ) for the materials investigated, including the differences found between the exposed and unexposed faces. A plot of the solar absorptance change (%) in Fig. 2 shows a maximum increase at or near the ram direction on all samples, coincident with maximum AO and UV degradation on the ram side. As θ increases, the absorptance quickly drops to values which are less than the back face reference values, well before $\theta = 90^\circ$. It was expected that α would only decrease to some value slightly higher than the "control" at or near 90° , since thermal AO and UV radiation degrades surfaces, to some extent, at all locations around the satellite. This unexpected result indicates that some other mechanism must be altering the surface characteristics, one that is not related to AO or UV surface degradation.

Contamination of the surface by vacuum-condensable silicone-based molecular compounds has been measured all over LDEF (ref. 1). The presence of this material on the surface would be consistent with a reduction in α for a high α material such as a graphite fibre composite. The contaminant tends to be light brown or tan in colour.

It is likely that, for these black graphite-based PMC's, the AO flux dropped low enough for contamination to build up between 60° and 80° . At angles less than 60° , the AO flux was high enough to remove the molecular contamination as it formed. At angles greater than approximately 80° , the flux was too low to remove all of the contaminant as it formed on the surface. Visual examination, IR and EDX spectra are inconclusive as to the presence of any uniform contamination on these rough sample surfaces. The contamination is clearly visible on aluminum portions of the trays and end fittings near the samples. Other work, specifically on contamination, has shown the brownish contamination at these higher θ angles (ref. 2).

A related effect can be seen in the emittance vs θ plot of Fig. 3. As expected, there is an increase in emittance of the samples subjected to ram AO and UV radiation. At higher θ 's, emittance decreases to values below the control (i.e., back face value). At the highest θ angles, however, emittance returns to the control value. The initial decrease in emittance appears to occur in the same range as the absorptance decrease, which means that the same AO erosion/contamination mechanism should apply. The return to control values at the highest θ angles indicates that the increase in UV irradiation on the trailing edge may be increasing the emittance of the samples. These results can be compared to α measurements for Al clamps and FEP/Ag from other experiments. Emittance effects are not as clear since the changes were quite small (refs. 3, 4).

Measurements made on FEP/Ag samples from the UHCRE (Ultra-Heavy Cosmic Ray Nuclei Experiment) show the same pattern of increase in absorptance at the leading edge, a decrease below the control value, but with a rapid increase on the trailing sides [3]. Here UV degradation dominates, increasing α at the leading and trailing edges while contamination probably lowers the absorptance below the control, around 90° .

Boeing's chromic acid anodized aluminum clamp measurements show the same basic effect [4]. In this case, absorptance decreases at high AO/UV flux levels, while the brown contamination increases absorptance. Again, contamination forces the α change beyond the control value. The transition from AO/UV effect to contamination effect occurs at 90° this time.

ATOMIC OXYGEN EROSION

The atomic oxygen fluence as a function of angular location around LDEF is summarized in Table 1. Although most of the angular variation can be described by a simple 'cosine' function, it is known that because of the random thermal motion associated with the AO, some exposure occurs well beyond the 90° position (ref. 5).

Summaries of the erosion depth measurements for the materials investigated at UTIAS, together with published data, are presented in Tables 5a and 5b, respectively. Cross-sectional SEM measurements were made at UTIAS to obtain the erosion loss. A plot of this data as a function of θ is given in Fig. 4. SEM micrographs illustrating the differences in erosion morphologies are given in Figs. 5 and 6 for 934/T300 graphite/epoxy samples located at 8° and 82° , respectively.

Cross-sectional SEM micrographs are shown in Figs. 7 and 8. Of special interest are the erosion depth profiles (when compared to the unexposed regions shown) and the relatively large surface 'pits,' probably caused by microparticle impacts.

In Fig. 9, it can be seen that a $\cos^{1.5}\theta$ function fits the 934/T300 erosion data rather well, except in the range of $\theta = 82^\circ$. Erosion is much larger than expected at this angle location. It has been previously noted that "significant differences" at high angles on FEP/Ag have also been measured (ref. 6). It is likely that surface morphology has an important effect by trapping incoming AO and increasing the probability of surface interaction. Large increases in interaction probability have been demonstrated as undercutting effects by Banks et al (ref. 7).

One can calculate the erosion yield as a function of angular location, $Y(\theta)$, from the relation $Y(\theta) = \frac{\text{erosion depth}}{\text{AO fluence}}$ (cm^3/atom). A summary of these values is given in Tables 5a and 5b. For design purposes, it is more convenient to work with the "normal" erosion yield parameter (Y_n), i.e., the value of Y that one would measure for a material whose plane was normal to the incident AO flux, $Y_n = Y(\theta)/\cos^m\theta$.

Tables 5a and 5b present the values of Y_n for $m = 0.5$. It is clear from Table 5a for the $\theta = 82^\circ$ data, that Y_n is far too high for epoxy-based composites. Since half of the erosion depth recorded at $\theta = 82^\circ$ was accounted for by an outer epoxy layer, one would indeed expect an erosion yield to be higher than that for the bulk graphite/epoxy material, but not as high as the values shown. Using a value of $m = 0.2$ gave Y_n results much lower at $\theta = 82^\circ$, although not significantly lower for the smaller values of θ

(see Table 5a and Fig. 9). Included in Fig. 10 is a correction factor for the effect of a 10 μ epoxy layer (as measured from the UTIAS samples located at $\theta = 82^\circ$).

A plot of the normal erosion yield values (Y_n) based on $m = 0.2$ is presented in Fig. 10. It is clear that for $0 < \theta \leq 70^\circ$ essentially constant yield values are obtained, independent of angular location θ because of the larger erosion losses that occurred. For these samples, one is essentially measuring a bulk property not significantly affected by the outer epoxy layer. However, for smaller erosion depths, a larger value for Y_n is obtained, consistent with the effect of the epoxy layer.

An estimate of the total erosion loss (h) for a polymer matrix composite laminate oriented at an angle θ to an incident normal AO flux (ϕ_n) for a given time 't' is given by

$h(\theta, t) = Y_{nc}\phi_n t(\cos \theta)^{1+m} + h_r \left(1 - \frac{Y_{nc}}{Y_{nr}}\right)$, where Y_{nc} , Y_{nr} are the normal erosion yields for the bulk composite and outer resin layer (of thickness h_r), respectively.

THE ROLE OF CHEMICAL CONTENT ON THE EROSION OF HYDROCARBON POLYMERS

A study was conducted to establish a relationship between the atomic oxygen erosion rate of hydrocarbon-based polymers and their chemical content and structure. Based on a comprehensive analysis of erosion data for a large number of samples exposed to the low Earth orbit (LEO) space environment and to simulated LEO environment conditions in ground-based hyperthermal facilities, an excellent linear correlation exists between the AO erosion rate and a structural parameter γ defined as the ratio of total number of atoms in a repeat monomer unit to the difference between the total carbon content and the total number of intermolecular oxygen in the same repeat unit, i.e., the relative content of effective carbon atoms in it (Fig. 11). The structural parameter γ actually represents the chemical content of the material, or the relative content of "effective carbon atoms." It would appear that the removal of these "effective carbon atoms" by oxidation is the limiting step for erosion by fast atomic oxygen. Figure 12 provides examples of three polymer materials and the calculation of γ .

CONCLUSIONS

1. Increases in solar absorptance and infrared emittance relative to control values have been measured as high as +12% and +18%, respectively in the ram direction. Absorptance decreased to slightly below the "control" value around $\theta \approx 60^\circ$, whereas the emittance decrease was as great as -12% in the range of $60 < \theta < 120^\circ$, rising again to the nominal "control" value for $160 \leq \theta \leq 180^\circ$.
2. The erosion loss has been found to vary around the circumference as $\cos^{0.5}\theta$ over much of the range of θ . However, at large θ values (i.e., $\theta > 70^\circ$), a better approximation is given by $\cos^{0.2}\theta$. Incorporating the effect of the outer epoxy layer yields a better estimate of erosion. Enhanced erosion at large θ angles is postulated to occur because of AO trapping resulting from the surface morphology and the increased reaction probability.
3. The average bulk normal erosion yield (Y_{nc}) for the fourteen different composite materials is $\sim 1 \times 10^{-24}$ cm³/atom based on a $\cos^{0.2}\theta$ relation (neglecting the 82° epoxy-dominated data and the

three questionable values in Tables 5a and 5b). The range of values measured for these various materials is given by $0.76 \leq Y_{nc} \leq 1.2 \times 10^{-24} \text{ cm}^3/\text{atom}$.

4. The erosion yield for hydrocarbon-based polymers exposed to hyperthermal atomic oxygen has been found to vary linearly with a chemical structure/content parameter γ . This functional relationship is useful for designing new materials in terms of their resistance to AO.

ACKNOWLEDGEMENT

The analysis of LDEF data and research results presented in this report were financed by the Space Mechanics Directorate of the Canadian Space Agency, under Contract No. 025SR.9 F009-1-1435, FC 5305-001-65 301-201-1400. Special thanks are given to Dr. D. G. Zimcik, Space Mechanics Directorate, Canadian Space Agency, for his support of this program. The authors also wish to recognize the efforts of Mr. G. Manuelpillai and Dr. W. D. Morison for their contributions to this research project. We all extend our thanks to the many LDEF investigators and their organizations who supplied us with LDEF samples for analysis. They include: Mr. Christopher Blair, Lockheed Missiles and Space Co.; Dr. David K. Felbeck, University of Michigan; Mr. Pete E. George and Mr. Harry Dursch, Boeing Defense and Space Group; Mr. Dick Vyhnaal, Rockwell International; Mr. Thomas Cookson, General Dynamics Space Systems; and Mr. Charles A. Smith, McDonnell Douglas.

The study of the erosion of hydrocarbon polymers and the development of the $Y_n(\gamma)$ graph was done in collaboration with Dr. Z. Iskanderova (UTIAS), Dr. Y. I. Gudimenko (Academy of Sciences, Institute of Physical Organic Chemistry, Minsk, Belarus), and Dr. J. Kleiman (UTIAS).

REFERENCES

1. G. A. Harvey, "Organic Contamination of LDEF," LDEF-69 Months in Space, Part 1, NASA Conference Publication 3134, June 1991, 179.
2. E. R. Crucher and K. J. Warner, "Molecular Films Associated with LDEF," LDEF — 69 Months in Space, Part 1, NASA Conference Publication 3134, June 1991, 155.
3. F. Levadou et al, "Preliminary Investigations into UHCRE Thermal Control Materials," LDEF — 69 Months in Space, Part 2, NASA Conference Publication 3134, June 1991, 875.
4. W. L. Plagemann, "Space Environmental Effects on the Integrity of Chromic Acid Anodized Coatings," LDEF — 69 Months in Space, Part 2, NASA Conference Publication 3134, June 1991, 1023.
5. R. J. Bourassa, J. R. Gillis, "LDEF Atomic Oxygen Flux and Fluence Calculations," NASA LDEF MSIG Report NAS1-18224, Task 12, January 1991.
6. B. A. Banks et al, "Atomic Oxygen Interactions with FEP Teflon and Silicones on LDEF," LDEF — 69 Months in Space, Part 2, NASA Conference Publication 3134, June 1991, 801.

7. B. A. Banks, S. K. Rutledge, B. M. Auer and F. Di Filippo, "Atomic Oxygen Undercutting of Defects on SiO₂ Protected Polyimide Solar Array Blankets," Proc. Materials Degradation in Low Earth Orbit, The Minerals, Metals and Materials Society, 1990, 15.
8. P. E. George and S. G. Hill, "Results from Analysis of Boeing Composite Specimens Flown on LDEF Experiment M0003," LDEF-69 Months in Space, First Post-Retrieval Symposium, June 2-8, 1991, NASA CP-3134, Part 2, p. 1115.
9. G. L. Steckel and T. D. Le, "M0003-10: LDEF Advanced Composites Experiment," LDEF — 69 Months in Space, First Post-Retrieval Symposium, June 2-8, 1991, NASA CP-3134, Part 2, p. 1041.
10. W. S. Slempp, P. R. Young, G. W. Witte Jr., and J. Y. Shen, "Effects of LDEF Flight Exposure on Selected Polymer Matrix Resin Composite Materials," LDEF — 69 Months in Space, First Post-Retrieval Symposium, June 2-8, 1991, NASA CP-3134, Part 2, p. 1149.
11. A. F. Whitaker and L. E. Young, "An Overview of the First Results on the Solar Array Materials Passive LDEF Experiment (SAMPLE), AO171," LDEF — 69 Months in Space, First Post-Retrieval Symposium, June 2-8, 1991, NASA CP-3134, Part 3, p. 1241.

Table 1
Samples Collected - θ Project

Material	Row	Angle	AO Fluence (atom/cm ³)	UV Dose (ESH)	Laminate	#	
P1700/T300	3	172	1.32x10 ¹⁷	11100	(0°,90°) ₄	1	Boeing
CE339/GY70					(0°) ₂ ,(90°) ₂	1	Lockheed
934/T300					0°	1	Boeing
PES-C/T300						1	M. Doug.
P1700/T300	4	158	2.31x10 ⁵	10400	(0°,90°) ₄	1	Boeing
F593/P75					(0°) ₁₆	1	Lockheed
934/T300					0°	1	Boeing
934/T300	1	112	2.92x10 ¹⁷	7500	Honeycomb	1	Rockwell
934/T300					(45°,0°) ₈ ,45°	1	Rockwell
934/T300	12	82	1.33x10 ²¹	6900	(0°) ₄	1	UTIAS
5208/T300					(±45°) ₂	1	UTIAS
5208/T300					(±20°) ₄	1	U of Mich
PMR15/C6000	7	68	3.28x10 ²¹	7200	(0°,±45°,90°) ₂	1	Rockwell
F593/P75	8	38	6.93x10 ²¹	9400	(0°) ₁₆	4	Lockheed
PS-C/T300						1	M. Doug.
PES-C/T300						1	M. Doug.
CE339/GY70						2	Gen. Dyn.
934/T300						2	Gen. Dyn
934/T300					0°	1	Boeing
P1700/T300	9	8	8.99x10 ²¹	11100	(0°,90°) ₄	1	Boeing
CE339/GY70					(0°) ₂ ,(90°) ₂	1	Lockheed
934/T300					0°	1	Boeing

Table 2a

UTIAS Samples

Measured Values

Material	Row	Angle	AO Fluence (atoms/cm ²)	UV Dose (ESH)	#	Solar Absorpt.		IR Emit.		AO Erosion Depth (microns)	Matrix * Microcracking
						- Front -	- Back -	- Front -	- Back -		
934/T300	12	82	1.33E+21	6900	1	0.814	0.830	0.703	0.796	21.5	None Observed
5208/T300	12	82	1.33E+21	6900	1	0.872	0.883	0.706	0.804	17.7	None Observed

* Does not include manufacturing process induced cracking

Lockheed Samples

Measured Values

Material	Row	Angle	AO Fluence (atoms/cm ²)	UV Dose (ESH)	#	Solar Absorpt.		IR Emit.		AO Erosion Depth (microns)	Matrix * Microcracking
						- Front -	- Back -	- Front -	- Back -		
CE339/GY70	9	8	8.99E+21	11100	1	0.985	0.881	0.918	0.805	65.4	None Observed
CE339/GY70	3	172	1.32E+17	11100	1	0.857	0.884	0.800	0.787	None	None Observed
F593/P75	8	38	6.93E+21	9400	4	Not Used Yet - Preserved for CTE/Outgas Testing					
F593/P75	4	158	2.31E+05	10400	1						

Rockwell Samples

Measured Values

Material	Row	Angle	AO Fluence (atoms/cm ²)	UV Dose (ESH)	#	Solar Absorpt.		IR Emit.		AO Erosion Depth (microns)	Matrix * Microcracking
						- Front -	- Back -	- Front -	- Back -		
934/T300	1	112	2.92E+17	7500	1	0.886	0.896	0.790	0.870	None	None Observed
934/T300	1	112	2.92E+17	7500	1	Composite in honeycomb, not used for these properties					
PMR15/C6000	.7	68	3.28E+21	7200	1						

Table 2b

Boeing Samples

Measured Values

Material	Row	Angle	AO Fluence (atoms/cm ²)	UV Dose (ESH)	#	Solar Absorpt.		IR Emit.		AO Erosion Depth (microns)	Matrix * Microcracking
						- Front -	- Back -	- Front -	- Back -		
934/T300	9	8	8.99E+21	11200	1	0.943	0.835	0.943	0.835	NA	N/A **
934/T300	8	38	6.93E+21	9400	1	0.886	0.832	0.886	0.832	NA	N/A
934/T300	3	172	1.32E+17	11100	1	0.769	0.804	0.769	0.804	None	N/A
934/T300	4	158	2.31E+05	10500	1	0.832	0.819	0.832	0.819	None	N/A
P1700/T300	9	8	8.99E+21	11200	1	0.983	0.895	0.983	0.895	NA	N/A
P1700/T300	3	172	1.32E+17	11100	1	0.871	0.889	0.871	0.889	None	N/A
P1700/T300	4	158	2.31E+05	10500	1	0.873	0.881	0.873	0.881	None	N/A

** samples mechanically tested previous to cross-sectioning

U of Mich. Sample

Measured Values

Material	Row	Angle	AO Fluence (atoms/cm ²)	UV Dose (ESH)	#	Solar Absorpt.		IR Emit.		AO Erosion Depth (microns)	Matrix * Microcracking
						- Front -	- Back -	- Front -	- Back -		
5208/T300	12	82	1.33E+21	6800	1	0.857	0.859	0.665	0.627	NA	None Observed

Table 2c

General Dynamics Samples

Measured Values

Material	Row	Angle	AO Fluence (atoms/cm ²)	UV Dose (ESH)	#	Solar Absorpt.		IR Emit.		AO Erosion Depth (microns)	Matrix *
						- Front -	- Back -	- Front -	- Back -		
CE339/GY70	8	38	6.93E+21	9400	1					56.3	None Observed
CE339/GY70	8	38	6.93E+21	9400	1					50.0	None Observed
934/T300	8	38	6.93E+21	9400	1					61.3	None Observed
934/T300	8	38	6.93E+21	9400	1					60.0	None Observed

Absorptance and emittance measurements not performed due to small size

McDonnell Douglas Samples

Measured Values

Material	Row	Angle	AO Fluence (atoms/cm ²)	UV Dose (ESH)	#	Solar Absorpt.		IR Emit.		AO Erosion Depth (microns)	Matrix *
						- Front -	- Back -	- Front -	- Back -		
PS-C/T300	8	38	6.93E+21	9400	1					65.0	Extensive
PS-C/T300	3	172	1.32E+17	11100	1					none	None Observed
PES-C/T300	8	38	6.93E+21	9400	1					55.0	None Observed

Absorptance and emittance measurements not performed due to small size

Table 3

Solar Absorptance Comparison

	Material	Front	Back	Difference	% difference	Angle
UTIAS	934/T300	0.814	0.830	-0.016	-1.9%	82
	5208/T300	0.872	0.883	-0.011	-1.2%	82
Lockheed	CE339/GY70	0.985	0.881	0.104	11.8%	8
	CE339/GY70	0.857	0.884	-0.027	-3.1%	172
Rockwell	934/T300	0.886	0.896	-0.010	-1.1%	112
	PMR15/C6000	0.876	0.899	-0.023	-2.6%	68
Boeing	934/T300	0.955	0.863	0.092	10.7%	8
		0.918	0.865	0.053	6.1%	38
		0.861	0.877	-0.016	-1.8%	172
		0.867	0.875	-0.008	-0.9%	158
	PMR15/C6000	0.980	0.910	0.070	7.7%	8
		0.900	0.910	-0.010	-1.1%	172
	P1700/T300	0.983	0.895	0.088	9.8%	8
		0.871	0.889	-0.018	-2.0%	172
0.873		0.881	-0.008	-0.9%	158	
U of Mich.	5208/T300	0.857	0.859	-0.002	-0.2%	82

Table 4

Emittance Comparison

	Material	Front	Back	Difference	% Difference	Angle
UTIAS	934/T300	0.703	0.796	-0.093	-11.7%	82
	5208/T300	0.706	0.804	-0.098	-12.2%	82
Lockheed	CE339/GY70	0.918	0.805	0.113	14.0%	8
	CE339/GY70	0.800	0.787	0.013	1.7%	172
Rockwell	934/T300	0.790	0.870	-0.080	-9.2%	112
	PMR15/C6000	0.750	0.840	-0.090	-10.7%	68
Boeing	934/T300	0.943	0.835	0.108	12.9%	8
		0.886	0.832	0.054	6.5%	38
	934/T300	0.769	0.804	-0.035	-4.4%	172
		0.832	0.819	0.013	1.6%	158
	PMR15/C6000	0.930	0.790	0.140	17.7%	8
		0.790	0.830	-0.040	-4.8%	172
	P1700/T300	0.922	0.822	0.100	12.2%	8
		0.817	0.825	-0.008	-1.0%	172
0.806		0.803	0.003	0.4%	158	
U of Mich.	5208/T300	0.665	0.627	0.038	6.1%	82

Table 5a

Erosion Yields - Various angles - As measured

Material	Row	Angle (deg)	Fluence (atom/cm ²)	Depth (micron)	Y (θ) (cm ³ /atom)	Y _n		Type	Source
						cos ^{0.5}	cos ^{0.2}		
934/T300	12	82	1.33E+21	21.5	1.6E-24	4.3E-24	2.4E-24	Ep/Gr	UTIAS
5208/T300	12	82	1.33E+21	17.7	1.3E-24	3.6E-24	2.0E-24	Ep/Gr	UTIAS
5208/T300	12	82	1.33E+21	20.1	1.5E-24	4.1E-24	2.2E-24	Ep/Gr	U. of Mich
CE339/GY70	9	8	8.99E+21	65.4*	7.3E-25	7.3E-25	7.3E-25	Ep/Gr	Lockheed
934/T300	9	8	8.99E+21	90.7	1.0E-24	1.0E-24	1.0E-24	Ep/Gr	Boeing
P1700/T300	9	8	8.99E+21	94.0	1.0E-24	1.1E-24	1.0E-24	Polysulfone/Gr	Boeing
934/T300	8	38	6.93E+21	82.2	1.2E-24	1.3E-24	1.0E-24	Ep/Gr	Boeing
PS-C/T300	8	38	6.93E+21	65.0	9.4E-25	1.1E-24	9.8E-25	Polysulfone/Gr	McDonnell Douglas
PES-C/T300	8	38	6.93E+21	55.0	7.9E-25	8.9E-25	8.3E-25	P-ethersulfone/Gr	McDonnell Douglas
CE339/GY70	8	38	6.93E+21	56.3	8.1E-25	9.2E-25	8.5E-25	Ep/Gr	General Dynamics
CE339/GY70	8	38	6.93E+21	50.1	7.2E-25	8.1E-25	7.6E-25	Ep/Gr	General Dynamics
934/T300	8	38	6.93E+21	61.3	8.8E-25	1.0E-24	9.3E-25	Ep/Gr	General Dynamics
934/T300	8	38	6.93E+21	60.0	8.7E-25	9.8E-25	9.1E-25	Ep/Gr	General Dynamics
PMR15/C6000	7	68	3.39E+21	30.1	8.9E-25	1.5E-24	1.1E-24	Polyimide/Gr	Rockwell

* Large surface erosion grooves

Table 5b

Erosion Yields — Various Angles — From Literature

Material	Row	Angle (deg)	Fluence (atom/cm ²)	Depth (micron)	Y (θ) (cm ³ /atom)	Y _n		Type	Source†
						cos ^{0.5}	cos ^{0.2}		
PMR15/C6000	9	8	8.99E+21	112.0	1.2E-24	1.3E-24	1.2E-24	Polyimide/Gr	Boeing
5208/T300	9	8	8.99E+21	114.3**	1.3E-24	1.3E-24	1.3E-24	Ep/Gr	NASA LaRC AO134
P1700/C6000	9	8	8.99E+21	76.2	8.5E-25	8.5E-25	8.5E-25	Polysulfone/Gr	NASA LaRC AO134
CE339/P75S	8	38	6.93E+21	78.0	1.1E-24	1.3E-24	1.2E-24	Ep/Gr	Aerospace Corp.
CE339/GY70	8	38	6.93E+21	75.0	1.1E-24	1.2E-24	1.1E-24	Ep/Gr	Aerospace Corp.
934/P75S	8	38	6.93E+21	55.0	7.9E-25	8.9E-25	8.3E-25	Ep/Gr	Aerospace Corp.
934/GY70	8	38	6.93E+21	60.5	8.7E-25	9.8E-25	9.2E-25	Ep/Gr	Aerospace Corp.
P1700/HMF322	8	38	6.93E+21	110.0*	1.6E-24	1.8E-24	1.7E-24	Polysulfone/Gr	MSFC AO171
934/P75S	8	38	6.93E+21	71.1	1.0E-24	1.2E-24	1.1E-24	Ep/Gr	MSFC AO171
934/HMS	8	38	6.93E+21	68.6	9.9E-25	1.1E-24	1.0E-24	Ep/Gr	MSFC AO171

*Possible contamination

**Measurement technique unknown

†See References 8 to 11

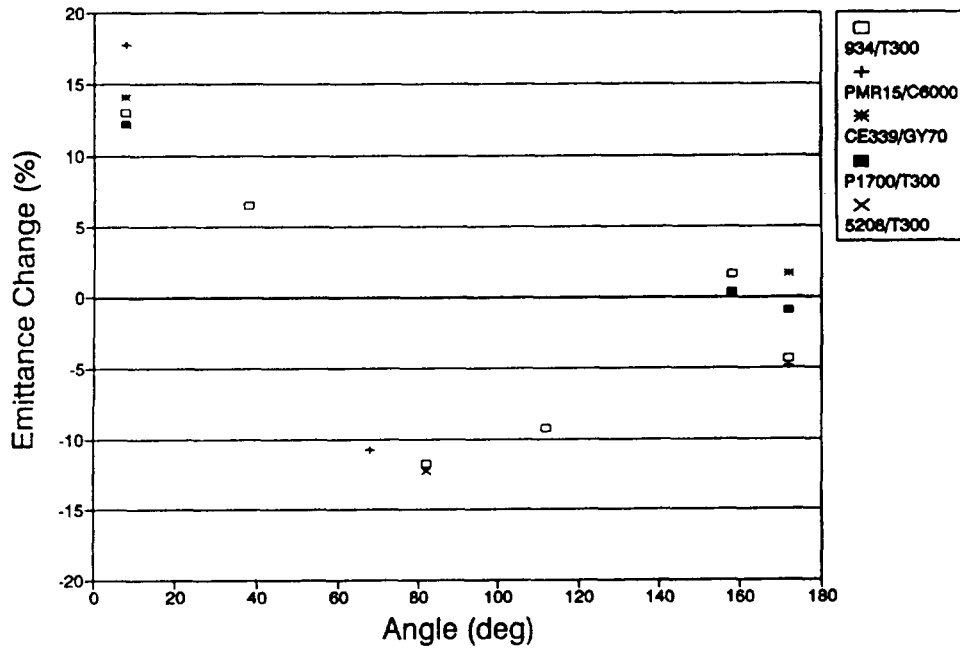


Figure 3. Percent Change in Emittance

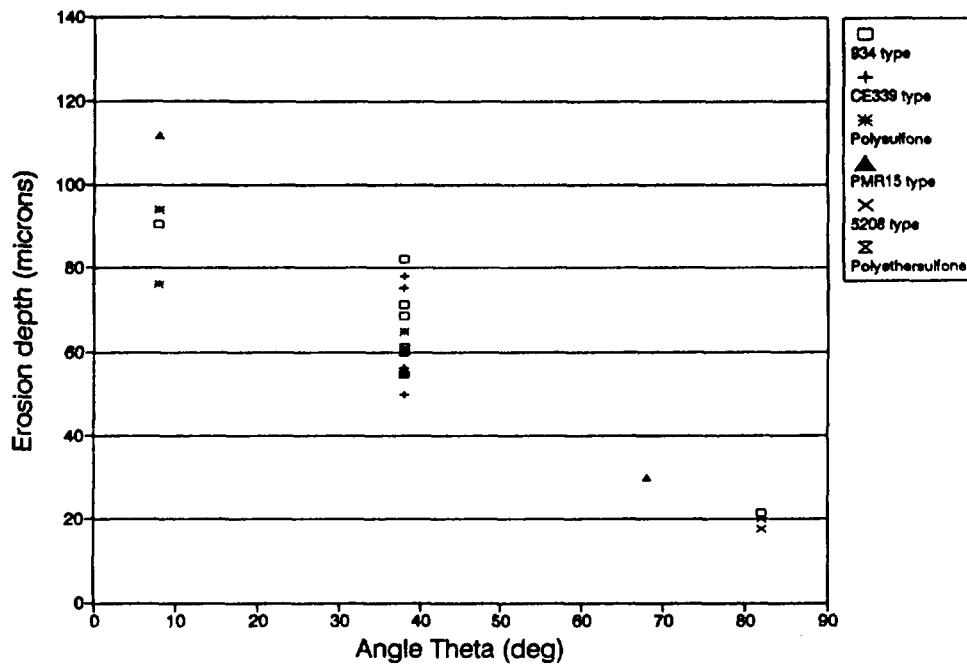


Figure 4. Erosion Depth of PMC Materials

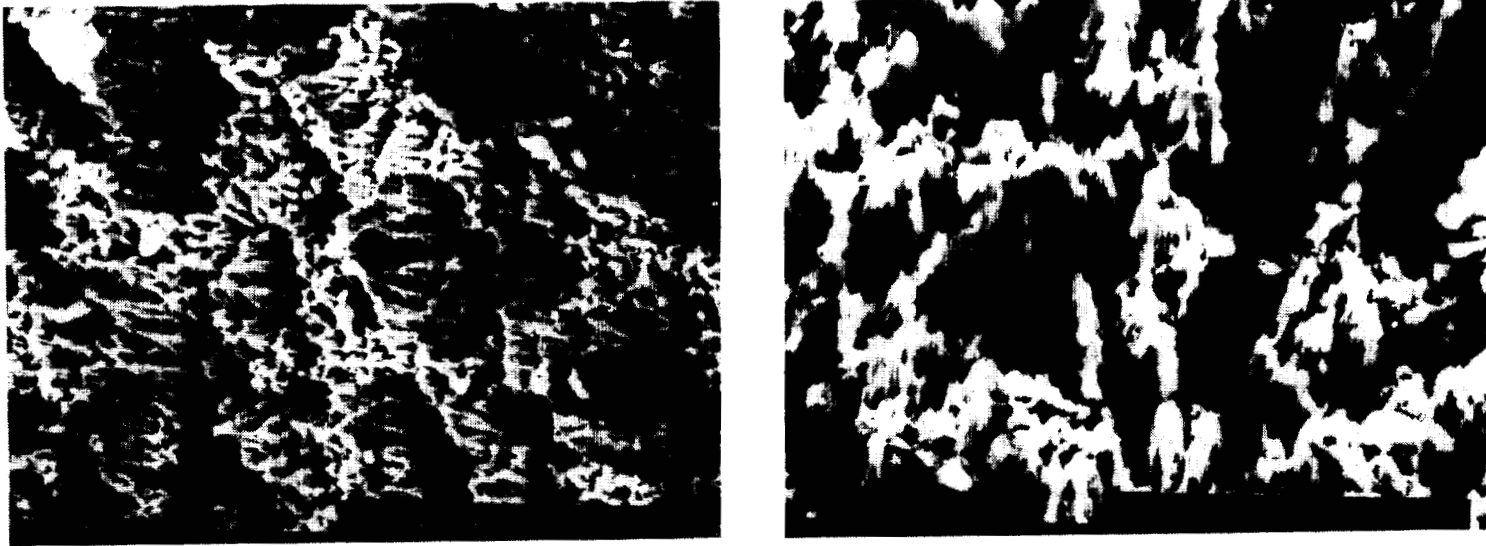


Fig. 5 Erosion of Graphite/Epoxy (T300/934) Material at 8°
(Ref: Boeing...) x750

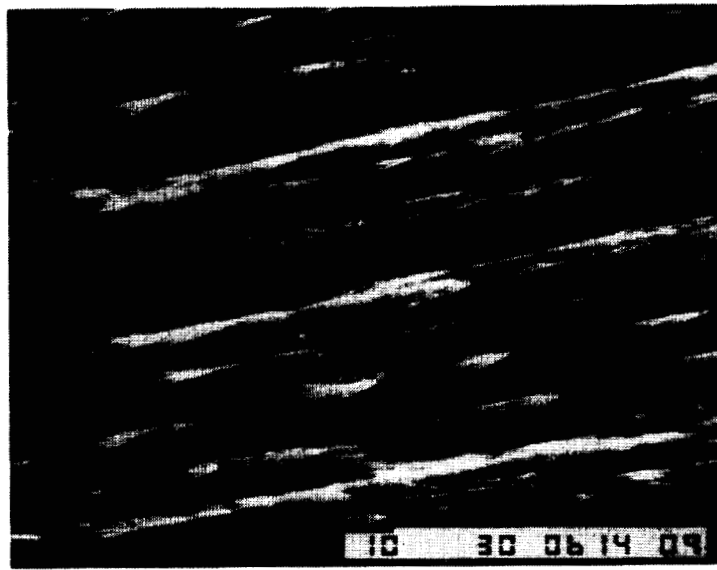


Fig. 6 SEM Photograph of Exposed Area of Graphite/Epoxy Laminate
(934/T300: $\pm 45^\circ$)_s at 82° (UTIAS) x750

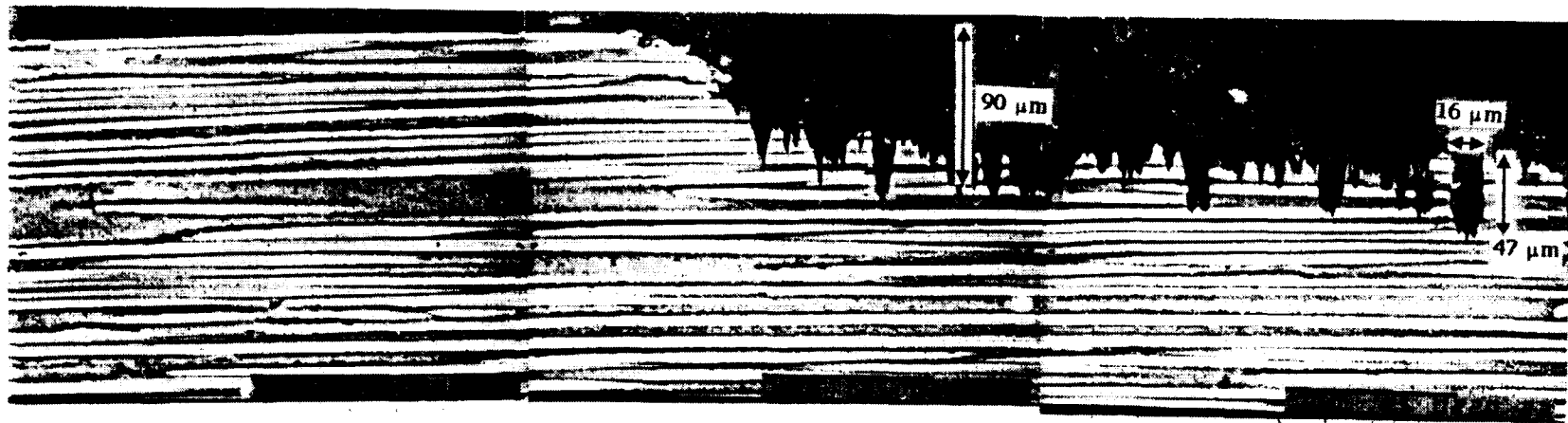


Fig. 7 SEM Micrograph Cross-Section of 934/T300 (0°) from RAM side showing Shielded Edge and the Effect of AO Erosion at 8° (Ref. Boeing...)

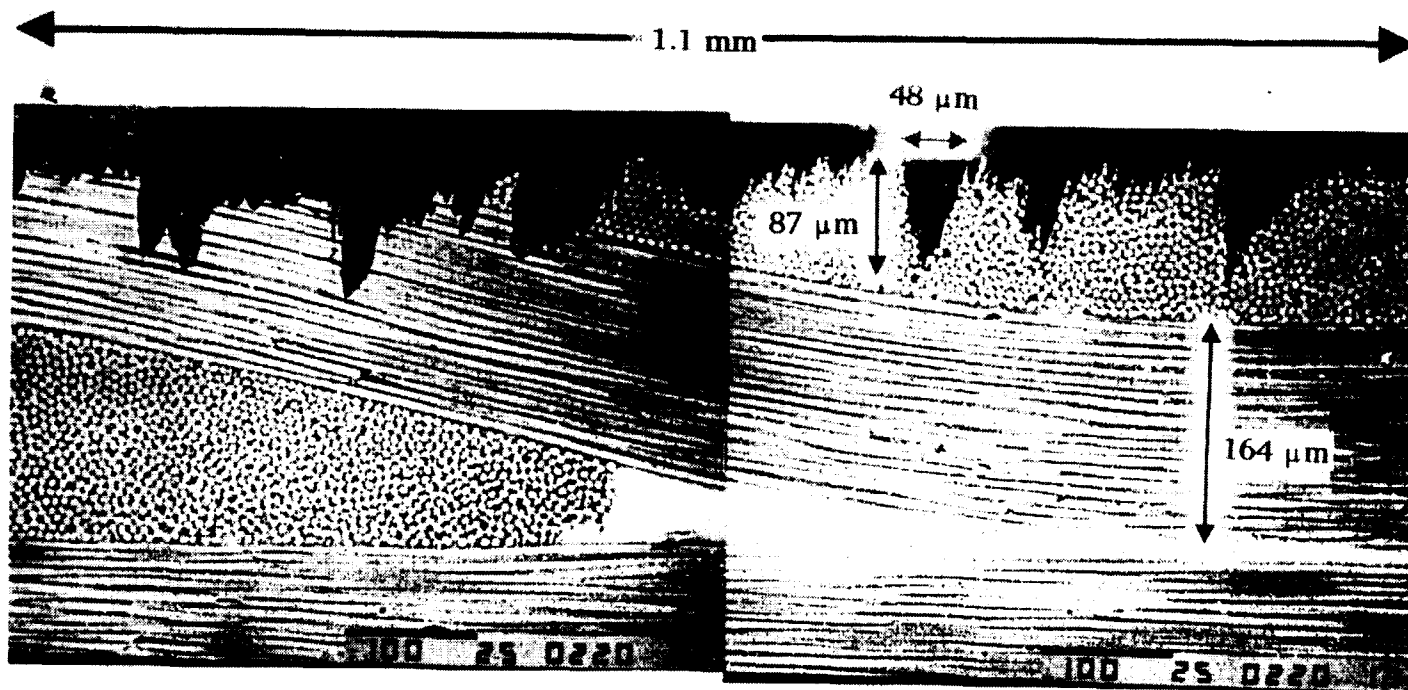


Fig. 8 SEM Micrograph of P1700/T300 Polysulfone/Graphite Cross-Section showing Eroded Section and Micro-particle Impact Sites
Location: Row 9 (8° off Ram) Layup: (0, 90)₄ Fabric (Ref: Boeing...)

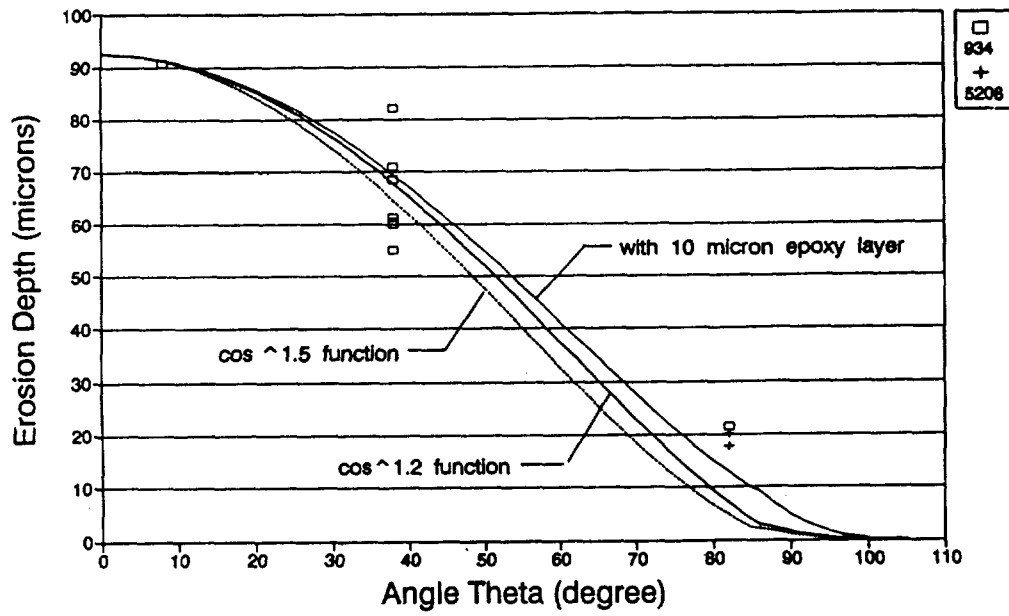


Figure 9. Erosion Depth of Epoxy Type Composite Samples - Epoxy Layer Effect

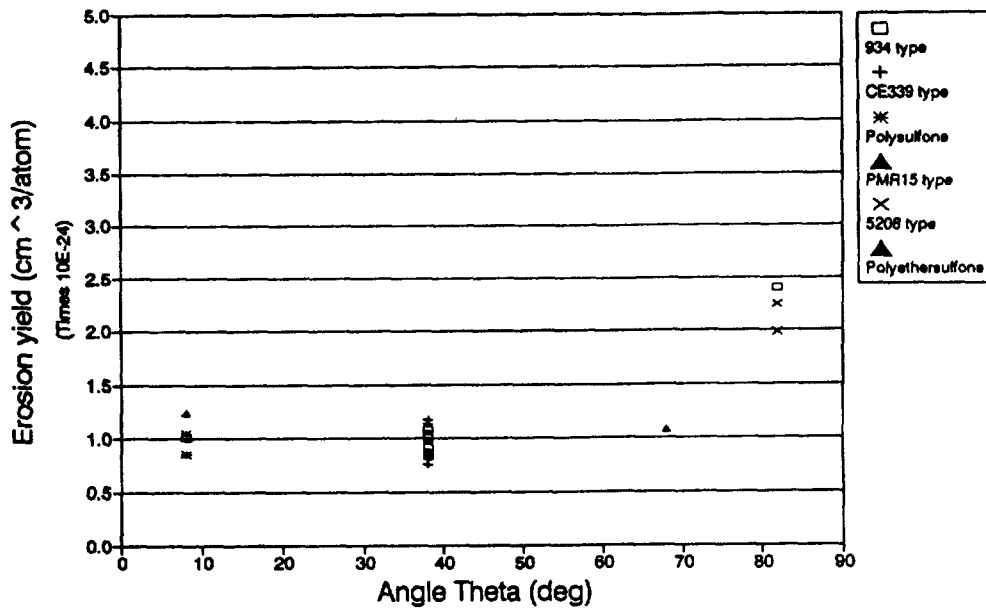


Figure 10. Normal Erosion Yield (Y_n) $\cos^{0.2}$

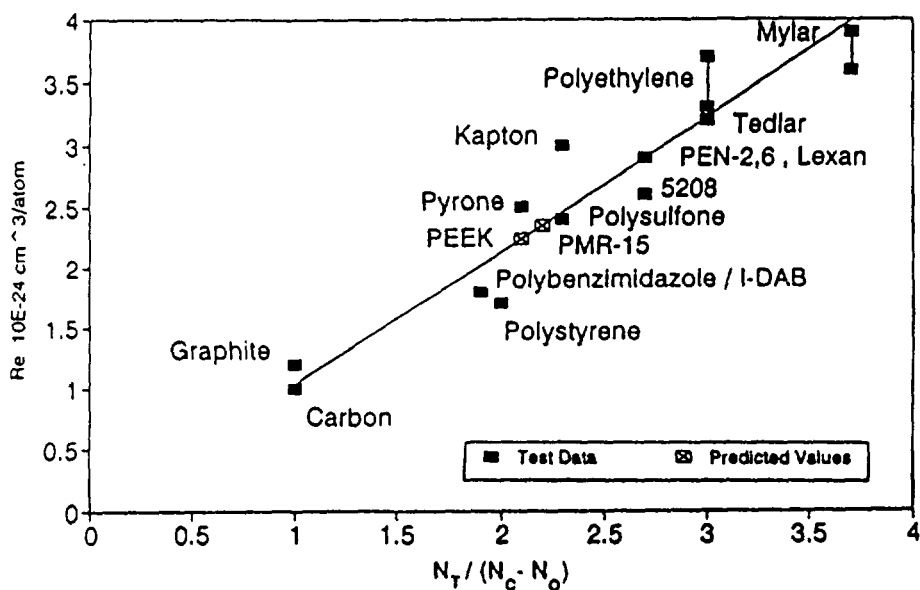
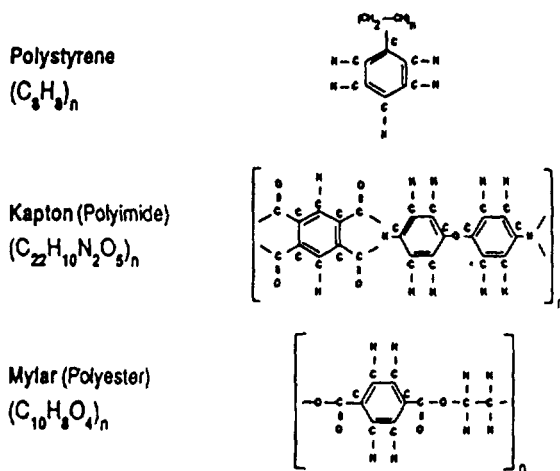


Figure 11. Effect of Polymer Structure on Erosion Yield in Presence of Hyperthermal Atomic Oxygen (2~5 eV).

Z. A. Iskanderova, Yu. I. Gudimenko, J. I. Kleiman, and R. C. Tennyson



POLYMERS	N_T	N_C	N_O	$\gamma = N_T / (N_C - N_O)$
Polystyrene	16	8	0	16/8 = 2
Kapton (Polyimide)	39	22	5	39/17 = 2.3
Mylar (Polyester)	22	10	4	22/6 = 3.7

N_T = Total number of atoms N_C = number of C atoms N_O = number of O atoms

Figure 12. Examples of Polymer Structures and Calculations of $N_T / (N_C - N_O)$.

**NONLINEAR VISCOELASTIC CHARACTERIZATION OF POLYMER
MATERIALS USING A DYNAMIC-MECHANICAL METHODOLOGY***

Thomas W. Strganac , Debbie Flowers Payne, and Bruce A. Biskup

Department of Aerospace Engineering

Texas A&M University

College Station, Texas 77843-3141

phone: (409) 845-7541

fax: (409) 845-6051

56-07

24420

14P

Alan Letton

Department of Mechanical Engineering

Texas A&M University

College Station, Texas 77843

phone: (409) 845-1534

fax: (409) 845-6051

ABSTRACT

Polymer materials retrieved from LDEF exhibit nonlinear constitutive behavior, thus the authors present a method to characterize nonlinear viscoelastic behavior using measurements from dynamic (oscillatory) mechanical tests. Frequency-derived measurements are transformed into time-domain properties providing the capability to predict long term material performance without a lengthy experimentation program. Results are presented for thin-film high-performance polymer materials used in the fabrication of high-altitude scientific balloons. Predictions based upon a linear test and analysis approach are shown to deteriorate for moderate to high stress levels expected for extended applications. Tests verify that nonlinear viscoelastic response is induced by large stresses. Hence, an approach is developed in which the stress-dependent behavior is examined in a manner analogous to modeling temperature-dependent behavior with time-temperature correspondence and superposition principles. The development leads to time-stress correspondence and superposition of measurements obtained through dynamic mechanical tests. Predictions of material behavior using measurements based upon linear and nonlinear approaches are compared with experimental results obtained from traditional creep tests. Excellent agreement is shown for the nonlinear model.

INTRODUCTION

The authors present a method to describe the nonlinear viscoelastic behavior of polymer materials used in the fabrication of high-altitude scientific balloons. The primary objectives of this research include the experimental measurement of nonlinear viscoelastic properties using dynamic (oscillatory) mechanical methods and the development of nonlinear constitutive laws which employ these measurements. Three primary issues are examined: (1) the superposition of

* Work partially supported by NASA Grant NAG5-673 (NASA-GSFC/Wallops Flight Facility)

material properties measured at different conditions, such that measurements at one condition (for example, temperature or load) are equivalent to measurements at another condition but on a compressed or expanded time scale; (2) the transformation of measurements obtained in the frequency domain into material properties in the time domain, thus characterization is performed on a much shorter time scale; and, (3) the nonlinear characterization of material behavior examined in a manner analogous to modeling temperature-dependent behavior using time-temperature correspondence and linear superposition principles.

Many investigators characterize thin-film materials using linear viscoelastic techniques. Wilbeck¹ has developed a constitutive relationship for thin polyethylene films such as those used in high-altitude scientific balloons. Wilbeck predicts the state of stress in the film given strain and temperature histories; however, he shows that the properties of these materials exhibit nonlinear behavior due to the dependence of the behavior on the load history. In several studies, the efforts of Schapery²⁻⁵ form the basis for the characterization of nonlinear behavior of viscoelastic materials. Smart and Williams⁶ compare Schapery's theory to the modified superposition principle (MSP) in which the creep behavior is separated into time-dependent and stress-dependent components. Predictions using the MSP are poor; however, Schapery's theory is shown to accurately model the constitutive behavior. In another investigation, Dillard, et. al⁷ compares Schapery's theory to several nonlinear viscoelastic models, including the MSP. Dillard's findings also suggest that Schapery's theory produces the most accurate results. Additionally, Dillard shows that Schapery's theory is appropriate for complex load histories.

A comparison of experimental results and predictions using Schapery's theory is presented by Crook⁸. Crook's research utilizes the experimental results from traditional creep tests as parameters for Schapery's theory. Crook accurately predicts the strain response of polycarbonate materials to a three-step stress input. In another study, Popelar, et. al⁹ analyzes a comprehensive set of experimental data obtained from stress relaxation and constant strain-rate tests. Again, the relaxation data are utilized to develop the nonlinear constitutive model, and the nonlinear response is accurately characterized by Schapery's theory.

These earlier studies have shown that Schapery's theory is the most general and the most adaptable of the examined techniques. Herein, we describe a technique to predict nonlinear viscoelastic response based on Schapery's theory but extended to incorporate results derived from dynamic oscillatory tests. Strganac, et. al^{10,11} and Letton, et. al¹² examine materials retrieved from NASA's Long Duration Exposure Facility (LDEF). The linear viscoelastic characteristics of these materials are determined using dynamic mechanical methods. Payne, et. al¹³ describe the initial efforts to examine nonlinear behavior of materials using superposition of measurements obtained from dynamic mechanical methods.

THEORETICAL APPROACH

The constitutive properties of viscoelastic materials are dependent upon the rate at which the load or deformation occurs. Additionally, nonlinear viscoelastic behavior exists if the material properties are dependent upon the magnitude of stress or strain as well as the rate at which the load or deformation occurs. The theory developed by Schapery allows the material properties to be expressed in terms of either stress- or strain-dependent behavior. This theory is a modification of the single integral solution for linear viscoelasticity at a constant temperature.

For linear theory, the stress and strain are related by the Boltzmann superposition integral,

$$\varepsilon(t) = \int_0^t D(t - \tau) \frac{\partial \sigma}{\partial \tau} d\tau \quad (1)$$

where ε is strain, σ is stress, $D(t)$ is the compliance, and t is time. A similar relation defines stress in terms of strain, but is not presented for brevity. By assuming a form of the compliance, such that $D(t) = D_0 + \Delta D(t)$, Eq. (1) may be expressed as

$$\varepsilon(t) = D_0 \sigma(t) + \int_0^t \Delta D(t - \tau) \frac{\partial \sigma}{\partial \tau} d\tau \quad (2)$$

where D_0 is the initial component and ΔD is the transient component of the compliance.

Time-temperature correspondence principles¹⁴ are typically employed to characterize the viscoelastic behavior of materials. The strength of the method is the superposition of data measured on different time scales - properties measured at one temperature are equivalent to those at a second temperature on a compressed or expanded time scale. Furthermore, transformations between measurements in the frequency domain and response in the time domain exist allowing for measurement of properties in the frequency domain and prediction of properties in the time domain. Thus, the properties measured at one temperature and frequency correspond to the properties at another temperature and frequency through a temperature-dependent shift factor

$$E^\dagger(\omega, T_1) = E^\dagger\left(\frac{\omega}{a_T}, T_2\right) \quad (3)$$

where E^\dagger represents either the dynamic modulus or a component of the dynamic modulus for the material, T is the temperature, and a_T is the temperature-dependent shift factor. This approach is similar to time-temperature correspondence principles in the time domain.

This shift factor is a measure of the temperature dependence of the relaxation process¹² for the material and is determined by the superposition of measurements at two distinct temperatures. The effect of a change in temperature is equivalent to measurements on a different frequency scale. This strategy allows the superposition of measurements taken over a range of

temperatures at a specific frequency interval. A master curve of the dynamic modulus as a function of frequency is formed for a reference temperature.

Traditional creep measurements require significant test time to adequately characterize the material response for a large time interval. However, the transformation of the modulus measured in the frequency domain to the modulus in the time domain provides rapid characterization and, consequently, long experimentation is eliminated. A numerical transformation from the frequency domain to the time domain is described by Ninomiya and Ferry¹⁴ for determining the relaxation modulus

$$E(t) = E'(\omega) - 0.40 E''(0.4 \omega) + .014 E''(10 \omega)_{t=\frac{1}{\omega}} \quad (4)$$

where E' is the storage modulus, E'' is the loss modulus, t is the relaxation time, and ω is the frequency.

We extend the approach of time-temperature superposition to time-stress superposition based upon the work of Schapery. Schapery modifies the constitutive equation to describe nonlinear viscoelastic responses by introducing a reduced time variable which is dependent upon the magnitude of the stress. If stress is the independent state variable, Schapery suggests the constitutive behavior may be described by

$$\epsilon(t) = g_0 D_0 \sigma(t) + g_1 \int_0^t \Delta D(\Psi - \Psi') \frac{\partial g_2 \sigma}{\partial \tau} d\tau \quad (5)$$

where g_0 , g_1 , and g_2 are stress-dependent material properties, Ψ and Ψ' are reduced time variables defined by

$$\Psi = \Psi(t) = \int_0^t \frac{dt}{a_\sigma} \quad (6)$$

$$\Psi' = \Psi'(\tau) = \int_0^\tau \frac{d\tau}{a_\sigma} \quad (7)$$

and a_σ is the stress-dependent shift factor.

The parameters g_0 , g_1 , and g_2 are unique for each material. These parameters are determined experimentally if traditional creep tests are used; but, with our approach, these parameters are integrated within the experimental measurements. The creep compliance (or relaxation modulus) developed from the experimental measurements will contain the effects of these parameters.

As will be fully described in the subsequent section, the dynamic modulus is measured as a function of preload and frequency, and these measurements are used to describe nonlinear behavior resulting from the preload. Using a method analogous to time-temperature correspondence based on temperature-dependent shift factors, time-stress correspondence¹³ is

employed to identify stress-dependent shift factors. Thus, the properties measured at one preload and frequency correspond to the properties at another preload and frequency

$$E^\dagger(\omega, \sigma_0) = E^\dagger\left(\frac{\omega}{a_\sigma}, \sigma_{02}\right) \quad (8)$$

where E^\dagger represents either the dynamic modulus or a component of the dynamic modulus for the material, σ_0 is the preload, and a_σ is the stress-dependent shift factor.

EXPERIMENTAL APPROACH

Dynamic oscillatory tests¹⁰ are used to measure the viscoelastic response. Experimental measurements are conducted with the Rheometrics Solids Analyzer II. Measurements are obtained through a sweep of frequencies ($0.1 \leq \omega \leq 100$ rad/sec) at a constant temperature and preload. Depending upon the nature of the analysis, either the temperature or preload is changed and new measurements are obtained through a sweep of frequencies. Temperatures range from -150°C (-238°F) to the melt temperatures. Preloads may approach the yield of the material. This test strategy is illustrated in Figure 1.

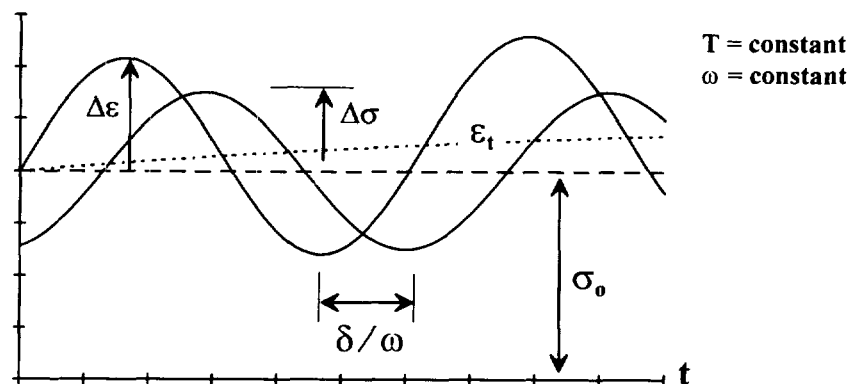


Figure 1. Force ($\Delta\sigma$) and damping (δ) is measured from an oscillatory deformation ($\Delta\epsilon$) input. A constant preload (σ_0) is applied.

Two parameters are measured directly - the force due to an oscillatory deformation input and the phase lag between input and output. Material damping is measured as the phase lag, δ , between the measured force (stress) response output,

$$\sigma(t) = \sigma_0 + \Delta\sigma e^{(i\omega t + \delta)} \quad (9)$$

and the oscillatory deformation (strain) input,

$$\epsilon(t) = \epsilon_t + \Delta\epsilon e^{i\omega t} \quad (10)$$

In Eqs. (9) and (10), σ_0 is the stress resulting from the preload which is held constant during the experiment, $\Delta\sigma$ is the measured stress response, ϵ_t is the strain (creep) which occurs during the dynamic oscillatory test, and $\Delta\epsilon$ is the magnitude of the oscillatory strain input.

Typically, dynamic oscillatory tests are used to measure the linear viscoelastic properties of the test specimen. A dynamic modulus, E^* , is derived from these measurements as

$$E^*(\omega, T) = \frac{\Delta\sigma e^{i(\omega t + \delta)}}{\Delta\epsilon e^{i\omega t}} = |E| e^{\delta} = |E| \cos \delta + i |E| \sin \delta \quad (11)$$

where $|E| \cos \delta$ is defined as the storage modulus, E' , and $|E| \sin \delta$ is defined as the loss modulus, E'' .^{14,15}

However, in our studies, two sources of nonlinear behavior are identified with the dynamic oscillatory tests.^{10,13} The first source is associated with the magnitude of the oscillatory strain, $\Delta\epsilon$. The second source is associated with the magnitude of the preload, σ_0 . Thus, the dynamic modulus should appear as

$$E^*(\omega, T, \sigma_0) = \frac{\sigma_0 + \Delta\sigma e^{i(\omega t + \delta)}}{\epsilon_t + \Delta\epsilon e^{i\omega t}} \quad (12)$$

A preload is used to maintain a tensile load on the specimen throughout the test; however, our results indicate a strong dependence of the measured response due to this preload. Typical measurements of the dynamic modulus are illustrated in Figure 2.

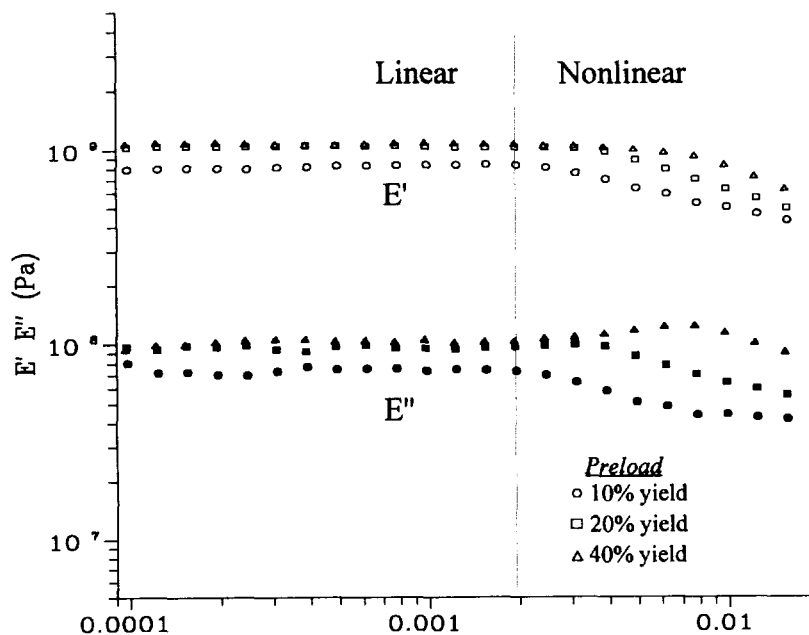


Figure 2. Measurements of the dynamic modulus are dependent upon the magnitude of the oscillatory deformation ($\Delta\epsilon$) and preload (σ_0).

In our measurements of the linear viscoelastic behavior for the material we require that the measured properties are independent of the magnitude of both the oscillatory strain and the preload. In our measurements of the nonlinear viscoelastic behavior for the material we require that the measurements are dependent of only the magnitude of the preload. Thus, in either case, the magnitude of the oscillatory strain is selected such that measurements of the dynamic modulus are independent of the magnitude of oscillatory strain. Nonlinearities are due only to preload.

In the linear analysis we measure the dynamic modulus at different temperatures.¹² In the nonlinear analysis we measure the dynamic modulus at different preloads (stresses).¹³ In both the linear analysis and nonlinear analysis the process of forming the master curve is identical. The experimental data consist of a collection of measurements obtained for the full range of test frequencies at a constant temperature (or preload for the nonlinear tests). This data establishes a family of curves relating the dynamic modulus to frequency. This family of temperature-dependent (or stress-dependent) curves are used to form a master curve which provides the dynamic modulus over a larger range of frequencies for a reference temperature (or reference preload). The temperature-dependent (or stress-dependent) shift factors are produced as a result of shifting and 'superposing' the measured data.¹² The properties measured at one temperature (or preload) and frequency correspond to the properties at another temperature (or preload) and frequency through the shift factor. The effect of a change in temperature (or preload) is equivalent to measurements on a different frequency scale. We note that the master curve provides the dynamic modulus over a larger range of time when the results are appropriately transformed from the frequency domain to the time domain.

RESULTS

We examine results for two thin-film polyethylenes - Stratofilmr and Astrofilmr - which are used in the fabrication of high-altitude scientific balloons. Stratofilmr (SF-372) is a linear-low density polyethylene manufactured by Winzen International, Inc. Astrofilmr (AF-E2) is a low density polyethylene manufactured by Raven Industries. These films are produced through a blown-film extrusion process which induces a directionality in the properties of the material. Thus, tests are conducted in the 'machine' direction and the 'transverse' direction; tests are not conducted through the thickness. The nominal length of each test specimen is 2.54 cm (1.0 in), the nominal width of is .635 cm (0.25 in), and the nominal film thickness is .0201 mm (0.0008 in).

Linear viscoelastic characteristics are measured for SF-372 and AF-E2 at temperatures ranging from -150°C (-238°F) to the melt temperature of the specimen. For the linear analysis, the dynamic modulus is dependent upon the frequency and temperature. Although a preload is used to maintain a tensile load on the specimen, in our measurements of the linear behavior we require that the measurements are independent of the preload.

The dynamic modulus for SF-372 and associated temperature-dependent shift factors are presented in Figure 3. The dynamic modulus for AF-E2 and associated temperature-dependent shift factors are presented in Figure 4.

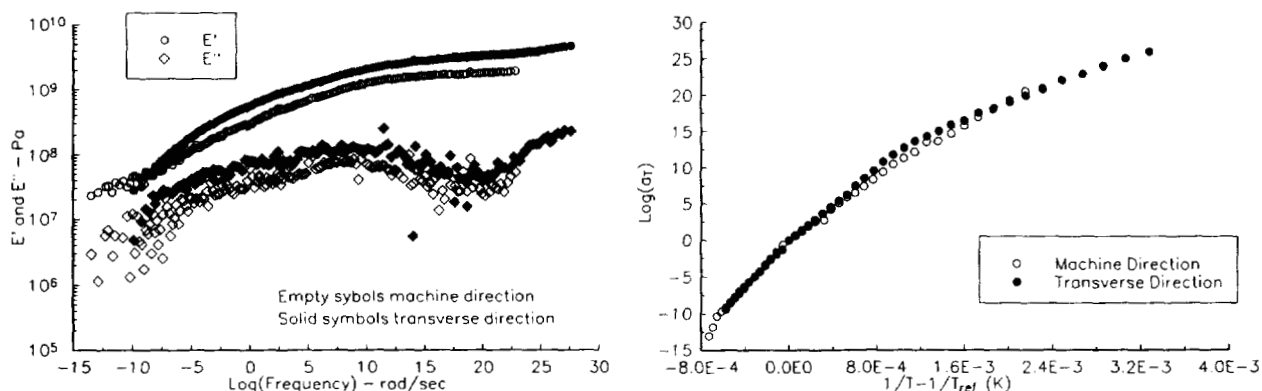


Figure 3. The master curve for SF-372, derived from temperature-frequency measurements of the dynamic modulus, is shown in the left view. The temperature dependent shift factors are presented in the right view ($T_{\text{ref}} = 20^\circ\text{C}$ (68°F)).

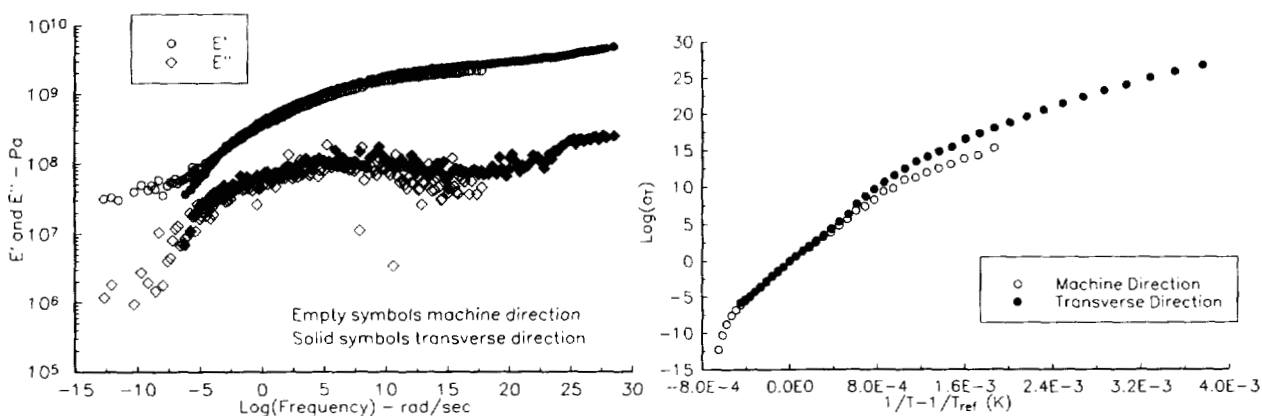


Figure 4. The master curve for AF-E2, derived from temperature-frequency measurements of the dynamic modulus, is shown in the left view. The temperature dependent shift factors are presented in the right view ($T_{\text{ref}} = 20^\circ\text{C}$ (68°F)).

Although the viscoelastic properties for both materials are measured under identical conditions (frequency and temperature range), the results presented in the above figures suggest otherwise. Two reasons for this aberration exist: first, the measured data does not behave in a linear manner (thus, the data cannot be superposed) at the extremely low temperatures (which relates to behavior at high frequency or short time scales); and, second, the melt temperature is not uniform for all specimens.

The relaxation modulus measured for SF-372 and AF-E2 is presented in Figure 5. These measured values of the dynamic modulus and the method of Ninomiya and Ferry are used to derive the relaxation modulus. Since measurements of the dynamic modulus are used in the derivation, differences in the range of time for the presented data exist for the same reasons as described in the preceding paragraph.

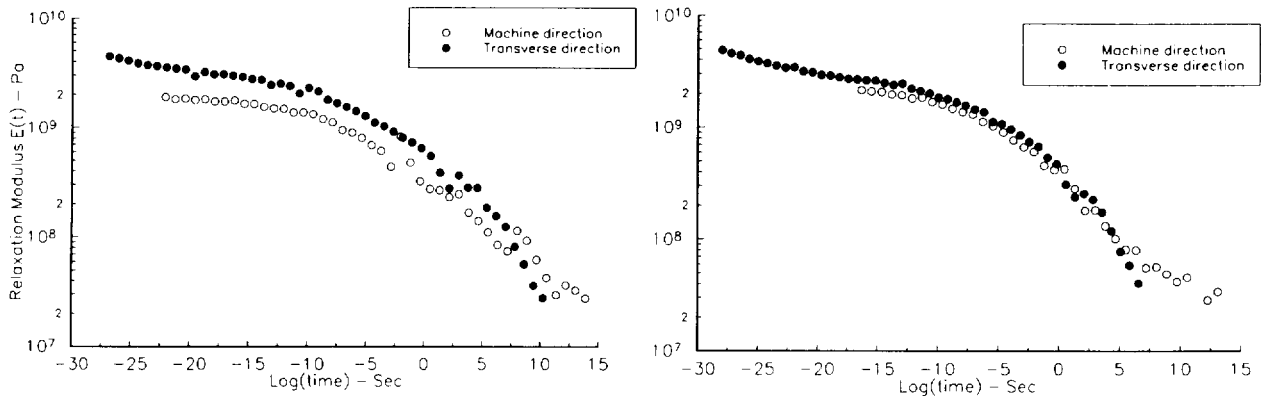


Figure 5. The relaxation modulus for SF-372 is shown in the left view. The relaxation modulus for AF-E2 is shown in the right view. The modulus is derived from measurements of the dynamic modulus (refer to Figures 3 and 4). $T_{ref} = 20^{\circ}\text{C}$ (68°F).

Creep response is predicted using the creep compliance derived from the dynamic oscillatory measurements. These predictions are compared with the creep response measured in traditional creep tests. Figure 6 provides a comparison of predictions and measurements for SF-372 and AF-E2.

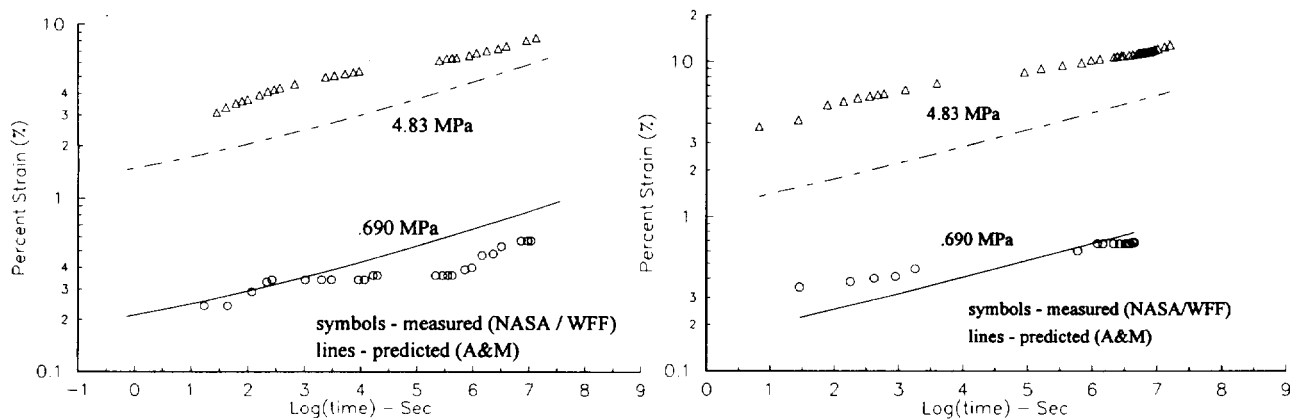


Figure 6. Creep is predicted using the compliance derived from measurements of the dynamic modulus. Comparisons are made with traditional creep measurements for SF-372 (left view) and AF-E2 (right view). The specimens are oriented in the machine direction. Measured creep data provided by NASA-GSFC/WFF.

Predictions for two preloads are shown in each figure. As expected due to the nonlinear effects induced by the large stresses due to preload, the predictions clearly deteriorate for both SF-372 and AF-E2 as the preload increases. Consequently, stress-dependent contributions must be included in the characterization of viscoelastic properties for materials exposed to higher stresses.

The yield stress for these materials is highly dependent upon the temperature.¹³ The yield stress for these materials is approximately 40 MPa (5800 psi) at $T = -100^{\circ}\text{C}$ (-148°F) and 9 MPa (1300 psi) at $T = 23^{\circ}\text{C}$ (73.4°F) (data courtesy of Winzen International, Inc., these measurements are determined from a 0.2% strain offset on the stress-strain curve). Thus, a preload which is 25% of the yield stress at $T = -100^{\circ}\text{C}$ (-148°F) exceeds the yield stress at room temperature. We introduce a convention in which we refer to the preload as a percentage of the yield stress; and, therefore, tests performed at different temperatures will be compared with preloads at identical percents of yield stress. Stress-dependent shift factors are also developed using this convention.

A limiting stress is noted in Figure 7, where the storage modulus is presented as a function of preload and frequency. At a preload of approximately 35% yield stress, a drop in E' is observed. This material 'stiffening' is not yet fully understood; consequently, the preload is limited to 30% of the yield stress to avoid complications associated with this region.

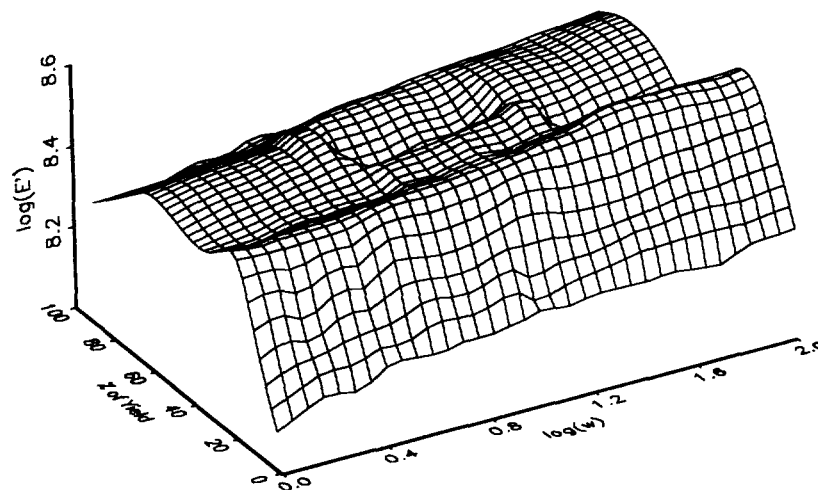


Figure 7. Viscoelastic properties are measured at several preloads and frequencies. The storage modulus is shown as a function of preload (measured as percent yield) and frequency ($T_{\text{ref}} = 20^{\circ}\text{C}$ (68°F)).

Nonlinear viscoelastic characteristics are measured for SF-372 for preloads ranging from 2% to 20% of the yield stress. For the nonlinear analysis, the dynamic modulus is dependent upon preload, as well as the frequency and temperature. In these measurements of nonlinear viscoelastic behavior we require that the measurements are dependent upon the magnitude of the preload and measurements are performed at a constant temperature of 23°C (73.4°F).

The results of a series of dynamic oscillatory tests performed at several preloads below 30% of the yield stress are shown in Figure 8. The effect of the stress level on the response of the material is evident. On the basis of time-stress superposition, the data are shifted to obtain the master curve and the corresponding stress-dependent shift factors are derived. The "linear" behavior of the results establishes confidence in the test and analysis procedure.

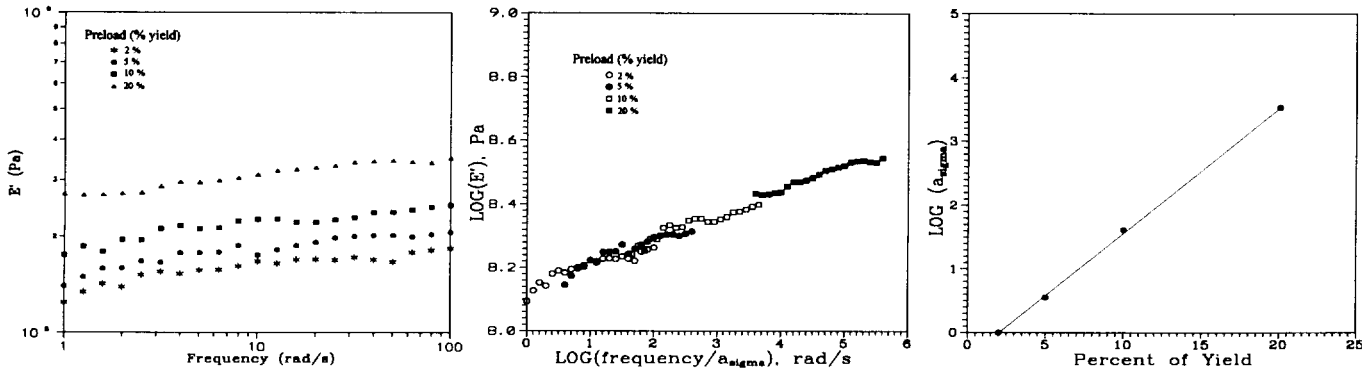


Figure 8. Stress-dependent measurements are obtained for preloads below 30% yield. The master curve of the storage modulus E' is shown (center view) for a reference preload of 2% yield. Stress-dependent shift factors provide correspondence between different stress levels.

Measurements obtained from dynamic oscillatory tests are compared to measurements obtained from traditional creep tests. A comparison of the creep compliance is presented in Figure 9. The reference stress (preload) is 20% of the yield stress at room temperature. For the dynamic oscillatory tests, the creep compliance is derived from the stress relaxation modulus found using measurements of the dynamic modulus and the transformation of Ninomiya and Ferry. For the comparison data, the creep compliance is derived from traditional creep measurements provided by Winzen International, Inc.

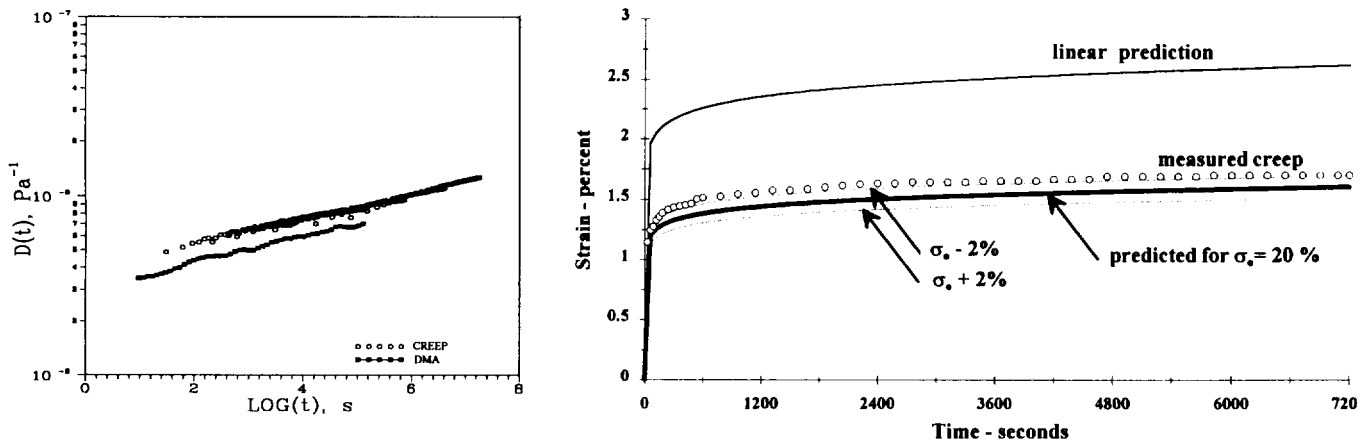


Figure 9. Compliance - derived from dynamic (oscillatory) measurements - is compared to compliance data derived from creep measurements (left view). Creep - predicted using the stress-dependent measurements - is compared with creep measurements (right view).

Measured creep data provided by Winzen International, Inc.

The creep compliance is fit to a function of the form $D(t) = D_0 + \Delta D(t)$, and this function is used to predict creep response. The difference between the two sets of data may be attributed to very small differences in the measured thickness of the test specimen and very small differences in the stress-dependent shift factors. Creep response, predicted using the nonlinear stress-dependent behavior due to preload (σ_0), is shown in Figure 9. Comparisons are made with creep measurements provided by Winzen International, Inc. Creep response is predicted for the linear case - the sensitivity to preload is evident. The material is SF-372 (machine direction), the reference stress is 2.07 MPa (300 psi), and the reference temperature is 20°C (68°F). The results from the dynamic oscillatory tests accurately predict the trends of the measured data; however, the predictions are slightly underestimated. The difference between the two sets of data reflects the difference in the creep compliance data. The predictions are sensitive to the stress-dependent shift factors.

CONCLUSIONS

Dynamic (oscillatory) mechanical tests are used as a basis to characterize the linear (temperature-dependent) and nonlinear (stress-dependent) viscoelastic behavior of thin polyethylene materials. Nonlinear stress-dependent behavior is characterized using correspondence and superposition principles. Dynamic oscillatory test measurements produce predictions consistent with the results of traditional creep tests. In addition, the effective transformation of measurements obtained in the frequency domain to response in the time domain allows for the nonlinear characterization of polymer materials without an extended test program. Results show that the response of the materials examined is best characterized by nonlinear viscoelastic methods.

ACKNOWLEDGMENTS

The authors thank the staff of Winzen International, Inc. for the experimental test data. The authors thank the staff of the Balloon Projects Branch at NASA-Goddard Space Flight Center / Wallops Flight Facility for their financial support and experimental test data.

REFERENCES

1. Wilbeck, J.S., "Nonlinear Viscoelastic Characterization of Thin Polyethylene Film", NASA CR - 156876, February 1981.
2. Schapery, R.A., "A Theory of Nonlinear Thermoviscoelasticity Based on Irreversible Thermodynamics", *Proceedings of the 5th U.S. Nat. Cong. Appl. Mech.*, L.E. Goodman, ed., June 1966.
3. Schapery, R.A., "On the Characterization of Nonlinear Viscoelastic Materials", *Polymer Engineering and Science*, Vol. 9, 1969, p. 295.
4. Schapery, R.A., "On a Thermodynamic Constitutive Theory and its Application to Various Nonlinear Materials", *Proceedings of the IUTAM Symposium on Thermoelasticity*, Springer-Verlag, 1969.
5. Schapery, R.A., "Irreversible Thermodynamics and Variational Principles with Applications to Viscoelasticity", Ph.D. Dissertation, California Institute of Technology, Pasadena, California, August 1962.
6. Smart, J. and Williams, J.G., "A Comparison of Single-Integral Nonlinear Viscoelasticity Theories", *J. Mech. Phys. Solids*, Vol. 20, 1972, p. 313.
7. Dillard, D.A., Straight, M.R., and Brinson, H.F., "The Nonlinear Viscoelastic Characterization of Graphite/Epoxy Composites", *Polym. Eng. Sci.*, Vol. 27, 1987, p. 116.
8. Crook, R.A., "Application of a Nonlinear Viscoelastic Model to the Design of Polymeric Structures", Ph.D. Dissertation, Texas A&M University, College Station, Texas, August 1991.
9. Popelar, C.F., Popelar, C.H., and Kenner, V.H., "Viscoelastic Material Characterization and Modeling for Polyethylene", *Polym. Eng. Sci.*, Vol. 30, 1990, p. 577.
10. Strganac, T.W., Letton, A., Farrow, D.A., Rock, N.I., Williams, K.D., "The Investigation of Balloon Materials Exposed to the Low Earth Orbit Environment", AIAA International Balloon Technology Conference, AIAA Paper No. 91-3657, Albuquerque, New Mexico, October 1991.
11. Strganac, T.W., Letton, A., Rock, N.I., Williams, K.D., Farrow, D.A., "Characterization of Polymer Films Retrieved from LDEF", *AIAA Journal of Spacecraft and Rockets*, accepted for publication by the AIAA (December 1993).
12. Letton, A., Farrow, D.A., and Strganac, T.W., "Viscoelastic Characterization of Thin-Film Polymers Exposed to Low-Earth Orbit", *Proceedings of LDEF - 69 Months in Space, Second Post-Retrieval Symposium*, NASA CP - 3194, Part 3, San Diego, California, June 1992, pp. 849-866.

13. Payne, D., Biskup, B., Letton, A., and Strganac, T.W., "On Nonlinear Viscoelastic Analysis of Thin Film Materials using a Dynamic Mechanical Approach", 34th AIAA Structures, Structural Dynamics, and Materials Conference, AIAA Paper No. 93-1578, La Jolla, California, April 1993.

14. Ferry, J.D., *Viscoelastic Properties of Polymers*, Third ed., John Wiley and Sons, New York, 1980.

15. Findley, W.N., Lai, J.S., and Onaran, K., *Creep and Relaxation of Nonlinear Viscoelastic Materials*, H.A. Lauwerier and W.T. Koiter, eds., North Holland Publishing Co., New York, 1976.

THE EFFECT OF SIMULATED LOW EARTH ORBIT RADIATION ON POLYIMIDES (UV DEGRADATION STUDY)

John S. Forsythe, Graeme A. George, David J.T. Hill, James H. O'Donnell,
Peter J. Pomery and Firas A. Rasoul

Polymer Materials and Radiation Group
The University of Queensland
Queensland, 4072, Australia

57-27
12F

ABSTRACT

UV degradation of polyimide films in air and vacuum were studied using UV-Visible, ESR, FTIR and XPS spectroscopies. The UV-Visible spectra of polyimide films showed a blue shift in the absorption compared to Kapton. This behaviour was attributed to the presence of bulky groups and kinks along the polymer chains which disrupt the formation of a charge transfer complex. The UV-Visible spectra showed also that UV irradiation of polyimides result extensively in surface degradation, leaving the bulk of the polymer intact. ESR spectra of polyimides irradiated in vacuum revealed the formation of stable carbon-centred radicals which give a singlet ESR spectrum, while polyimides irradiated in air produced an asymmetric signal shifted to a lower magnetic field, with a higher g value and line width. This signal was attributed to oxygen-centred radicals of peroxy and/or alkoxy type. The rate of radical formation in air was two fold higher than for vacuum irradiation, and reached a plateau after a short time. This suggests a continuous depletion of radicals on the surface via an ablative degradation process. FTIR, XPS and weight loss studies supported this postulate. An XPS study of the surface indicated a substantial increase in the surface oxidation after irradiation in air. The sharp increase in the C-O binding energy peak relative to the C-C peak was believed to be associated with an aromatic ring opening reaction.

INTRODUCTION

Spacecraft in low earth orbit are subjected to significant levels of high energy radiation, including UV and VUV wavelengths. The effects of UV radiation are enhanced over those at the surface of the earth, where the only incident wavelengths are greater than 290 nm (1). In low earth orbit the incident UV wavelengths extended below 290 nm into the VUV region, where the Lyman- α emissions of atomic hydrogen occur at 121 nm (2). In addition to electromagnetic radiation, in low earth orbit polymer materials may also be subjected to atomic oxygen particle radiation, which will result in direct oxidation of the polymer (3).

Thus, polymeric materials for space applications must exhibit a resistance to radiation damage by UV and atomic oxygen. One class of materials which may have this characteristic are the polyimides.

Polyimides are prepared from the reaction of a tetracarboxylic acid dianhydride with a phenylene diamine. Ring opening of the dianhydride readily occurs resulting in the formation of a polyamic acid. The polyamic acid was casted onto a glass plate and cured over night at 300° C to achieve maximum imidization (4).

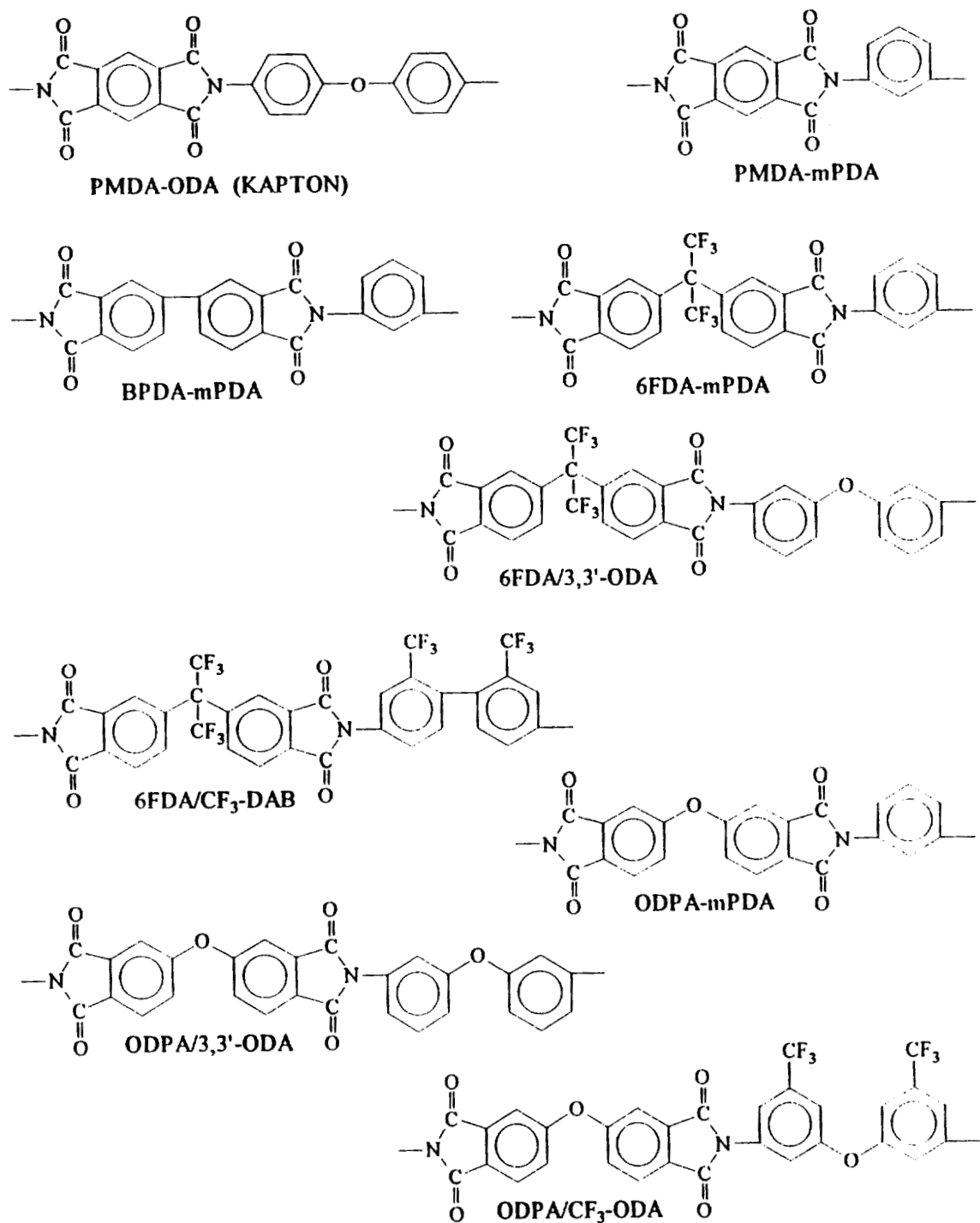


Figure 1: The chemical structures of polyimides.

As part of a materials evaluation program for space applications, we have studied the effects of UV induced degradation processes in eight different polyimide films prepared from different dianhydrides and diamines (see Fig 1). Weight loss due to photochemical degradation in an oxidising environment was also determined for comparison with thermal degradation. The study involved the photogeneration of radical species in the polymer

matrices as the initial steps in the degradation process. In this paper molecular level information for the initial stages of the photodegradation processes obtained from ESR, FTIR and UV-Visible spectroscopies will be discussed. The synergistic effect of UV radiation in air on polyimide surfaces, assessed using X-ray Photoelectron Spectroscopy (XPS) will be also considered.

EXPERIMENTAL

The polyimide films were exposed to unfiltered UV radiation. The light source used in this study was an Oriel high power mercury/xenon lamp with an output intensity of 9.1 mW/cm². The high energy UV wavelength cut off point was about 240 nm. Films irradiated with this lamp were studied using UV/Visible and FTIR spectroscopies, weight loss measurements and XPS spectroscopy.

For the ESR studies, the polyimide films were irradiated in situ in the ESR cavity using a system of lenses and mirrors to focus the radiation on the sample, and a water filter was used to eliminate the infrared radiation which could otherwise cause heating of the sample.

RESULTS AND DISCUSSIONS

UV-Visible Spectroscopy:

The UV-Visible spectra of the un-irradiated polyimides showed a large blue shift from the spectrum of Kapton, see Fig 2, with a strong absorption occurring at wavelengths below 400 nm. The reduction in colour of the polyimide films compared to Kapton can be attributed to the effective disruption of the charge transfer complex, giving the polyimides an almost colourless appearance, as in the case of the 6FDA polyimide (5).

It has been recognised that the charge transfer complex governs the colour, thermoplastic flow, dielectric constant and even the UV stability of linear aromatic polyimides (6). In Kapton, both of the imide linkages are attached to the central aromatic ring of the pyromellitic acid, which becomes electron deficient due to the electron withdrawing effect of the four adjacent carbonyl groups. On the other hand, the diamine phenyl rings become electron rich due to electron donating effects of the lone pair of electrons on the nitrogen and the oxygen of the diphenyl ether (ODA) group (7). This relationship causes polarisation and consequently formation of an intramolecular charge transfer complex between the polymer chains (8, 9).

In order to reduce the colour of polyimide films, several approaches have been employed to disrupt the formation of the charge transfer complex in those

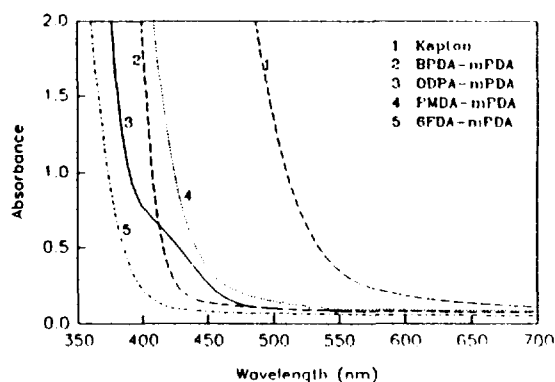


Figure 2: The UV-Visible absorption spectra of polyimides

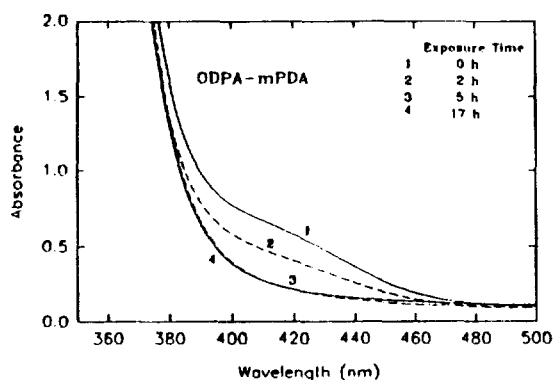


Figure 3: The changes in the UV-Visible absorption spectra with irradiation time of ODPDA-mPDA polyimide

decreases the electron affinity of the polyimides based on this anhydride, the introduction of a bulky group, such as CF_3 , and the location of the imide groups on different aromatic rings, as in the case of BPDA (see Fig 1). The effects of these strategies is evident in the UV absorption spectrum of PMDA-mPDA polyimide film, for example, which showed a substantial blue shift from Kapton. This behaviour could be explained by the fact that *m*-phenylene diamine in the PMDA polyimide causes much less polarisation than the ODA in Kapton, despite both imide linkages being attached to the same central aromatic ring (5, 6).

An important feature of the UV-Visible spectra of the polyimide films is their high absorption in the UV region. It has been estimated by Von Sonntag et al. (12) that for the aromatic polyimides the penetration depth of UV radiation is only about 10 nm for a 95% reduction of the UV intensity. It could therefore be argued that UV irradiation of these polyimide films would result extensively in surface degradation, leaving the bulk of the material intact.

With the exception of ODPDA based polyimides, the UV absorption spectra of the polyimides become slightly red shifted upon exposure to UV radiation in air. This shift may be attributed to the formation of an oxidised species, such as carbonyl groups, on the surface of the films. ODPDA polyimides showed a small hump in the visible region of the absorption spectrum before exposure to UV radiation, which could be associated with the oxygen bridge in the dianhydride moiety, (see Fig 3). Interestingly, the hump disappeared after approximately 2 h of exposure to UV radiation, then a slight red shift appeared after 5 h exposure, as observed with the other polyimides. This would indicate that the ODPDA polyimides may initially undergo chain scission which disrupts the charge transfer complex, and results in the initial blue shift, then upon further irradiation, the photo-oxidation process causes the red shift through formation of carbonyl groups on the surface.

ESR Studies:

Samples of the polyimides in quartz tubes were irradiated at room temperature in vacuum and in air using a high power mercury/xenon lamp.

polymer systems. The use of bulky groups and kinks along the polymer chain are two commonly used approaches by making it physically difficult for the polymer chains to pack close enough to each other to allow the complex to form (10). Furthermore, the introduction of electron withdrawing groups in the diamine and electron donating groups in the dianhydride decreases the charge separation in the polymer, and consequently reduces the possibility of charge transfer complex formation (11). Examples of these approaches are the introduction of oxygen bridges in the dianhydride, as in the ODPDA, which

Typical ESR spectra of the radicals formed on the exposure of the polyimides to UV radiation in vacuum and air are shown in Fig 4a and 4b respectively. The free radical concentration for the polyimides changes substantially upon UV irradiation in vacuum to produce a symmetrical ESR signal having a g value of 2.004 and a peak-to-peak line width of 8 G. Both the g value and the line width are somewhat larger than those typical of a carbon centred free radical ($g = 2.003$ and $\Delta H_{pp} = 3$ G respectively) (13). The slightly larger g value in the polyimides may be associated with unpaired electrons that are delocalised in the aromatic rings containing nitrogen and oxygen, since the interaction of unpaired electrons with nitrogen and oxygen generally causes the g value to increase, due to their larger spin-orbit coupling constant (14). However, from the ESR spectra alone it is not possible to assign the initial bond cleavage, but it has been postulated by George et al. (13), and later by others (15), that one of the initial photochemical reactions is cleavage of the imide linkage, which contains the comparatively weak C-N bond.

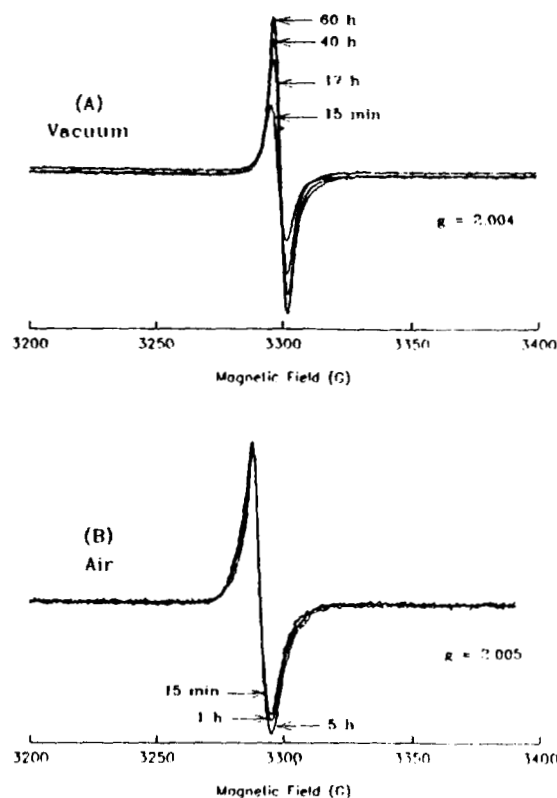


Figure 4: The ESR spectra of BPDA-mPDA polyimide exposed to UV radiation in vacuum (A) and air (B).

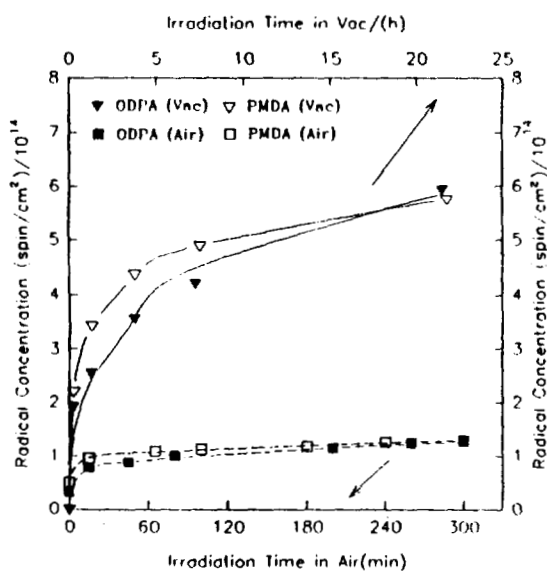


Figure 5: The changes in radical concentration of polyimide films exposed to UV radiation in air and vacuum.

The ESR spectra of polyimides irradiated in an oxygen environment are different from those formed for vacuum irradiation. Samples irradiated in air produced an asymmetric ESR signal shifted to a lower magnetic field, with a g value of 2.005 and a line width of about 14 G, see Fig 4b. It was also noticed that the rate of radical formation for polyimides irradiated in the presence of oxygen increased by 2 fold over that for the polymers irradiated in vacuum (see Fig. 5). Moreover, the asymmetric shape of the ESR spectra of polymers irradiated in air suggest that oxygen plays an important role in the radical formation process, and that oxygen centred radicals contribute to the observed spectrum. Therefore, the ESR spectrum in Fig. 4b could result from radicals being present in both photo-oxidised and

unphoto-oxidised forms (16). That is, UV irradiation of the polymers in air results in an initial bond cleavage producing radicals on the surface of the films, and these radicals subsequently undergo reaction with oxygen to produce peroxy and alkoxy radicals, which give rise to the oxidised species observed in the UV spectra of the films.

It is worth mentioning that upon irradiation of Kapton in an oxygen environment, a relatively high concentration of radicals are produced compared with the concentrations observed for the other polyimides; see Fig 6. It is also worth noting that un-irradiated Kapton exhibits a weak asymmetrical ESR signal, with characteristics similar to those found for Kapton following irradiation in an oxygen environment. George et al. (13) claimed that most of the radicals (peroxy and alkoxy) formed by UV irradiation of Kapton in air are located at, or very near, the surface of the polymer, while most of the radicals formed by UV irradiation in vacuum are located at a greater depth in the polymer. This claim was demonstrated by the observed decrease in the ESR signal intensity (60-70%) for polymers irradiated in air, followed by soaking of the polymer film in water and or acetone (13, 17).

Although the mechanism for formation of these complex surface radicals is unresolved at present, it is clear from the ESR spectra that the radicals observed after irradiation in the presence of oxygen are created at a substantially faster rate than those observed after irradiation in the absence of oxygen. Generally, it can be seen from Fig 5 that the radical concentration rapidly reaches a plateau on irradiation in oxygen (after about 1 h). These observations could be explained either by the formation of a stable photo-oxidised surface, which prevents further radical formation, or by the depletion of surface radicals via an ablative degradation process.

A transmission FTIR study of the changes in the films on irradiation in air showed that the intensity of all of the absorption peaks decreased with irradiation time, and that no significant new peaks were formed. This observation is consistent with the second of the postulates above. Irradiation in air results in the formation of photo-oxidised species which are lost from the surface by volatilisation. This means that the concentration of the photo-oxidised species does not build up on the surface, so that no significant absorption from new function groups appears in the IR spectra, and that, as the film surface is eroded away, the film thickness decreases and the intensities of the observed absorption peaks decreases with irradiation time. Hoyle and coworker (18) observed a similar decrease in the intensity of the FTIR absorption spectra of polyimides irradiated in air. These observations are also supported by the observed weight loss in the films with irradiation time. Kapton films exposed to a low earth orbit environment on the leading edge of the

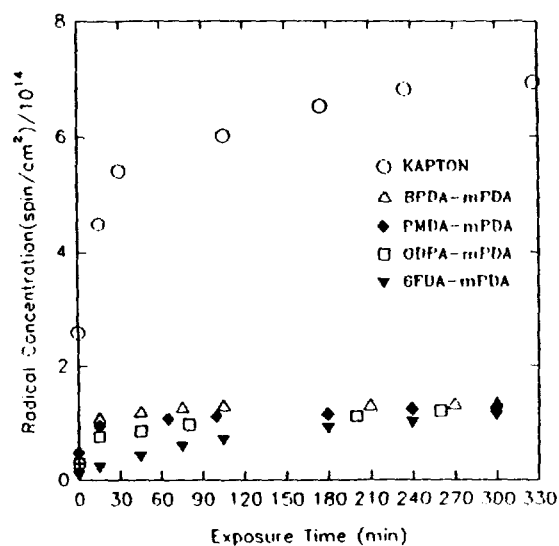


Figure 6: The effect of UV exposure time in air on the radical concentration of Kapton and polyimides.

LDEF showed no new IR absorption peaks, no peaks were missing and that there were no significant shifts in the frequency of various bands (19, 20). The films were also eroded by the environment. This is consistent with our observations for UV irradiation in air.

The radical intermediates formed on irradiation are thermally stable and the ESR signal intensity decays only slowly over an extended period of time. One week after irradiation, only 20% of the radicals have decayed. The slow decay rate might suggest the involvement of various aromatic type radicals, which could be produced either in the absence or the presence of oxygen. This slow radical decay could explain the post irradiation effects observed for polyimide samples after retrieval from LDEF.

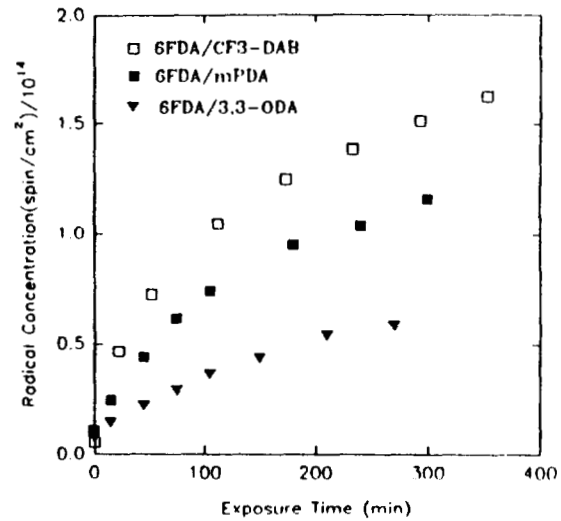


Figure 7: The changes in radical concentration of 6FDA polyimides with UV exposure time in air.

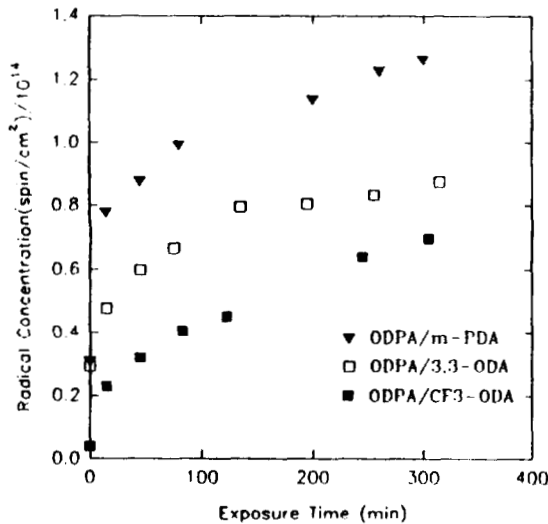


Figure 8: The changes in radical concentration of ODPA polyimides with UV exposure time in air.

Irradiation of polyimide films in air could provide valuable information on the relative UV stability of polymers compared to Kapton. A close examination of the ESR results of various polyimides revealed that polymers exhibiting a lower radical concentration upon exposure to UV radiation in air are more susceptible to oxidation, and undergo faster erosion and material loss by volatilisation. The build up in the radical concentration with time for two series of polyimides with the same dianhydride and various diamines are shown in Figs 7 & 8. These observations are consistent with the behaviour expected for an ablative degradation process.

A simplified free radical chain mechanism for the oxidation of polyimides can be proposed to explain the observed results, in which peroxy and/or alkoxy radicals are formed. These radicals could be formed by direct reaction of oxygen with the radicals produced either on the aromatic rings or at single bonds in the polymer chain (13). The saturation of the radical concentration after long irradiation times could be explained by radical recombination, or by radical loss by volatilisation, in the case of irradiation in the presence of oxygen.

Irradiation of polyimide films in air could provide valuable information on the relative UV stability of polymers compared to Kapton. A close examination of the ESR results of various polyimides revealed that polymers exhibiting a lower radical concentration upon exposure to UV

Surface Analysis:

Surface analysis of polyimide films were conducted using XPS spectroscopy. A typical XPS multiplex spectrum (at 25 eV pass energy) for the C1s, O1s and N1s regions of an un-irradiated polyimide film is shown in Fig. 9 for BPDA-mPDA. The theoretical ratios of O1s/C1s and N1s/C1s were in agreement with the measured ratios, which suggests that there is no significant contamination of the polymer surface. The C1s region exhibits two distinct peaks at 285 eV and 288.5 eV, which represent the C-C plus C-H and C-O binding energies respectively. The C-N band, which is less sensitive in the XPS analysis than the C-C band, occurs at 285.2 eV. It is over shadowed in intensity by the stronger C-C peak. For the fluorinated polyimides, an additional peak arises in the C1s region for the C-F binding energy, which appears at 292.5

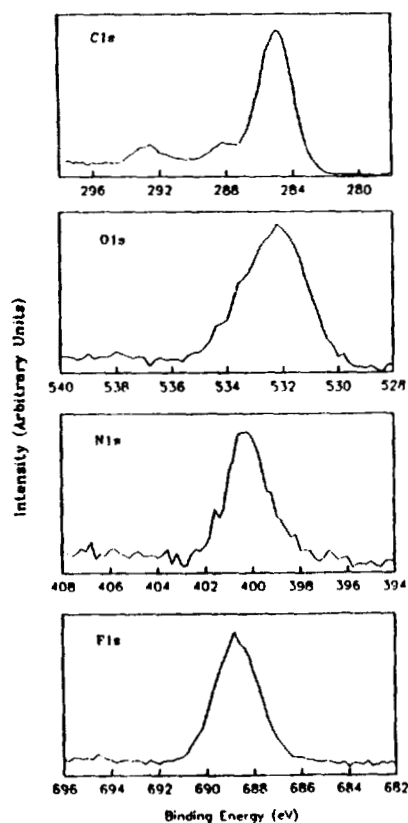


Figure 10: XPS spectra of unirradiated 6FDA/3,3'ODA polyimide film.

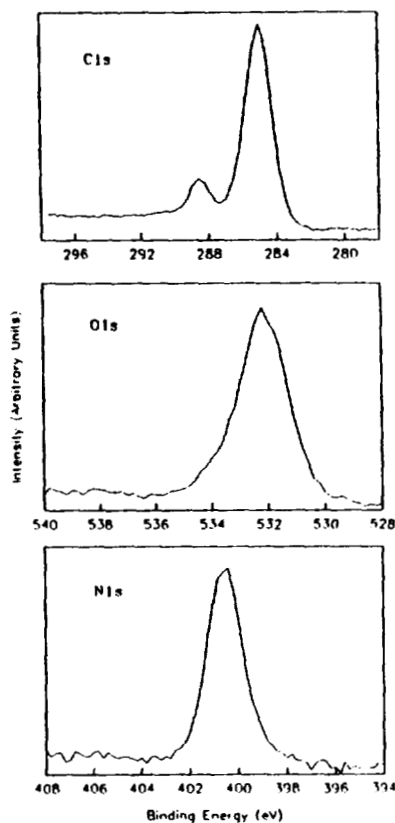


Figure 9: XPS spectra of unirradiated BPDA-mPDA polyimide film.

eV. Fig 10 shows the C1s, O1s, N1s and F1s regions of the un-irradiated 6FDA-3,3'ODA polyimide.

Exposure of the polyimide films to UV radiation in the presence of oxygen resulted in oxidation of the polymer surface. Figs 11 & 12 below show the changes in the C1s and O1s regions due to exposure to UV radiation in air. It is clear from Fig. 11 that the C1s region has changed substantially after exposure. The intensity of the C-O binding energy peak has increased relative to that of the C-C peak, which indicates an increase in the surface oxidation. Comparing the O1s

region of the exposed polymer films with the same region of the unexposed polymer, (Fig 12) shows a broadening of the O1s peak, which suggests the presence of different oxidation species on the polymer surface, while the N1s and F1s peaks do not show any significant change. Fig 13 shows a plot of the changes in O1s/C1s ratios with irradiation time for 6FDA-mPDA in comparison to Kapton. The ratio of O1s/C1s increased sharply after only a few minutes of exposure to UV radiation in air, and then reached a plateau for both polymers after about 30 minutes. This supports the proposal based on the FTIR and the ESR studies that there is continual degradation of the surface during irradiation in the presence of oxygen, producing volatile low molecular weight species. On the other hand, examination of

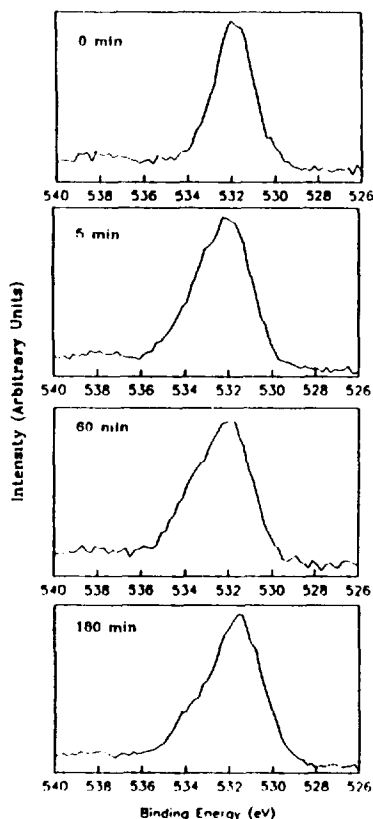


Figure 12: XPS spectra (O1s region) of 6FDA-mPDA polyimide film exposed to UV radiation in air.

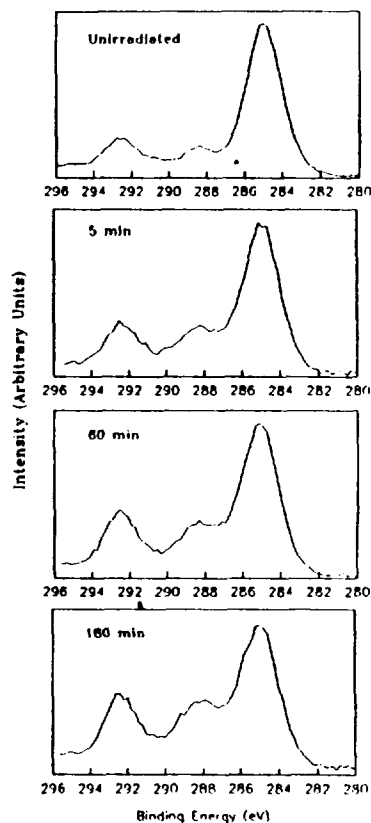


Figure 11: XPS spectra (C1s region) of 6FDA-mPDA polyimide film exposed to UV radiation in air.

the changes in the N1s/C1s ratios reveals a concomitant increase in this ratio, which could be related to a reduction in the carbon atom concentration on the polymer surface. This could occur due to surface ablation (21) and loss of low molecular weight oxidised species, such as CO and CO₂, from the polymer surface. Furthermore, it has been reported by Srinivasan et al. (17) that polyimide film exposed to UV radiation for 10 minutes and then soaked for 1 h in water showed a decrease in the O1s/C1s ratio to essentially the value for the un-irradiated polyimide, indicating that the highly photo-oxidised species are effectively removed by dissolution.

The increase in the O1s/C1s ratios on the surface of the polymers can only be accounted for by the opening of the aromatic

rings during photo-oxidation. Similar aromatic ring opening during photo-oxidation has been reported for other polymers, including polystyrene (22). These reactions in polystyrene have been reported to involve the complexation of oxygen with surface aromatic groups and the subsequent photolysis of this complex (23). A similar mechanism could apply in the polyimides.

Contact Angle Measurements

Further evidence of surface oxidation was obtained from contact angle measurements. The water/polymer contact angles are sensitive to the surface chemistry and therefore provide information pertaining to the surface chemistry, before and after UV exposure in air. After 15 hours UV exposure, the contact angles for all the polyimides studied, except ODPA/3,3'ODA, have diminished considerably (Table 1), indicating that the surface had become more hydrophilic, and therefore more oxidised.

The water/polymer contact angles were referenced against teflon/water, which agreed well with the literature value of 112 degrees.

It should be noted that ODPA/3,3'-ODA polyimide initially had a small contact angle. This result may be due in part to the absence of fluorine on the surface, although Kapton also lacked fluorine and had a significantly larger contact angle. Errors from inconsistencies in the size of the drop may have been a contributing factor on this result. After irradiation of the ODPA/3,3'-ODA polyimide, there was a measured increase in the contact angle. This observation was inconsistent with the other polyimides, and it was thought that surface roughening may have been responsible for this result.

Table 1: Measured water/polyimide contact angles

Polymer	Contact Angles (degrees)	
	Before Exposure	After Exposure
6FDA/3,3'-ODA	72	54
6FDA/CF ₃ -DAB	75	46
ODPA/3,3'-ODA	31	35
ODPA/CF ₃ -ODA	69	25
Kapton	63	45
Teflon	113	N/A

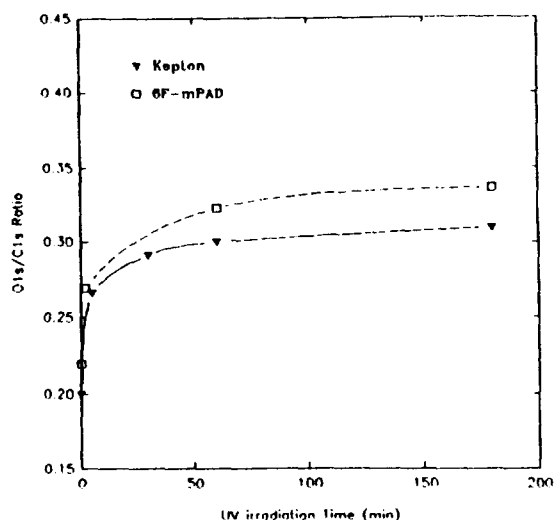


Figure 13: The changes in the O1s/C1s ratio of Kapton and 6FDA-mPDA polyimide exposed to UV radiation in air.

CONCLUSIONS

In summarising the results of the present investigation, we have shown that polyimides are highly absorbing in the UV region of the spectrum. Therefore, it can be argued that UV irradiation of these polyimides results extensively in surface degradation, leaving the bulk of the polymer unchanged. Furthermore, the stability of polyimides can be associated with their chemical structure and their capacity for forming a charge transfer complex.

The ESR spectra of polyimides irradiated in vacuum reveals the formation of stable radicals which give a singlet ESR spectrum, with a g-value and line width somewhat larger than those typical of carbon-centred free radicals. This suggests that the unpaired electrons are delocalised over the aromatic rings containing nitrogen and oxygen, which are responsible for the slight increase in the g-values due to their larger spin-orbit coupling constant. The primary photodegradation mechanism was believed to involve the cleavage of the imide linkages at the comparatively weak C-N bonds. The radical concentration for irradiation in vacuum increased rapidly to a plateau for long exposure times.

The ESR spectra of polyimides irradiated in air produced an asymmetric signal shifted to a lower magnetic field with a higher g-value and a higher line width than that for the polyimides irradiated in vacuum. This ESR signal was attributed to oxygen centred radicals of the peroxy and/or alkoxy type. The rate of radical formation was two fold higher than for vacuum irradiation, and reaches a plateau after only one hour. This suggests a continuous depletion of radicals on the surface via an ablative degradation process. FTIR and weight loss studies supported this postulate. Furthermore, polyimides exhibiting low radical concentration upon irradiation in air are more susceptible to oxygen attack, and have higher rates of degradation than those producing a high radical concentration. This could be due to the fast depletion of radicals from the polymer surface via volatilisation.

Further supporting evidence for the proposed ablation mechanism comes from an XPS study of the surface. The intensity of the C-O binding energy peak increased substantially relative to that of C-C during irradiation, which indicated an increase in the surface oxidation. Furthermore, the broadening of the O1s peak after exposure to UV radiation in air suggested the presence of different oxidised species on the polymer surface. The initial sharp increase in the O1s/C1s ratio with exposure time, and then the levelling off after about 30 minutes consistent with the postulate of an ablative degradation process. The N1s/C1s ratio showed a similar behaviour, which could only be related to a reduction in carbon atom concentration on the polymer surface. This can only occur by opening of the aromatic rings and the loss of low molecular weight oxidised species from the polymer surface.

REFERENCES

- 1- A.E. Stiegman, D.E. Brinza, M.S. Anderson, T.K. Minton, and E.G. Liang, Jet Propulsion Laboratory Publication, 91-10, California Institute of Technology; Pasadena, California, USA.
- 2- D. Heath, and M. Thekaekara, 1977, *The Solar Output and its Variation*, Colorado

Associated University Press, Boulder, CO, 193.

- 3- L.E. Murr & W.H. Kinard, *American Scientist*, 81, 1993.
- 4- A.I. Bouise, *J. Appl. Polym. Sci.*, 1986, 32, 4043.
- 5- A. K. St. Clair and W. S. Slemp, 1991, *23rd International SAMPE Technical Conference*.
- 6- T.L. St. Clair, 1990, in *Polyimides*, D. Wilson, H.D. Stenzenberger, P.M. Hergenrother, Eds., Blackie Glasgow.
- 7- R.A. Dine-Hart and W.W. Wright, *Makromolek. Chem.*, 1971, 143, 189.
- 8- H. Ishida, S.T. Wellinghoff, E. Baer and J.L. Koenig, *Macromolecules*, 1980, 13, 826.
- 9- E.D. Wachsman, P.S. Martin and C.W. Frank, 1989, in *Polymeric Materials for Electronic Packaging and Interconnection*, ACS Symposium Series 407, J.H. Lupinski and R.S. Moore, Eds., Am. Chem. Soc., Washington, D.C., P. 26.
- 10- A.K. St. Clair, T. L. St. Clair and K. I. Shevket, 1984, *Proceedings of the ACS Division of polymeric materials: Science and Engineering* vol. 51, p. 62.
- 11- A.K. St. Clair & T.L. St. Clair, 1986, US Pat. 4595548.
- 12- I.C. Lewis and L.S. Singer, 1981, *Chemistry and Physics of Carbon*, Marcel Dekker, New York, 17, 1.
- 13- M. A. George, B.L. Ramakrishna, & W.S. Glaunsinger, *J. Phys. Chem.*, 1990, 94, 5159.
- 14- C. Von Sonntag, H.D. Schuchmann, 1977, *Adv. Photochem.*, 10, 6784.
- 15- T.K. Minton, S.Y. Chung, D.E. Brinza, & T.A. More, 1993, *3rd LDEF Post Retrieval Symposium Abstracts*.
- 16- B. Ranby and J.F. Rabek, 1977, *ESR Spectroscopy in Polymer Research*, Springer-Verlag, New York.
- 17- S. Lazare, P.D. Hoh, J.M. Baker and R. Srinivasan, *J. Am. Chem. Soc.* 1984, 106, 4288.
- 18- C.E. Hoyle and E.T. Anzures, *J. Appl. Polym. Sci.* 1991, 43, 1.
- 19- P.R. Young, W.S. Slemp and C.R. Gautreux, 1992, *37th International SAMPE*, Anaheim, CA, March, 9-12.
- 20- P.R. Young and W.S. Slemp, 1992, *LDEF Materials Workshop 91*, NASA Conference Publication 3162, part 1, 357.
- 21- C.E. Hoyle, D. Creed, R. Nagarajan, P. Subramanian and E.T. Anzures, *Polymer*, 1992, 33, 3162.
- 22- R.C. Clough, M. Kristiansen and P.R. Ogilby, *Macromolecules*, 1990, 23, 2698.
- 23- D.J. Carlsson, R. Brousseau, C. Zhang and D.M. Wiles, *Polym. Degrad. Stab.*, 1987, 17, 303.

Acknowledgment: We would like to acknowledge support of this work by the National Aeronautics and Space Administration (NASA), Langley Research Centre.

THE SURFACE PROPERTIES OF FLUORINATED POLYIMIDES EXPOSED TO VUV AND ATOMIC OXYGEN

John S. Forsythe, Graeme A. George, David J.T. Hill, James H. O'Donnell,
Peter J. Pomery and Firas A. Rasoul

Polymer Materials and Radiation Group
The University of Queensland
Queensland, 4072, Australia

ABSTRACT

The effect of atomic oxygen flux and VUV radiation alone and in combination on the surface of fluorinated polyimide films was studied using XPS spectroscopy. Exposure of fluorinated polyimides to VUV radiation alone caused no observable damage to the polymer surface, while an atomic oxygen flux resulted in substantial oxidation of the surface. On the other hand, exposure to VUV radiation and atomic oxygen in combination caused extensive oxidation of the polymer surface after only 2 minutes of exposure. The amount of oxidised carbon on the polymer surface indicated that there is aromatic ring opening oxidation. The changes in the O1s/C1s, N1s/C1s and F1s/C1s ratios suggested that an ablative degradation process is highly favourable. A synergistic effect of VUV radiation in the presence of atomic oxygen is clearly evidenced from the XPS study. The atomic oxygen could be considered as the main factor in the degradation process of fluorinated polyimide films exposed to a low earth orbit environment.

INTRODUCTION

A need exists for high temperature (200-300°C) stable, flexible polymeric film and coating materials that have high optical transparency in the 300-600 nm region of the solar spectrum for applications in space components, such as insulation blankets, solar cells and thermal control coating systems. Although several classes of polymers are available which are transparent and colourless, such as polyesters or aliphatic polyimides, many of these materials have limited long-term thermal stability. On the other hand, commercially available aromatic polyimides are thermally stable, however they have poor transparency in the visible region of the solar spectrum of interest for space applications. Furthermore, the transparency of these commercial polyimides is reduced dramatically after exposure to the space environment. Several series of linear aromatic polyimide films having maximum optical transparency have been prepared by St. Clair et al. (1). The optical transparency was achieved by using highly purified monomers and the incorporation of meta-linked diamines, bulky electron-withdrawing groups and flexible linkages into the molecular structure, in order to reduce the electronic interactions between polymer chains (2).

Spacecraft in low earth orbit are subjected to significant levels of high energy radiation, including UV and VUV wavelengths. The effects of UV radiation are enhanced over those at the surface of the earth, where the only incident wavelengths are greater than 290 nm. In low earth orbit the incident UV wavelengths extend below 290 nm into the VUV region, where the Lyman α emissions of atomic hydrogen occur at 121 nm. In addition to electromagnetic radiation, in low earth orbit polymer materials may also be subjected to

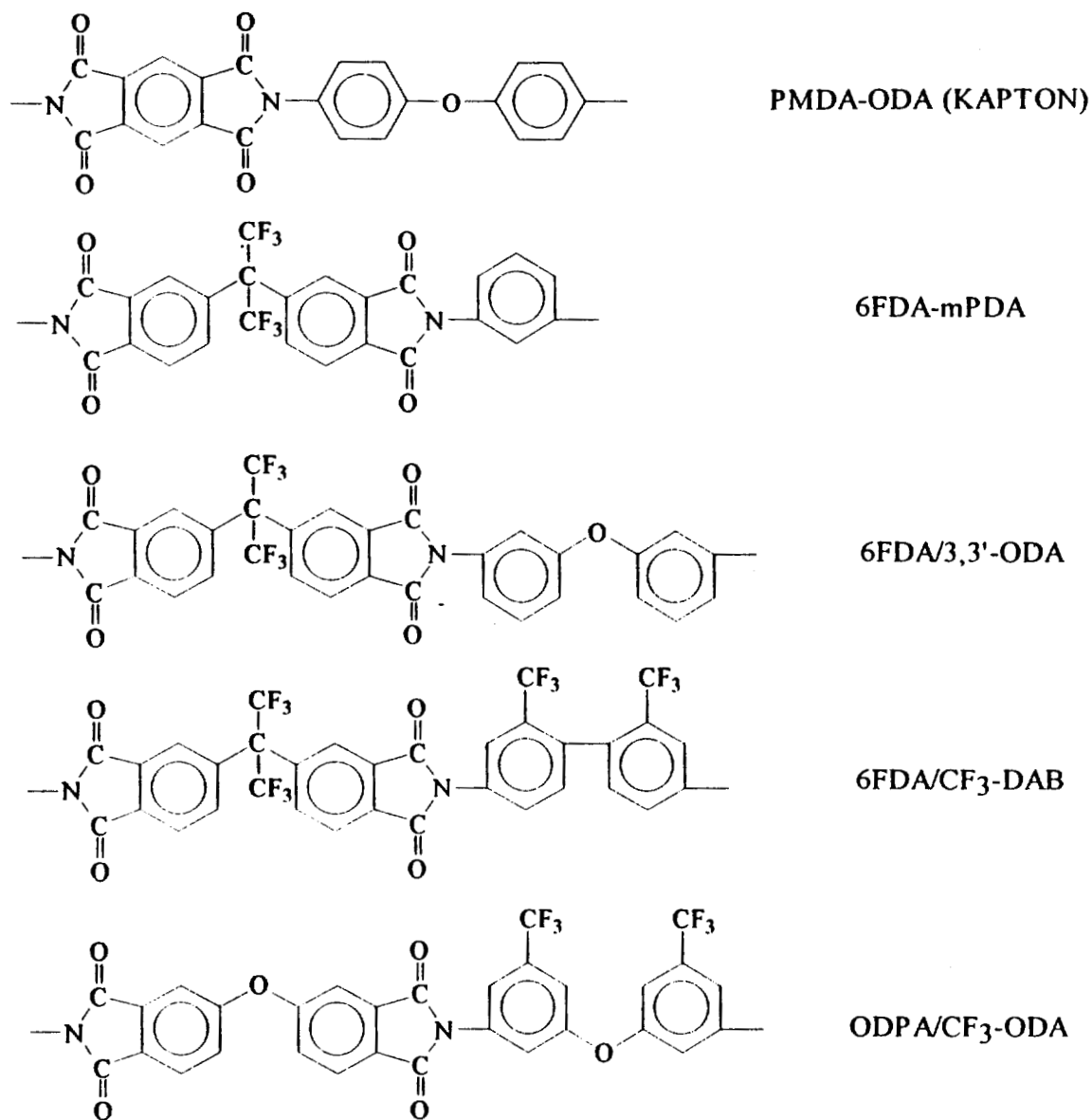


Figure 1: The chemical structure of fluorinated polyimides and Kapton.

bombardment by atomic oxygen, which will result in direct oxidation of the polymer. Thus polymeric materials for space applications must exhibit a resistance to damage by both VUV radiation and atomic oxygen attack.

As part of a materials evaluation program for space applications, we studied the effects of a simulated low earth orbit environment of VUV and atomic oxygen on a series of fluorinated polyimide films compared to a Kapton reference (see Fig. 1). The major objective of this paper is to assess the effect of atomic oxygen, VUV radiation alone and atomic oxygen and VUV radiation in combination on polyimides surfaces, by using X-ray photoelectron spectroscopy (XPS).

EXPERIMENTAL

Atomic oxygen and VUV radiation was generated in a specially designed oxygen plasma apparatus, by applying a radio frequency (RF) to oxygen molecules in a flowing system. Pressures of 0.2 torr were used in the apparatus and identical RF power and oxygen flow rates were used in each experiment. Irradiation of the fluorinated polyimide films by VUV in the absence of the atomic oxygen was

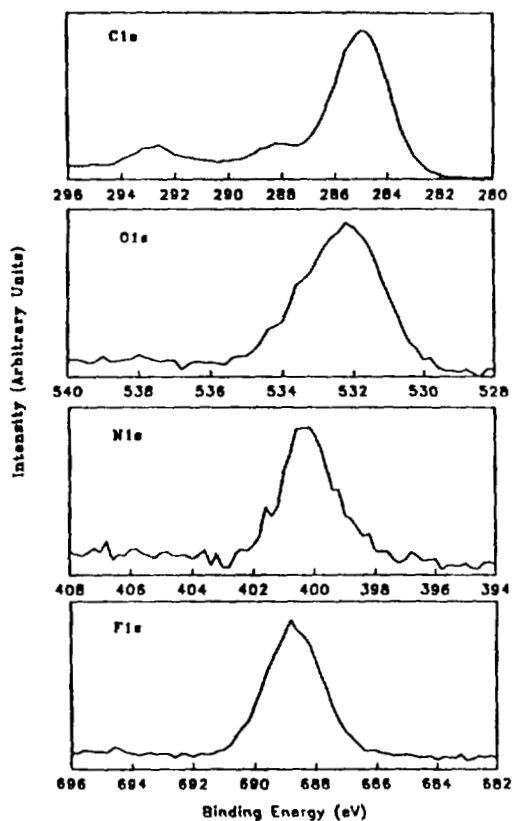


Figure 3: XPS multiplex spectra for C1s, O1s, N1s and F1s regions of unirradiated 6FDA/3,3'-ODA polyimide film.

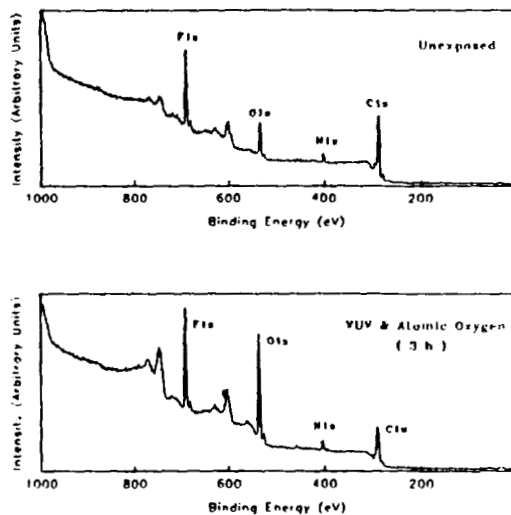


Figure 2: XPS survey spectra of fluorinated polyimide films before and after exposure to VUV and atomic oxygen.

achieved by the insertion of a MgF_2 window in front of the sample. Exposure of the films to atomic oxygen in the absence of VUV was accomplished by placing the films in a detachable side arm, where only the flow of atomic oxygen was allowed to reach the sample. The XPS spectra were obtained from a Perkin-Elmer PHI Model 560 ESCA/SAM multi-technique analysis system. Un-monochromated $\text{Mg K}\alpha_{1,2}$ (1253.6 eV) X-ray radiation source (400 watt, 15 KV) was used.

RESULTS AND DISCUSSION

Surface analyses of fluorinated polyimide films were conducted using XPS spectroscopy. Typical XPS survey spectra (at 100 eV pass energy) of irradiated and un-irradiated polymer films are shown in Fig 2. It is clearly illustrated from the irradiated polyimide film that the ratio of the O1s/C1s has changed substantially after exposure to VUV and atomic oxygen. The multiplex spectrum (at 25 eV pass energy) of un-irradiated polyimide film for the C1s, O1s, N1s and F1s regions are shown in Fig. 3 for 6FDA/3,3'-ODA in comparison to Kapton (Fig 4). The measured ratios of O1s/C1s, N1s/C1s and F1s/C1s were comparable with the theoretical values, which suggests no significant contamination of the polymer surface. The

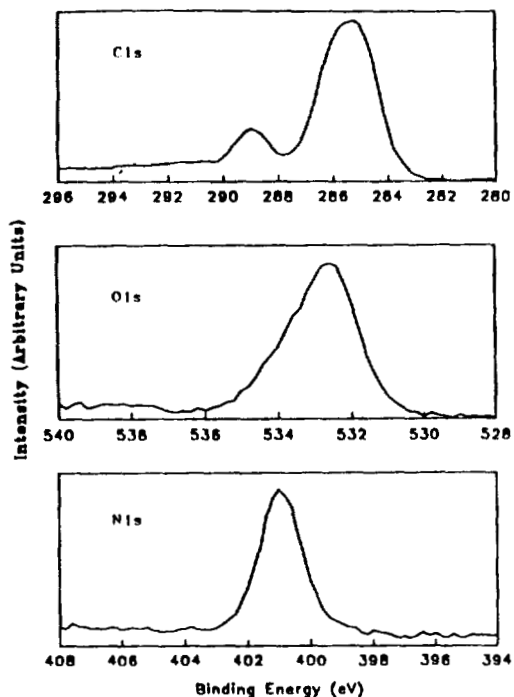


Figure 4: XPS multiplex spectra for C1s, O1s, and N1s regions of unirradiated Kapton.

binding energy peak has increased relative to that of C-C, which indicates an increase in surface oxidation. Comparing the O1s region of the exposed polymer film with the same region of the unexposed polymer, shows a broadening of the O1s peak, which suggests the possible presence of different oxidation species on the polymer surface, while the N1s and F1s peaks dose not show any significant change.

Fig. 7 shows a plot of the changes in O1s/C1s ratios with the irradiation time for four different fluorinated polyimide structures in comparison to Kapton. The ratio of O1s/C1s increased sharply after only a few minutes of exposure to VUV and atomic oxygen, and then rapidly reached a plateau for all five polymers after about 10 minutes. The rapid oxidation of the entire surface, and the plateau appearance of the O1s/C1s ratio after short time of exposure to VUV and atomic oxygen could be explained either by

C1s region exhibits three distinct peaks at 285 eV, 288.5 eV and 292.5 eV, which represent the C-C plus C-H, C-O and C-F binding energies respectively. The C-N group, which is less sensitive in the XPS analysis than C-C, occurs at 285.2 eV, and is over shadowed by the stronger C-C peak.

Exposure of fluorinated polyimide films to VUV radiation in the presence of atomic oxygen resulted in extensive oxidation of the polymer surface. Fig 5 shows the changes in the C1s, O1s, N1s and F1s regions due to exposure to VUV and atomic oxygen, while Fig 6 shows the XPS spectra of Kapton exposed to similar conditions. It is clear from Fig. 5 and 6 that the C1s region has changed dramatically after only 2 minutes of exposure. The intensity of the C-O

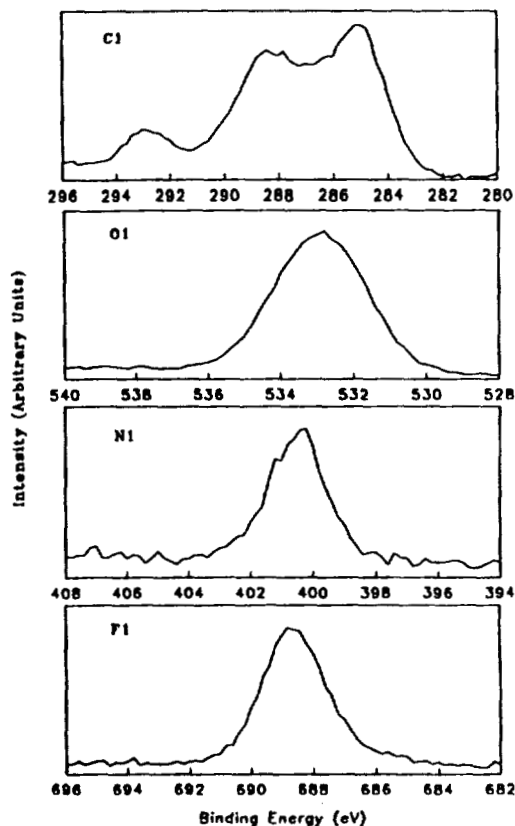


Figure 5: XPS multiplex spectra for C1s, O1s, N1s and F1s regions of 6FDA/3,3'-ODA polyimide film exposed to VUV radiation and atomic oxygen.

formation of an oxidised protective layer which is resistant to further oxidation, or by a simultaneous oxidation and ablation processes affecting the polymer surface. The results obtained from the FTIR, ESR and UV absorption spectroscopies suggested that there was a continuous ablation of the polymer surface, which agreed with the latter postulate (3). The initially formed oxidised species on the polymer surface undergo further reaction upon exposure to UV radiation to produce low molecular weight oxidised products, which are removed from the surface by volatilisation. This would result in a continuous renewal of the surface, with a continuous weight loss by erosion.

On the other hand, examination of the changes in the N1s/C1s and the F1s/C1s ratios, revealed a similar rapid increase and levelling off, which could only be related to a reduction in the carbon atom concentration on the polymer surface. This must occur by surface ablation and loss of low molecular weight oxidised species from the polymer surface.

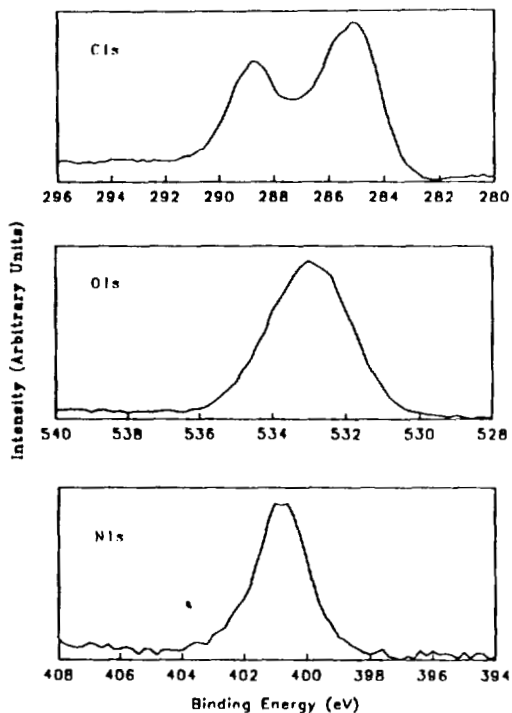


Figure 6: XPS multiplex spectra for C1s, O1s and N1s regions of Kapton exposed to VUV radiation and atomic oxygen.

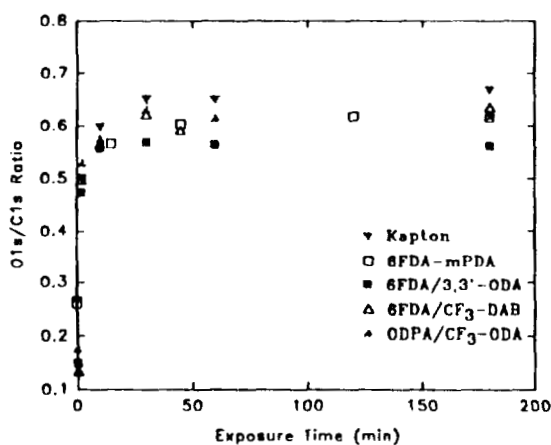


Figure 7: The O1s/C1s ratio of fluorinated polyimide films exposed to VUV radiation and atomic oxygen.

the polymer surface at equilibrium was greater than that for any other carbon functional group. This level of oxidation strongly suggested a ring opening mechanism for the aromatic groups in the polyimides exposed to VUV and atomic oxygen.

Kapton film specimens which flew on the space end of the LDEF and received 5.8 years of

FTIR and weight loss experiments of irradiated polymers later confirmed that an ablative type mechanism is responsible for the degradation of polyimides exposed to a VUV and atomic oxygen environment. Furthermore, it has been reported in the literature that Kapton exposed to UV radiation in air for 10 minutes and then soaked for 1 h in water, showed a decrease in the O1s/C1s ratio to essentially the value for the un-irradiated Kapton, indicating that the highly photooxidised species are effectively removed by washing (4,5). These results reinforce our speculation that surface oxidation and ablation must be the main degradation process for polyimides. Interestingly, it was observed that the oxidised carbon concentration present on the

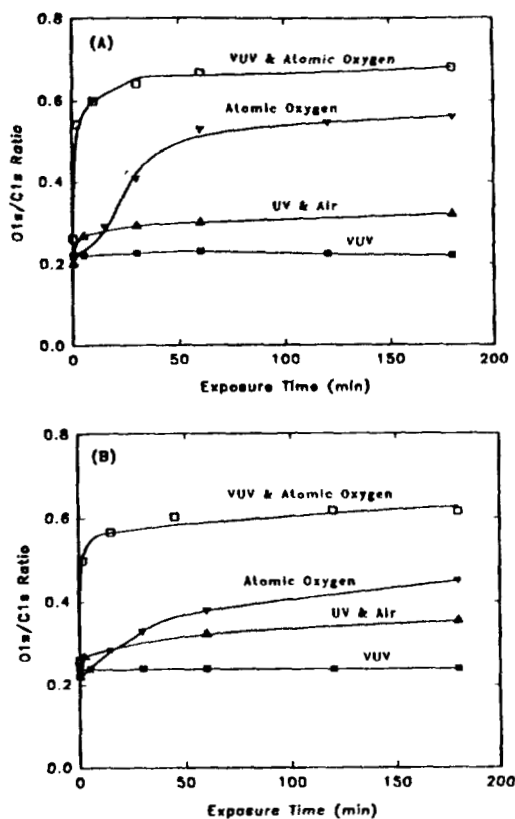


Figure 8: The change in the O1s/C1s ratio with exposure time of Kapton (A) and 6FDA-mPDA polyimide film (B).

could act as protective layer against further degradation of polyimide films exposed on the LDEF (11).

Exposure of polyimides films to UV or VUV radiation alone caused minimal or no damage to the polymer surface (see Fig 8), while atomic oxygen causes extensive damage to the polymer surface. The XPS analysis of the fluorinated polyimide films showed that the atomic oxygen flux produces a significant amount of surface oxidation. This was evidenced by an increase in the C=O peak at 288.1 eV and the C-O peak at 285.6 eV. Generally, the XPS spectra in the C1s region showed clearly that polymers exposed to VUV and atomic oxygen were characterised by different oxidised species from the polymers exposed to atomic oxygen alone (see Figs 9

exposure to LEO environment, with the atomic oxygen flux perpendicular to the edge of the film and parallel to its surface, showed a significant decrease in light transmission which was attributed to surface roughening and a diffuse appearance (6). The XPS spectra of LDEF exposed polyimide film showed a drastic increase in oxygen and also the appearance of a distinct silicon peak. Silicon was believed to be associated with the surface contamination of the spacecraft. Whiteside and coworkers (7) related the increase in the oxygen peaks with the silicon contamination. Young suggested that polyimides which received exposure on the LDEF showed surface erosion, however, the presence of silicon on the polymer surface could lead to the formation of silicate upon exposure to atomic oxygen. Silicate is known to be an effective barrier to atomic oxygen (8,9,10), and

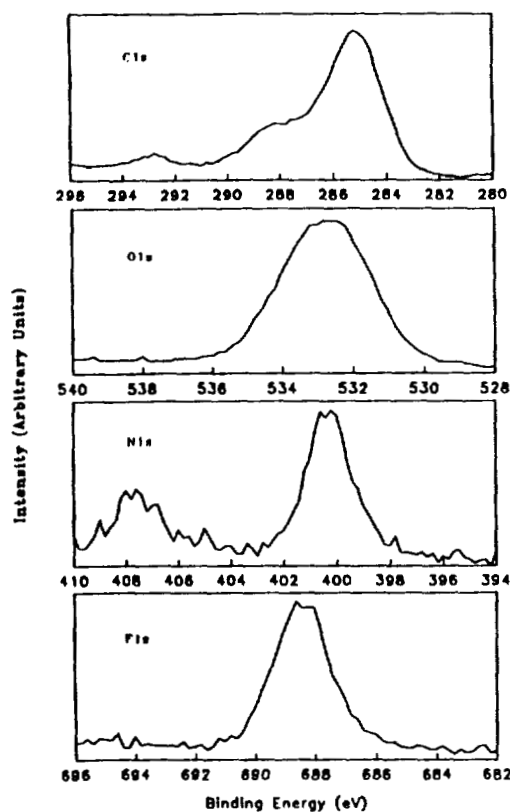


Figure 9: XPS multiplex spectra for C1s, O1s, N1s and F1s regions of 6FDA,3,3'-ODA polyimide film exposed to atomic oxygen flux.

and 10 for 6FDA/3,3'-ODA and Kapton respectively). Consequently, the O1s region peak in the atomic oxygen exposure experiment is broad and occurs at a slightly higher binding energy than the peak obtained for the combined VUV and atomic oxygen, which confirmed the formation of different oxidation species. The XPS spectrum in the N1s region of polyimides exposed to atomic oxygen alone also showed two distinctive peaks with binding energies of 400.2 and 407.8 eV. The peak at 407.8 disappeared after about 1 h of further exposure to the atomic oxygen flux. From the binding energy, the transient species was identified as -NO_2 (12), which suggested that the imide linkage was susceptible to oxidation. The susceptibility of the imide group in Kapton to atomic

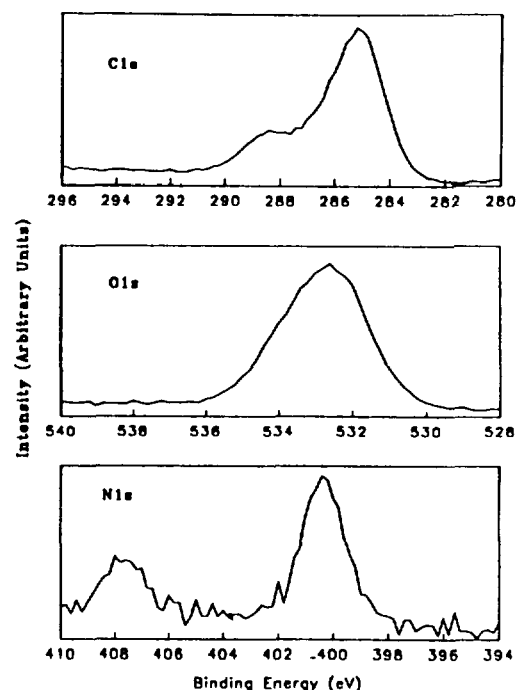


Figure 10: XPS multiplex spectra for C1s, O1s and N1s regions of Kapton exposed to atomic oxygen flux.

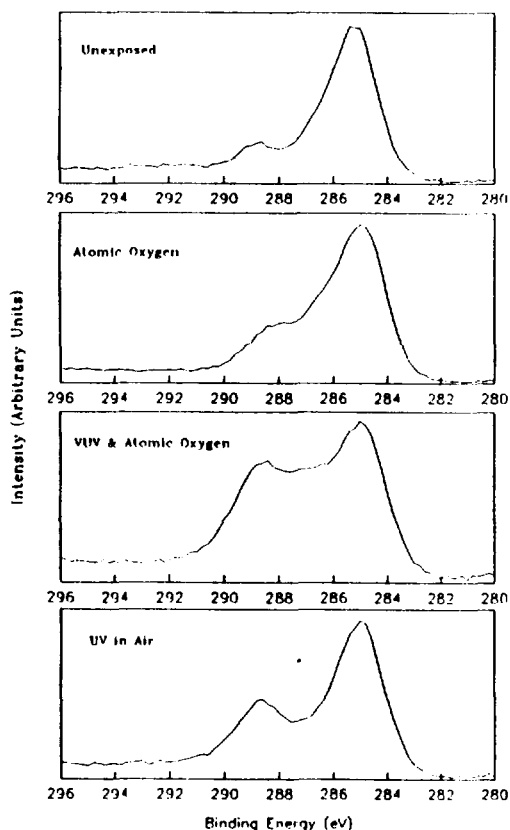


Figure 11: XPS multiplex spectra for C1s regions of ODPA/3,3'-ODA polyimide films exposed to different conditions.

oxygen attack has been suggested by others (13) and recently demonstrated by Minton et al. (14).

The above results suggest that atomic oxygen could be considered to be the main factor in the degradation process of polyimides films exposed to a low earth orbit environment. However, there is evidence for a synergistic effect of VUV radiation in the presence of atomic oxygen, which increases the damage to the polymer surface by photodegradation of oxidised species. Fig 8 clearly illustrates the effect of different exposure conditions on the O1s/C1s ratios of the fluorinated polyimide films in comparison to Kapton. The synergistic effect of VUV and atomic oxygen is obvious, while there is minimal or no observable damage of the polymer surface as result of exposure to either UV or VUV radiation alone. Consequently, atomic oxygen alone causes significant damage to the polymer surface, however the nature of the oxidation species are different from those which appear from the exposure to VUV and atomic oxygen in combination (Figs 11 & 12).

The effect of UV irradiation in air on the O1s/C1s is also presented in Fig 8 for comparison (3). The XPS spectra of the C1s and the O1s regions of polymer films exposed to UV in air suggested that the formation of the C=O group is more favourable, while polymers exposed to atomic oxygen alone or VUV and atomic oxygen in combination showed a more intense peak in the region of C-O, see Figs 11 & 12.

CONCLUSIONS

The effect of an atomic oxygen flux and VUV radiation alone and in combination on the surface of fluorinated polyimide films was studied using XPS spectroscopy. Exposure of fluorinated polyimide films to VUV radiation in the presence of an atomic oxygen flux resulted in extensive oxidation of the polymer surface after only 2 minutes exposure. The amount of oxidised carbon on the polymer surface indicated that there is aromatic ring opening during oxidation. The ratio of O1s/C1s reached a plateau after a few minutes of exposure, which suggested that an ablative degradation process is highly favourable. The variation in the N1s/C1s and F1s/C1s ratios confirmed this postulate.

Exposure of fluorinated polyimide films to VUV radiation alone caused no damage to the surface, while an atomic oxygen flux resulted in substantial oxidation of the surface. Atomic oxygen exposure produces oxidation species different from those observed for VUV and atomic oxygen in combination, as evidenced from the broadening and the shift to higher binding energy of the O1s peak. Polyimides exposed to UV in air seem to favour the formation of C=O, while VUV and atomic oxygen exposure favour the formation of C-O groups. Furthermore, a new peak at 407.8 eV developed in the N1s region as a result of exposure to atomic oxygen, and was identified as $-\text{NO}_2$. This peak diminished after 1 h of further exposure to the atomic oxygen flux. The formation of $-\text{NO}_2$ suggested that the imide linkage could be sensitive to oxidation by atomic oxygen. The atomic oxygen could be considered as the main factor in the degradation process of polyimide films exposed to a low earth orbit environment. Obvious evidence of a synergistic effect of VUV radiation in the presence of atomic oxygen, which increases the damage to the polyimide surface, could also be drawn from the XPS study.

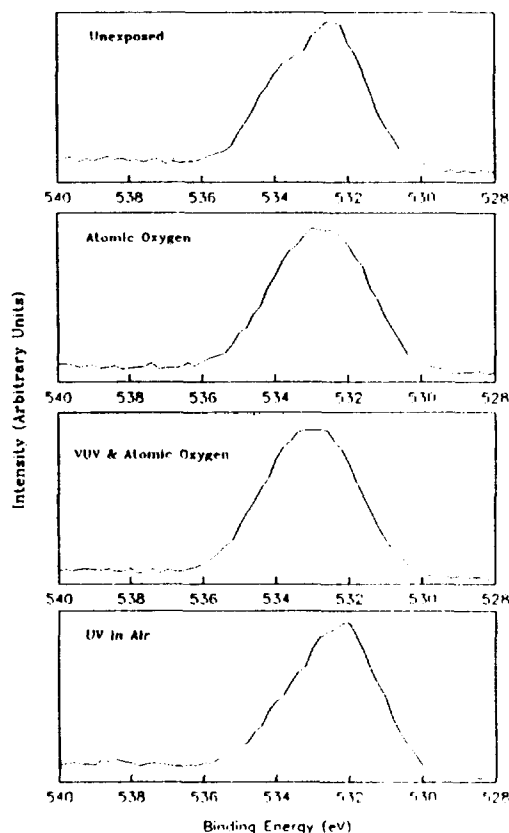


Figure 12: XPS multiplex spectra for O1s regions of ODPA/3,3'-ODA polyimide films exposed to different conditions.

REFERENCES

- 1- A.K. St. Clair, T. L. St. Clair and K. I. Shevket, 1984, *Proceedings of the ACS Division of polymeric materials: Science and Engineering* vol. 51, p. 62.
- 2- A.K. St. Clair and W.S. Slemph, 1991, *Proceeding of the 23rd International SAMPE Technical Conference*.
- 3- J.S. Forsythe, G. George, D.J.T. Hill, J.H. O'Donnell, P.J. Pomery and F.A. Rasoul, 1994, *Paper Presented at the 3rd LDEF Symposium, Williamsburg, Virginia, Nov. 8-12 1993*.
- 4- M. A. George, B.L. Ramakrishna, & W.S. Glaunsinger, *J. Phys. Chem.*, 1990, 94, 5159.
- 5- S. Lazare, P.D. Hoh, J.M. Baker and R. Srinivasan, *J. Am. Chem. Soc.* 1984, 106, 4288.
- 6- P.R. Young and W.S. Slemph, 1992, *LDEF Materials Workshop 91, NASA CP-3162*, Part 1, 357.
- 7- M. Lee, W. Rooney and J. Whiteside, 1993, *2nd Post-Retrieval Symposium, LDEF-69 Months in Space, San Diego, California, June 1-5, 1992, NASA Conference Publication 3194*, Part 3, 957.
- 8- P.R. Young, W.S. Slemph, W.G. Witte and J.Y. Shen, 1991, *SAMPE International Symposium*, 36 (1), 403.
- 9- M.J. Meshishnek, W.K. Stuckey, J.S. Evangelsides, L.A. Feldman, R.V. Peterson, G.S. Arnold and D.R. Peplinski, 1988, *Section 5-1 to 5-33, NASA TM 100459, Vol. II*.
- 10- W.S. Slemph, B. Santos-Mason, G.F. Sykes, Jr. and W.G. Witte, 1988, *Section 5-1 to 5-15, NASA TM 100459, Vol. I*.
- 11- P.R. Young, A.K. St. Clair and W.S. Slemph, 1993, *38th International SAMPE Symposium and Exhibition, Anaheim, California, May 10-13*, 664.
- 12- G. Beamson and D. Briggs, 1992, *High Resolution XPS of Organic Polymers- The Scienta ESCA 300 Data Base*, John Wiley & Sons, Chichester.
- 13- C.E. Hoyle, D. Creed, R. Nagarajan, P. Subramanian and E.T. Anzures, 1992, *Polymer*, 33 (15), 3162.
- 14- T.K. Minton, S.Y. Chung, D.E. Brinza and T.A. Moore, 1994, *Paper presented at the 3rd LDEF Symposium, Williamsburg, Virginia, Nov. 8-12 1993*.

Acknowledgment: We would like to acknowledge support of this work by the National Aeronautics and Space Administration (NASA), Langley Research Centre.

Collection and Review of Metals Data Obtained
From LDEF Experiment Specimens and Support Hardware*

Roger Bourassa and Gary Pippin
Boeing Defense & Space Group
P. O. Box 3999
Seattle, Washington 98124-2499
Phone: (206)773-8437

SJ-26
14-1-2
208

INTRODUCTION

LDEF greatly extended the range of data available for metals exposed to the low-Earth-orbital environment. The effects of low-Earth-orbital exposure on metals include meteoroid and debris impacts, solar ultraviolet radiation, thermal cycling, cosmic rays, solar particles and surface oxidation and contamination. This paper is limited to changes in surface composition and texture caused by oxidation and contamination. Surface property changes afford a means to study the environments (oxidation and contamination) as well as in-space stability of metal surfaces.

In this paper we will compare thermal-optical properties for bare aluminum and anodized aluminum clamps flown on LDEF. We will also show that the silicon observed on the LDEF tray clamps and tray clamp bolt heads is not necessarily evidence of silicon contamination of LDEF from the Shuttle. The paper concludes with a listing of LDEF reports that have been published thus far that contain significant findings concerning metals.

BARE ALUMINUM AND ANODIZED ALUMINUM CLAMPS

The retaining clamps on LDEF Experiment Trays C9 and C3 offer an opportunity to compare the behavior of bare and chromic acid anodized (CAA) aluminum when exposed to space in low-Earth-orbit (LEO). Figure 1 shows a photograph of Tray C9. The four corner clamps that hold this tray in place on the vehicle are bare 6061-T6 aluminum. The remaining four clamps on Tray C9 are anodized aluminum. Figure 2 shows a close-up of the bare aluminum Clamp C09-3 on Tray C9 and is adjacent to the CAA Clamp C08-5 on Tray C8. Both Clamp C09-3 and Clamp C08-5 are bolted to Longerons 8-9 at an angle of 23 degrees to ram. A striking difference in the appearance of the anodized and bare aluminum surfaces is shown in the photographs.

Tray clamps on LDEF were protected by their location from possible line-of-sight sources of contamination from the LDEF vehicle itself as shown in Figure 3. It is assumed that very little contamination from the vehicle reached the clamp surfaces. Two bare aluminum clamps, (C09-7, leading edge and C03-5, trailing edge) and two CAA clamps (C09-2, leading edge and C03-6, trailing edge) were selected for laboratory testing and comparison of thermal-optical properties. The locations of the four clamps included in the comparison of bare and anodized aluminum surfaces are shown in Figure 4. Solar radiation and atomic oxygen exposure data for these clamps are shown on Table 1.

* This work was carried out under contract NAS1-19247, NASA Langley Research Center

Solar absorptance and thermal emittance are shown on Table 1 for the thermal-optical properties comparison. Data for flight clamps are from post-flight measurements. Data for control clamp #4 were taken after the clamp was removed from storage. Solar absorptance was measured in accordance with ASTM E903-82 and ASTM E424-17. Thermal emittance was measured in accordance with ASTM E408-71.

Flight exposure caused little change in the thermal-optical properties of either bare or CAA clamp surfaces (Table 1). A bare ground control clamp was not available. However, thermal-optical properties for the exposed surfaces of bare flight clamps may be compared with those of unexposed surfaces (back surfaces) of the same clamps. Thermal-optical properties of exposed surfaces of CAA flight clamps may be compared with those of the ground control clamp.

The thermal-optical properties of bare clamp surfaces and CAA clamp surfaces differ significantly. Average solar absorptance for bare flight clamp surfaces (leading edge and trailing edge) is 210 percent that of CAA flight clamp surfaces. Average thermal emittance for bare flight clamp surfaces (leading edge and trailing edge) is 45 percent that of CAA flight clamp surfaces.

Figures 5 through 9 give Auger electron spectroscopy profiles (AES) for principal elements on the surfaces of the clamps. The conversion of sputter time to depth is estimated at approximately 120 Angstroms/minute. Figures 5 and 6 suggest that magnesium near the surface of bare aluminum plate is higher than the bulk average value deeper in the material. This variation in composition at the surface of metal alloys is caused by the manufacturing process. This surface composition change with depth is not evident on CAA aluminum because the surface is etched before anodizing and the anodizing process converts aluminum to aluminum oxide.

Figures 5 and 6 show that based on post-flight determinations the depth at which magnesium and aluminum concentrations are equal is approximately 890 Angstroms (7.4 minutes sputter time) for the leading-edge bare clamp C09-7 and approximately 1150 Angstroms (9.6 minutes sputter time) for the trailing-edge bare clamp C03-5. The difference is attributed to the removal of carbon by atomic oxygen for the leading-edge clamp.

Figures 5 and 6 show lower carbon concentrations for Clamp C09-7 than for Clamp C03-5 at depths greater than 200 Angstroms (2 minutes sputter time). Clamp C03-5 was shielded from exposure to atomic oxygen. However, surface concentrations of carbon obtained by post-flight measurements are the same for both bare clamps, C09-7 (leading edge) and C03-5 (trailing edge). It is likely that the carbon content of the clamp surfaces increased due to exposure to the post-flight, ambient ground atmosphere.

Figure 7 shows ESCA atomic concentrations for a CAA treated control clamp. The control clamps were stored in a laboratory at NASA-Langley during the LDEF mission. Figures 8 and 9 when compared with Figure 7 for the control clamp surface show that the CAA treated clamp surfaces were unaffected by exposure to the LEO environment whether exposed on leading or trailing surfaces of LDEF.

ESCA DETERMINATIONS ON BOLT-HEAD SURFACES

Figure 3 shows that the tops of the stainless steel bolts that held the clamps in place were shielded from possible contamination from sources on-board LDEF. This positioning of the bolt heads makes them useful for studying possible contamination of LDEF surfaces by the Shuttle. The location of the bolts also prevented them from being shielded from atomic oxygen and solar ultraviolet radiation exposures. Likewise, the bolt head tops were not exposed to either the atomic oxygen flux or solar radiation reflected from other LDEF surfaces. Thus, prediction of oxidation and radiation environments for the bolt head tops is simplified.

ESCA determinations were made on the tops of the clamp bolt heads. Figure 10 shows that the atomic concentration of silicon increases everywhere around the LDEF vehicle relative to the control bolts. However, no trend in the absolute amount of silicon on the bolt heads is necessarily indicated by Figure 10. The alloy from which the bolts are manufactured has a small concentration of silicon. The apparent increase in silicon atomic concentration may be caused by the removal of carbon atoms by atomic oxygen. Carbon concentrations tend to decrease with increasing atomic oxygen exposure.

Figure 11 is a plot of the ratio of silicon-to-iron concentrations for locations around the vehicle. If it is assumed that the quantity of iron present on the bolt-head surfaces is constant (unaffected by atomic oxygen) then the amount of silicon on the bolts would vary with the silicon-to-iron ratio as plotted in Figure 11.

If LDEF were being contaminated by silicon from the Shuttle during deployment or recovery then a definite trend in relative silicon-to-iron composition with position on the vehicle would be expected. No consistent trend is seen in this ratio. The variation in the silicon-to-iron ratio shown by the plot may be explained by random errors in the analytical procedure and preflight condition of the bolt surfaces. These ESCA data do not necessarily support the premise of silicon contamination of LDEF from outgassing from the Shuttle.

Figure 12 shows both atomic oxygen fluence and carbon atomic concentrations on bolt heads as a function of position on LDEF. Figure 12 shows that the reduction in carbon atomic concentration on the stainless steel bolt heads is a sensitive indicator of atomic oxygen exposure, notwithstanding the universal availability of carbon in the atmosphere that might change the surface carbon concentration following the LDEF flight. Note that this finding for stainless steel surfaces is opposite to the finding for bare aluminum clamp surfaces discussed above. For bare aluminum surfaces, the concentration of carbon following flight tended to be independent of atomic oxygen exposure. This effect was attributed to post-flight reaction of the aluminum surfaces with carbon in the ground atmosphere.

AES PROFILES ON BOLT-HEAD SURFACES

It was decided that a comparison of Auger electron spectroscopy profiles for control bolts and flight bolts would be useful in explaining the surface composition changes caused by the LEO environment. Figure 13 shows the locations on LDEF of six flight bolts chosen for the comparison. Figure 14 shows the average silicon-to-iron ratios obtained for four unexposed control bolts. The range of the ratio at any given depth is quite wide, but the average values form a smooth curve.

Five of the flight bolts (E9-4c, D7-7a, A6-6c, D2-4c, and H11-7a) were exposed to significant amounts of atomic oxygen, as shown on Table 2. Figure 15 shows silicon-to-iron ratios for each of these bolts compared with the average silicon-to-iron ratio for the four control bolts shifted by 45 Angstroms. The surfaces of the flight bolts show less silicon relative to iron than do the control bolts. However, the silicon-to-iron ratios for the control bolts and flight exposed bolts compare when the curves are shifted by 45 Angstroms relative to each other as shown in Figure 15. It is suggested that possibly a thin layer (45 Angstroms) of silicone material on the surface of the flight bolts may have been removed by oxidation during the mission.

The sixth flight bolt, D5-8c, received only a negligible amount of atomic oxygen. Figure 16 shows the silicon-to-iron concentration ratio at two locations for flight bolt D5-8c as a function of depth by AES profile analysis. Silicon-to-iron atomic concentration ratios for bolt D5-8c bracket the control bolt average values. This result is consistent with the fact that the head of this bolt (D5-8c) was not exposed to significant atomic oxygen during the flight. It ended the flight in a condition comparable to the average condition of the control bolts which were not exposed.

The data developed from the AES profiles on the stainless steel bolt-head surfaces does not support the premise of silicon contamination of LDEF by the Shuttle.

SUMMARY OF OBSERVATIONS

Table 3 lists papers published to date that contain information concerning metals flown on LDEF. The table includes papers presented at the First Post-Retrieval Symposium, the Materials Workshop '91, and the Second Post-Retrieval Symposium. A paper presented at the Third Post-Retrieval Symposium, and three other papers are also included. Additional information will become available when papers presented at the LDEF Materials Results For Spacecraft Applications Conference and the Third Post-Retrieval Symposium are published.

A number of observations concerning the effects of the LEO environment on metals have been made and confirmed by investigators reporting thus far. Some of the principal findings, including those discussed herein, can be summarized as follows:

- (1) Metals are highly variable in their response to the LEO environment.
- (2) Gold and platinum are nonreactive.
- (3) Osmium, which forms a volatile oxide, is rapidly eroded.
- (4) Silver, which forms a nonprotective oxide, is rapidly eroded.
- (5) Other metals (Al, Cu, Ga, Ge, Ir, Mo, Ni, Ti, and Sn) show some level of reaction unless protected.
- (6) Contamination is a major contributor to exposure effects on metal surfaces.

- (7) Absorptance is significantly greater for bare aluminum than for CAA aluminum. Emittance is significantly less for bare aluminum than for CAA aluminum.
- (8) The surface properties of both bare aluminum and CAA aluminum are little changed by exposure to LEO environmental conditions.
- (9) Magnesium in aluminum alloys is preferentially oxidized relative to aluminum.
- (10) An oxide coating forms on exposure of copper to atomic oxygen that impedes further oxidation.
- (11) The oxide coating adversely affects the optical properties of copper.
- (12) Copper without surface protection may be used for extended periods of time in applications where thermal management and optical performance requirements are not critical.

BIBLIOGRAPHY

- Bourassa, Roger J., and J. R. Gillis, "LDEF Atomic Oxygen Fluence Update," NASA Conference Publication 3162, Part 1, p59, 1992.
- Levine, Arlene S. (Editor): LDEF -69 Months in Space: First Post-Retrieval Symposium. NASA Conference Publication 3134, 1992.
- Stein, Bland A., and Philip R. Young (Compilers): LDEF Materials Workshop '91, NASA Conference Publication 3162, 1992.
- Levine, Arlene S. (Editor): LDEF -69 Months in Space: Second Post-Retrieval Symposium. NASA Conference Publication 3194, 1993.
- Clark, Lenwood G., William H. Kinard, David J. Carter, Jr., and James L. Jones, Jr., "The Long Duration Exposure Facility (LDEF) Mission Experiments," NASA SP-473, 1984.
- Banks, Bruce A., and Linda Gebauer, "LDEF Yaw and Pitch Angle Estimates," NASA Conference Publication 3134, Part 1, p71, 1991.
- Bourassa, R. J., and J. R. Gillis, "Atomic Oxygen Exposure of LDEF Experiment Trays," NASA Contractor Report 189627, 1992.
- Bourassa, R. J., and H. G. Pippin, "Model of Spacecraft Atomic Oxygen and Solar Exposure Microenvironments," LDEF Materials Results for Spacecraft Applications Conference, October 1992.
- Bourassa, R. J. and J. R. Gillis, "Solar Exposure of LDEF Experiment Trays," NASA Contractor Report 189554, 1992
- Assie', Jean-Pierre, and Alfred Perotto, "Effects of Ultra-Vacuum and Space Environment of Contact Ohmic Resistance LDEF Experiment A0138-11," NASA Conference Publication 3134, Part 3, p1607, 1991.
- Assie', Jean-Pierre, and Eric Conde', "Microwelding (or Cold Welding) of Various Metallic Materials Under the Ultra-Vacuum LDEF Experiment A0138-10," NASA Conference Publication 3134, Part 3, p1613, 1991.
- "Atomic Oxygen Effects Measurements for Shuttle Mission STS-4," Journal of Geophysical Research, Vol. 10, July 1983, pp 569-571.
- "Atomic Oxygen Effects Measurements for Shuttle Missions STS-8 and 41G," NASA Technical Memorandum 1000459, Volumes I, II, III.
- Christl, Ligia C., John C. Gregory and Palmer N. Peters, "Measurements of Erosion Characteristics for Metal, and Polymer Surfaces Using Profilometry," NASA Conference Publication 3134, Part 2, p723, 1991.
- Cromer, T. F., H. L. Grammer, J. P. Wightman, P. R. Young, and W. S. Slemp, "Surface Characterization of Selected LDEF Tray Clamps," NASA Conference Publication 3194, Part 3, p1015, 1993.

- Cromwell, B. K., Capt. S. D. Shepherd, C. W. Pender, and B. E. Wood, "Spectral Infrared Hemispherical Reflectance Measurements for LDEF Tray Clamps," NASA Conference Publication 3194, Part 3, p1001, 1993.
- de Rooij, A., "Some Results of the Oxidation Investigation of Copper and Silver Samples Flown on LDEF," NASA Conference Publication 3162, Part 2, p479, 1992.
- Dursch, H. W., W. S. Spear, E. A. Miller, G. L. Bohnhoff-Hlavacek, and J. Edelman, "Analysis of Systems Hardware Flown on LDEF - Results of the Systems Special Investigation Group," NASA Contractor Report 189628, April 1992.
- Franzen, W., J. S. Brodtkin, L. C. Sengupta, and P. L. Sagalyn, "Ellipsometric Study of Oxide Films Formed on LDEF Metal Samples," NASA Conference Publication 3134, Part 2, p1005, 1991.
- Frederickson, A. R., R. C. Filz, F. J. Rich, and P. Sagalyn, "Patterns of Discoloration and Oxidation by Direct and Scattered Fluxes on LDEF, Including Oxygen on Silicon," NASA Conference Publication 3134, Part 2, p1189, 1991.
- Golden, Johnny L., "Anodized Aluminum on LDEF: A Current Status of Measurements on Chromic Acid Anodized Aluminum," NASA Conference Publication 3162, Part 1, p211, 1992.
- Golden, Johnny L., "Changes in Oxidation State of Chromium During LDEF Exposure," NASA Conference Publication 3162, Part 2, p491, 1992.
- Golden, Johnny L., "Selected Results for LDEF Thermal Control Coatings," NASA Conference Publication 3194, Part 3, p1099, 1993
- Hurley, Charles J., and Michele Jones, "Long Duration Exposure Facility M0003-5 Recent Results on Polymeric Films," NASA Conference Publication 3162, Part 1, p417, 1992.
- Kauder, Lonny, "Preliminary Results for LDEF/HEPP Thermal Control Samples," NASA Conference Publication 3134, Part 2, p797, 1991.
- Levadou, Francois, and Gary Pippin, "Effects of the LDEF Environment on the Ag/FEP Thermal Blankets NASA Conference Publication 3162, Part 1, p 311, 1992.
- Linton, Roger C., and Rachel R. Kamenetzky, "Second LDEF Post-Retrieval Symposium Interim Results of Experiment A0034," NASA Conference Publication 3194, Part 3, p1151, 1993.
- Linton, Roger C., Rachel R. Kamenetzky, John M Reynolds, and Charles L. Burris, "LDEF Experiment A0034: Atomic Oxygen Stimulated Outgassing," NASA Conference Publication 3134, Part 2, p763, 1991.
- Mason, J. B., H.W. Dursch, and J. Edelman, "Systems Investigation Group Overview," NASA Conference Publication 3134, Part 3, p1217, 1991.
- Meshnishnek, M. J., S. R. Gyetvay, and C. H. Jagers, "Long Duration Exposure Facility Experiment M0003 Deintegration Findings and Impacts," NASA Conference Publication 3134. Part 2, p1073, 1991.

Miglionico, C., et. al., "Effects of Space Environment on Structural Materials," NASA Conference Publication 3134, Part 2, p663, 1991.

Mirtich, Michael J., Sharon K. Rutledge, Nicholas Stevens, Raymond M. Olle, and James Merrow, "Ion Beam Textured and Coated Surfaces Experiment (IBEX)," NASA Conference Publication 3134, Part 2, p989, 1991.

Peters, Palmer N., John C. Gregory, Ligia C. Christl, and Ganesh N. Raikar, "Effect on LDEF Exposed Copper Film and Bulk," NASA Conference Publication 3134, Part 2, p755, 1991.

Pippin, Gary, and Russ Crutcher, "LDEF Materials Data Analysis: Representative Examples," NASA Conference Publication 3194, Part 3, p1187, 1993.

Pippin, H. G., Owen Mulkey, Juris Verzemnieks, Emmett Miller, Sylvester Hill, and Harry Dursch, "Survey of Results From The Boeing Modules on the M0003 Experiment on LDEF," NASA Conference Publication 3134, Part 2, p1109, 1991.

Plagemann, W. L., "Space Environmental Effects on the Integrity of Chromic Acid Anodized Coatings," NASA Conference Publication 3134, Part 2, p1023, 1991.

Presentation Nov 1991

Presentation Oct 1992

Raikar, Ganesh N., John C. Gregory, Ligia C. Christl, and Palmer N. Peters, "The Interaction of Atomic Oxygen With Copper: An XPS, AES, XRD, Optical Transmission and Stylus Profilometer Study," NASA Conference Publication 3194, Part 3, p1169, 1993.

Robertson, J. B., "Effect of Space Exposure on Pyroelectric Infrared Detectors," NASA Conference Publication 3162, Part 2, p501, 1992.

Saxton, J. M., I. C. Lyon, E. Chatzitheodoridis, P. Van Lierde, J. D. Gilmour, and G. Turner, "Oxygen Isotopes Implanted in the LDEF Spacecraft," NASA Conference Publication 3194, Part 3, p791, 1993.

Slemp, Wayne S., Philip R Young, William G. Witte Jr., and James Y. Shen, "Effects of Flight Exposure on Selected Polymer Matrix Resin Composite Materials" NASA Conference Publication 3134, Part 2, p1149, 1992.

Spear, W. S., and H. W. Dursch, "LDEF Mechanical Systems," NASA Conference Publication 3134, Part 3, p1549, 1991.

Stein, B. A. and H. G. Pippin, "Preliminary Findings of the LDEF Materials Special Investigation Group," NASA Conference Publication 3134, Part 2, p617 1991.

Stein, Bland A., "LDEF Materials: An Overview of the Interim Findings," NASA Conference Publication 3162, Part 1, p1, 1992.

Stein, Bland A., "LDEF Materials Overview," NASA Conference Publication 3194, Part 3, p741, 1993.

Tredway, W. K., and K. M. Prewo, "Analysis of the Effect of Space Environmental Exposure on Carbon Fiber Reinforced Glass," United Technologies Research Center Report R91-112542-4, 1991.

Whitaker, Ann F., "Selected Results for Metals From LDEF Experiment A0171," NASA Conference Publication 3162, Part 2, p467, 1992.

Wilkes, Donald R., Ann Whitaker, James M. Zwiener, Roger C. Linton, David Shular, Palmer Peters, and John Gregory, "Thermal Control Surfaces on the MSFC LDEF Experiments," NASA Conference Publication 3162, Part 1, p187, 1992.

Wilkes, Donald R., M. John Brown, Leigh L. Hummer, and James M. Zwiener, "Initial Materials Effects Observed on the Thermal Control Surfaces Experiment (S0069)," NASA Conference Publication 3134, Part 2, p899, 1991.

Young, Philip R., and Wayne S. Slemo, "Characterization of Selected LDEF-Exposed Polymer Films and Resins," NASA Conference Publication 3162, Part 1, p357, 1991.

TABLE 1. THERMAL-OPTICAL PROPERTIES OF BARE AND ANODIZED ALUMINUM CLAMPS

SAMPLE	EXPOSURE	SURFACE TREATMENT	AVERAGE SOLAR ABSORPTANCE	AVERAGE THERMAL EMITTANCE	FIGURE NUMBER
C03-5 Trailing Edge	Back Surface No Direct Exposure	Bare	0.71	0.13	
C03-5 Trailing Edge	Longeron 3-4 2.66E+03 AO/cm ² 11,000 ESH Solar	Bare	0.74	0.08	5
C09-7 Leading Edge	Back Surface No Direct Exposure	Bare	0.72	0.09	
C09-7 Leading Edge	Longeron 9-10 9.02E+21 AO/cm ² 11,200 ESH Solar	Bare	0.69	0.06	6
Control #4	Ground Control	CAA	0.32	0.18	7
C03-6 Trailing Edge	Longeron 3-4 2.66E+03 AO/cm ² 11,000 ESH Solar	CAA	0.35	0.14	8
C09-2 Leading Edge	Longeron 8-9 8.36E+21 AO/cm ² 10,500 ESH Solar	CAA	0.33	0.17	9

Note: A bare ground control clamp is not available.

TABLE 2. FLIGHT BOLTS USED IN THE AUGER ELECTRON SPECTROSCOPY PROFILE STUDY OF SILICON CONCENTRATION

BOLT NUMBER	ANGLE degrees	AO FLUENCE atoms/cm ²	NUMBER OF PROFILES
A6-6c	83	1.16E+21	1
D2-4c	142	1.54E+17	2
D5-8c	128	9.60E+12	2
D7-7a	53	5.45E+21	1
E9-4c	8	8.99E+21	1
H11-7a	89	4.59E+20	1

Table 3. Metals Related Information

LDEF First Post-Retrieval Symposium Reference	Metals Related Information	Experiment
MEASUREMENTS OF EROSION CHARACTERISTICS FOR METAL AND POLYMER SURFACES USING PROFILOMETRY Ligia C. Christl, John C. Gregory and Palmer N. Peters p723	Roughness, erosion depths and material growth. 128 solid surfaces, including: iridium, gold, silver, copper, osmium, platinum, tungsten, aluminum, and molybdenum.	A0114
EFFECT ON LDEF EXPOSED COPPER FILM AND BULK Palmer N. Peters, John C. Gregory, Ligia C. Christl and Ganesh N. Raikar p755	Discussion of methods for characterizing exposed surfaces. Atomic concentrations of elements on surfaces of exposed copper film and bulk copper.	A0114
LDEF EXPERIMENT A0034: ATOMIC OXYGEN STIMULATED OUTGASSING Roger C. Linton, Rachel R. Kamenetzky, John M. Reynolds and Charles L. Burris p763	Optical degradation of the gold, silver, and osmium mirrors.	A0034
PRELIMINARY RESULTS FOR LDEF/HEPP THERMAL CONTROL SAMPLES Lonny Kauder p797	Atomic oxygen resistant vapor deposited aluminum coatings for Kapton.	
INITIAL MATERIALS EVALUATION OF THE THERMAL CONTROL SURFACES EXPERIMENT (S0069) Donald R. Wilkes, M. John Brown, Leigh L. Hummer and James M. Zwiener n899	Effects of natural and induced environments on silver/Inconel reflecting surface coatings for FEP Teflon film.	S0069
LONG DURATION EXPOSURE FACILITY EXPERIMENT M0003-5 THERMAL CONTROL MATERIALS Charles J. Hurley p961	Physical and optical performance of gold, silver, and aluminum mirrors and metallized films.	M0003-5
ION BEAM TEXTURED AND COATED SURFACES EXPERIMENT (IBEX) Michael J. Mirtich, Sharon K. Rutledge, Nicholas Stevens, Raymond Oile and James Merrow p989	Functional durability and properties of ion beam textured silicon, titanium, copper, Inconel, and stainless steel materials exposed to the space environment.	
ELLIPSOMETRIC STUDY OF OXIDE FILMS FORMED ON LDEF METAL SAMPLES W. Franzen, J. S. Brodtkin, L. C. Sengupta and P. L. Sagalyn p1005	Optical constants of six metals (aluminum, copper, nickel, tantalum, tungsten and zirconium) exposed to space.	M0002-2
PRELIMINARY RESULTS FROM THE LDEF/UTIAS COMPOSITE MATERIALS EXPERIMENT R. C. Tennyson, G. E. Mabson, W. D. Morison and J. Kleiman p1057	Time to outgas, dimensional changes, coefficients of thermal expansion, atomic oxygen erosion and damage due to micrometeoroid/debris impacts on a stainless steel tube.	A0180
SURVEY OF RESULTS FROM THE BOEING MODULES ON THE M0003 EXPERIMENT ON LDEF H. G. Pippin, Owen Mulkey, Juris Verzemnieks, Emmett Miller, Sylvester Hill and Harry Dursch p1109	Optical properties of anodized and polished aluminum discs.	M0003
EFFECTS OF SPACE ENVIRONMENT ON COMPOSITE MATERIALS AND THERMAL COATING (A0138-9) Michel Parcelier and Jean Pierre Assié p1163	A sputter-deposited coating consisting of 1000 Angstroms of nickel overcoated with 600 Angstroms of silicon dioxide protected an epoxy/graphite composite panel from atomic oxygen erosion on LDEF.	A0138-9
PATTERNS OF DISCOLORATION AND OXIDATION BY DIRECT AND SCATTERED FLUXES ON LDEF, INCLUDING OXYGEN ON SILICON A. R. Frederickson, R. C. Filz, F. J. Rich and P. Sagalyn p1189	Discoloration pattern on polished single crystal silicon.	M0002-1
EFFECTS OF ULTRA-VACUUM AND SPACE ENVIRONMENT OF CONTACT OHMIC RESISTANCE LDEF EXPERIMENT A0138-11 Jean-Pierre Assié and Alfred Perotto p1607	Comparison of aluminum conductors and contacts with conventional conductors and contacts under different conditions of production and storage in space vacuum. Nickel plated aluminum, silvered copper, and tinned copper conductors.	A0138-11

Table 3. Metals Related Information (Continued)

LDEF Materials Workshop '91 Reference	Metals Related Information	Experiment
LDEF ATOMIC OXYGEN FLUENCE UPDATE Roger J. Bourassa and J. R. Gillis p59	Solar absorptance and thermal emittance of copper grounding straps as function of atomic oxygen and ultraviolet radiation exposure.	
THERMAL CONTROL SURFACES ON THE MSFC LDEF EXPERIMENTS Donald R. Wilkes, Ann Whitaker, James M. Zwiener, Roger C. Linton, David Shular, Palmer Peters, and John Gregory p187	Optical, thermal, physical, and chemical effects of space exposure on silverized Teflon and chromic acid anodized thermal control surfaces.	A0034 A0114 A0171 S0069 S1005
ANODIZED ALUMINUM ON LDEF: A CURRENT STATUS OF MEASUREMENTS ON CHROMIC ACID ANODIZED ALUMINUM Johnny L Golden p211	Solar absorptance and thermal emittance of chromic acid anodized aluminum at various locations on LDEF including pre-flight, and post-flight measurements.	
CHARACTERIZATION OF SELECTED LDEF-EXPOSED POLYMER FILMS AND RESINS Philip R. Young and Wayne S. Slemp p357	A sputter-deposited coating consisting of 1000 Angstroms of nickel overcoated with 600 Angstroms of silicon dioxide protected an epoxy/graphite composite panel from atomic oxygen erosion on LDEF.	A0138-9
LONG DURATION EXPOSURE FACILITY M0003-5 RECENT RESULTS ON POLYMERIC FILMS Charles J. Hurley and Michele Jones p417	Physical and optical performance of gold, silver, and aluminum mirrors and metallized films.	M0003-5
SELECTED RESULTS FOR METALS FROM LDEF EXPERIMENT A0171 Ann F. Whitaker p467	Atomic oxygen effects on multicrystalline silver, cold rolled silver ribbon, copper, molybdenum, and titanium (75A) metal surfaces	A0171
SOME RESULTS OF THE OXIDATION INVESTIGATION OF COPPER AND SILVER SAMPLES FLOWN ON LDEF A. de Rooij p479	Oxidation of silver film on FEP Teflon through holes in thermal control blankets caused by micro-meteoroid impacts. Thickness of copper oxide layer on grounding straps. Analysis also indicates that silicone contamination of copper straps occurred early in the LDEF mission.	
CHANGES IN OXIDATION STATE OF CHROMIUM DURING LDEF EXPOSURE Johnny L. Golden p491	Oxidation of black chromium plate.	A0076

Table 3. Metals Related Information (Concluded)

LDEF Second Post-Retrieval Symposium Reference	Metals Related Information	Experiment
LDEF MATERIALS OVERVIEW Bland A. Stein p741	Summary of LDEF findings.	
SPECTRAL INFRARED HEMISPHERICAL REFLECTANCE MEASUREMENTS FOR LDEF TRAY CLAMPS B. K. Cromwell, Capt. S. D. Shepherd, C. W. Pender, and B. E. Wood p1001	Infrared hemispherical reflectance of tray clamp surfaces show essentially no dependence on atomic oxygen fluence. There did appear to be a slight dependence on solar radiation exposure.	
SURFACE CHARACTERIZATION OF SELECTED LDEF TRAY CLAMPS T. F. Cromer, H. L. Grammer, J. P. Wightman, P. R. Young, and W. S. Slemp p1015	Documents changes in the surface chemistry of tray clamps taken from different locations on LDEF.	
SECOND LDEF POST-RETRIEVAL SYMPOSIUM INTERIM RESULTS OF EXPERIMENT A0034 Roger C. Linton and Rachel R. Kamenetzky p1151	Space environmental effects on thin film mirrors including mirrors with silver, osmium, gold surfaces and mirrors with silicon monoxide and magnesium fluoride overcoated aluminum surfaces.	A0034
THE INTERACTION OF ATOMIC OXYGEN WITH COPPER: AN XPS, AES, XRD, OPTICAL TRANSMISSION AND STYLUS PROFLOMETER STUDY Ganesh N. Raikar, John C. Gregory, Ligia C. Christl, and Palmer N. Peters p1169	Analysis of data on a thin film copper sample exposed on Row 9 show that 55 nm of copper was converted stoichiometrically to cuprous oxide.	
LDEF MATERIALS DATA ANALYSIS: REPRESENTATIVE EXAMPLES Gary Pippin and Russ Crutcher p1187	Solar absorptance and thermal emittance of copper grounding straps as function of atomic oxygen and ultraviolet radiation exposure.	

Other Reports With Metals Related Information

Reference	Metals Related Information	Experiment
CHANGES IN CHEMICAL AND OPTICAL PROPERTIES OF THIN FILM METALS MIRRORS ON LDEF P. N. Peters, J. C. Gregory and G.N. Raikar	Reports composition and thickness of oxides formed on thin films of Au, Ga, Cu, Ni, Os, Sn, Mo, Al, Ir, and Ge deposited on silica optical flats.	A0114
ANALYSIS OF SYSTEMS HARDWARE FLOWN ON LDEF - RESULTS OF THE SYSTEMS SPECIAL INVESTIGATION GROUP H. W. Dursch, W. S. Spear, E. A. Miller, G. L. Bohnhoff-Hlavacek, and J. Edelman	Exposure on LDEF caused no discernible effect on the bulk microstructure of aluminum alloy 6061-T6.	Tray E10
ATOMIC OXYGEN EFFECTS MEASUREMENTS FOR SHUTTLE MISSION STS-4 Journal of Geophysical Research, Vol. 10, July 1983, pp 569-571	Atomic oxygen reactions on Ag, C, and Os.	
ATOMIC OXYGEN EFFECTS MEASUREMENTS FOR SHUTTLE MISSIONS STS-8 AND 41G NASA Technical Memorandum 1000459 Volumes I, II, III	Protection of composites by thin atomic oxygen resistant metallic coatings (Volume I, p5-1) Atomic oxygen effects on metals (Volume I, p2-2).	

Note: Additional reports from the LDEF Materials Results Spacecraft Applications Conference will be added when available.

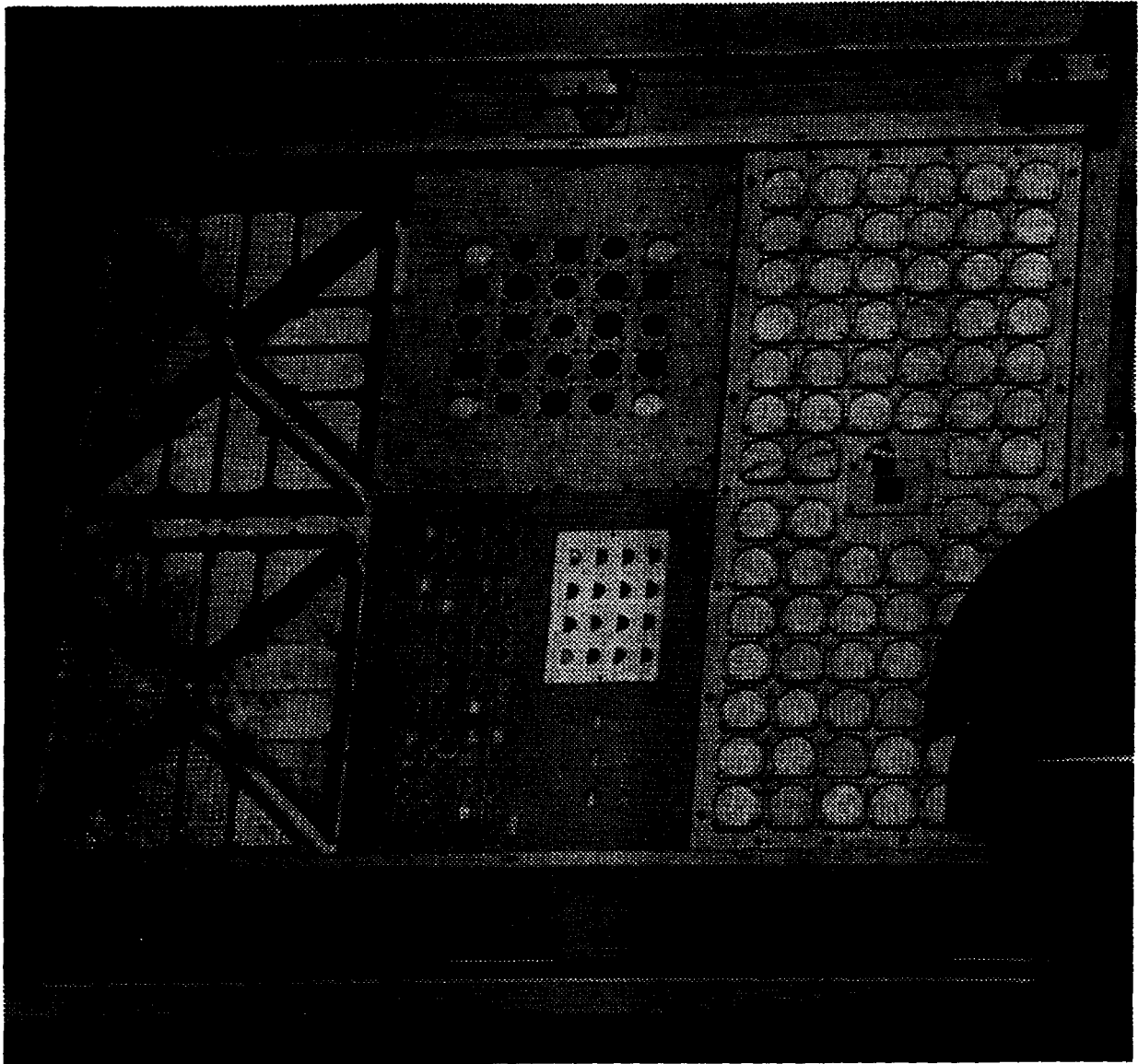


Figure 1. NASA on-orbit photograph showing four unanodized aluminum clamps at the corners of experiment Tray C9.

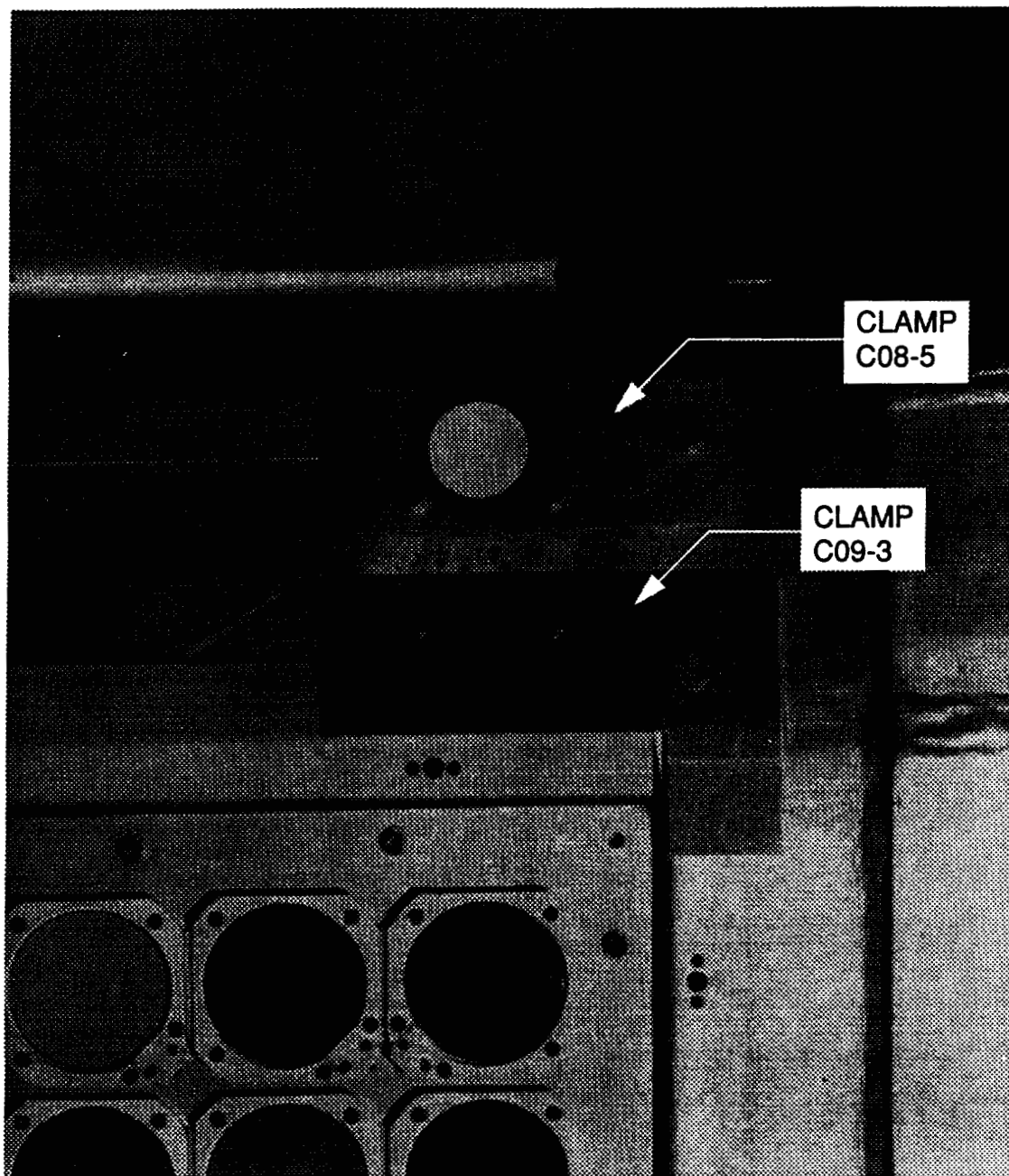


Figure 2. NASA KSC photograph of unanodized aluminum clamp C09-3 and adjacent CAA treated clamp C08-5 (with paint dot).

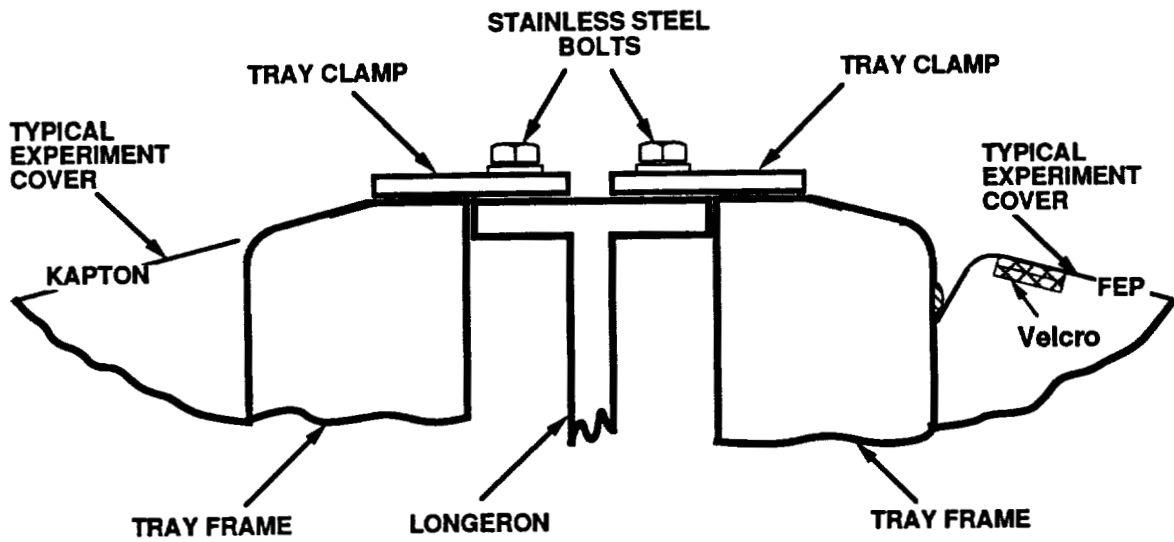


Figure 3. Position of Clamp Bolts

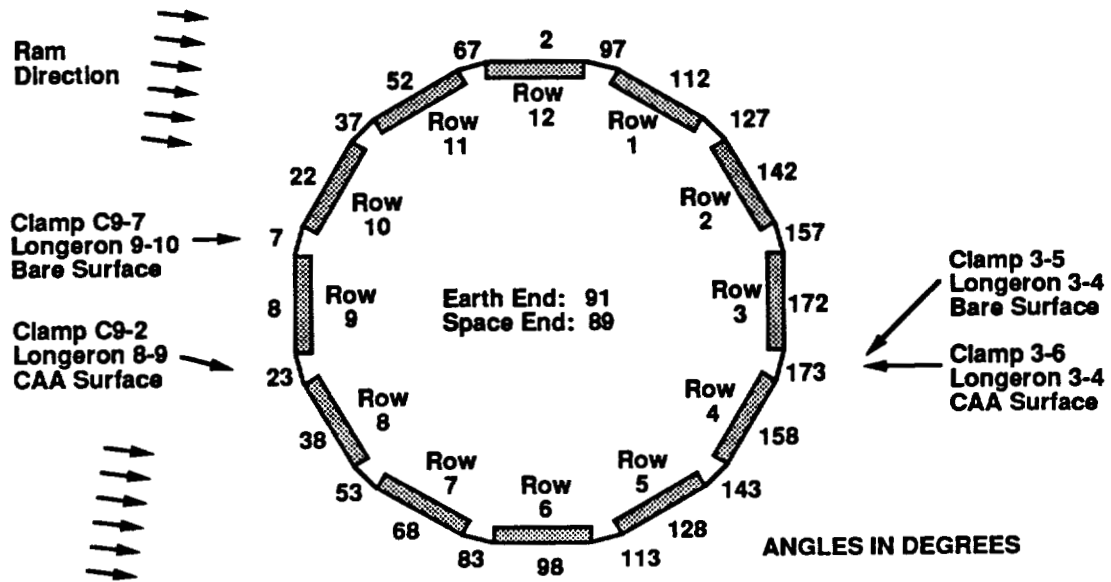


Figure 4. Clamp Locations For Comparison Of Bare And Anodized Surfaces

Material: Clamp, C03-5
 Surface: Bare
 Exposure: LDEF Trailing Edge, Longeron 3-4, 173 degrees from ram

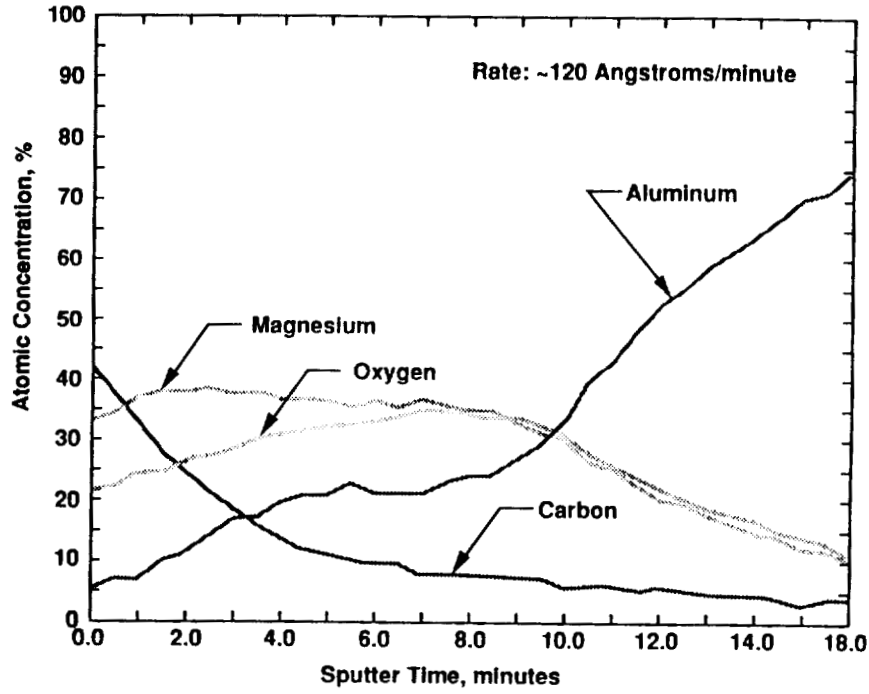


Figure 5. Auger Electron Spectroscopy Profile (Clamp C03-5)

Material: Clamp, C09-7
 Surface: Bare
 Exposure: LDEF Leading Edge, Longeron 9-10, 7 degrees from ram

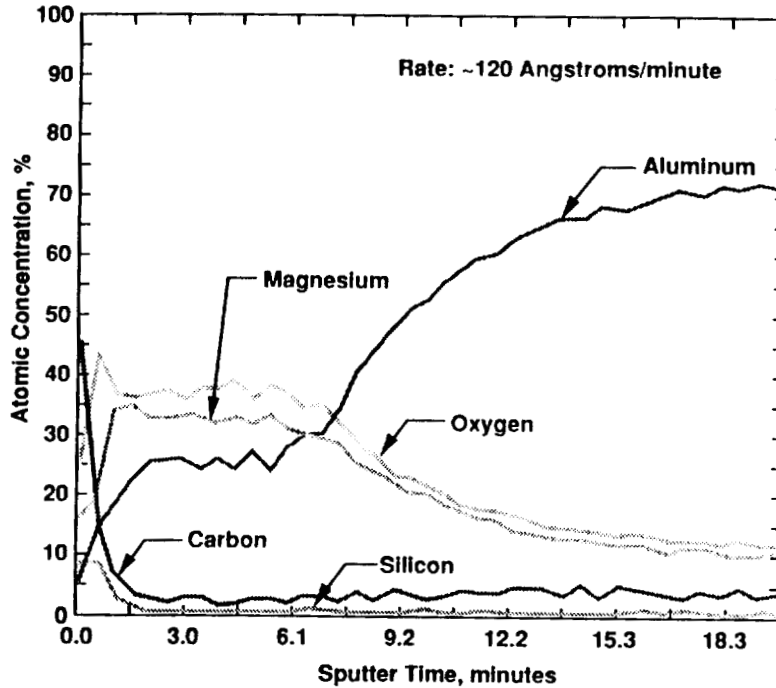


Figure 6. Auger Electron Spectroscopy Profile (Clamp C09-7)

Material: Ground Control Clamp, #4
Surface: CAA
Exposure: None

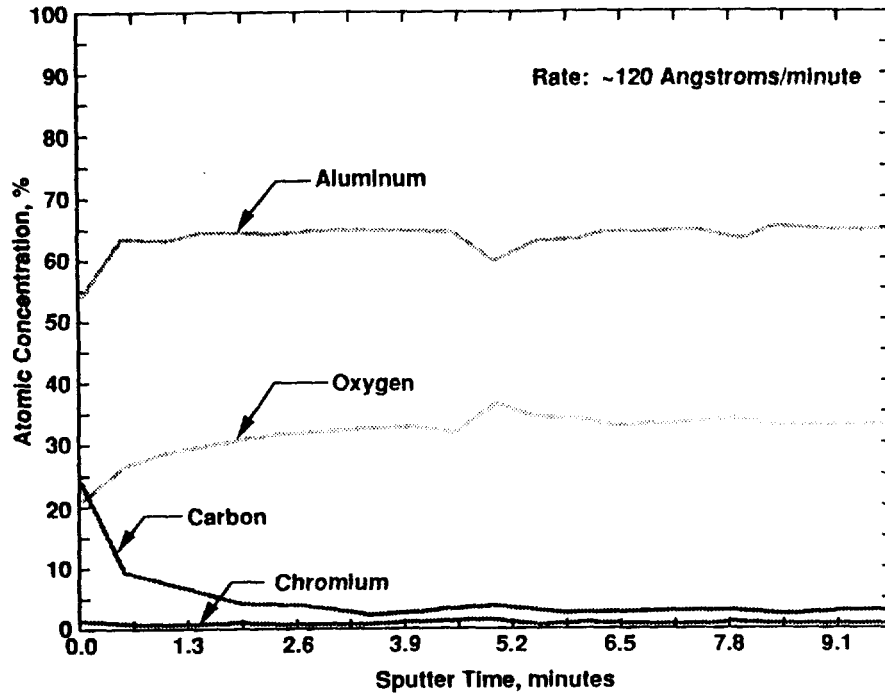


Figure 7. Auger Electron Spectroscopy Profile (Ground Control Clamp No. 4)

Material: Clamp, C03-6
Surface: CAA
Exposure: LDEF Trailing Edge, Longeron 3-4, 173 degrees from ram

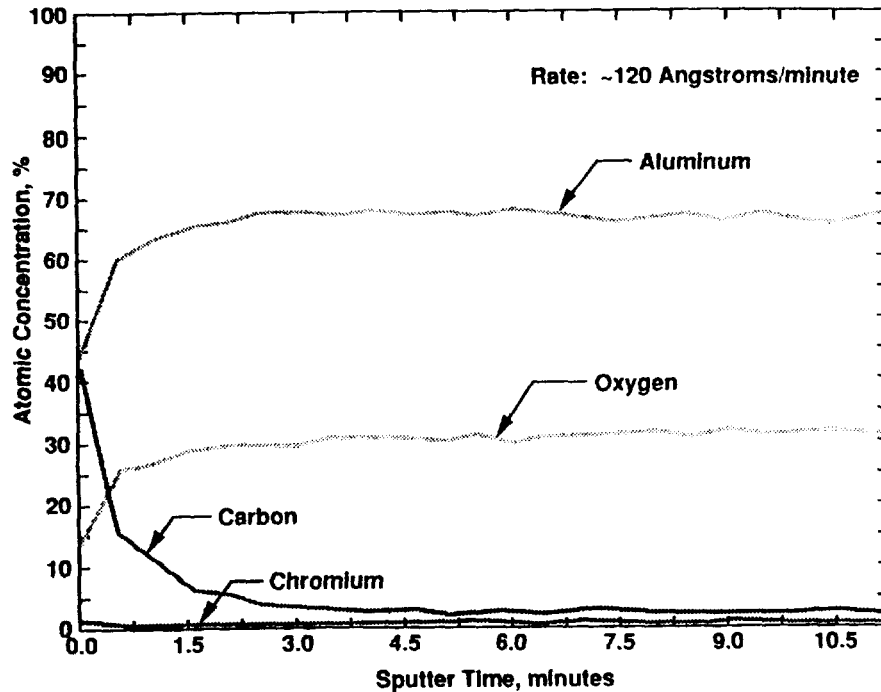


Figure 8. Auger Electron Spectroscopy Profile (Clamp C03-6)

Material: Clamp, C09-2
 Surface: CAA
 Exposure: LDEF Leading Edge, Longeron 8-9, 23 degrees from ram

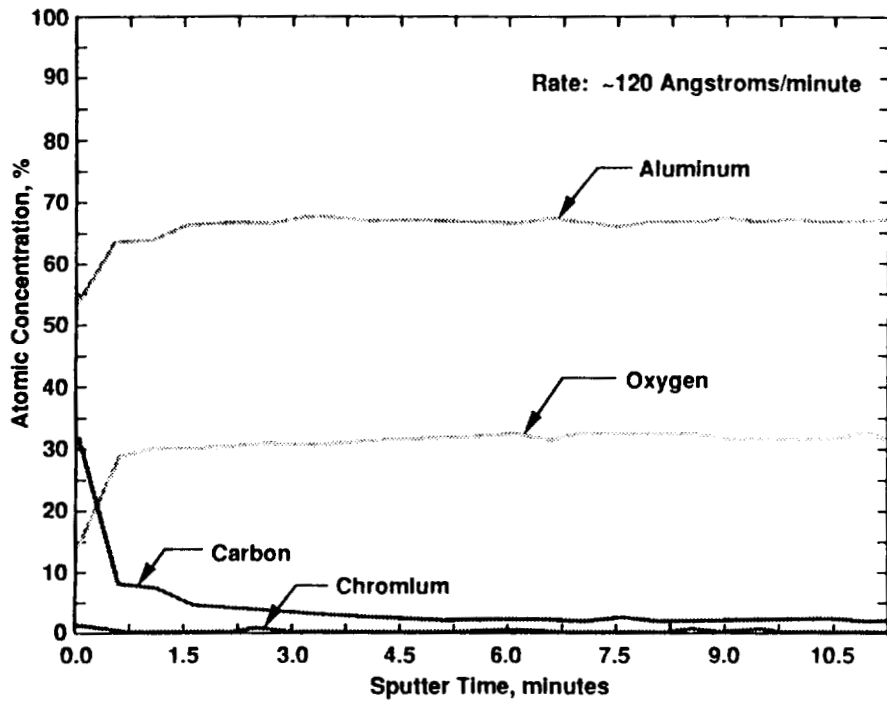


Figure 9. Auger Electron Spectroscopy Profile (Clamp C09-2)

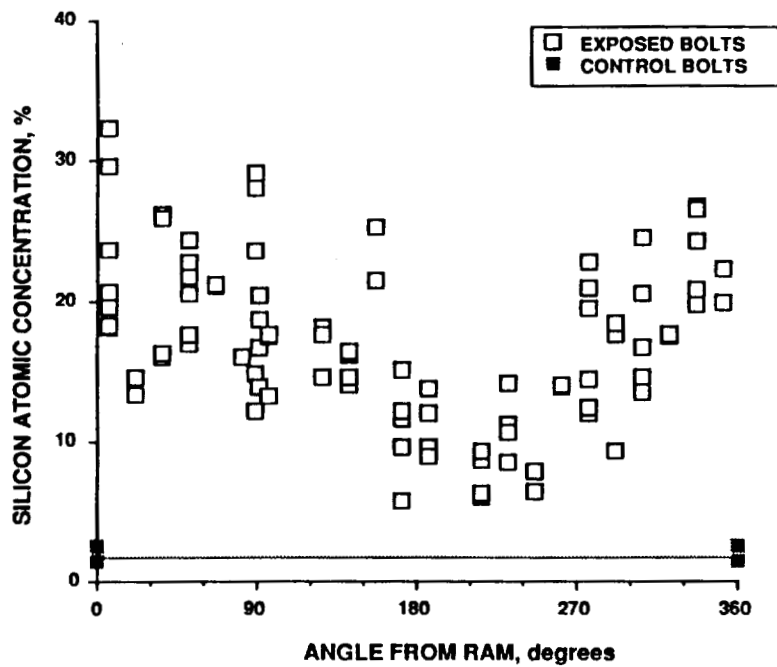


Figure 10. Silicon Concentrations On Bolt Head Surfaces Determined by ESCA

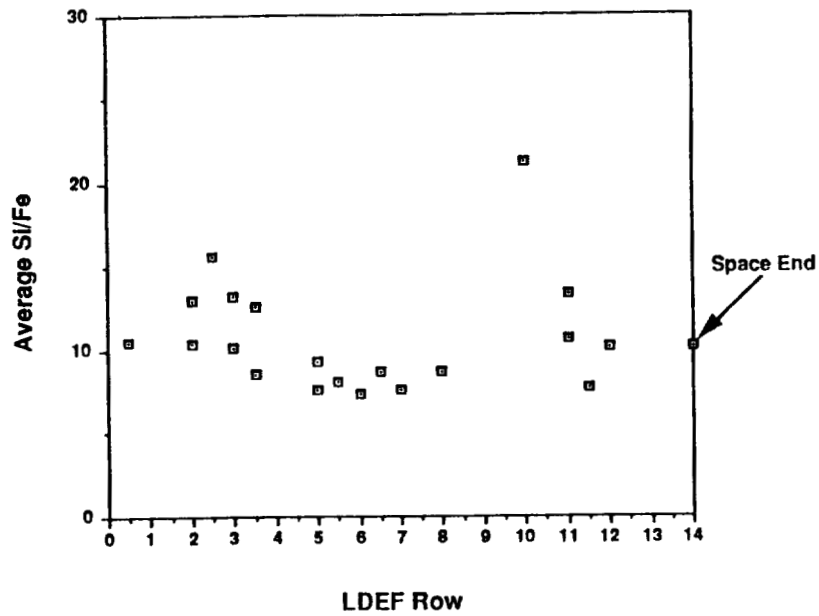


Figure 11. Surface Silicon to Iron Ratio Concentration by ESCA as a Function of Location

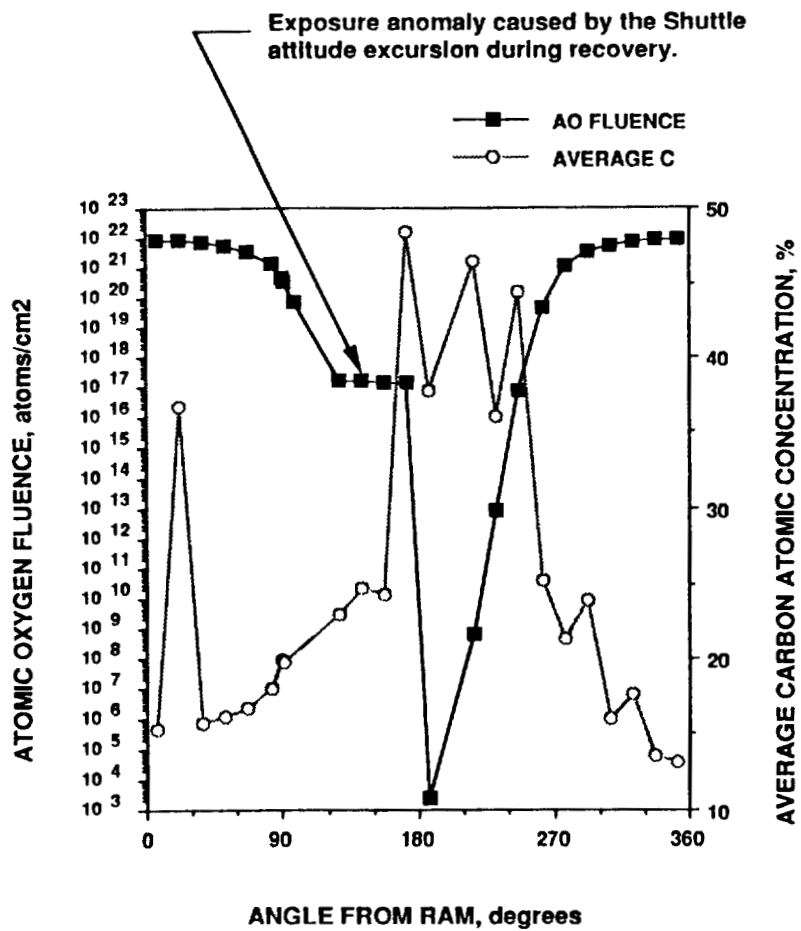


Figure 12. Atomic Oxygen Fluence and Carbon Concentrations on Bolt Heads Determined by ESCA

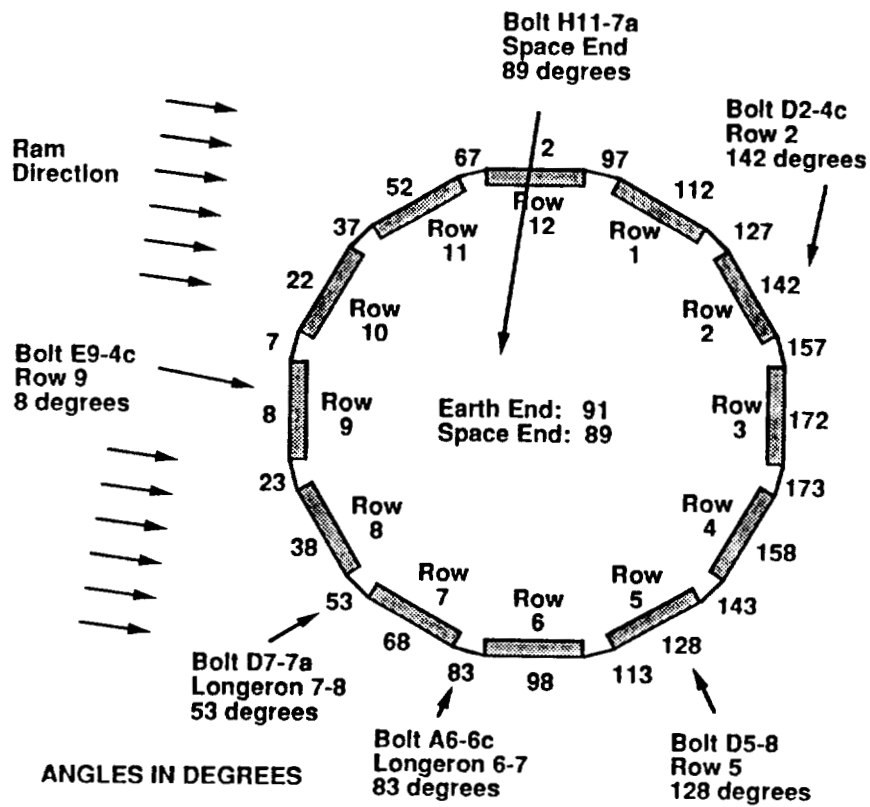


Figure 13. Bolt Locations for AES Profile Study of Silicon Contamination

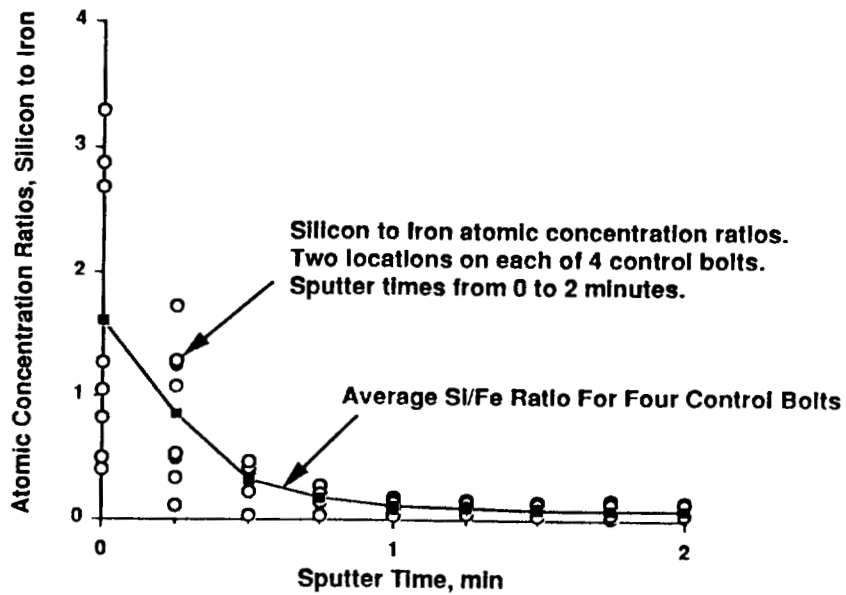


Figure 14. Average Silicon to Iron Concentration for Control Bolts

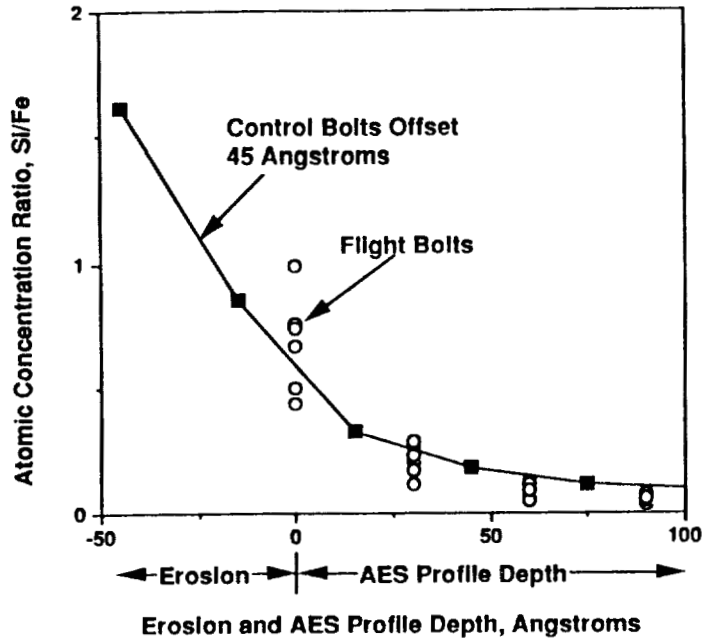


Figure 15. Silicon to Iron Concentrations for Flight Bolts Compared with Control Bolts

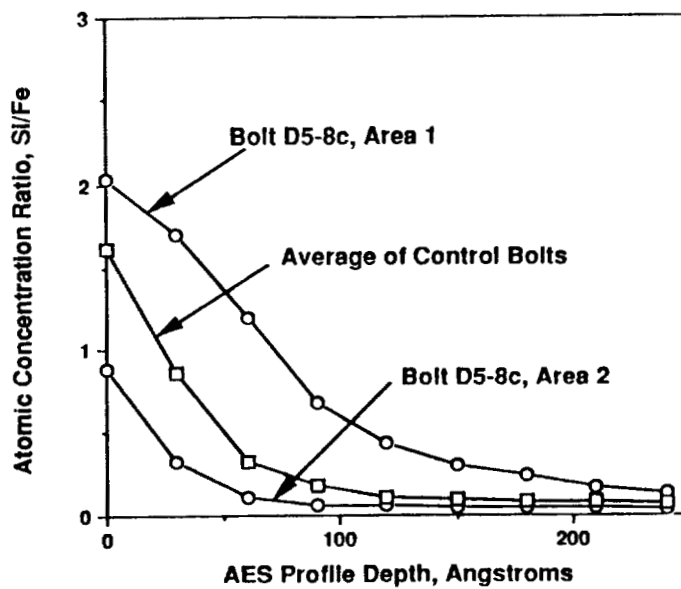


Figure 16. Silicon to Iron Concentrations on Control and Non-Atomic-Oxygen Exposed Flight Bolts

MEASUREMENTS OF THE OPTICAL PROPERTIES
OF THIN FILMS OF SILVER AND SILVER OXIDE

Palmer N. Peters
Robert C. Sisk
Yolanda Brown*
NASA/George C. Marshall Space Flight Center
Huntsville, AL 35812
Phone: 205/544-7728; FAX: 205/544-7754

S10-27
444-27
151

John C. Gregory
Pallob K. Nag
Ligia Christl
University of Alabama in Huntsville
Huntsville, AL 35899
Phone: 205/895-6076, FAX: 205/895-6349

SUMMARY

The optical properties of silver films and their oxides are measured to better characterize such films for use as sensors for atomic oxygen. Good agreement between properties of measured pure silver films and reported optical constants is observed. Similar comparisons for silver oxide have not been possible because of a lack of reported optical constants, but self-consistencies and discrepancies in our measured results are described.

INTRODUCTION

Silver, because of its electrical and optical properties, has many uses; however, silver's tendency to tarnish limits its optical film applications, and its susceptibility to destruction by atomic oxygen in low Earth orbits severely limits its applications in space.¹⁻⁴ Such changes in properties, however, have been used as sensors of atomic oxygen.⁵⁻⁸ While silver films are inexpensive and relatively simple sensors compared to mass spectrometers, or other complicated instruments, they exhibit some complexities that affect interpretation of exposure results. Optical measurements, such as reflectance and transmittance of silver films, are also relatively simple to do, but to accurately quantify oxygen atom exposure it is necessary to know the optical constants of the materials and to be able to model the material distributions. The studies reported here were performed to help measure such constants and to develop models, which are presently lacking.

One difficulty that arises is that silver is not useful for very heavy exposures. While measured effects have been found to be fairly linear over a specified range, excessive exposure leads to nonlinearity, cracking, debonding, and loss of the oxide's specular appearance.^{3,9} Using silver films of limited thickness can solve the above problems, if the possibility of saturation is recognized. Another problem can arise when the silver films are too thin; below approximately 25 nm thickness silver films have been found to exhibit an increase in extinction coefficient k and a decrease in the index of refraction n , with k peaking between 10 and 20 nm, and the absorption was dependent upon deposition rates.¹⁰ Such films were found to be discontinuous and treated as incompletely coagulated particles. The formation of both

*Summer Intern from Florida A&M

oxides of silver, AgO and Ag₂O, causes a large expansion of the silver lattice,^{2,3} which, for excessively thick films, causes the debonding and loss of specular characteristic. The resulting brown-gray or black-gray oxides fit the descriptions given for them in handbooks.¹¹ However, for thinner, specular oxide films the properties are more characteristic of coated optics.

The high reflectance and strong absorption of light by pure silver results in a rapid loss of intensity and minor interference between wavefronts reflected from top and bottom interfaces of a silver film; approximate linearity of optical density with thickness results and a simple Beer's Law model is reasonably appropriate, where $I=I_0e^{-at}$ is used to determine the transmittance; however, the greater transparency of silver oxide causes obvious interference effects, which cannot be neglected in interpretation of the measurements. Determination of a suitable model and optical constants to describe measured results on the partially oxidized films has not been easy for a number of reasons. For silver films initially thin enough to be transparent, a strong effect of exposure to oxygen atoms is an increase in light transmittance as the pure silver is thinned by oxidation. The kinetics of this oxidation process are still being investigated, and there are difficulties with determining the exact distributions of oxide and unreacted silver as a function of depth, because attempts to measure such distributions can tend to decompose the relatively unstable oxides. A simplified model of a layer of pure oxide on pure silver on glass, although tentative, is much easier to treat theoretically and has some merit, as will be discussed. Interference effects associated with the silver oxide films can exhibit colors which are dependent upon the oxide thickness, much like oil on water or antireflection films on optics. These effects produce maxima and minima in the reflectance and transmittance versus wavelength or film thickness plots. We have previously noted that not being able to properly correct for interference effects was a potential problem in previous studies.⁷

In summary, we have relied upon optical changes to measure the effects of atomic oxygen exposure for a number of applications, and appropriate optical constants are needed for calculations in the modeling. Due to a lack of published optical constants for silver oxide, we have embarked upon extracting such constants from silver films prepared in the same manner as films we have used; these films are oxidized at ambient temperature with a thermal oxygen, rf-discharge source, and thickness, reflectance and transmittance measurements are made. Subsequent studies will consider effects of source and exposure parameters.

EXPERIMENTAL

Following prolonged pumpdown and approximately 30 minutes presputtering, silver films were deposited on Corning 7059 glass substrates using rf sputtering from a 6 inch diameter silver target with argon at 4 microns pressure and using 200 watts forward power; similar conditions previously produced niobium films with the order of one-percent oxygen, probably associated with the low residual water peak observed in the residual gas just before the presputtering was used to getter the system. Silver is probably a poorer getter than niobium, but its sputter yield, and thus deposition rate, are several times higher; relatively low oxygen content might also be expected in the deposited silver films, although contamination levels have not been accurately measured; however, reasonable agreement with published optical properties have been observed.

Film thicknesses were initially estimated by the time of deposition and accurately measured by stylus profilometry traces across fine scratches produced in the silver to expose the substrate; a technique previously reported.^{3,12} Diffuse transmission measurements were made using four relatively broadband filters centered around yellow, green, blue, and red wavelengths in a densitometer having a 1 mm diameter source aperture. Both optical density and transmittance were determined.

Reflectances were measured from 250 nm to 2500 nm with the source beam incident at 15° off-normal to the sample, which covered a 12.5 mm diameter hole in an integrating sphere (AZ Technology LPSR-200 instrument). Comparisons were made to several standards to assure calibration within instrument specs.

MODELING

The films were treated as one or more layers, each of homogeneous material, on a Corning 7059 glass substrate. The initial silver film was treated as one layer on the substrate, and any oxide was treated as a second uniform film of given thickness on top of the silver. This simplified model ignores the possibility of the oxide density decreasing with distance from the top surface, but there appears to be some support for the uniform layering in the results observed.

Measurements on most intermediate thickness films exhibit a consistent ratio between the thickness of a silver oxide film and its initial silver thickness; this agrees with published density changes being accommodated by an appropriate increase in thickness of about 58%. Large deviations from this 58% expansion and anomalies in the optical constants when the films are on the order of 10 nm thickness indicate that a separate model is needed for the thinnest films. This may be accounted for by several factors: the films may consist of aggregate particles which create a lower film density, the probability is higher that thinner films might contain more contamination from the substrate as deposited, and the thinnest films may be more poorly represented by the bulk or thicker film physical and optical properties used in the calculations. Also, for films exceeding several hundred nanometers thickness debonding or surface roughening problems are more likely to appear, which would require additional modeling.

Although in many cases film properties are sensitive to deposition techniques and measured optical properties may only be applicable to films produced under the same conditions at the same facility, the properties of pure silver films from our facility seem to agree with those from other facilities; thus, the use of published optical constants for silver seems appropriate for calculations on films of intermediate thickness. While our extracted results show some self-consistency, more studies are required to clarify discrepancies, further verify the results, and to determine to what extent the constants are dependent upon exposure conditions and other parameters during formation of the oxides.

DISCUSSION

As deposited, the silver films exhibited optical properties of pure silver, as characterized by measurements of reflectance and transmittance in air and by comparison to calculated reflectance and transmittance using published optical constants. The results of these comparisons are shown in Figs. 1 through 4. Figure 1 compares the reflectance of pure silver as measured from a 168 nm film (line with open squares) with values calculated for a number of wavelengths (*); also shown in Fig. 1 is the reflectance of the same film after exposure to a beam from an oxygen discharge. Figure 2 shows measured optical densities for pure silver films of different thicknesses using four different broadband filters in the densitometer. The near linear behavior approximates Beer's Law described earlier, except for very thin films. Figure 3 shows the transmittances of the same films obtained from the measured optical densities, and Fig. 4 was obtained by calculating transmittance versus film thickness using published optical constants (single wavelengths near the filter centers were used in the calculations). The published constants, which are for thicker films, are not appropriate for films below 20 nm thickness, because silver films this thin tend to be inconsistent and produce variable properties due to variations in the aggregates that form. Thus, the calculations in Fig. 4 do not show the deviations in properties observed in very thin films that are most sensitive to deposition parameters; however, peaks, as observed near 13 nm in Fig. 3, have been reported for certain deposition conditions.¹⁰ The absorption coefficient for pure silver is sufficiently large that a rapid decay in light intensity occurs with depth in the film, limiting the transmission to films about 100 nm or less in thickness and subduing any interference effects. Silver transmits the shorter wavelengths better than the other colors, with the results that white light appears more blue when viewed through the silver and the measured transmittance is greater when shorter wavelength filters are used in the densitometer, as seen in Fig. 3.

When the silver films are oxidized, the lattice expands. For continuous films approaching bulk densities, lateral motion across the surface of the substrate is restricted, which favors vertical displacement,

or increasing film thickness; volume increases due to oxidation thus cause a proportional thickness increase. Figure 5 shows the expansion on oxidation (i.e. the ratio of oxidized film thickness to original silver film thickness) versus the original silver film thickness; to obtain this data, a number of different film thicknesses of silver were completely oxidized. The films near 20 nm and below show too little thickness change compared to the theoretical 1.58 value calculated from volume changes produced by oxidizing the films. This would be observed if the silver film consisted of aggregates, rather than being continuous, and expanded in three dimensions instead of thickness alone; adjacent voids would permit the lateral swelling. This interpretation is also consistent with the optical anomalies described above for films below 20 nm in thickness.

Figure 6 shows the general increase in transmittance with exposure time in seconds; different samples of approximately 31 nm thickness were separately exposed to the beam, each for a progressively longer time to obtain the increasing oxide thickness; this was done because returning the same sample to the beam after air exposure multiple times gave poor results. Because the oxide is relatively transparent, interference effects superimposed upon a slow decay in transmittance due to absorption are to be expected, as illustrated in Fig. 7, where measured transmittance is plotted versus silver oxide thickness on 7059 glass. Again, numerous samples were used, but this time each was of different initial silver film thickness before being totally oxidized. Figure 8 is a theoretically predicted version of Fig. 7 for a wavelength of 550 nm, where constant values of $n=3.1$ and $k=0.2$ were associated with all oxide thicknesses. Some of the disagreement between measured and calculated results may be related to the granular structures in thin films; however, other explanations seem necessary for all the observed discrepancies; the apparent lack of peak shifts with wavelength for the measured data seems strange, but the sparse data may not be providing satisfactory locations of the peaks and dispersion would influence peak location, as mentioned later. Another uncertainty is that uniformly complete oxidation is assumed in this case, which does not allow for variations in density or other parameters due to under or over exposure or other influences.

The effects of oxygen atom exposure on silver as a function of time were simulated by exposing 10 films, each over 500 nm thick, for increasingly longer periods. These results are shown in the Table, and the measured reflectances for the 10 films vs. wavelength are shown in Fig. 10. Attempting to obtain optical constants for silver oxide at a wavelength of 550 nm by adjusting n and k to produce the reflectances measured for each of the 10 oxide thicknesses shown in Fig. 10 causes problems similar to those in trying to fit the transmittance data of Fig. 7 by the calculations in Fig. 8; no pair of n and k values appears to satisfy all of the data points, and exact causes for all of the discrepancies have not been satisfactorily analyzed yet, but film structure, homogeneity and other factors that may be influenced by exposure conditions are being considered, and the accuracies of the oxide thicknesses, which are estimates in some cases, cannot be neglected in the analysis. It should be pointed out that reflectance measurements on a silver film flown on STS-4 gave a value of n estimated to be greater than 3, and results obtained from orbital exposure are not inconsistent with some of these ground-based results. Improper application of the same constants to a wide range of wavelengths gives qualitative agreement between measurements and calculations, but the interference maxima and minima locations are shifted, when comparing such calculated curves to the measured curves; this would be expected for a material with dispersion.

We have made limited extractions of optical constants as a function of wavelength from our measurements, but recent determinations of constants for two samples have been made using an ellipsometer with variable angle of incidence and wavelength;[#] these results suggest considerably more dispersion exists than in a typical glass, especially in the visible. If such dispersion is sensitive to exposure conditions, some of the observed discrepancies may be due to this. The ellipsometry and other results will be expanded and reported in the future.

Several computer programs to calculate reflectances and transmittances were written utilizing different techniques reported in the literature.¹⁴ All programs have given the same results where their applications overlapped. Metals, dielectrics, and semiconductors are treated, but each layer is considered to have uniform isotropic properties.

The assumption of uniform properties within each layer seems arbitrary, especially when

[#]Ellipsometry measurements by Mr. John Reynolds

partially oxidized silver films are treated as layers of pure oxide over pure silver, but the results appear to agree with some features of such a model, and while nonuniformities and anisotropies in the layers may be contributing to observed discrepancies, such effects are difficult to characterize. In the model used here, the total film thickness associated with a partially oxidized film is obtained by multiplying the thickness of silver consumed by 1.58 and adding the remaining unaltered silver thickness. The uniform layering is suggested not only by comparison of optical calculations and measurements, but also by stylus profilometry traces across scratches in films which indicate a sharp plateau at depths in the films where the boundary between the oxide layers and the silver should be expected, see Fig. 9; this suggests layering with fairly sharp changes in the mechanical properties at the interface. With further confirmation and study, such a model will also enable conclusions to be drawn about the kinetics of the silver oxidation process, at least under conditions like those described above.

The 5% precision for the measurement determining the 1.6 ± 0.05 times thickness increase upon oxidation (see Fig. 5) does not permit selecting which oxide forms, AgO or Ag₂O, since only 3% difference in the results would be predicted by substituting one oxide for the other. However, x-ray diffraction (XRD) results indicate our films are predominantly Ag₂O, as shown in Fig. 11.

It should be noted that the oxidation of silver at ambient temperature by active oxygen species involves numerous parameters, all of which are not known. There appears to be a variable lag between the initiation of exposure to our oxidizing beam and the appearance of rapid oxidation. There is also a similar effect if a partially oxidized film has been exposed to air and returned for additional exposure to the beam. The lag appears to be too long to remove a monolayer of combustible contaminant, but silicone contaminants at monolayer levels or effects of water vapor on the surface might be contributors. Heavy layers of contamination seem unlikely, unless polymerization, or some other fixation process is converting vapors adsorbed in the laboratory to films not easily evaporated during pumpdown in the oxygen source chamber. The major difficulty resulting from the above variable lags in starting time for the oxidation is that the use of timing for estimating the oxidation thickness is rather inaccurate, especially if thinly oxidized films are desired.

The ratio of Ag₂O to AgO in the oxidized films may be a parameter influenced by the type of O-atom source and exposure conditions. Conversion from AgO to Ag₂O after exposure may be a factor also, since slow changes over a period of months appear to occur and are accelerated by stresses, such as exposure in a scanning electron microscope, elevated temperature, and other parameters. Further investigations of factors influencing the ratio of the two oxides in the oxidation process are needed. Any differences in optical properties that exist between the two oxides are also needed, especially if the oxide ratios change with time, with in-depth location, or are different for thick and thin films.

CONCLUSIONS

Although the properties of silver oxide are relatively complicated, it appears that, with proper precautions, inexpensive, uncomplicated hardware can be used to perform optical measurements on silver films to gage exposure to atomic oxygen. The physical and optical properties of silver films below 20 nm and above 400 nm may be unsuitable for obtaining meaningful data; even in the intermediate thickness range there are some complications associated with nonlinearity between exposure time and measured effect. While it seems feasible to deposit pure silver films reproducibly, the initial oxidation of the films may be variably delayed during exposure by contaminants from open air or from some other cause; thus, very low levels of timed exposure may not produce the expected effect. Whether in situ film deposition might solve this problem is not known. Also, the properties of intermediate thickness films, which have specular surfaces and are relatively transparent, are significantly different from the brown-gray and black-gray powders usually described in the handbooks; this is not too different from the properties of transparent oxides of iron used for photolithography masks and the opaque red, or black, oxides associated with rust or powdered iron oxide; the optical properties of silver oxide have not received appreciable investigation at this time, probably because formation of these films has not been a common practice, but much better

characterization of the optical properties of silver oxide are needed for really accurate interpretation of optical measurements. Attempts to evaporate, sputter, or even bombard the oxides with appreciable energy results in decomposition ($T=100^{\circ}\text{C}$ decomposes AgO and 280°C decomposes Ag_2O). Silver oxide's optical properties appear to be useful enough in the intermediate thickness films to justify the effort required to determine them. The results of this study give some preliminary values for such optical constants and a layer model for the oxidation. Additional studies now in progress hopefully will confirm these results using different measurements and expand and better define their range of application.

REFERENCES

1. Gregory, J.C.; and Peters, P.N.: Interaction of Atomic Oxygen with Solid Surfaces at Orbital Altitudes, *Proceedings, First LDEF Mission Working Group Meeting (NASA, Langley Research Center)*, 1981, p.48.
2. Peters, P.N.; Linton, R.C.; and Miller, E.R.: Results of Apparent Atomic Oxygen Reactions on Ag, C, and Os Exposed During the Shuttle STS-4 Orbits, *Geophysical Research Letters*, Vol.10, 1983, p.569.
3. Peters, P.N.; Gregory, J.C.; and Swann, J.T.: Effects on Optical Systems from Interactions with Oxygen Atoms in Low Earth Orbits, *Applied Optics*, Vol. 25, April 15, 1986, pp.1290-1298.
4. Whitaker, A.F.; Little, S.A.; Harwell, R.J.; Griner, D.B.; DeHaye, R.F.; and Fromhold, A.T.: Orbital Atomic Oxygen Effects on Thermal Control and Optical Materials-STs-8 Results, *AIAA-85-0416, AIAA 23rd Aerospace Sciences Meeting*, 1985.
5. Henderson, W.R.; and Schiff, M.I.: A Simple Sensor for Atomic Oxygen in the Upper Atmosphere, *Planetary Space Science*, Vol.18, 1970, p.1527.
6. Thomas, R.J.; and Baker, D.J.: Silver Film Atomic Oxygen Sensors, *Canadian Journal of Physics*, Vol.50, 1972, p.1676.
7. Gregory, J.C.; and Peters, P.N.: A Measurement of the Angular Distribution of 5 eV Atomic Oxygen Scattered off a Solid Surface in Earth Orbit, *Rarefied Gas Dynamics*, ed. by V. Boffi and C. Cercignani, B.G. Teubner Stuttgart, 1986, pp.644-656.
8. Peters, P.N.; and Gregory, J.C.: Pinhole Cameras as Sensors for Atomic Oxygen in Orbit; Applications to Attitude Determination of the LDEF, *Proceedings of LDEF First Post-retrieval Symposium*, ed. by A.S. Levine, NASACP-3134, Part 1, June 1991, pp.61-67.
9. Edwards, D.L.; Williams, J.R.; Fromhold, A.T.; Barnes, P.A.; Wey, J.P.; Neely, W.C.; and Whitaker, A.F.: The Oxidation of Polycrystalline Silver Films by Thermal, Ground-State Atomic Oxygen, *Nuclear Instruments and Methods in Physical Research*, B79, 1993, pp.676-679.
10. Heavens, O.S.: Results of Measurements on Silver Films, *Optical Properties of Thin Solid Films*, Dover, New York, 1991, pp.166, 167, and 192-194.
11. Weast, R.C., ed.: Physical Constants of Inorganic Compounds, *Handbook of Chemistry and Physics*, The Chemical Rubber Co., Cleveland, Ohio, 1971, p.B-135.
12. Christl, L.C.; Gregory, J.C.; and Peters, P.N.: Measurements of Erosion Characteristics for Metal and Polymer Surfaces Using Profilometry, *Proceedings of First LDEF Post-Retrieval Symposium*, Kissimmee, Fla., June 2-8, 1991; ed. by A.S. Levine, NASA CP-3134, pp.723-735.
13. Lynch, D.W.; and Hunter, W.R.: Optical Constants of Metals, *Handbook of Optical Constants of Solids*, ed. by E.D. Palik, Academic Press, Orlando, 1985, pp.353-357.
14. Heavens, O.S.: *Ibid.* pp.46-95.

Table : Effects of increasing the O exposure on silver films

EXPOSURE TIME (MIN.)	UNEXPOSED FILM THICKNESS (nm)	EXPOSED FILM THICKNESS (nm)	OXIDE FILM CALCULATED THICKNESS (nm)	OXIDE FILM MEASURED THICKNESS (nm)
5	554.8	567.1	33.5	NA
8	553.7	555.5	4.9	NA
10	544.4	558.0	37.0	NA
12	550.3	575.2	67.8	NA
15	502.7	555.7	144.3	136.8
17	540.8	576.5	97.2	NA
20	518.5	586.5	185.2	203.8
22	552.7	597.8	122.8	170.3
25	516.3	570.0	146.2	154.5
27	513.8	604.2	246.1	204.5

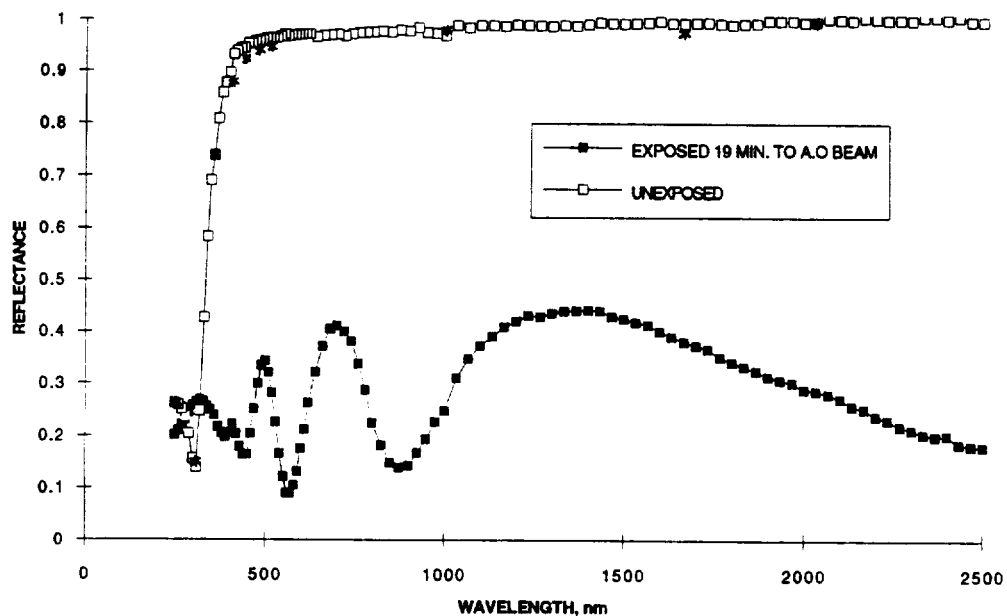


Fig. 1. Measured reflectance of a typical pure silver film compared to calculated values from literature optical constants (*), and the measured reflectance of the same film after conversion to a more transparent oxide exhibiting interference effects.

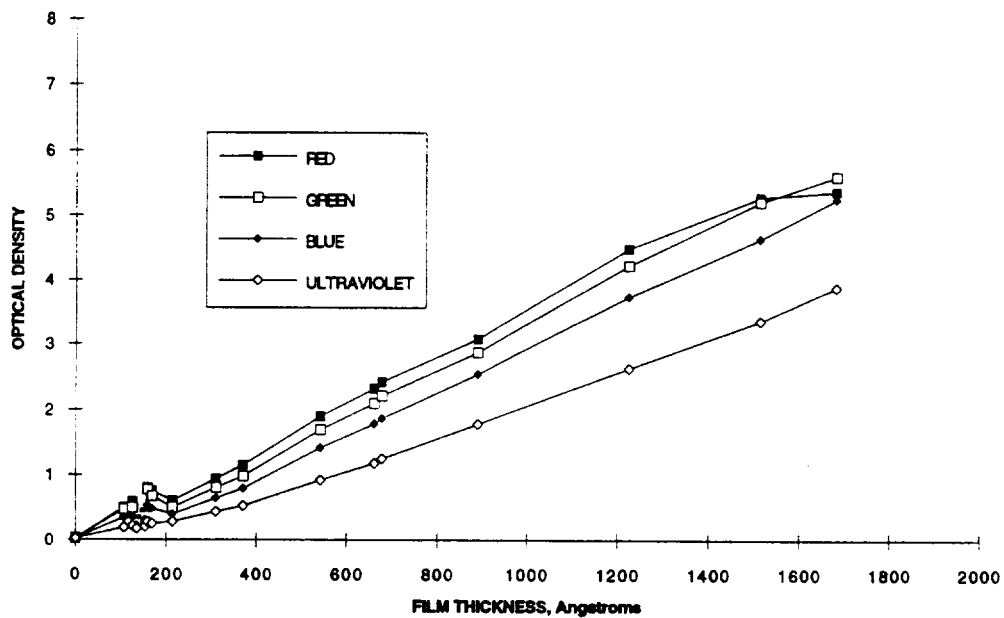


Fig. 2. Measured optical density of pure silver films vs. thickness, showing approximation to Beer's Law for films with strong absorption (interference effects negligible).

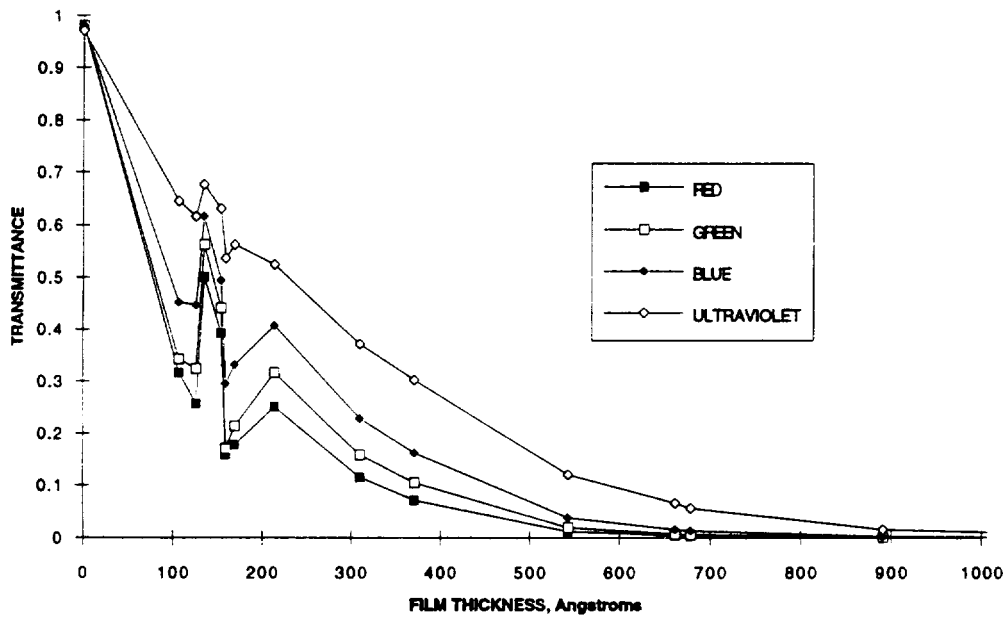


Fig. 3. Measured transmittance vs. film thickness of pure silver on glass. See text for explanation of anomaly near 150 angstroms thickness.

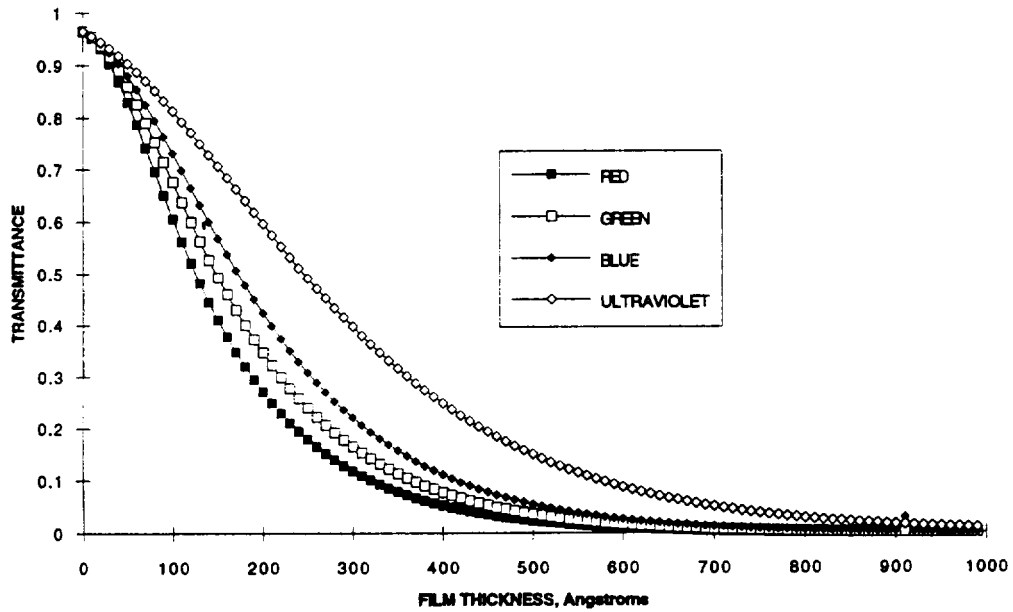


Fig. 4. Calculated transmittance vs. film thickness of pure silver on glass; each curve calculated for a wavelength representative of the middle of the color shown.

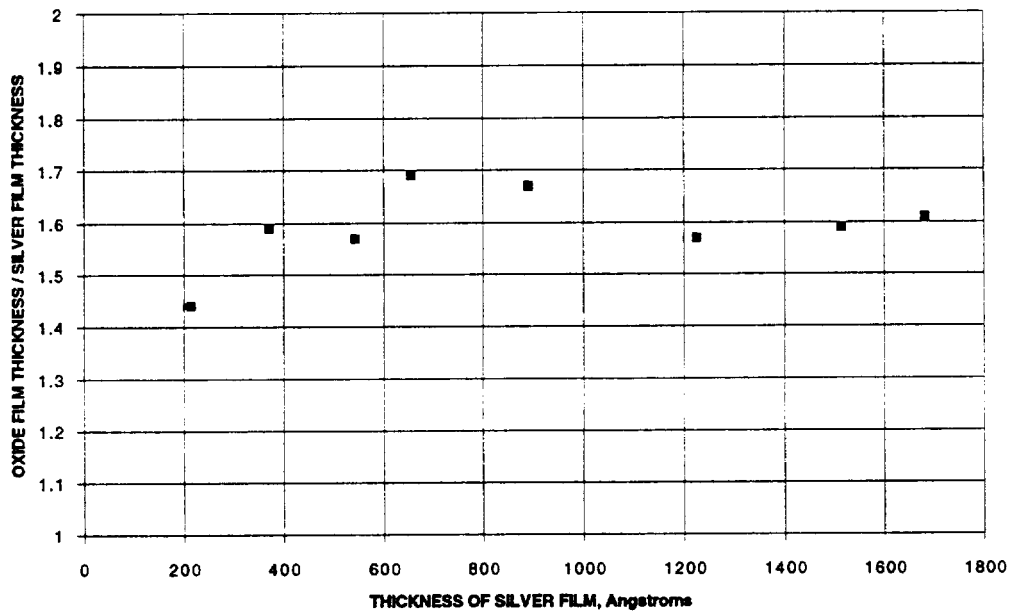


Fig. 5. Expansion in thickness of a number of silver films due to oxidation of sufficient time to convert the whole film to an oxide.

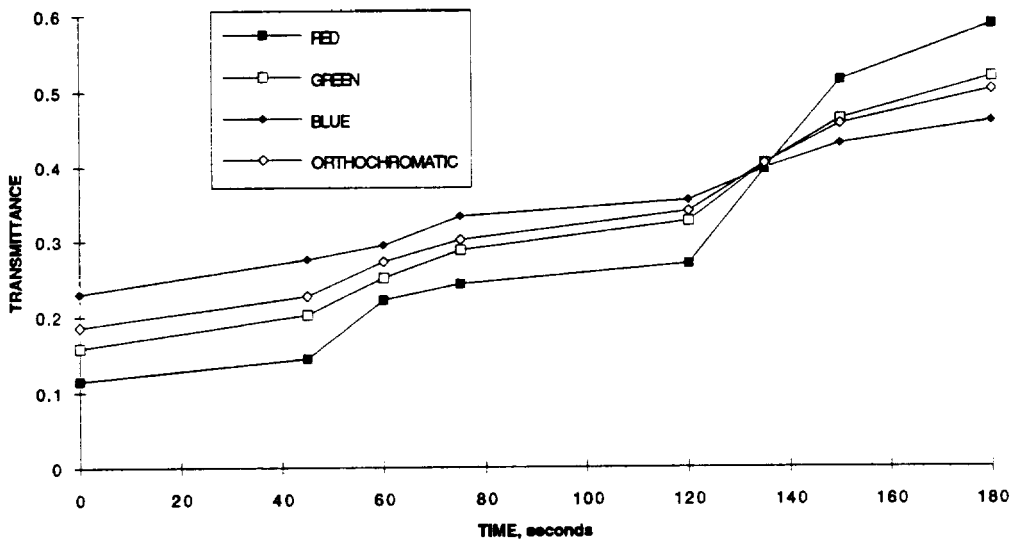


Fig. 6. Measured transmittance vs. exposure time of silver films to oxidation source.

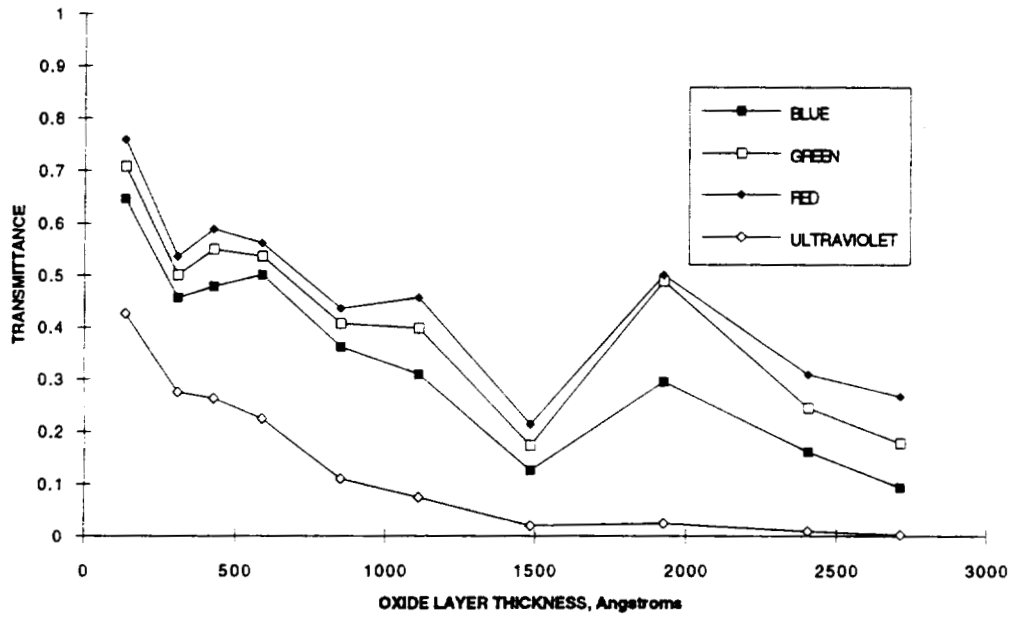


Fig. 7. Measured transmittance vs. silver oxide thickness on glass.

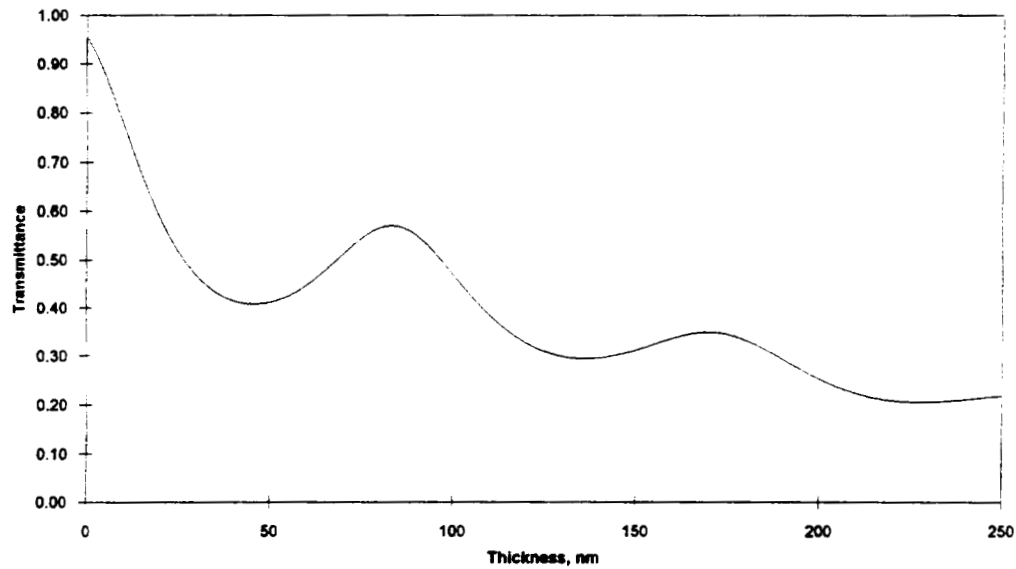


Fig. 8. Calculated transmittance vs. thickness of films for a wavelength of 550 nm, assuming pure silver oxide having $n=3.1$ and $k=0.2$ on glass whose $n=1.53$.

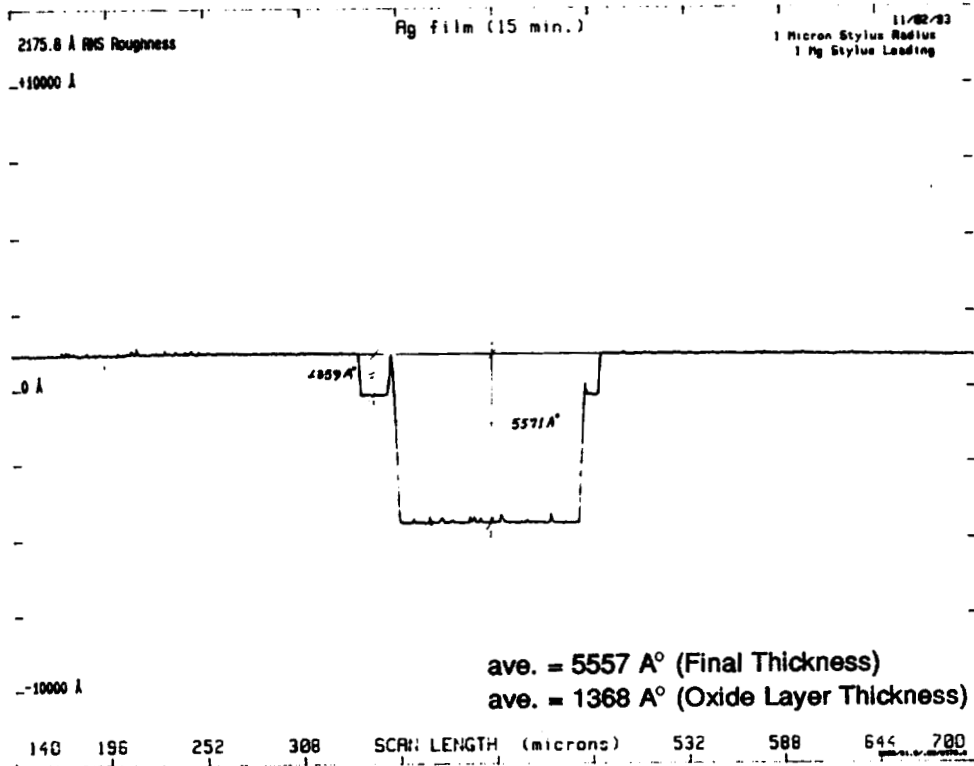


Fig. 9. Stylus profilometry measurement showing typical thickness of one of the thicker films used to measure reflectance of oxide on silver; half of such films exhibited the secondary step interpreted as silver oxide thickness on top of silver.

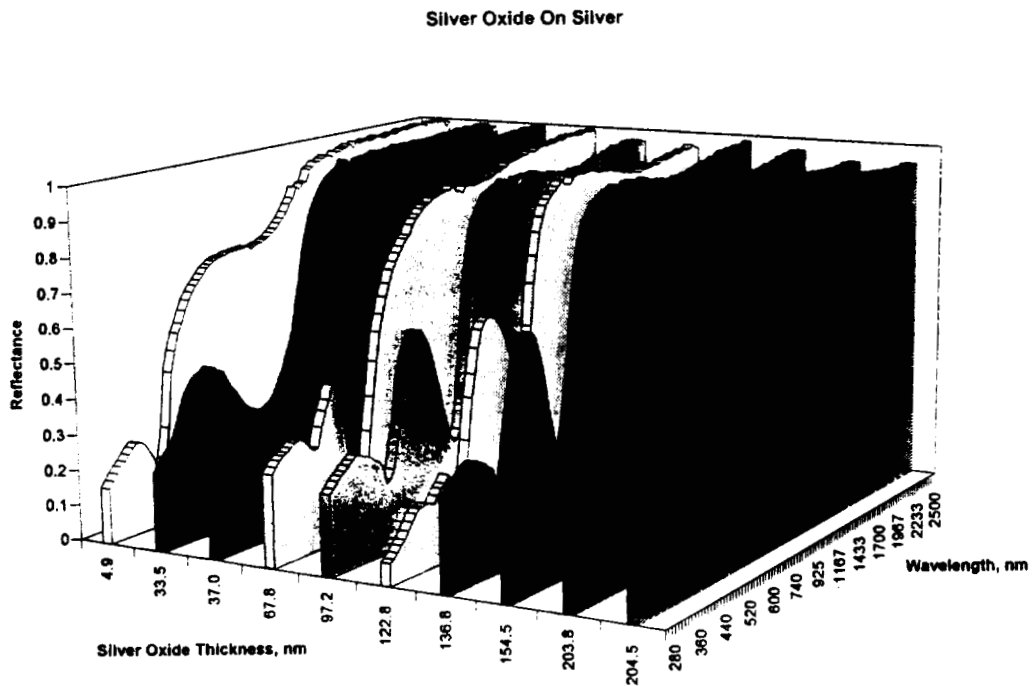


Fig. 10. Reflectance vs. wavelength for ten silver films, all initially thicker than 500 nm, each exposed once for a period ranging from 5 minutes to 27 minutes. See Table and the text for details of estimating silver oxide thickness.

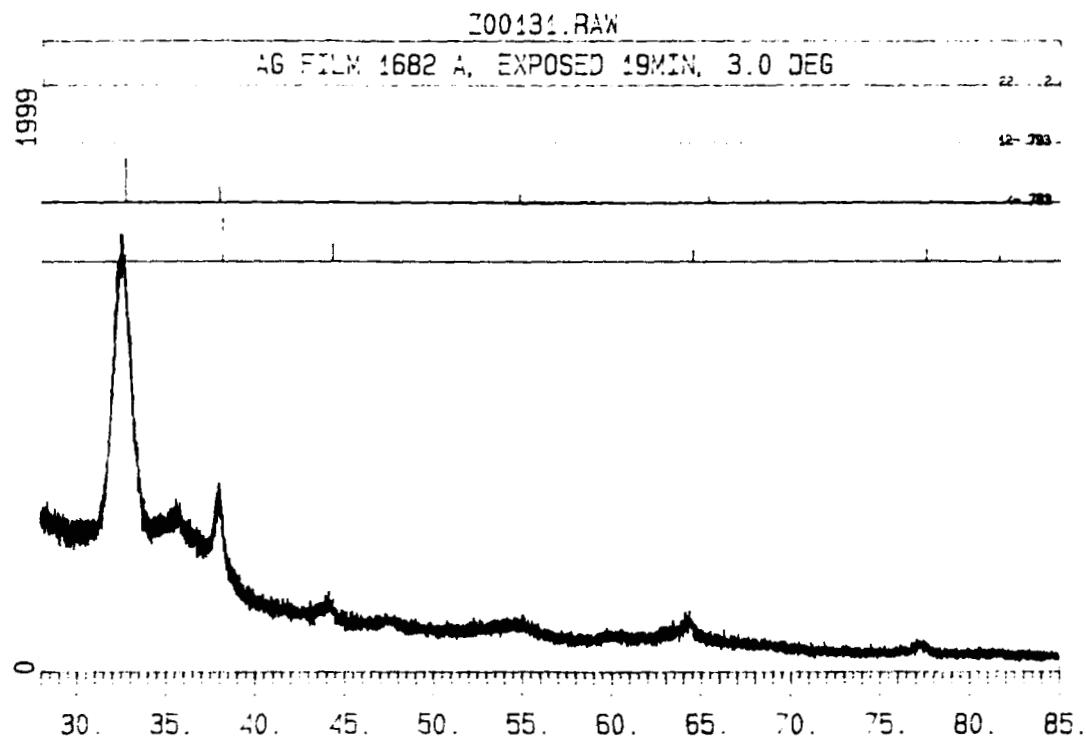


Fig. 11. X-ray diffraction of a silver film, initially 168 nm thick, exposed sufficiently that conversion to silver oxide was assumed. Pattern is most closely represented by Ag_2O .

**CHANGES IN CHEMICAL AND OPTICAL PROPERTIES
OF THIN FILM METAL MIRRORS ON LDEF**

Palmer N. Peters and James M. Zwiener
NASA/George C. Marshall Space Flight Center
Huntsville, AL 35812
Phone: 205/544-7728; FAX: 205/544-7754

S11-27

L-425

23f

John C. Gregory, Ganesh N. Raikar and Ligia C. Christl
University of Alabama in Huntsville
Huntsville, AL 35899
Phone: 205/895-6076, FAX: 205/895-6349

Donald R. Wilkes
AZ Technology, Huntsville, AL
Phone: 205/880-7481, FAX: 205/880-7483

SUMMARY

Thin films of the metals Cu, Ni, Pt, Au, Sn, Mo and W deposited on fused silica flats were exposed at ambient temperature on the leading and trailing faces of the LDEF. Reflectances of these films were measured from 250 to 2500 nm and compared with controls. The exposed films were subjected to the LDEF external environment including atomic oxygen, molecular contamination and solar ultraviolet. Major changes in optical and infrared reflectance were seen for Cu, Mo, Ni and W films on the leading face of LDEF and are attributed to partial conversion of metal to metal oxide. Smaller changes in optical properties are seen on all films and are probably caused by thin contaminant films deposited on top of the metal.

The optical measurements are correlated with film thickness measurements, x-ray photoelectron spectroscopy, optical calculations and in the case of Cu, with x-ray diffraction measurements. In a few cases, comparisons with results from a similar UAH experiment on STS-8 have been drawn.

INTRODUCTION

Earlier Results

The LDEF Experiment A0114¹ was designed to investigate the effects of atomic oxygen on orbiting spacecraft. Subsequently, degradation of surfaces was noted on early space shuttle missions and a dedicated part of mission STS-8 was carried out at a low altitude to further the investigations. Effects on optics were reported as part of the STS-8 results². The UAH portion of the EOIM-2 experiment flown on STS-8 was essentially a subset of the LDEF A0114 experiment in which approximately half of each sample surface was exposed with the other half covered by aluminum of the mounting plate, but unlike the free-flying LDEF, STS-8 had to be controlled to maintain the space shuttle's cargo bay in the orbital direction. To compare the effects resulting from the two missions properly, it is necessary to examine similarities and differences in parameters influencing both the experiments.

Mission and Sample Specific Effects

Due to a much longer exposure time, the total exposure to oxygen atoms for the LDEF leading surfaces was about 25 times that for the STS-8 surfaces; however, the rate (flux) of oxygen atoms was much higher on the lower altitude STS-8 surfaces. The initial reaction rates on virgin surfaces should correlate with the oxygen atom flux, which depends upon the atom density. The atom density depends upon the phase of the cyclic solar activity and the altitude of the orbit. The long term effects can be highly specific to individual samples as well as the mission. Some materials form such protective oxides that the predominant effect, if any, is a slight increase in oxide thickness. Other materials that form volatile species (e.g. osmium) erode rapidly, destroying thin films and producing roughness on bulk surfaces, which greatly modifies or destroys their optical properties. Materials forming nonvolatile but nonprotective oxides, such as silver, exhibit strong destructive surface changes which are more difficult to characterize, but for most optical applications these materials can be discarded. Nonreactive surfaces, such as gold, or those with protective oxides are the best candidates for optical applications. Contamination of these surfaces is a predominant cause of optical degradation, and the space environment can produce both desired and undesired effects on the optics. The vacuum induces outgassing of contaminants from spacecraft materials, but since the optical surfaces are initially well cleaned, transport to, and contamination of, the optics from other sources is more likely. The effect of atomic oxygen on deposited combustible contaminants such as hydrocarbons is to oxidize them into volatile species. However, many contaminants are from silicone-based materials, chosen for space applications due to their high mechanical stability and adhesive properties. These contaminants appear to be modified to form stable coatings after reaching the optical surfaces and being exposed to the space environment. Since silicone-based contaminants can greatly reduce atomic oxygen effects by providing a protective coating, it might be expected that the ratio of silicone contaminant deposition rate to atomic oxygen flux would be a factor in the overall effects. Sources of contamination and contamination transport to sensitive surfaces are complex issues⁵, and it is difficult to accurately predict rates of deposition. However, if contaminant depositions are similar at all altitudes and levels of solar activity, then missions initially carried out at high altitude during solar minimum (as with the LDEF) might experience greater subsequent protection from atomic oxygen due to contaminants than a mission carried out at low altitudes during solar maximum throughout the mission. Although later exposure of the LDEF at lower altitudes and higher solar activity provided most of the total fluence, earlier produced protective coatings could have had a strong influence on the later outcome of surface degradation, especially if surface renewal by heavy erosion or flaking did not occur. Such comparisons between STS-8, the LDEF, and other missions are needed and their results better understood to improve predictions of future effects.

Other Parameters

There are other factors that influence the comparison of the LDEF and STS-8 missions. The LDEF samples were prepared first, but were flown later, and exposed to ground-based environments longer than the STS-8 samples (the covered half of each sample acted as a control but it is difficult to isolate any ground-based effects). In both the experiments, thin films were deposited on optical flats to enable precise measurements of changes in film thickness using a stylus profilometer and to enhance optical measurements. However, while available $\sim \lambda/2$, flats of variable quality were used on the LDEF, uniformly superior optical flats were purchased later for STS-8. As a result better characterization of changes in film thickness was possible with the STS-8 samples. Contamination levels were generally more widespread on the LDEF samples than the STS-8 samples. Silicone-based contamination of <6 nm was observed from an isolated, nearly point source on only one STS-8 sample, while ~ 2 - 5 nm contamination appears typical on our non-etched LDEF samples. Limited stability has been observed for a few of the effects of atomic oxygen; thus, measurements on some surfaces would be different in situ (in orbit) than after recovery and perhaps as a function of time after recovery. Also, some measurements, such as

observation with a scanning electron microscope, or other processes which deposit appreciable energy to the surface, can modify areas scanned on some sensitive atomic oxygen exposed samples. The importance of chronological order of measurements from least likely to more severely degrading has been better recognized after the STS-8 studies. These studies produced a few such modified effects and greater precautions have been taken to avoid such effects on the LDEF samples by dividing or shielding parts of the samples, if modification is anticipated.

SAMPLE PREPARATION

The deposited films were optically thin in many cases, with the thickness in the range of 20 to 100nm. An important effect of such thin films is that a very small change in film thickness represents a large percentage property change. As described below, much greater measurement precisions were obtained for stylus profilometry and optical transmission measurements by using films on the order of a few tens of nanometers thick. Ideally, both opaque, as well as such thin films should be used to separate out effects of the substrate in the optical properties and the possibility that thinner films might absorb more solar radiation and reach a higher equilibrium temperature while in orbit. Another advantage of opaque films, is that interface layers, such as chrome, can be put down to improve film adhesion to the fused silica substrates since the optical reflectance of an opaque film would not involve this interface; because of the increased difficulty of interpreting very small changes when additional layers are present, interface or buffer layers were not used with these transparent films. Although paints and smooth bulk samples were also flown, their properties are reported separately, only the effects on metal films deposited on optical flat are reported here.

A typical sample was prepared by cleaning a fused silica flat after verifying that it was flat to $\sim \lambda/2$ or better. Planar diode sputtering and e-beam evaporation were predominately used for in-house film depositions. Some of the coatings were obtained from external sources.

EXPOSURE

The samples were mounted in a 9 mm thick aluminum plate⁴. Flat bottom holes the diameter of the optical flats plus clearance were machined two-thirds of the way through from the back, and the front 3 mm thickness was machined so a "half-moon opening" exposed approximately one-half of the front surface of each sample, while elastomer disks or O-rings were compressed behind the 3 mm thick samples to hold the samples in place. Attempts to produce hot and cold plates dependent upon thermal control coatings and isolation of the hotter plate appear to have created such modest temperature differences that little evidence of any temperature effect was observed. Similar samples were positioned on the LDEF's C9 (leading) and C3 (trailing) surfaces. During free flight, only portions of the LDEF trunnions and scuff plates had any line of sight to the A0114 surfaces and their solid angles from the samples were small. Deployment and recovery effects were relatively small on C3 surfaces, but not negligible. Present estimates⁵ of the total fluence are 8.72×10^{21} for the C9 surfaces and 1.32×10^{17} for the C3 surfaces, with most of this total occurring in the last year, since the LDEF started much higher during a period of solar minimum and ended much lower during a period of solar maximum. Non-orbiting environmental exposure effects, if any, are much harder to quantify.

MEASUREMENT TECHNIQUES

Characteristics

As previously observed, exposure to atomic oxygen in orbit can effectively "thin" some metallic films while changing their optical properties. A material whose oxide evaporates (e.g., osmium) exhibits a huge loss in film thickness and has limited usefulness if exposed to atomic oxygen. Other films of interest for optical applications often exhibit very small changes in optical properties (a small increase in light transmission and a small decrease in reflectance for instance). Several factors could be responsible for the observed effect: extremely low loss of metal atoms due to very low probability formation of a volatile oxide or a very low sputtering yield, both of which would result in a small decrease in overall film thickness. Formation of a very thin, stable, transparent oxide can also similarly change the optical properties. However any metal oxide formed tends to increase the overall film thickness slightly, although the pure metal is effectively "thinned". An additional cause for the changes observed could be an overlying contaminant layer which would increase the overall film thickness without loss of "metal thickness". A combination of these factors may be present, and difficulties can be experienced in separating the causes of the effects. A variety of measurements have been performed, in addition to the optical measurements, to identify the causes where possible.

Stylus Profilometry

One measurement of choice for determining film thicknesses is stylus profilometry, which is independent of the sample's optical properties. Stylus profilometry measurements are complimentary to optical measurements, which may pose difficulty in determining film thicknesses accurately if the indices of refraction are inhomogeneous, have anisotropies or numerous unknown layers. We have experienced problems in many cases with single frequency ellipsometry measurements; more complex techniques will have to be used to satisfactorily measure these film thicknesses optically. Stylus profilometry has difficulties if the surface is not smoother than the precision desired, and longer range waviness can create problems if sharp steps in the thickness being measured are not present. Shadowing effects at mask edges generally produce too broad a step to measure very small changes in film thickness. We developed a technique for stylus measurements of film thicknesses that overcomes this problem if the film can be removed in fine scratches without damaging the substrate. Films relatively softer than fused silica can be removed over small regions by using a fine wire to scrape lines through the metal, leaving a bare substrate; uniform, flat bottoms are indicative of successful scratches. Each scratch produces a square well pattern in the stylus trace and multiple, parallel scratches in the film produce a "square-wave-type" pattern which can be modulated by waviness in the surface of the flat, but still provide precise thickness measurements, since the top to bottom of each scratch indicates uniformity in the film thickness. Softer intermediate hardness films in layers have even produced multiple step heights, with ledges at film interfaces and a flat bottom at the substrate. The precision is limited somewhat by surface smoothness, with average changes of less than 1 nm in thickness being detectable with high quality flats and very smooth films. It should be noted that the scratches are actually produced perpendicular to the mask edge of sufficient length that stylus traces perpendicular to the scratches and parallel to the mask edge can provide several measurements of thickness in both the exposed and covered areas to verify that the change is not due to a taper in the film thickness as deposited. Consistent differences in thickness measured between exposed and nearby unexposed areas can be attributed to exposure. Much poorer precisions result if poorly defined steps or chance pinholes in the films must be used to estimate the exposed and unexposed thicknesses, since surface waviness obscures the poorly defined steps and widely spaced pinholes may measure a small variation in original film thickness unrelated to exposure as well as exhibit poor steps. Some films were too hard to scratch without damaging the substrate; using patterned films may solve such problems in future experiments. The results of previously measured film thicknesses

are reported here to help interpret the optical changes. One artifact, recently determined, from these types of measurements will be described, however. To avoid spoiling the central region of the films, where optical measurements are performed, the scratches were made at the boundary between exposed and unexposed areas as far removed from the sample center as possible; one of the chosen locations was near the corners of the "half-moon shaped" exposed area on the straight section of the boundary. The straight boundary has the advantage of producing the sharpest step with least shadowing because this straight edge on the aluminum mask had a knife edge nearly in contact with the sample surface. To accurately define the mask boundaries before the samples were removed, two small very fine, V-shaped notches were produced with a diamond microscribe traced around each corner. When stylus measurements were made too close to these scribed markings, fine debris from the silica substrates appears to have produced a higher density of spikes in the stylus measurement than would otherwise occur. This can be incorrectly attributed to other sources of particles or changes in surface roughness that result in increased scattering of the optical surfaces. While some local debonding of an iridium film was observed and reported previously (no interface layer was used), the density of spikes observed in the stylus measurements was greater than the density of debonded points and may have been related to debris near the boundary marks where the stylus measurements were made. Why the iridium predominantly debonded in the exposed area in a fairly uniform pattern of microscopic crazed peaks is speculative; possibly this was due to greater stresses on the exposed film and would presumably be less likely if a chrome, or other, interface layer was first deposited on the substrate to produce better adhesion. It should be noted that adhesion, except at these spikes was good, however, since the remainder of the film was not easily removed by scratching or other techniques. The softer gold and also platinum films did not exhibit similar local debonding; although bonding of gold to the fused silica was undoubtedly poor, stresses in the gold film were most likely much lower.

X-Ray Photoelectron Spectroscopy

X-ray photoelectron spectroscopy⁶ was used to investigate the surface contamination and oxide species present on the exposed and unexposed surfaces of a number of samples. The unexposed region of each sample was used as control. The samples were mounted on the sample stub with double-sided tape. Mg ka or Al ka source was chosen for x-ray radiation. System pressure during analysis was $\sim 2.5 \times 10^{-9}$ Torr. A pass energy of 89.5 eV was used to acquire the survey scans from 0 to 1100 eV binding energy to identify various elements present on the surface. A pass energy of 17.9 eV was used for high resolution elemental scans for surface composition in terms of atomic percentage. The XPS core levels were measured with a pass energy of 8.95 eV to obtain chemical state information from the details of binding energy and peak shape. Sample charging was measured by the displacement of the adventitious surface C 1s peak at 284.8 (± 0.2) eV. Carbon 1s due to hydrocarbon contamination and oxygen 1s peaks due to oxide species plus other carboxyl and moisture contaminants can be easily differentiated. Enhanced levels of oxygen and other impurities and a decrease in the substrate peaks on the exposed areas compared to covered areas was one indication of exposure effects. Details of the spectra, such as extra peaks (including satellite peaks), peak broadening, energy shifts, and peak ratios can be interpreted in terms of oxides formed, their oxidation states and relative amounts of contamination, especially when different measurement angles are compared.

Optical Measurements

Four types of optical measurements have been performed on the samples reported: optical density measurements using a small area white light source with a scanning microdensitometer, diffuse optical density measurements over a 1 mm aperture using four broad band color filters, diffuse reflectance (from a 12.5 mm diameter area) versus wavelength from 250 nm to 2500 nm, and infrared emissivity measurements. Only the reflectances versus wavelength are reported in detail here. Ellipsometry measurements have been attempted on a number of samples, but so far

the results have been generally disappointing. Only the scanning microdensitometer provided good evidence of the relative uniformity of the films in the covered and exposed areas; however, its measurement did not resolve variations smaller than its spot size nor gradients along the optical path. The disappointing ellipsometry measurements suggest that such depth variations or perhaps inhomogeneities within the film plane smaller than the microdensitometer spot, exist and create some measurement problems.

Other Measurements

On some metals where appreciable, but incomplete, reaction occurred on leading exposed surfaces, it was practical to analyze the structure of the modified surface, using x-ray diffraction, but only when a thin film attachment was used. The results of this type of XRD measurement were most useful for copper, which showed intermediate reactivity.

RESULTS

Sample C3-04, tin , Trailing Edge

Stylus profilometry measurements, of the trailing edge (wake side) tin sample exhibited considerably less precision in the measured film thicknesses than for the leading edge (ram side) tin surface (see Table I). This result usually indicates a greater roughness in the measured surface. Although the film appears to be possibly thicker in the exposed area, the measurement precision is poorer than any suggested difference. XPS showed a higher concentration of Na in both exposed and covered areas, presumably due to NaCl contamination, sources of which are unknown. Si concentration was higher in the exposed area than in the covered area. Both C and O concentration was similar in both the areas.

The reflectance, Fig. 1, exhibits considerable improvement at shorter wavelengths (tin was the only film showing significant improvement) after exposure. Interestingly, improvement in reflectance is observed to be higher for the trailing tin sample than the leading tin sample. Although it is possible for some overcoats to enhance reflectance and hydrocarbon contaminant removal could accomplish the same result, no completely satisfactory explanation for these results is offered from the existing data.

Sample C9-04, tin, Leading Edge

Table I indicates that the exposed area of the leading tin sample had an apparent thinning. Table II shows that there were increases in oxygen and silicon, and a decrease in carbon in the exposed area. Carbon, from hydrocarbons (hydrogen is not observed), is a common atmospheric contaminant. Its decrease in the exposed area is consistent with removal by atomic oxygen; the remaining carbon in the exposed area could have come from post flight exposure. Traces of Na, Cl, and F may indicate minute amounts of salt contamination. The significantly higher levels of silicon and oxygen and much smaller level of tin in the exposed area indicates appreciable overlying contamination consistent with models assuming silicone contamination from the LDEF followed by modification of the surface, perhaps to silica, by the atomic oxygen. Again, a slight increase in reflectance in the exposed area is observed in Fig. 1; removal of hydrocarbon contamination could be a contributor to better reflectance, while the SiO₂ -type contamination would presumably decrease the reflectance; however, appreciably greater hydrocarbon removal would seem necessary to explain the larger change in sample C3-04, which received the least oxygen; therefore other mechanisms are apparently involved.

Sample C3-09, tungsten, Trailing Edge

The tungsten film was too hard to be scratched effectively without damaging the silica substrates; therefore, only a thickness in the covered area is listed in Table I; such thicknesses are usually estimates based on deposition parameters and the best measurements permitted by stylus measurements of any pinholes in the film where dust particles resided during deposition.

In such cases where the scratching techniques were not applicable for determining changes in thickness of the exposed area, attempts were made to use stylus tracing from unexposed to exposed areas to look for a step at the mask boundary. The precision of such step measurements was strongly dependent upon finding a region with well-defined, reasonably sharp steps at the former location of a mask knife edge. Such satisfactory steps are found sometimes; this tungsten sample showed a step up of 18.6 (± 3.1) nm in going from the covered area to the exposed area of the sample. This might be interpreted as an increase in film thickness due to exposure, but substrate surface changes cannot be ruled out. Table II indicates a considerably lower percentage atomic concentration of tungsten for the exposed than the covered area, and considerably more Si, consistent with a silicone-based overcoat. The level of W measured would not be observed through 18.6 nm of overlying contamination. A "swelling" of the film by oxidation also seems unlikely, since this trailing film received minimal oxygen exposure and little difference in oxygen concentration is observed between exposed and covered areas by XPS. It would be easier to assume the 18.6 nm step was unrelated to exposure, if it were not for similar steps being observed on other samples independent of whether they were on leading or trailing surfaces. It should be noted that where actual film thicknesses were measured (by the scratch technique) that thickness changes were much smaller than these large steps. If the similar steps are indeed related to exposure, further studies are needed to determine whether the films, the fused silica substrate, or both are involved; the change is a much smaller percentage of the substrate thickness than the film thickness, and may be within the stability limits of fused silica under appreciable stresses for a long length of time (about 6 ppm change). The substrates were compressed on the holder for ~ 6 years. Regardless, it is premature to associate the larger measured steps with surface preparation, contamination, film swelling or any specific mechanism at this time. Calculated values for the reflectance of tungsten using literature optical constants gave results both higher and lower than we measured for covered tungsten, and the calculated values were more irregular than for other films.

Sample C9-09, tungsten, Leading Edge

The leading tungsten sample did not permit accurate stylus determination of its film thickness since there were no good pinholes nor other film thickness steps to measure. The thickness has been estimated to be between 60 and 70 nm. Again, a measurable, somewhat more precise, step of 19.4 (± 0.7) nm was observed in stylus traces from covered to exposed areas, which, within the precision of the measurements was the same as that observed on the trailing sample. It is assumed that this step also does not represent a contaminant thickness, since Table I shows the tungsten atomic concentration to be only slightly less in the exposed than the covered area. The reduction in carbon and increase in oxygen in the exposed area agrees with high fluences of atomic oxygen to the leading surfaces. The relatively large amount of Si concentration on the covered area as seen in Table II was not expected, nor understood, and is atypical. However, grains of silica debris or pinholes to the silica substrate in the analyzed area could account for higher Si. The fairly uniform reduction in reflectance at long wavelengths in Fig. 4 for the exposed area is not consistent with calculated effects of a thin overlying contaminant (see gold as such an example), but this and the high tungsten concentration are more consistent with appreciable tungsten oxide; this oxidation occurred to a lesser extent than for some of the other films, such as copper.

Sample C3-10, platinum, Trailing Edge

As would be expected, this trailing platinum film exhibited nothing attributable to oxidation. The precision of the stylus measurements of film thickness was relatively good in both covered and exposed areas; values of 38.4 (± 1.3) nm thickness in the covered and 43.6 (± 2.3) nm thickness in the exposed areas were obtained, as shown in Table I. The difference of ~ 5 nm is similar to changes on other films believed to be contaminated by films of silicone-based origin. However, the measured reflectance versus wavelength, as shown in Figure 5, shows no difference between covered and exposed areas, which is puzzling, since calculated reflectance changes for gold films with < 5 nm contaminant thickness are noticeable (as discussed later). Repeated measurements confirmed the same reflectances, and the stylus measurements were on the correct samples (note thickest Pt has highest reflectance). XPS showed a higher concentration of Si and O in the exposed area than in the unexposed area and vice versa is true for C (see Table II). This indicates formation of a thin layer of silica based on XPS chemical shifts. Other contaminants were found in very minute quantities.

Sample C9-10, platinum, Leading Edge

This leading platinum sample shows precise thickness measurements, with both covered and exposed areas indicating ~ 59 nm film thicknesses, as shown in Table I. This indicates no apparent contamination on the exposed area using stylus measurements, however, there is significantly more Si indicated on the exposed area from XPS measurements and the Pt is greatly reduced, as if overcoated, as shown in Table II. The same XPS measurements also show more carbon on the covered area, and presumably hydrocarbon contaminants were oxidized and removed from the exposed area. One seemingly unlikely explanation for no thickness change would be that the increase in SiO_2 was balanced by an equivalent removal of hydrocarbon.

The measured reflectances were consistently higher than those calculated using literature optical constants and the measured film thickness as shown in Fig. 6 ; a platinum film from another source measured in the middle of these sets of data. The XPS measurements on the C9-10 film definitely indicate contamination, similar to that observed later on gold, and the reflectance loss on the exposed area is similar to that for gold, but no completely satisfactory answer is offered for not having measured the contaminant by stylus, nor explaining a stylus measured increase for the trailing exposed surface with no reflectance change.

The platinum does differ from gold in that oxide layers may be contributing to the observed changes, but more details are needed to fit the platinum with a satisfactory model.

Sample C3-16, copper, Trailing Edge

Good to fair precisions were obtained for the film thicknesses on this trailing copper sample. Although ~ 0.8 nm increase in thickness of the exposed area film is suggested in Table I, this value is less than the precision of the stylus measurements for this sample. Table II shows slightly higher copper in the exposed area, little difference in oxygen, slightly less carbon, and a small increase in Si. Measured reflectances in both covered and exposed areas in Fig. 7 differ only at shorter wavelengths from calculated values, using literature optical constants and our stylus measured film thickness. Reflectance measurements on 1 year old copper films in our laboratory showed fairly good agreement with the literature. Some environmental degradation is suspected, even in the covered areas, after a decade, but we cannot verify this, since as-coated reflectances were not measured. The very small difference between covered and exposed area reflectances may be contaminant or oxide related, but all effects are too small for our measurements to be definitive.

Sample C9-16, copper, Leading Edge

The effects on the leading copper film were gross, as evident visually, since the exposed area no longer had a metallic appearance. Table I shows that this sample grew in thickness over 30 nm in the exposed area. X-ray diffraction using a thin film attachment, showed that copper oxide was formed and identified it, mostly as Cu_2O .⁷ However, pure copper and a trace of CuO were also present. Our best estimate was that the film consisted of the equivalent of ~ 92 nm of oxide and ~ 13 nm of copper; however, ellipsometry and other measurements so far have not provided any evidence of layers. The reflectance was greatly reduced, as shown in Fig. 8, and the transmission of light was much greater in the exposed area, as previously reported. Attempts to calculate reflectances using literature values of optical constants for copper and its oxides on fused silica gave no agreement; no combination of copper on silica covered by copper oxide gave the amount of reflectance loss observed. It appears that the converted film has its own optical constants and we believe that these are not uniform, perhaps having a gradient from the surface to the substrate, or at least having some distribution of copper within the oxide film. Any contamination effect seems negligible compared to the chemical changes on this sample; however, carbon is less and Si and oxygen greater in the exposed area. The higher Cu peak in the exposed area is associated with the Cu_2O .

Sample C3-24, molybdenum, Trailing Edge

Molybdenum was another film which did not scratch satisfactorily for thickness measurements. This trailing film was estimated to be 35.1 (± 4.3) nm thick in Table I, and only stylus traces from unexposed to exposed areas were available to estimate any changes in the surface. Again, a large 18.6 (± 3.1) nm, step was observed, which is still not considered contamination, and is not satisfactorily explained. This film is estimated to be nearly the same thickness as for C9-24, but it shows considerably less reflectance, Fig. 9, than the covered area of C9-24, Fig. 10. XPS measurements showed considerable Si contamination in the exposed area which has converted into silica. There was hardly any Si in the covered area. However there was a large increase in N concentration in the covered area which is difficult to explain. It is hypothesized that the molybdenum films may have been deposited with oxide incorporated; this could explain the reduction in reflectance of covered films compared to calculated values.

Sample C9-24, molybdenum, Leading Edge

The leading molybdenum sample also could not be scratched, but its thickness was estimated to be 35.4 (± 1.9) nm, in Table I. Stylus traces from the covered to exposed areas did not give detectable steps, but a yellow-green color on the exposed area suggests an oxide interference. The absence of detectable steps indicates that they were not very sharply defined at the mask boundary compared to the substrate surface variations. Table II, shows appreciable oxygen and carbon in the covered area, suggesting appreciable oxidation of the original film plus hydrocarbon contamination. Appreciable carbon was removed by the ram oxygen in the exposed area; since residual carbon is seen on the numerous other samples exposed to ram oxygen, it may result from postflight exposure as opposed to carbides, etc. Considerably more Si and additional oxygen are present, consistent with contamination on the LDEF, but the effects of oxidation are considered to be the dominating factor. As discussed later, it is believed that initial oxide incorporation could have occurred in some of the films during deposition, lowering their reflectances compared to values calculated from literature constants, and the ram exposure further reduced the reflectance, as in Fig. 10.

Sample C3-45, nickel, Trailing Edge

The thicknesses of the nickel films were poorly known, since no suitable steps were obtained for film thickness measurements. The best estimate for the thickness, which was poor, was ~ 40 nm. Based on this thickness and literature values for the optical constants, calculated reflectances were found to be considerably higher than the measured reflectances, as shown in Fig. 11. Better agreement is obtained for considerably thinner films, but we believe that the nickel is thicker than necessary to obtain reasonably good agreement, suggesting that even the covered areas of the film contain more oxide than the nickel of the literature. Table II shows a smaller concentration of Ni in the exposed area of C3-45, indicating some contaminant overcoat, Si-based film being likely, with some reduction in the total carbon. The slightly higher oxygen could be associated with partially converted Si, but the uniformly small decrease in reflectance of the exposed area is more typical of slight oxidation of the nickel film.

Sample C9-45, nickel, Leading Edge

Table II shows that the ram side nickel film has a higher Ni concentration in the exposed than in the covered area; this appears to be characteristic of the heavier oxidized films where the metal concentration is associated with its oxide. The carbon is significantly reduced, as expected from the ram atomic oxygen removing hydrocarbons. The Si and oxygen are both also increased in the exposed area consistent with Si-based contamination and perhaps oxygen modification. The major decrease in reflectance of the exposed, ram nickel film in Fig. 12, however, is believed to be a result of increased oxidation of the nickel film.

Sample C3-46, gold, Trailing Edge

The modeling for the trailing gold sample is similar to that for the leading gold, which is discussed next in greater detail, because more results have been measured for it. The stylus profilometry results in Table I indicate that the film thickness for the covered area was 33.3 (± 0.5) nm and for the exposed area it was 35.3 (± 1.3); from the following discussion for C9-46, this thickness difference suggests that ~ 2 nm of contamination was acquired on C3-46 and XPS measurements seem to support this assumption (see Table II). The same model as for C9-46 can be used. It appears that roughly one-half as much contamination was acquired on C3-46 as on C9-46. From Fig. 13 it is seen that the reflectance loss is correspondingly less for the exposed C3-46 than the exposed C9-46 area in Fig. 14.

Sample C9-46, gold, Leading Edge

Fortunately, there are fewer parameters influencing gold than most materials. Two primary modes of degradation are apparent for the gold: (1) thinning of the film by physical sputtering, and (2) effects of contamination. Although gold has a high sputtering yield compared to most materials, the ~ 5 eV impact energies of oxygen atoms and higher energies for N₂ and heavier molecules, due to the orbital velocity, do not provide enough momentum exchange to produce significant sputtering. On STS-8 the fluence levels were below those needed to detect any effect of sputtering. McKeown⁸ reported sputtering of gold at levels less than 5×10^{-6} atom/molecule of the upper atmosphere striking the gold; the measurements were performed with quartz oscillators on Discoverer satellites with a perigee of ~ 200 km and ~ 10 eV particle-surface interaction energies (more typical of N₂). With atomic oxygen dominating the fluence at higher orbits the gas-surface interactions should produce even less sputtering yield. Using 5×10^{-6} atom of Au/atom of O multiplied by 8.72×10^{21} atoms of O/cm² for the total fluence produces 4.36×10^{16} atoms of Au/cm², as a conservative upper limit for the amount of gold that might be sputtered. Using the bulk density of gold, its atomic weight, and Avogadro's number, it can be shown that this amount

of sputtering would correspond to an upper limit of 7.4 nm thinning of the gold film. The slightly lower density associated with most films compared to bulk could increase the thickness sputtered slightly. Table I shows, from stylus measurements, that C9-46 had a film thickness of 31.7 (± 0.6) nm in the covered area and 35.4 (± 0.4) nm in the exposed area. This increase in thickness is assumed to be from contamination, and the XPS measurements in Table II support this conclusion, since the gold peak is greatly reduced, as if overcoated, and the Si and O peaks are much higher in the exposed than the covered area. The reflectance of C9-46, in Fig. 14, shows a decrease at short wavelengths. If we assume, for lack of better optical constants, that 3.7 nm of SiO₂ represents the contaminant on 31.7 nm of gold on a fused silica substrate, then the reflectances calculated using literature optical constants⁹ for pure gold and gold plus the SiO₂ are shown in Fig. 15. The loss in reflectance thus calculated represents a large fraction of the loss measured. If we assume that a loss in hydrocarbon contamination (C was much less in Table II) was made up by additional SiO₂, then it appears feasible to explain most of the total loss, if not all, as being due to contamination; the assumption of optical constants of SiO₂ might be slighting the calculated reflectance for the given contaminant thickness also. Although an increase in thickness of the exposed film was measured, rather than a thinning, it is still desirable to estimate the effect of sputtering, since any thinning could be overcompensated for by contamination thickening. Figure 16 shows the measured reflectances of C9-46 for the covered and exposed areas and calculated reflectances for two gold thicknesses: a 31.7 nm film thickness (covered area) and an assumed gold film thickness of 24.2 nm, which would result if 7.5 nm of gold had been sputtered from this film as an upper limit. Note that the measured reflectance of the covered area agrees with the literature, but the assumption of 7.5 nm thinning of the gold totally disagrees with the measured reflectance of the exposed area; not only is the reflectance at 250 and 300 nm wavelength not reduced by thinning, while the measured change is greatest there, but the thinning reduces the reflectance at longer wavelengths, where no change is measured. Lack of apparent sputtering may be explained in two ways: (1) the sputter yields are, as expected, even lower than the already very low upper limit on the yield, and (2) contaminants prevented, or greatly reduced, any sputtering that might have ordinarily taken place. Thus, the effects on the gold are rather well-modeled by assumptions of no sputtering and the presence of several nanometers of contamination.

CONCLUSIONS

A wide range of effects from atomic oxygen interaction with low Earth orbiting satellites occurs on metal films. Such films have numerous applications to electrical circuits, to thermal control coatings and to various optical systems; degradation of the physical, electrical, or optical properties of the films can be disastrous to mission objectives under some circumstances.

For very sensitive materials such as osmium, and silver, which have been previously reported^{10,11}, the effects of oxygen atom ram exposure are so severe that the use of these materials should be questioned unless great care is taken to protect the materials. The effects on films reported here, while less severe, still vary from possibly insignificant to unacceptable in terms of application and optical degradation. The films appear to be separable into those which are relatively insensitive to atomic oxygen, such that contamination probably dominates any effects, and those which are oxidized appreciably, causing their optical constants to be changed enough to challenge their use if exposure to ram oxygen is permitted.

In the insensitive materials category gold represents the best modeled material reported here. Measured optical properties of gold agreed well with accepted literature values; its reflectances, film thicknesses, and other measurements supported a model which discarded physical sputtering effects, at least for this LDEF mission, and attributed the smaller changes in the optical properties to a few nanometers of contamination. This contamination was apparently silicone-based and perhaps specific to this mission, but with the potential of being generated on

many missions because of the wide spread use of silicone compounds for space applications. Evidence of slightly higher Si contamination and degradation of the leading surfaces compared to the trailing was observed, but otherwise these samples were relatively insensitive to position on the satellite relative to the ram; if contamination had been limited to hydrocarbons, the ram facing surfaces would probably have been slightly improved in optical properties by removal of such contaminants, but the oxygen appears to have reacted with the silicone-based contaminants to form a more permanent film, perhaps similar to SiO₂. While a similar model was attempted with other films exhibiting small effects, probably because of thin protective oxides, not all of the measurements gave agreement. The results indicate that refinements are needed in measurements, interpretations, and modelling, especially as the number of parameters influencing the film properties increases over those for gold.

Those films more sensitive to oxidation appear to also acquire the same contamination, but the degradations are so dominated by the effects of metal oxidation that the sample's position relative to the ram direction becomes increasingly more important because of the sample's susceptibility to damage. The most extreme degradation reported here was also one of the best characterized sensitive materials, namely copper. The predominant features of the sensitive materials are small changes to the trailing films and large reflectance losses across a broad wavelength range for leading surfaces, associated with metal oxidation. The optical properties of these oxides, however, do not appear to be similar to those produced under equilibrium conditions for thermally grown oxide films. Problems with using ellipsometry and other optical methods of characterization to model these films suggest that perhaps variable concentrations of free metal may be distributed within the oxides, or at least the oxides do not provide uniform optical constants distributed in layers that are easily interpreted.

There is evidence that contamination by the modified silicone-based materials offers some protection from atomic oxygen degradation. The amount of protection of course would depend upon the contamination thickness and film integrity. Since rates of contamination and fluxes of atomic oxygen to the surfaces are strongly mission dependent, it is advisable to not only account for anticipated fluences of atomic oxygen, but also levels of contamination that might be expected for a given mission; the latter effects can utilize extensive studies of outgassing properties of materials that have been studied, but the transport mechanisms associated with depositing the contaminant on various surfaces and the fixation processes need to be studied in greater detail.

REFERENCES

1. Gregory, J.C.; and Peters, P.N. The Interaction of Atomic Oxygen with Surfaces at Orbital Altitudes, *The Long Duration Exposure Facility (LDEF)*, Clark, L.G, Kinard, W.H., Carter, D.J., and Jones, J. L., ed.: NASA SP-473, 1984.
2. Peters, P.N.; Gregory, J.C.; and Swann, J.T.; Effects on Optical Systems from Interactions with Atomic Oxygen in Low Earth Orbits, *Applied Optics*, **25**, 1290-1298 (1986).
3. Jemiola, J.M.; ed; *Proceedings of the USAF/NASA International Spacecraft Contamination Conference*, AFML-TR-78-190, NASA-CP-2039, March 1978.
4. Gregory, J.C.; and Peters, P.N.; Interaction of Atomic Oxygen with Solid Surfaces at Orbital Altitudes, *Proceedings of the First LDEF Mission Working Group Meeting*, NASA Langley Research Center, P.48, 1981.

5. Bourassa, R.; and Pippin, H.; Model of Spacecraft Atomic Oxygen and Solar Exposure Microenvironments, *Proceedings of LDEF Materials Results for Spacecraft Applications Conference, Oct 27-28, 1992*.
6. Chastin, Jill.; ed: *Handbook of X-ray photoelectron Spectroscopy*, 1992, Perkin-Elmer Corporation.
7. G.N. Raikar, J.C. Gregory, P.N. Peters, *Oxidation of Copper by Atomic Oxygen*, accepted for publication by **Oxidation Of Metals** 1994.
8. McKeown, D.; Surface Erosion in Space; *Rarefied Gas Dynamics*; ed: Laumann, J.A.; Academic Press, pp.315-326, 1963.
9. Palik, E.D.; ed: *Handbook of Optical Constants of Solids*, Academic Press, 1985.
10. Peters, P.N.; Linton, R.C.; and Miller, E.R; Results of Apparent Atomic Oxygen Reactions on Ag, C, and Os Exposed during the Shuttle STS-4 Orbits, *Geophysical Research Letters*, **10**, 569-571, 1983.
11. Gull, T.R.; Herzig, J.F.; Osantowski, F.F.; and Toft, A.R.; Low Earth Orbit Environmental Effects on Osmium and related Optical Thin-Film Coatings, *Applied Optics*, **24**, 2660-2665, 1985.

Table I. Measured film thicknesses and solar absorptances

A0114 SAMPLE*	MATERIAL	FILM THICKNESS		SOLAR ABSORPTANCE	
		COVERED, nm	EXPOSED, nm	α_s^\dagger COVERED	α_s^\dagger EXPOSED
C3-04	TIN	131.3 ± 3.7	136.1 ± 6.3	0.311	0.295
C9-04	TIN	125.0	121.4 ± 0.6	0.313	0.295
C3-09	TUNGSTEN	52.2 ± 2.2	#	0.427	0.420
C9-09	TUNGSTEN	60.0 to 70.0	#	0.430	0.485
C3-10	PLATINUM	38.4 ± 1.3	43.6 ± 2.3	0.271	0.271
C9-10	PLATINUM	58.9 ± 0.9	60.7.0 ± 0.1	0.259	0.271
C3-16	COPPER	70.8 ± 1.0	71.6 ± 2.6	0.290	0.297
C9-16	COPPER	71.5 ± 7.2	105.8 ± 0.6	0.368	0.857
C3-24	MOLYBDENUM	35.1 ± 4.3	#	0.506	0.516
C9-24	MOLYBDENUM	35.4 ± 1.9	#	0.453	0.689
C3-45	NICKEL	#	#	0.571	0.583
C9-45	NICKEL	#	#	0.568	0.676
C3-46	GOLD	33.3 ± 0.5	35.3 ± 1.3	0.268	0.275
C9-46	GOLD	31.7 ± 0.6	35.4 ± 0.4	0.275	0.288

Notes:

* C3=Trailing edge (wake side), C9=Leading edge (ram side).

The C3-exposed surfaces received an estimated 1.32×10^{17} oxygen atoms/cm² total fluence.

The C9- exposed surfaces received an estimated 8.72×10^{21} oxygen atoms/cm² total fluence

See text for details

† The solar absorptance measured by the AZ Technology LPSR-200 spectro-reflectometer is actually (1-Reflectance) over the solar emission band. For thin films which are partially transmitting: (1-Reflectance) = Absorptance + Transmittance. Thus the values of α_s given here may not be the same as for solid metal (and should be quite different in the cases of C-9 exposed Cu, Mo, Ni and W.)

Table II: XPS Data for LDEF Thin Metal Films

Sample	Material	Side	Surface Atomic Concentration in %													
			Sn	W	Pt	Cu	Mo	Ni	Au	O	C	Si	Na	Cl	F	N
C3-09	Sn	Exposed	4.5							28.3	52.7	7.1	5.4	0.4	0.7	1.0
		Covered	13.1							24.6	53.7	2.7	4.0	0.5	0.4	0.9
C9-04	Sn	Exposed	2.7							54.3	15.3	25.2	1.3	0.3	0.4	0.6
		Covered	14.9							24.6	52.7	2.8	3.3	0.4	0.6	0.7
C3-09	W	Exposed		5.3						43.2	31.7	12.7	nd	nd	nd	7.0
		Covered		11.2						37.7	36.7	2.9	nd	nd	nd	11.5
C9-09	W	Exposed		9.5						48.8	16.2	16.7	0.3	0.4	0.6	7.3
		Covered		11.7						27.2	38.1	12.0	0.4	0.2	0.5	9.9
C3-10	Pt	Exposed			9.4					47.7	18.0	19.9	0.3	0.7	nd	3.9
		Covered			25.0					16.7	40.3	8.5	1.1	1.8	nd	6.6
C9-10	Pt	Exposed			4.9					51.0	18.2	21.0	0.7	0.7	nd	3.9
		Covered			14.3					23.6	46.4	6.5	0.5	0.7	0.3	8.1
C3-16	Cu	Exposed				8.7				23.9	62.9	5.4	nd	0.9	nd	nd
		Covered				5.5				23.3	66.8	3.6	nd	1.1	nd	nd
C9-16	Cu	Exposed				4.3				37.4	44.4	13.9	nd	nd	nd	nd
		Covered				2.7				21.6	65.8	9.3	nd	0.6	nd	nd
C3-24	Mo	Exposed				4.0				46.9	24.7	15.2	0.4	0.2	1.2	7.4
		Covered				12.2				36.3	32.2	0.9	1.0	0.3	0.6	16.3
C9-24	Mo	Exposed				7.9				48.7	25.6	17.8	nd	nd	nd	nd
		Covered				19.6				38.0	39.1	3.3	nd	nd	nd	nd
C3-45	Ni	Exposed					4.3			36.2	47.8	10.0	nd	0.5	1.6	nd
		Covered					10.5			27.8	58.9	2.0	nd	0.7	tr	nd
C9-45	Ni	Exposed					14.7			54.6	13.2	15.4	nd	nd	2.2	nd
		Covered					12.6			34.5	45.7	6.3	0.5	0.4	nd	nd
C3-46	Au	Exposed						16.5		41.0	19.7	16.5	0.4	0.5	nd	5.3
		Covered						42.2		12.7	34.4	6.3	0.2	0.4	nd	3.7
C9-46	Au	Exposed						4.5		56.4	15.6	22.0	tr	0.9	0.8	nd
		Covered						22.9		18.8	54.7	2.5	3.0	0.3	1.0	nd

Note: nd= not detected, tr=trace

C3-04, TIN

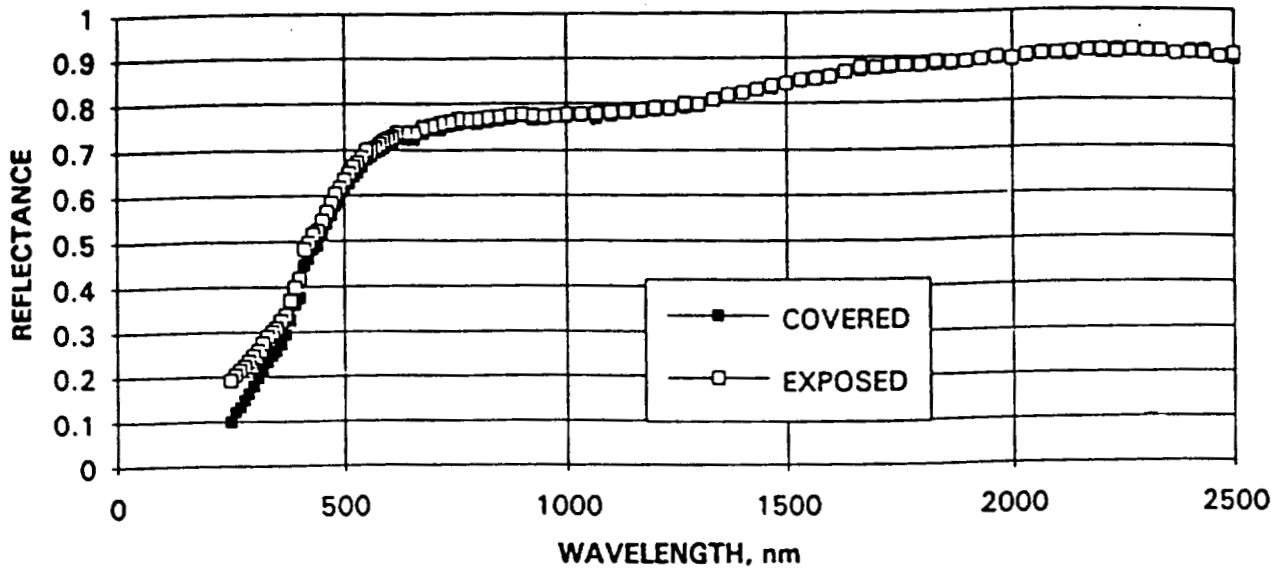


Fig. 1 Reflectances of covered and exposed areas on the trailing (wake side) tin film.

C9-04, TIN

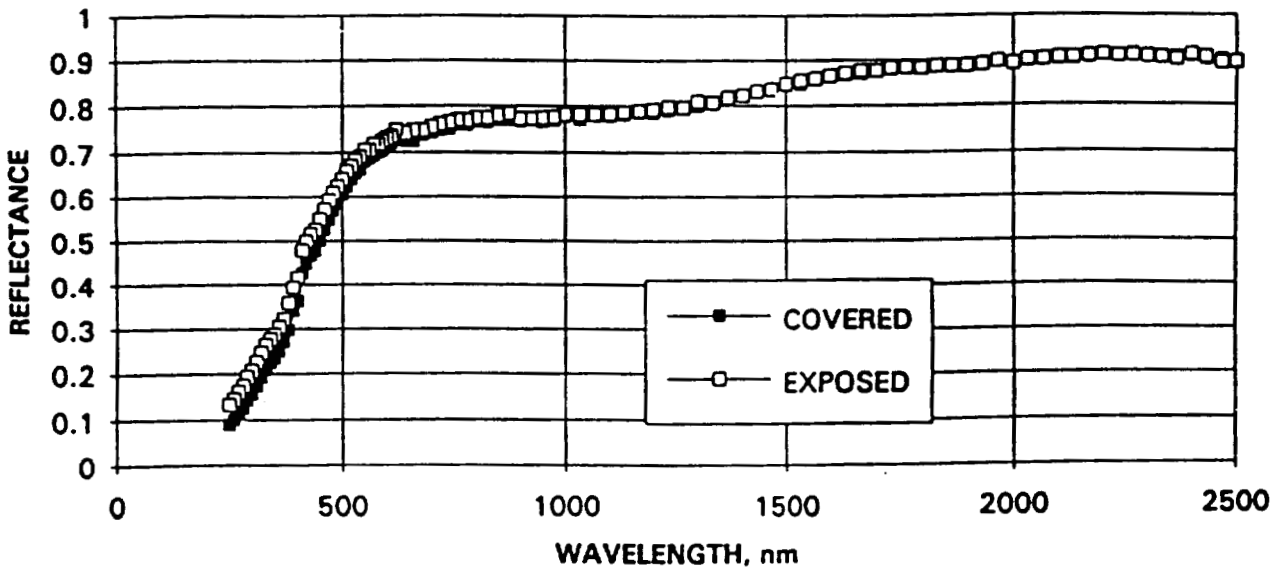


Fig. 2 Reflectances of covered and exposed areas of the leading (ram side) tin film.

C3-09, TUNGSTEN & CALCULATIONS

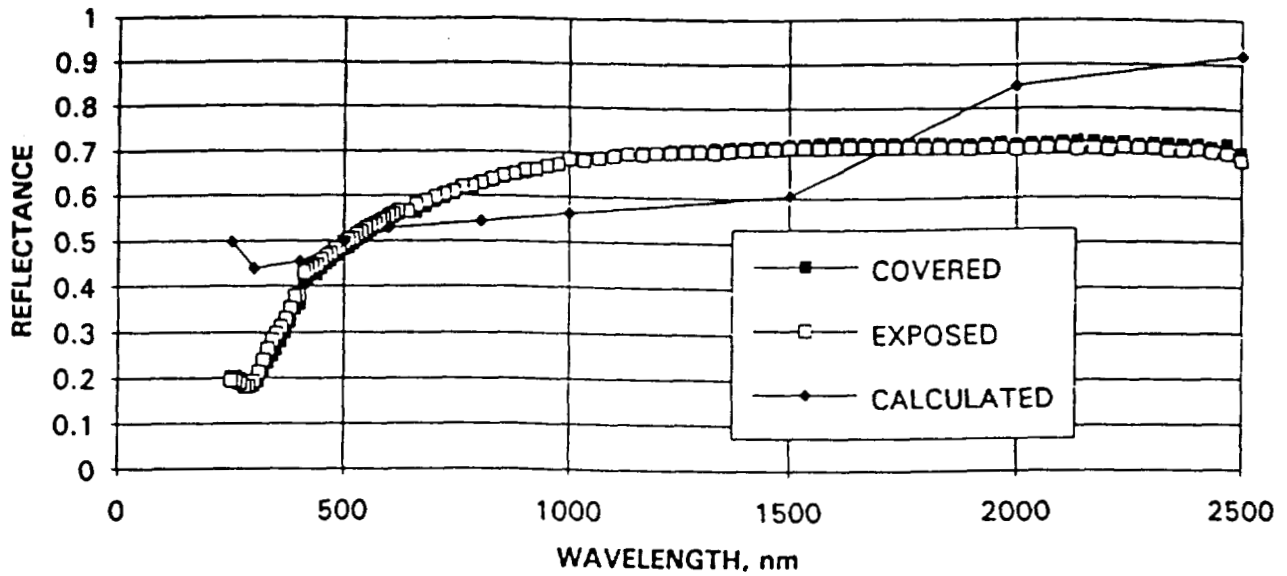


Fig. 3 Reflectances of covered and exposed areas of the trailing (wake side) tungsten film and calculated reflectances using the measured film thickness and optical constants from the literature.

C9-09, TUNGSTEN

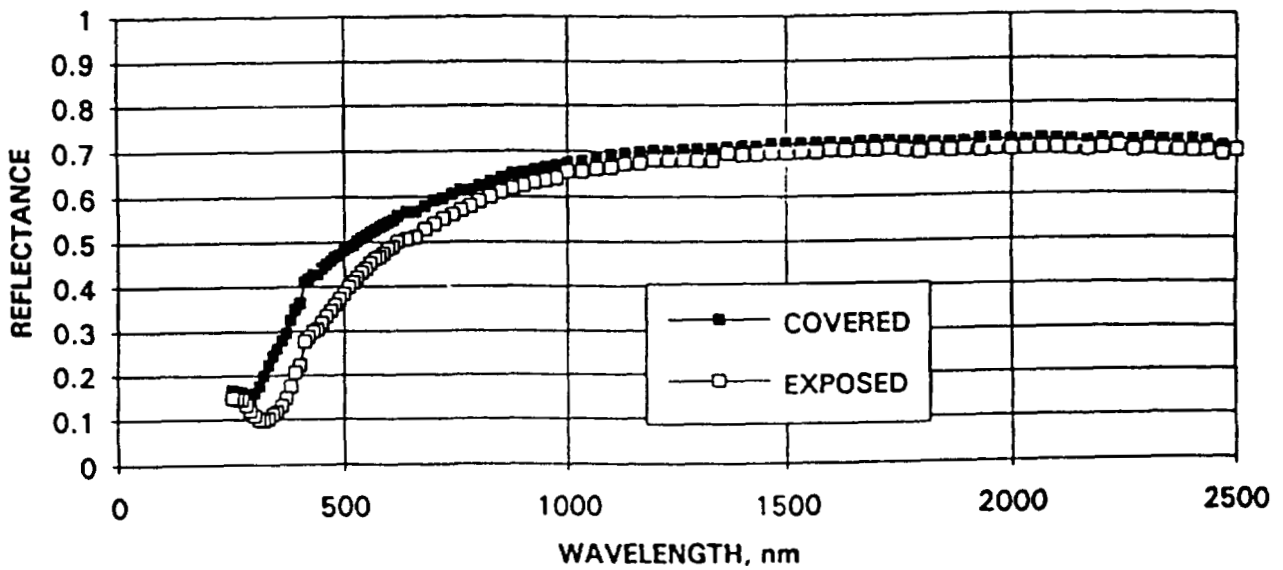


Fig. 4 Reflectances of covered and exposed areas of the leading (ram side) tungsten film.

C3-10, PLATINUM

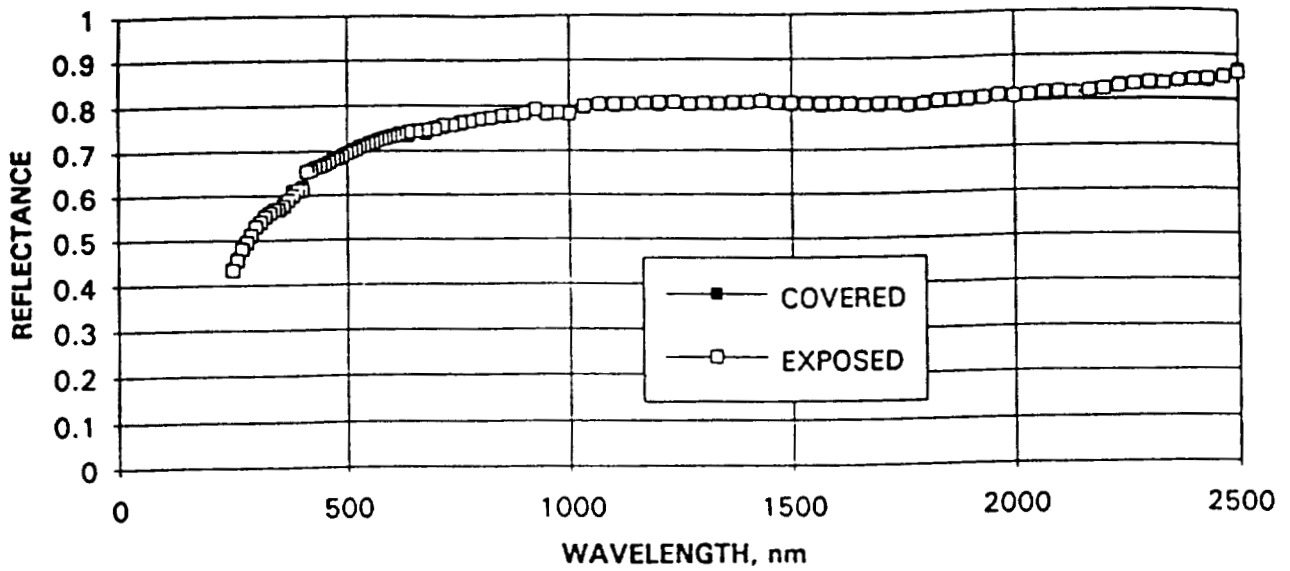


Fig. 5 Reflectances of covered and exposed areas of the trailing (wake side) platinum film.

C9-10, PLATINUM & CALCULATIONS

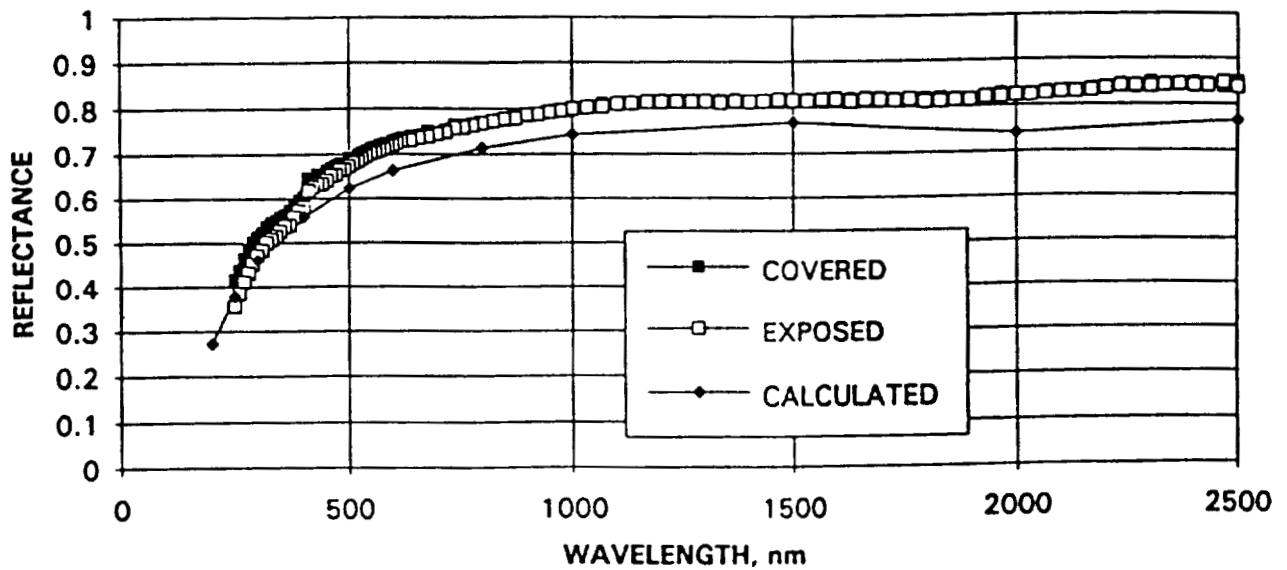


Fig. 6 Reflectances of covered and exposed areas of the leading (ram side) platinum film and calculated reflectances using the measured film thickness and optical constants from the literature.

C3-16, COPPER

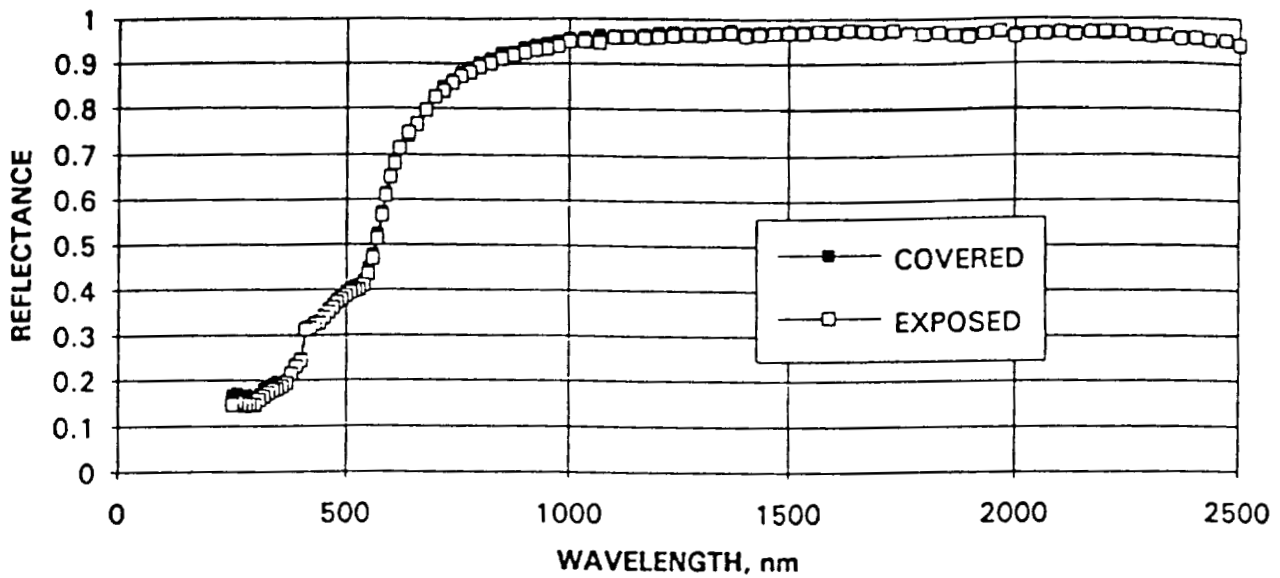


Fig. 7 Reflectances of covered and exposed areas of the trailing (wake side) copper film.

C9-16, COPPER

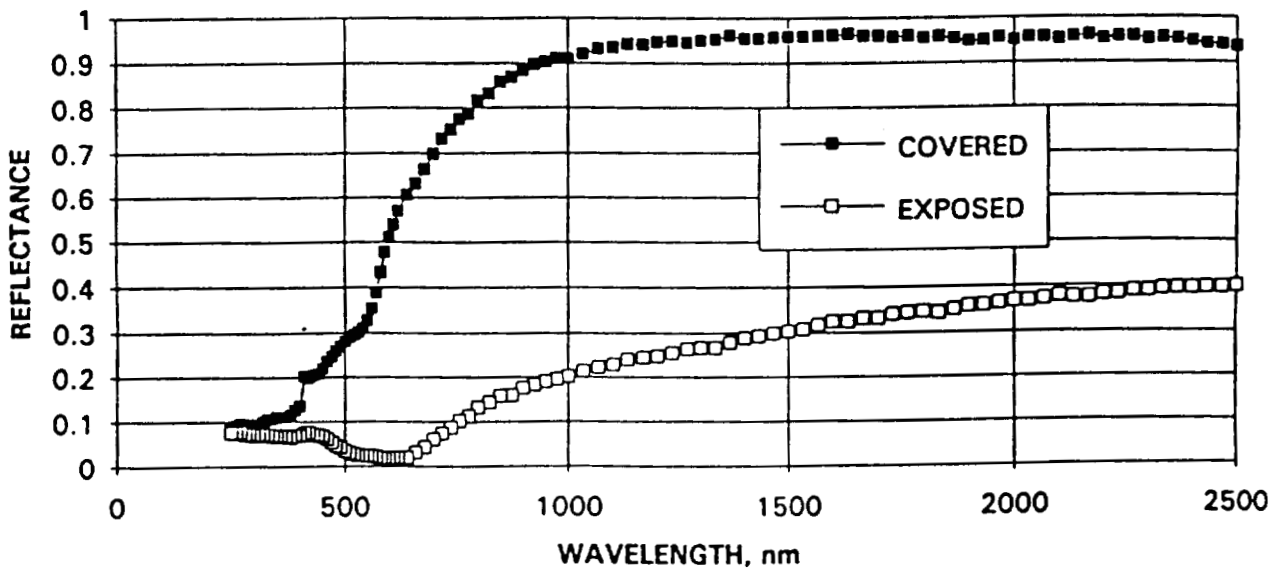


Fig. 8 Reflectances of covered and exposed areas of the leading (ram side) copper film.

C3-24, MOLYBDENUM

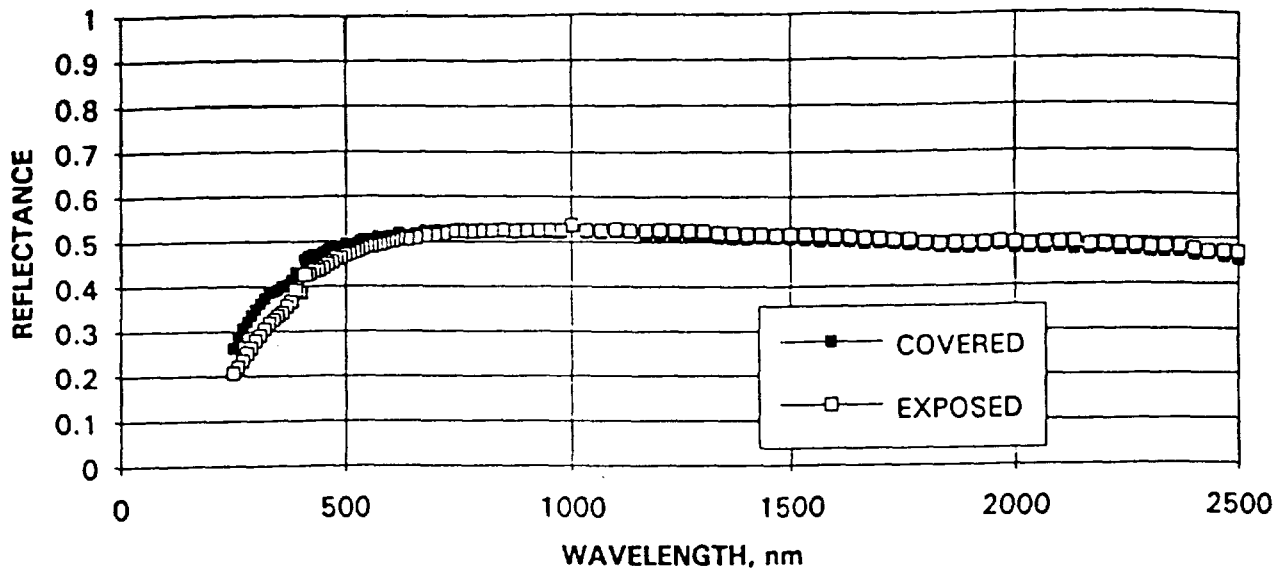


Fig. 9 Reflectances of the covered and exposed areas of the trailing (wake side) molybdenum film.

C9-24, MOLYBDENUM & CALCULATIONS

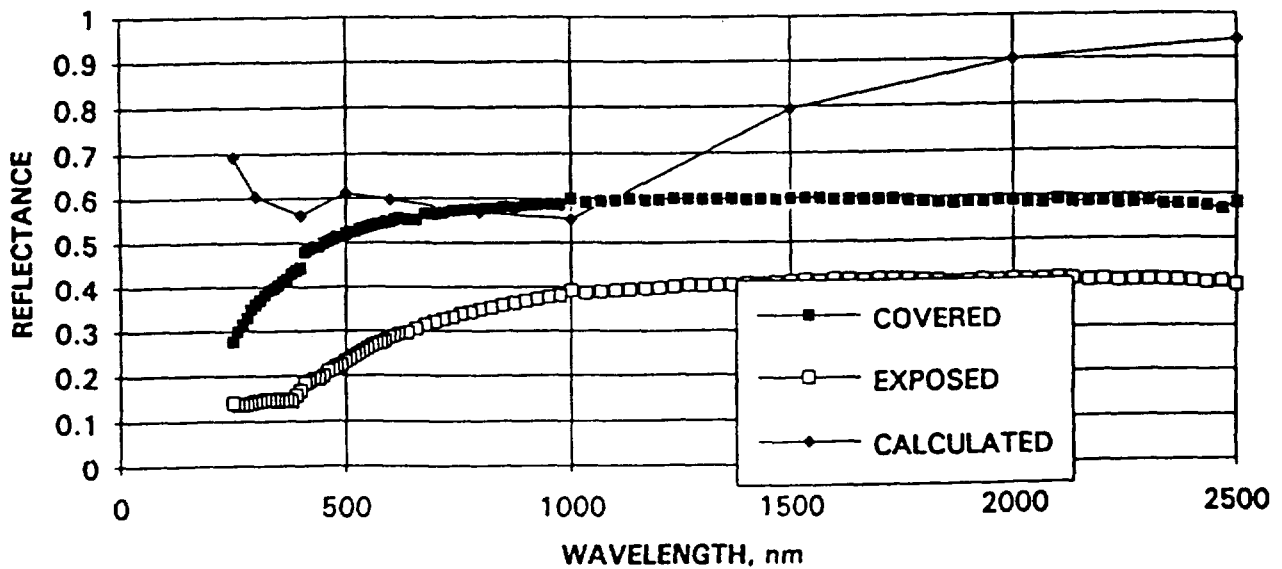


Fig. 10 Reflectances of the covered and exposed areas of the leading (ram side) molybdenum film and calculated reflectances using measured thickness of covered area and optical constants from the literature.

C3-45, NICKEL & CALCULATIONS

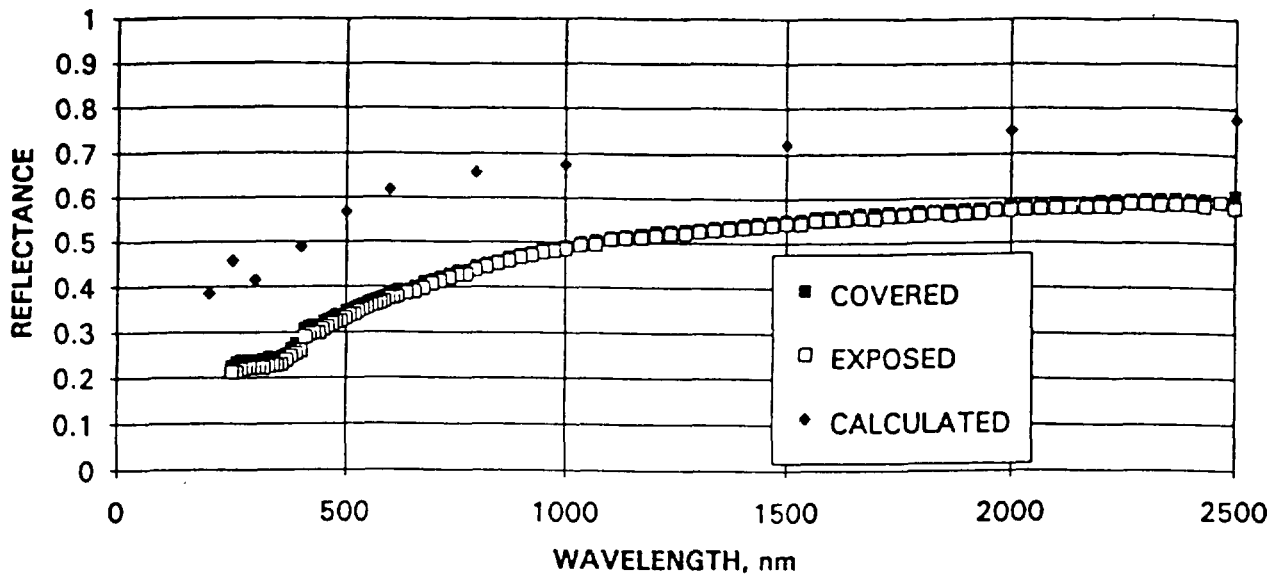


Fig. 11 Reflectances of covered and exposed areas of the trailing (wake side) nickel film and calculated reflectances using 40 nm film thickness (see text about uncertainty) and optical constants from the literature.

C9-45, NICKEL

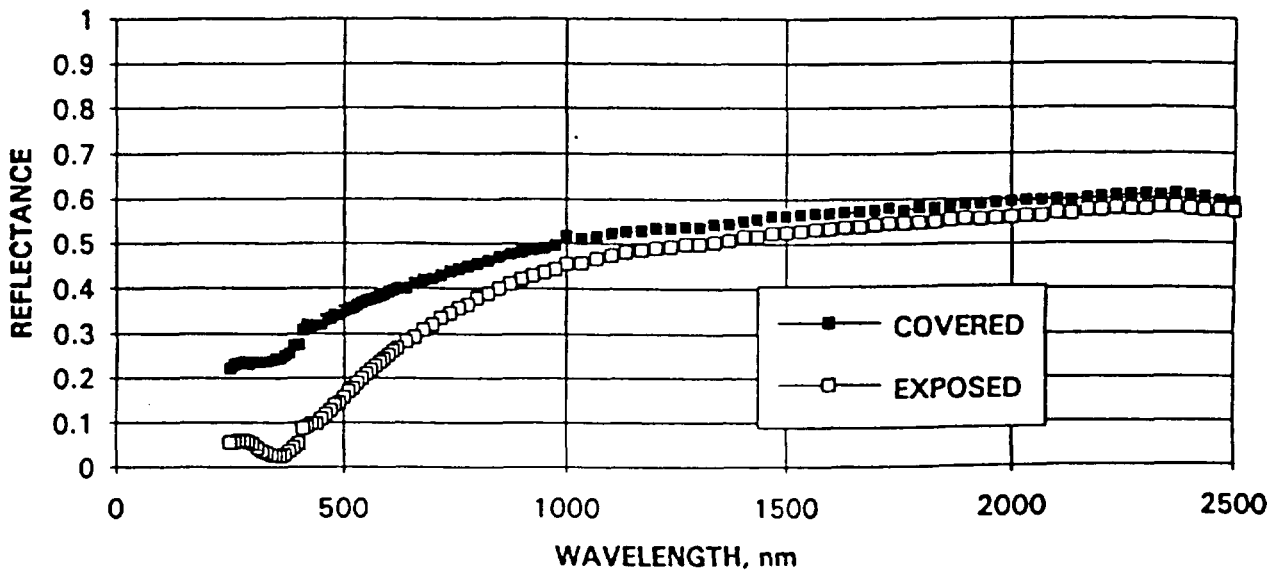


Fig. 12 Reflectances of covered and exposed areas of the leading (ram side) nickel film.

C3-46, GOLD

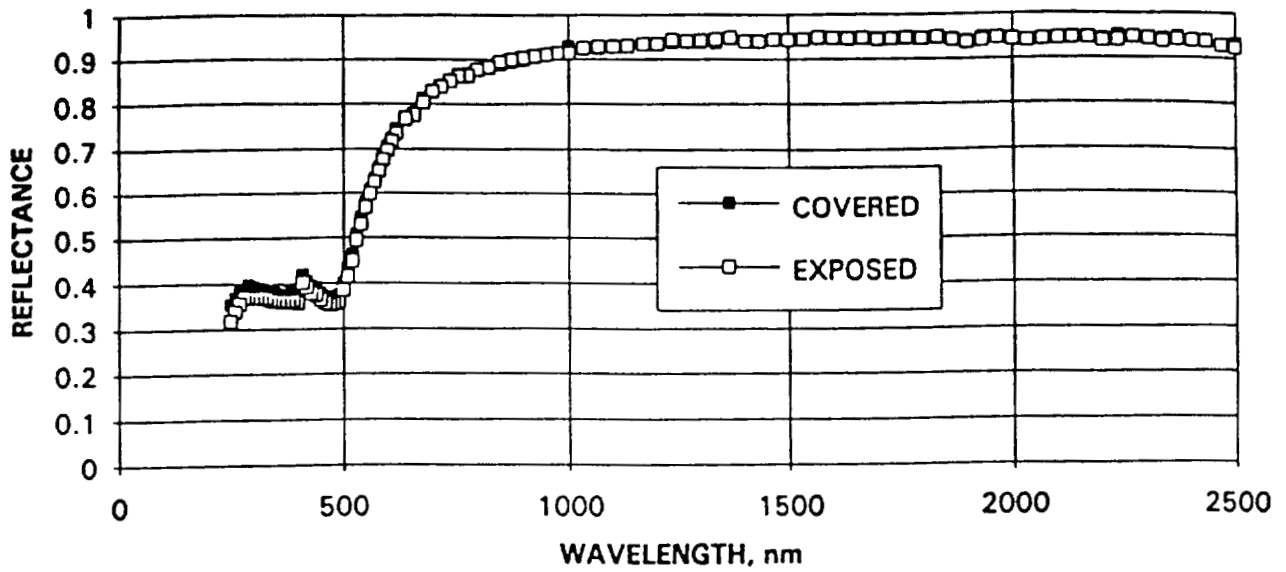


Fig. 13 Reflectances of the covered and exposed areas of the trailing (wakeside) gold film.

C9-46, GOLD

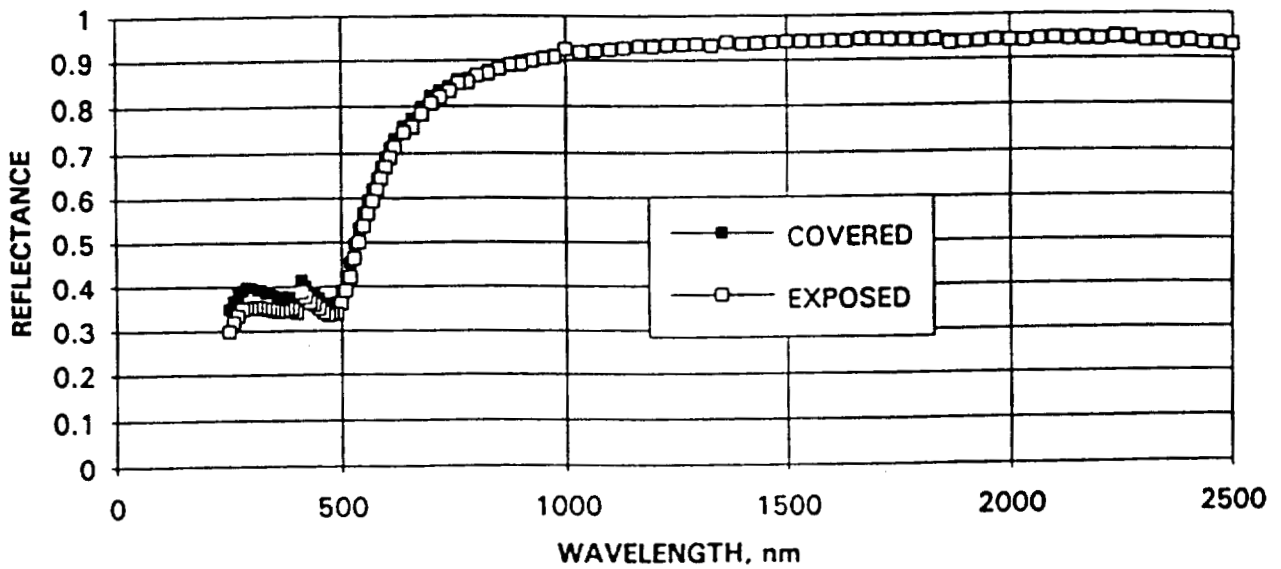


Fig. 14 Reflectances of the covered and exposed areas of the leading (ram side) gold film.

GOLD CALCULATIONS

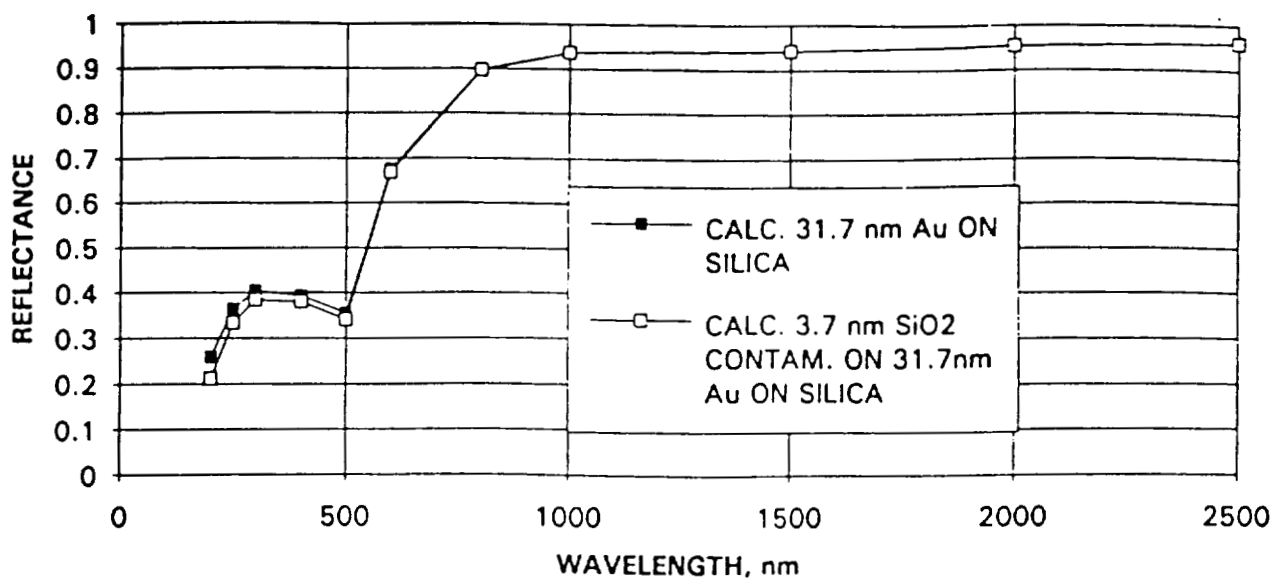


Fig. 15 Calculated reflectances of a gold film of 31.7 nm thickness and same film with 3.7 nm thickness of SiO₂ contamination on top; both on fused silica substrate.

C9-46, GOLD AND SPUTTER CHECK

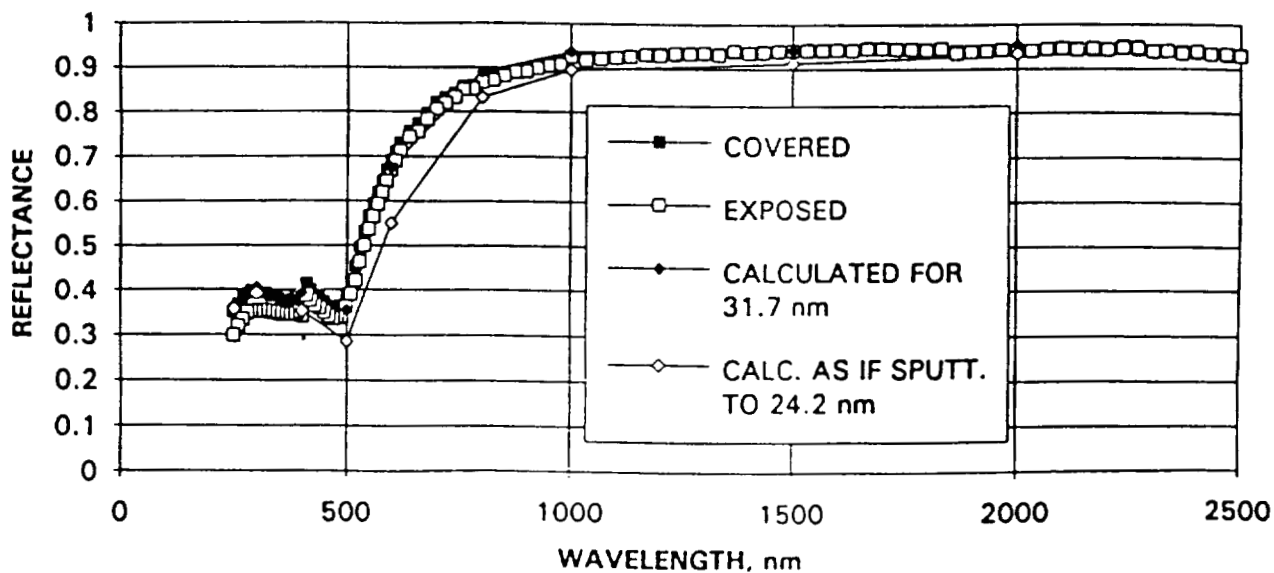


Fig. 16 Measured reflectances of covered and exposed areas of the ram side gold film compared to calculated reflectances of 31.7 nm and 24.2 nm gold film thicknesses; thinner gold would result if upper limit placed on sputtering occurred.

FURTHER INVESTIGATIONS OF EXPERIMENT A0034

ATOMIC OXYGEN STIMULATED OUTGASSING

Roger C. Linton
 Miria M. Finckenor
 Rachel R. Kamenetzky
 EH15/Space Environmental Effects
 Marshall Space Flight Center, AL
 Phone (205) 544-2526 FAX (205) 544-0212

5/2-27
 10/1

ABSTRACT

Thermal control coatings within the recessed compartments of LDEF Experiment A0034 experienced the maximum leading edge fluence of atomic oxygen with considerably less solar UV radiation exposure than top-surface mounted materials of other LDEF experiments on either the leading or the trailing edge. This combination of exposure within A0034 resulted in generally lower levels of darkening attributable to solar UV radiation than for similar materials on other LDEF experiments exposed to greater cumulative solar UV radiation levels. Changes in solar absorptance and infrared thermal emittance of the exposed coatings are thus unique to this exposure. Analytical results for other applications have been found for environmentally induced changes in fluorescence, surface morphology, light scattering, and the effects of coating outgassing products on adjacent mirrors and windows of the A0034 experiment. Some atmospheric bleaching of the thermal control coatings, in addition to that presumably experienced during re-entry and recovery operations, has been found since initial post-flight observations and measurements.

INTRODUCTION

This passive LDEF experiment, occupying one-sixth of Tray C9 on the leading edge and Tray C3 on the trailing edge, consisted of an aluminum framework housing 25 individual compartments sandwiched between a base plate and a top cover providing apertures for each individual compartment (Fig. 1). Most, but not all, of the 25 compartments in each flight unit contained a thermal control coating, sized larger in diameter than the opposing top cover aperture. Each compartment also contained a mirror mounted on an adjoining side wall intended to collect outgassed molecular species or particulates from the underlying coating. These mirrors were facing transverse to RAM-impinging AO on the leading edge and shielded from all but the most oblique incidence angles to solar radiation by the aperture covers. At least one compartment in each flight unit was left empty, except for the contaminant collector mirror, as a means of assessing contamination attributable to external sources. Each of the four corner compartments in each flight unit was sealed with aluminum covers to assess, as a control,

the outgassing of coatings stimulated by thermal vacuum exposure in the absence of UV radiation and atomic oxygen. Another level of experimental control was provided by sealing six other compartments in each flight unit with UV-grade quartz windows. The basic experimental control was provided by duplicating the leading edge flight unit on the trailing edge to assess outgassing in the absence of atomic oxygen.

The thermal control coatings exposed in this experiment are S13G, S13G/LO, A276, Z306, Z93, and zinc orthotitanate. S13G paint is a potassium silicate-treated zinc oxide in a methyl silicone binder. S13G/LO is a lower outgassing version of S13G. A276 is a glossy white titanium dioxide paint in a polyurethane binder. Z306 is similar to A276, with the addition of carbon for a glossy black color. Z93 paint is zinc oxide pigment in the original PS7 potassium silicate binder. Effects of LEO environmental exposure and subsequent changes in optical properties, including solar absorptance, infrared thermal emittance, and spectrofluorescence, are detailed in previous symposia proceedings (refs. 1-3).

Most of the contaminant collector mirrors in the flight units were quartz substrates coated with an opaque layer of aluminum protected by silicon monoxide. Four other mirrors in each flight unit consisted of thin film reflector coatings: silver, osmium, gold, and magnesium fluoride overcoated aluminum. These four mirrors in each flight unit were all mounted in compartments with open apertures. The silver and osmium mirrors were flown to provide a passive indicator of scattered atomic oxygen impingement in the compartments, while the gold and MgF_2/Al mirrors were intended to provide a means of assessing the role of mirror material in the degree of optical effects of contamination.

ENVIRONMENTAL EXPOSURE

During the 5.8 year flight, the A0034 trays were exposed to the LEO environment of atomic oxygen, ultraviolet radiation, particulate radiation, thermal cycling, hard vacuum, and micrometeoroid/space debris impacts. Atomic oxygen exposure is estimated to have been 8.99×10^{21} atoms/cm² and 1.32×10^{17} atoms/cm² (ref. 4) for leading and trailing edge trays, respectively. UV radiation exposure was limited, as discussed previously, by the tray cover apertures to approximately 2000 equivalent sun hours. Particulate radiation exposure was approximately 3.0×10^5 rads. Both trays experienced over 33,000 thermal cycles during the mission and a vacuum estimated between 10^{-6} and 10^{-7} torr. Damage by micrometeoroids or space debris consisted primarily of impact craters in the aluminum tray covers.

ESCA ANALYSIS

ESCA analysis was performed on a number of the collector mirrors adjacent to thermal control coatings. Figure 2 demonstrates the difference in atomic concentrations of silicon, oxygen, and carbon for mirrors exposed to S13G paint under various exposure conditions. Depth profiling analyses have indicated that the original coating of silicon

monoxide has been oxidized for both flight exposed and control samples. Mirrors exposed to S13G outgassing on the leading edge have the least carbon on the surface as a result of reflected atomic oxygen from the underlying paint. The most striking observation is the level of carbon found on the trailing edge windowed sample. A similar (48% atomic concentration) level of carbon has been found for mirrors exposed to other paints on the trailing edge without a covering window sealing the compartments. This is presumed to be the result of outgassing.

Figure 3 compares collector mirrors adjacent to two of the thermal control coatings, S13G and zinc orthotitanate, to a collector mirror in an empty open compartment on the leading edge. Pre-flight, it was presumed that the atomic oxygen-stimulated outgassing from the S13G sample would result in high atomic concentration levels of carbon and oxygen as compared to the zinc orthotitanate and certainly higher than carbon and oxygen levels found in a compartment without an adjacent thermal control coating. Post-flight observations indicated that any contaminant deposition was likely etched off the collector mirrors by atomic oxygen, as the ESCA analysis revealed little evidence for contamination and lacked a trend in compositional analysis. The ESCA survey indicates that the small levels of carbon on the mirrors from leading edge open compartments are likely adventitious.

These results may be compared to previously reported ESCA data for Experiment A0034 (ref. 3). These mirrors and the compartment window covers are being re-investigated to include sputter etch depth profiling. The photoelectron binding energies and surface chemistries of all of the mirrors are being compiled for analysis and will be reported in a future paper.

LABORATORY INVESTIGATIONS

Small areas of these contaminated windows, foil wrapped to outline the desired exposure area, were exposed to thermal energy atomic oxygen in the laboratory to investigate atomic oxygen "cleaning" susceptibility. The relatively thick layers of photolyzed contaminant on windows from compartments with Chemglaze A276 or Z306 polyurethane based paints were readily removed by only minutes of exposure to an atomic oxygen flux of approximately 2×10^{16} atoms/cm²/second. In contrast, the silicone-based contaminant films on windows exposed to outgassing from the S13G and S13G-LO RTV-based coatings were not "cleaned", even after hours of exposure, changing only in appearance by silicate formation at the surface and hardening. No visible effect was observed for exposure to this laboratory-generated atomic oxygen of the contaminant films on windows exposed to Z93 coatings.

Visible changes in appearance of most of the exposed thermal control coatings have been minimal since the time of initial post-flight characterization. Repeat measurements of diffuse reflectance indicate some bleaching, particularly for the solar UV-darkened A276 coating sample flown under a UV-grade quartz window, and for the Z306 coating samples exposed either under a window or open to leading edge environment. These results are averaged for all of the A0034 coatings in Table 1.

Some atmospheric bleaching of UV-darkened thermal control coatings exposed in vacuum has long been noted, particularly for the zinc-oxide pigmented paints (ref. 5), and the acceleration of this bleaching by subsequent near-ultraviolet irradiation has also been noted (ref. 6). Laboratory demonstrations have been performed to investigate this phenomenon for LDEF coatings darkened by flight exposure on A0034. Solar absorptance of a sample of S13G, flown in an open compartment on the trailing edge, increased from 0.18 to 0.26 during the 5.8 year exposure. Bleaching of quadrants of this sample were induced by laboratory exposure to UV radiation in air then in vacuum. The source of illumination was a commercial long wave (365 nm) Blak-Ray B100-A lamp. Alternate portions of the coating were shielded by tightly wrapped aluminum foil (fig. 4) during black light illumination. Bleaching in air was slightly more effective at lowering the solar absorptance ($\alpha = 0.236$) than bleaching in vacuum ($\alpha = 0.244$). The small difference between the air and vacuum bleaching indicates that the effect is not dominated by air/ozone interaction with the coating. The area with combined bleaching in air and vacuum had a solar absorptance measurement of 0.223.

The visual appearance of the coating quadrant exposed to the black light both in air and then vacuum was effectively indistinguishable from the flight control samples of S13G. These patterns of bleaching are most striking for visual observations under black-light illumination, showing the progressive restoration of the original fluorescent yellow emission. Spectrofluorescence measurements concur with the visual observations, as seen in figure 5. The decreased intensity of spectral bands of fluorescent emission in the A0034 zinc-oxide pigmented coatings (ref. 1) has been partially restored by the laboratory bleaching. These curves, for the protected (unexposed) areas of the coating, indicate that thermal heating during black light illumination is only a small factor in the bleaching.

Fluorescence effects of exposure for the A0034 thermal control coatings were investigated by comparative black-light observations and detailed spectral measurements using an SLM Aminco SPF-500C dual-monochromator spectrofluorometer. The effects of exposure to solar UV radiation and atomic oxygen in the LDEF flight thermal vacuum environment are revealed in material dependent patterns of stimulated, quenched, and wavelength shifted fluorescence (ref. 7). All of these effects have been shown, in laboratory testing, as a consequence of exposure to UV radiation of both near and vacuum-ultraviolet wavelengths and also indicated by similar analytical results of coatings exposed on both the leading and the trailing edge of LDEF. However, subsequent testing of similar coatings in the laboratory also indicate that exposure to atomic oxygen, in the absence of UV radiation, can decrease ("quench") the intensity of spectral bands of emission, and that all of the effects of exposure on fluorescence for UV-irradiated coatings can be significantly modified in degree or nature by subsequent or coincident exposure to atomic oxygen. Additionally, comparison to flight exposures of similar materials on Shuttle experiments (refs. 7, 8) indicates that the fluorescence effects found in LDEF-exposed coatings are similar in nature, differing only in degree, for these relatively brief missions. Fluorescence, then, is a highly sensitive indicator, though not necessarily accurate gauge, of material interaction with the space environment.

Chemglaze A276 paint exposed on A0034 is a good example of altered fluorescence dependent on exposure. The control sample of A276 fluoresces bluish-purple. When the

polyurethane binder was eroded by the full, open exposure to LEO atomic oxygen, this fluorescence was totally quenched. When exposed under a quartz window, fluorescence was stimulated to a yellow/orange color (fig. 6). Laboratory exposure of A276 to near-UV stimulates the same fluorescence with as little as 100 equivalent sun hours irradiance.

CONCLUSIONS

In retrospect, several features of the experiment design and approach proved flawed for passive assessment of orbital atomic oxygen stimulated outgassing. The impingement of atomic oxygen on the contaminant collector mirrors on both the leading and trailing edge units is clearly shown by the oxidation and/or erosion of the silver and osmium mirrors and the associated evidence of "cleaning," revealed by ESCA analysis. This AO impingement altered to an unknown degree the basic comparative measure of deposits attributable to outgassing from the adjacent coatings. Outgassed species from the thermal control coatings formed contaminant films on the quartz windows, which were then photopolymerized by solar UV radiation, significantly degrading the transmission of the windows at UV wavelengths (200 to 400 nm). This outgassing, deposition, and solar UV-induced polymerization presumably occurred early in the LDEF mission, as would be expected, since the windowed thermal control coatings were considerably less degraded (darkened) than the companion type coatings exposed to the greater levels of solar UV radiation under open apertures.

This highly visible evidence of contamination on the inside of the optically degraded windows contrasts strikingly with the absence of visible contamination on the collector mirrors in the covered compartments. This indicates UV radiation-enhanced deposition and the intrinsically more severe optical degradation of photolyzed contaminant films. The ranking of leading edge coatings by type for outgassing (ref. 1), as determined from measurements of optical degradation of these windows, was completely reversed from the ranking of similar coatings and exposure on the trailing edge. The only obvious discriminators between contaminated windows over specific coatings on the leading and trailing edges are the greater levels of contamination and visible darkening on leading edge windows. Photomicroscopy and FTIR analysis revealed characteristic contaminant layer morphologies and chemical signatures that are different for each type of coating.

ACKNOWLEDGMENTS

The authors gratefully acknowledge the contributions of Mr. Carl Miller of Raytheon Co. under contract NAS8-39924. The authors also note the support of Ms. Whitney Hubbs, Mr. John Reynolds, and Mr. Don Burch of the Physical Sciences Branch, Engineering Physics Division, of the MSFC Materials and Processes Laboratory in this effort.

REFERENCES

1. Linton, Roger C., Rachel R. Kamenetzky, John M. Reynolds, and Charles L. Burris, "LDEF Experiment A0034: Atomic Oxygen Stimulated Outgassing," LDEF-69 Months in Space: First Post-Retrieval Symposium, NASA CP-3134, Arlene S. Levine, editor, Kissimmee, FL, June 1991.
2. Wilkes, Donald R., Ann Whitaker, James M. Zwiener, Roger C. Linton, David Shular, Palmer Peters, and John Gregory, "Thermal Control Surfaces on the MSFC LDEF Experiments," LDEF Materials Workshop '91, NASA CP-3162, Bland A. Stein and Philip R. Young, editors, Langley, VA, November 1991.
3. Linton, Roger C. and Rachel R. Kamenetzky, "Second LDEF Post-Retrieval Symposium Interim Results of Experiment A0034," LDEF-69 Months in Space: Second Post-Retrieval Symposium, NASA CP-3194, Arlene S. Levine, editor, San Diego, CA, June 1992.
4. Bourassa, R.J. and H.G. Pippin, "Model of Spacecraft Atomic Oxygen and Solar Exposure Microenvironments," LDEF Materials Results for Spacecraft Applications, NASA CP-3257, Ann F. Whitaker and John Gregory, editors, Huntsville, AL, October 1992.
5. Zerlaut, G.A., J.E. Gilligan and N.A. Ashford, Investigation of Environmental Effects on Coatings for Thermal Control of Large Space Vehicles, Final Report for NASA contract NAS8-5379, p. 146, October 1971.
6. Blair, Paul M., Jr., William F. Carroll, Stephen Jacobs, and Lubert J. Leger, "Study of Thermal Control Surfaces Returned from Surveyor III," AIAA 71-479, AIAA 6th Thermophysics Conference, Tullahoma, TN, April 1971.
7. Linton, Roger C., Ann F. Whitaker, and Rachel R. Kamenetzky, "Fluorescence Observations of LDEF Exposed Materials as an Indicator of Induced Material Reactions," LDEF Materials Results for Spacecraft Applications, NASA CP-3257, Ann F. Whitaker and John Gregory, editors, Huntsville, AL, October 1992.
8. Linton, R.C., J.A. Vaughn, M.M. Finckenor, R.R. Kamenetzky, R.F. DeHaye, and A.F. Whitaker, "Orbital Atomic Oxygen Effects on Materials: An Overview of MSFC Experiments on the STS-46 EOIM-3," AIAA 93-4102, AIAA Space Programs and Technologies Conference and Exhibit, Huntsville, AL, September 1993.

Table 1.
Solar Absorptance Measurements of A0034 Thermal Control Coatings

Material	Flight Condition	α_s		
		Pre-Flight	Initial Post-Flight	Present Condition
S13G	Leading Open	0.17	0.17 - 0.18	0.22
	Leading Window	0.17	0.17 - 0.18	0.18
	Leading Covered	0.17	0.17	0.17
	Trailing Open	0.18	0.25 - 0.26	0.25
	Trailing Window	0.18	0.20	0.19
	Trailing Covered	0.18	0.18	0.18
S13G/LO	Leading Open	0.18	0.19	0.19
	Leading Window	0.18	0.19	0.19
	Leading Covered	0.18	0.18	0.18
	Trailing Open	0.17	0.27 - 0.28	0.26
	Trailing Window	0.17	0.21	0.20
	Trailing Covered	0.17	0.17	0.17
A276	Leading Open	0.23	0.20	0.22
	Leading Window	0.23	0.35	0.31
Z306	Leading Open	0.96	0.96	0.93
	Leading Window	0.96	0.95	0.93
Z93	Leading Open	0.16	0.17	0.17
	Leading Window	0.16	0.17	0.17
	Trailing Open	0.16	0.17	0.17
	Trailing Window	0.16	0.16	0.16
	Trailing Covered	0.16	0.16	0.16
	Trailing Covered	0.16	0.16	0.16
Zinc Orthotitanate	Leading Open	0.16	0.16 - 0.17	0.17
	Trailing Open	0.16	0.18 - 0.19	0.18
	Trailing Window	0.16	0.19	0.18
	Trailing Covered	0.16	0.16	0.16

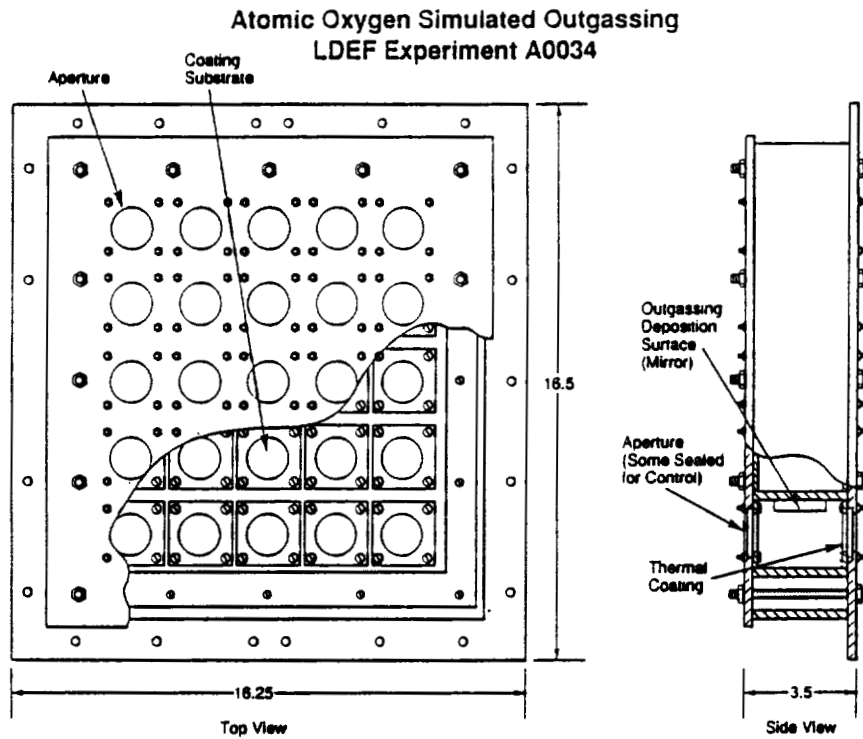


FIGURE 1. SCHEMATIC OF LDEF EXPERIMENT A0034

ESCA Analysis - A0034 Collector Mirrors
S13G Thermal Control Coating

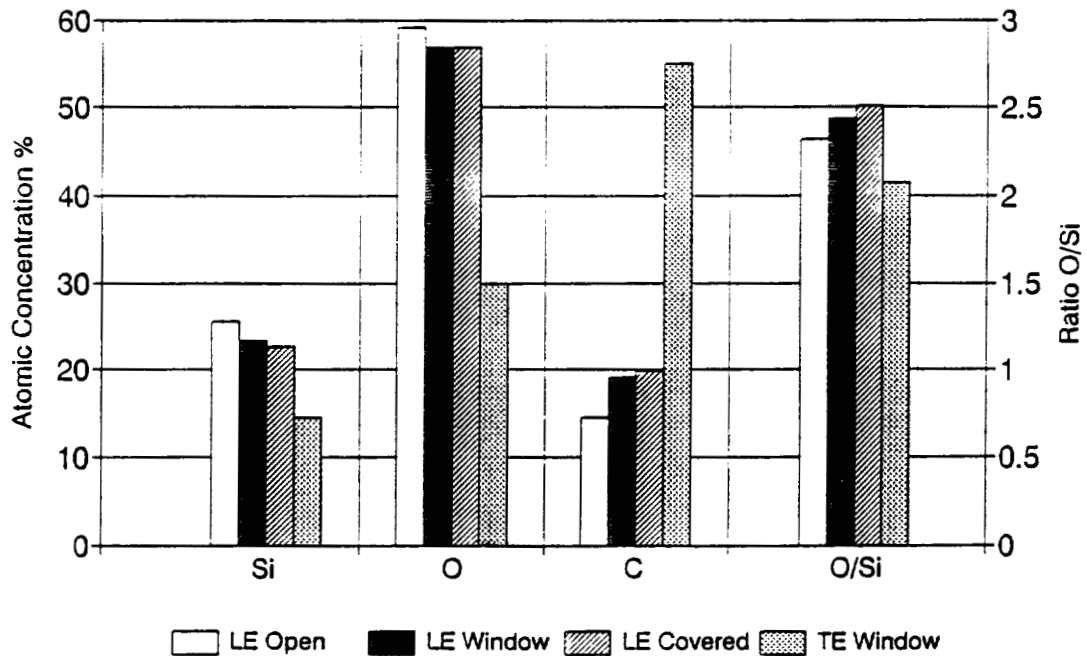


FIGURE 2. ESCA RESULTS OF COLLECTOR MIRRORS ADJACENT TO S13G UNDER VARIOUS FLIGHT EXPOSURE CONDITIONS

ESCA Analysis - A0034 Collector Mirrors Leading Edge Open Compartments

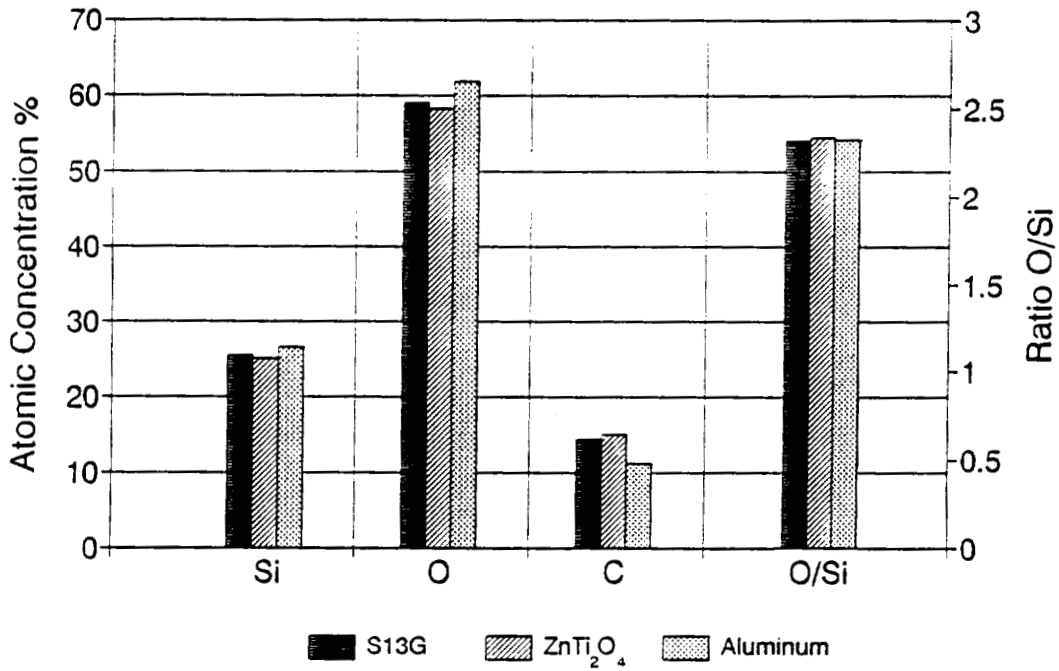


FIGURE 3. ESCA RESULTS OF COLLECTOR MIRRORS ADJACENT TO THERMAL CONTROL COATINGS IN OPEN COMPARTMENTS

Bleaching of LDEF (A0034) Thermal Control Coatings Black-Light Illumination Induced

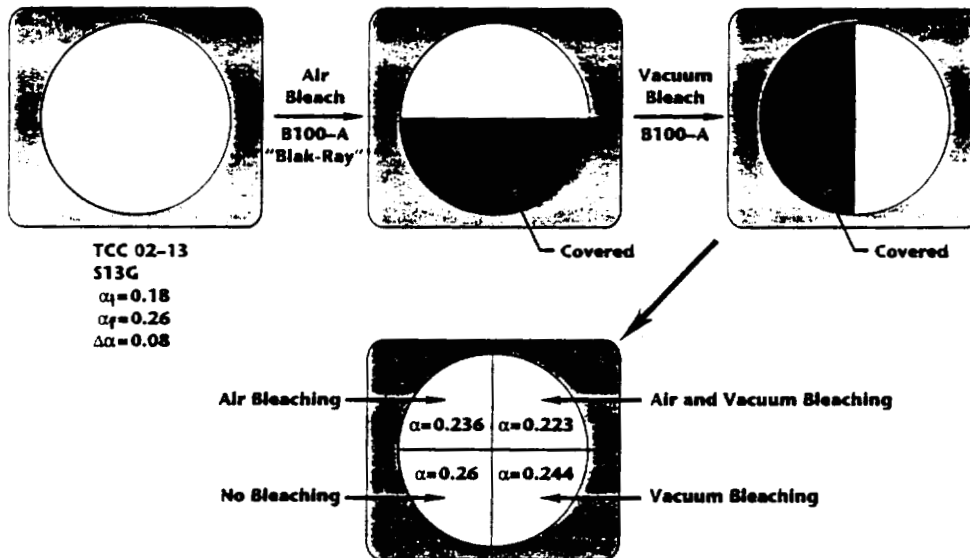


FIGURE 4. LABORATORY BLEACHING EXPOSURE

Spectrofluorescence

S13G Bleaching

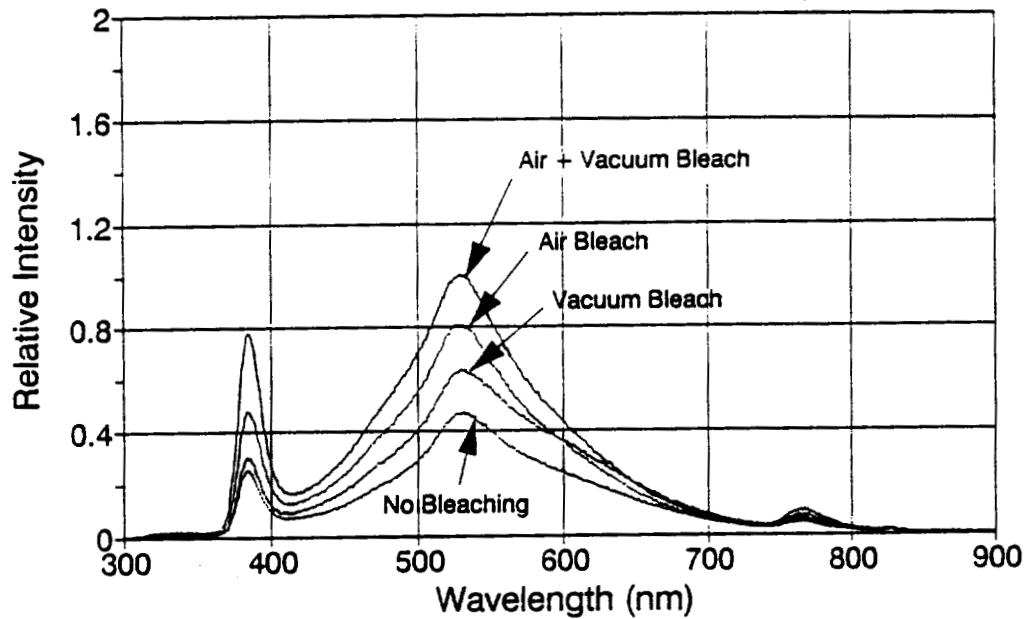


FIGURE 5. SPECTROFLUORESCENCE OF S13G FOLLOWING BLEACHING

A276 Thermal Control Coating

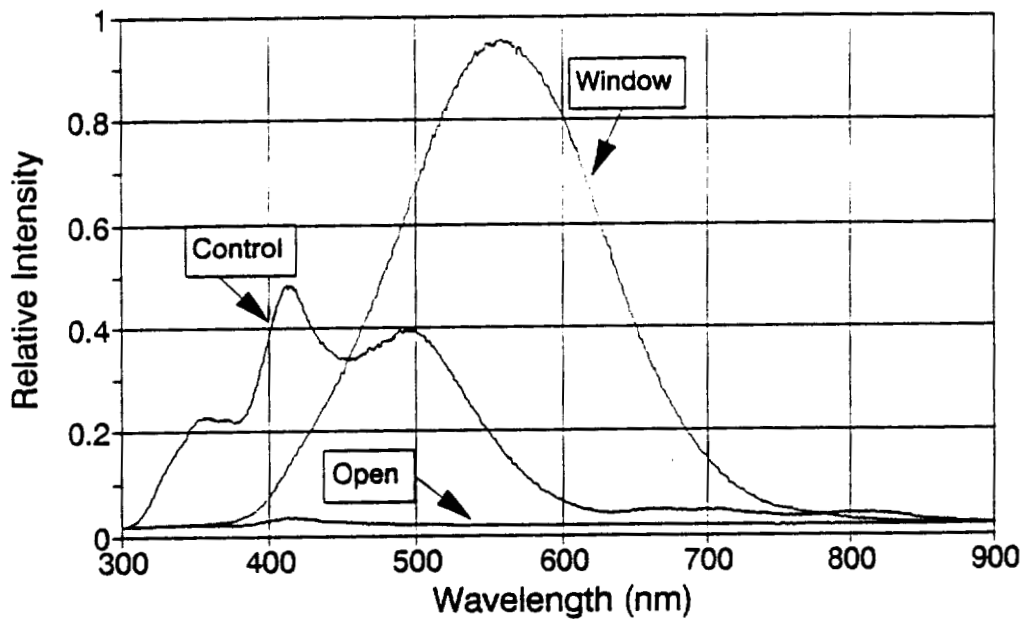


FIGURE 6. SPECTROFLUORESCENCE OF A0034 A276 THERMAL CONTROL COATINGS

ATOMIC OXYGEN INTERACTIONS WITH PROTECTED ORGANIC MATERIALS ON
THE LONG DURATION EXPOSURE FACILITY (LDEF)

Bruce A. Banks, Kim K. de Groh,
NASA Lewis Research Center
Cleveland, Ohio 44135
Telephone: (216) 433-2308, Fax: (216) 433-2221

513-23

44927

178

Justine L. Bucholz
Ohio Aerospace Institute
Brook Park, Ohio 44142
Telephone: (216) 433-2308, Fax: (216) 433-2221

and

Michael R. Cales
Cleveland State University
Cleveland, Ohio 44115
Telephone: (216) 433-2310, Fax: (216) 433-2221

ABSTRACT

The Long Duration Exposure Facility (LDEF) has provided an excellent opportunity to understand the nature of directed atomic oxygen interactions with protected polymers and composites. Although there were relatively few samples of materials with protective coatings on their external surfaces on LDEF which were exposed to a high atomic oxygen fluence, analysis of such samples has enabled an examination of the shape of atomic oxygen undercut cavities at defect sites in the protective coatings.

Samples of front-surface aluminized (Kapton) polyimide were inspected by scanning electron microscopy to identify and measure crack defects in the aluminum protective coatings. After chemical removal of the aluminum coating, measurements were also made of the width of the oxidized undercut cavities below the crack defects. The LDEF flight undercut cavity geometries were then compared with Monte Carlo computational model undercut cavity predictions.

The comparison of the LDEF results and computational modeling indicates agreement in specific undercut cavity geometries for atomic oxygen reaction probabilities dependent upon the 0.68 to 3.0 power of the energy. However, no single energy dependency was adequate to replicate flight results over a variety of aluminum crack widths.

INTRODUCTION

Atomic oxygen in low Earth orbit readily oxidizes most polymeric materials (1-5).

It is now widely known that the use of unprotected polymeric materials in low Earth orbit may cause unacceptable recession during high atomic oxygen fluence missions. Either new materials should be used which are inherently immune to atomic oxygen attack or conventional materials may continue to be used provided they are covered with atomic oxygen resistant coatings.

Protective coatings for polymers typically used in low Earth orbit, such as SiO_x on polyimide Kapton, have been developed and extensively tested in ground laboratory atomic oxygen systems. However, few high fluence in-space exposure studies of such protected polymers have been conducted (7,8).

On the LDEF spacecraft, relatively few polymers that had metal or metal oxide protective coatings on their exposed surfaces were exposed to high fluence atomic oxygen. A small sample of aluminized (Kapton) polyimide was exposed to high fluence atomic oxygen on LDEF and then used for characterization of the undercut cavities at defect sites in the protective coating. These data were then used for comparison with an *ab initio* Monte Carlo computational model which was developed to predict the shape of the atomic oxygen undercut cavities that occur at defects in protective coatings on polyimide Kapton. The detailed mechanistic assumptions of the computational model could then be varied to examine the degree to which the observed LDEF results matched the model predictions for various mechanistic assumptions.

Understanding the detailed mechanistic interactions which occur between atomic oxygen and protected materials in low Earth orbit will allow more reliable predictions of the long term durability of protected materials in low Earth orbit, based on ground laboratory testing.

METHODS, MATERIALS, AND PROCEDURE

LDEF Aluminized Kapton Samples

A front-surface aluminized (Kapton H) polyimide sample exposed on LDEF as part of the Solar Array - Materials Passive LDEF Experiment located on row 8A was used for the experimental data presented in this investigation. The sample consisted of approximately 1,000 Å of vapor deposited aluminum on a 0.0254 mm thick Kapton substrate. The sample was oriented such that it received a total atomic oxygen fluence of 7.15×10^{21} atoms/cm² arriving at 38.1° from the perpendicular to the surface.

The sample was examined for crack or scratch defects in the aluminization to allow a two-dimensional characterization of the crack width and the associated undercutting. A two-dimensional geometry was desired because the Monte Carlo computational model was also two-dimensional.

Scanning electron microscope photographs were taken of defects with a variety of widths in the aluminized Kapton. The sample was then chemically treated with a dilute hydrochloric acid solution to remove the aluminum. Additional scanning electron micrographs were taken at the identical defect sites to allow measurement of the width of the undercut cavities associated with the defect sites.

The crack-width data, undercut-width data, and undercut-cavity shape were then used as the basis for modeling this behavior with Monte Carlo predicted undercutting geometries based on specific atomic oxygen interaction mechanistic assumptions such as reaction probabilities and fractional energy loss upon impact.

Monte Carlo Computational Model

An *ab initio* Monte Carlo computational model was developed to predict the undercut cavity shape as a result of atomic oxygen interaction with polyimide Kapton at the site of crack defects in the protective aluminum coating. The model allows the atomic oxygen to enter the crack from a fixed direction (as was the case for LDEF), a sweeping direction (as would occur in the case of a solar array surface where the surface rolls with respect to the atomic oxygen arrival direction), or an isotropic arrival direction (as occurs in ground laboratory oxygen plasma exposure tests to simulate low Earth orbital atomic oxygen conditions). For the fixed direction arrival case, the model also allows a thermally distributed arrival direction to be assumed because the atoms are hot ($\approx 1227\text{K}$ for the LDEF mission) (8), which causes transverse velocity variations to occur.

The mathematical model of Kapton underneath the crack defect consisted of an orthogonal array of cells in which the details of the atomic oxygen interaction with each cell were based on mechanisms which were mathematically defined. Figure 1 illustrates the geometry of the Monte Carlo computational model. Figure 2 is a flow chart of the Monte Carlo computational model showing the decision-making process and the iterations used to predict the undercut cavity shape.

The location of atoms being brought into the defect in the aluminum coating is randomly selected. When the atomic oxygen model atom impinges upon the Kapton surface, a random selection is made as to whether or not the oxygen reacts with the Kapton. This selection is based on a prescribed initial impact reaction probability. In general this reaction probability was set at

0.138 (for normal incidence) based on previous experimental and computational investigations (9).

The probability of reaction upon energetic impact was also assumed to be dependent upon the arrival angle, Θ , with respect to the perpendicular to the surface with a $(\cosine \Theta)^{1/2}$ dependence (9,10). The angle-dependent reaction probability was based on the impinging direction with respect to the local surface normal which was based on the average of adjoining Monte Carlo computational model cells.

Oxygen atoms which impinged upon aluminum were treated as if a glass surface was struck where no reaction was possible. However, depending upon the program operator's choice, recombination or ejection and scattering distributions could be prescribed as similar to those used for atomic oxygen ejection from Kapton.

Energy loss upon impact was defined in terms of a fraction of energy loss between the arriving energy and that energy which would be associated with thermally accommodated atomic oxygen. Thus, the atomic oxygen was assumed to be at 4.5 eV upon initial impact and ultimately thermally accommodated down to approximately 0.04 eV after numerous collisions. The atomic oxygen reaction probability was explored for a dependence upon energy proportional to the arriving energy raised to a numerical exponent ranging from 0.68 to 4.

The atomic oxygen which did not react was ejected at an angle which could be selected based on choices made by the Monte Carlo program operator. These choices included elastic scattering, cosine distributed scattering, or a combination of elastic scattering and thermally accommodated cosine distributed emission. One could also select a random probability of recombination of atomic oxygen if it did not react with the Kapton.

The Monte Carlo computational model ray traced each atom until it either reacted with Kapton or exited the undercut cavity. Exiting could be accomplished by leaving through the defect in the aluminum, or, in the case of high fluence exposure, exiting from an aperture produced in the bottom of the Kapton which was not protected.

Undercutting profiles were predicted by the Monte Carlo model and measurements were then made from the undercut profiles produced by the model and compared with actual LDEF data.

The use of the Monte Carlo computational simulation requires a calibration in which actual in-space erosion for a given atomic oxygen fluence is correlated with computational modeling erosion. This is accomplished by using a wide defect in the protective coating to simulate the erosion which would occur in space, using

the Monte Carlo computational model.

The mean depth of erosion for simulated unprotected Kapton was then used to predict the number of atoms, N, required to simulate the actual LDEF in-space damage which would occur at the site of a narrow crack for which experimental data exists from LDEF. Thus the number of atoms required to enter the simulated defect to cause the same damage as would occur during the LDEF mission is given by

$$N = \frac{MEFW}{HDC}$$

where:

M = number of atoms
entering a wide defect for computation simulation
calibration

E = in-space erosion yield of polyimide Kapton, cm³/atom

F = atomic oxygen fluence in space for the LDEF coupon,
atoms/cm²

W = narrow crack width in Monte Carlo cell units representing
the LDEF protective coating cracks

H = wide crack width in units of Monte Carlo cells for
simulation of unprotected Kapton for Monte Carlo calibration

D = depth of erosion in units of Monte Carlo cells for the wide
defect calibration Monte Carlo simulation

C = Monte Carlo simulation cell edge length, cm/cell.

With the above equation one could then use the Monte Carlo model to predict the atomic oxygen undercutting which would occur in space. The above equation also allows calculation of the scale for the Monte Carlo computational geometry. In the above equation a Kapton in-space erosion yield, E, of 3×10^{-24} cm³/atom was assumed.

RESULTS AND DISCUSSION

The aluminized Kapton sample retrieved from LDEF had cracks which were oriented in such a direction that if one looks down the length of the crack, the average angle of atomic oxygen arrival was 25.9° from the perpendicular to the coated Kapton surface. Figure 3 shows scanning electron micrographs of this sample at a crack defect site in the aluminized coating, before and after removal of the aluminized coating.

As can be seen from Figure 3, the width of undercutting significantly exceeds the width of the crack defect in the aluminized coating.

Figure 4 shows a clear view of the undercut cavity of a similar defect site after removal of the aluminized coating. As can be seen from Figure 4, the undercut cavity is asymmetrical. The left side of the undercut cavity has a chamfer near the top while the right side of the undercut cavity, which does not contain a chamfer, is undercut at such an angle that the cavity wall is not visible in this image. This is thought to be largely due to the fact that incoming atomic oxygen scatters off the edges of the aluminized coating causing the scattered atomic oxygen to preferentially attack the near surface Kapton opposite the side of the defect.

In Figure 4, the atomic oxygen was arriving from the upper left direction. Thus the undercut cavity has rather straight walls on its right side and is more undercut on the left side because of atomic oxygen scattering effects. It was apparent from the micrographs of wide cracks (of the order of $3\mu\text{m}$ on this sample) that the atomic oxygen undercut cavity extended all the way through the 0.0254 mm thick Kapton sample. Narrow cracks in the aluminized layer did not allow sufficient atomic oxygen fluence entry into the undercut cavities to erode all the way through the Kapton, as shown in Figure 5.

Figure 5 also shows the chamfering effects of atomic oxygen reflected from the aluminized coating. The bottom of the undercut cavity is also observable at this rather narrow crack defect site.

Figure 6 shows the results of measurements from the scanning electron micrographs of a variety of crack widths in the aluminized coating and their associated undercut widths, for cracks all oriented in approximately the same direction. This plot, along with the asymmetrical shape of the undercut cavities observed in the scanning electron micrographs, was used as a basis of comparison with Monte Carlo model predictions to assess the validity of mechanistic assumptions for atomic oxygen interaction with polymers and protective coatings.

The Monte Carlo modeling of the LDEF atomic oxygen arrival used the assumptions of reference (8). The angular distribution of atomic oxygen arrival associated with 1227K hyperthermal atoms is shown in Figure 7 as a polar plot of the atomic oxygen arrival flux as a function of the arriving direction.

As can be seen from Figure 7, the arriving atomic oxygen has an angular distribution similar to a searchlight which clearly would indicate that undercut cavities should widen with depth, if a sufficient atomic oxygen fluence has passed through the defect.

Although computational simulations of the LDEF environmental interactions with aluminized Kapton were conducted assuming a variety of atomic oxygen scattering processes (including specular, cosine, and a mix of cosine and specular), only a cosine ejection distribution was found to produce undercut profiles which replicated observed LDEF results.

Figure 8 shows two Monte Carlo predicted undercut cavities. These two predictions were selected for providing reasonable undercut cavity matches to both the undercut shape and the undercut cavity width versus defect width plot of Figure 6. Such models were then developed for reaction probability energy dependent exponents ranging from 0.68 to 3.

As can be seen from Figure 8, atomic oxygen reflected from the aluminized protective coating does produce a slight pocket in the Kapton near the aluminum coated surface as shown in the observed LDEF scanning electron micrographs.

For each reaction probability energy-dependent exponent, a variety of fractional energy losses upon impact were evaluated in an attempt to reproduce the LDEF-observed undercut cavity width versus protective coating defect width data. The results of these efforts are shown in Figure 9. The Monte Carlo predictions are shown as error bars on the figure. The error bars represent the range of undercut widths that could be predicted based on the range of interpretations possible for the width of the undercutting profile. No individual reaction probability energy dependent exponent and its associated fractional energy loss upon impact was found to produce an ideal match to the observed experimental data.

A rather weak energy dependence as shown in Figure 9a produces far too much undercutting for small width defects. Increasing the energy dependence up to an exponent of 3, Figure 9d did produce crack width to undercut width ratios which replicated flight results; however, predicted undercutting for large width cracks was not sufficiently wide to match observed data. Thus, although undercut widths could be predicted which matched LDEF results for specific width cracks, no single energy dependent exponent for reaction probability was found to provide acceptable profile matches over all width cracks. Based on these results further adjustments in the quantification of the mechanistic assumption parameters are necessary.

One of the difficulties associated with performing the Monte Carlo computational calculations is that typically ten hours were needed to produce each predicted Monte Carlo undercutting profile. This is largely a result of Monte Carlo model atoms bouncing around within the undercut defect cavities with a very low reaction probability after they have thermally accommodated. Each atom is required to either react or exit the defect before

another atom is brought into the model cavity. No recombination was assumed to occur in these studies. As the reaction probability decreases with each collision, many impacts are required before the next atom is allowed to enter. Thus, the process of computation slows down greatly as the undercut cavity grows. Although this is an inconvenience, the accuracy of the prediction should not be compromised.

The Monte Carlo model does predict many of the features experimentally observed but will require additional investigation to more clearly quantify the energy dependence and fractional energy loss.

SUMMARY

A retrieved LDEF sample of front surface aluminized Kapton was analyzed by scanning electron microscopy to characterize the atomic oxygen undercut geometries and the dependence of undercut cavity width on the aluminized protective coating crack width.

The undercut cavities observed indicate that atomic oxygen scatters off the edges of the protective coating to produce accentuated atomic oxygen erosion of the Kapton opposite the impinged edge. A Monte Carlo computational model was developed which is capable of simulating a variety of atomic oxygen environments including that of the LDEF spacecraft. This model was used to predict undercut cavity profiles in an attempt to replicate the observed LDEF data.

Although the results of the computational modeling were found to replicate the shape of some of the undercut cavities at defect sites, such replication was not observed over a wide range of crack defect widths. Further study is needed to develop mechanistic information which accurately predicts observed experimental results.

ACKNOWLEDGEMENT

The authors gratefully acknowledge the kind assistance provided by Dr. Ann Whitaker at NASA Marshall Space Flight Center who provided the sample of aluminized Kapton used in this study.

REFERENCES

1. L. J. Leger, "Oxygen Atom Reaction with Shuttle Materials at Orbital Altitudes," NASA TM-58246, 1982.
2. A. F. Whitaker, "LEO Atomic Oxygen Effects on Spacecraft Materials," paper presented at the AIAA Shuttle Environment and Operations Meeting, Washington, D.C., October 31-November 2, 1993, AIAA-83-2632-CP.

3. D. E. Brinza, "Proceedings of the NASA Workshop on Atomic Oxygen Effects," JPL Publication 87-14 (June 1, 1987), Pasadena, CA, Nov. 10-11, 1986.
4. B. A. Banks, M. J. Mirtich, S. K. Rutledge, and D. M. Swec, NASA TM-83706, Paper presented at the 11th International Conference on Metallurgical Coatings sponsored by the American Vacuum Society, San Diego, CA, April 9-13, 1984.
5. W. S. Slemple, D. R. Young, G. W. Witte, Jr., and J. Y. Shen, "Effects of the LDEF Flight Exposure on Selected Polymer Matrix Resin Composite Materials," LDEF-69 Months in Space, First Post-Retrieval Symposium, June 2-8, 1991, NASA CP-3134, Part II, p.1149.
6. B. A. Banks, S. K. Rutledge, K. K. de Groh, M. J. Mirtich, L. Gebauer, R. Olle, and C. M. Till, "The Implications of the LDEF Results on Space Station Freedom Power System Materials," paper presented at the 5th International Symposium on Materials in a Space Environment, Cannes-Mandelieu, France, Sept. 16-20, 1991.
7. S. K. Rutledge, R. M. Olle, and J. M. Cooper, "Atomic Oxygen Effects on SiO_x Coated Kapton for Photovoltaic Arrays in Low Earth Orbit," paper presented at the IEEE/Photovoltaic Specialists Conference, Las Vegas, Nevada, Oct. 7-11, 1991.
8. B. A. Banks, S. K. Rutledge, K. K. de Groh, B. M. Auer, M. J. Mirtich, L. Gebauer, C. M. Hill, and R. F. Lebed, "LDEF Spacecraft, Ground Laboratory and Computational Modeling Implications on Space Station Freedom's Solar Array Materials and Surfaces Durability," paper presented at the IEEE/Photovoltaic Specialists Conference, Las Vegas, Nevada, Oct. 7-11, 1991.
9. B. A. Banks, S. K. Rutledge, K. K. de Groh, C. R. Stidham, L. Gebauer, and C. M. LaMoureaux, "Atomic Oxygen Durability Evaluation of Protected Polymers using Thermal Energy Plasma Systems," paper presented at the International Conference on Plasma Synthesis in Processing of Materials, Denver, Colo., February 21-25, 1993.
10. C. R. Tennyson, G. R. Cool, and D. G. Zimcik, "Space Environmental Effects on Polymer Matrix Composites as a Function of Sample Location on LDEF," paper presented at the LDEF Materials Results for Spacecraft Applications Conference, Huntsville, AL, Oct.27-28, 1992.

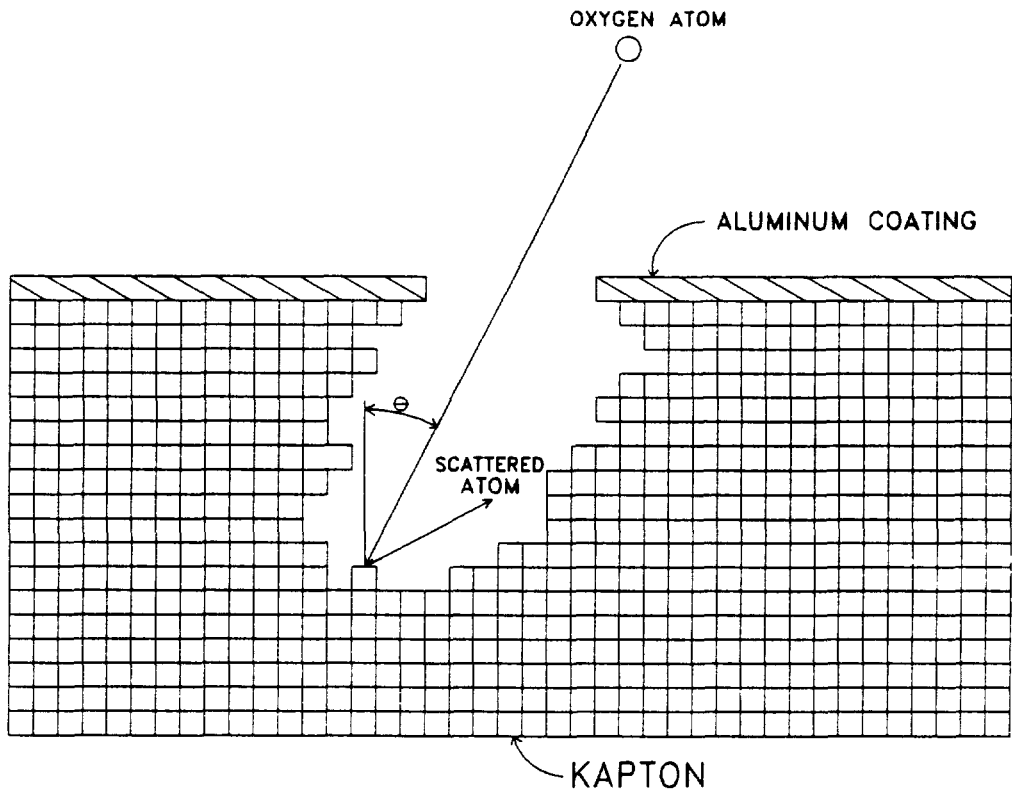


Figure 1. Monte Carlo computational model geometry.

GENERAL OUTLINE

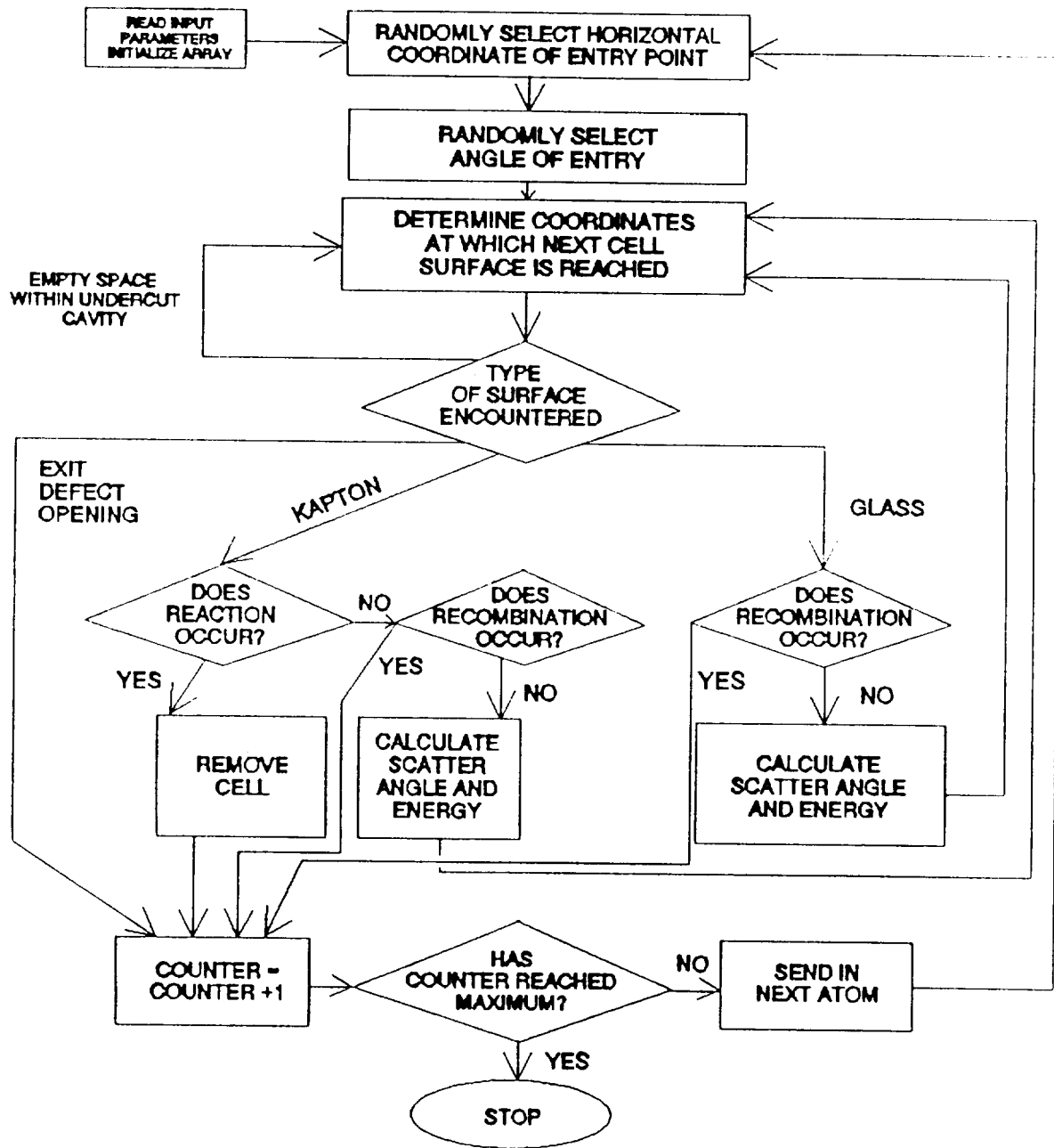
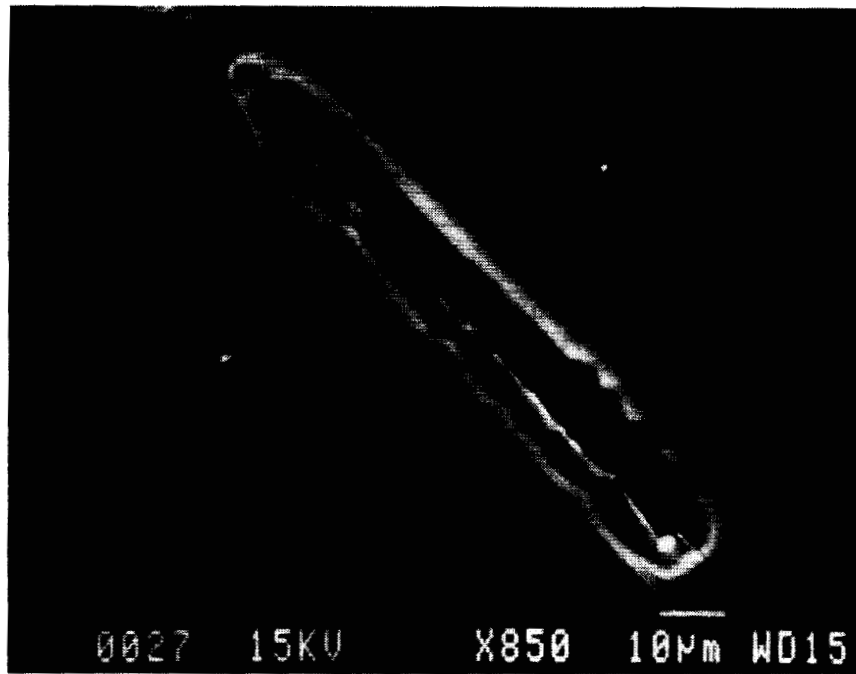
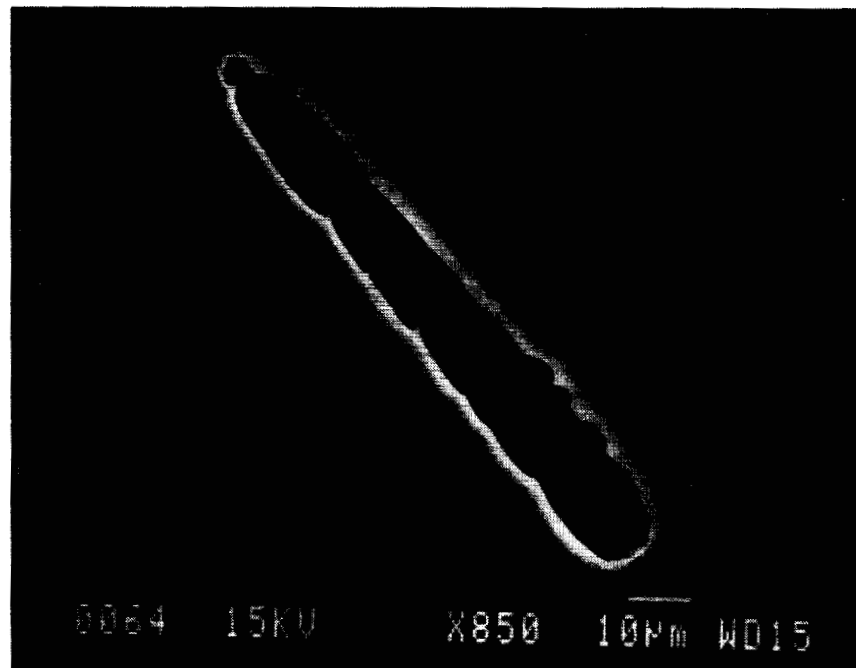


Figure 2. Monte Carlo computational model flow chart.



a. Al coating present



b. Al coating removed

Figure 3. Scanning electron photomicrograph of retrieved LDEF aluminized Kapton sample

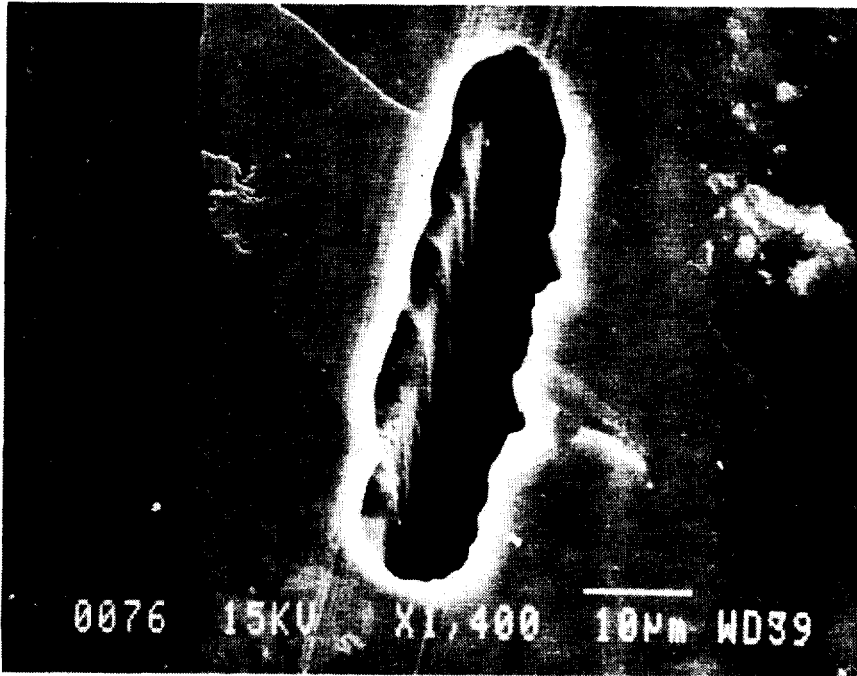


Figure 4. Undercut cavity associated with a wide defect in the aluminized Kapton after removal of the aluminized coating.



Figure 5. Undercut cavity beneath a narrow crack in the aluminized coating after removal of the aluminized coating.

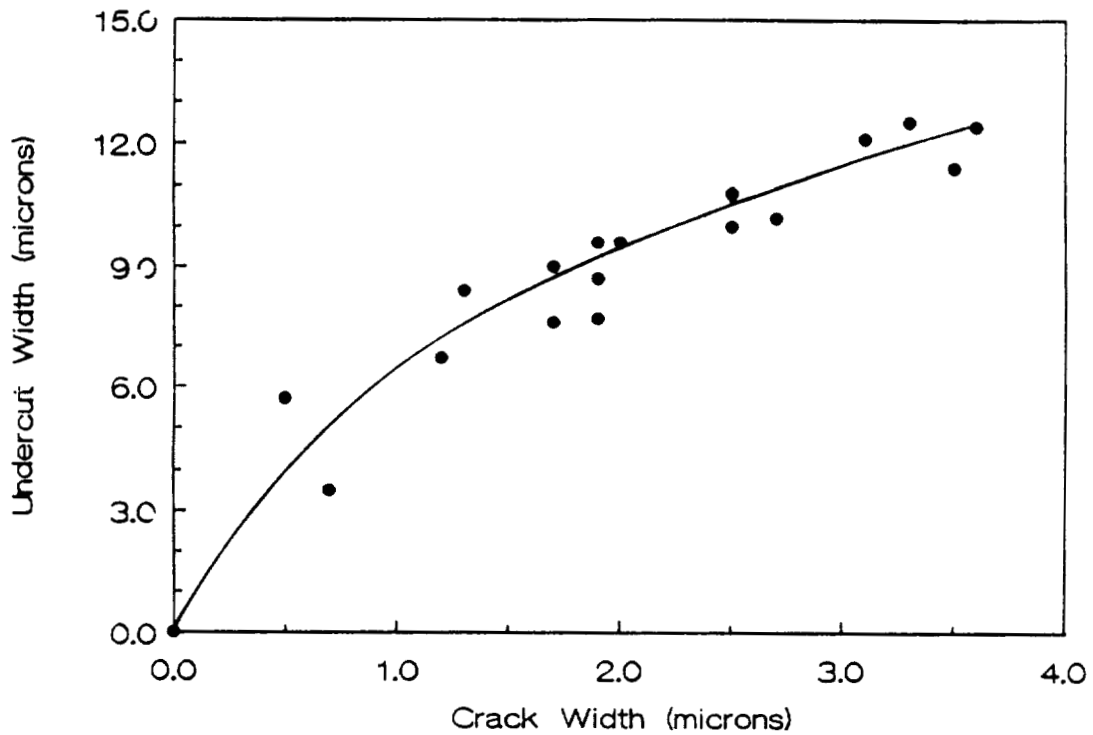


Figure 6. Observed retrieved LDEF sample undercut cavity width dependence upon crack width in the aluminized coating

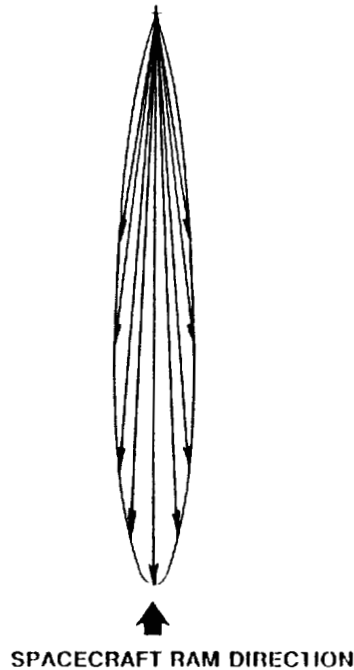
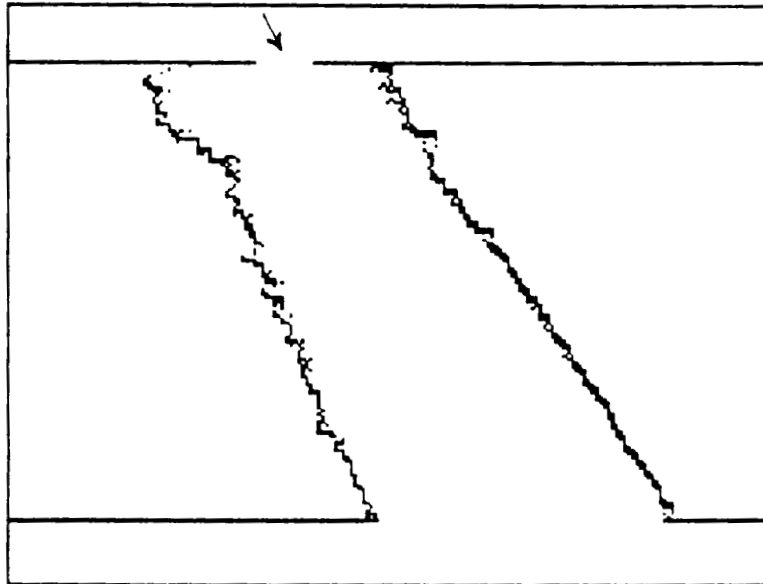
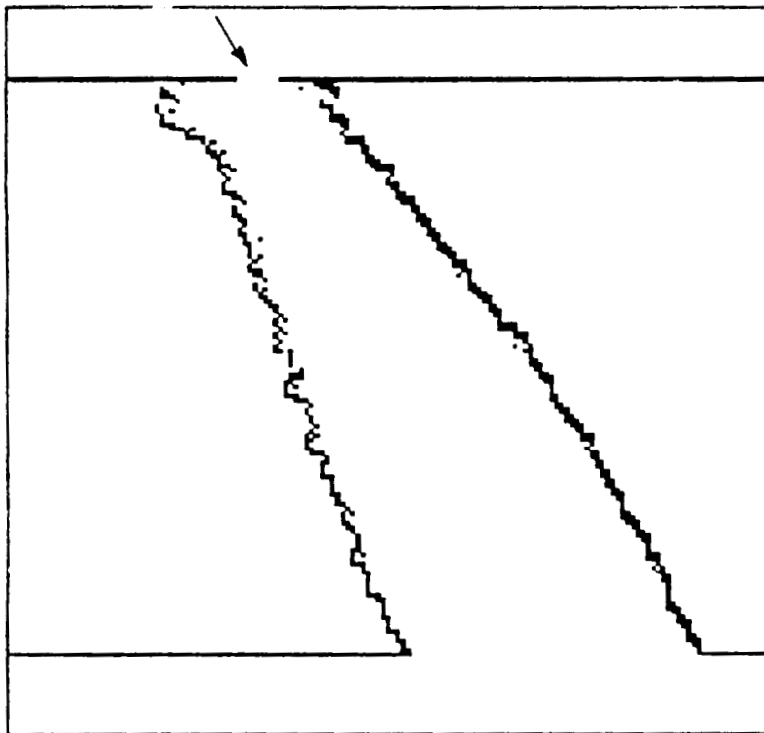


Figure 7. Polar plot of LDEF atomic oxygen arrival resulting from a combination of the spacecraft's orbital velocity, Earth's upper atmosphere co-rotational velocity, the 28.5° inclination of the orbit, and the fact that the spacecraft is ramming into a 1227K gas of atomic oxygen.

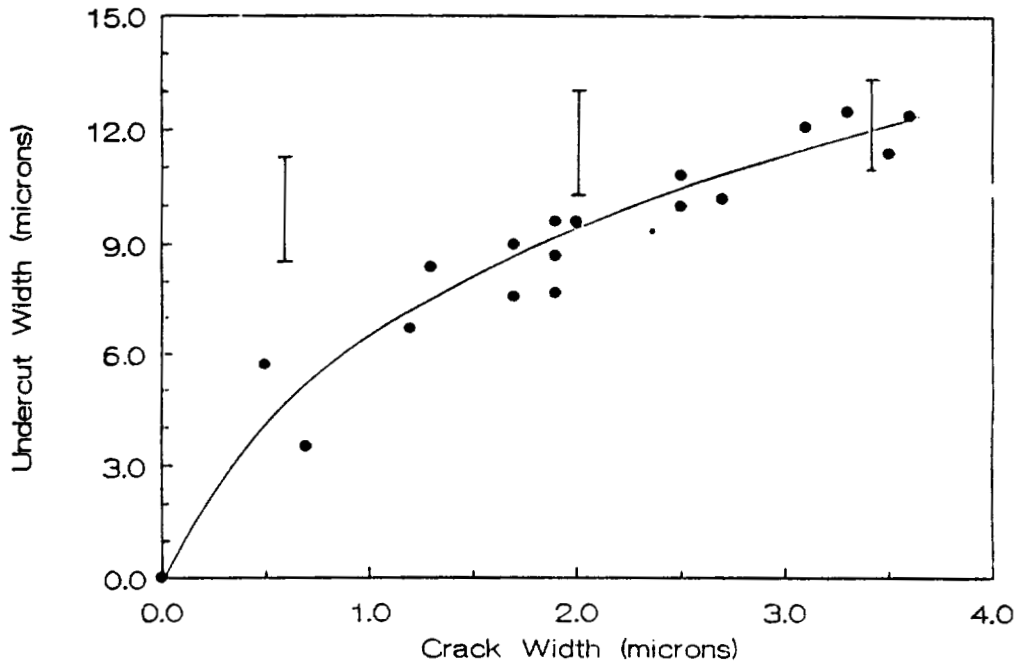


a. 3.4 μm wide crack defect, reaction probability dependent upon $(\text{energy})^{0.68}$, fractional energy loss upon impact equal to 0.4.

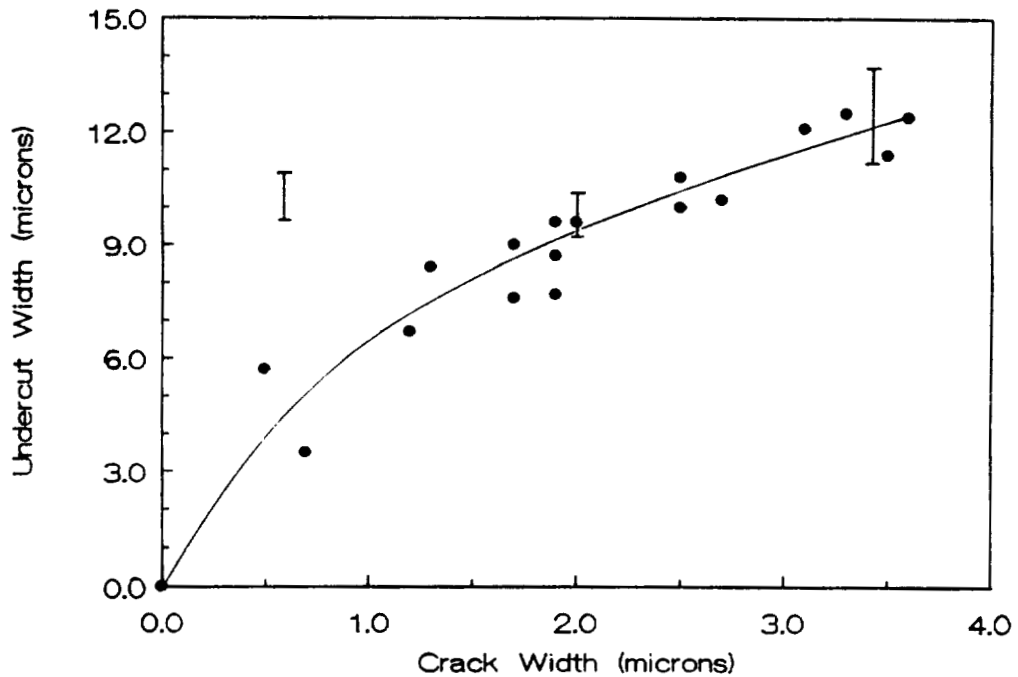


b. 2 μm wide defect in the aluminized coating, reaction probability dependent upon $(\text{energy})^3$, fractional energy loss upon impact equal to 0.2.

Figure 8. Monte Carlo computational model predictions for undercut cavities associated with crack defects in LDEF aluminized Kapton.

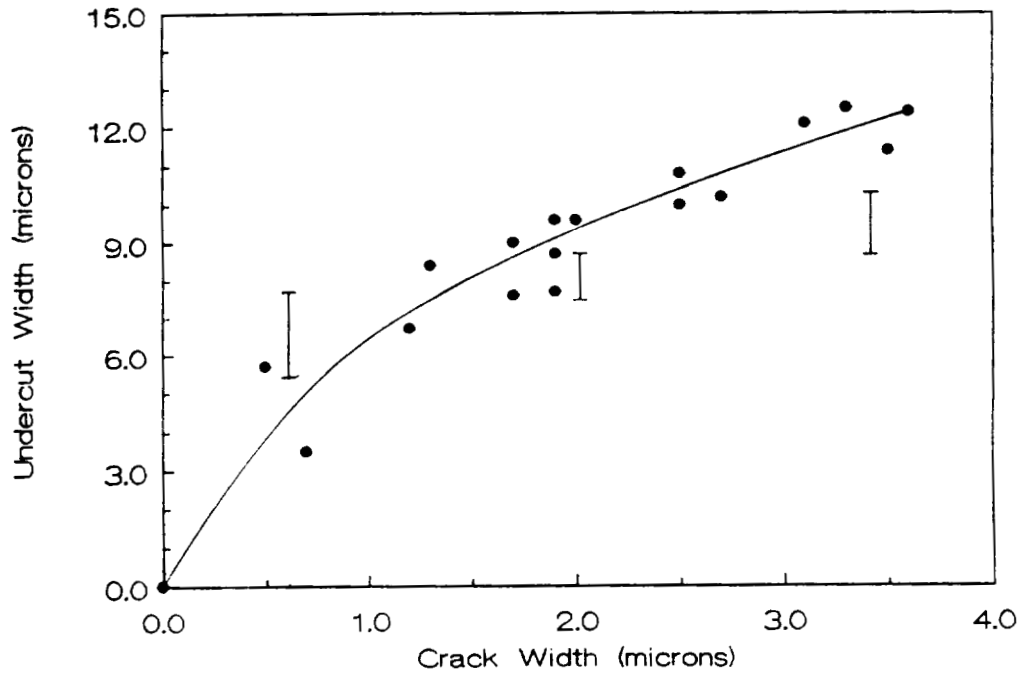


a. Reaction probability proportional to $(\text{energy})^{0.68}$,
fractional energy loss upon impact = 0.4

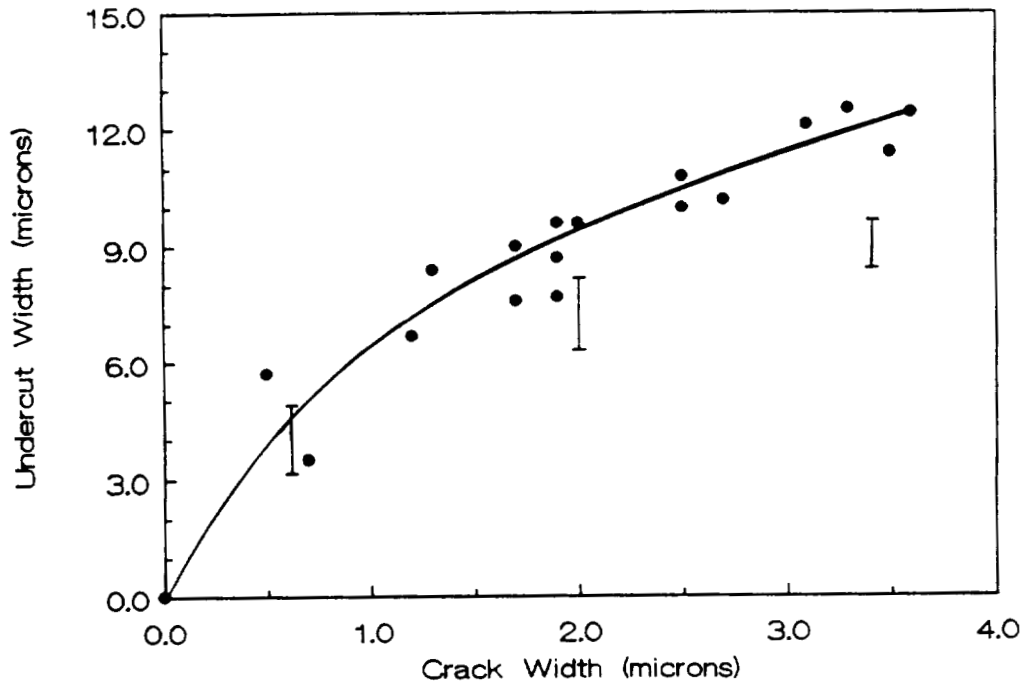


b. Reaction probability proportional to $(\text{energy})^1$,
fractional energy loss upon impact = 0.2

Figure 9. Comparison of Monte Carlo computational model predicted undercutting (shown as error bars) with experimentally observed LDEF data.



c. Reaction probability proportional to $(\text{energy})^2$,
fractional energy loss upon impact = 0.2



d. Reaction probability proportional to $(\text{energy})^3$,
fractional energy loss upon impact = 0.2.

Figure 9. Comparison of Monte Carlo computational model predicted undercutting (shown as error bars) with experimentally observed LDEF data.

514-24
44423
15PTREND ANALYSIS OF IN-SITU SPECTRAL REFLECTANCE DATA
FROM THE THERMAL CONTROL SURFACES EXPERIMENT (TCSE)

D.R. Wilkes, P.S. LeMaster, R.J. Mell, and E.R. Miller
AZ Technology, Inc.
3322 Memorial Parkway SW, Suite 93
Huntsville, AL 35801
Phone: 205/880-7481, Fax: 205/880-7483

J.M. Zwiener
NASA/Marshall Space Flight Center
Marshall Space Flight Center, AL 35812
Phone: 205/544-2528, Fax: 205/544-7329

SUMMARY

The Thermal Control Surfaces Experiment (TCSE) on the LDEF was a comprehensive experiment that combined in-space measurements with extensive pre- and post-flight analyses of thermal control surfaces to determine the effects of exposure to the low Earth orbit (LEO) space environment. The TCSE is the first space experiment to directly measure in-situ total hemispherical reflectance of thermal control surfaces in the same way they are routinely measured in the laboratory. In-space optical measurements performed by the TCSE provide the unique opportunity for trend analysis of the performance of materials in the space environment. Such trend analysis of flight data offers the potential to develop an empirical lifetime prediction model for several thermal control surfaces. For material research, trend analysis of the TCSE flight data, particularly the spectral data, can provide insight into the damage mechanisms of space exposure.

Trend analysis for the TCSE samples has been limited to those materials that were not significantly eroded by the atomic oxygen (AO) environment. The performance of several materials on the LDEF mission was dominated by AO effects. Trend analysis was performed on both the detailed spectral reflectance measurements (in-space, pre-flight, and post-flight) and on the integrated solar absorptance (α_s).

Results of this analysis for the five selected TCSE materials are presented along with the spectral flight data. Possible degradation and effects mechanisms will be discussed to better understand and predict the behavior of these materials in the LEO space environment.

INTRODUCTION

The long term effects of the natural and induced space environment on spacecraft surfaces are critically important to future spacecraft--including the Space Station. The damaging constituents of this environment include thermal vacuum, solar ultraviolet radiation, atomic oxygen, particulate radiation, and the spacecraft induced environment. The behavior of materials and coatings in the space environment continues to be a limiting technology for spacecraft and experiments. The Thermal Control Surfaces Experiment (TCSE) was flown on the National Aeronautics and Space Administration (NASA) Long Duration Exposure Facility (LDEF) to study these environmental effects on thermal control surfaces.

The TCSE was a comprehensive experiment that combined in-space measurements with extensive pre- and post-flight analyses of thermal control surfaces to determine the effects of exposure to the low Earth orbit (LEO) space environment.¹ The TCSE is the first space experiment to directly measure in-situ total hemispherical reflectance of thermal control surfaces in the same way they are routinely measured in the laboratory.

EXPERIMENT DESCRIPTION

The TCSE was a completely self-contained experiment package, providing its own power, data system, reflectometer, and pre-programmed controller for automatically exposing, monitoring, and measuring the sample materials (see Figure 1). The primary TCSE in-space measurement was total hemispherical reflectance as a function of wavelength from 250 to 2500 nm using a scanning integrating sphere reflectometer. The measurements were repeated at preprogrammed intervals until battery power depletion.

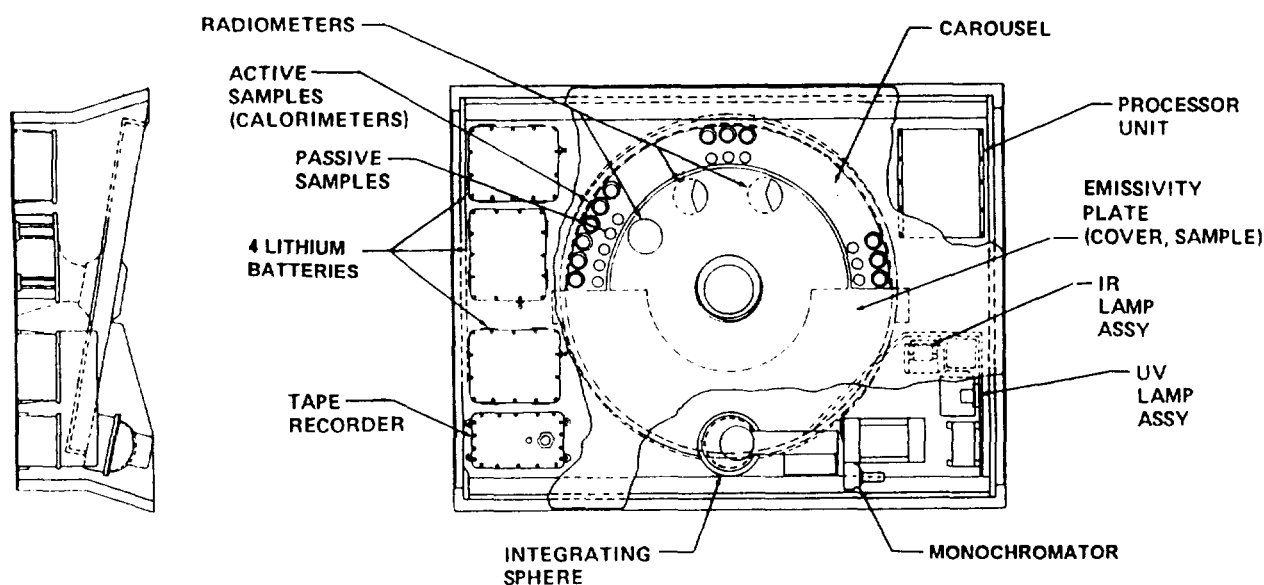


Figure 1. TCSE Assembly.

The LDEF, with the TCSE on board, was placed in low Earth orbit by the Shuttle Challenger on April 7, 1984. LDEF was retrieved by the Shuttle on January 12, 1990 after 5 years 10 months in space. The LDEF was gravity-gradient stabilized and mass loaded so that one end of LDEF always pointed at the Earth and one side pointed into the velocity vector or RAM direction. The TCSE was located on the

leading edge (row 9) of LDEF and at the Earth end of this row (position A9). The LDEF leading edge (and the TCSE) was offset from the RAM vector by 8.1°. This LDEF/TCSE orientation and mission duration provided the following exposure environment for the TCSE samples:

Total space exposure	5 years 10 months
Atomic oxygen fluence ²	8.3 x 10 ²¹ atoms/cm ²
Solar UV exposure ²	1.0 x 10 ⁴ ESH
Thermal cycles	3.3 x 10 ⁴ cycles
Radiation (at surface) ³	3.0 x 10 ⁵ rads

The TCSE operated for the first 584 days of the LDEF mission before its batteries were depleted. Although the flight recorder malfunctioned, data were recovered for the last 421 days of this operational period. The recovered data included eleven sets of reflectometry data. The battery power was fully expended while the sample carousel was being rotated, leaving the carousel in a partially open position. This carousel position permitted exposure of 35 of the samples for the complete LDEF mission (69.2 months), while 14 samples were exposed for only 19.5 months and were protected from the direct space environment for the subsequent four years.

DEGRADATION TREND ANALYSIS

Long duration of space missions requires significant extrapolation of flight and ground simulation data to provide predictions of end-of-life properties for thermal control surfaces. This is particularly true for NASA programs such as the Space Station, AXAF and the Hubble Space Telescope. The in-space optical measurements performed by the TCSE offer the unique opportunity to perform a trend analysis on the performance of materials in the space environment. Trend analysis of flight data provides the potential to develop an empirical prediction model for some of the thermal control surfaces. For material research, trend analysis of the TCSE flight data can provide insight into the damage mechanisms of space exposure.

The trend analysis for the TCSE samples has been limited to those materials that were not significantly eroded by the atomic oxygen (AO) environment. The performance of several materials on the LDEF mission was dominated by AO effects. This is particularly true for unprotected A276 and Tedlar where the AO eroded away the surface layers faster than they were degraded by Solar UV. This resulted in a fresh surface with unchanged or slightly improved optical properties.

Trend analyses have been performed on five materials:

- Z93 White Paint
- YB71 White Paint
- S13G/LO White Paint
- A276 White Paint and protective overcoats
- Silver Teflon

These analyses were performed on both detailed spectral reflectance data and derived integrated solar absorptance (α_s). This data includes both in-space and ground based pre-flight and post-flight measurements. The solar absorptance data was analyzed using regression analysis to develop an empirical lifetime model for these materials. Empirical prediction models must be used with caution, however, because they can be misleading and have no scientific basis. The TCSE data provides the only in-situ optical data providing time history of the optical changes to materials exposed to the space environment. The analysis of this data provides the first insight into these time dependent material changes and enables the development of a prediction model. Other in-situ optical measurement experiments should be performed to verify this data and to provide data on new and improved materials. Several standard regression analyses were evaluated including polynomial, exponential, logarithmic and

power fit functions. For integrated α_s the power regression analysis provided a better fit of the experimental data. The power regression line takes the form:

$$\alpha_s = e^{(a+b \ln(t))}$$

While the analysis of solar absorptance data is of great benefit to spacecraft designers, it is the analysis of the spectral data that provides the best insight into the different damage mechanisms of the space environment on materials. For most materials, there are more than one, and potentially many, competing mechanisms of damage due to the combined space environment. In many cases different damage mechanisms exhibit effects in different spectral ranges. The trend analysis of reflectance changes at different wavelengths will aid in separating different mechanistic effects.

In the following discussions, the results of the trend analyses are presented for the five selected materials. Data is shown for both integrated solar absorptance and spectral reflectance. Some of this α_s data has been previously reported⁴ but is repeated to relate the spectral data to the integrated α_s data. The format of the data presentation is described in the first section for Z93 White Paint.

Z93 White Paint

Figure 2 shows the performance of Z93 for the LDEF mission. Solar absorptance is plotted versus exposure time. There appear to be at least two mechanisms that affected the Z93 solar absorptance during the LDEF mission. The first is a short term improvement (decrease) in α_s typical of silicate coatings in thermal vacuum. This improvement is normally associated with loss of water from the ceramic matrix. In ground simulation tests this process takes a much shorter time than the TCSE flight data suggests. This slower loss of water may be due to the cold temperature of the TCSE Z93 sample mounted on a thermally isolated calorimeter. The temperature of the Z93 sample ranged from approximately -55°C to $+6^\circ\text{C}$ but remained well below 0°C most of the time.

The short term improvement is dominant for the first year of exposure after which a long term degradation mechanism becomes dominant. The results of the power regression analysis for the short and long term effects are also shown in Figure 2. Figure 3 plots the long term regression model for Z93 on a log scale allowing extrapolation out to 30 years. The regression analysis projects a 30 year end-of-life value for Z93 of $\alpha_s = 0.185$. This predicted value is statistically a most probable value and not a worse case value.

Figures 4 and 5 show the spectral reflectance data for Z93. All spectral reflectance data presented in this paper are plotted as normalized change in reflectance.

$$\Delta R/R = (\rho - \rho_0)/\rho_0$$

where ρ_0 = initial reflectance (time = 0)

ρ = reflectance at time t

Figure 4 plots normalized reflectance change versus exposure time for five selected wavelengths while Figure 5 plots normalized reflectance change versus wavelength at four different exposure times. These data show that the short term improvement in reflectance of Z93 (attributed to loss of water) is broad banded with the major changes occurring in the infrared as expected. It is somewhat surprising to also see this improvement at the shorter wavelengths. The longer term degradation mechanism occurs mainly below 1000 nm. Even though the changes are small, they are significant because the solar energy curve peaks in this spectral range.

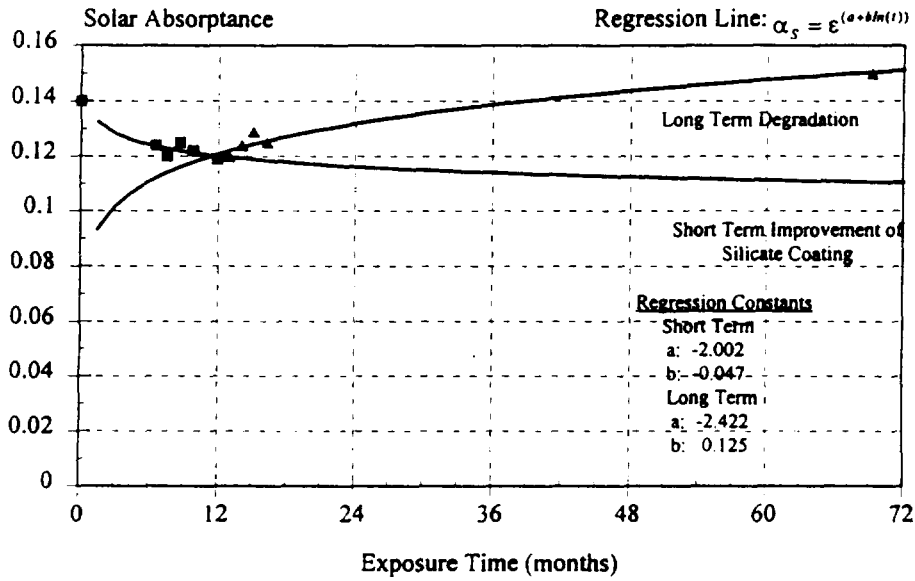


Figure 2. Power Regression Analysis of Z93.

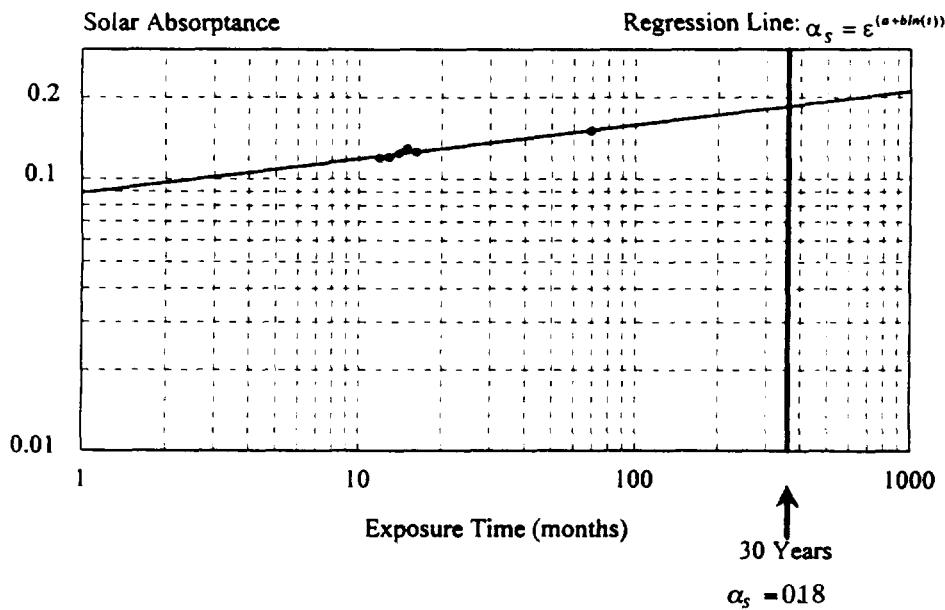


Figure 3. Z93 Degradation Model.

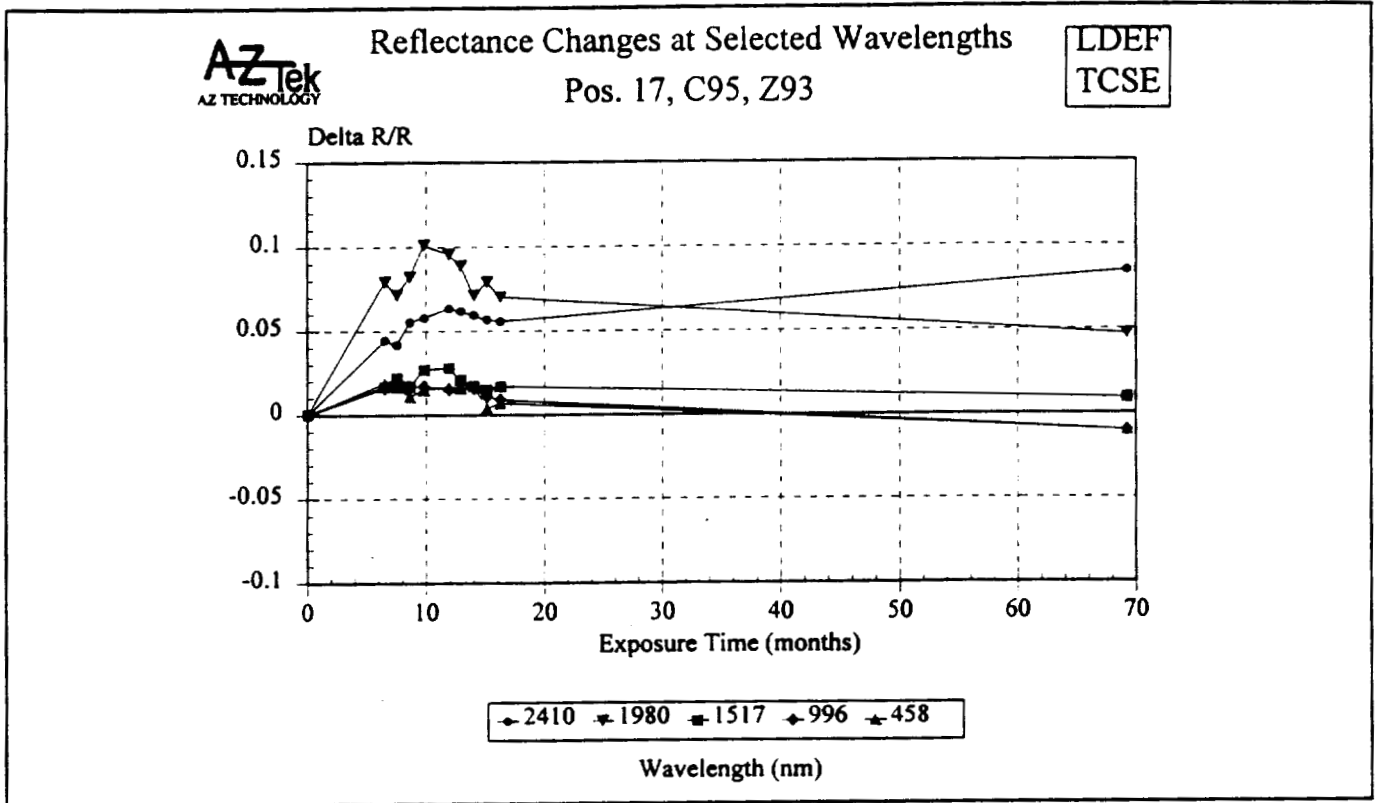


Figure 4. Z93 Reflectance Changes at Selected Wavelengths.

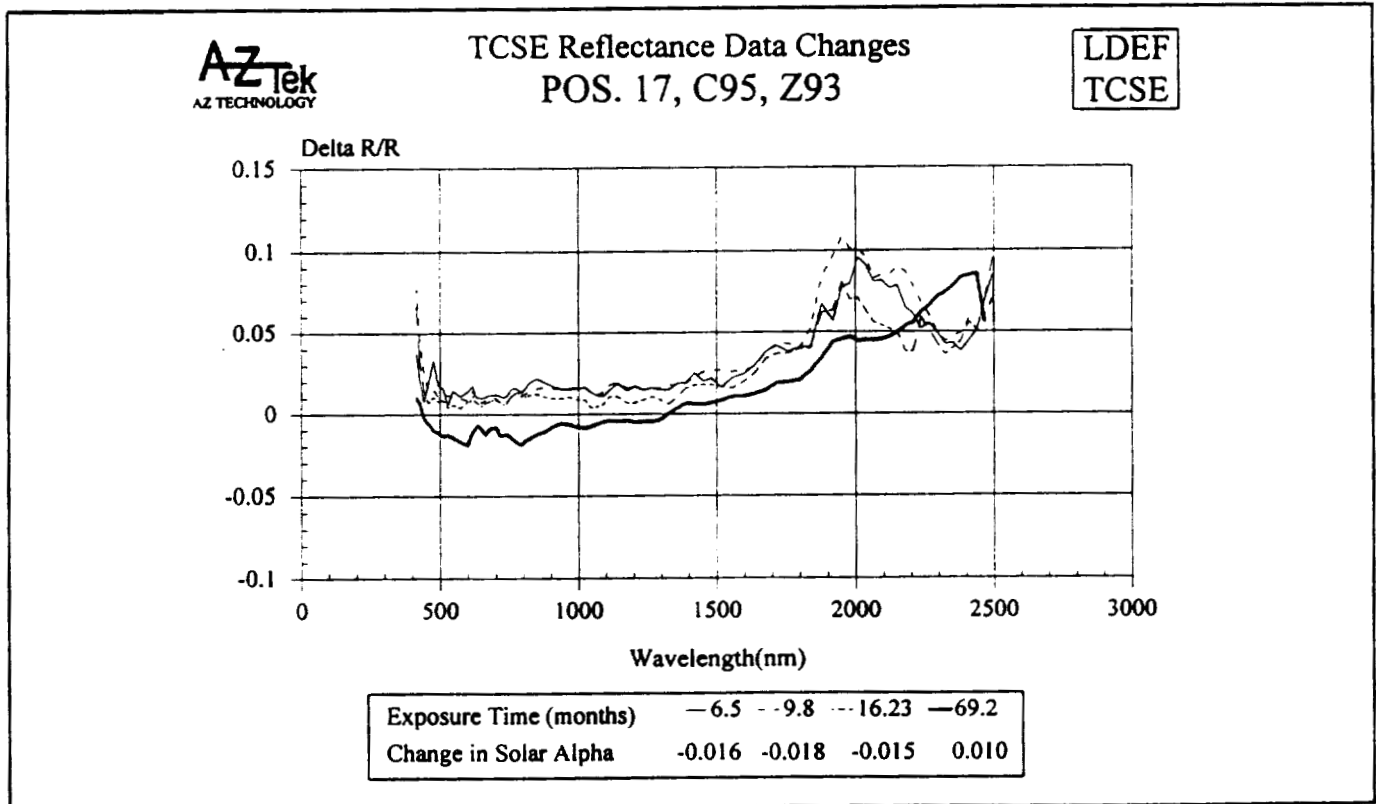


Figure 5. Z93 Reflectance Data Changes.

YB71 White Paint

YB71 exhibited very similar changes to Z93 during the LDEF mission as shown in Figure 6. The reflectance changes for the first fifteen months are nearly identical for both materials (see Figures 5 and 6). This is not surprising as both white coatings use the same potassium silicate binder. What is surprising, however, is the greater degradation of spectral reflectance (and solar absorptance) of the YB71 over Z93. In ground simulation testing before the LDEF mission, YB71 was more stable than Z93.

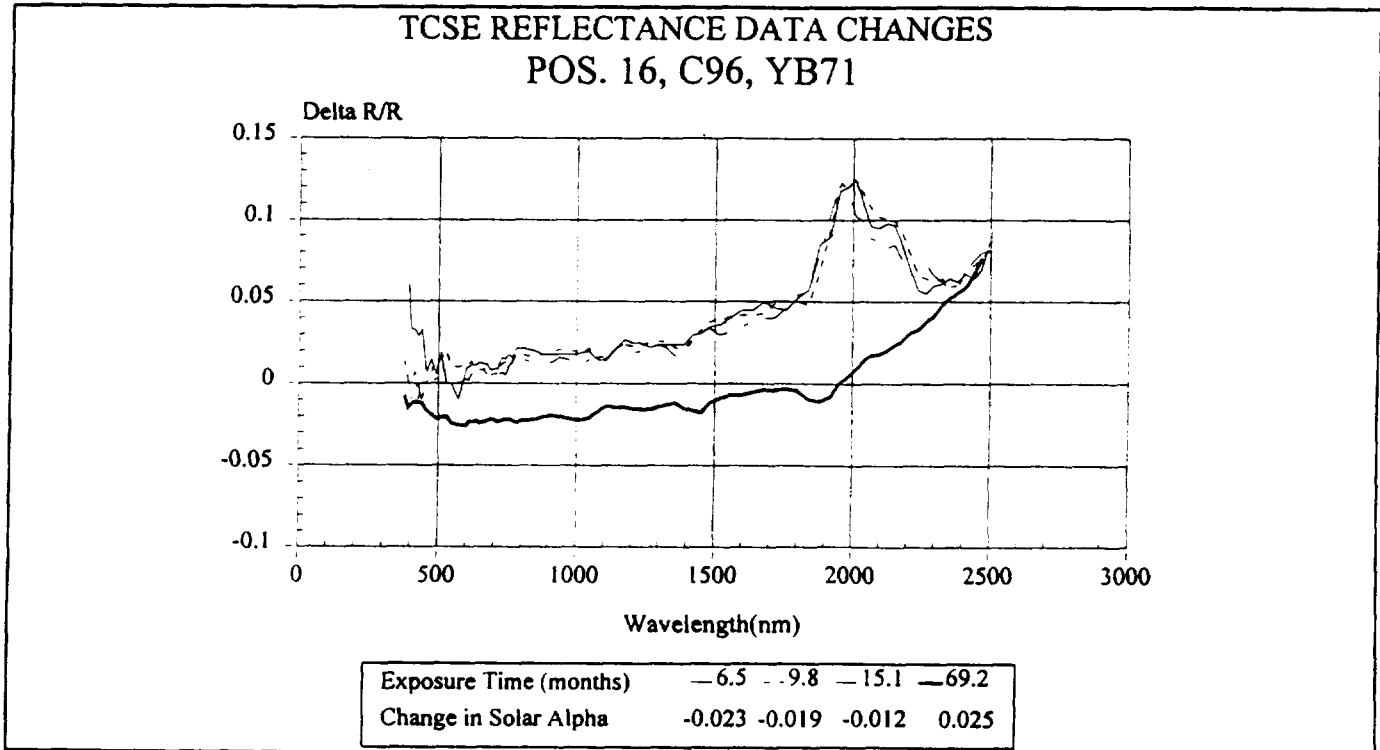


Figure 6. YB71 Reflectance Data Changes.

S13G/LO White Paint

Figure 7 shows the solar absorptance changes for S13G/LO over the LDEF mission. As with most of the TCSE active samples, there is an initial period in which the rate of change is different than the subsequent changes. This indicates a different dominant damage mechanism than later in the mission. The regression analysis provides a good fit if the initial data point is ignored. The degradation model for S13G/LO is shown in Figure 8. Significant changes in S13G/LO were expected but actual changes were somewhat larger than expected.

Figures 9 and 10 show the spectral reflectance changes for S13G/LO. The only significant changes occurred below 1000 nm which resulted in the large changes in integrated solar absorptance.

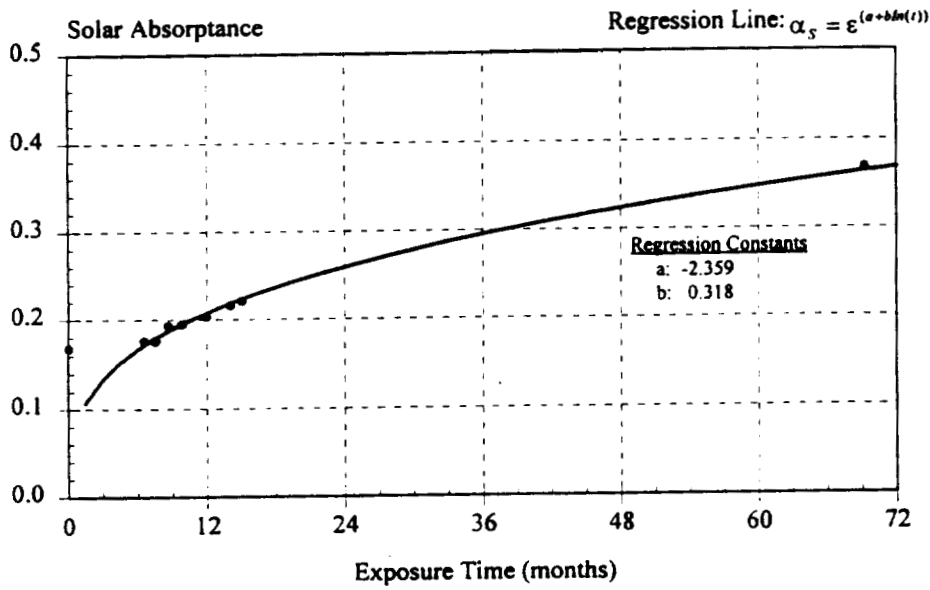


Figure 7. Power Regression Analysis of S13G/LO.

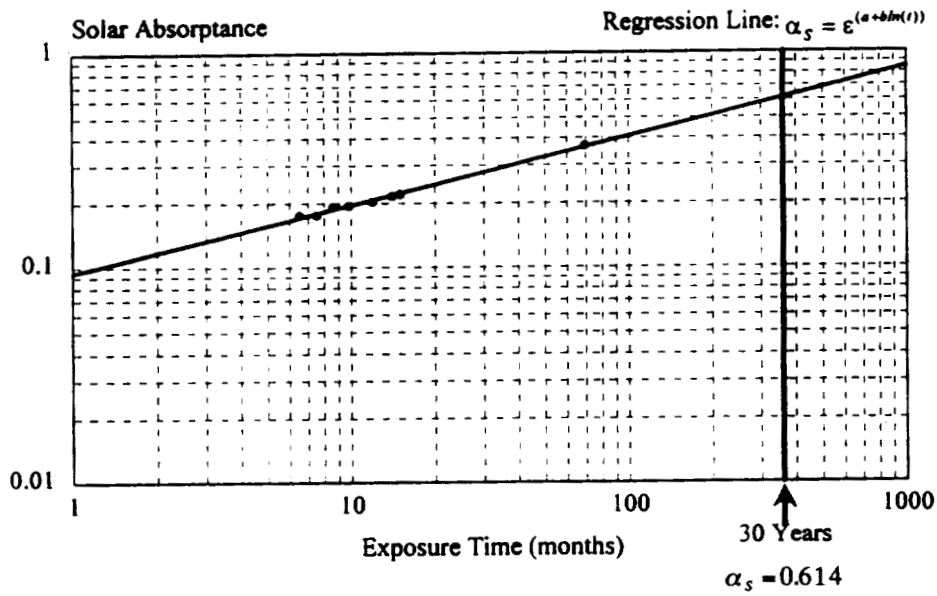


Figure 8. S13G/LO Degradation Model.

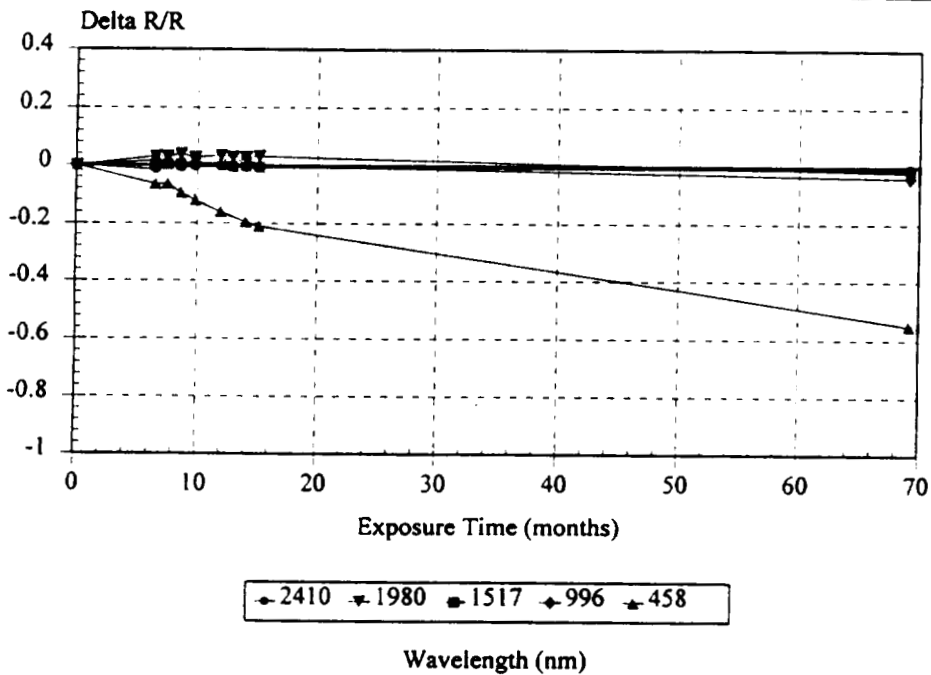


Figure 9. S13G/LO Reflectance Changes at Selected Wavelengths.

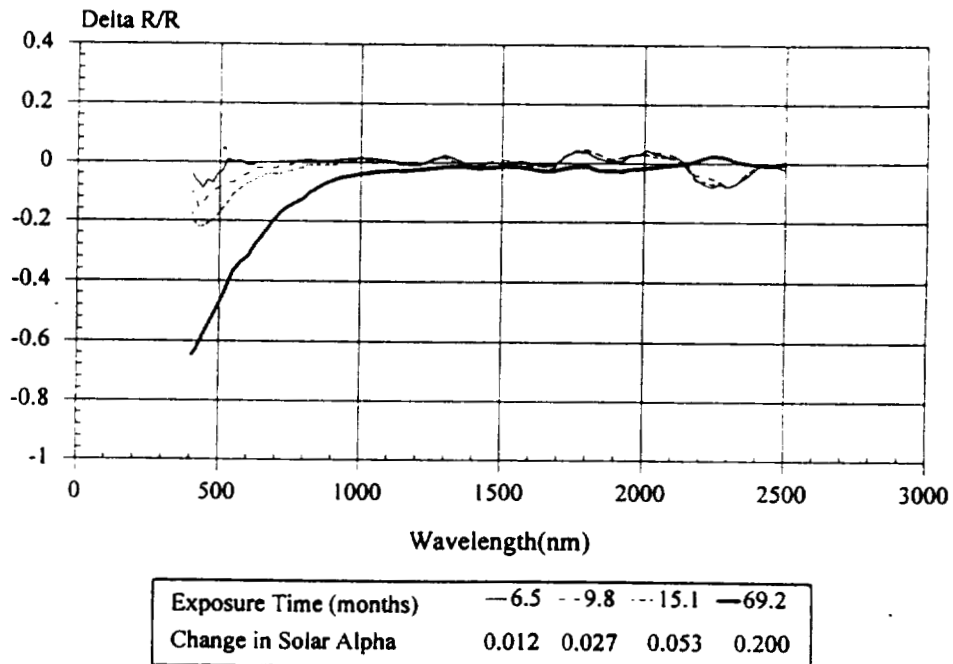


Figure 10. S13G/LO Reflectance Data Changes.

A276 White Paint and Protective Overcoats

Chemglaze A276 is a widely used white coating that was known to erode in atomic oxygen (AO) even before the LDEF mission. To evaluate their effectiveness, RTV670 and OI650 clear silicone protective overcoats were applied to A276. Figures 11-13 show the performance of the three coating systems during the LDEF exposure. Figure 13 shows that without a protective overcoating, A276 had relatively small changes for the first sixteen months. Exposure to the very large AO fluence during the subsequent four years eroded the damaged surface layer exposing a pigment dominated surface with even better reflectance than the pre-flight surface. The A276 with the protective overcoatings degraded significantly. Figure 14 compares post-flight reflectance changes for the three A276 surfaces and an LDEF trailing edge A276 sample from Dr. Palmer Peters and Dr. John Gregory's AO114 experiment. The AO114 trailing edge sample saw only a small amount of AO and was significantly damaged by solar UV exposure. Some of the damage to the TCSE overcoated samples may be in the overcoat itself. However, as shown in Figure 14, the damage spectra of the UV degraded AO114 A276 samples are very similar to the TCSE overcoated samples in both magnitude and spectral range.

Silver Teflon

Samples of both 5 mil and 2 mil thick silver Teflon were flown on the TCSE active sample array. The 5 mil material was optically very stable for the LDEF mission. AO exposure resulted in the loss of approximately 1 mil of Teflon and a textured diffuse surface. Figure 15 shows the variation of solar absorptance versus exposure time for 5 mil silver Teflon. As with several other materials, an improvement (decrease) in solar absorptance was measured early in the mission. This was followed by a small degradation for the remainder of the mission. Power regression analysis provides a fair fit to this long term degradation. Figure 16 extends this degradation model and predicts an excellent 30 year solar absorptance of 0.1.

Figure 17 shows the spectral reflectance changes over the mission duration. A slight increase in the 1700 to 2500 nm infrared range early in the mission is offset by the long term degradation below 1400 nm.

The 2 mil silver Teflon active sample was the same material that was applied to the TCSE front cover. This material suffered from an internal contamination and optical degradation that has been previously documented.⁵ The silver and inconnel backing layer was cracked during the application process allowing the acrylic adhesive to migrate into the layer between the silver and the Teflon. Solar UV then darkened the adhesive resulting in an overall optical degradation. Figure 18 shows the spectral reflectance changes of the 2 mil silver Teflon. The data up to 15 months is nearly identical to the 5 mil material. The degradation during the subsequent four years indicates that the internal contamination required several years to become significant.

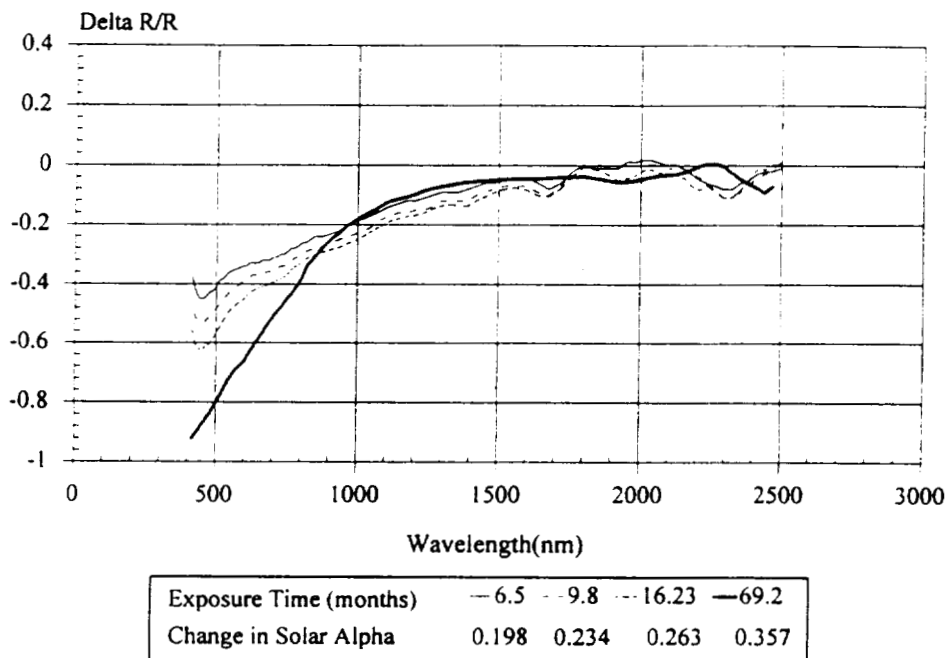


Figure 11. A276/RTV670 Reflectance Data Changes.

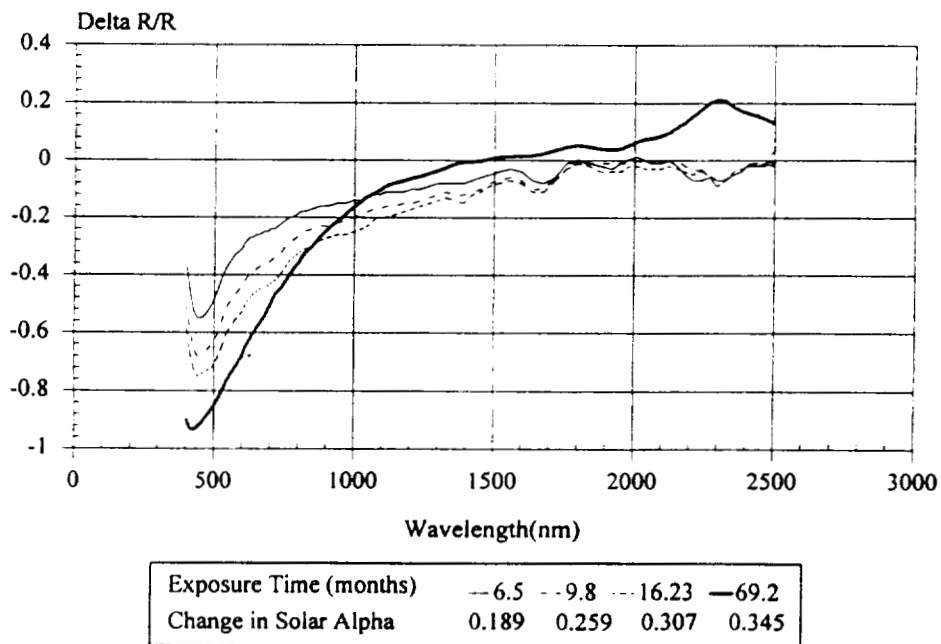
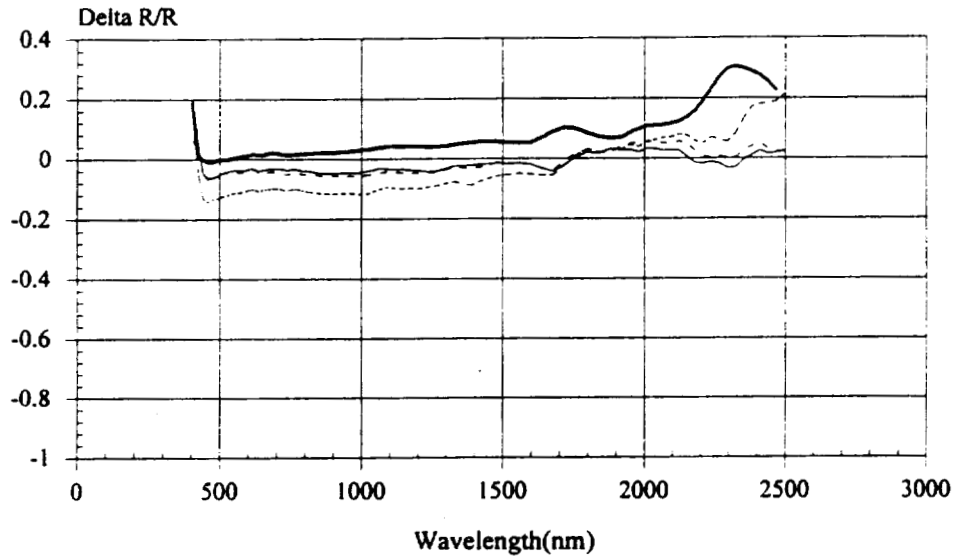
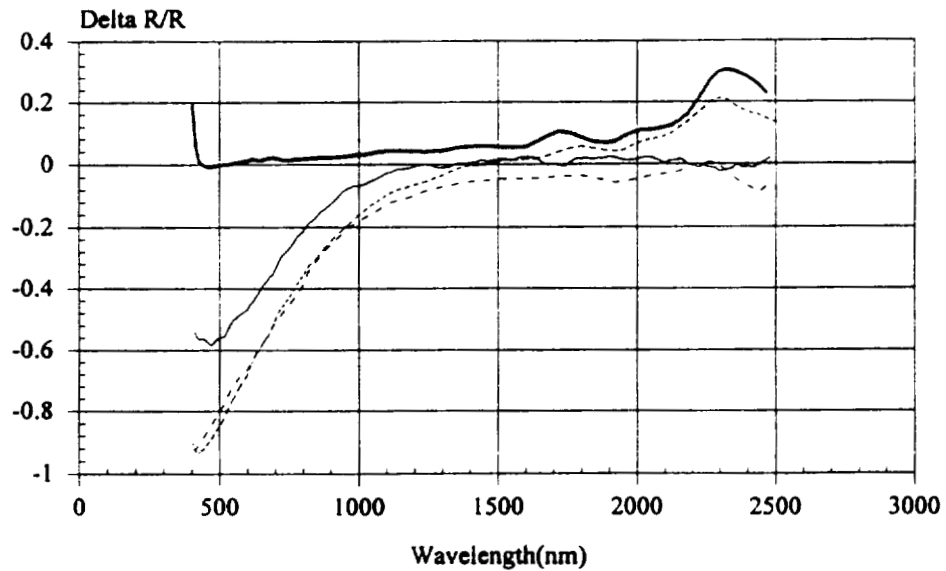


Figure 12. A276/OI650 Reflectance Data Changes.



Exposure Time (months)	6.5	9.8	16.23	69.2
Change in Solar Alpha	0.023	0.026	0.077	-0.017

Figure 13. A276 Reflectance Data Changes.



— AO114 Trailing	- TCSE A276/RTV670	--- TCSE A276/OI650	- - - TCSE A276
$\Delta\alpha_s$ 0.208	0.357	0.345	-0.017

Figure 14. TCSE and AO114 Post-Flight Measurements.

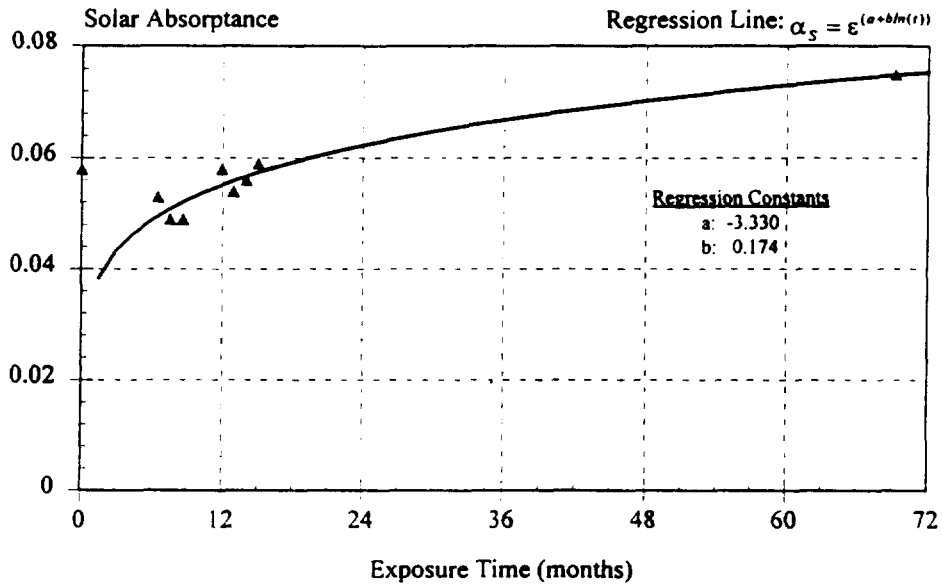


Figure 15. Degradation Rate Study of 5 mil Silver Teflon.

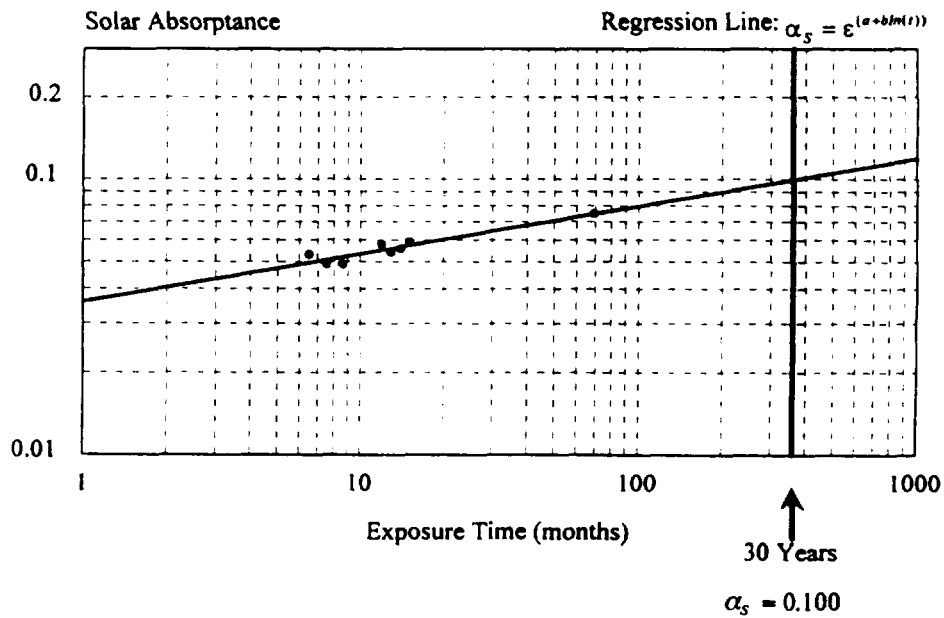
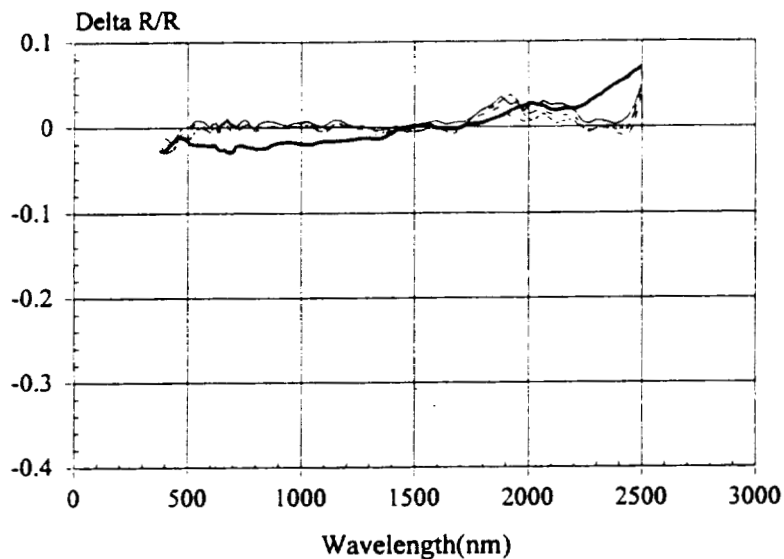


Figure 16. 5 mil Silver Teflon Degradation Model.



TCSE Reflectance Data Changes
POS. 12, C76, 5 mil Silver Teflon

LDEF
TCSE



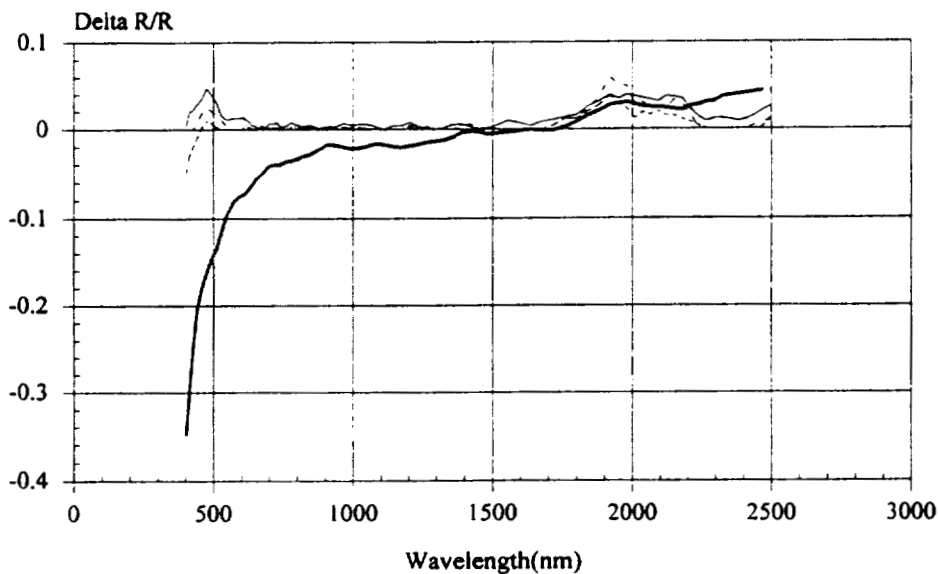
Exposure Time (months)	— 6.5	-- 11.9	--- 15.1	— 69.2
Change in Solar Alpha	-0.005	0.000	0.001	0.017

Figure 17. 5 mil Silver Teflon Reflectance Data Changes.



TCSE Reflectance Data Changes
POS. 13, C90, 2 mil Silver Teflon

LDEF
TCSE



Exposure Time (months)	— 6.5	-- 11.9	--- 15.1	— 69.2
Change in Solar Alpha	-0.011	0.000	0.006	0.086

Figure 18. 2 mil Silver Teflon Reflectance Data Changes.

CONCLUSION

The TCSE in-space spectral reflectance measurements and analysis of this data demonstrate the benefit of active type materials space experiments. This time dependent data provides insight into how thermal control surfaces behave in the space environment and enables the development of lifetime prediction models.

The results of this effort are based on one space mission and in most cases only one sample of a material. While the quality of the data is excellent, the lifetime prediction models should be used with caution. The extrapolated data is statistically a most likely value and not a worst case value.

The study of the trends in the TCSE spectral reflectance data provides a unique view of how materials degrade in the space environment. This data and the post-flight surface analysis demonstrate the very complex nature of the behavior of materials operating in this environment. Many issues remain in understanding the effects of the space environment on materials. Additional flight opportunities are needed for active optical experiments measuring these effects. To address this need, the In-Space Technical Experiments Program (IN-STEP) Optical Properties Monitor (OPM) is being developed for a 1997 mission. The OPM is an in-space optical laboratory for the in-situ study of materials.⁶

REFERENCES

1. Wilkes, D.R. and Hummer, L.L.; "Thermal Control Surfaces Experiment Initial Flight Data Analysis," Final Contract Report NAS8-38689, June 1991.
2. Private communication with H.G. Pippin and R.J. Bourassa of Boeing Defense and Space Group. This data was developed using their LDEF microenvironment model which is described in the following reference.
Bourassa, R.J., Pippin, H.G., Gillis, J.R.; "LDEF Microenvironments, Observed and Predicted," *Second LDEF Post-Retrieval Symposium*, NASA CP-3194, 1993, pp. 13-25.
3. Benton, E.V. and Heinrich, W.; "Ionizing Radiation Exposure of LDEF," University of San Francisco Report USF-TR-77, August 1990.
4. Wilkes, D.R., Miller, E.R., Zwiener, J.M., and Mell, R.J.; "The Continuing Materials Analysis of the Thermal Control Surfaces Experiment (S0069)," *Second LDEF Post-Retrieval Symposium*, NASA CP-3194, 1993, pp. 1061-1073.
5. Zwiener, J.M., Wilkes, D.R., Hummer, L.L., Miller, E.R.; "Unusual Materials Effects Observed on the Thermal Control Surfaces Experiment (S0069)," *First LDEF Post-Retrieval Symposium*, NASA CP-3134, 1991, pp. 919-933.
6. Wilkes, D.R.; "Next Generation Optical Instruments and Space Experiment Based on the Thermal Control Surfaces Experiment (S0069)," *Second LDEF Post-Retrieval Symposium*, NASA CP-3194, 1993, pp. 1521-1533.

WHISKER/CONE GROWTH ON THE
THERMAL CONTROL SURFACES EXPERIMENT #S0069

James M. Zwiener
James E. Coston Jr.
NASA Marshall Space Flight Center
Huntsville, AL 35812
Phone: 205/544-2528, Fax: 205/544-5103

515-27

44

201

Donald R. Wilkes
Edgar R. Miller
Richard J. Mell
AZ Technology
Huntsville, AL 35801
Phone: 205/880-7481, Fax: 205/880-7483

SUMMARY

An unusual surface "growth" was found during scanning electron microscope (SEM) investigations of the Thermal Control Surface Experiment (TCSE) S0069 front thermal cover. This "growth" is similar to the cone type whisker growth phenomena as studied by G. K. Wehner (Univ. of Minn.) beginning in the 1960's. Extensive analysis has identified the most probable composition of the whiskers to be a silicate type glass. Sources of the growth material are outgassing products from the experiment and orbital atomic oxygen, which occurs naturally at the orbital altitudes of the LDEF mission in the form of neutral atomic oxygen. The highly ordered symmetry and directionality of the whiskers are attributed to the long term (5.8 year) stable flight orientation of the LDEF.

INTRODUCTION

During scanning electron microscope (SEM) investigations of the front thermal control cover on the LDEF Thermal Control Surface Experiment (TCSE) S0069 an interesting "growth" was discovered on its exposed Teflon surface. The authors of the paper were utilizing a field emission scanning electron microscope to investigate the atomic oxygen (AO) damage to the silver Teflon coating as a function of AO incident angle. This "growth" has lead to a great deal of interest within the LDEF material investigator community and by various news media sources^{1,2,3,4}, of which some publications were of a rather dubious accuracy and intent^{5,6,7}.

EXPERIMENT DESCRIPTION

Objective

The overall objective of the TCSE on the LDEF was to determine the effects of the combined near-Earth orbital environment including the LDEF induced environment on space-

craft thermal control surfaces. In flight optical measurements were performed to evaluate optical changes in thermal control coatings as a function of time on orbit. This unique data also enabled the development of lifetime prediction models for these materials.

Mission Summary

On April 7, 1984 the LDEF was placed in a 463 km (250 N miles), 28.5 degree inclination low Earth orbit by the Space Shuttle *Challenger*. After 5 years 10 months in space, on January 12, 1990, the LDEF was retrieved by Space Shuttle *Columbia* at an altitude of 330 km (178 N miles).

Figure 1 is a schematic of the LDEF in orbit. The LDEF was a gravity-gradient stabilized and mass loaded so that one end of the spacecraft always pointed at the Earth and one side always pointed into the velocity vector or RAM direction. Spacecraft deployment was as planned with the TCSE located on the leading edge (row 9) of the LDEF and at the Earth end of this row (position A9). Actual LDEF orientation was slightly offset from this planned orientation. As shown in Figure 2, the LDEF was rotated about the long axis where row 9 was offset from the RAM direction by about 8 degrees^{8,9}. This LDEF/TCSE orientation resulted in total exposures of 8×10^{21} atoms/cm² atomic oxygen¹⁰, 1×10^4 ESH solar ultraviolet¹¹, 3.3×10^4 thermal cycles¹², and 3×10^5 rads of particulate radiation¹³.

Hardware Description

The TCSE was the first experiment to measure the optical properties of thermal control surfaces in space in the same way they are routinely measured in the laboratory¹⁴. The configuration of the experimental system consisted of a completely self-contained experiment package providing its own power, data system, reflectometer, and preprogrammed controller for automatically exposing, monitoring, and measuring the sample materials.

The primary in-space measurement was provided by a total hemispherical reflectometer recording total reflectance as a function of wavelength at 100 wavelength points from 250 to 2500 nm. The reflectometer design consisted of two light sources, tungsten and deuterium lamps, used with a scanning prism monochromator with selectable slit widths to provide the monochromatic energy for the spectral measurement. The 115 mm (4.5 inch) diameter integrating sphere collected both the specular and diffuse reflected monochromatic light from a wall mounted sample to provide the angularly integrated measurement capability. Kodak barium sulfate (BaSO₄) was used for the sphere coating. Reflected energy was measured with a UV enhanced silicon photodiode detector and a lead sulfide detector.

FRONT THERMAL CONTROL COVER

Summary of Previous Results

Optical Properties of Front Thermal Control Cover

The front thermal control cover has a Sheldahl 0.05 mm (0.002 inch) thick Ag/FEP thermal control material applied with 3M 966 acrylic adhesive to an aluminum substrate of 6061 alloy, 1.6 mm (0.063 inch) thick. The Ag/FEP is composed of an outer Teflon support

layer, a silver high reflective layer deposited on the backside of the Teflon, an inconel protective layer deposited on the silver, and 3M 966 acrylic pressure sensitive adhesive. The silver layer provides the high visible reflectance, while the Teflon layer provides a high far-infrared emittance value, providing an excellent surface for minimizing average surface temperatures during orbital sunlight/shadow cycles.

Covered areas that were protected from AO and solar ultraviolet radiation have no apparent damage and are still highly specular¹⁵. Areas exposed to the space environment are clearly delineated and have a diffuse, whitish appearance with brown discoloration. This brownish discoloration varies from light brown to dark brown. Changes in Ag/FEP visual appearance are the result of two damage mechanisms: AO erosion and internal damage associated with cracking of the silver/inconel layer during application¹⁵.

Exposed regions on the front cover without the brownish discoloration experienced only small increases from the original solar absorptance value from 0.08 to 0.10. The worse case brownish area had a solar absorptance as high as 0.49. Thermal emittance was unchanged in the covered areas whereas the exposed regions degraded from 0.68 to 0.48. Change in emittance resulted from loss of Teflon by AO erosion^{15,16}.

Atomic Oxygen Erosion Effects

AO erosion of the exposed Ag/FEP surface, sample S1 in Figure 3, is typical of that observed on other LDEF experiments^{17,18}. Erosion of the exposed Teflon surface creates a nonuniform etching pattern. This results in a roughened surface which scatters incident light in a manner similar to a sandblasted piece of glass, providing an overall diffuse whitish color. SEM photographs of the Teflon surface on either side of the whisker/cone growth region are also shown in Figure 3. The covered region of sample T51 appears to show contamination deposits or layers. Apparent AO erosion on sample T51 in the exposed region near the growth shows a radical variation in the normal Teflon erosion surface morphology. All three images are at approximately the same magnification, yet erosion near the growth area is composed of roughly parallel ridges. These ridges are parallel to the local overlapping covers. Close inspection of the sample T51 image for the exposed region near the growth reveals what appears to be growth on the top of the central ridges, as would be expected if the ridges provide the nucleation site for growth initiation. Crystal or dendritic growth always initiates (all other parameters being equal) at surface defect sites or on sharp pointed protrusions.

Brownish Streaking Effect

Optical microscope investigations of the silver Teflon covered area showed that the silver/inconel layer is cracked¹⁵. When the Ag/FEP material is stressed, the silver/inconel layer cracks. Uniform parallel cracks are formed during normal application. A shattering type crack pattern is formed when the Ag/FEP is bent around protrusions or when air bubbles are squeezed out.

An overall surface contamination was not found on the brownish discolored areas; only very localized surface contamination occurred along overlapping panels and vents. The brownish discoloration observed is actually a result of the silver/inconel cracks. The closer grouped cracks give the appearance of a long dark smeared brownish streak when viewed without magnification. The overall brownish streaking on the front cover is the result of a series of events, starting with the initial cracking of the silver/inconel layer during application to the TCSE front thermal control cover. Subsequent long-term exposure to thermal cycling and solar ultraviolet caused the brownish discoloration of the acrylic adhesive, exposed by the silver/inconel cracks to the solar UV transmitting through the Teflon. The intensity of the

brownish discoloration is a direct function of the crack density which was caused by what we now know to be inappropriate application and handling techniques.

Location of Growth

Figures 4 and 5 show the location on the front thermal control cover where the whisker/cone growth was found. The arrow in Figure 4 points at a gap between two of the front thermal control covers. Within this gap a dark contamination deposit is apparent on the Teflon surface in Figure 5 on which the growth was located. This dark deposit, in contrast to the brownish streaks, was found to be a surface contamination deposit.

All regions on the front cover having overlaps had a very narrow contamination deposit within their gaps. This deposit was ~3 mm in width by ~50 mm in length. Other growth areas may exist on the front panel, but this is the only one found. In fact, a front cover sample section immediately below the growth region was provided to Dr. Stuckey/The Aerospace Corp. for analysis but no growth was found on the contamination deposit on this sample.

WHISKER/CONE GROWTH CHARACTERISTICS

The growth region is oriented parallel to the front thermal panel gap shown in Figure 4. SEM images in Figure 6 show that the growth is well ordered, oriented, directional, localized and varies in whisker concentration across the growth region. The growth surface shows no indication of surface facets. There are several stages of growth apparent in the SEM pictures. The base of the growth is a thin brittle dark layer on the Teflon which can be easily removed. In places the base layer has separated from the Teflon substrate. Individual whisker/cones are translucent when viewed with a visible wavelength optical microscope.

There are two major growth orientations: one is normal to the surface aligned with the LDEF major axis; the other is parallel to the surface facing inward on one side and outward on the other side. The overall growth pattern appears to have some of the characteristics of a dendritic type growth with nucleation occurring along defect sites. The growth dimensions are on the order of 7 microns height and a fraction of a micron in diameter. A few growth units are larger, many are smaller. Individual growth units have a hollow tube down their center and have an inverted cone morphology. The growth surface does not appear eroded by the space environment, including atomic oxygen exposure.

ANALYSIS

Biological Viability Testing Results

Analysis performed to date has indicated that the growth is not a standard fungus or mold type growth or contamination that could have occurred on the ground after flight.

Biological testing results were negative in that the unknown growth material did not respond to culturing on a nutrient agar. In addition, the acridine orange direct count epi fluorescence tests, which stain DNA to determine if the growth material is biological, were also negative. These tests were repeated for two different samples, one of which had not been exposed to the SEM vacuum and electron beam irradiation. Results were negative in both cases.

Electron Microprobe Elemental Analysis

Elemental analysis was performed on three areas of sample T-51. The "interior area" was shielded from the exterior LDEF environment. The "growth area" was located in a gap between the front panel covers (Figure 4) which formed a vent path from the experiment interior and was partly shielded from atomic oxygen and solar ultraviolet. The so called "no growth" area was exposed to the full space environment during the LDEF mission. Results of these analyses are shown in Figures 7, 8, and 9.

EDAX data for the interior location defined as the "unexposed/covered no growth region" on Figure 7a shows the presence of carbon (C), oxygen (O), fluorine (F), and silicon (Si). Although sulfur (S) is identified on the scan, it is very weak and may be questionable.

In comparison, the EDAX data for the "no growth" exposed region on Figure 7b shows strong peaks for fluorine (F), and very weak peaks for silicon (Si) and no sulfur (S). A small hint of carbon (C) can be seen on scan, although it is not labeled. The small silicon peak may be from residual growth or contamination not obvious during the initial viewing of the SEM images. This data is consistent with a Teflon surface eroded by atomic oxygen.

EDAX data for the growth region was based on focusing the SEM beam on a grouping of the inverted cone whiskers. EDAX scans for this region are shown in Figure 8a and b from two different instruments. A very strong silicon (Si) peak is detected, along with sulfur (S), oxygen (O), fluorine (F), and magnesium (Mg), when using the Hitachi S-4000. Notice that the fluorine (F) is greatly reduced from the "no growth" regions, and is probably background from the Teflon substrate. Also, notice that the carbon peak virtually disappears on exposed as compared to the unexposed regions. This same sample was run in the Cambridge 250 Mark II, having a higher energy analysis capability in order to confirm the magnesium and sulfur peaks. Surprisingly the magnesium peak turned out to be arsenic (As). Both peaks for arsenic are present as shown in Figure 8b. Therefore, the peak in Figure 8a identified as Mg is most likely As.

In order to determine if the fluorine peak in Figure 8a was from the growth or was background scatter from the Teflon substrate, another series of EDAX scans were made, carefully focusing on the thickest growth area. Results of these scans are shown in Figure 9a. The fluorine (F) peak is now totally eliminated, proving that fluorine is not a typical component of the growth and the previous fluorine peak was from background scatter. Silicon (Si) is still the main peak and assumed to be the main component. Sulfur (S) shows as a clean peak, indicating its presence. Oxygen (O) still shows but is weak. Interestingly, carbon (C) now shows up, but is also very weak. The arsenic (As) peak also is present, but is very weak.

Another set of scans were taken of the underside of the base material layer on which the growth is located. This layer is the darker material located at the base of the inverted cones as can be seen in Figure 6. On sample T51, some of the growth was disturbed while taking samples for the biological tests, thereby exposing the underside of some of the base material. Figure 9b is the result of a series of EDAX scans of this material. Most of the previously identified elements remain at the same ratio, except that the sulfur (S) peak is greatly reduced and the fluorine (F) peak now returns. This data indicates that some fluorine (F) is incorporated in the base material but is not incorporated in the whisker/cones. Also, it appears that sulfur was principally incorporated into the whisker/cone growth during the growth process and not from the base material.

FTIR; Total Attenuated Microprobe Analysis

Infrared analysis of this phenomenon has been very complicated because of the complex chemistry across the sample surface and the very small size of the dendritic growth. The problem of size has been alleviated through the use of an infrared microprobe system, but the complex chemistry across the sample still remains. For the purposes of this analysis, the scope will be limited to the Teflon substrate and the whisker/cone growth material.

Molecular microanalysis utilizing a scanning infrared microprobe microscope was performed by Nicolet Instrument Corporation in Stamford, Connecticut. Figure 10 shows the infrared spectra for Teflon flight control, Teflon flight sample exposed with no growth, and the whisker/cone growth (labeled dendritic growth). Teflon's characteristic absorption bands can be seen for both flight and control samples. The infrared spectra for the whisker/cone growth show almost no structure. The large absorption band at 1057 cm^{-1} indicates a strong presence of Si-O-Si. The small absorption bands at 3601 , 3628 , 3705 , and 3732 cm^{-1} indicate a weak presence of Si-OH. This data indicates that the whisker/cone growth is primarily a SiO_x glass type material.

In addition to the infrared spectra, contact with the probe crystal during surface probing indicates that the whisker/cones are hard and brittle in comparison to the surrounding fluorocarbon polymer. Again, this is consistent with a glassy or silicate type material.

CONTAMINATION SOURCES

Sulfur

During post flight investigation, when the S0069 cover was removed, very odiferous fumes were detected. Gas samples were taken using organic (activate charcoal) vapor monitors located inside the S0069 TCSE instrument with the shipping cover in place. Three monitors were located inside the instrument and one control was placed outside. Analysis identified the gas as dimethyldisulfide. Batteries were then removed and double bagged. Gas samples were taken from the bag using a vacuum bottle technique and analyzed at MSFC. As before, the gas was identified as dimethyldisulfide.

Figure 11 is a mosaic of photographs showing the returned flight batteries in the S0069 experiment tray (four batteries were used; one is hidden under the carousel). One of the batteries is shown with and without its lid in place. Individual cells are potted in the battery case, as can be seen in Figure 11. For these batteries it was found through investigations at MSFC* that after approximately three years (even in cold storage) the individual nickel cell safety pressure release would rupture. Figure 11 shows an individual cell with the pressure release ruptured. Dimethyldisulfide gas is vented by these cells when they rupture. In conjunction with the cell rupture, the battery case seal leaked when the o-rings (ethylene propylene) failed from compression set. Figure 11 clearly shows the magnitude of the compression set. A cross section of the flight o-ring compared to an unused o-ring shows that the flight o-ring has taken the shape of its groove indicating 100% compression set. The dimethyldisulfide gas vented from the batteries is the most likely source of the sulfur detected in the growth.

*Private communication with M. Martin/EB11 and M. Mendrek/EH24 MSFC.

Silicon/Silicone/Silicate

Silicone contamination has been identified at several locations on the LDEF^{19,20,21}. Although no principle source of silicone has been identified internal to the S0069 instrument, it does appear from the data that a silicone source existed. Silicone under exposure to atomic oxygen converts to a silicate²².

The possibility that the silicone source was external to the S0069 experiment has to be considered. Sources have been identified both internal to the LDEF and from the Shuttle²³. The S0069 experiment did not have a direct line-of-sight to these sources and at orbital pressures the mean free path for molecular collisions is several kilometers, which would make it unlikely that the localized thick (several microns) silicone deposits found could have formed from returned flux. In addition there appears to have been a flow of contamination from the interior of the S0069 experiment to the exterior. If the internal contamination deposits were from external sources, then the molecules would have to enter through vents and gaps in the front thermal panels normal to the RAM direction.

Rantanen²⁴ has performed calculations using the Integrated Spacecraft Environments Model (ISEM) which indicates potentially significant backscatter of outgassing contamination from the LDEF, back onto its RAM facing side. Further analysis is required to resolve this issue, but it may be that the silicone contamination layers originated from sources both internal and external to the S0069 experiment.

Oxygen/Carbon/Fluorine/Arsenic

The principal source of oxygen is presumed to be from orbital atomic oxygen. Fluorine identified in the growth base material could originate from the Teflon eroded by atomic oxygen. Carbon is reasonably plentiful, located both in the Teflon and from practically all non-metallic materials used in the TCSE instrument. Thermal vacuum bakeout of the S0069 instrument prior to flight should have reduced hydrocarbon sources to very low levels, consistent with ASTM E595²⁵. The potential source of Arsenic has not been identified.

DISCUSSION

Dr. R. Warner*, Univ. of Minn., suggested that the growth may be similar to that reported by his colleague, Dr. G. K. Wehner. In Wehner's 1985 survey paper²⁶ he discusses the conditions for cone formation during whisker growth by ion bombardment of metal surfaces. One of the earliest reported observations of cone formations is by Guenterschulze and Tollmien²⁷ in their 1942 paper where they reported formation of cone forests on cathodes.

There are several growth characteristics reported by Wehner that are necessary for whisker and cone formations to occur. Most of the experiments reported were performed in a low energy ion sputtering high vacuum environment. Ion energies less than 500ev were capa-

*Private communication with Dr. R. Warner, in October 1992.

ble of achieving whisker growth with dissimilar metals. When the ion energies neared the sputtering threshold, whisker growth was observed. Whisker growth occurs when dissimilar metals are physically close (seed and substrate). Redeposition of sputtered materials results in unique formations of long thin and short thick cones. Inverted cones can also be formed. Whisker/cone orientation is not related to ion impact direction at low ion energies.

For the LDEF growth, the sputtering source was the orbital atomic oxygen (AO), which, being neutral, is capable of "sputtering" or erosion of materials at much less energy than the sputtering threshold, although the rates are very slow^{28,29}. Atomic oxygen impacts the RAM face of the LDEF (Figure 2) at ~8 Km/sec or with a kinetic energy of ~5 ev. Wehner found that for metals, whisker growth occurred at low energies only when surface temperatures were elevated. Surface temperatures on the front cover were measured to be below ambient during the first 18 months and thermal model predictions indicated low temperatures throughout the mission.

The major difference between these ground experiments and the flight growth is that metals were used in the studies reported by Wehner, while the growth found on the TCSE experiment is non-metallic and initially polymeric which tends to undergo conversion at low temperatures. As a consequence, cones reported by Wehner were mostly faceted as one would expect, while the TCSE cones were not faceted. Interestingly, both hollow and inverted cone formations were reported, but no inverted hollow cones were reported by Wehner.

Taking into account all the growth conditions between flight and ground experiments makes the growth mechanism less likely to be the true "ion sputtering" related phenomena as reported by Wehner, but a very similar low energy neutral atomic oxygen related erosion phenomena.

CONCLUSIONS

Proposed Growth Scenario

After LDEF orbital insertion, exposure to atomic oxygen initiates surface erosion of the Teflon surface on the front thermal control cover. Since the LDEF was inserted in a high orbit and the solar cycle was in a low period, the AO flux was also low. Therefore the erosion rate was low. At the vent/gap interface where growth occurred, the Teflon surface erosion was in the form of roughly parallel ridges versus the normal peak and valley hill type surface texture found in the exposed areas. In time, outgassing molecules of silicone and other contaminants reached this narrow gap between the front thermal covers, which provided a vent, resulting in deposition of thin layers of contamination. Solar ultraviolet photons incident on the Teflon interacted with the thin silicone contamination layer to form longer chain, lower vapor pressure, silicone materials. This photodeposition process continued, resulting in a thick, brown varnish type layer. Away from the gap, the silicone contamination flux was dispersed to such low levels that the AO erosion of Teflon dominated and no silicone buildup could be sustained.

As the atomic oxygen level increased, resulting from the LDEF orbital decay and solar cycle heading towards a high period, the silicone was transformed to a silicate^{20,22}. At about 3 years into the mission the battery cells ruptured, venting a continuous source of dimethylsulfide gas. At this period in time, all growth elements existed. Figure 12 is a schematic of the growth environmental conditions and associated hardware orientation.

Initially, hollow whiskers are formed which slowly form inverted cones as growth

progresses. Growth is driven by redeposition of silicate contamination by atomic oxygen erosion or "sputtering". Simultaneously, dimethyldisulfide outgassing molecules react with AO freeing sulfur, possibly in the form of a sulfate (SO_3), which is then incorporated into the whisker/cone growth. Sulfate has a solubility in silica of $<0.6\%$ ³⁰; therefore, the sulfur concentration should be low, as was found from the EDAX data.

The proposed scenario fits the existing data and knowledge of events. As other observations of similar growth are reported and analyzed³¹ a better understanding of the growth process can be developed. With a better understanding of this intriguing whisker/cone growth phenomena, intentional growth can be performed, thereby providing a means to process material on a microscale with unique surface morphologies and physical characteristics.

ACKNOWLEDGEMENTS

The authors would like to recognize the interest and support of the following individuals: scanning electron microscope and EDAX analysis by James Coston/MSFC; biological tests by Dr. E. Rodgers/MSFC and Dr. D. Obenhuber, Sverdrup Inc.; and battery offgassing sampling and analysis by R. Crowder, SEA Inc. and J. Perkins/EH32 MSFC. Technical assistance was provided by Dr. John Reffner of Nicolet Instrument Corp., and Dr. Pamela Martoglio of Spectratech Applied Systems for the total attenuated microprobe FTIR analysis.

REFERENCES

1. Zwiener, J. M.; "Unusual "Growth" Found on LDEF Surface", LDEF Newsletter, vol III, no. 4, August 15, 1992, pp. 4-7.
2. Burkey, M.; "LDEF reveals 'unusual growth'," The Huntsville Times, Monday, October 19, 1992.
3. Burkey, M.; "Space Growth," Final Frontier, February 1993, p. 6
4. Baker, S.; "Mystery Stuff form Outer Space," OMNI, December 1993, p. 87.
5. Strauss, S., "It's not of this Earth", Mystery growth formed in space baffles NASA scientists," Houston Chronicle, Wednesday, Sept, 9, 1992, p. 9A.
6. "Stowaway from Space; Mysterious growth rides in on shuttle - terrifies experts," National Examiner, January 12, 1993
7. Rothstein, A.; presented highly edited NASA video on Sightings, FOX TV #54, May 12, 1993
8. Banks, B. A.; "LDEF Yaw Estimated at Eight Degrees", LDEF Spacecraft Environmental Effects Newsletter, Vol II, Number 1, March 15, 1991.
9. Gregory, J. C. and Peters P. N. "Measurement of the Passive Attitude Control Performance of a Recovered Spacecraft", J. of Guidance, Control, and Dynamics, vol. 15, no. 1, Jan.-Feb. 1992, pp. 282-284.
10. Bourassa, R. J. and Gillis, J. R. "Atomic Oxygen Flux and Fluence Calculation for Long Duration Exposure Facility (LDEF) LDEF Supporting Data", NASA Contractor Report 189554, Contract NAS1-18224, January 1991.
11. Bourassa, R. J. and Gillis, J. R. "Solar Exposure of LDEF Experiment Trays", NASA Contractor Report 189554, Contract NAS1-18224, February 1992.
12. Berrios, W. M.; "Long Duration Exposure Facility Post-Flight Thermal Analysis, Orbital/Thermal Environment Data Package," NASA LaRC, Hampton VA, October 3, 1990.
13. Benton, E. V. and Heinrich, W., "Ionizing Radiation Exposure of LDEF", University of San Francisco Report USF-TR-77, August 1990.
14. Wilkes, D.R., Hummer, L.L., and Zwiener, J.M.; "Thermal Control Surfaces Experi-

- ment Flight System Performance," LDEF-69 Months in Space First Post-Retrieval Symposium, NASA Conference Publication 3134, Part III, June 1991, pp. 1577-1585.
15. Zwiener, J.M., Wilkes, D.R., Hummer, L.L., and Miller, E.R.; "Unusual Materials Effects Observed on the Thermal Control Surfaces Experiment (S0069)," LDEF-69 Months in Space First Post-Retrieval Symposium, NASA Conference Publication 3134, Part II, June 1991, pp. 919-933.
 16. Wilkes, D.R., Brown, J.M., Hummer, L.L., and Zwiener, J.M.; "Initial Materials Evaluation of the Thermal Control Surfaces Experiment S0069," LDEF-69 Months in Space First Post-Retrieval Symposium, NASA Conference Publication 3134, Part III, June 1991, pp. 899-917.
 17. Hemminger, C. S.; "Space Environmental Effects on Silvered Teflon Thermal Control Surfaces," LDEF-69 Months in Space First Post-Retrieval Symposium, NASA Conference Publication 3134, Part II, June 1991, pp. 831-845.
 18. Rousslang, K., et. al.; "Results fo Examination of Silvered Teflon from the Long Duration Exposure Facility," LDEF-69 Months in Space First Post-Retrieval Symposium, NASA Conference Publication 3134, Part II, June 1991, pp. 845-859.
 19. Hemminger, C. S.; "Surface Contamination on LDEF Exposed Materials," LDEF Materials Workshop, NASA Conference Publication 3162, Part 1, November 19-22, 1991, pp. 159-174.
 20. Harvey, G.A.; "Silazane to Silica" LDEF-69 Months in Space, Second Post-Retrieval Symposium, NASA Conference Publication 3194, Part III, June 1992, pp. 797-810.
 21. Pippin, G. and Crutcher, R.; "Contamination on LDEF: Sources, Distribution, and History" LDEF 69 Months in Space, Second Post-Retrieval Symposium, NASA Conference Publication 3194, Part III, June 1992, pp. 1023-1032.
 22. Banks, B. A., Gebauer, L., and Hill, C. M.; "Atomic Oxygen Interactions with FEP Teflon and Silicones on LDEF," LDEF-69 Months in Space First Post-Retrieval Symposium, NASA Conference Publication 3134, Part II, June 1991, pp. 801-806.
 23. Harvey, G.; "Sources and Transport of Silicone NVR," LDEF Materials Workshop, NASA Conference Publication 3162, Part 1, November 19-22, 1991, pp. 174-184.
 24. Rantanen, R. & Carruth, M.R.; "Modeling of LDEF Contamination Environment," LDEF Materials Results for Spacecraft Applications Conference, NASA Conference Proceedings (scheduled for publication by mid 1994).
 25. American Society for Testing and Materials Standard Test Method, "Total Mass Loss (TML) and Collected Volatile Condensable Materials (CVCM) from Outgassing in a Vacuum Environment," ASTM E 595-77.
 26. Wehner, G. K.; "Cone formation as a result of whisker growth on ion bombarded metal surfaces," J. Vac. Sci. Technol. A 3(4), Jul/Aug 1987, p. 1821 thru 1835.
 27. Guentersschulze, A. and Tollmien, W. V.; Z. Phys, vol. 119, 1942, p. 685.
 28. Hansen, R.H. et. al., "Effects of Atomic Oxygen on Polymers," Journal of Polymer Sciences: part A, vol. 3, 1965, pp. 2205-2211.
 29. Whitaker, A. F., et. al.; "Atomic Oxygen Effects on LDEF Experiment A0171," LDEF-69 Months in Space, Second Post-Retrieval Symposium, NASA Conference Publication 3194, Part III, June 1992, pp. 1125-1135.
 30. Holland, L., "The Properties of Glass Surfaces," Chapman and Hall, Ltd., London 1964, pp. 207-208.
 31. Edelman, J. "LDEF is not Unique Surface Growths on Other Missions", LDEF Newsletter volume IV, no. 1, March 30, 1993, (information provided by Dr. R. L. Kruse, Monsanto, Springfield, Mass. and Dr. D. Schwam, Case Western Reserve University, for the LDCE 1,2, & 3 flown on STS-46, July 1992).

LDEF Orbital Flight Orientation

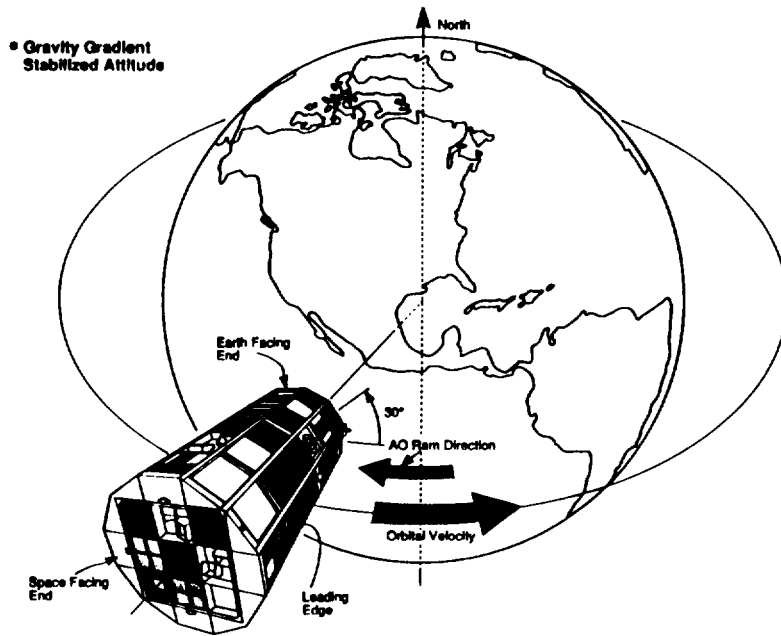


Figure 1. Schematic of the LDEF in Earth Orbit.

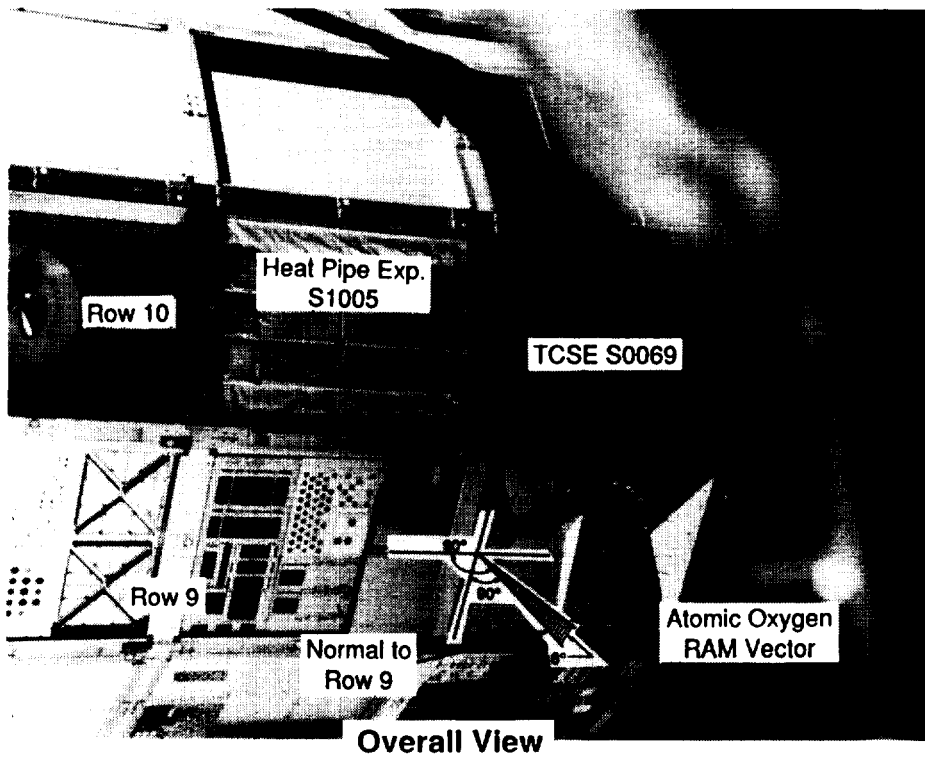
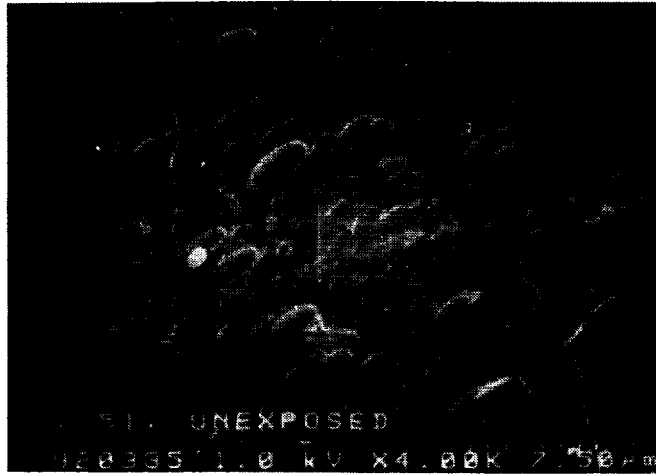
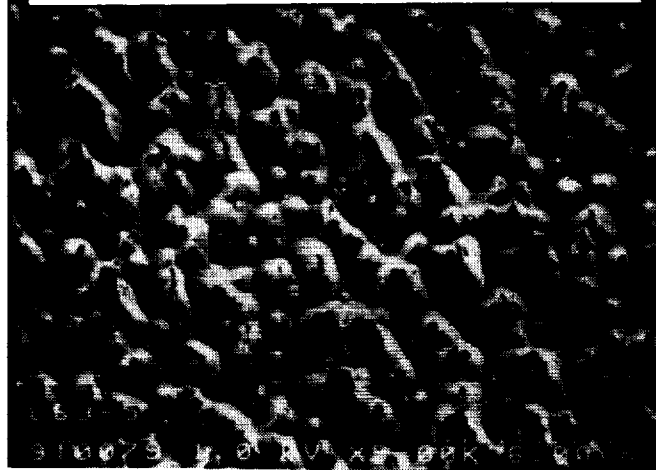


Figure 2. S0069 TCSE Experiment on LDEF During Retrieval

SAMPLE T51: COVERED REGION NEAR GROWTH



SAMPLE S1: TYPICAL AO SURFACE DAMAGE



SAMPLE T51: EXPOSED REGION NEAR GROWTH

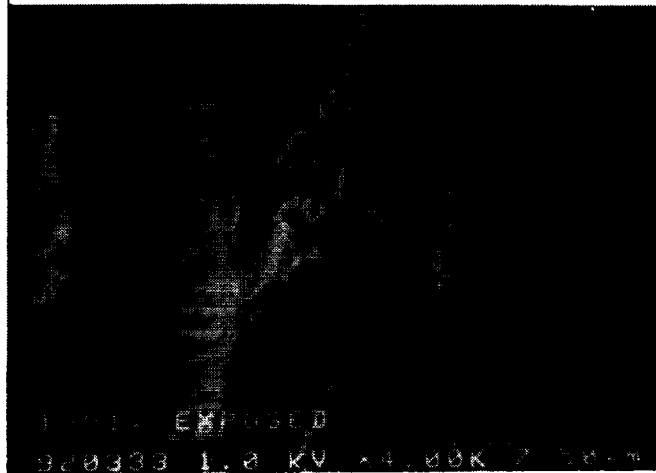


Figure 3. SEM Images of Teflon Surfaces on S0069 for covered and exposed locations.

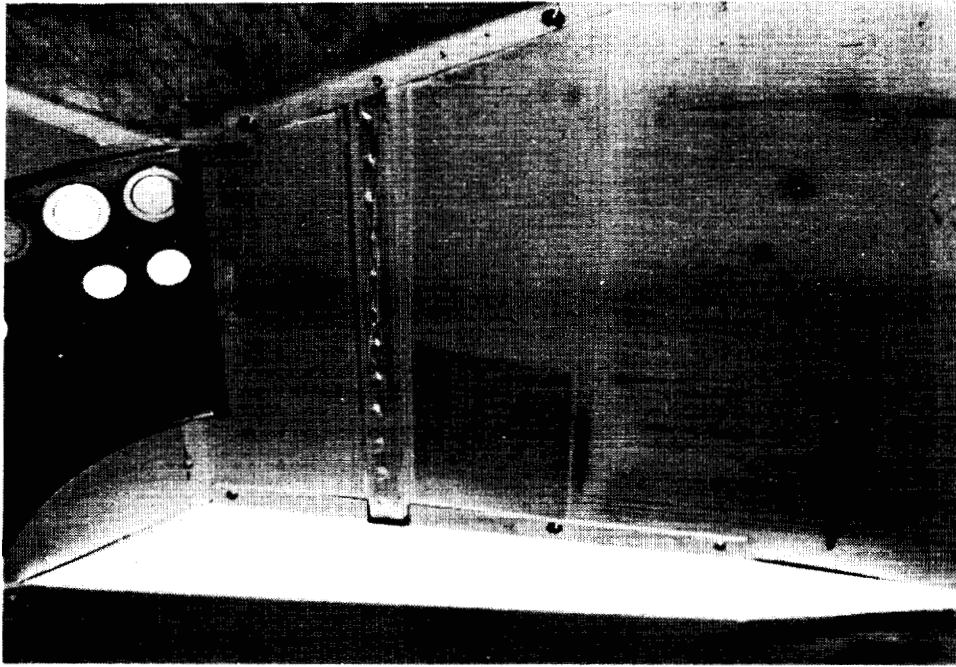


Figure 4. Front Surface of S0069 TCSE Instrument in the Laboratory after Retrieval Showing the Brown Streaks and the Gap (vent) between the Front Covers.



Figure 5. Front Thermal Control Cover Removed from the S0069 Instrument Showing Covered Regions, Exposed Regions, and location of Whisker/Cone "Growth".

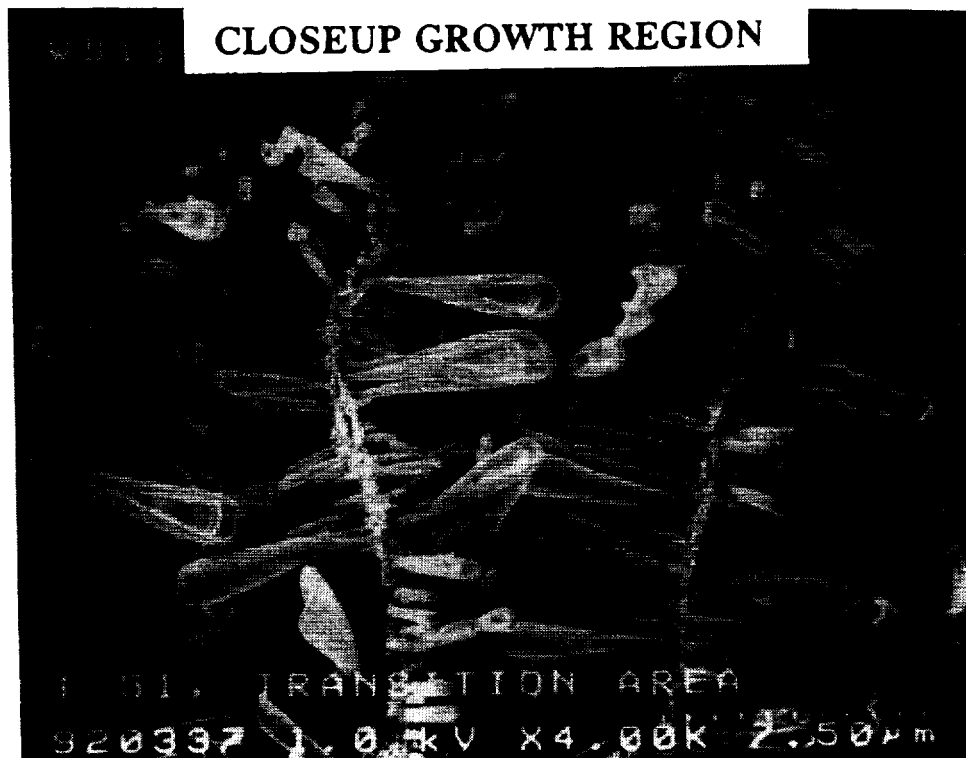
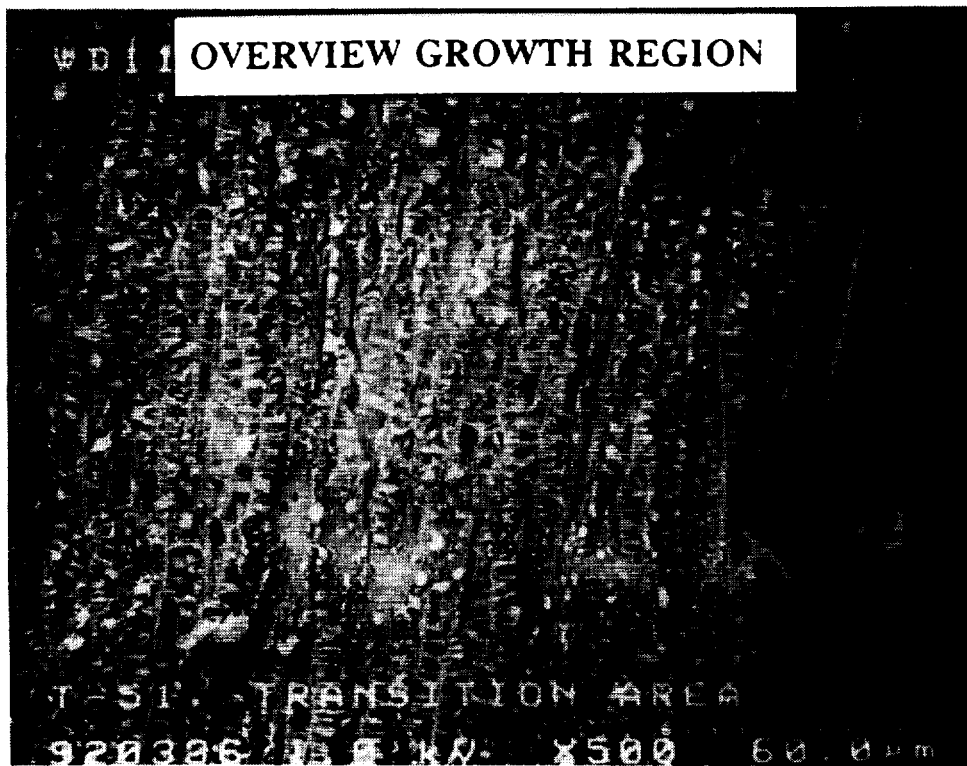


Figure 6. SEM Images of the Whisker/Cone Growth.

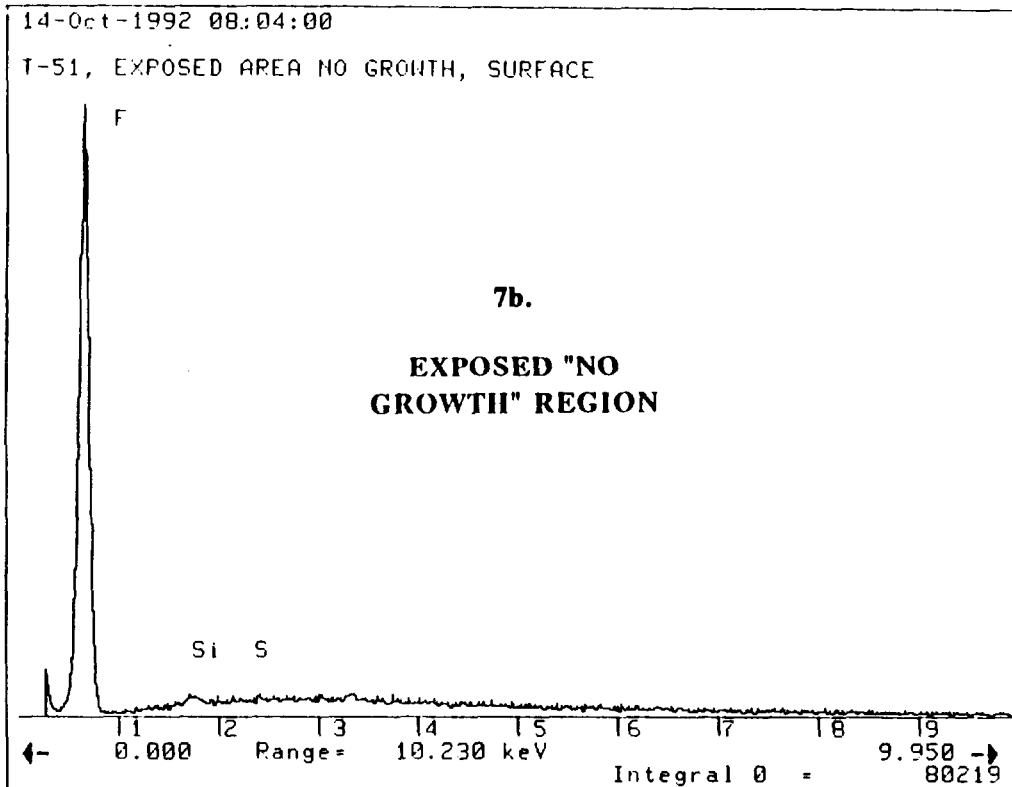
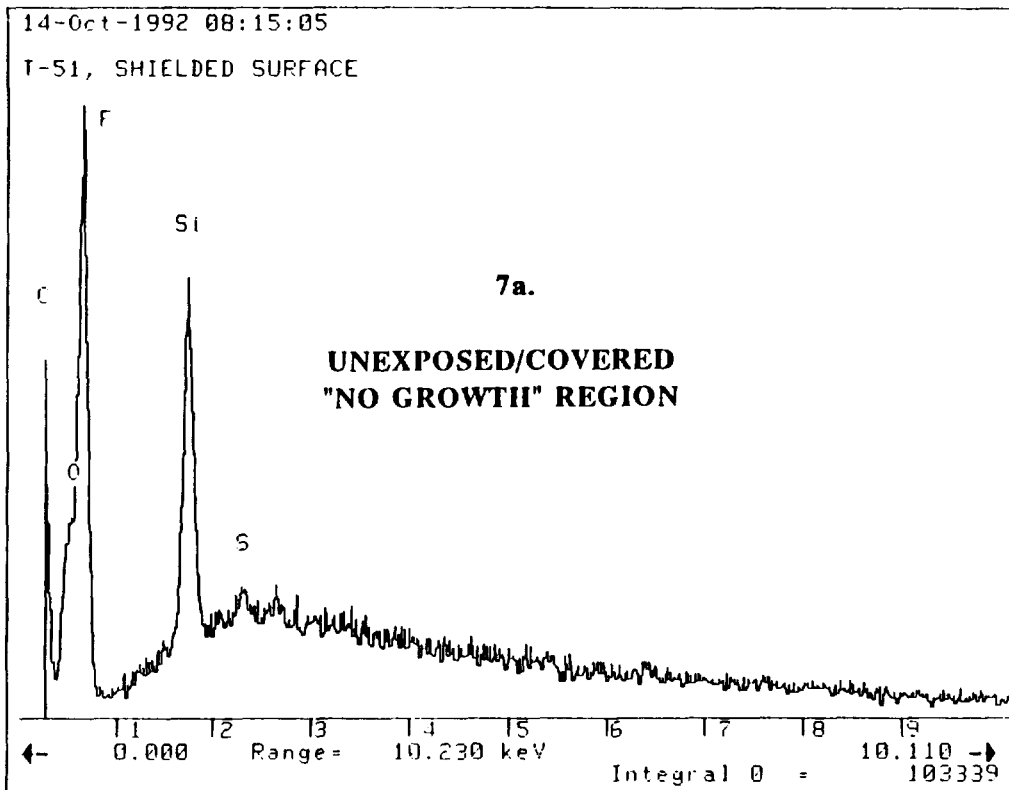
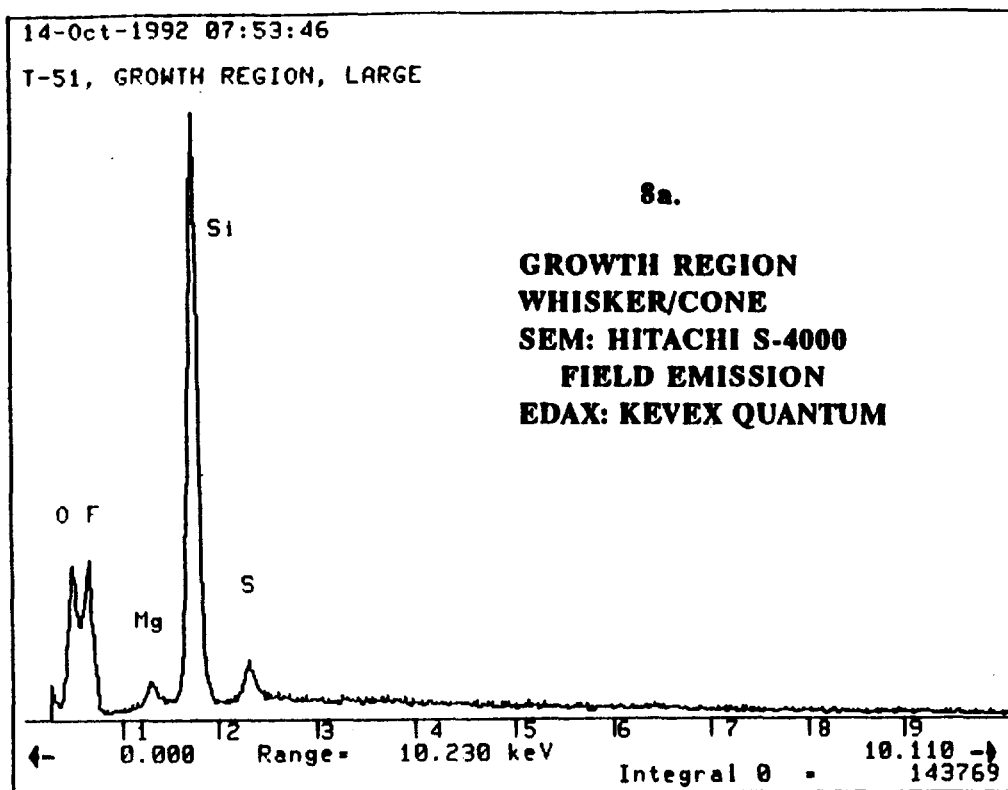


Figure 7. EDAX Data for the Silver Teflon Surface of Sample T51.



MSFC, M&P LABORATORY
 Cursor: 0.000keV = 0

MON 23-FLG-93 09:29

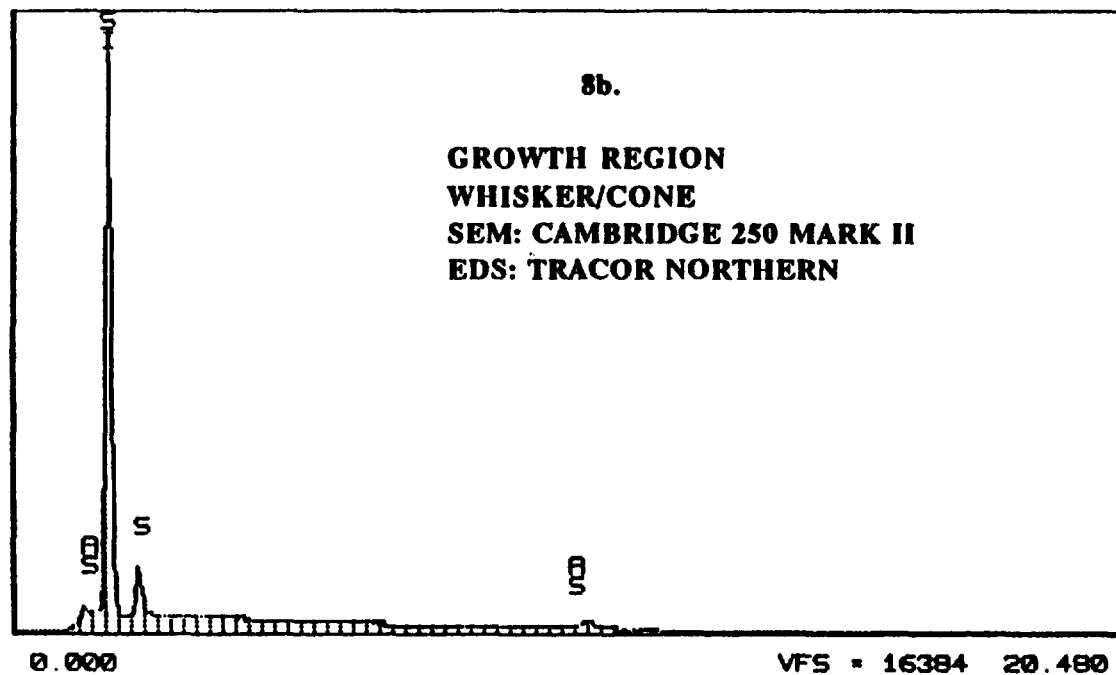


Figure 8. EDAX Data for the Whisker/Cone Growth on Sample T51.

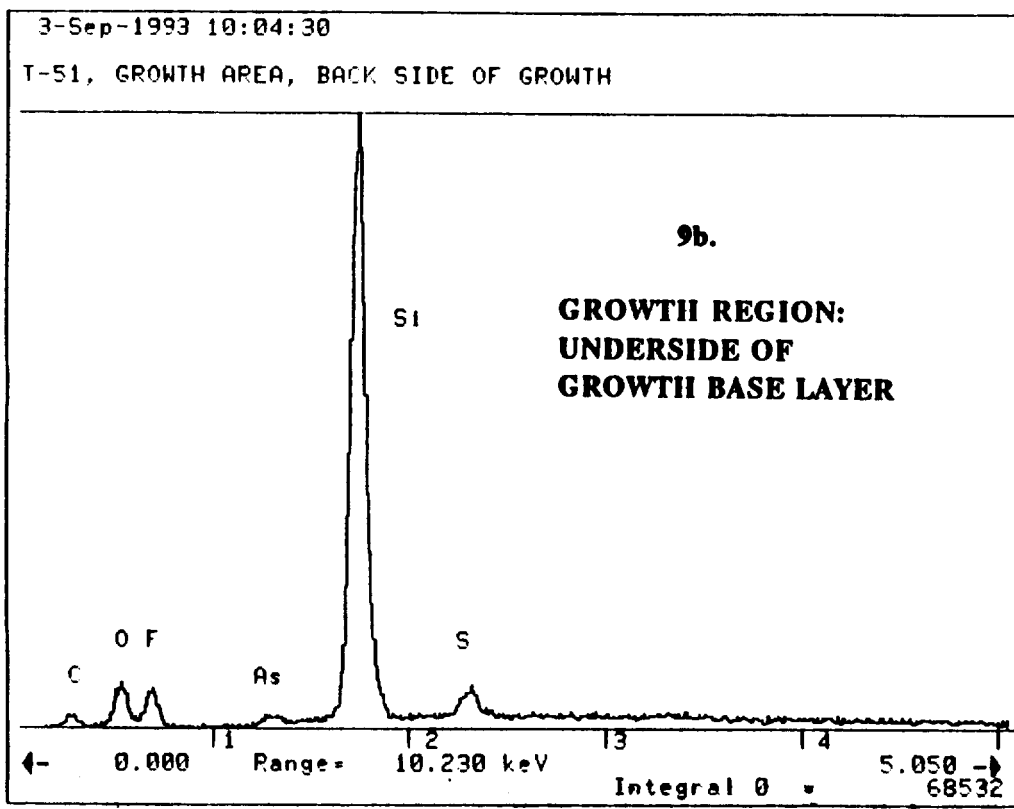
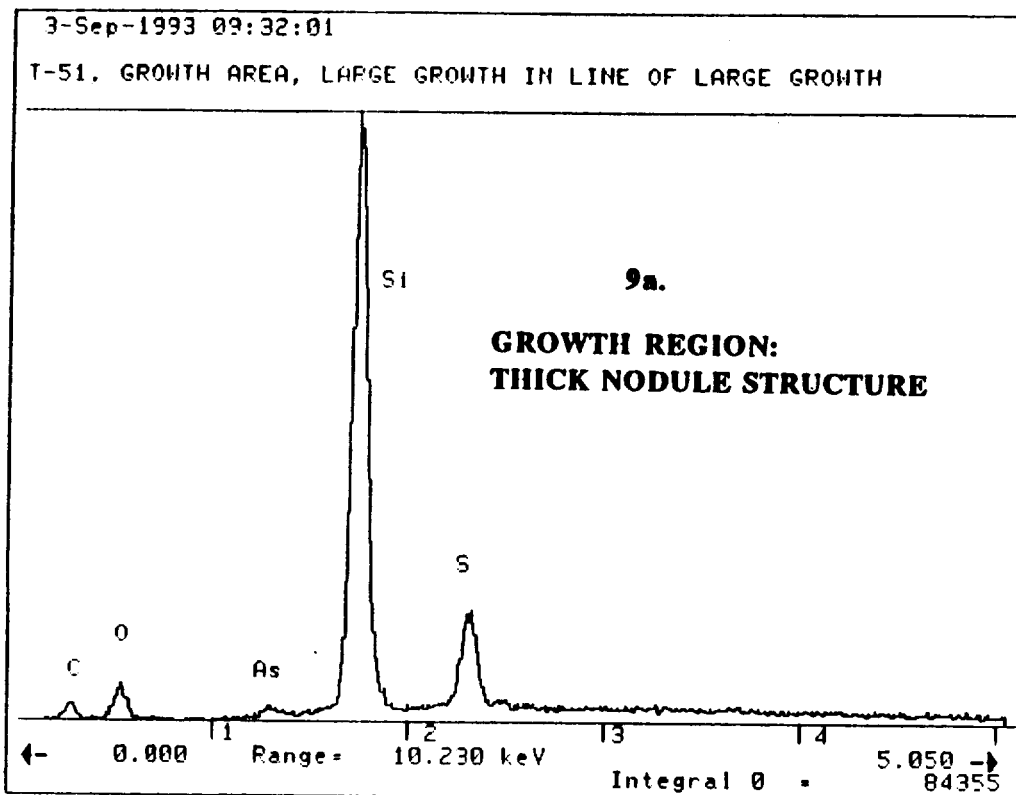


Figure 9. Comparison of EDAX Data for Whisker/Cones and Growth Base Layer.

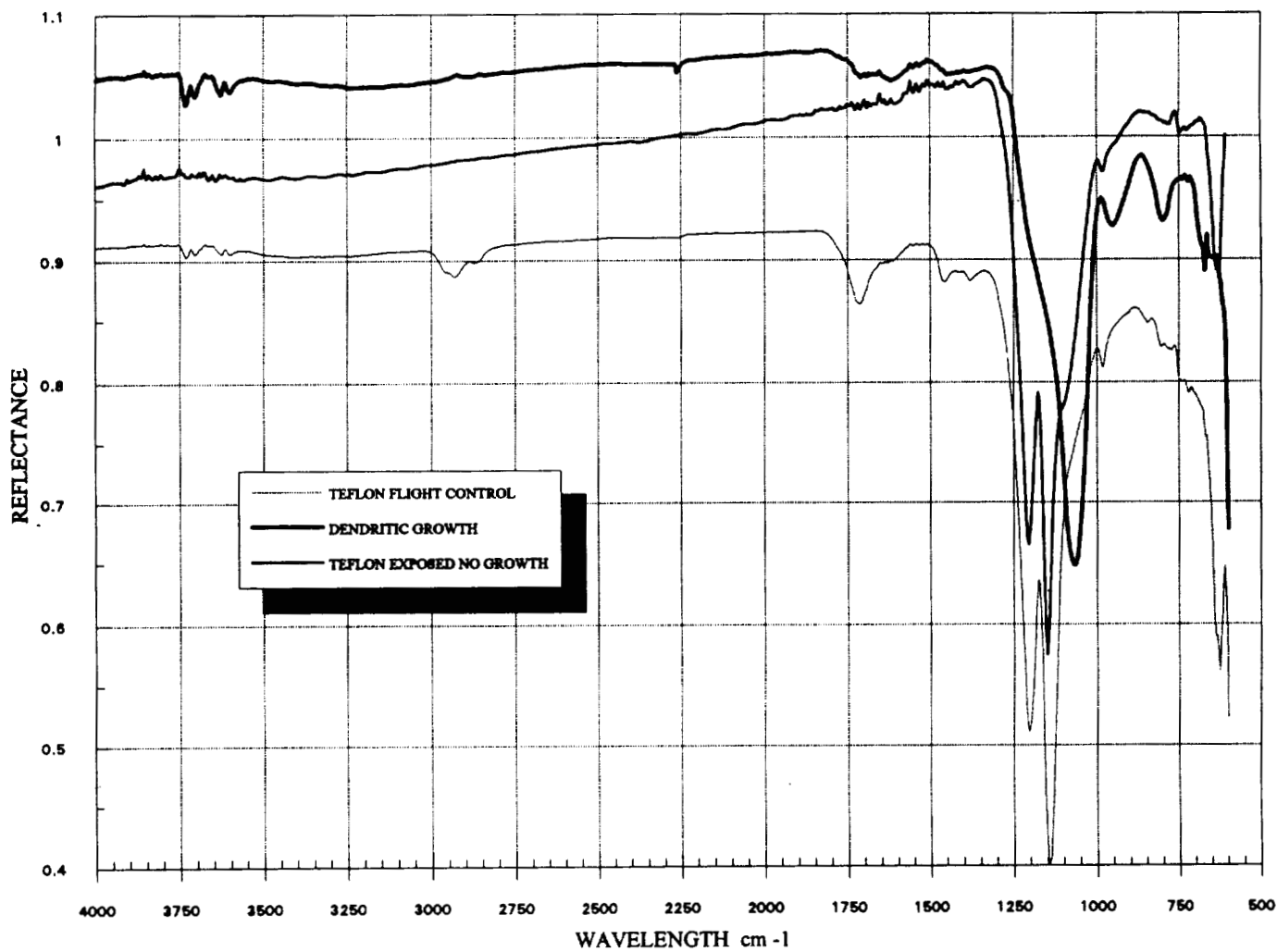


Figure 10. FTIR, Total Attenuated Microprobe Analysis Data for Sample T51.



Figure 11. S0069 Lithium Monofluorographite Batteries and Leakage of Dimethydisulfide Gas.

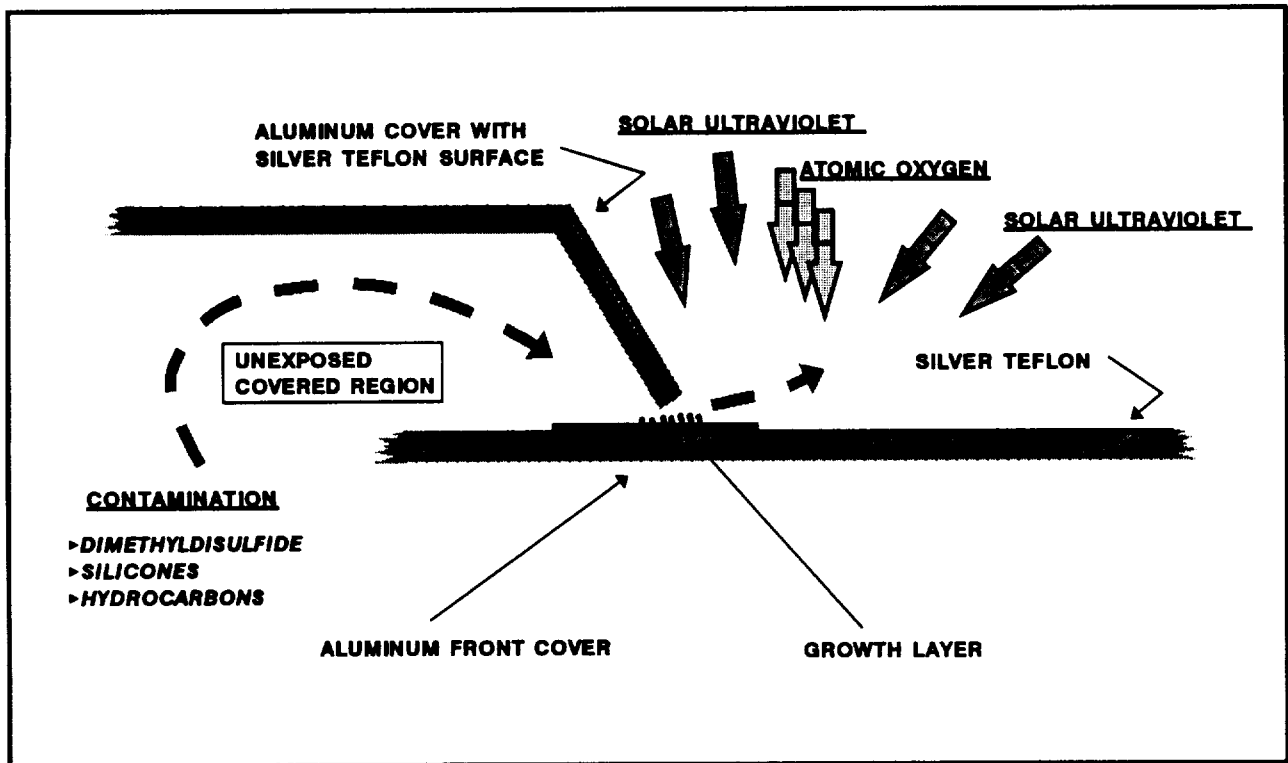


Figure 12. Schematic of Space Environmental Growth Conditions for the Whisker/Cone Growth.

DURABILITY OF REFLECTOR MATERIALS IN THE SPACE ENVIRONMENT

Ann F. Whitaker
Project and Environmental Engineering
Marshall Space Flight Center, AL 35812

Miria M. Finckenor
David Edwards
Rachel R. Kamenetzky
Roger C. Linton
Space Environment Effects
Marshall Space Flight Center, AL 35812

516-27

447-2
1-21

ABSTRACT

Various reflector configurations were flown as part of the Long Duration Exposure Facility (LDEF) A0171 experiment. These reflectors consisted of nickel substrates with aluminum, enhanced aluminum (multiple layers of aluminum and silver), silver, and silver alloy coatings with glassy ceramic overcoatings. These samples have been evaluated for changes in reflectance due to 5.8 years in the space environment. The reflector materials have also been evaluated using angstrometer, Rutherford backscattering (RBS), and electron spectroscopy for chemical analysis (ESCA) techniques.

INTRODUCTION

Multi-layered reflector materials, such as the samples flown on the LDEF satellite, have been tailored for highly efficient reflectance in the near-ultraviolet through visible and near-infrared wavelengths (approximately 350 nm - 1400 nm). Spacecraft applications include solar concentrators and energy dispersion systems where reflection of solar radiation is required. Analysis of the protective glassy ceramic layers utilized on these samples may have transferrable applications in other areas, such as solar cell covers.

EXPERIMENT DESCRIPTION

The Solar Array Materials Passive LDEF Experiment (SAMPLE), A0171, was exposed to the low Earth orbit space environment on the LDEF satellite. The duration of this exposure to atomic oxygen, ultraviolet radiation, thermal cycling, meteoroid/debris impacts, and particulate

radiation was approximately 69 months. The experiment was positioned 38 degrees off the RAM direction at its location on Row 8 position A. The exposure conditions are given in Table 1.

The SAMPLE experiment tray is shown in Figure 1. Solar reflector materials were included in the 300 flight specimen complement. Approximately half of the reflector samples received full surface exposure while the remainder were configured with a mask that covered half the surface area. These half-covered samples are hereafter referred to as half-moon samples. These samples flew on Plate IV of the A0171 experiment and are shown in Figure 2.

Nickel substrates were coated with either silver or aluminum then a glassy ceramic protective layer. The samples exposed on LDEF were:

- Silver coated with SiO₂
- Silver coated with MgF₂ and sapphire
- Silver alloy coated with a multi-layer dielectric of MgF₂ and Al₂O₃
- Aluminum coated with SiO₂
- Aluminum coated with SiO
- Enhanced aluminum coated with SiO and SiO₂
- Enhanced aluminum coated with MgF₂ and sapphire

These flight samples and the control samples which were stored in the laboratory for the duration of the mission have been evaluated for changes in visual and microscopic appearance, optical properties, surface roughness, and layer thickness. Changes in the film morphology were determined by precision angstromer traces, ellipsometry measurements, and Rutherford backscattering analysis. ESCA analysis was also performed to determine composition and extent of contamination, if any.

Table 1. Experiment A0171 Exposure Conditions

High Vacuum	- 10 ⁻⁵ - 10 ⁻⁷ Torr (Estimated)
UV Radiation	- 10,041 ESH
Proton Fluence	- 10 ⁹ p+/cm ² (0.05 - 200 MeV)
Electron Fluence	- (10 ¹⁸ - 10 ¹²) e-/cm ² (0.05 - 3.0 MeV)
Atomic Oxygen	- 7.15 x 10 ²¹ atoms/cm ²
Micrometeoroid/ Space Debris	- 2 to 5 impacts per 25 cm ² , < 1mm
Thermal Cycles	- ~32,000 cycles (temp. unknown)

VISUAL OBSERVATIONS

Visual observations of the reflector materials post-flight revealed few changes. The most significant changes occurred in the reflector samples of silver overcoated with magnesium fluoride and sapphire. These samples were more diffuse due to space environment exposure. The exposed areas appeared scratchy and non-reflective. One sample in particular (fig. 3) was darker, with increased oxidation in atmosphere. The flight silver samples with silicon dioxide coatings had a few pits but remained reflective. The silver alloy reflectors overcoated with a dielectric multilayer suffered some scratches but also remained reflective. The aluminum reflectors with silicon dioxide or silicon monoxide coatings appeared unchanged (fig. 4), as did the enhanced aluminum reflectors. Black light observations did not reveal any obvious molecular contaminant deposition.

OPTICAL PROPERTY MEASUREMENTS

A variety of instruments are available for optical measurements in the Engineering Physics Division of the Materials and Processes Laboratory at the Marshall Space Flight Center. Post-flight reflectance measurements were performed on both control and flight samples with several instruments as follows - a Varian Cary model 2300 spectrophotometer, a Beckman model DK-2A spectrophotometer, a Perkin-Elmer model Lambda 19 spectrometer, and an AZ Technology Laboratory Portable Spectroreflectometer (LPSR). Thermal emittance measurements were made with a Gier-Dunkel DB 100 portable infrared reflectometer.

Reflectance and thermal emittance measurements for selected samples are given in Table 2. The reflectance measurement given for each material is the integrated reflectance from 350 nm to 1400 nm. The exposed reflectance measurements shown are for the worst case (highest ΔR_s) in each sample group. The range of reflectance change for each sample group is also given. Small decreases in reflectance were noted for the majority of exposed samples. Changes in reflectance were consistent within each sample group with the exception of the silver samples coated with magnesium fluoride and sapphire. These reflectance changes are in agreement with the visual observations, with the most obviously degraded sample experiencing a 17% drop in solar reflectance (fig. 5). Thermal emittance measurements on all samples showed no significant changes due to space exposure.

CHANGES IN SURFACE MORPHOLOGY

Precision angstromer traces were made on all the samples using a Wyko Topo-3D surface profiler. A decrease in film height was noted in the exposed areas of the flight samples. A typical trace of a half-moon sample is shown in fig. 6. The changes in thickness of the exposed materials are given in Table 3 and range from 25 up to 160 Å. For applications of these materials where the total coating thickness is 1000 to 2000 Å, the percentage change is considerable, and the effect can be substantial for space optics. If these changes in thickness are assumed to be the result of atomic

oxygen interaction, then the calculated reaction efficiencies, based on the angstromer measurements of a change in layer height, range from 0.4 to $2.3 \times 10^{-28} \text{ cm}^3/\text{atom}$.

Roughness of the samples was measured using a TMA Technologies μScan instrument. RMS roughness measurements are given in Table 3. Measurements of unexposed areas of the half-moon samples agreed well with control surface measurements. These roughness measurements also agree with visual observations, particularly of the oxidized silver/ MgF_2 -sapphire samples.

Ellipsometry measurements were made using a Gaertner Waferskan model L115B. For given N, the refractive index, and K, the extinction coefficient, calculations based on the Fresnel equations indicate a reflectance equal to the measured reflectance for an aluminum reflector coated with 1300 Å of silicon monoxide. The top layer thickness measurements are nominally in agreement with the measurements indicated by RBS analysis, as discussed in the next section.

RUTHERFORD BACKSCATTERING ANALYSIS

Rutherford Backscattering (RBS) analysis was performed on a number of the half-moon reflector samples. RBS is based on the concepts of coulomb scattering and heavy ion energy loss in matter. In most applications, alpha particles are used as the incident beam. A collimated beam of mono-energetic alpha particles impinges on a target, and a small fraction of these particles is scattered due to coulomb interactions with atomic nuclei in the target. Scattering may occur at the front surface of the target or at depths within the target. If the alpha particle penetrates the target instead of scattering from the front surface, the alpha particle loses energy continuously during the penetration due to coulomb interactions with atomic electrons. This measured energy loss produces information related to the depth within the sample at which a scattering event takes place.

During this investigation, a 2 MeV beam energy, a 0.015" beam diameter, and 2 microcoulomb total charge to the sample were used. The incident alpha particles impinged normal to the sample, with the scattered alpha particles measured through an angle of 160 degrees. RBS spectra were obtained from both the exposed and unexposed areas of the reflector samples.

The nickel substrate, being massive relative to the coating materials, dominates the RBS spectrum up to approximately 1200 KeV. The presence of this nickel signal complicates the analysis with respect to the lighter elements.

Results from the RBS analysis are given in Table 4. A typical RBS spectra of the exposed and unexposed areas of an apparently unaffected silver/silicon dioxide reflector is shown in Figure 7. Slight diffusion was apparent at the silicon dioxide-silver and silver-nickel substrate interfaces in both spectra, but the thickness of the SiO_2 layer was not significantly changed. Enhanced aluminum with magnesium fluoride-sapphire overcoating showed the most significant change in RBS spectra. Figure 8 shows the diffusion of the silver in the enhanced aluminum into the nickel substrate and into the coating layer. However, this observation was not consistent among the samples. This diffusion was observed in sample #51 but not #60. These samples received the same amount of space exposure; therefore the cause of this variation is not obvious. Analysis of these samples is continuing.

To sum up the Rutherford backscattering analysis results, the silver and silver alloy samples, in general, revealed some diffusion between the silver-substrate and silver-protective coating interfaces for both exposed and unexposed material. Space environment effects on these

materials, as indicated by surface profilometry and other measurements, were not obviously revealed by RBS analysis. The aluminum and enhanced aluminum samples with SiO_x coatings appeared to be stable in the space environment. The enhanced aluminum with a magnesium fluoride-sapphire protective coating appeared to be affected by space exposure, but this observation was not consistent among the samples nor in agreement with angstromer traces.

ESCA ANALYSIS

An aluminum/SiO₂ reflector, a silver/MgF₂-sapphire reflector, and other material samples from this experiment plate were selected for ESCA analysis. The aluminum reflector was half-exposed to the environment, so three measurements were made on the unexposed and exposed areas. Only one of the three measurements on the exposed area has a significantly higher carbon content (C 1s peak) than that of the control area (see Table 5). The silicon to oxygen ratio is near 0.5, in agreement with the SiO₂ top layer chemistry.

The silver/MgF₂-sapphire reflector was fully exposed to LEO, therefore only exposed ESCA data is given in Table 5. Aluminum, from the sapphire layer, was found in atomic percentages of 12 and 16% in the two measured areas. Silver was also found in atomic percentages of 3 and 7%. Magnesium and fluoride peaks were not reported. The level of oxygen found is in agreement with the sapphire Al₂O₃ layer and formation of silver oxide and/or silicon oxide during the flight. This oxidation layer was not significant enough to appear on RBS spectra. For the silver reflector, carbon levels are typical of LDEF flight samples, though some of the carbon may have been deposited during post-flight storage before ESCA analysis was performed. From these measurements and results from other Plate IV materials, there is some variability in contaminant deposition in exposed sample areas. Visual inspection indicate these reflectors appear to be reasonably clean.

CONCLUSIONS

Degradation of the solar reflectors, when it occurred, was not uniform across the material. When designing for the low Earth orbital environment, solar reflector materials require careful selection. The best performance of a solar reflector material in terms of property maintenance was obtained from a fully oxidized coating over aluminum. All of the coatings experienced densification, decreased thickness, and increased surface roughness, but the measured solar reflectivity values were better than expected based on visual observations. Intercoating diffusion was observed with Rutherford backscattering analysis.

REFERENCES

Whitaker, A.F., Kamenetzky, R.R., Finckenor, M.M., and Norwood, J.K. Atomic Oxygen Effects on LDEF Experiment A0171. Second LDEF Post-Retrieval Symposium, San Diego, CA, June 1992.

ACKNOWLEDGMENTS

The authors gratefully acknowledge Bob Patterson of TRW, for supplying the samples from Cascade Optical Coating, Inc. and Optical Coating Laboratory, Inc. The authors also wish to thank Ms. Whitney Hubbs and Mr. John Reynolds of the Physical Sciences Branch for performing spectrophotometer and ellipsometer measurements, and Mr. J.K. Norwood of the Nondestructive Evaluation Branch and Mr. Perry Gray of Microcraft, Inc. for Wyko analysis.

Table 2. Optical Property Changes of Solar Reflectors

Solar Reflector/Coating	Control R_s	Exposed R_s	ΔR_s (%)	Control ϵ_{IR}	Exposed ϵ_{IR}
Ag/SiO ₂	0.94	0.93	-1	0.03	0.03
Ag/MgF ₂ -Sapphire	0.93	0.76	-4 to 17	0.02	0.02
Ag Alloy/Dielectric	0.92	0.90	-1 to 2	0.02	0.02
Al/SiO ₂	0.87	0.87	<-1	0.03	0.03
Al/SiO	0.87	0.85	-2	0.02	0.02
Enhanced Al/SiO-SiO ₂	0.88	0.86	-2	0.02	0.02
Enhanced Al/MgF ₂ -Sapphire	0.89	0.88	<-1	0.05	0.05

Table 3. Changes in Film Morphology

Solar Reflector/Coating	Decrease in Film Thickness (Å)	Control RMS Roughness (Å)	Exposed RMS Roughness (Å)
Ag/SiO ₂	40	45	60
Ag/MgF ₂ -Sapphire	150	25	75
Ag Alloy/Dielectric	160	30	40
Al/SiO ₂	50	45	40
Al/SiO	150	30	35
Enhanced Al/SiO-SiO ₂	125	30	30
Enhanced Al/MgF ₂ -Sapphire	25	25	30

Table 4. Rutherford Backscattering Analysis Results

Solar Reflector/Coating	Observations
Ag/SiO ₂	No appreciable change Slight diffusion at interfaces
Ag/MgF ₂ -Sapphire	Visually apparent damage is not uniform enough to appear on RBS spectra
Ag Alloy/Dielectric	Slightly increased diffusion at layer interfaces where exposed to space environment
Al/SiO ₂	No appreciable change
Al/SiO	No appreciable change
Enhanced Al/SiO-SiO ₂	Little difference between exposed and unexposed spectra. Protective layer appears to be mainly SiO ₂
Enhanced Al/MgF ₂ -Sapphire	Silver of enhanced aluminum material diffused into surrounding layers. Results not consistent in sample group.

Table 5. ESCA Survey Results

Location	Si (at%)	O (at%)	Ratio Si/O	C (at%)
Aluminum/SiO₂				
Unexposed #1	32	54	0.59	14
#2	33	51	0.65	16
#3	31	53	0.58	16
Exposed #1	27	47	0.57	26
#2	31	50	0.62	19
#3	30	55	0.55	15
Silver/MgF₂-Sapphire				
Exposed #1	15	50	0.30	20
#2	14	41	0.34	22



Figure 3
Silver reflector with MgF₂-sapphire coating

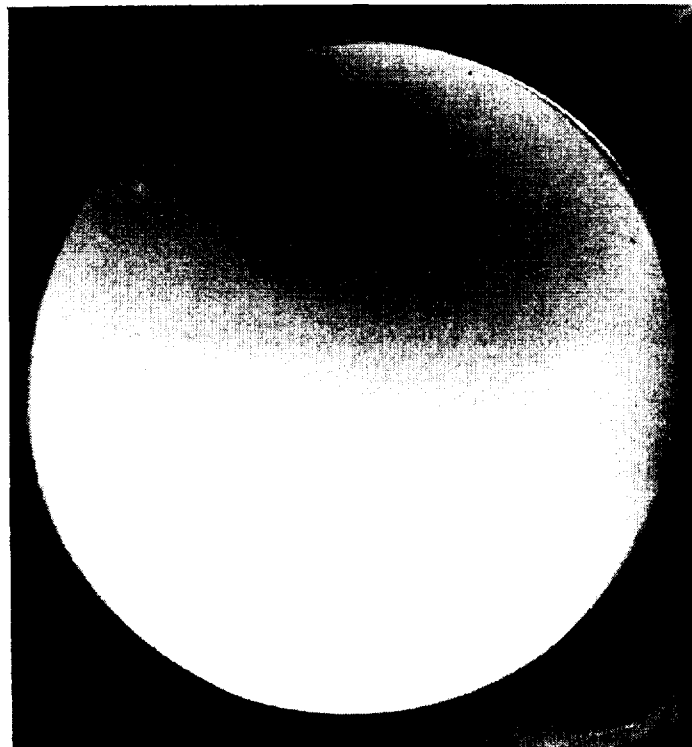


Figure 4
Aluminum reflector with SiO₂ coating

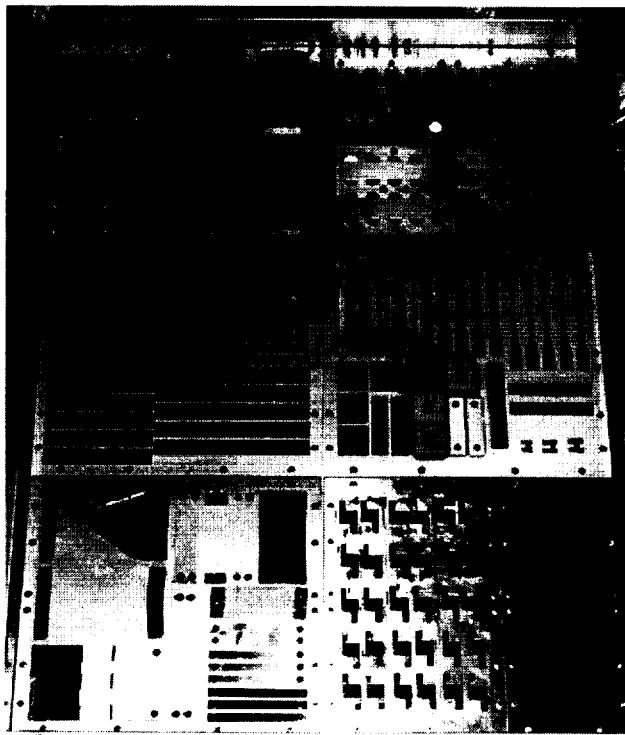


Plate IV

Figure 1
LDEF Experiment A0171 (SAMPLE)

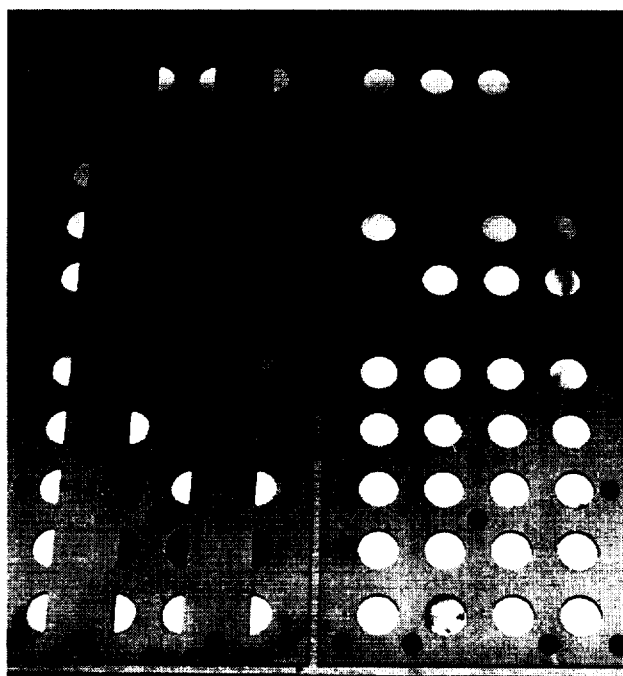


Figure 2
A0171 Plate IV - Thermal Control Coatings

Silver Reflector

Magnesium Fluoride-Sapphire Coating

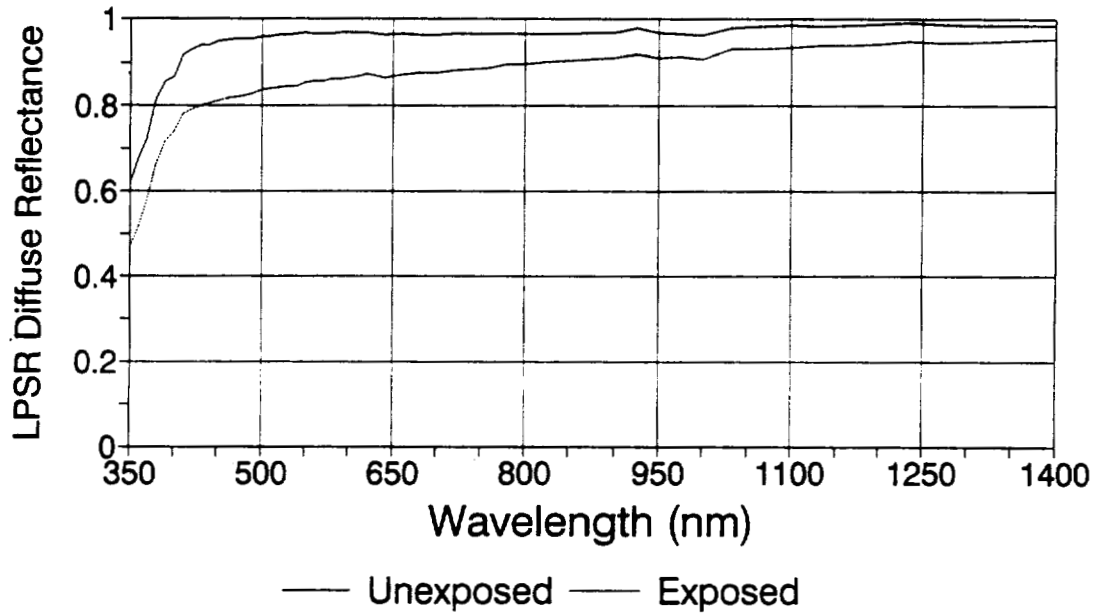


Figure 5

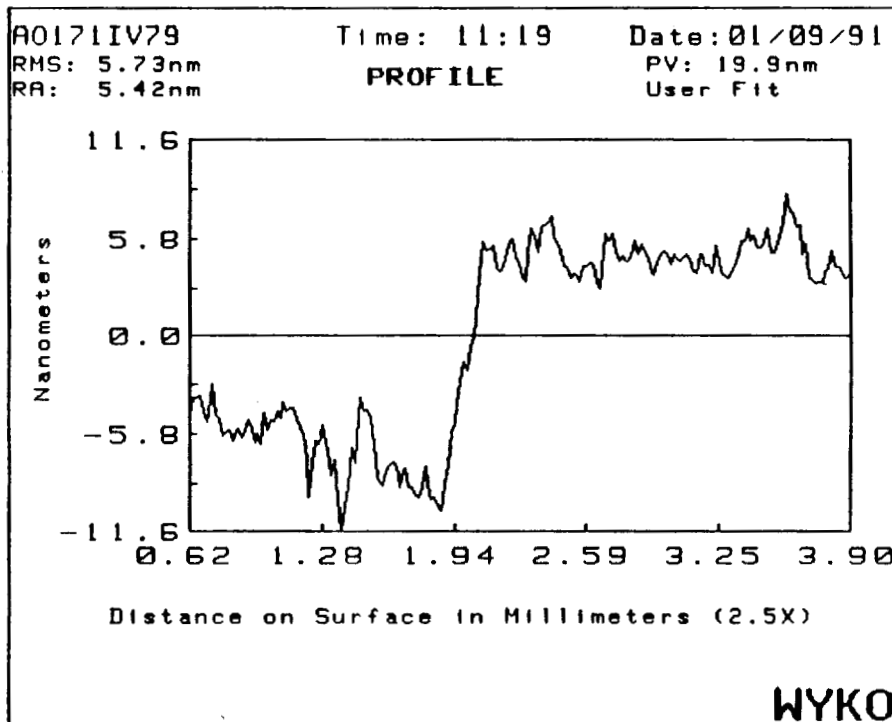


Figure 6

Angstromer trace of
 silver reflector with SiO₂ coating
 Transition between exposed/unexposed areas

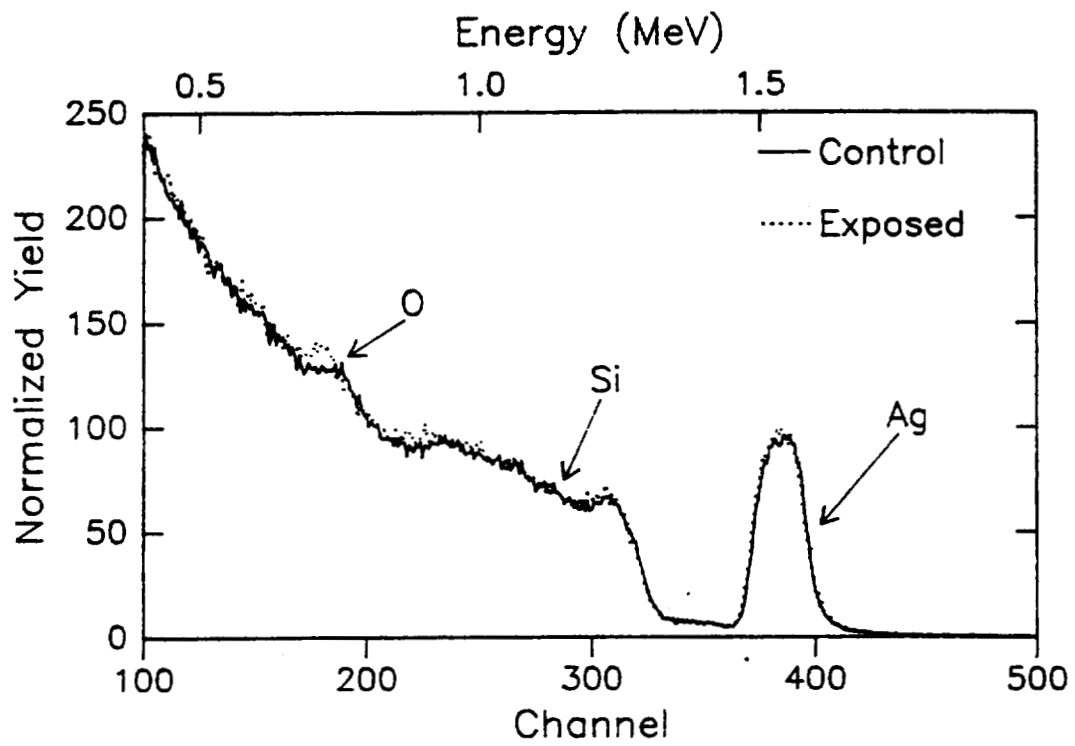


Figure 7: RBS Spectra of Ag/SiO₂

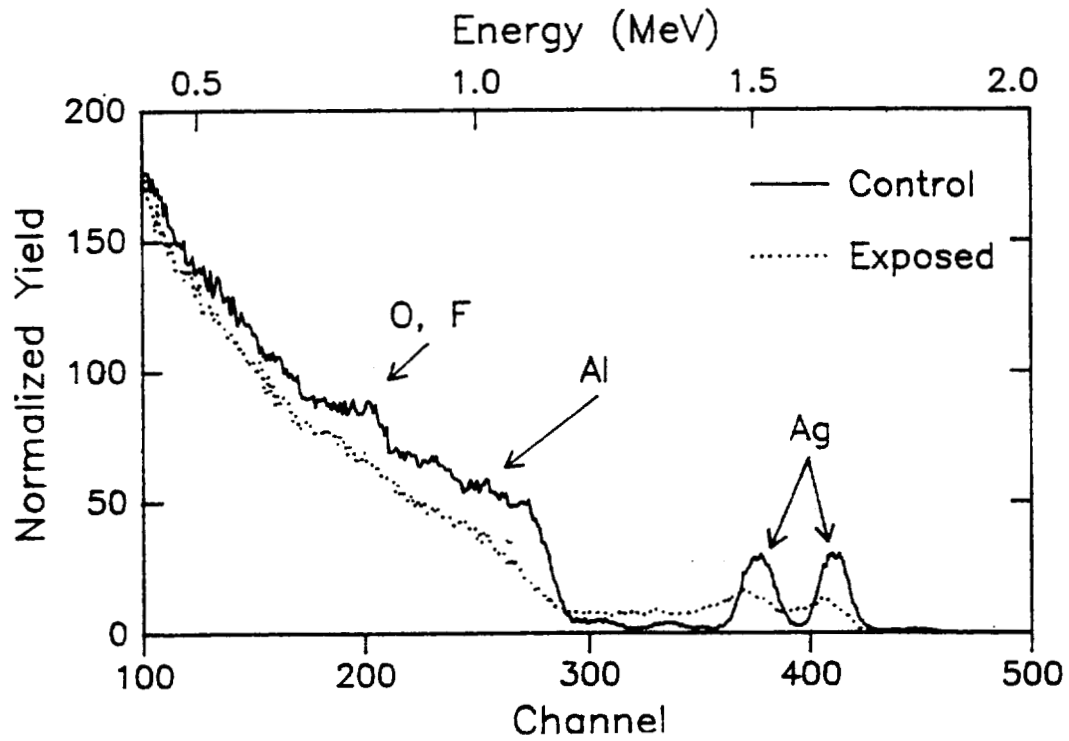


Figure 8: RBS Spectra of Enhanced Al/MgF₂-Sapphire Sample Indicating Interlayer Diffusion

FOUR SPACE APPLICATION MATERIAL COATINGS ON THE
LONG-DURATION EXPOSURE FACILITY (LDEF)

John J. Scialdone and Carroll Clatterbuck
NASA Goddard Space Flight Center
Greenbelt, MD 20771
Phone: 301/286-6731; Fax: 301/286-2562

517-27
44431
JIP

SUMMARY

Four material coatings of different thicknesses were flown on the LDEF to determine their ability to perform in the harsh space environment. The coatings, located in the ram direction of the spacecraft, were exposed for 10 months to the low-Earth orbit (LEO) environment experienced by the LDEF at an orbit of 260 nautical miles. They consisted of Indium Oxide (In_2O_3), Silicon Oxide (SiO_x), clear RTV silicone, and Silicone with Silicate-treated Zinc Oxide (ZnO). These coatings were flown to assess their behavior when exposed to atomic oxygen and to confirm their good radiative properties, stability, electrical conductivity, and resistance to UV exposure.

The flown samples were checked and compared with the reference unflown samples using high-magnification optical inspection, ESCA analysis, weight changes and dimensional changes. These comparisons indicated the following.

The 1000\AA SiO_x coating eroded uniformly, with minor changes in its radiative properties. The 100\AA In_2O_3 coating eroded completely down to the Kapton® backing, with resultant losses of reflectance. The RTV-615 showed erosion, with carbon (C) content losses, while the Si remained constant, with a doubling of the oxygen (O) concentration. The RTV-615 silicone with K_2SiO_3 -treated ZnO changed from flat to glossy white in appearance. It lost C, was etched, and increased its O content. The upper layers showed no remaining Zn or K. Losses of reflectance occurred within certain wavelength bands.

It was not possible to evaluate the experimental oxygen reaction rate using the calculated atomic oxygen fluence of 2.6×10^{20} atoms/cm² for the exposure of these coatings during the flight. The bakeout of the coatings was not carried out prior to the flight. Hence, the coating weight and dimensional losses included losses by outgassing products.

Kapton® is a registered trademark of the E.I. du Pont de Nemours Company

1. INTRODUCTION

Four coating samples prepared by the Materials Branch at GSFC were flown on the Long Duration Exposure Facility (LDEF) spacecraft, launched in 1984. The samples were mounted with many others in the Experiment Environmental Control Canister (EECC). The canister was identified as Experiment No. S0010, and was located in Tray B9, which was situated at an angle of 8.1° from the ram vector, as shown in Figure 1. The assembly of the test specimens in the flight canister and in the control canister was managed by NASA's Langley Research Center (LaRC).

The flight canister, shown in Figure 2, was provided with a drawer that opened and closed on command to expose the samples to the space environment while in flight. The container provided a clean, low-pressure inert gas environment while closed. A timer opened and exposed the samples 1 month after launch, and remained open for 10 months, at which time the drawer returned to the closed position to protect the samples during the remainder of the mission. The hermeticity of the drawer and canister was reconfirmed on the LDEF return, some 5 1/2 years after launch.

Table 1 shows the environmental exposure conditions as reported in Reference 1. The atomic oxygen fluence for the spacecraft (particularly for Row 9) and other data on the space environment are shown in Figures 3 and 4, taken from Reference 2 and 3.

For the 10-month exposure at an altitude of 260 nautical miles, the oxygen fluence is estimated to have been (from Figure 3 of the above reference) 2.6×10^{20} atoms/cm². The UV radiation exposure was 126,000 hours, as indicated in Table 1. The other environmental parameters are given in Table 1.

The four samples were located on the tray in the same row that included samples from the GSFC Optics Branch. Those samples consisted of various metallic coatings such as Au (gold), Pt (platinum), Os (osmium), Ir (iridium), and Al (aluminum) with MgF (magnesium fluoride) and SiO_x (silicon oxide).

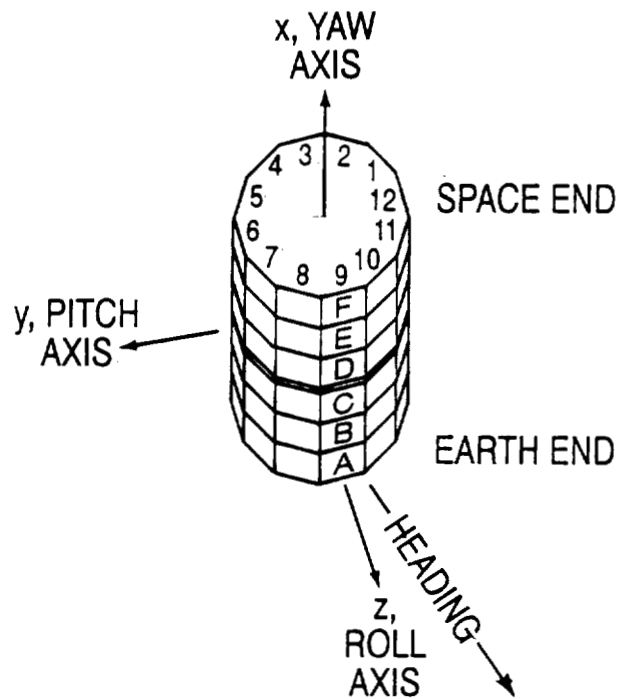


Figure 1. LDEF sketch and orbital configuration.

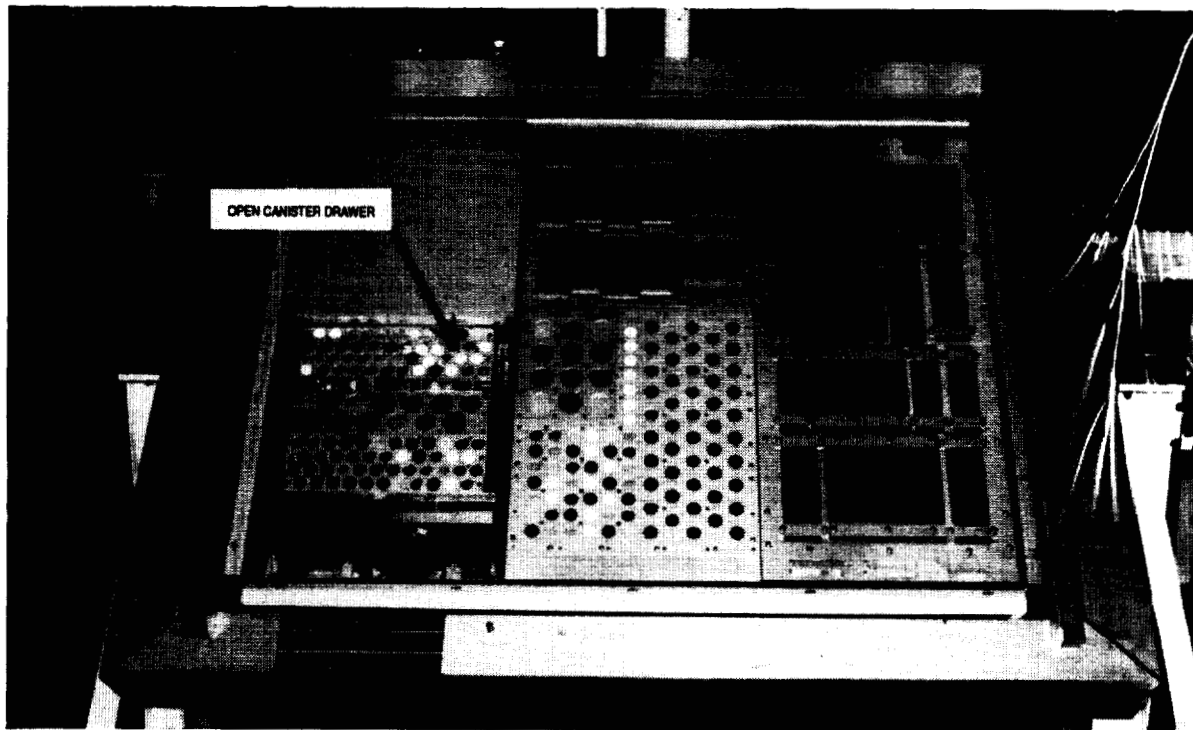


Figure 2. Photograph of Experiment Environmental Control Canister (EECC) with test specimen installed (Photo L-83-10,250).

Table 1. Preliminary Environmental Exposure Conditions

Atomic Oxygen* 0 to 10^{22} atoms/cm ² (wake to ram)	Vacuum 10^{-6} – 10^{-7} torr
UV radiation 100-400 nm; 16,000 hrs	Thermal cycles ~34,000 cycles: -20 to 190°F, ±20°
Particulate radiation e ⁻ and p ⁺ : 2.5×10^5 rad surface fluence Cosmic: <10 rads	Altitude 255-180 nautical miles
Micrometeoroid and debris 6000 particles from 0.1 mm to 2 mm	Orbital inclination 28.5°

*Updated value of $9.09E+21$ as in Figure 4.

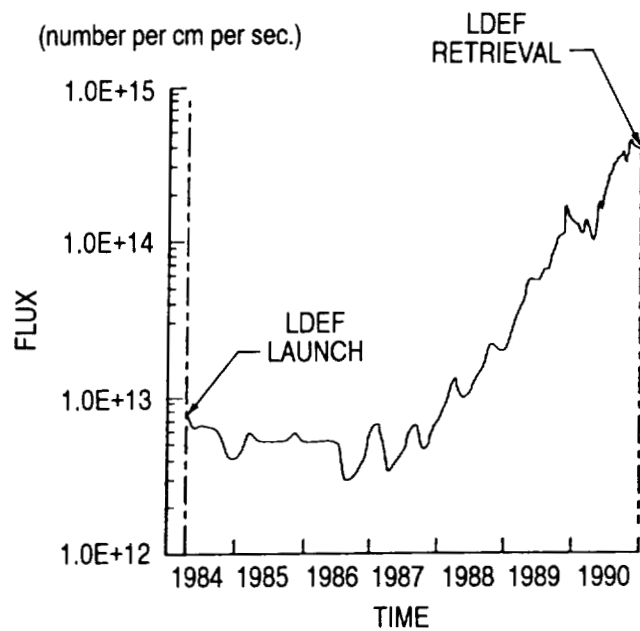


Figure 3. History of oxygen fluence on LDEF leading surfaces.

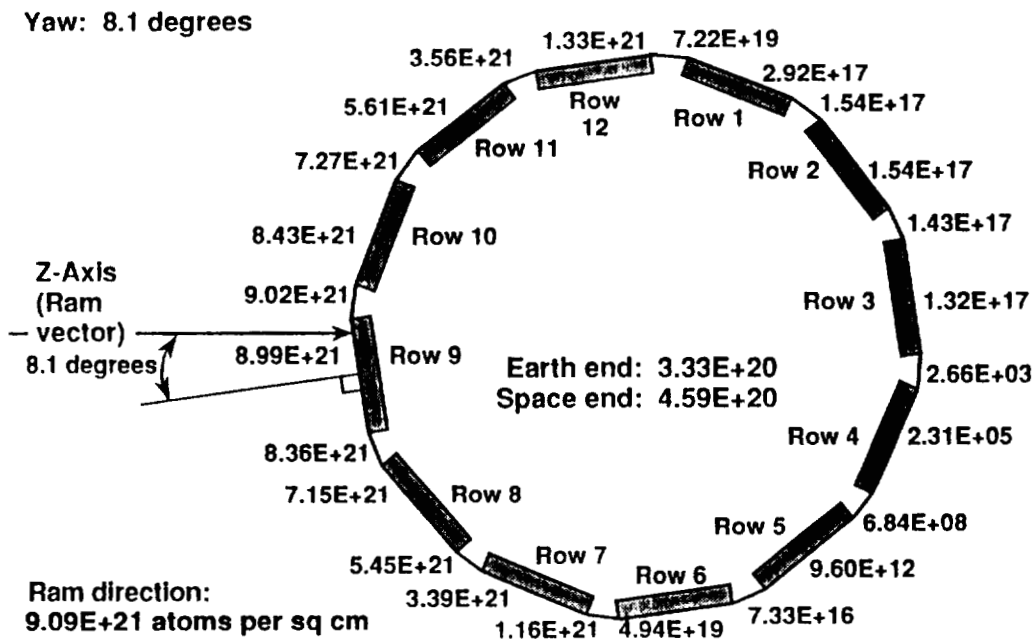


Figure 4. Calculated distribution of the total atomic oxygen fluence on each of the LDEF surfaces.

2. DESCRIPTION OF COATING SAMPLES

The four coating samples are shown schematically in Figure 5, indicating their compositions and the known dimensions. It is not known if, previous to the flight, those samples were baked out in vacuum to reduce their outgassing. We are assuming that they were not. The descriptions of the samples, the primary uses and advantages of the coatings, and available data on the samples follow.

Kapton®/VDA, 1000Å SiO_x (Sample #3)

This sample was composed of 1000 Å of SiO_x deposited on the vacuum-deposited aluminum (VDA) face of Kapton, which was attached to the aluminum support disk with 3M Corporation's Y-966 transfer adhesive. Data on the sample indicate that the weight of the assembled components was 4.345883 g and its total thickness was 0.1294 in. (0.3287 cm). The weight of the support disk was approximately 4.25987 g and its thickness was 0.1148 in. (0.2916 cm). No other data was given. The surface was described as "shiny metallized." This combination is often used as an environmental protective coating, is resistant to atomic oxygen exposure, and provides improved radiative properties after space environment exposure.

Kapton/VDA with 100 Å In₂O₃ (Sample #2)

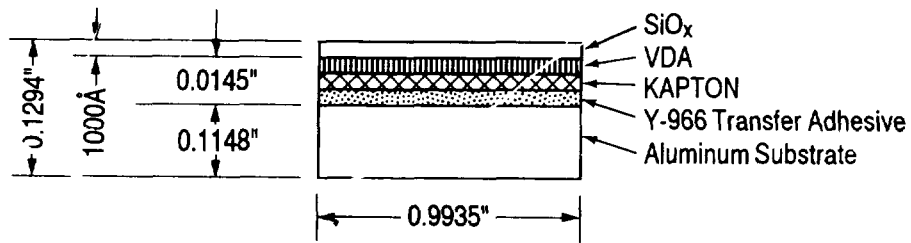
This sample consisted of 100 Å of indium oxide deposited on Kapton. The Kapton was attached with its vacuum-deposited Al face to the aluminum support disk with 3M's Y-966 adhesive. The data sheet indicates that the assembled sample weight was 4.328355 g and its thickness was 0.1271 in. (0.3228 cm). The support disk weight was approximately 4.259878 g and its thickness was 0.1160 in. (0.2946 cm). The surface was described as "yellow" and "shiny." The indium oxide coating provides sufficient electrical conductivity, has little effect on substrate solar absorption and emittance, and remains stable during long exposure in space to UV radiation and particle bombardment.

RTV-615 Silicone on Aluminum (Sample #2C)

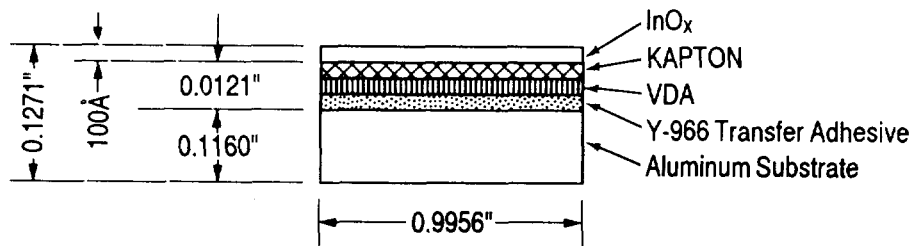
This sample consisted of devolatilized General Electric Corporation (GE) RTV-615 two-part silicone with an A/B parts-by-weight mix ratio of 10/1, which was bonded to the aluminum disk via GE primer SS4155. The data describe it as a clear silicone. The total thickness of the assembly was 0.1253 in. (0.3183 cm). The weight of the support disk was 4.25987 g and its thickness was 0.1127 in. (0.2862 cm). No other description was given. This combination is an environmental protective coating used as a sealant and is particularly resistant to atomic oxygen.

Kapton® is a registered trademark of the E.I. du Pont de Nemours Company

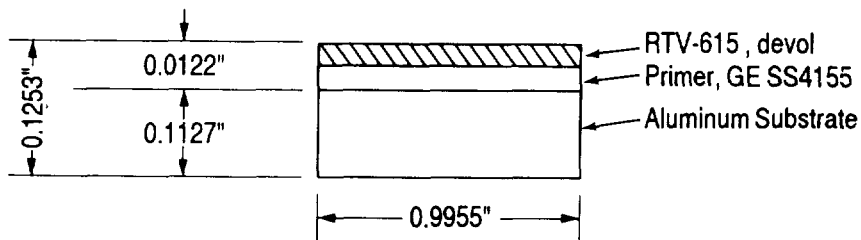
1. KAPTON®/VDA with 1000Å SiO_x coating



2. KAPTON®/VDA with 100Å In₂O₃ coating



3. RTV-615 Silicone on Aluminum



4. RTV-615 Silicone-Treated ZnO

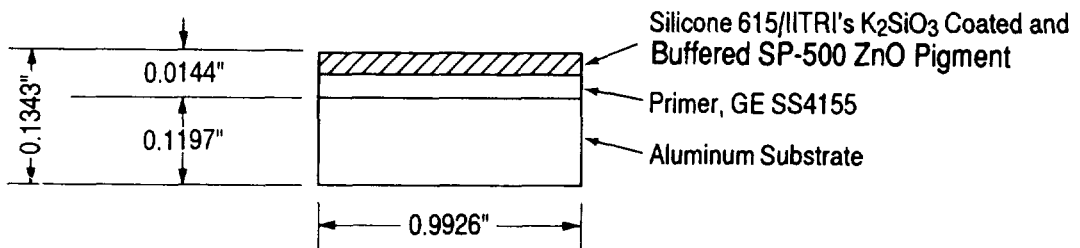


Figure 5. Side views of LDEF specimens (not drawn to scale).

RTV-615/Silicone-Treated ZnO (zinc oxide) (Sample #1A)

This sample consisted of GE's devolatized RTV-615 two-part silicone with 68% of IITRI's K_2SiO_3 coated and buffered SP-500 ZnO pigment. The RTV-615 silicone had an A/B parts-by-weight mix ratio of 10:1. The material was bonded to the aluminum disk via GE primer, SS4155. The total weight was 4.55060 g and the total thickness was 0.1343 in. (0.3411 cm). The weight of the support disk was 4.25987 g and its thickness was 0.1197 in. (0.3040 cm). No other data were given. This combination is a thermal control coating and is used as a white paint for spacecraft and other structures. It is resistant to UV radiation exposure.

3. DATA AND MEASUREMENTS TAKEN

The effect of the space environment on these samples is indicated by providing the following descriptive parameters.

- The sample weight loss per unit area ($g\ cm^{-2}$)--This is the difference between the weight of the flight and control samples before and after the mission, ratioed to the exposed area of the flight samples.
- The sample thickness loss (cm)--This is obtained from the difference in thickness of the flight samples before and after the mission. Depending on the magnitude of the difference, one can determine the degree of coating loss attributable to the space environment.
- A percent thickness loss--This is based on the same assumptions used for the measurements of the coating thickness.
- A comparison of the spectral reflectance and the integrated absorption and emittance of the coatings before and after space environment exposure--The measurements were made using the P.E. λ -9 spectrophotometer.
- Surface analysis of the samples--The ESCA probe was used to provide elemental/chemical composition of the samples within a depth of 100 Å (up to some 50 monolayers) employing x rays to emit electrons.
- Photographic and microscopic documentation--This shows the reference and flight sample surface appearance and related evaluation of the changes that may have occurred following space exposure.

4. SAMPLE ANALYSES

1000 Å of SiO_x on VDA Kapton

Visual Inspection--The surface was highly reflective with some raised areas. The flight sample surface was slightly duller than the reference sample, with extremely fine discontinuities over the entire surface.

High-Magnification Inspection--The shape of the discontinuities was not discernible at 200 X magnification. There were no pinholes in the vacuum-deposited Al.

ESCA Analysis--The composition of both the flight and reference samples was similar, as shown by the spectrogram in Figure 6. The concentrations of Si and O remain constant through the thicknesses of both samples. Erosion may have been uniform over the surface. Peaks of silicone and oxygen are found within the various thicknesses.

Radiative Analysis--The reflectances vs. wavelengths are shown in Figure 7. The exposed sample shows an improved reflectance below 450 nm and above 700 nm. The integrated properties are $\alpha = 0.127$ and $\epsilon = 0.023$ for the flight sample, and $\alpha = 0.155$ and $\epsilon = 0.025$ for the reference sample.

Physical Analysis--The mass loss of the flight sample was 3.3×10^{-5} g or about 8.9×10^{-6} g cm⁻² of the exposed area. The thickness change amounted to 3.032×10^{-3} cm, corresponding to about 0.994% of the total sample thickness.

Oxygen Erosion--The change in thickness, 3.032×10^{-3} cm, is considerably more than the SiO₂ thickness of 1000 Å (1×10^{-5} cm). Some of the VDA Kapton was eroded. One cannot establish a reaction rate constant because the measured mass loss and thickness may include changes due to the sample's outgassing losses.

100Å In₂O₃ on VDA/Kapton

Visual Inspection--Figures 8 and 9 reveal uniformly oriented serrations in the highly reflective, gold-colored Kapton surface. Brushed marks on the aluminized surface are opaque with a golden hue and an aluminized color visible on only a few small areas.

High-Magnification Inspection--An etched, frosted appearance is visible at the brush marks under the undamaged areas.

ESCA Analysis--The flown coating sample (Figure 10) has a rough surface with visible erosion and delamination. The non-exposed surface appears shiny at the outer edge, with no visible damage. The exposed surface is severely eroded and gray in color, with scratch marks around the eroded area. The scratched and eroded areas are made up mostly of Kapton, with some traces of indium. The indium at those locations measured up to 0.95 atomic % while at the unexposed surfaces, the indium was 7 atomic %.

Mon Jun 22 13:58:34

M-Probe ESCA Console

User ID: LDEF

Filename	Spot	Res	Flood eV	Scans	Description
G080205.MRS	200x750 μ	3	1.0	1	LDEF.SiO _x +KAPTON,flight,60 sec sput
G080107.MRS	200x750 μ	3	1.0	1	LDEF.SiO _x +KAPTON,ref,60 sec sput

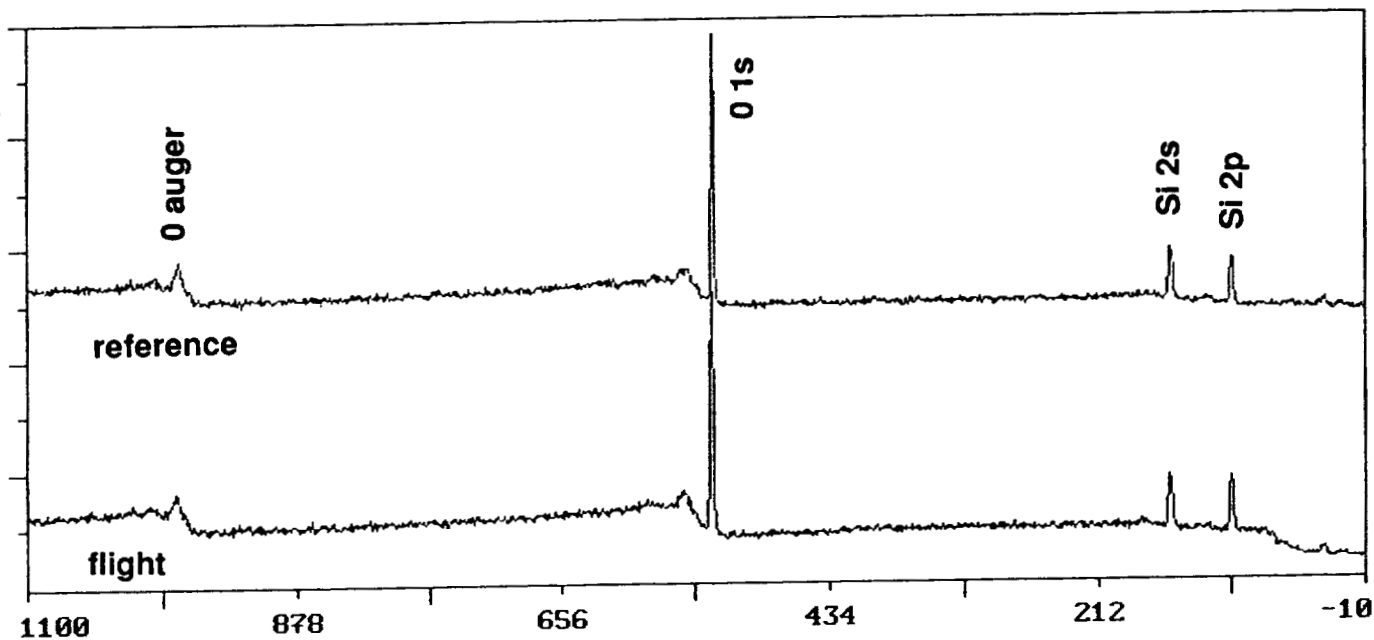


Figure 6. ESCA spectrum of 1000 Å of SiO_x on VDA/Kapton.

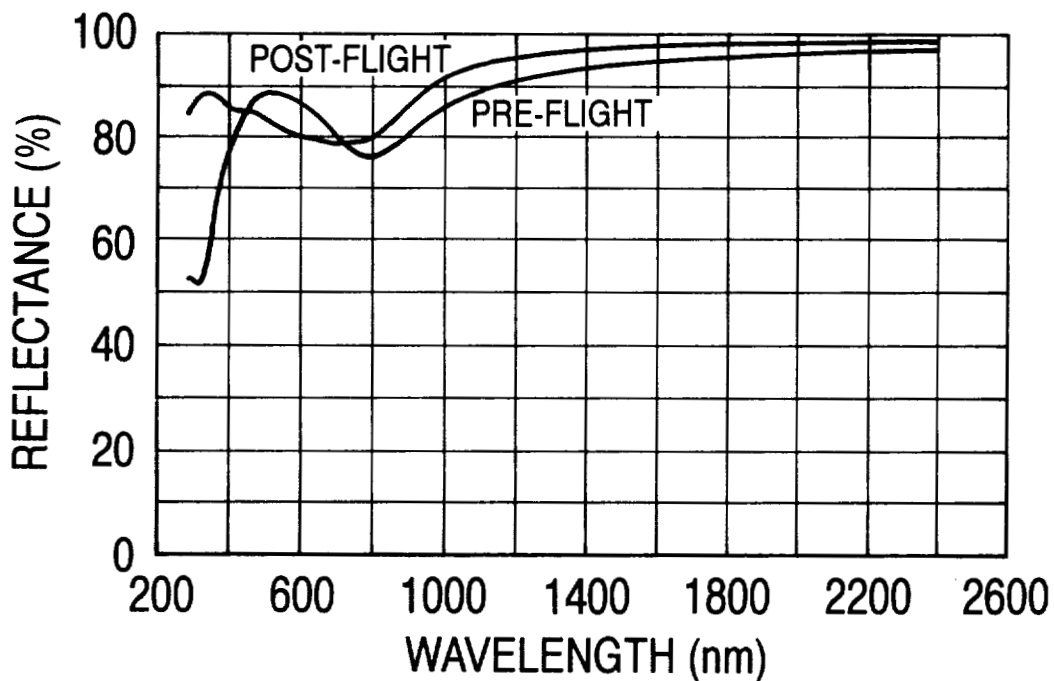


Figure 7. Reflectance of 1000 Å SiO_x coating on VDA/Kapton sample.

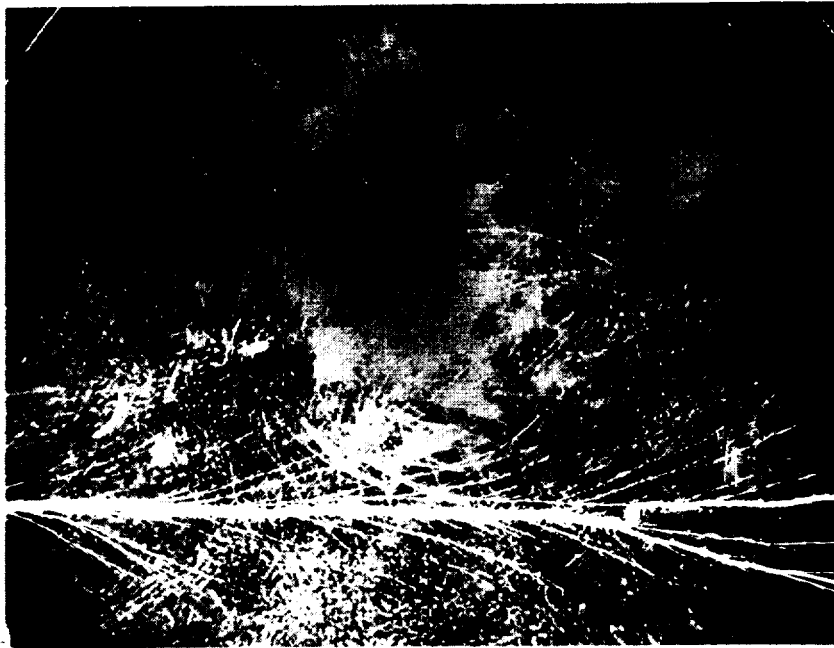


Figure 8. 100 Å In_2O_3 on VDA/Kapton (5.5X).

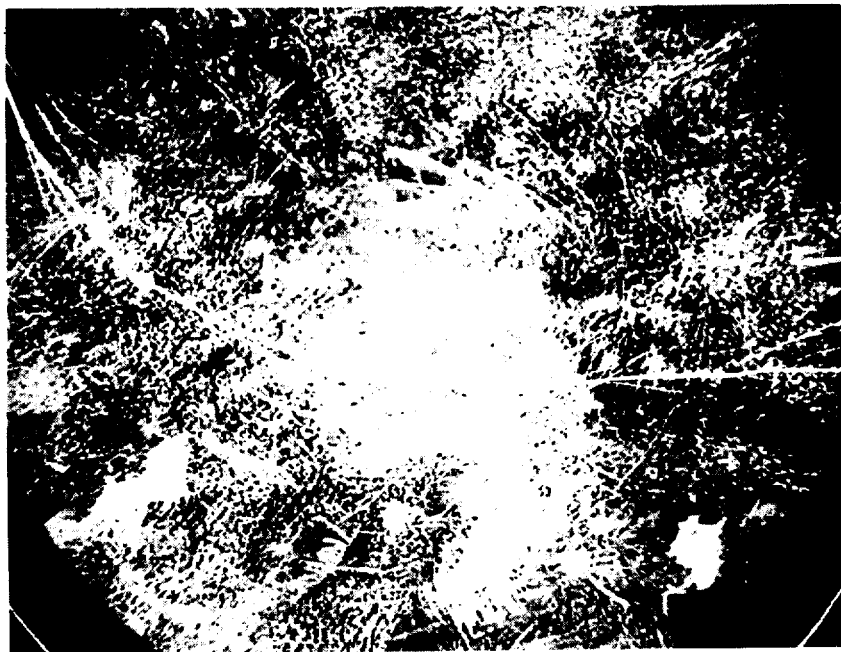


Figure 9. VDA/Kapton/ InO_x (5.5X).

Mon Jun 22 13:50:46

M-Probe ESCA Console

User ID: LDEF

Filename	Spot	Res	Flood eV	Scans	Description
G072910.MRS	200x750 μ	3	1.0	1	LDEF,UDA#2-KAPTON,center,60sec sput
G072903.MRS	200x750 μ	3	1.0	1	LDEF,UDA#2-KAPTON,reference, 60 sec

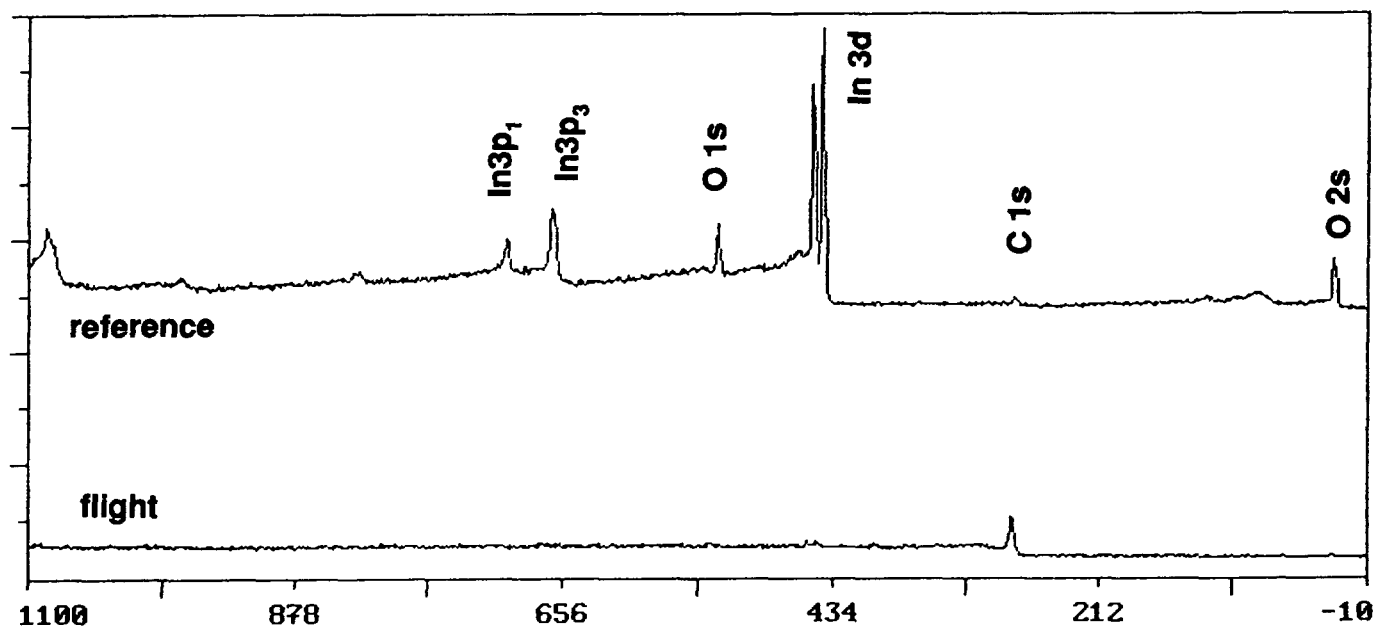


Figure 10. ESCA spectrum of sample with 100 Å of In₂O₃ on VDA/Kapton.

Radiative Analysis--Figure 11 shows the reflectances of the exposed and reference samples. About 10% reflectance loss occurred at wavelengths below 450 nm and about 5% loss occurred between 600 and 1600 nm. The integrated values are 0.391 absorption and 0.547 emittance for the flown sample and are 0.363 and 0.564, respectively, for the reference sample.

Physical Analysis--The mass loss for the sample was 0.001867 g, or about 5.37×10^{-4} g cm⁻² of exposed area. The thickness change amounted to about 5.08×10^{-3} cm, corresponding to about 1.538% of the total thickness.

Oxygen Erosion--The 100 Å (10^{-6} cm) of In₂O₃ and a considerable amount of the VDA/Kapton were eroded. In addition, considerable material and thickness must have been lost by outgassing in space. Not knowing if bakeout in vacuum was performed on the material before launch, it is not possible to estimate the reaction efficiency of the indium. However, the various analyses have indicated that the indium was completely eroded. The reaction rate for the Kapton is known to be about 3×10^{-24} cm³/atom from other orbital tests.

Devolatized RTV-615 Bonded on Al with SS 4155 Primer

Visual Inspection--The surface is clear and transparent with no noticeably changed features (Figures 12 and 13).

High-Magnification Inspection--Optical magnification shows banded networks with areas of contamination (possibly impacts) at focal points of several bands (Figures 12 and 13). The network of crack lines may have originated from solar exposure and from additional material losses causing thermal cracking.

ESCA Analysis--The erosion pattern is similar to that of the sample consisting of the same RTV with K₂SiO₃ and ZnO pigment. The flight sample shows carbon content of 1.5 atomic %, while the reference sample has 35 atomic %. The Si concentration did not change, while the O concentration doubled in the flight sample (Figure 14).

Radiative Analysis--The flight sample experienced a loss of about 5% in reflectance throughout the measured range of wavelength with respect to that of the reflectance sample. The integrated properties are $\alpha = 0.489$ and $\epsilon = 0.819$ for the flight sample, and $\alpha = 0.432$ and $\epsilon = 0.824$ for the reference sample (Figure 15).

Physical Analysis--The mass loss was 0.0037 g, or about 8.983×10^{-3} g cm⁻² of the exposed area. The thickness change amounted to about 8.63×10^{-3} cm, corresponding to about 2.617% of the total thickness.

Oxygen Erosion--The change in thickness, 0.0034 in. (8.63×10^{-3} cm), is considerably less than the thickness of the RTV and primer 0.0167 in. (4.24×10^{-2} cm). Under the assumptions that the loss was the result of the oxygen erosion, we could calculate the reaction efficiency.

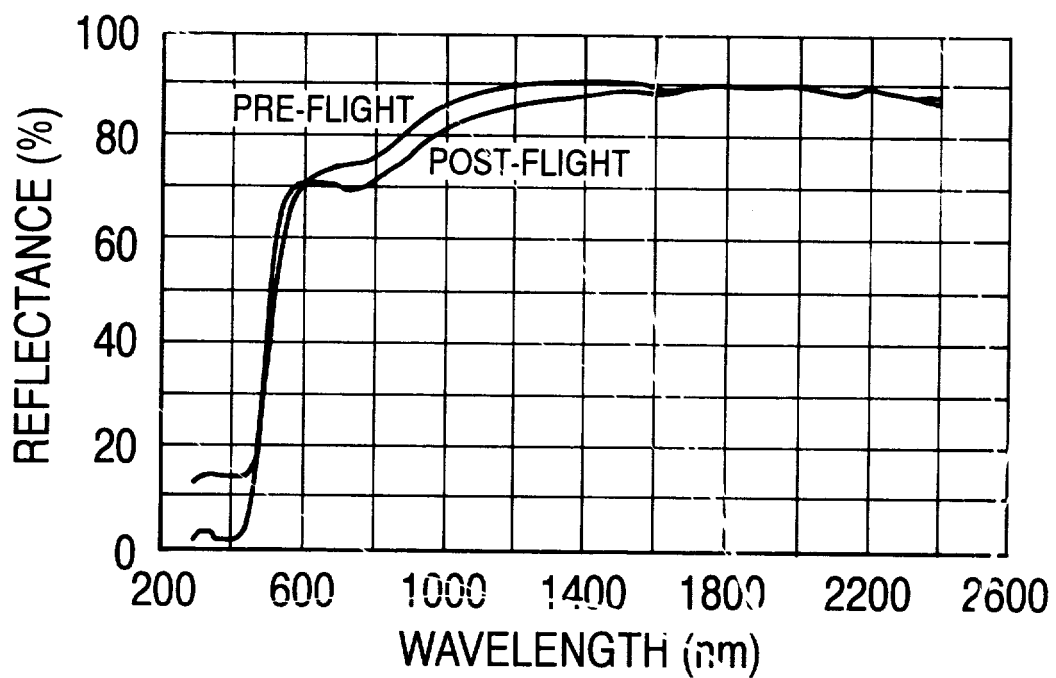


Figure 11. Reflectance of 100 Å InO₃ coating on VDA/Kapton sample.



Figure 12. Devolatilized RTV-615 bonded on Al with SS 4155 Primer (200X).



Figure 13. Devolatilized RTV-615 bonded on Al with SS 4155 Primer (25X).

Mon Jun 22 14:22:28 M-Probe ESCA Console User ID: LDEF
 Filename Spot Res Flood eV Scans Description
 G091305.MRS 400x1000µ 3 1.0 3 LDEF.RTU-clear.flight.60 sec sput
 G091205.MRS 400x1000µ 3 1.0 3 LDEF.RTU-clear.reference.1 min sput.

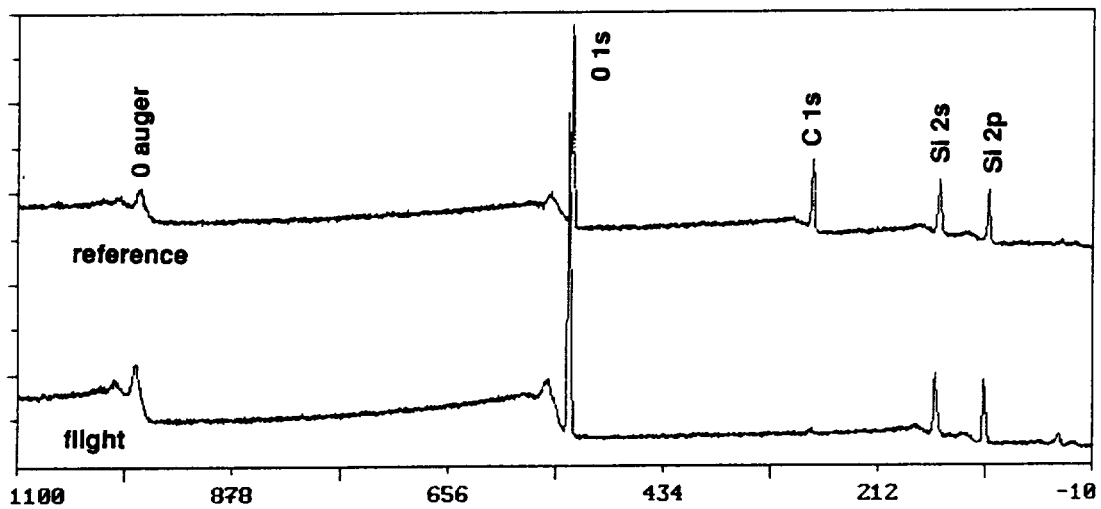


Figure 14. ESCA spectrum of sample with RTV-615 bonded on Al with SS 4155 primer.

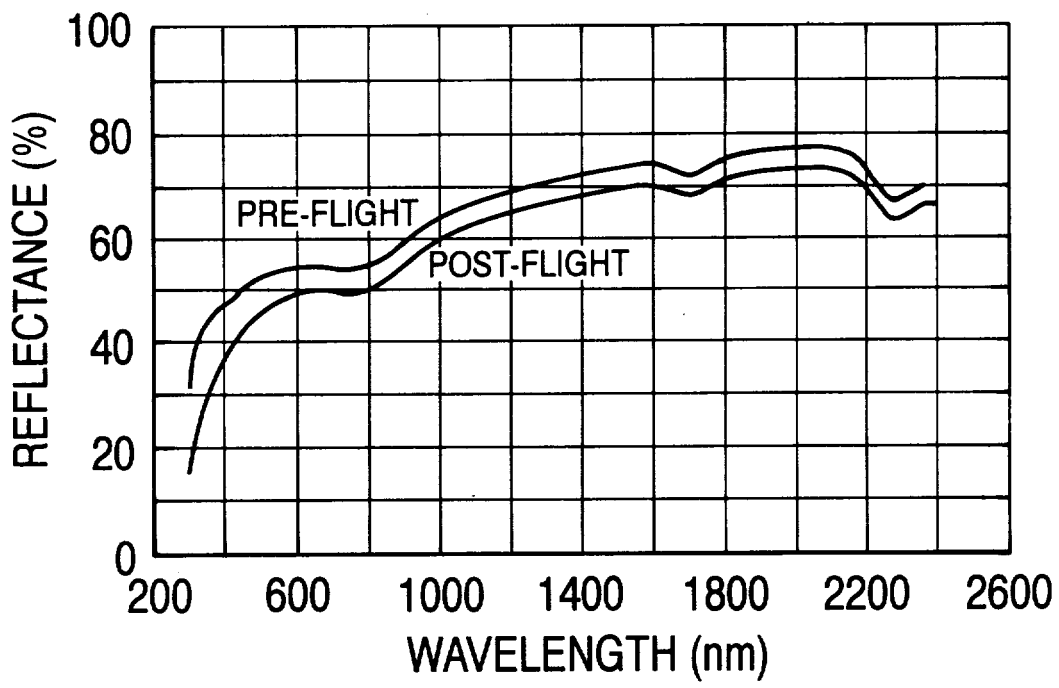


Figure 15. Reflectance of RTV-615 clear coating on aluminum.

However, calculations to estimate the reaction efficiency using the above data indicate a considerable oxygen erosion, much larger than the value of $6.25 \times 10^{-26} \text{ cm}^3/\text{atom}$ reported in reference 4. The discrepancy in order of magnitude must be assumed to have been produced by loss of material from outgassing.

RTV-615/Silicate-Treated ZnO

Visual Inspection--The flight sample surface appears slightly glossy and white, with raised agglomerated particles originating from the glossy matrix surface. The reference sample is flat white.

High-Magnification Inspection--The exposed flight sample surface is shown in Figures 16 and 17.

ESCA Analysis--This analysis (Figure 18) indicated considerable difference in the concentrations of carbon (C) between the flight and the reference specimens. The concentrations of Si between the two are about equal and constant through the thicknesses. The O and C concentrations differ. The C concentration decreases by 21 atomic % and O increases by 18 atomic % after 1 minute of etching. On the other hand, for the reference sample, the C decreases by 7 atomic % concentration and the O increases by 2 atomic % for the same etching time. No Zn or K peaks were found, even though the silicone was filled with potassium silicate and ZnO, indicating that they had eroded or that they had penetrated into deeper layers.

Radiative Analysis--The reflectance versus wavelength is shown in Figure 19. It shows some loss between 400 and 700 nm and between 1800 and 2100 nm. The integrated absorption is 0.201 and the emittance is 0.891 for the flown sample and 0.190 and 0.907, respectively, for the reference sample.

Physical Analysis--The mass loss was $8.27 \times 10^{-4} \text{ g}$, or about $2.33 \times 10^{-4} \text{ g cm}^{-2}$ of exposed surface. The thickness change amounted to $3 \times 10^{-3} \text{ in.}$ ($7.78 \times 10^{-3} \text{ cm}$), corresponding to about 2.142% of the total thickness.

Oxygen Erosion--Both the RTV and the silicate were eroded. The actual erosion and mass thickness are not known because of the possible loss by outgassing, and the calculation for the reaction efficiency could be erroneous. But, as indicated, the erosion did occur.

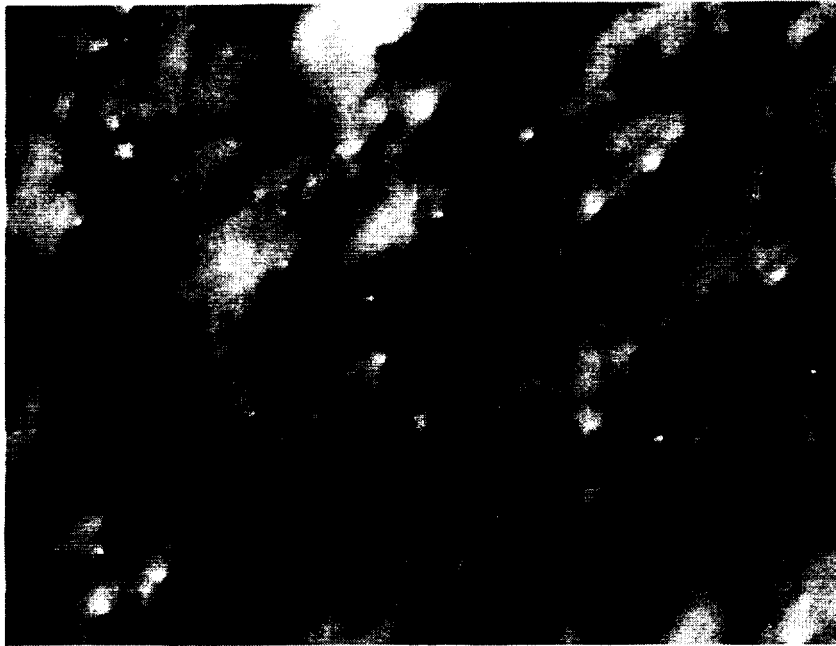


Figure 16. RTV-615/Silicone-Treated ZnO (38.5X).

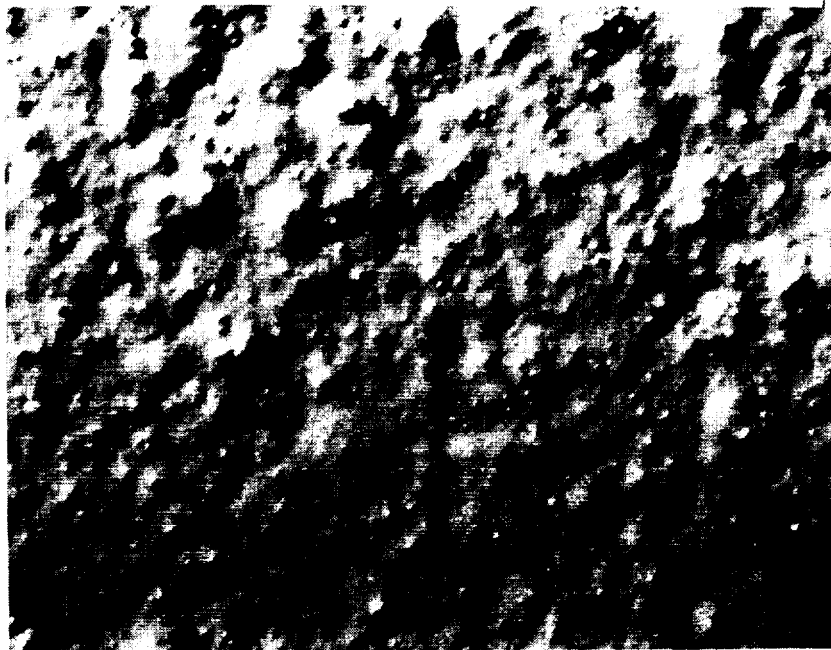


Figure 17. RTV-615/Silicone-Treated ZnO (16.5X).

Mon Jun 22 14:20:25 M-Probe ESCA Console User ID: LDEF
 Filename Spot Res Flood eV Scans Description
 G091107.MRS 400x1000µ 3 1.0 3 LDEF.RTU-white,flight.3 min sput
 G090807.MRS 400x1000µ 3 1.0 3 LDEF.RTU-white,ref.3 min sput.new lo

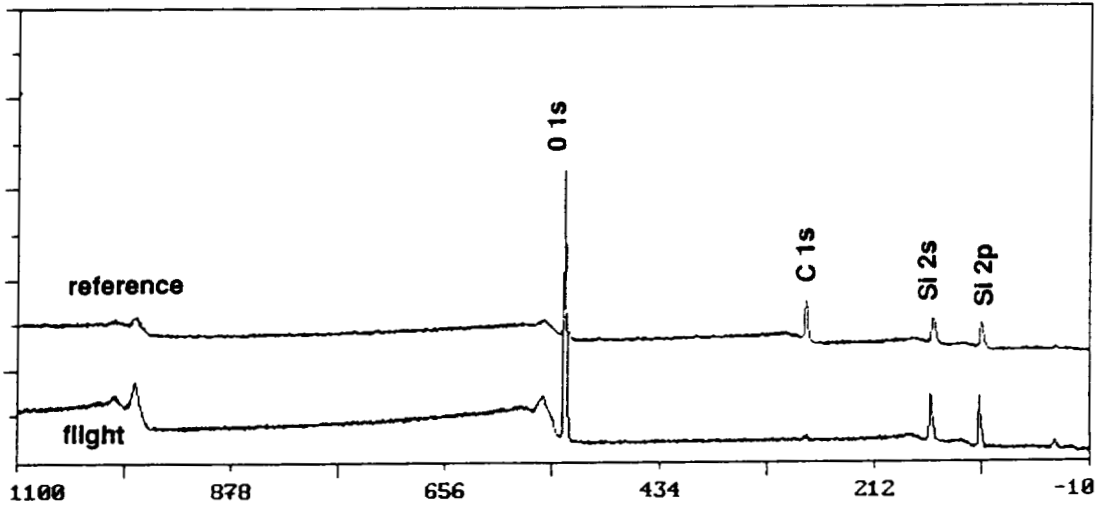


Figure 18. ESCA spectrum of sample with RTV-615 Silicone Treated with ZnO bonded on Al.

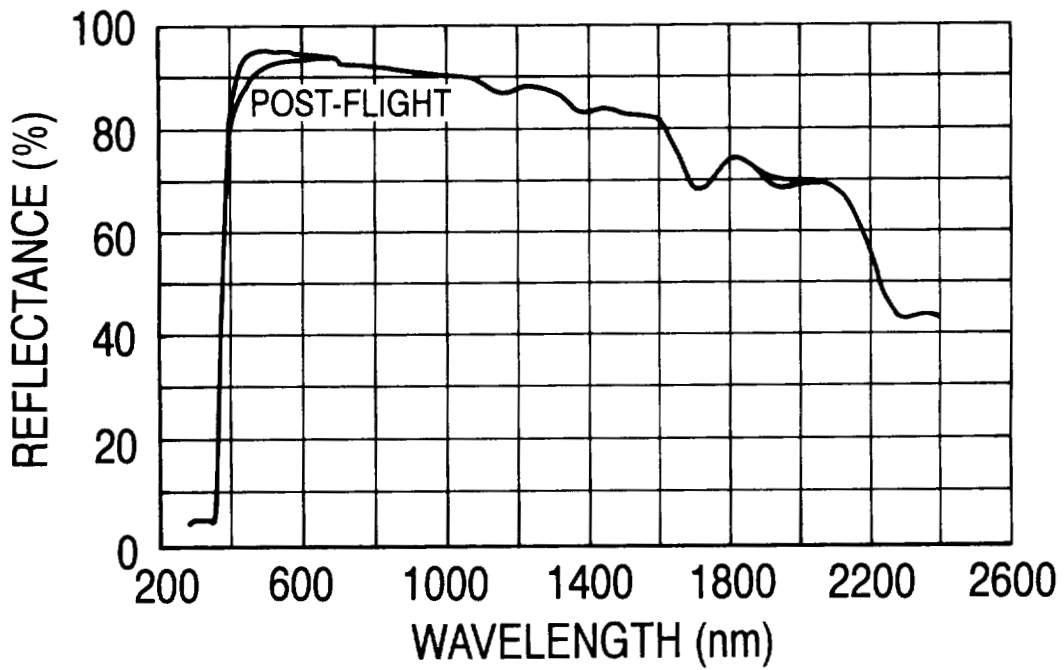


Figure 19. Reflectance of RTV-615/Silicone-Treated ZnO.

5. CONCLUSIONS

The four material coatings aboard the LDEF that were exposed directly to the space environment at an orbit of 260 nautical miles for 10 months, beginning 1 month after launch, have exhibited the following.

- **1000 Å of SiO_x on Kapton**--The sample of SiO_x was uniformly eroded. The concentrations of O and Si remained constant. Some improved reflectance occurred below 450 nm and above 700 nm.
- **100 Å In₂O₃ on VDA/Kapton**--The sample was severely eroded, with the indium reduced to less than 0.95 atomic % in comparison to the unexposed sample at 7 atomic %. The color changed from gold to gray. Kapton was exposed to the eroded areas and it exhibited substantial erosion. Losses of 5% to 10% in reflectance resulted below 450 nm and between 600 and 1600 nm.
- **RTV-615 Devolitized on Aluminum**--The sample surface shows erosion and banded networks originating from focal points. Carbon content dropped significantly. The Si concentration remained constant while the O concentration doubled with respect to the reference sample. Reflectance losses of about 5% occurred throughout the analyzed spectrum.
- **RTV-615 Silicate-Treated ZnO**--The flight sample surface changed from flat white to slightly glossy white. The C concentration decreased by about 21 atomic % while the O concentration increased by 18 atomic %, as the surface was etched. A comparable etching of the reference sample indicates a C drop of 7 atomic % and an O increase of 2 atomic %. No Zn and K were found, indicating either erosion or penetration deeper into the coating. Some loss of reflectance is noted at the wavelengths between 400 and 700 nm, and between 1800 and 2100 nm. The silicone was eroded.

An evaluation of the O reaction efficiency for the coatings exposed to a total O fluence of about 2.6×10^{20} atoms cm⁻² was not possible. The material losses and recessions must have included outgassing products, but these could not be determined. However, from the above analyses, general indications of these coatings' performance in orbit was possible.

6. ACKNOWLEDGMENTS

The authors are grateful to the following coworkers for their contributions to this work: Gloria Oh, for the ESCA analyses; Wanda Peters, for the reflectance measurements; and Diane Kolos, for the microscopic examination of the samples.

7. REFERENCES

1. Young, Philip R. and W. S. Slemm, *Analysis of the LDEF-Exposed Silvered FEP Teflon Thermal Blanket Material*, NASA TM 104096, December 1991.
2. Kinard, William H. and G. D. Martin, *Long Duration Exposure Facility Space Environment*, NASA CP 3134, p. 34, 1991.
3. Stein, Bland A., LDEF Materials Overview, *LDEF--69 Months in Space*, NASA CP 3194, pp. 741-789, April 1993.
4. Banks, B., et al., *Atomic Oxygen Effects on Materials*, NASA CP 3035, June 1988.

Organic Matrix Composite Protective Coatings for Space Applications*

Harry Dursch and Pete George
Boeing Defense and Space Group
P.O. Box 3999, M/S 82-32
Seattle, WA 98124
Phone: 206-773-0527, Fax: 206-773-4946

5/18-23
44432
18f

ABSTRACT

Successful use of composites in low Earth orbit (LEO) depends on their ability to survive long-term exposure to atomic oxygen (AO), ultraviolet radiation, charged particle radiation, thermal cycling, and micrometeoroid and space debris. The AO environment is especially severe for unprotected organic matrix composites surfaces in LEO. Ram facing unprotected graphite/epoxy flown on the 69-month Long Duration Exposure Facility (LDEF) mission lost up to one ply of thickness (5 mils) resulting in decreased mechanical properties. The expected AO fluence of the 30 year Space Station Alpha mission is approximately 20 times that seen on LDEF. This exposure would result in significant material loss of unprotected ram facing organic matrix composites. Several protective coatings for composites were flown on LDEF including anodized aluminum, vacuum deposited coatings, a variety of thermal control coatings, metalized Teflon, and leafing aluminum. Results from the testing and analysis of the coated and uncoated composite specimens flown on LDEF's leading and trailing edges provide the baseline for determining the effectiveness of protectively coated composites in LEO. In addition to LDEF results, results from Shuttle flight experiments and ground based testing will be discussed.

INTRODUCTION

As with all other spacecraft materials, successful use of composites in space depends on their ability to survive the various environments encountered during the spacecraft mission. Both AO and particulate radiation can cause a loss of mechanical properties. Thermal cycling induced microcracking results in dimensional stability and mechanical/thermal property changes. The very low vacuum levels of space cause moisture desorption resulting in dimensional changes and possible contamination of sensitive optics. High velocity impacts from meteoroid or space debris may result in cratering, penetration, or structural damage. Choosing the right coating can control or eliminate these environmental effects. The location on the spacecraft (internal vs external), orientation of the composite surface to the spacecraft's ram direction (orbital velocity vector), and the mission profile determine both the need for and the type of protective coating.

* Authorship of this paper was funded by NAS1-19427, Task 8. Testing of LDEF coated composites at Boeing Defense & Space was funded by Boeing IR&D.

PRECEDING PAGE BLANK NOT FILMED

The effects of the various space environments on unprotected organic matrix composites are summarized in the following paragraphs (references 1-4 contain papers discussing additional details).

- Atomic oxygen: AO induced erosion of bare composites is the most detrimental LEO environmental effect. Leading edge erosion has been well documented on the numerous bare composite specimens flown on LDEF's leading or near leading edges (total ram facing AO fluence was 9.09×10^{21} atoms/cm²). Typical depth of erosion loss of unprotected ram facing graphite epoxy (Gr/Ep) was approximately 0.005 inches or one ply of material. This loss resulted in reduced mechanical properties due to the reduced cross-section. AO did not cause any bulk changes in composites.

- Ultraviolet radiation: Minimal effect on composites. Limited to darkening of the surface resin layer

- Meteoroid and Debris: Composites retrieved from LDEF showed numerous impacts with the diameter and depth dependant upon the size and collision velocity of the impactor. Impact features on these composites generally took the form of broken fibers with missing matrix material. In some cases the diameter of the affected volume increased with depth (ref. 5)

- Particle Radiation: The threshold particle radiation dosage for organic matrix composite property degradation is approximately 10^8 to 10^9 rads, well above the total dosage seen by LDEF.

- Thermal Cycling: Thermistors on bare composite specimens flown on LDEF's indicated a maximum and minimum of approximately +180°F and -50°F over the first 4000 cycles of the 32,422 cycles seen by LDEF (ref. 6).

Figures 1 - 3 show three different Boeing built graphite fiber composite spacecraft structures, each possessing different protective coating requirements. Figure 1 is a photo of the Gr/Ep Hubble Space Telescope truss structure. This internal structure is shielded from any external environment with its temperature determined by the various layers of the spacecraft between it and the external spacecraft surfaces. This 252 lb structure highlights a property that composites provide, dimensional stability. The 16 ft focal length between the primary and secondary mirror supports is designed and manufactured to remain within 0.00005 of an inch during the temperature cycling associated with the LEO environment. Figure 2 shows a Gr/Ep antenna designed for use in a geosynchronous orbit (GEO) environment. The 6 ft diameter reflector has a base coating of vacuum deposited aluminum (VDA) overcoated with white inorganic coatings (YB-71 and Z-93). The VDA enhances the rf reflectivity and also serves as a good primer for the two inorganic coatings which provide passive thermal control. This coating scheme was subjected to twenty +250°F to -320°F thermal cycles and then exposed to high levels of particle radiation exposure. Test results met all program requirements. Although this coating scheme provides an excellent AO barrier, because of the GEO mission profile, AO protection was not a requirement. Figure 3 shows a prototype graphite/cyanate ester satellite bus structure designed for small launch vehicles such as Pegasus. This structure requires an exterior coating that 1) rejects heat generated by experiments mounted on decks within the structure and 2) provides protection for the thin exterior composite facesheet from AO induced erosion.

PROTECTIVE COATINGS

The use of a well designed and stable protective coating on externally mounted organic matrix composites both protects the underlying composite substrate from the exterior environment and alters the bare composite optical properties, resulting in reduced temperature extremes. Table 1 shows various protective coatings along with the range of optical properties possible with each coating.

Material	Solar Absorptance	Thermal Emittance
Bare Composite		
T300/934	0.90	0.73
Adhesively Bonded Aluminum Foil		
Bare aluminum foil	0.08 - 0.17	0.03
Chromic acid anodized - 1145 Al alloy	0.20 - 0.39	0.15 - 0.62
Chromic acid anodized - 6061 Al alloy	0.48 - 0.57	0.18 - 0.69
Sulfuric acid anodized - 5657 Al alloy	0.15 - 0.20	0.78 - 0.84
Vacuum Deposition		
Sputtered Al (420Å - 2520Å) smooth Gr/Ep surface	0.16	0.05 - 0.09
Sputtered Al (420Å - 2520Å) rough Gr/Ep surface	0.24	0.19 - 0.30
Vacuum deposited Al	0.22	0.04
Thermal Control Paints		
Z-93	0.14 - 0.17	0.92
YB-71	0.07 - 0.13	0.89 - 0.90
YB-71/Z-93	0.10	0.85
S13G/LO	0.15 - 0.19	0.88 - 0.91
A-276	0.21	0.87
Other Coatings		
Silverized Teflon (5 mil thick)	0.06	0.81
Silverized Teflon (2 mil thick)	0.07	0.66
Plasma sprayed aluminum	0.28	0.80

Table 1. Composite Protective Coatings

Ground based testing provides the initial screening for these coatings. Actual on-orbit exposure data is needed to verify ground based results and develop the necessary design confidence prior to these coatings being applied to spacecraft surfaces. Coatings flown on LDEF provide this data which has become the baseline for predicting coating performance in a LEO environment. It is interesting to note that LDEF was deployed prior to a thorough understanding of the effects of AO on organic composites. The coatings flown on LDEF composite specimens were selected as thermal control coatings. However, the majority of these coatings provided excellent AO protection. The following lists identify composite coatings that have been flown in space and undergone post-flight testing and analysis.

Protectively coated composites flown on LDEF:

- A-276 white titanium dioxide pigment in polyurethane binder with epoxy polyamide primer.
- BMS 10-60: white titanium dioxide pigment in polyurethane binder
- S13G: white zinc oxide in RTV 602 silicone binder (unknown if this was S13G/LO)
- White zinc oxide coating manufactured by General Dynamics
- Z-306: black carbon in polyurethane binder
- Tin/indium eutectic coating
- Leafing aluminum with epoxy binder with an epoxy polyamide binder
- Sputtered coatings: aluminum, aluminum/nickel, SiO₂/nickel, SiO₂/aluminum/nickel, SiO₂/chromium
- Aluminum thermal control tape

Composite coatings (without composite substrates) flown on LDEF:

- Chromic acid anodized aluminum
- Sulfuric acid anodized aluminum
- Z-93: white zinc oxide in a potassium silicate binder
- YB-71: white zinc orthotitanate (ZOT) in a potassium silicate binder
- YB-71 overcoated Z-93 combination
- Adhesively bonded silverized Teflon

Protectively coated composites flown on Shuttle experiments:

- Sputtered coated composites flown on STS-8, STS-41G, and STS-46 (EOIM-3)

TEST RESULTS

The following sections describe the results of ground based testing and testing of retrieved specimens for each category of protective coatings. Table 2 shows representative changes in optical properties of coatings flown on LDEF. The pre-flight values were taken prior to LDEF's deployment, the control values represent data taken on lab specimens after LDEF's retrieval, and the shielded specimens were either specimens facing LDEF's interior protected from the external environment or backsides of composite substrates on LDEF's exterior.

Specimen	Optical property	Preflight	Postflight (69 month exposure)			
			Control	Shielded	Leading	Trailing
Bare composite - graphite/epoxy	α	0.90		0.90	0.93	0.87
	ϵ	0.73		0.81	0.93	0.82
S13G-LO (ref. exp. S0069)	α	0.18			0.37	
	ϵ	0.90			0.89	
S13G/composite (McDonnell Douglas ctg)	α		0.14		0.19-0.21	0.34
	ϵ		0.90		0.88	0.89
Zinc Oxide (General Dynamics ctg)			0.48	0.46-0.59*	0.37	0.68
			0.89	0.88	0.92	0.88
A-276 (ref. exp. S0069)	α	0.25			0.24	
	ϵ	0.90			0.93	
TiO ₂ (A-276?)/composite (McDonnell Douglas ctg)	α			0.31	0.29	
	ϵ			0.90	0.94	
TiO ₂ (A-276?)/composite (General Dynamics ctg)			0.22	0.38-0.45*	0.35	0.59
			0.87	0.87	0.89	0.86
Leafing Aluminum/ composite	α		0.67	0.66	0.60	0.75
	ϵ		0.79	0.78	0.73	0.78
Z-93 (ref. exp. S0069)	α	0.14			0.15	
	ϵ	0.91			0.92	
YB-71 (ref. exp. S0069)	α	0.13			0.15	
	ϵ	0.90			0.89	
YB-71 over Z-93 (ref. exp. S0069)	α	0.10			0.11	
	ϵ	0.85			0.87	
CAA Al (tray clamps)	α	0.32	0.36	0.34	0.33	0.35
	ϵ	0.16	0.18	0.16	0.15	0.15
CAA Al (Exp S0010) - thick CAA	α	0.34			0.35	
	ϵ	0.75			0.75	
Silverized Teflon - 5 mil thick	α		0.07		0.07	0.08
	ϵ		0.81		0.78	0.81

* solar absorptance range due to varying amounts of contamination

Table 2. Optical Properties of Protective Coatings Flown on LDEF.

Anodized Aluminum Foil

Ground Based Testing

A series of NASA LaRC funded research tasks led to the selection of chromic acid anodized (CAA) aluminum foil as the optimum protective coating for Space Station's composite (now aluminum) truss structure. Reference 7 summarizes the findings of these studies into the development of sputter coatings applied directly to composite substrates and on adhesively bonded anodized aluminum foil. Other coatings evaluated included nickel-based coatings. Co-cured 0.002 inch thick CAA foil adhesively bonded to the 2 inch diameter composite tubes with a 0.003" thick layer of epoxy film adhesive was selected as the preferred coating for the following reasons:

- Environmental durability to the LEO environment including retention of foil to composite bond strength and retention of optical properties following 5000 hours of simulated UV exposure.
- Optical tailorability. As shown in Table 1, optical properties can be tailored to individual mission requirements by altering the anodizing parameters and/or aluminum alloy.
- Diameter of impact hole doesn't change with time limiting the amount of composite substrate subject to AO exposure following a meteoroid or space debris impact.
- Provides moisture/outgassing barrier.
- Anodizing and bonding process specifications developed.
- Excellent handling and abrasion resistance.
- Low cost and ease of manufacture.
- Excellent thermal conductivity minimizing temperature gradients due to shadowing of nearby structures.

Testing of Retrieved Hardware

No composites protectively coated with anodized aluminum foil have been flown on retrieved spacecraft hardware. However, CAA aluminum was used as part of LDEF's passive thermal management. The trays, tray clamps, space end thermal covers, and exposed surfaces of the primary structure were all CAA aluminum. This resulted in over 50% of the exposed surfaces on LDEF consisting of CAA aluminum. In addition, several LDEF experimenters flew CAA, sulfuric acid anodized, and dyed sulfuric acid anodized specimens that were anodized to a variety of thicknesses and optical properties. Results indicate that the CAA was very stable in its optical properties, but that contamination caused small increases in absorptance on surfaces exposed to low AO fluences. Sulfuric acid anodized surfaces appeared stable, although very little surface area was available for evaluation and no specimens were exposed to a high AO fluence environment. Only one type of dyed sulfuric acid anodize (Martin Black Anodize) was flown on LDEF. This specimen had increased infrared absorptance characteristics following its trailing edge exposure on LDEF (ref. 8).

Vacuum Deposition

Testing of Retrieved Hardware

Composite substrates sputter coated with a variety of materials and thicknesses were flown on the leading edge experiment S0010, Exposure of Spacecraft Coatings. The combination of materials sputtered onto the Gr/Ep substrates were: aluminum, aluminum/nickel, SiO₂/nickel, SiO₂/aluminum/nickel, SiO₂/chromium, and aluminum/chromium. Figure 4 shows post-flight photos of two 1-in² Gr/Ep specimens flown on this experiment. The specimen on the left was uncoated while the specimen on the right was sputter coated with 600Å SiO₂ over 1000Å nickel. The outer-edge region of both specimens was protected by an aluminum holding fixture. The textured appearance is

the pattern of the breather cloth left in the resin rich surface during specimen fabrication. The 45-degree band pattern, for the uncoated specimen is most likely due to tow-to-tow material variations resulting in different erosion rates. The coated specimen exhibited no mass loss while the uncoated specimen lost 3-4 mils of material. Post-flight testing and analysis showed that while a total coating thickness of 400 Å retarded AO induced Gr/Ep erosion, total coating thicknesses as thin as 800 to 1000 Å eliminated any mass loss (ref. 9). Additional results also showed that rough surface morphology of composites can result in numerous protective coating defects of these ultra-thin coatings (ref. 10).

Space Shuttle flight STS-8, launched in September 1983, flew three sputtered coatings deposited on Gr/Ep substrates. Table 3 shows the various materials, thicknesses, and pre-flight and post-flight optical properties. Post-flight test results show the three coatings were generally unaffected by the 42 hour ram facing (3.5×10^{20} atoms/cm²) Shuttle exposure (ref. 11).

Specimens	Pre-flight α/ϵ	Post-flight α/ϵ
1600 Å of 0.999% pure nickel	0.52/0.45	0.52/0.45
600 Å SiO ₂ over 1600 Å nickel	0.50/0.27	0.49/0.27
800 Å Al ₂ O ₃ over 1800 Å aluminum	0.29/0.78	0.29/0.78

Table 3. Optical Properties of STS-8 Specimens

Thermal Control Paints with Composite Substrates

Testing of Retrieved Hardware

Over 55 organic matrix/graphite composite substrates overcoated with thermal control coatings were flown on LDEF. The specific coatings, A-276, BMS 10-60, S13G, Z306, leafing aluminum, zinc oxide mfg by General Dynamics, and an indium-tin eutectic were exposed to leading edge, trailing edge, and shielded environments on LDEF. Laboratory control specimens were also kept for the duration of LDEF's 69 month mission.

M0003-10 Results

LDEF Experiment M0003-10, Advanced Composites Experiment, included specimens supplied by McDonnell Douglas Space Systems Company (MDSSC) and General Dynamics Space Systems Division (GDSSD) to determine the effectiveness of protective coatings. MDSSC evaluated the TiO₂ (post-flight analysis shows this coating to most likely be A-276), S13G (unable to determine if this was S13G/LO), and leafing aluminum coated graphite/polyimide, Gr/Ep, and graphite/thermoplastic substrates. GDSSD evaluated TiO₂ (post-flight analysis and discussions with retired GDSSD personnel determined this coating was most likely A-276), ZnO (this was a proprietary coating developed by GDSSD somewhat similar to the S13G coatings), and an indium-tin eutectic coating (developed by GDSSD as a moisture barrier to prevent on-orbit composite dimensional changes associated with moisture desorption) protecting graphite-fiberglass fabric/polysulfone and graphite/epoxies. Most of the samples were composite strips 3.5 inches long x 0.5 inches wide with the coating applied to all six sides. Pre- and post-flight mass loss data was taken by The Aerospace Company (M0003 experiment integrator). Additional post-flight characterization occurred at Boeing Defense & Space including optical properties, cross-sectioning, and coating adhesion.

The optical properties for the TiO₂ coated specimens were typical of results found on A-276 coatings mounted throughout LDEF and provide an interesting study into the synergistic effects of the LEO environment. The leading edge AO fluences were high

enough to cause enough erosion of the polyurethane paint binder, removing the UV darkened binder seen on the trailing edge specimens. This AO induced erosion kept the UV damaged paint near original pre-flight absorptance levels. However, this erosion leaves the surface layers of the TiO₂ pigment in the A-276 without any binder. While the optical properties had not changed, the surface layers had lost their physical integrity and are easily damaged upon contact. The trailing edge specimens increased in solar absorptance due to the UV exposure darkening the polyurethane resin (no AO "cleansing" of the A-276). Tape peel testing on a leading edge specimen removed the pigment down to the stable binder. No material was removed during tape peel testing of shielded or control specimens. No erosion of the substrates was observed. Post-flight inspection showed that all the GDSSD woven graphite-fiberglass fabric/polysulfone (W-722/P-1700) specimens (coated, uncoated, lab control, and flight) had significant cracking. It is unknown if the cracking was present following cure or whether it slowly developed over time. The cracking was most likely due to coefficient of thermal expansion (CTE) mismatches between the fiberglass, graphite, and polysulfone matrix. On the coated specimens, these cracks extended up through the TiO₂ coating as shown in Figure 5. Photomicrographs taken at 400x appear to show minor AO induced erosion of the composite through the larger cracks on the leading edge.

Figure 6 shows leading edge and trailing edge MDSSC S13G coated composite specimens. The control and trailing edge optical properties were typical of LDEF data with the trailing edge specimen taking on a strongly discolored yellow appearance. The leading edge specimen took on a lightly discolored brown appearance but it experienced a much smaller increase in absorptance than other leading edge S13G/LO specimens. Unlike the A-276, tape peel tests showed no material removed from any of the specimens. Similar cracking was visible in the GDSSD ZnO coated W-722/P-1700 specimens as occurred in their TiO₂ coated specimens.

Figure 7 shows leading edge, trailing edge, and shielded leafing aluminum coated composite specimens. The leafing aluminum coating consists of aluminum flakes in an epoxy binder applied to a primed composite substrate. No other leafing aluminum specimens were flown on LDEF. Like the A-276 coated composites, the leafing aluminum specimens illustrate the synergistic effects of the LEO environment. The decrease in absorptance and increase in emittance for the leading edge specimen is attributed to removal of the epoxy binder exposing additional aluminum flakes. The increase in absorptance for the trailing edge specimen was caused by UV darkening on the epoxy binder. Tape peel testing removed some of the unsupported aluminum flakes on the leading edge specimen. No material was removed during tape peel testing of the control or trailing edge specimens. No erosion of the underlying composites was noted.

The indium-tin eutectic coating was developed as a composite moisture barrier. Minor visual differences between leading and trailing edge specimens with the exposed surfaces becoming dull and discolored compared to the control specimen. No erosion of the underlying composites was noted.

Pre- and post-flight mass loss data was taken by The Aerospace Company for all composite specimens flown on Experiment M0003-10 and all laboratory control specimens. These measurements were made after the samples had equilibrated in a constant temperature and humidity environment which eliminated moisture variations. The majority of the coated composite data is shown in Table 4. Analysis of this data illustrates the effectiveness of the coatings in protecting the underlying composite substrate from AO induced erosion. LDEF data showed that leading edge bare composites underwent a 2% to 4% mass loss. The coatings reduced this mass loss to negligible amounts similar to shielded or lab control specimens.

Specimen location	Uncoated - % mass change (# of specimens)	Coated - % mass change (# of specimens)
Leading edge - exposed	- 2.15 (1)	+ 0.02 (2)
Leading edge - shielded	- 0.41 (2)	- 0.07 (2)
Trailing edge - exposed	- 0.19 (1)	+ 0.73 (1)
Trailing edge - shielded	- 0.05 (2)	- 0.56 (1)
Lab control	- 0.17 (3)	- 0.05 (3)

Indium-Tin Eutectic Coating on GY70/X-30 Graphite/Epoxy flown by GDSSC.

Specimen location	Uncoated - % mass change (# of specimens)	Coated - % mass change (# of specimens)
S13G - Celion 6000/polyimide	-	+ 0.14 (1)
S13G - T300/5208	-	- 0.12 (1)
S13G - T300/P-1700	-	- 0.02 (1)
Leafing Al - T300/P-1700	-	- 0.41 (2)
TiO ₂ - T300/P-1700	-	- 0.18 (1)

Various coatings with various substrates flown by MDSSC. All specimens located on leading edge-exposed. No lab controls or uncoated specimens.

Specimen location	Uncoated - % mass change (# of specimens)	Coated - % mass change (# of specimens)
S13G - Trailing edge exposed	-	- 0.04 (2)
Leafing Al - Trailing edge exposed - Trailing edge shielded	- - -	- 0.11 (1) + 0.05 (1)
TiO ₂	-	+ 0.01 (1)

T300 Graphite/Polyether Sulfone with various coatings flown by MDSSC. No lab controls or uncoated specimens.

Specimen location	Uncoated - % mass change (# of specimens)	ZnO Coated - % mass change (# of specimens)	TiO ₂ Coated - % mass change (# of specimens)
Leading edge - exposed	- 2.80 (2)	- 0.37 (6)	- 0.33 (6)
Leading edge - shielded	- 0.63 (2)	- 0.12 (6)	- 0.13 (6)
Trailing edge - exposed	- 0.08 (3)	- 0.04 (3)	- 0.03 (3)
Trailing edge - shielded	- 0.09 (3)	- 0.03 (3)	- 0.02 (3)
Lab control	- 0.07 (4)	- 0.01 (4)	- 0.03 (4)

Graphite-Fiberglass Fabric (W-722)/P-1700 with ZnO and TiO₂ coatings flown by GDSSD

Table 1. Mass changes for coated composite substrates flown on M0003-10 (data courtesy of The Aerospace Corporation).

M0003-8 Results

The electronics module cover for the leading edge experiment M0003-8 was an 11.75" x 16.75" Gr/Ep panel with thermal control coatings in three of the four quadrants. The following paragraphs summarize findings presented in reference 12. This panel was coated with two white urethane coatings, A-276 and BMS 10-60, and a black urethane coating, Z306. The fourth quadrant was left bare. One inch diameter mounting washers located at the corners and along each side shielded the underlying composite and coating. Temperature extremes were predicted, using pre- and post-flight optical properties, for each quadrant with the results showing maximum and minimum temperatures of 235°F to -70°F for the uncoated quadrant, 205°F to -70°F for the Z306 coated quadrant, and 60°F to -75°F for both the A-276 and BMS 10-60 quadrants. The bare composite lost an average of over 0.003 inches and the white coated quadrants showed no underlying composite erosion due to shielding by the AO stable TiO₂ pigment. The Z306 coating was severely eroded as both the carbon pigment and the polyurethane matrix were eroded by the AO. Some initial attack of the substrate under the Z306 coating was apparent. Extensive microcracking was observed in the black Z306 and bare quadrants. These cracks extended approximately one inch into the two white coated quadrants. The cracks, which appear to be related to thermal stresses, propagate up through the white coatings.

Figure 8 is a 3D plot of the data collected during a laser profilometry scan of a portion of the module cover. The approximately 1 inch square contains a circular region shielded from AO attack by one of the mounting washers. The A-276 coating covers the rear left half of the panel segment. This shows several interesting features including three distinct height levels, contaminant shielded area, and an impact site.

The five most prominent impact sites in this panel were cross-sectioned to investigate coating and substrate damage (figure 9 shows four of these five impacts). All five impacts happened to occur in the A-276 coated quadrant and were severe enough to have breached the coating, exposing the underlying composite. The deepest crater (upper right-hand corner) was over 0.015" deep (three plies). These impacts have many of the same features along with some distinct dissimilarities. Four of the five displayed an inverted hat shape (three very strongly) with the fifth impact site (lower right-hand corner), which does not have this shape, displays extensive crushing and displacement of material. No indications of A-276 coating undercutting by AO were visible in any of the five sites.

As shown in figure 9, pin-hole or impact damage through coatings will expose the underlying composite to AO attack. Reference 13 discusses an analytical approach used to determine reduction in properties of two-inch diameter Gr/Ep tubes from impact damage and subsequent AO induced erosion. Results show a hole diameter ≤ 0.2 " completely through a 0.06" thick tube causes a maximum reduction in the tube's EI (stiffness x inertia) of only 7%.

Space Shuttle flight STS-46, launched in July, 1992, flew an experiment titled Evaluation of Oxygen Interactions with Materials Experiment-3 (EOIM-3) for 42 hours of ram facing exposure (2.3×10^{20} atoms/cm²). Included in the 82 different materials flown on EOIM-3 were three ceramic coated graphite/thermoplastic (PEEK) composites coated with boron nitride/alumina ($\alpha = 0.39/\epsilon = 0.80$), alumina (0.35/0.82), or a plasma sprayed alumina. No measurable changes in optical properties and no visual or mass loss changes occurred for the coated PEEK substrates (ref. 14). AO erosion of the unprotected PEEK was ≈ 2 microns. Post-flight ESCA did show a differentiation of constituents may have occurred during the application of the boron nitride coating. In addition to these EOIM-3 results, two bare Gr/Ep specimens that were previously flown on LDEF were flown again on EOIM-3. One specimen was from the LDEF's trailing edge and the other had been shielded on LDEF, exposed only to vacuum. EOIM-3 post-flight testing showed the LDEF shielded specimen eroded much faster than the specimen that had been exposed on LDEF's

trailing edge. ESCA analysis revealed that silicone contamination existed on the trailing edge specimen which provided some protection against AO erosion (ref. 15).

Ground Based Testing

Reference 16 discusses the results of The Aerospace Corporation's study into the effects of thermal cycling of YB-71 coated Gr/Ep substrates. A second goal of the study was to evaluate the quality of different coating application processes. Five specimens of Gr/Ep coated with VDA were distributed to five participants interested in testing zinc orthotitanate (ZOT) application procedures and the ability of ZOT coatings to withstand thermal cycling from -275°F to +265°F. The participants were Boeing, Hughes Aircraft Company, TRW, JPL, and IITRI (manufacturer of YB-71). While results showed a variation in coating adhesion between the five sets of specimens, all the ZOT coatings performed adequately up to the maximum number of thermal cycles, 440.

Thermal Control Paints without Composite Substrates

Testing of Retrieved Hardware

The Z-93 and YB-71 coatings flown on LDEF were almost unchanged after the 69 month mission. The YB-71 overcoated Z-93 specimen also was impervious to the LEO environment (ref.17) LDEF results show that either coating is an excellent choice for long term LEO exposure. In fact, Z-93 has been selected as the radiator coating for the International Space Station Alpha.

Ground Based Testing

Thermal control coatings possessing a low solar absorptance and high thermal emittance are needed for the Space Station solar dynamic power module radiator surfaces. Eleven candidate materials including white thermal control coatings (Z-93, YB-71, and S13G/LO), silverized Teflon with oxide protective coatings, sulfuric acid anodized aluminum, and a plasma sprayed aluminum oxide coating, were evaluated. Results of extensive ground based testing showed the Z-93 and YB-71 to be the most durable and best performing coatings for this application since they maintained their optical properties and did not show cracking following AO exposure and thermal cycling (ref. 18).

Silverized Teflon

Testing of Retrieved Hardware

Silverized Teflon consists of a 2 mil or 5 mil thick first surface Teflon layer with a 1500Å layer of silver deposited onto the Teflon and a 100Å layer on inconel on the backside to protect the silver. Adhesively backed silverized Teflon is available from Sheldahl and has proven to be an excellent AO barrier. LDEF Experiment S0069 used pressure sensitive acrylic adhesive to adhere the 2 mil thick silverized Teflon to an aluminum facesheet. Post-flight observations showed a brownish discoloration of the silverized Teflon ranging from light to dark brown. The absorptance varied from 0.10 to 0.49 depending on the amount of discoloration. Post-flight testing and analysis showed that the technique used to apply the material to the aluminum covers excessively stressed the material resulting in cracking of the silver and inconel layers. This exposed the adhesive to UV (Teflon is transparent to UV) causing the discoloration. An improved application technique has been developed. Keeping the silverized Teflon flat during release paper removal and reducing squeegee pressure during application of the material to the substrate seems to have eliminated the damage to the silver and inconel (ref.19).

Post flight testing of LDEF ram facing 5 mil thick Teflon thermal blankets showed a Teflon thickness decrease of approximately 1 mil. Ram facing Ag/Teflon took on a milky

appearance and increased surface roughness resulting in decreased specularly. Minimal changes in solar absorptance or thermal emittance occurred for either leading or trailing edges specimens (ref. 20).

Silverized Teflon was also used on hardware retrieved from the Solar Maximum Measurement (SMM) experiment. This hardware was retrieved by the Space Shuttle STS-41C after 50 months in LEO (this Shuttle mission also deployed LDEF). SMM was launched in February 1980 in a 310 nm orbit. After 10 months attitude control malfunctions required that SMM be placed in a spin stabilized orbit until it was repaired 40 months later. By this time the orbit had decayed to 265 nm. Post-flight investigation of the silverized Teflon on the exterior surfaces of retrieved hardware showed changes similar to those found on similar material flown on LDEF. There was no change in absorptance or emittance but the outer surface of the Teflon had become rougher, described by SSM investigators as "bristle like" (ref.21).

SUMMARY

Adhesively bonded coatings - Ground based testing has shown adhesively bonded anodized aluminum foil co-cured or secondarily bonded to composites to be an excellent protective coating. On-orbit optical properties of chromic acid anodized aluminum have proven to be very stable and these properties can be easily tailored to a specific mission requirement by varying anodizing parameters and/or aluminum foil alloy. Aluminum foil also offers the best meteoroid and debris impact resistance of any of the coatings. If a breach of the coating does occur, the foil will limit the amount of AO reaching the underlying substrate. The limited information concerning sulfuric acid anodizing also shows this to be a stable coating but without the wide range of optical properties available in the chromic acid anodizing process. Anodized foil is best suited for tubular or flat structures as it can be difficult to apply to irregular shaped surfaces. In addition, the chromium anodizing facilities are slowly being phased out due to the health hazards associated with chromium.

Silverized Teflon is a widely used thermal control material possessing very low absorptance/emittance ratios. LDEF results showed that the application technique used for applying adhesively bonded silverized Teflon is critical in ensuring good on-orbit durability. Silverized Teflon has shown good long term on-orbit performances with the suitability of using this material to protectively coat composites dependant upon the charged particle or AO fluences seen during the mission (ref. 20).

Vacuum deposited coatings - LDEF results show that extremely thin sputtered coatings offer excellent atomic oxygen protection. Coatings as thin as 800Å eliminated any AO induced erosion of the composite substrate. Sputtering a layer of SiO₂ over the base metal layer provides the required emittance. For these coatings to be effective all composite surface irregularities must be adequately coated. The limitation to these coatings is the complexity associated with the need for vacuum during the coating process.

Thermal control coatings - Most space qualified thermal control coatings will provide the needed environmental protection and optical property retention for short term missions. The organic based coatings, such as S13G/LO and A-276, offer a good coefficient of thermal expansion (CTE) match with composite substrates and good coating/composite adhesion strength. For longer term missions two IITRI coatings, YB-71 and Z-93, provide the necessary protection and retention of optical properties. While no Z-93 or YB-71 coated composites have been retrieved from space for post-flight testing, LDEF data has shown excellent optical property retention and good bond strength retention to aluminum substrates. Successful application of these brittle ceramic coatings to an organic composite

substrate is rather complex, requiring careful application on a contaminate free surface. The application process used on the antennas shown in figure 2 consisted of a layer of VDA applied to the composite surface followed by a layer of hand rubbed Z-93 and then a spray application of YB-71. Boeing is currently developing a ZOT application specification eliminating the need for VDA and hand-rub application of the Z-93. Future flight experiments will be needed to verify this approach.

ACKNOWLEDGEMENTS

Richard Mell, AZ Technologies for providing assistance in verifying the type of the coatings flown on M0003-10. The Aerospace Corporation's Corporate Archives for providing timely assistance in acquiring photos and post-flight observation information on the various coated composites flown on M0003-10.

REFERENCES

- 1) Levine, A.S: "LDEF 69 Months in Space, First LDEF Post-Retrieval Conference", NASA CP-3134, February 1992.
- 2) Stein, B. A, Young, P.R.: "LDEF Materials Workshop '91", NASA CP-3162, November 1991.
- 3) Levine, A.S: "LDEF 69 Months in Space, 2nd LDEF Post Retrieval Symposium", NASA CP-3194, June 1992.
- 4) Whitaker, A.F, and Gregory, J.: "LDEF Materials Results for Spacecraft Application Proceedings", NASA CP 3257, October 1992.
- 5) See, T., et al: "Meteoroid and Debris Impact Features Documented on the LDEF: A Preliminary Report.", August 1990, NASA JSC Report # 24608.
- 6) Steckel, G.L, and Le, T.D.: "M0003-10 Advanced Composites Experiment", LDEF 69 Months in Space, First LDEF Post-Retrieval Conference, NASA CP-3134, February 1992, Volume 2, page 1041.
- 7) Teichman, L.A, Slemp, W.S., and Witte, W.G.: "Evaluation of Selected Thermal Control Coatings for Long-Life Space Structures", NASA TM 4319, January 1992.
- 8) Golden, J.L.: "Anodized Aluminum on LDEF", LDEF Materials Results for Spacecraft Application Proceedings, NASA CP 3257, October 1992, page 61.
- 9) Slemp, W.S, Young, P.R., and Witte, G.: "Effects of LDEF Flight Exposure on Selected Polymer Matrix Resin Composite Materials", LDEF 69 Months in Space, First LDEF Post-Retrieval Conference, NASA CP-3134, February 1992, Volume 2, page 1149.
- 10) Banks. B.: "Issues/Considerations and Performance Prediction of LEO Protective Coatings", Protection of Materials and Surface Finishes from the Low Earth Orbit Space Environment, Canadian Space Agency Forum, February 1992.

- 11) Visentine, J.T.: "Atomic Oxygen Effects Measurements for Shuttle Missions STS-8 and 41-G", NASA Technical Memorandum 100459 - Volume 1, September 1988.
- 12) George, P.E., Dursch, H.W., and Hill, S.G.: "Space Environmental Effects on LDEF Composites: A Leading Edge Coated Graphite/Epoxy Panel", 2nd LDEF Post Retrieval Symposium, NASA CP-3194, June 1992, Volume 3, page 923.
- 13) Bowles, D.E., Tenney, D.R.: "Composite Tubes for the Space Station Structure", 18th International SAMPE Technical Conference, October 1986.
- 14) Chung, S.Y. et al: "Flight- and Ground-Test Correlation Study of BMDO SDS Materials: Phase 1 Report", JPL Publication 93-31, December 1993.
- 15) Golden, J.L, et al: "Analysis of Selected Specimens from the STS-46 EOIM-3 Experiment" 3rd LDEF Post-Retrieval Symposium, NASA CP-3275, 1995.
- 16) Binegar, G.A. and Welch, J.W.: "Thermal Cycling Performance of YB-71 Zinc Orthotitanate (ZOT) Coatings Applied to Graphite/Epoxy Panels", The Aerospace Corporation Report No. TOR-0090(5404-21)-1, September 1990.
- 17) Wilkes, D.R, Brown, M.J., and Hummer, L.L: "Initial Materials Evaluation of the Thermal Control Surfaces Experiment (S0069)", LDEF 69 Months in Space, First LDEF Post-Retrieval Conference, NASA CP-3134, February 1992, Volume 2, page 899.
- 18) Dever, J.A., et al: "Evaluation of Thermal Control Coatings for use on Solar Dynamic Radiators in Low Earth Orbit", NASA TM-104335, June 1991.
- 19) Zwiener, James, et al: "Unusual Materials Effects Observed on the Thermal Control Surfaces Experiment (S0069)", LDEF 69 Months in Space, First LDEF Post-Retrieval Conference, NASA CP-3134, February 1992, Volume 2, page 919.
- 20) Pippin, H.G., Stuckey, W.S., Hemminger, C.; "Performance of Silvered Teflon Control Blankets on Spacecraft", LDEF Materials Results for Spacecraft Application Proceedings, NASA CP 3257, October 1992, page 21.
- 21) Proceedings of the Solar Maximum Repair Mission Study Workshop, NASA GSFC Report 408-SMRM-79-0001, May 1985.

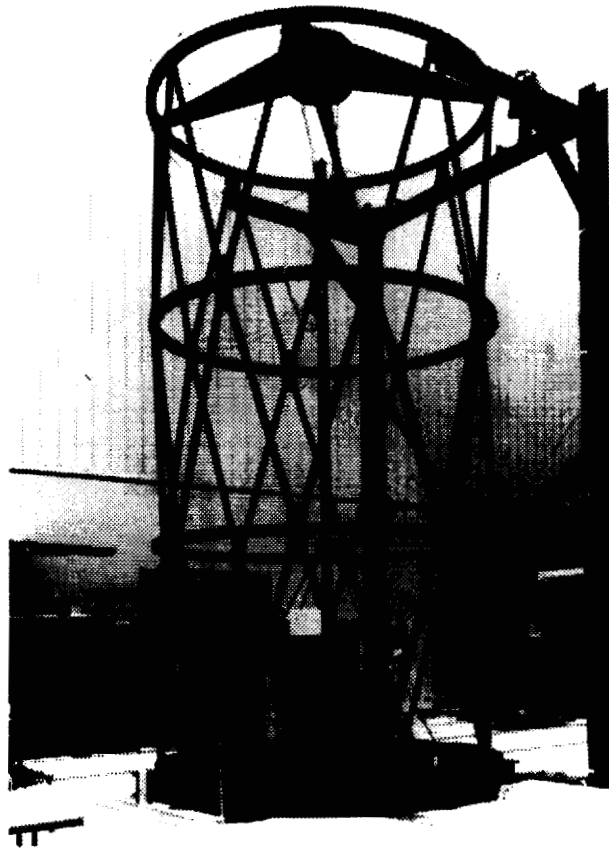


Figure 1. Hubble Space Telescope Optical Truss Assembly

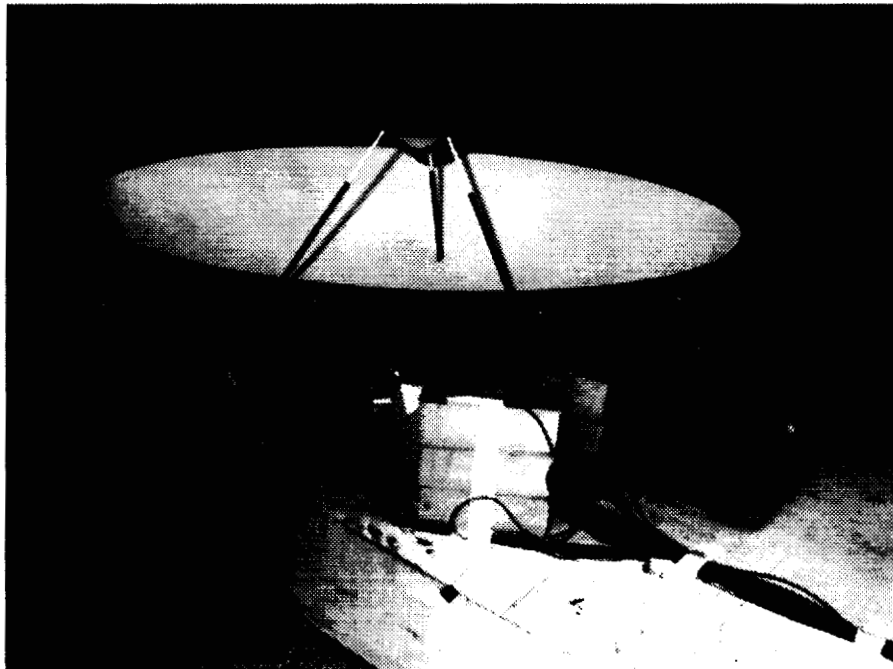


Figure 2. 6 Ft. Diameter Graphite/Epoxy Antenna

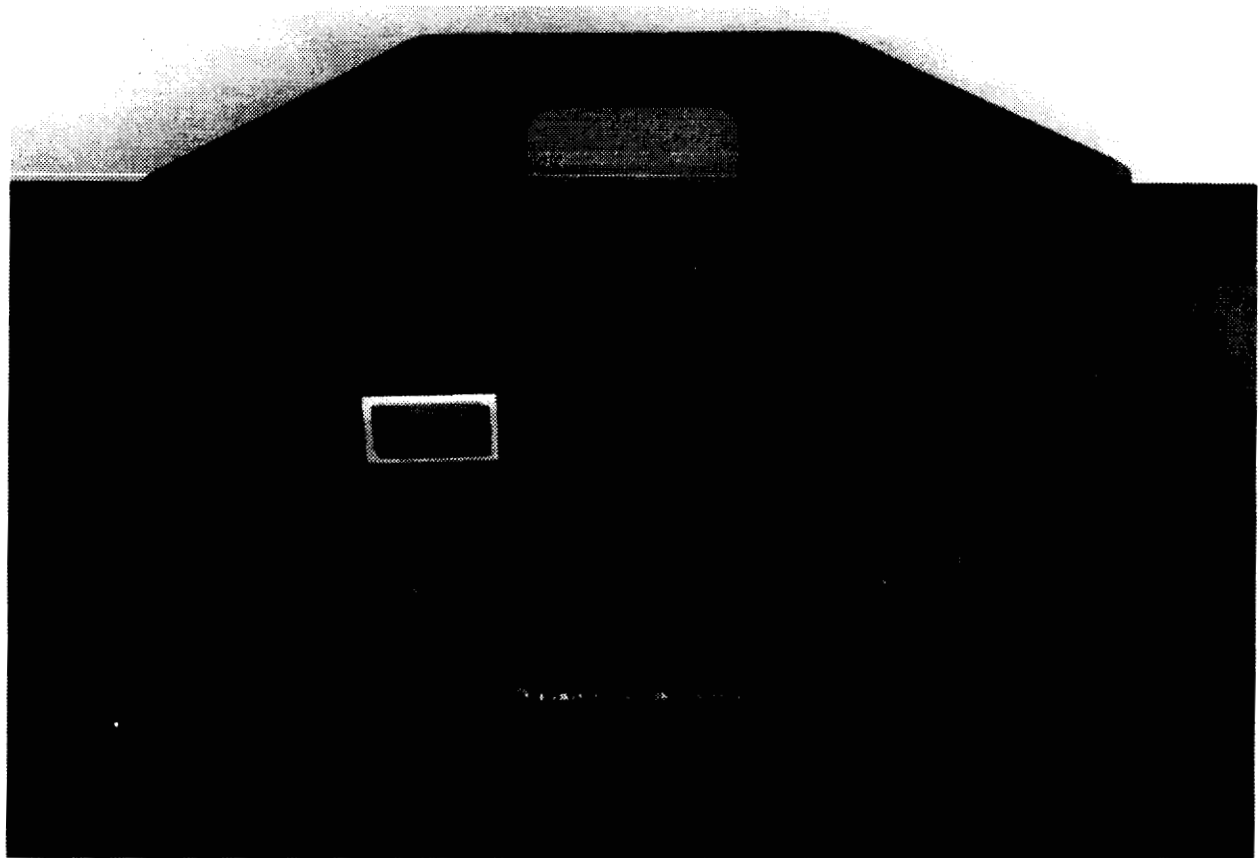


Figure 3. Prototype Composite Spacecraft Bus Structure

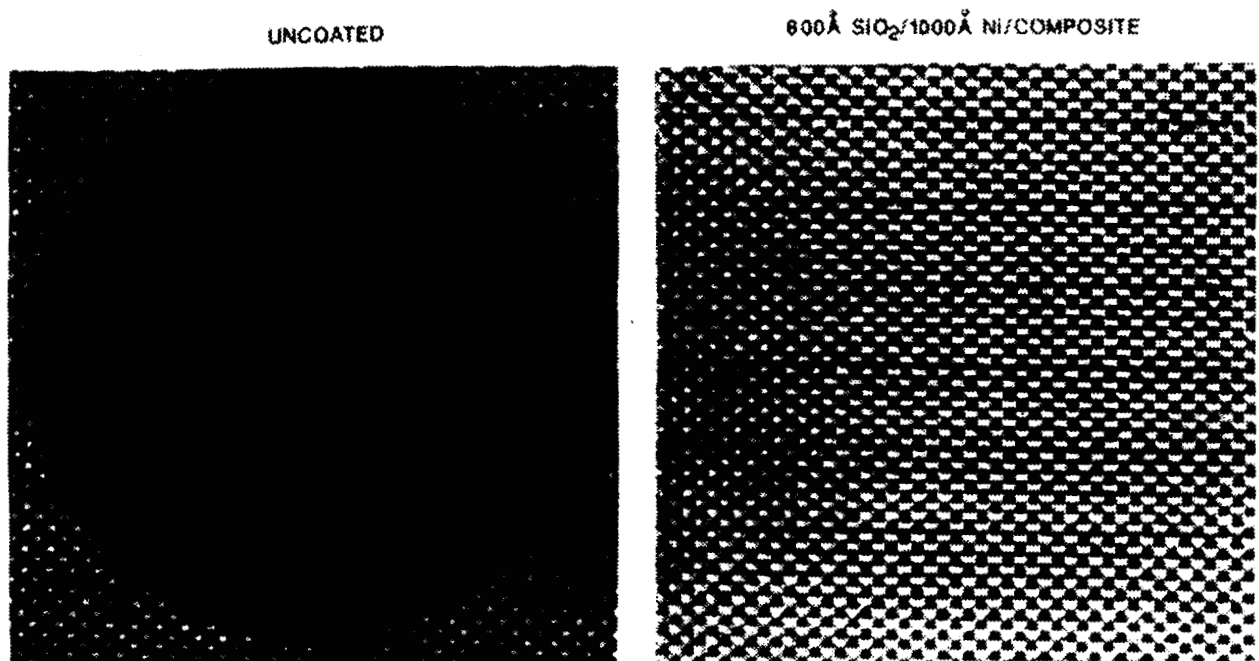


Figure 4. Bare And Protected Graphite/Epoxy Specimens Flown On LDEF's Leading Edge (Photo Courtesy of NASA LaRC)

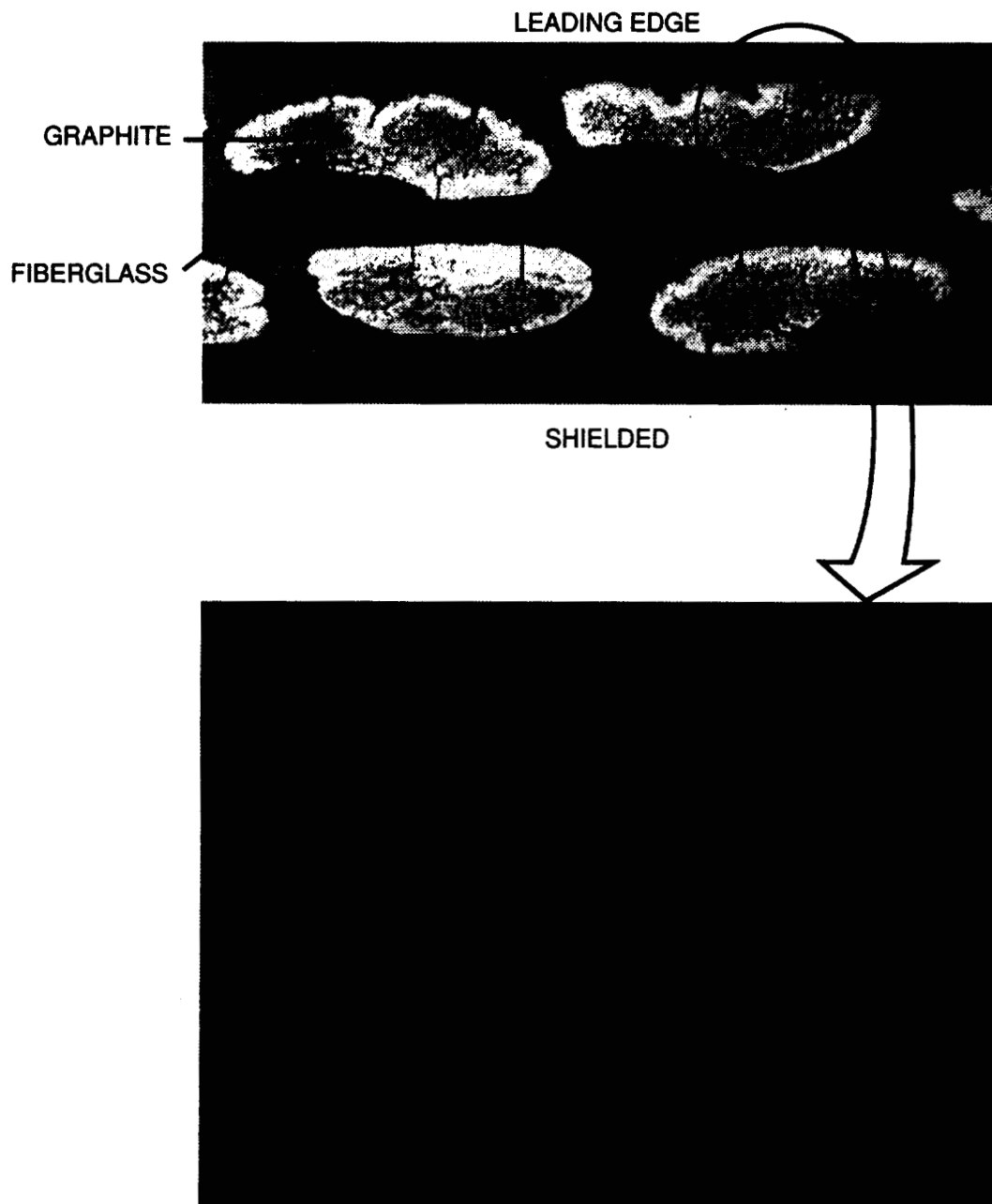


Figure 5. A-276 Coated Graphite-Fiberglass/Polysulfone Composite

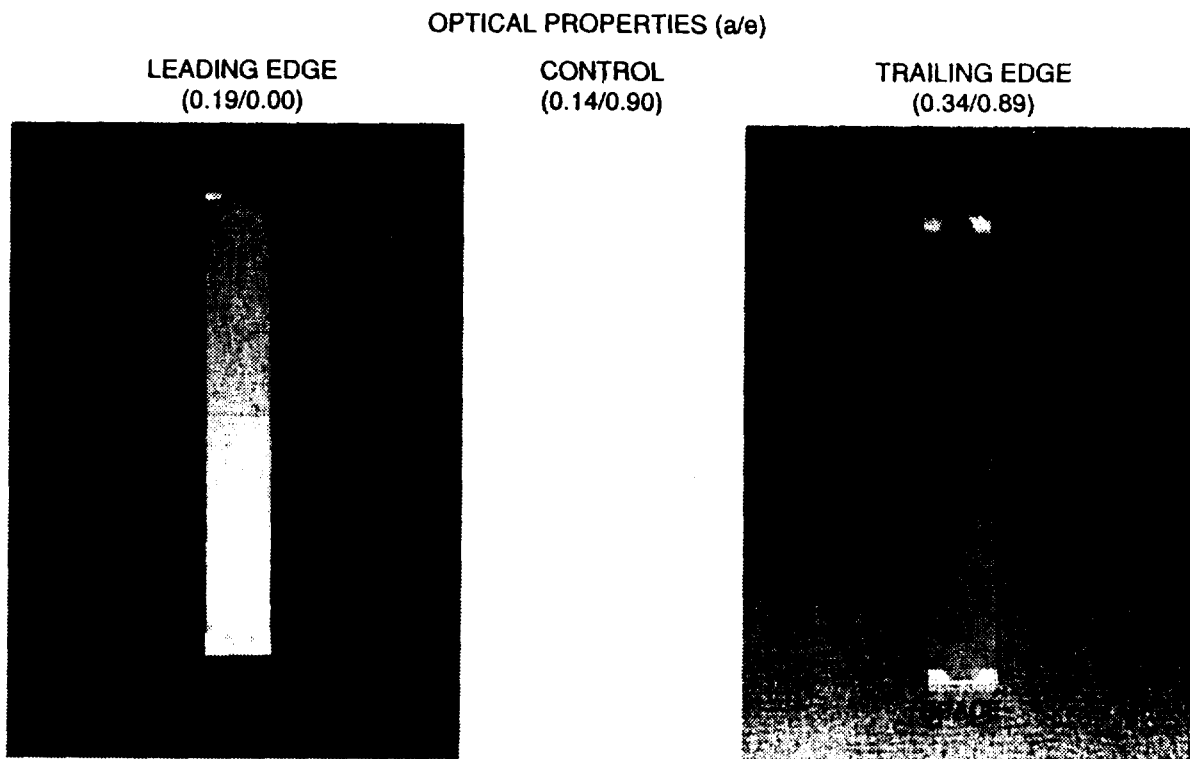


Figure 6. Effects Of LDEF Exposure On S-13G (Photos Courtesy of The Aerospace Corporation)

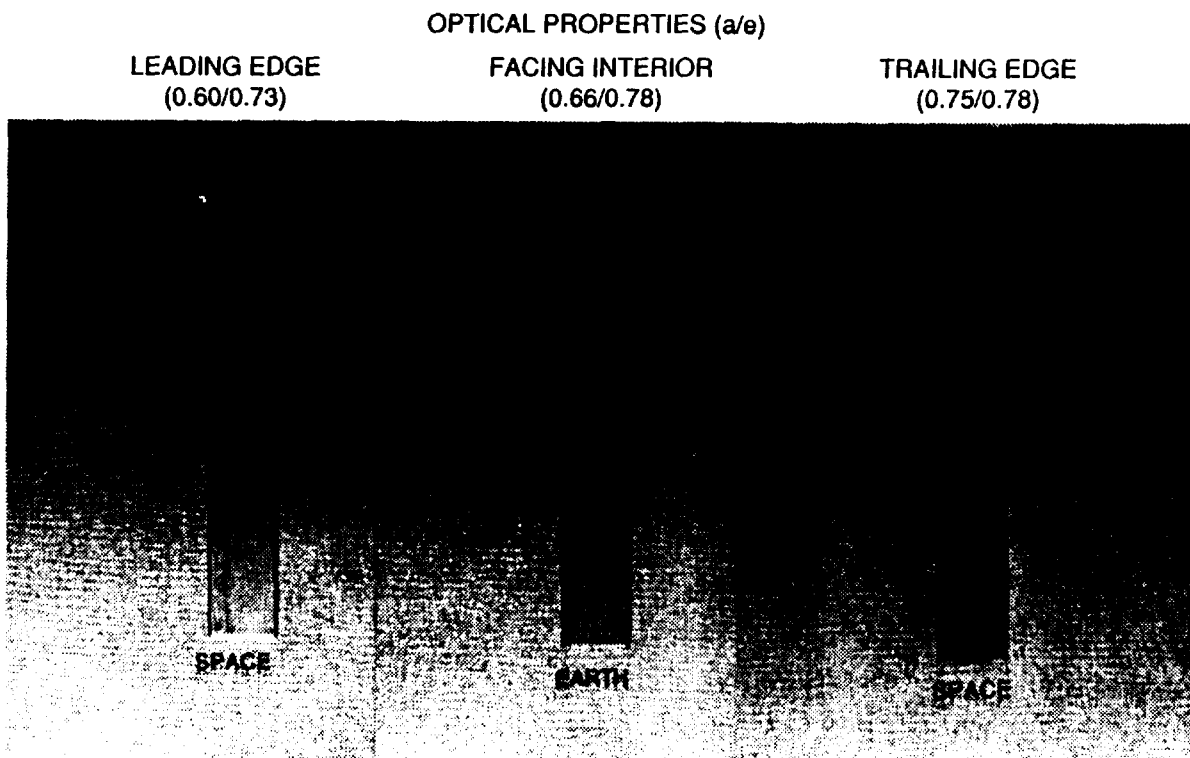


Figure 7. Effects Of LDEF Exposure On Leafing Aluminum (Photo Courtesy of The Aerospace Corporation)

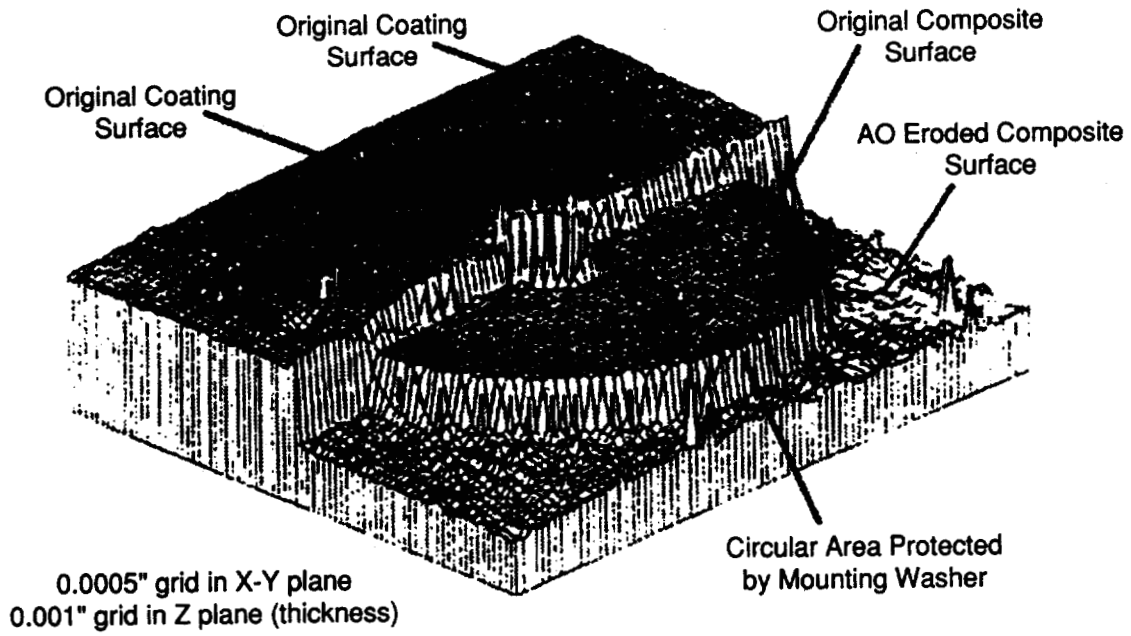


Figure 8. Three-dimensional Plot of Profilometry Measurements Taken From A Partially Coated Graphite/Epoxy Panel

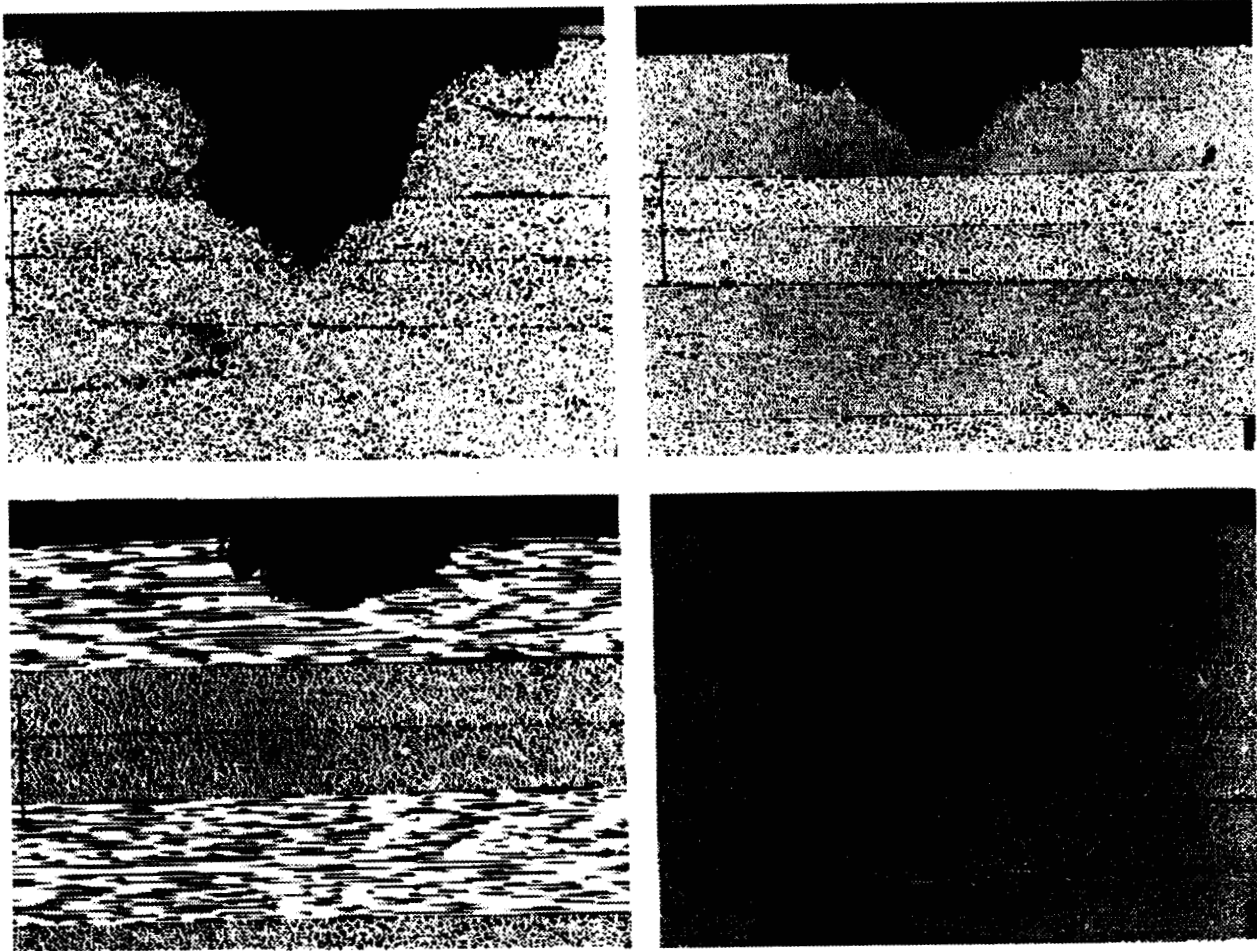


Figure 9. Impact Craters In Graphite/Epoxy

STRUCTURE AND PROPERTIES OF POLYMERIC COMPOSITE MATERIALS DURING 1501
DAYS OUTER SPACE EXPOSURE AT "SALYUT-7" ORBITAL STATION

Oleg V. Startsev
Altai State University
66, Dimitrov St., Barnaul, 656099, Altai,
Russia
Phone: 385/222-1807, Fax: 385/222-2875
E-mail: vup@mezon.altai.su

519-27
44433
15P

Eugene F. Nikishin
"Salyut" Design Office 18, Novozavodskaya St., Moscow, 121087,
Russia
Phone: 095/142-53-05

SUMMARY

Specimens of polymeric composite materials for aviation and space applications such as glass fiber reinforced plastics (GFRP), carbon fiber reinforced plastics (CFRP), organic fiber reinforced plastics (OFRP), hybrid plastics (HP) based on epoxy compounds were exposed to the space environment on the surface of "Salyut-7" orbital station. The space exposure lasted 1501 days as a maximum. The data relating to the change in mechanical properties, mass losses, glass transition temperature, linear thermal expansion coefficient, and microstructure after various periods of exposure are given. It has been found that the change in properties is caused by the processes of binder postcuring and microerosion of the exposed surface of plastics. The phenomenon of strengthening of the surface layer of hybrid composites, due to which the nature of destruction changes at bending loads, has been revealed.

INTRODUCTION

On the initiative of the "Salyut" Design Office and the All-Union Institute of Aviation Materials, a comprehensive study on the effectiveness of modern polymeric composite materials (PCM) after direct long duration exposure to the space environment at "Salyut" and "Mir" orbital stations has been conducted in Russia since 1978. A major goal of the study is to obtain data on the effective degree of space environment factors (SEF) on PCM.

Physical methods with a high resolution have been used along with the traditional techniques for measuring mechanical parameters. A selection of these experimental results has been reported in [1-6]. This review includes general regularities concerning the behaviour of PCM on the "Salyut-7" orbital station's surface, the results obtained, analysis and conclusions relating to the ageing mechanism, the effect of composition, production technology, and protective screens on the change in the properties of PCM during long term exposure to the space environment.

EXPERIMENTAL

Table 1. Characteristics of PCM Specimen

No	Name and Composition of PCM (Epoxy Matrix+ Filler)	Type of PCM ¹	Laying	Size of Specimens, mm	Exposure time, days
1	Organite 7T (5-211BN + SVM cloth article 5303/74)	OFRP	laminated plastic	92x5x2	304, 382 ² , 686
2	KMU-31 (5-211B + carbon thin ribbon LU-3)	CFRP	0 ⁰ , 90 ⁰ ,layer ratio is 1:1	92x5x2	304, 382 ² , 686
3	SK-5-211B (5-211B + glass fiber cloth T-10-80)	GFRP	laminated plastic	92x5x2	304, 382 ² , 686
4	VPS-7 (EDT-10P + glass fiber cloth T-10)	GFRP	laminated plastic	92x5x2	304, 382 ² , 686
5	KMU-2 with one-sided foil coating ³ (SP-97 + carbon ribbon LU-3)	CFRP	0 ⁰ , 90 ⁰ foil AD1M 0.03 mm	66x25x0.46	456 ⁴ , 1501
6	KMU-3ln ⁵ (5-211B + carbon ribbon LU-3)	CFRP	0 ⁰ , 90 ⁰ +0.01mm glass fiber cloth layer	66x50x0.46	456 ⁴ , 1501
7	KMU-4l (ENFB + carbon ribbon LU-P)	CFRP	0 ⁰ , 90 ⁰	66x8x1.75	456 ⁴ , 1501
8	KMU-4l (ENFB + carbon ribbon LU-P)	CFRP	±45 ⁰ , 0 ⁰ , 90 ⁰	66x8x1.75	456 ⁴ , 1501
9	KMU-3l/VK-9/ KMU-3l (5-211B + carbon thin film LU-3/adhesive VK-9/5-211B + carbon ribbon LU-3)	HC (CFRP + CFRP)	0 ⁰ , 90 ⁰ ; layer ratio is 1:1	33x8x3	102, 456 ⁴ , 1501
10	VPS-7/VK-9/KMU-3l(EDT-10P ⁶ + (glass-fiber cloth T-10/ adhesive VK-9/ 5-211B + carbon ribbon LU-3)	HC (GFRP + CFRP)	laminated VPS-7; 0 ⁰ , 90 ⁰ in KMU-3l; layer ratio is 1:1	33x8x3	102, 456 ⁴ , 1501
11	VPS-7/VK-9/ VPS-7 (EDT-10P + (glass fiber cloth T-10/ adhesive VK-9/ EDT-10P + glass fiber cloth T-10	HC (GFRP + GFRP)	laminated systems; layer ratio is 1:1	33x8x3	102, 456 ⁴ , 1501

Notes: 1 - the type of PCM: OFRP - organic fiber reinforced plastic, CFRP - carbon fiber reinforced plastic, GFRP glass fiber reinforced plastic, HC - hybrid composite; 2 - specimens subjected to the test after 304 days of exposure; 3 - exposure with foil: in an inner and outer double layer; 4-specimens subjected to the test after 102 days of exposure; 5 - exposure with glass fiber cloth on the inside in two ways: in a single layer and in a double layer; 6 - exposure with an outer VPS-7 layer.

Materials

Materials of various classes of PCM for aviation and space applications, including GFRP, OFRP, CFRP and hybrid composites, have been selected to conduct the study. The class of CFRP is presented to a much greater extent. Hybrid plastics representing homogeneous and heterogeneous adhesive systems have been first studied. Materials, their composition, exposure conditions and exposure times are listed in Table 1. Before and after the experiments the specimens were stored at a temperature of $293 \pm 3 \text{ K}$ and at a relative humidity of $60 \pm 20\%$.

Exposure Conditions

During the space exposure, easy-to-remove holders with the samples of PCM were located at a distance of 50 mm from the orbital station's screen-vacuum-insulated body near the transfer module (Fig.1). Exposure conditions were characterized by the following parameters: the ambient pressure in

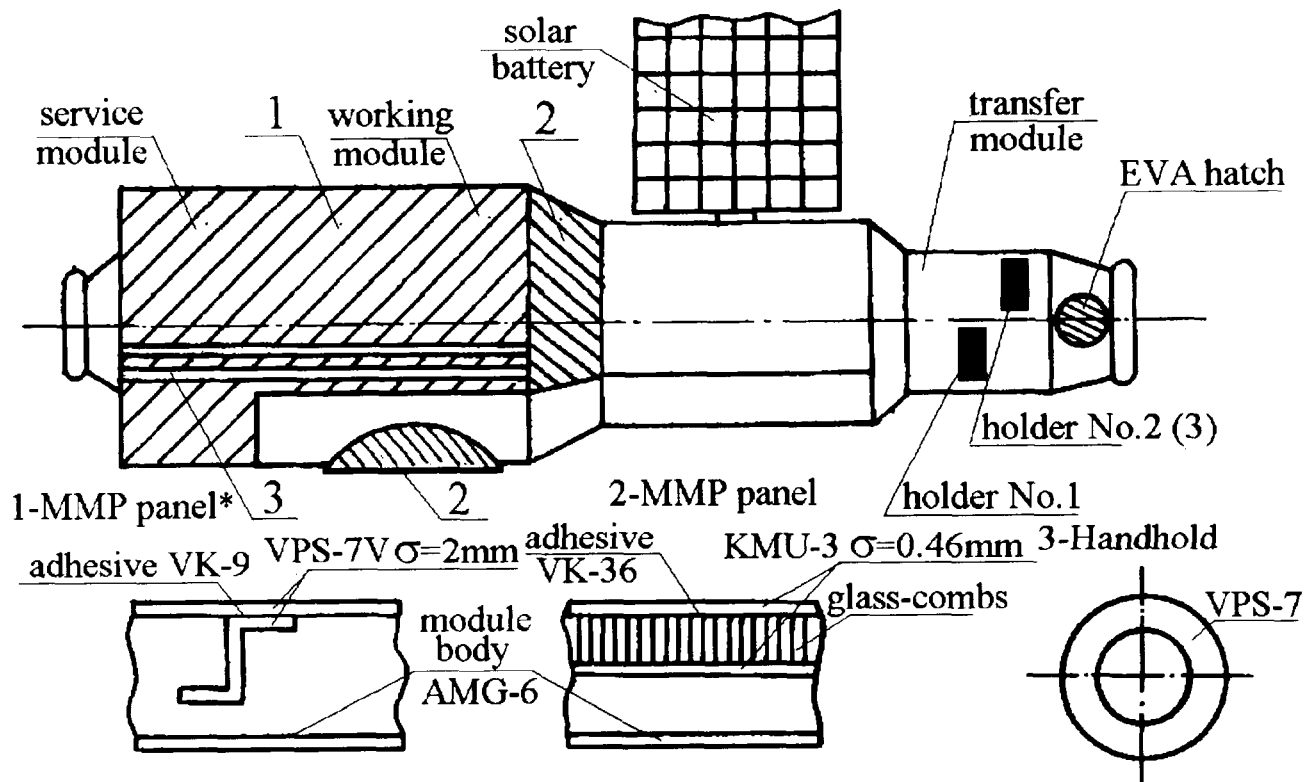


Fig.1. Scheme of locating the PCM specimens at "Salyut-7" orbital station (MMP - micrometeoroid protection)

proximity to the panels with samples was $1.3 \times 10^{-2} \text{ Pa}$; the impact of extra-atmospheric Sun was cyclic with a cycle time of 90 min, of which, on the average, 20 min were in solar illumination; the maximum duration of experiments was 1501 days (2.4×10^4 cycles, 334 equivalent solar days); the averaged concentration of atomic oxygen was estimated as $10^{10} \text{ N} \times \text{cm}^3$ (N - number of atoms). The concentration of O^+ and O_2^+ charged particles was 1-3 orders below. The kinetic energy of atoms was approximately 5

eV; the fluence of atomic oxygen was $7.7 \times 10^{18} m^{-2} s^{-1}$ at an altitude of 300 km and at a velocity of 7.7 km/s; the power of ionizing radiation dose was approximately 0.5 rad/day; the intensity of solar UV-radiation was $1.4 kW/m^2$ in the wavelength range from 0.1 to $0.4 \mu m$; the proton flux with an energy from 0.1 to 4 MeV was $10^8 p^+/cm^2 s$; the electron flux with an energy from 0.1 to 4 MeV was $10^8 e^-/cm^2 s$.

Methods of Study

Two groups of methods were used to conduct the study [1-6]. Methods for which small samples are required were preferred.

The first group was composed of methods characterizing the operating parameters of PCM. The strain-stress characteristics were estimated following the recommendations given in the paper [7]. To determine the mechanical parameters at bending, a scheme of three-point bending of a right-angled bar was used. Loading of samples was performed on the rupture-test machine, a movable bearing velocity which was $13 \pm 1 mm/min$. From the bending tests the four parameters were estimated: E_x^- - modulus of compression, E_{bx} - flexural modulus, σ_{nx} - strength along the normal stresses, σ_{tx} - strength along the tangential stresses. The mass loss was measured using ADV-200M analytical balance with an accuracy of $10^{-7} kg$. The density was estimated by the method of hydrostatic weighing in distilled water at 295 K.

The second group was composed of methods for studying the structure and physical-chemical processes of ageing of PCM. The special requirements imposed upon these methods were the precision and the reproducibility of measurements.

When evaluating thermal expansion, a linear quartz dilatometer with optical reading system [4], the error of measurement of which didn't exceed $1 \mu m$, was used. The linear thermal expansion coefficient α_T was calculated from the measurements of thermal expansion $\Delta l/l_0$ (l_0 is the initial length of a sample).

The microstructure of materials was studied using MBS-9 light microscope and JSM-35C scanning electron microscope designed by JEOL (Japan). The investigation techniques and the interpretation of epoxy matrices' microphotos have been reported in [8].

More comprehensive and precision measurements were taken by dynamic mechanical analysis (DMA). For this purpose, some further steps [9] were provided in the construction of an inverted torsion pendulum and in the measurement techniques to increase the precision of measurements of dynamic shear modulus G' and mechanical loss tangent $tg \delta$ in the temperature range from 77 to 573 K.

RESULTS AND DISCUSSION

Microscopy Data

Even in the first series of experiments [1] it was ascertained that for uncoated PCM under the impact of SEF the stripping of filler fibers occurs due to the destruction and removal of the epoxy matrix surface layer. Depending on the type and chemical composition of fibers, their structure and surface either remain unchanged (glass fiber) or are subjected to etching (which is characteristic of plasma etching in carbon fibers and organic fibers), or even a partial destruction and removal of fibers occur (carbon and organic fibers) on long duration exposure.

Microcracks disposed mainly along the fibers are detected on the surface of specimens (both a right side facing an incident particle flux and a rear side). It has been ascertained that these microcracks are caused by temperature cycling. The composition of epoxy binder, the character of fiber laying, the level of inner tensions, the difference between linear thermal coefficients of a binder and a filler, the exposure duration and other factors have an effect on the formation and the growth of microcracks.

The VPS-7 glass fiber reinforced plastic is the most stable material in the degree of surface conservation among all the studied PCM. However, the surface of GFRP in hybrid No. 10 is damaged to a much greater extent than that one in monoplastic or in hybrid No. 11. It is explained [6] by further temperature stresses in the layer of VPS-7 due to the distinction between values of hybrid layers (See below).

Stable microstructural changes of epoxy matrix on the surface, in the volume and at the fiber interface are observed under the effect of SEF, along with the erosion effects. With increase in exposure time τ , the following processes occur: the aggregation of microparticles (it was reported in [8] before), loosening of initially closely packed matrix in the surface layer, and the reduction in size of overmolecular formation with higher density of packing.

At the surface of binder thin film the boundaries between particle aggregates become more prominent.

Aluminium-foil coating of the KMU-2 surface practically retains the initial structure of the CFRP surface, thus supporting the applicability of such a protection of PCM from the effect of SEF.

Mass Losses

Mass losses of the specimens under the effect of SEF are determined by two components

$$\Delta M = \Delta M_1 + \Delta M_2, \quad (1)$$

where ΔM_1 , mass losses due to moisture desorption and low molecular products residues are proportional to the volume of the specimen; $\Delta M_2 = \frac{\Delta m}{S} \times S_{\text{exp}}$, mass losses due to microerosion effect and etching are proportional to the square of unexposed surface of the specimen S_{exp} .

With increase of τ to $\tau_1 = 100 \div 300$ days the rate of the change of $\frac{\Delta m}{S}$ decreases [6], because the fibers of reinforcing filler with higher erosion stability are stripped as the surface layer of a binder moves farther and farther. Table 2 illustrates that the magnitude $\frac{\Delta m}{S}$ correlates with the thickness of stripped surface layer Δh_{12} of composites in time $\Delta \tau = \tau_2 - \tau_1$, where $\tau_1 \geq 102$ days; $\tau_2 \geq 1501$ days [6].

Table 2. Microerosion of Unprotected Surface of PCM

PCM*	Exposure time, days			$\bar{V} = \frac{\Delta m}{S \Delta \tau} \times 10^3, \text{ g/m}^2 \text{ day}$	$\Delta h_{12}, \mu\text{m}$	Δh in 10 years, μm (Calculation by the formula(2))
	initial time	final time	duration			
1	382	686	304	254	78	269
2	382	686	304	156	49	167
3	382	686	304	38	12	35

4	382	686	304	10	3	7
5	0	456	456	91	35	111
6	0	456	456	104	43	127
7	102	456	354	58	17	
	102	1501	1399	19	23	
	456	150	1045	6.3	6	44
8	102	456	354	44	13	
	102	1501	1399	12	14	
	456	1501	1045	1.3	1	22
9	0	456	456	128	85	
	102	456	354	149	44	
	102	1501	1399	55	63	
	456	1501	1045	23	19	145
10	102	456	354	26	8	
	102	1501	1399	13	15	
	456	1501	1045	8.3	7	39
11	102	456	354	13	2	
	102	1501	1399	4	5	
	456	1501	1045	0.12	3	8

* See Table 1.

The last column of Table 2 represents the estimation of the stripped surface layer thickness h after 10 years of exposure by the relationship

$$\Delta h = \Delta h_1 + K\bar{v} \times (\tau - \tau_2), \quad (2)$$

assuming that at $\tau_2 > 300 \div 1500$ days the rates of mass loss $\bar{v} = \frac{\Delta m}{S(\tau_2 - \tau_1)}$ are constant. The coefficient of proportionality - $K = 0.82 \mu m \text{ m}^2/g$ [6].

From the data given in Table 2 conclusions about comparative erosion stability of tested PCM are evident.

Erosion stability increases in the following sequence: organic fiber reinforced plastics - carbon fiber reinforced plastics - glass fiber reinforced plastics. For CFRP erosion stability increases in the sequence No. 2 \rightarrow No. 6 \rightarrow No. 5 \rightarrow No. 7 \rightarrow No. 8. Erosion stability depends on the way of laying, showing an increase in the plastic with diagonal reinforcement (No.7 and No.8). Erosion stability of GFRP in hybrid No.11 is higher than in hybrid No. 10. As will be show below, in a hybrid composed of heterogeneous materials the distinctions between α_T produce additional temperature stresses and strengthen the destruction of a binder on the surface. The screening either with aluminium foil or polytetrafluoroethylene thin film [1-3] protects the surface of PCM from the effect of erosion. An increase in volumetric content of a filler has a beneficial effect on erosion stability.

Density

The density of PCM remains stable during 1501 days of exposure, changing no more than 1-2% due to surface effects, which is in agreement with microscopy data.

Mechanical Properties

In a few series of experiments [1, 3, 6] it was shown that after exposure the strength parameters of PCM (with the exception of OFRP) don't decrease or even increase (Fig. 2a). The phenomenon of enhancement of strength measured at $T = 393$ K is more noticeable as compared to the initial magnitude at the same temperature (Fig. 2b). The dependences of elasticity modulus at strength, compression and shear are different. For example, E_x^- and G_{xy} shear modulus in plane of the sheet don't change or increase, but the G_{xy} modulus of interlayer shear is reduced by 20-24% for the PCM studied in the paper [3] (Fig. 2c,d). The same characteristics measured at 393 K are generally higher than the initial values at this temperature. For instance, the increase in E_{bx} by 1.5-2 times is recorded in hybrids No.9 and No.10 (Fig. 2e,f). By and large, it is a rather diversified and complicated situation due to a wide scatter (up to 20-30%) of parameters.

The investigations have established two main reasons for such an ambiguous dependence of the PCM mechanical properties parameters. The first reason is connected with the general regularities of mechanical measurements. As the specimens of PCM were of comparatively small size (Table 1), the nature of PCM destruction had a significant effect on the results of measuring [7]. For example, Table 3 shows the fact that for hybrids No.9 and No.10 as distinct from No.11, the nature of destruction at bending load changes after space exposure [6].

Table 3. The Nature of Fracture of Hybrid Composites

PCM*	In the initial state	After 1501 days of exposure
No.9	Cross fracture due to normal stresses or delamination flaws along the adhesive-bonded joint due to tangential stresses.	Cross fracture due to normal stresses in the exposed layer. Lack of any adhesive bonded joints fracture.
No.10	Cross fracture or delamination flaws of CRFP; delamination flaws along the adhesivebonded joints due to tangential stresses.	Dominant fracture of CRFP layer due to tangential stresses. Lack of any adhesive-bonded joints fracture.
No.11	Cross fracture due to normal stresses or delamination flaws along the adhesive-bonded joint due to tangential stresses.	Similar to the initial state.

* Designations are given in Table 1.

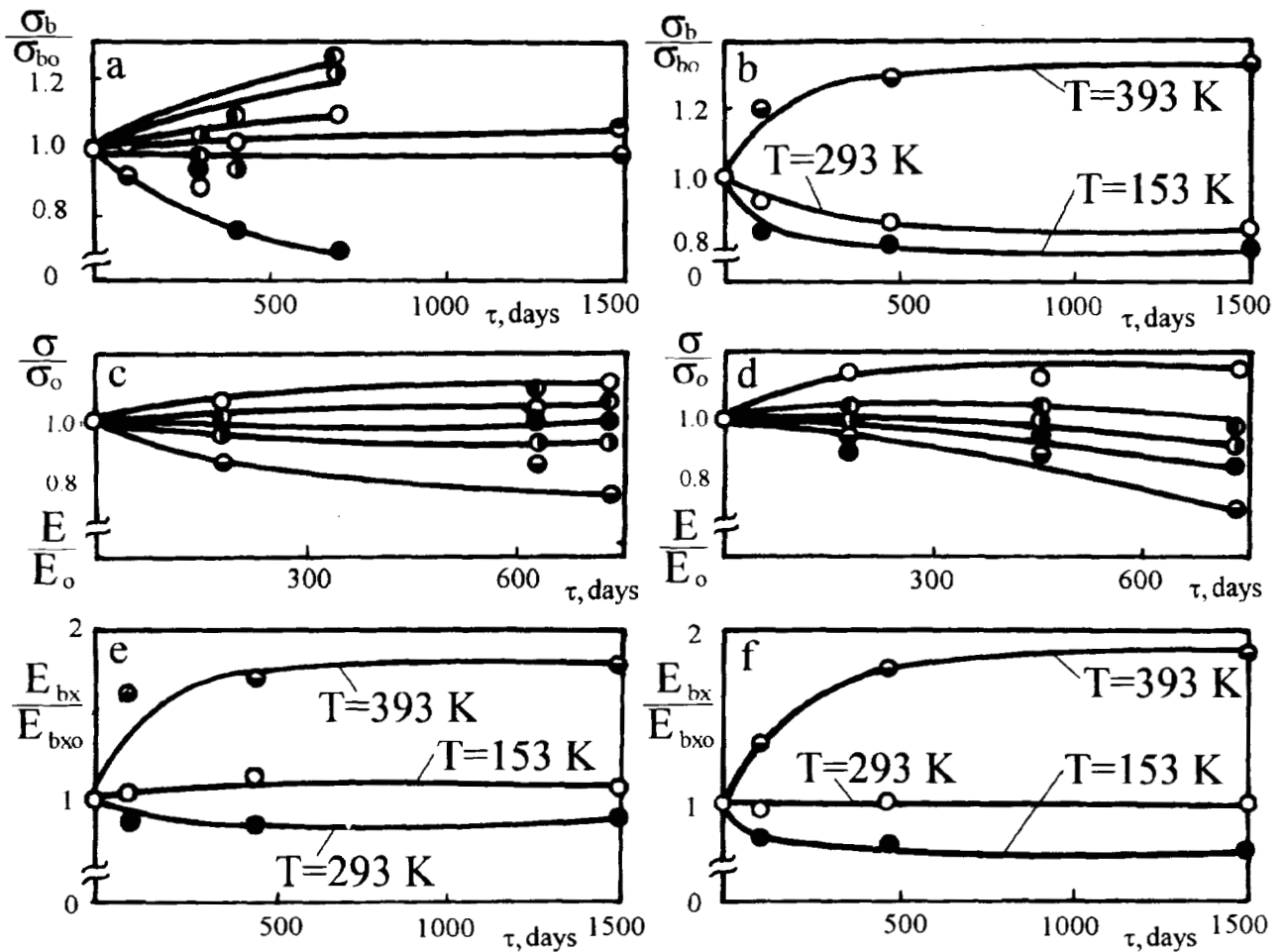


Fig. 2. Exposure-time dependences of the mechanical properties parameters of PCM as compared to the initial magnitude:

a - bending strength (● - N1; ◐ - N2; ◑ - N3; ○ - N4; ◒ - N7; ◓ - N8)

b - bending strength for hybrid No. 10 at various temperatures

c, d - strength (○ - σ_x^- , ● - σ_b) and modulus (◐ - E_x^- , ◑ - G_{xy} , ◒ - G_{xz}) of glass fiber reinforced plastic (c) and carbon fiber reinforced plastic (d) according to the data [3]

e, f - flex modulus at various temperatures for hybrids No. 9 (e) and No. 10 (f)

Taking into account the results obtained in [5, 10], such a change in the nature of fracture is a sign of increasing hardness and strength of carbon fiber reinforced plastic which is a component of hybrid. Strengthening as will be shown below is caused by binder postcuring.

The second reason responsible for a various character of the curves in Fig. 2 e, f derives, according to the data of [10-14], from the superposition of destruction and binder postcuring processes and it will be analysed below.

DMA Data

The investigations performed by DMA method have provided the most detailed body of information on physical and chemical transformations in PCM under the effect of SEF. In a number of papers it has been ascertained a direct relationship between the type of DMA-curves and the structure and the composition of PCM [11-13], chemical structure of a binder [10, 11] and the processes of plasticization [14], ageing [15-16], etc. It is general practice to examine the temperature-dependences of dynamic shear modulus G' , mechanical loss tangent $\operatorname{tg} \delta$, sound velocity $c_t = \sqrt{G'/\rho}$, where ρ - density of material [11].

Fig. 3 depicts an example of DMA-curves for PCM No.1, No.2, No.3 in the initial state and after two exposure periods. A comprehensive analysis of these curves is given in the paper [11]. It has been ascertained that the existence of two temperature regions of decreasing G' , to which the maximums in the curves $\operatorname{tg} \delta(T)$ correspond, is a general regularity. One can obtain an amount of information on the local molecular mobility (β -peak $\operatorname{tg} \delta$ at 200K) and the segmental mobility of a binder (α -peak at $400 \pm 10K$) according to the change in $\operatorname{tg} \delta$ peak height, their position on the temperature scale, as well as according to the interfaces of relaxation regions. The filler has an effect on the character of DMA-curves. For instance, for OFRP (Fig. 3a), α' -peak $\operatorname{tg} \delta$ at 530 K reflecting segmental mobility process and glass transition region of SVM-fiber [11].

As the exposure time increases, G' decreases for PCM No.1 and No.2 in glassy state. The temperature of α -peak $\operatorname{tg} \delta$ increases by 20-30 K, but α' -peak height and position remain intact (Fig. 3a, b, c). These and other changes in DMA-curves are in good agreement with the general scheme of changes commonly observed on postcuring of PCM binder [2, 10, 15, 16]. In Table 4 are given [6] the changes in glass transition temperatures for disordered matrix of a binder (T_{g1}) and for more ordered domains (T_{g2}) of all PCM under maximum duration of SEF effect. Despite different exposure times, the comparison of temperature shifts is rather correct, because the main process of transformations in a binder finishes for 500-700 days (Fig. 4). On evidence from Table 4, for all PCM, one can observe no case of reducing T_{g1} and T_{g2} , which could point to the destruction of a binder [6, 15, 16]. Thus, the process of postcuring dominates clearly over that of possible degradation of exposed surface layer.

The analysis of Table 4 and similar data allow a number of concrete practical conclusions. For instance, the glass transition temperatures of a binder 5-211B of various CFRP kinds (No.No. 2, 6, 9, 10) in the initial state fluctuate in the range from 0 to 40 K. It depends on the composition and production technology [10]. From Table 4 it is evident, that $328 \leq T_{g1} \leq 364 K$, $361 \leq T_{g2} \leq 401 K$. After 456-1501 days outer space exposure the scatters in magnitudes T_{g1} and T_{g2} decrease to 10-15 K. It is apparent, that, on postcuring, a binder keeps to its limiting value of cross-linking degree.

The minimum shifts of T_{g1} and T_{g2} occurred in those materials which were the least heated under solar radiation. The closer the temperature of the heating composite is to the glass transition region of binder, the greater the shift of glass transition temperatures is.

Using composites No. 1 and No. 2 (Fig. 3 a,b) as an example, a manifestation of "anomalous" reduction of G' in glassy state with an increase in crosslinking degree is illustrated [17]. The graph inversion of $G'(T)$ occurs close to T_{g1} . Such an effect is clearly defined in KMU-3l (No.7) carbon fiber reinforced plastic (Fig. 5). Its phenomenological theory is given in the book [18]. Its mechanical mechanism is also known: with increasing cross-linking degree due to additional steric limitations in glassy state, molecular packing level is decreased while the increase of free volume is observed, so G' decreases,

which is often treated by mistake in the literature as the result of microdamages buildup at ageing.

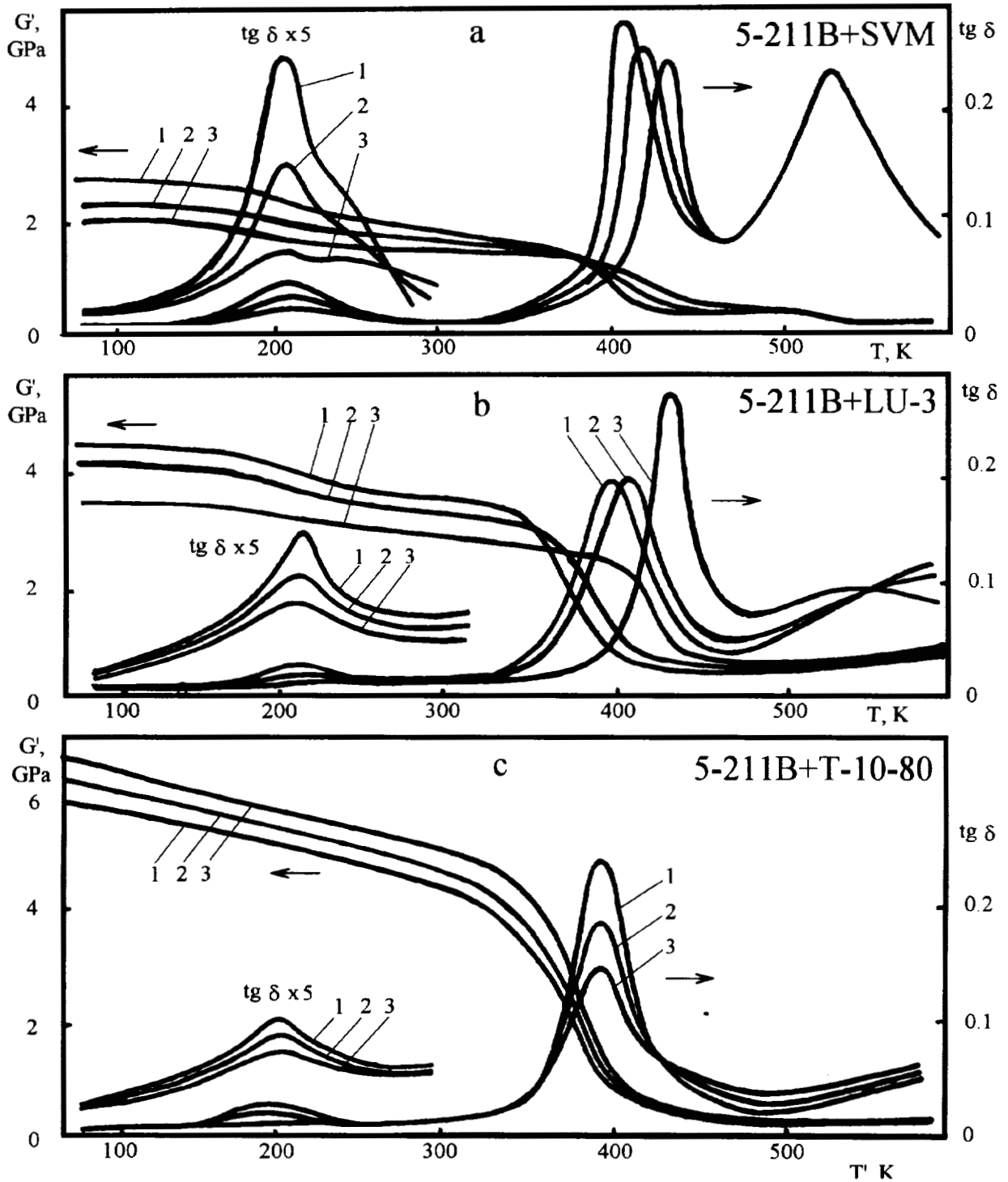


Fig.3. DMA - curves of PCM No.1(a), No.2(b), No.3(c) in the initial state (1) and after 304 (2) and 686 (3) days outer space exposure

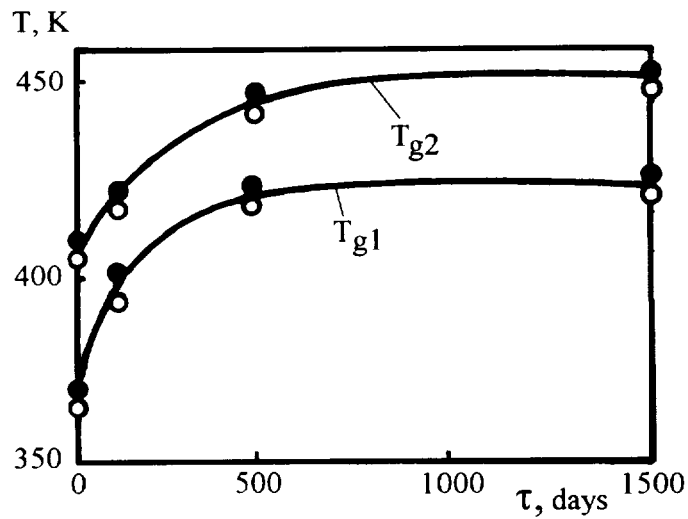


Fig. 4. Exposure - time dependences of glass transition temperatures T_{g1} and T_{g2} for KMU - 4I carbon fiber reinforced plastic: empty circles - No.7. (laying $0^0, 90^0$), dark circles - No.8. (laying $0^0, 90^0, \pm 45^0$)

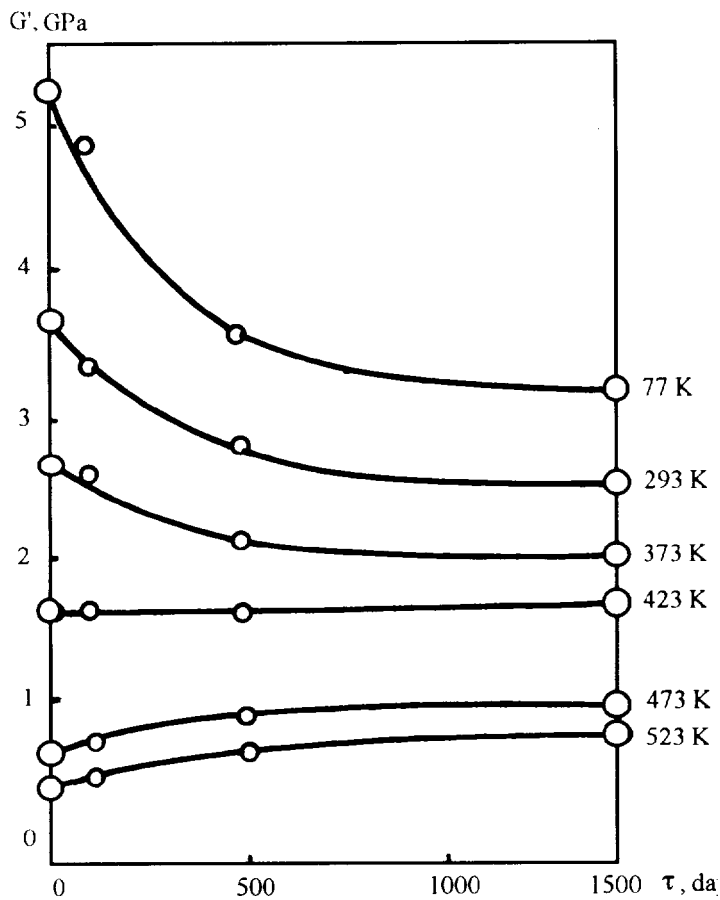


Fig. 5. Exposure - time dependences of dynamic shear modulus for KMU - 4I carbon fiber reinforced plastic measured at various temperatures

Table 4. Effect of exposure to the space environment on glass transition temperatures of PCM binder [6]

PCM, Exposure Conditions	τ , days	T_{g1} , K		T_{g2} , K		ΔT_{g1} , K	ΔT_{g2} , K
		initial state	after exposure	initial state	after exposure		
1	686	328	345	399	418	17	19
2	686	328	390	366	411	62	45
3	686	330	330	368	368	0	0
4	686	311	319	333	340	8	7
5	456	560	562	573	573	2	0
5 (with Al-foil coating)	456	560	563	573	575	3	2
6	1501	364	395	401	423	31	22
6 (screened)	1501	364	395	401	413	31	12
7	1501	365	413	403	447	48	44
8	1501	367	415	403	450	45	47
9 (exposed layer)	1501	351	411	361	427	60	66
9 (unexposed layer)	1501	351	411	361	419	60	58
10 (exposed layer)	1501	309	335	349	371	40	36
10 (unexposed layer)	1501	351	396	371	413	45	17
11 (exposed layer)	1501	320	323	361	373	3	12
11 (unexposed layer)	1501	320	326	361	371	6	10

Taking into account this phenomenon, the reason for increasing mechanical properties parameters of exposed PCM at higher temperature is evident: it is caused by binder postcuring.

Hence, from measuring mechanical properties parameters at 293 K and DMA-data for initial and exposed PCM specimens, one can predict the character of change in strain-stress parameters over a wide range of temperatures.

Linear Dylatometry

PCM based on epoxy compounds have comparatively low linear thermal expansion coefficients α_T [13, 19]. Fig. 6 depicts an example of outer space exposure effect on the thermal expansion Δ/l_0 of the layers for VPS-7 GFRP and KMU-31 CFRP which are components of hybrid No.10. In the initial samples

of PCM in glassy state (when $T < T_{g1}$) one can observe thermal expansion. Due to the relaxation of internal stresses the slope of the curve $\Delta l/l_0 (T)$ reduces for GFRP at $T > T_{g1}$, but due to a negative value of carbon fibers the process of shrinkage (Table 5) is observed in CFRP [13, 19].

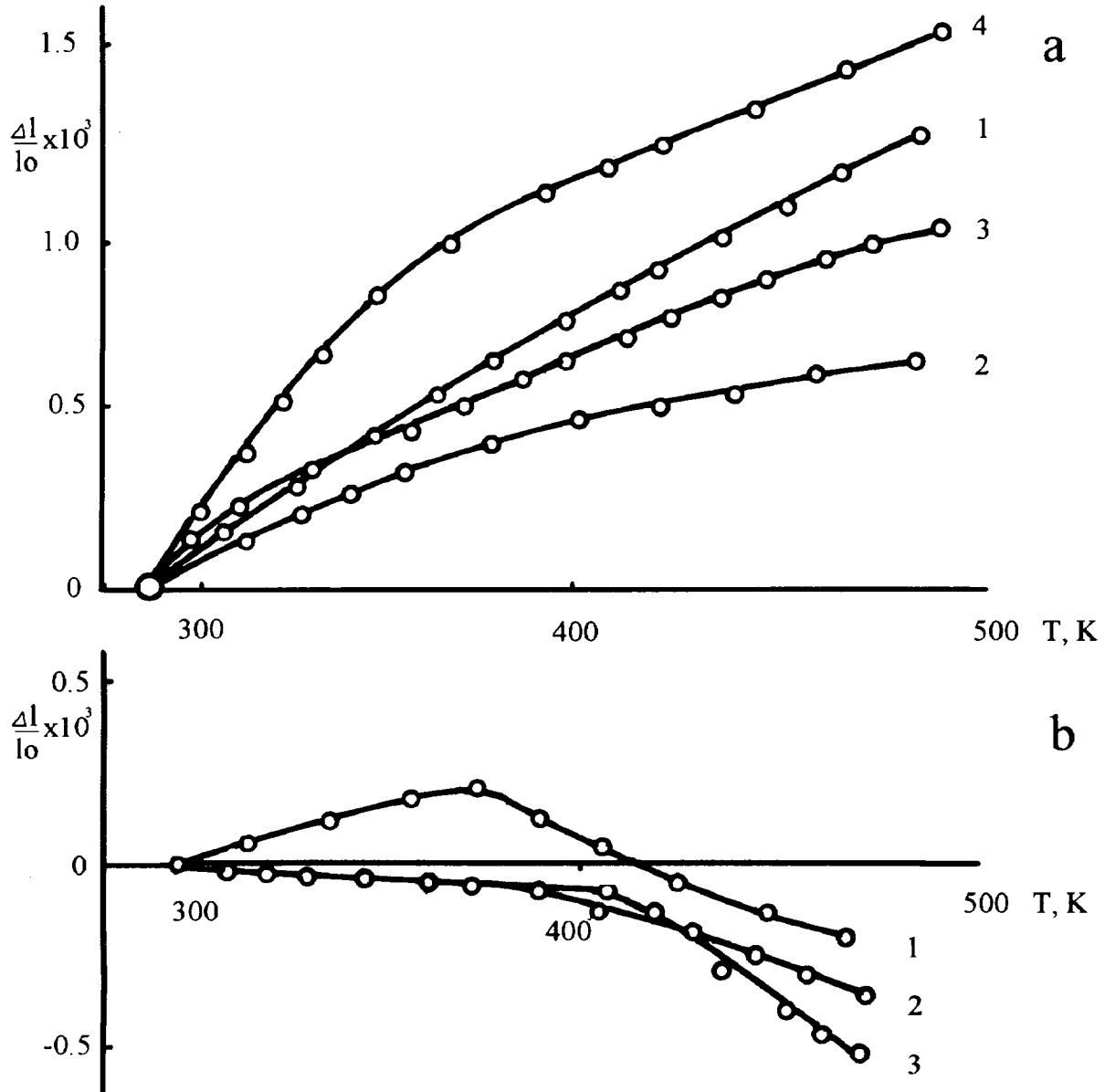


Fig.6. Thermal expansion of VPS-7 glass fiber reinforced plastic (a) and KMU - 31 carbon fiber reinforced plastic (b) which are components of hybrids No.9 - No.11:

a - initial state (1), unexposed layer in hybrid No.11 (2), exposed layer in hybrid No.11 (3), exposed layer in hybrid No. 10 (4);

b - initial state (1), exposed layer in hybrid No.9 (2), unexposed layer in hybrid No.10 (3)

Table 5. Effect of outer space exposure on linear thermal expansion coefficient [6]

PCM	Composition, Exposure Conditions	$\alpha_T \times 10^6, K^{-1}$			
		$T < T_{g1}$		$T > T_{g1}$	
		initial	after 1501 days	initial	after 1501 days
VPS-7	unexposed layer of hybrid No. 11	7.3	5.7	4.7	2.1
	unexposed layer of hybrid No. 9	7.3	10.3	4.7	3.5
	unexposed layer of hybrid No. 10	7.3	19	4.7	3.4
KMU-31	unexposed layer of hybrid No. 10	1.3	-0.8	-0.3	-3.3
	unexposed layer of hybrid No. 9	1.3	-0.5	-0.3	-7
KMU-41	No. 7	1.4	0.6*	-4.2	-2.4*
	No. 8	0.9	0.9*	-2.4	-1.6*

* - after 102 days of exposure

After 1501 days of exposure $\Delta l/l_0$ of VPS-7 unexposed layer is nearly halved as compared to initial specimens (Fig. 6a). In the exposed layer of hybrid No. 11 the magnitude α_T of VPS-7 increases greatly at $T < T_{g1}$, (Table 5), during which the range of increase is greater in the exposed layer of VPS-7 in hybrid No. 10 due to softening the binder structure under the effect of SEF. Such a result is in excellent agreement with the microscopy data, as well as with the information on mass losses, change in mechanical properties and heat resistance.

Even approximate estimations show the following facts: for hybrid No. 10 due to VPS-7 layer expansion and KMU-31 shrinkage in the process of temperature cycling with the cycle amplitude in excess of 200 K, additional internal stresses occur. Their value ranges up from 15 to 25 MPa, i. e. 0.1-0.2 of fracture stress at temperatures of 373-393 K. From Fig. 6 it is evident that the level of internal stresses increases in hybrid No. 10 with increasing the exposure time.

In a similar way the thermal expansion of KMU-41 CFRP with orthogonal structure of layers (No. 7) decreases, while the effect of SEF is attenuated by inserting layers above $\pm 45^\circ$ in the reinforcement scheme (Table 5).

Conclusion

Binder postcuring is the main process which has an effect on the properties of PCM on long duration exposure to SEF. The phenomenon of postcuring depends on the composition and structure of composite material, its production technology, the initial degree of cross-linking, the maximum temperature of thermal cycles and the exposure time. The binder postcuring has a beneficial effect on the mechanical properties parameters of PCM. Excepting ORFP, strain-stress parameters of composite materials measured

at room temperature don't reduce after 456-1501 days of exposure to the space environment, and even increase at higher temperatures.

More detailed conclusions about the mechanism of physical, chemical and structural transformations are given in the papers [1-6]. The use of physical thermal methods of analysis allows us to gain a considerable body of information on the regularities concerning the behaviour of PCM under outer space conditions.

REFERENCES

1. E. A. Barbashov, M. I. Dushin, Yu. N. Ivonin, V. I. Kosin, E. F. Nikishin, B. I. Panshin, B. V. Perov. In the book: *Space Technology and Study of Materials* Ed. by A. S. Okhotin, Moscow, Acad. of Sci. USSR Publ., pp. 78-84 (1982).
2. G. M. Gunayev, M. I. Dushin, Yu. N. Ivonin, L. A. Kvacheva, V. V. Mikhailov, E. F. Nikishin, O. V. Startsev, *Mechanics of Compos. Mater. (Riga)*, 19, 211 (1983).
3. I. G. Jigun, Yu. N. Ivonin, R. P. Shlitsa, E. F. Nikishin, *Mechanics of Compos. Mater. (Riga)*, 23, 813 (1987).
4. O. V. Startsev, V. P. Rudnev, Yu. N. Ivonin, E. F. Nikishin, E. A. Barbashov, V. A. Bogatov, B. V. Perov, *Polym. Sci., USSR*, 29A, 2577 (1987).
5. Yu. M. Vapirov, Thesis (1989).
6. O. V. Startsev, E. F. Nikishin, *Mechanics of Compos. Mater. (Riga)*, 29, 457 (1993).
7. Yu. M. Tarnopolsky, T. A. Kinthis. *Methods of Static Tests of Reinforced Plastics*, Moscow, 272 pp. (1981).
8. I. S. Deev, L. P. Kobets, *Mechanics of Compos. Mater. (Riga)*, 22, 3 (1986).
9. O. V. Startsev, Yu. M. Vapirov et al. Patents of the USSR No. 1045070 (1983), No. 1099236 (1984), No. 1221542 (1986), No. 1359685 (1987).
10. *Problems of Aviation Science and Technique. Series: Aviation Materials. Climatic Ageing of Polymeric Composite Materials.* Ed. by B. V. Perov and O. V. Startsev, Moscow (All-Union Institute of Aviation Materials), 100 pp. (1990).
11. O. V. Startsev and I. I. Perepechko, *Mechanics of Compos. Mater. (Riga)*, 20, 387 (1984).
12. O. V. Startsev, I. I. Perepechko et al., *Dokl. Acad. Nauk USSR*, 267, 1412 (1982).
13. O. V. Startsev, Yu. M. Vapirov et al., *Polym. Sci. USSR*, 28A, 1842 (1986).
14. O. V. Startsev, I. I. Perepechko et al., *Polym. Sci. USSR*, 25B, 457 (1983).
15. O. V. Startsev, V. P. Meletov et al., *Mechanics of Compos. Mater. (Riga)*, 22, 462 (1986).
16. O. V. Startsev, Yu. M. Vapirov et al. *Mechanics of Compos. Mater. (Riga)*, 22, 637 (1986).
17. O. V. Startsev, G. P. Mashinskaya and V. A. Yartsev, *Mechanics of Compos. Mater. (Riga)*, 20, 593 (1984).
18. I. I. Perepechko. *Introduction to Polymer Physics*, M., Khimiya, 312 pp. (1978).
19. G. M. Gunayev. *Structure and Properties of Fiber Reinforced Plastics*, M., Khimiya, 232 pp. (1981).

OVERVIEW OF THE LDEF MSIG DATABASING ACTIVITIES

Joan G. Funk
 NASA Langley Research Center
 Hampton, Va 23681-0001
 Phone: 804/864-3092, Fax: 804/864-4449

ABSTRACT

The Long Duration Exposure Facility (LDEF) and the accompanying experiments were composed of and contained a wide variety of materials, representing the largest collection of materials flown in low Earth orbit (LEO) and retrieved for ground-based analysis to date. The results and implications of the mechanical, thermal, optical, and electrical data from these materials are the foundation on which future LEO spacecraft and missions will be built. The LDEF Materials Special Investigation Group (MSIG) has been charged with establishing and developing databases to document these materials and their performance to assure not only that the data are archived for future generations but also that the data are available to the spacecraft user community in an easily accessed, user-friendly form. This paper gives an overview of the current LDEF Materials Databases, their capabilities and availability. An overview of the philosophy and format of a developing handbook on LEO effects on materials is also described.

INTRODUCTION

The LDEF is a reusable, unmanned spacecraft designed to accommodate a wide variety of technology and science experiments which require long-term exposure to a known LEO environment. The LDEF was designed to be transported into LEO via the Space Shuttle, free-fly for an extended time period, and be retrieved by the Space Shuttle for return to Earth. The LDEF was deployed on April 7, 1984 into a nearly circular 257 nautical mile orbit with a 28.4 degree inclination. On January 29, 1990, the LDEF was retrieved at a decreased altitude of 179 nautical miles after 69 months in space. During the mission life, the LDEF was exposed to the range of solar conditions including solar minimum and maximum. As LDEF was gravity gradient stabilized, the leading edge of the spacecraft saw the greatest atomic oxygen (AO) exposure, 5.8×10^{22} atoms/in², with the trailing edge of the spacecraft having only minimal AO exposure. The environment that the LDEF was exposed to is described in reference 1.

The LDEF MSIG was formed to investigate the effects of long-term LEO exposure on structure and experiment materials which were not original test specimens. A significant part of the MSIG's charter is to establish and develop electronic databases which will eventually contain the wide variety and vast quantity of electrical, thermal, optical, and mechanical materials data being generated by the MSIG members and other LDEF investigators (ref. 1, 2). The MSIG chose to accomplish this task by a three-pronged approach as shown in figure 1. The first approach was to build on the Optical Materials Database developed by the Boeing Defense & Space Group under the auspices of the Systems Special Investigation Group (ref. 3). The Optical Materials Database was expanded and four other IBM/Macintosh software-based databases, commonly referred to mini-databases, were developed.¹ The second approach utilized a pre-existing global access database system, the Materials and Processes Technical Information System (MAPTIS), as the host for the LDEF Materials Database. The third approach was to develop a version of the LDEF Materials Database for use with PDA Engineering's

¹ Work done under NASA Langley Research Center contract NAS1-19247.

M/VISION^{2,3} software. An overview of the capabilities and requirements of the databases is discussed. Information on availability and how to access these databases is also given.

MINI-DATABASES

Under contract to the SSIG and MSIG, Boeing Defense & Space Group has developed a series of databases containing results from LDEF on specific topics. These databases were developed to provide the user community with early access to LDEF data. The databases were developed for use with IBM and Macintosh versions of Filemaker⁴ Pro software. Filemaker Pro is a flat file database which means that the user can retrieve multiple data types such as tabular data, text, graphs, diagrams, and or picture files. The databases' simple interface allows for easy use of the database by the novice user. The individual databases are password protected, allowing the user full access privileges to read, print, or download the data but not allowing the user to edit the data. The software allows the user to search and retrieve specific information in a variety of layouts. Data can be exported to a variety of formats including ASCII. All data is traced back to its original data source. A more detailed report of the capabilities of these mini-databases can be found in reference 3.

The mini-databases cover the optical materials, silverized Teflon thermal blankets, treated aluminum hardware, thermal control paints, and the LDEF environment areas of interest. The Optical Materials Database is a compilation of the results on the optical materials flown on LDEF and was originally developed by the SSIG. The Silverized Teflon Thermal Blankets Database covers the results from the silverized Teflon thermal blankets utilized on LDEF. The Treated Aluminum Hardware Database is a compilation of data from the various types of aluminum hardware flown on or as part of the LDEF structure including different alloys, surface conditions, etc. The Thermal Control Paints Database contains information on the wide variety of paints flown on LDEF. The LDEF Environments Database contains information on the environment that LDEF was exposed to, including thermal profiles, and solar UV, and AO exposures levels. An order form for the mini-databases is given as figure 2.

MAPTIS VERSION OF THE LDEF MATERIALS DATABASE

NASA Marshall Flight Center has incorporated the LDEF Materials Database as a part of their automated storage, retrieval, and display database system. The preliminary version of the LDEF Materials Database was released on MAPTIS in June of 1992 and an updated version is currently available to all interested parties in the international space community. The goal of MAPTIS is to provide an efficient, reliable means of supplying the information needed for the selection and application of materials and processes to produce the hardware required for NASA's and industry's current and future space missions. MAPTIS uses ORACLE Corporation's relational data management system and can be accessed via modem and a 1-800 phone number or via Internet. There are several different databases in MAPTIS, one of which is the LDEF Materials Database.

The LDEF Materials Database allows the user to view and search a listing of the materials flown on LDEF, a listing of materials by specific material or material type, a listing of materials by property and property value, and original data source. All of the data is traced back to the original reference. Only tabular data is given as output of the MAPTIS version of the LDEF Materials Database. An order

² The use of trademarks or names of manufacturers in this report is for accurate reporting and does not constitute an official endorsement, either expressed or implied, of such products or manufacturers by the National Aeronautics and Space Administration.

³M/VISION is a registered trademark of PDA Engineering.

⁴Filemaker Pro is a registered trademark of Claris Corporation.

form for the MAPTIS version of the LDEF Materials Database is given in figure 3.

M/VISION VERSION OF THE LDEF MATERIALS DATABASE

M/VISION is a materials software system, developed and marketed by PDA Engineering, which facilitates the organization and visualization of materials engineering data. M/VISION allows the user to analyze, manipulate, query, and graph materials data. The M/VISION software includes graphics, spreadsheet, imaging, and modeling capabilities as well as databasing capabilities. Multiple data types, such as tabular data, graphs, and raster images (e.g., C-scans, photomicrographs, etc ...) can be stored in a single M/VISION database. M/VISION is a hybrid hierarchical/relational database with both hierarchical and standard Structure Query Language (SQL) interfaces. An integrated engineering spreadsheet is included in the software that provides the user an efficient means to manipulate and visualize the information in the database. Databases can be manipulated via user-written FORTRAN and C codes.

A version of the LDEF Materials Database that runs on M/VISION is current available to the international space materials community to run on their own licensed M/VISION software. The user can examine data based on specific materials, environmental parameters such as UV or AO exposure, experiment number, and data source. Once again all data is referenced to the original data source. Data from the LDEF Materials Database can be operated on and graphed using this software tool. An order form for the M/VISION version of the LDEF Materials Database is given in figure 4.

HANDBOOK

The results from LDEF and other LEO experiments and spacecraft are being used to determine the "rules of thumb" governing the relationship between the LEO environment and materials effects and life performance. The "rules of thumb" and the data to support them are being compiled into a handbook by TRW, Inc. under contract to NASA Langley Research Center. The principal audience for the handbook is the LEO spacecraft designer. The handbook is expected to be available in early 1995.

SUMMARY

Data from the materials and systems flown on LDEF experiments or as part of the LDEF structure is available in a variety of formats to suit the needs of the international space user community. All forms are available free-of-charge by filling out the request forms found in figs. 2-4.

ACKNOWLEDGMENT

The author would like to thank Dr. Gary Pippin and Gail Bohnhoff-Hlavacek of Boeing Defense & Space Group for their work on the mini-databases, Marshall Space Flight Space Center and their contractor's BAMSI, Inc. specifically John Strickland and Frankie Leath for their work on the LDEF Materials Database and PDA Engineering for their support of the M/VISION version of the LDEF Materials Database. The support of the LDEF principal investigators in allowing us to utilize their data is gratefully acknowledged.

REFERENCES

1. Levine, Arlene S., ed.: *LDEF- 69 Months In Space: First Post-Retrieval Symposium*, NASA CP-3134, January 1992.
2. Stein, Bland A.: "An Interim Overview of LDEF Materials Findings," NASA TM-107664, August 1992.
3. Bohnhoff-Hlavacek, Gail: "Databases For LDEF Results," *Second LDEF Post-Retrieval Symposium*, NASA CP-3194, Part 3, April 1993, pp. 1223-1233.

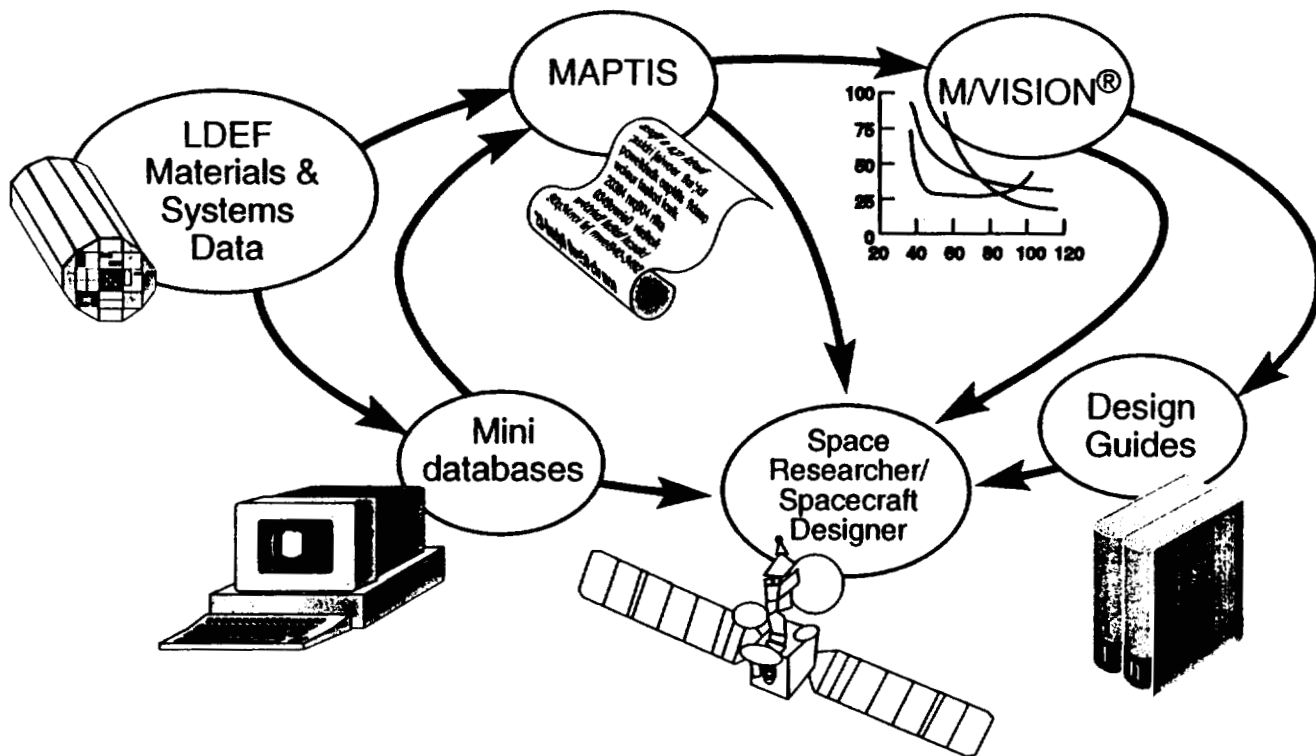


Figure 1. LDEF Materials databasing approach.

User Request Form for the Long Duration Exposure Facility (LDEF)

Materials Mini-Databases

Date: ___/___/___

Format: _____ IBM-compatible or _____ Macintosh

(runs on Claris Corporation's FileMaker® Pro version 2.0 or later software)

Databases requested:

- _____ LDEF Optical Materials Database
- _____ LDEF Treated Aluminum Database
- _____ LDEF Thermal Control Coatings Database
- _____ LDEF Silverized Teflon® Database
- _____ LDEF Environment Database

Name: _____

Company: _____

Address: _____

City: _____ State: _____ Zip Code: _____

Phone Number: (_____) _____ - _____

Complete and return this form along with one High Density Diskette (1.44MB) for each database requested to Gary Pippin, Boeing Defense & Space Group, P.O. Box 3999, M/S 82-32 , Seattle, WA 98124. If you have any questions contact Gary Pippin (206)773-2846 or Joan Funk at (804)864-3092.

Figure 2. Request form for the mini-databases.

**User Request Form for the Long Duration Exposure Facility (LDEF)
Materials Database on
the Materials and Processes Technical Information System (MAPTIS)**

Date: ___/___/___

Employee Name: _____
(first) (mi) (last)

Company/Mail Code: _____

Work Address: _____

City: _____ State: _____ Zip Code: _____

Office Telephone Number: (____)____-____ FAX: (____)____-____

Do you have access to a NETWORK? (Yes/No) _____ Network: _____

Check one only:

Govt Contractor _____ Industry User _____ NASA (MSFC) _____

Bamsi/BCSS Programmer _____ EH02 Personnel _____ NASA (other) _____

Signature _____ Date: ___/___/___

Do Not Write Below This Line- System Information

User name: _____ Uic:[_____,_____]

Password: _____

NPSS/PSCN ID: _____ Initial Password: _____

Creation Date: ___/___/___ By: _____

Deletion Date: ___/___/___ By: _____

Complete and fax this form to Rene Hitson at (205)544-5786. If you have any questions contact Rene Hitson at (205)544-6972 or Joan Funk at (804)864-3092.

Figure 3. Request form for the MAPTIS version of the LDEF Materials Database.

**User Request Form for the Long Duration Exposure Facility (LDEF)
Materials Database in the M/VISION ® Format**

Date: ___/___/___

Employee Name: _____
(first) (mi) (last)

Company/Mail Code: _____

Work Address: _____

City: _____ State: _____ Zip Code: _____

Office Telephone Number: (____)____-____ FAX: (____)____-____

Do you have access to a NETWORK? (Yes/No) _____ Network: _____

Check one only:

Govt Contractor _____ Industry User _____ NASA (MSFC) _____

Bamsi/BCSS Programmer _____ EH02 Personnel _____ NASA (other) _____

Signature _____ Date: ___/___/___

Do Not Write Below This Line- System Information

User name: _____ Uic:[_____,_____]

Password: _____

NPSS/PSCN ID: _____ Initial Password: _____

Creation Date: ___/___/___ By: _____

Deletion Date: ___/___/___ By: _____

Complete and fax this form to Rene Hitson at (205)544-5786. If you have any questions contact Rene Hitson at (205)544-6972 or Joan Funk at (804)864-3092.

Figure 4. Request form for the M/VISION version of the LDEF Materials Database.

REPORT DOCUMENTATION PAGE			Form Approved OMB No. 0704-0188	
Public reporting burden for this collection of information is estimated to average 1 hour per response, including the time for reviewing instructions, searching existing data sources, gathering and maintaining the data needed, and completing and reviewing the collection of information. Send comments regarding this burden estimate or any other aspect of this collection of information, including suggestions for reducing this burden, to Washington Headquarters Services, Directorate for Information Operations and Reports, 1215 Jefferson Davis Highway, Suite 1204, Arlington, VA 22202-4302, and to the Office of Management and Budget, Paperwork Reduction Project (0704-0188), Washington, DC 20503.				
1. AGENCY USE ONLY (Leave blank)	2. REPORT DATE February 1995	3. REPORT TYPE AND DATES COVERED Conference Publication		
4. TITLE AND SUBTITLE 69 Months In Space: Third LDEF Post-Retrieval Symposium			5. FUNDING NUMBERS 233-03-02-03	
6. AUTHOR(S) Arlene S. Levine, Editor				
7. PERFORMING ORGANIZATION NAME(S) AND ADDRESS(ES) NASA Langley Research Center Hampton, VA 23681-0001			8. PERFORMING ORGANIZATION REPORT NUMBER L-17430B	
9. SPONSORING/MONITORING AGENCY NAME(S) AND ADDRESS(ES) National Aeronautics and Space Administration Washington, DC 20546-0001			10. SPONSORING/MONITORING AGENCY REPORT NUMBER NASA CP-3275, Part 2	
11. SUPPLEMENTARY NOTES				
12a. DISTRIBUTION/AVAILABILITY STATEMENT Unclassified—Unlimited Subject Category 99			12b. DISTRIBUTION CODE	
13. ABSTRACT (Maximum 200 words) This volume is a compilation of papers presented at the Third Long Duration Exposure Facility (LDEF) Post-Retrieval Symposium. The papers represent the data analysis of the 57 experiments flown on the LDEF. The experiments include materials, coatings, thermal systems, power and propulsion, science (cosmic ray, interstellar gas, heavy ions, micrometeoroid, etc.), electronics, optics, and life science. In addition, papers on preliminary data analysis of EURECA, EOIM-3, and other spacecraft are included.				
14. SUBJECT TERMS Space Experiment			15. NUMBER OF PAGES 354	
			16. PRICE CODE A16	
17. SECURITY CLASSIFICATION OF REPORT Unclassified	18. SECURITY CLASSIFICATION OF THIS PAGE Unclassified	19. SECURITY CLASSIFICATION OF ABSTRACT Unclassified	20. LIMITATION OF ABSTRACT	